Genetic and Functional Studies of Mutations affecting cell adhesion proteins in Arrhythmogenic Right Ventricular Cardiomyopathy (ARVC)

PhD thesis

June 2008

HATIM Y EBRAHIM

Department of Medicine

UNIVERSITY COLLEGE LONDON

ProQuest LLC
789 East Eisenhower Parkway
P.O. Box 1346
Ann Arbor, MI 48106-1346

Declaration of Originality of this work

I, Hatim Y Ebrahim, confirm that the work presented in this thesis is my own. Where information has been derived from other sources, I confirm that this has been indicated in the thesis.

Hatim Y Ebrahim

June 2008

Acknowledgements

I would like to thank Professor William J McKenna for the opportunity to undertake my PhD work in his group and for providing facilities, resources, and his tremendous support, guidance, and encouragement through all stages of my work. I am grateful to Dr Petros Syriss for his direction and guidance in the genetic screening and family studies of ARVC probands. I would like to thank Professor Chris Fry and Dr Rosaire Gray for their support with the electrophysiological studies and interpretation of the data. The expert technical assistance of Mr Peter Balson with electron microscopy analysis of stable cell lines and interpretation of the data is much appreciated. I am most grateful to Professor Kathleen Green (Northwestern University, Illinois, USA) for her advice on the desmoplakin project and for kindly providing plasmid vector encoding full-length desmoplakin, which made the desmoplakin functional study possible. I thank Dr Lisa Godsel (Northwestern University, Illinois, USA) for her guidance and discussions in desmoplakin functional study. I am indebted to Drs. Petros Syrris and Katja Ghemlick for critical reading of my thesis. Finally, the forbearance and support of my wife, Fatema and of my son, Juzer throughout my PhD allowed this work to fruition.

Quote - interdependent interactions in systems

"The systems view looks at the world in terms of relationships and integration. Systems are integrated wholes whose properties cannot be reduced to those of smaller units. Instead of concentrating on basic building blocks or basic substances, the systems approach emphasizes basic principles of organization. Every organism - from the smallest bacterium through the wide range or plants and animals to humans is an integrated whole and thus a living system. ...But systems are not confined to individual organisms and their parts. The same aspects of wholeness are exhibited by social systems- such as an anthill, a beehive, or a human family - and by ecosystems that consist of a variety of organisms and inanimate matter in mutual interaction. What is preserved in a wilderness area is not individual trees or organisms but a complex web of relationships between them.

All these natural systems are wholes whose specific structures arise from the interactions and interdependence of their parts. The activity of systems involves a process known as transaction- the simultaneous and mutually interdependent interaction between multiple components."

- Fritjof Capra
the Turning Point

Abstract

ARVC is a cardiac disease associated with ventricular cardiomyocyte fibro-fatty replacement and sudden death. It presents with incomplete penetrance and variable clinical expression. Desmoplakin (DP) and plakoglobin (PG) gene mutations were previously identified.

This study aimed: to identify desmosomal (DS) gene mutations in an ARVC cohort by DNA sequencing; study the gene transmission and disease expression in affected families and determine functional implications of three identified mutations (A733fsX740PKP-2, S140FPKP-2 and Q273fsX288DP) using wild-type and mutant cDNA plasmid cloning and cell line protein expressions.

Eight PKP-2 mutations were identified of which four were novel: frame-shifts disrupting Armadillo domains (ARM) 4, 5 and 8, and a non-sense disrupting ARM 2. One missense and two frame-shift novel DP mutations occurred. Pedigree analysis showed incomplete gene penetrance and variable ARVC expression.

Stable cells over-expressing A733fsX740PKP-2 showed increased cellular adhesion and apoptosis following mechanical stretch recovery, and absence of cell junction Connexin-43 (Cx43) protein without significant change in cell-input resistance. Desmosomal lengths were statistically unaltered, but intermittent pale DS coupling occurred. Truncated PKP-2 showed reduced PG interaction.

Stable cells over-expressing S140FPKP-2 showed no differences in cell proliferation, adhesion, apoptosis following mechanical stretch recovery, and in cell junction Cx43 protein localization. DS lengths, however, were significantly increased, and missense PKP-2 showed reduced β-catenin interaction.

Stable cells over-expressing Q273fsX288 DP showed reduced DS widths, vimentin filament retraction, and lower monolayer adhesion. PG and PKP-2 interacted normally with truncated DP.

Altered DS morphologies featured prominently in all three mutant protein expressions. Reduced inter-protein interactions of truncated and missense PKP-2 proteins with PG and β-catenin respectively suggests PG and β-catenin signalling may be affected. Q273fsX288DP expression lacking DP distal domains correlated with loss of DS filament association. These data suggests that expression of mutant desmosomal proteins leads to abnormal DS formation, thus providing the substrate for arrhythmia and cardiomyopathy.

CONTENTS

Abbreviations

α-catenin	alpha-catenin
α-actinin	alpha-actinin
AJ	Adherens junction (also abbreviated fa -*fascia adhaerens* in Figure 1.2)
ARM	Armadillo repeat
as	conserved, splice site acceptor sequence in an intervening (intron) sequence
APC	Adenamatous polyposis coli protein
ARVC	Arrhythmogenic Right Ventricular Cardiomyopathy
ATP	Adenosine 5'-triphosphate
α-MHC	alpha myosin heavy chain
β-actin	Beta-actin
β-catenin	Beta catenin
βTRCP	Ubiquitin lygase
bp	Base pairs
Ca^{2+}	Calcium cation
CBC	Cap-binding complex
cDNA	Complementary deoxyribonucleic acid
C-terminus	Carboxyl terminus
C-TAK1	Cdc25C-associated kinase1 enzyme
Cul1	Cullin 1
Cx	Connexin
Da	Dalton
DAPI	4', 6-Diamidino-2-phenylindole
DCM	Dilated cardiomyopathy
Dcp	Decapping enzymes
del	nucleotide sequence deletion (human genome variation society nomenclature)
DM	Dense midline of desmosome
DMEM	Dulbecco's Modification of Eagle's Medium
DMSO	Dimethyl Sulfoxide
DNA	Deoxyribonucleic acid
dNTP	Deoxyribonucleoside Triphosphate
DP	Desmoplakin (also abbreviated Dsp in Figure 1.2)
DP-NTP	584 amino acid desmoplakin N-terminal peptide
ds	conserved, splice site donor sequence in an intervening (intron) sequence
DS	Desmosome or desmosomal (also abbreviated DES and d in Figures 1.2 and 1.8)
DSC-2	Desmocollin-2
DSG-2	Desmoglein-2
Dsh	Disheveled protein involved in canonical Wnt signalling
DTT	Dithiothreitol
dup	nucleotide sequence duplication (human genome variation society nomenclature)
EB	Elution buffer

ECG	Electrocardiogram
ECL	Enhanced Chemiluminescence
EDTA	Ethylenediaminetetraacetic acid
EF	Ejection fraction
EM	Transmission Electron Microscopy
EJC	Exon-exon junction complex
ESE	Exonic splicing enhancer (positively enhancing selection of neighbouring splice site)
ESS	Exonic splicing silencer (negatively inhibiting selection of neighbouring splice site)
FBS	Foetal bovine serum
Flp-In HEK	Flp-In Human Embryonic Kidney 293 cells
Frz	Frizzled receptors
GJ	Gap junction (abbreviated Gj in Figure 1.8)
GJIC	Gap junction intercellular communication
GSK	Glycogen synthase kinase
HEK 293T	Human embryonic kidney 293T cells
hnRNP	heterogenous ribonucleotide protein
HRP	Horse Radish Peroxidase
hrs	Hours
ICD	Implanted cardioverter-defibrillator
ID	Intercalated disc
IDP	Inner dense plaque of desmosome
IF	Intermediate filament
IFL	Immunofluorescence staining localization by confocal microscopy
IHC	Immuno-histochemical staining
IMS	Industrial methylated spirit alcohol
IP	Immunoprecipitation
IVS	Intervening (or intron sequence) non-coding DNA sequence
K^+	Potassium cation
kb	Kilobases
KD	Kilo Dalton
LB	Luria Broth
LBBB	Left bundle branch block
LEF	Lymphoid enhancing factor
LV	Left ventricle
mPKP2	Stable HEK 293 cells over-expressing missense S140F PKP-2
MRI	Magnetic resonance image
mRNA	Messenger ribonucleic acid
Na^+	Sodium cation
NAS	Nonsense associated altered splicing
No.	Number
NMD	Nonsense-mediated messenger RNA decay
NRVC	Neonatal rat ventricular cardiomyocytes

N-terminal	Amino terminal
ODP	Outer dense plaque of desmosome
ORF	Nucleotide open reading frame used in protein translation
P_{90}, P_{60}, P_{30}	90-cm^2, or 60-cm^2, or 30cm^2 tissue culture dishes
PAGE	Polyacrylamide gel electrophoresis
PBS	Phosphate buffered saline
PCR	Polymerase chain reaction
PG	Plakoglobin (abbreviated Pg in Figure 1.2)
PKP-2	Plakophilin-2 (abbreviated Plp in Figure 1.2)
PM	Plasma membrane
PRD	plakin repeat domain of desmoplakin
PTC	Premature termination codon
RBBB	Right bundle branch block
RNA	Ribonucleic acid
RV	Right ventricle
RyR2	Ryanodine receptor 2
SAECG	Signal averaged electrocardiogram
S.D.	Standard deviation
SD	Sudden cardiac death
SDS	Sodium Dodecyl sulphate
SDM	Site-directed mutagenesis
Skp1	S-phase kinase associated protein 1A
SPK	Striate Palmoplantar Keratoderma
SR1-9	Plectin Spectrin repeats 1-9, and homologous repeats found in other Spectraplakins
SSSS	Staphylococcus aureus scalded skin syndrome
T_{75}, T_{25}	75-cm^2 or 25-cm^2 tissue culture flask
TBE	Tris buffered EDTA solution
TBST	Tris buffered saline with 0.05% tween-20
TCF	T-cell factor
tDP	Stable HEK 293 cells over-expressing truncated Q273fsX288DP
TGFβ	Transforming growth factor beta
TGM	Tris glycine methanol transfer buffer used in western blotting
Tm	DNA Melting temperature of a nucleotide fragment
tPKP2	Stable HEK 293 cells over-expressing truncated A733fsX740 PKP2
Ub	Ubiquitination
UPF	Up-frameshift proteins involved in non-sense mediated mRNA decay
UTR	Untranslated 5' and 3' regions of a gene
VT	Ventricular tachycardia
wPKP2	Stable HEK 293 cells over-expressing PKP2 isoform 2a
wDP	Stable HEK 293 cells over-expressing DP isoform I
WB	Western immunoblotting
Wnt	Mammalian soluble factors homologous to Drosophila Wingless protein

Chapter 1 – Introduction

1.1 Arrhythmogenic right ventricular dysplasia/ cardiomyopathy

1.1.1 ARVC disease, diagnosis and treatment

Arrhythmogenic right ventricular cardiomyopathy (ARVC) is a primary myocardial disease[1] affecting the heart muscle. The condition was described affecting the right ventricle by Dalla Volta[2] *et al* and later recognized by Fontaine[3] *et al* as a separate condition (ARVD) associated with right ventricular tachyarrhythmias. The World Health Organization classification of cardiomyopathies assigned the term ARVC to include a broad spectrum of diseases featuring ventricular tachycardia, sharing similar basic histology, but having different clinical manifestation and outcomes[1,4,5]. The most common form of this condition, ARVD/C, results in morphological and functional abnormalities of the right ventricle. This is a progressive familial disease (in up to 50% of cases[6]), genetically heterogeneous, inherited in a predominantly autosomal dominant fashion with incomplete penetrance[7] and a major cause of sudden cardiac death (SD). Autosomal recessive syndromes such as Naxos disease is a variant of the disease. ARVC is characterised by gradual loss of myocytes mainly in the right ventricle with transmural substitution of the myocardium with fat and fibrous tissue. This pathological process begins from the epicardium and extends to the endocardium. Although ARVC affects primarily the right ventricle, the left ventricle may also be affected during the course of disease progression, in which case it is difficult to distinguish it from Dilated Cardiomyopathy[8] (DCM). ARVC affecting only the left ventricle is also recognized[9-11].

The important morphological change in ARVD/C is a diffuse or segmental absence of myocardium in the right ventricular free wall, which undergoes replacement with fatty and/or fibrous tissue[5,12,13]. Two types of ARVD/C (fatty or fibro-fatty) were proposed based on histology of the right ventricle[12]; the fatty form consisted solely of fat replacement of the right ventricle. The fibro-fatty type is associated with a mixture of fibrotic tissue and fat interspersed in regions of myocyte atrophy, and is accompanied by myocardial thinning mainly in the infundibulum, outflow tract and the lateral apical regions of the right ventricular wall[4,13,14] (referred to as "triangle of dysplasia"), and significant secondary aneurysmal dilatation and myocardial lymphocytic

infiltration. The subtricuspid area, the epicardial left ventricle, and to a lesser extent the ventricular septum are all involved in the fibro-fatty ARVC type. In contrast, in the purely fatty ARVD form, there is a partial or complete replacement of the right ventricular wall with adipose tissue confined to the apex and infundibular regions and accompanied by normal or thickened myocardium without fibrosis, myocyte atrophy or inflammatory infiltrates[4,13-15]. The left ventricle and the intraventricular septum are very infrequently involved in the fatty ARVD form. The inverse relationship between wall stress and wall thickness may explain the increased susceptibility of the thin-walled RV, and the predilection of early ARVC for its thinnest portions (triangle of dysplasia).

Fontaine[5] et al, suggested that the fatty ARVD form could represent an early stage in disease progression, and that focal myocarditis with myocyte cell death and replacement fibrosis may transform the purely fatty ARVD form to the fibro-fatty ARVC. Studies of hearts from fibro-fatty ARVC, fatty ARVD and control patients who died from non-cardiac causes were compared by Burke[14] *et al*, this showed that patients with fibro-fatty ARVC were younger than those with fatty ARVD, more likely to have a family history of premature SD, and to be males. However, they were less likely to have coexisting conditions (such as atherosclerosis, diabetes epilepsy, asthma mitral prolapse or alcohol abuse) predisposing them to SD. Thiene *et al* however, believed that ARVD with pure fatty replacement as well as fibro-fatty cardiomyopathy represented a very significant cause of sudden cardiac death in patients less than 35 years of age[13].

The assignment of a purely fatty form of ARVC in elderly patients and in obese young women requires caution as right ventricular fat infiltration is a frequent (>50%) normal finding[14,16,17]. Sheppard believed that fatty infiltration is an incidental finding in many hearts not related to death in many cases, and that this did not represent a spectrum of ARVD/C. In the UK ARVD is a very rare condition with only three pathologically confirmed cases per 600 sudden deaths found in a recent study[16].

Clinical manifestation in ARVC shows phenotypic variation, depending on cardiac instability and progressive venous dysfunction. It may present without symptoms, or manifest clinically with ventricular or supra-ventricular arrhythmias of right ventricular origin ranging from isolated premature ventricular beats to sustained

ventricular tachycardia (SVT) or ventricular fibrillation (VF) that leads to SD[4,13,15]. SD may be the first clinical manifestation of the ARVC and could be a major cause of death in young people[18,19]. Other clinical symptoms evident include global or regional dysfunction with structural alterations of the RV, ECG depolarization/repolarization changes (observed in right precordial leads), and progression to right or biventricular heart failure mimicking DCM.

ARVC prevalence varies according to the study population and it is estimated to be 1 in 5,000 individuals, affecting threefold more males than female[20,21] and usually manifests in adolescents and adults, although paediatric and even *in-utero* cases have also been reported[5,22]. In addition, the disease shows heterogeneity in relation to age-related progression, and an incomplete penetrance (30%[23]). It has been estimated that in the young Italian population 12-25% of SD may be attributed to undiagnosed ARVC2[13,24-26] but this is known to vary (10-40%) in different ethnic populations[27,28].

Four clinicopathological phases of ARVC disease are recognised:

1) The early or concealed phase is generally asymptomatic, and may be characterised by subtle right ventricular structural changes with or without minor ventricular arrhythmias during which SD from arrhythmia may be the first manifestation of disease, especially in young people during competitive sports or intense physical exercise[13].
2) The overt arrhythmic phase (or unstable phase) shows symptomatic ventricular arrhythmias generally of left bundle-branch block, possibly leading to cardiac arrest and associated with clearly discernible right ventricular morphological and functional abnormalities[26]. Patients typically present with palpitation, syncope and presyncope[29]
3) The diffuse right ventricular dysfunctional phase results in extension of muscle disease leading to a global right ventricular failure with relative preservation of left ventricular function[25].
4) The final phase leads to progressive bi-ventricular pump failure caused by pronounced left ventricular involvement. This ARVC phase mimics biventricular dilated cardiomyopathy of other causes leading to atrial fibrillation and thromboembolism.

Clinical diagnosis of ARVC is complicated, as a single diagnostic test alone is not sufficient to establish the disease with certainty. A definitive diagnosis of ARVC

requires histological confirmation showing the presence of transmural fibro-fatty replacement of right ventricular myocardium in surgical, autopsy, or in endomyocardial biopsy samples. Demonstration of intramyocardial fat is not sufficient *per se* for a diagnosis of ARVC; pure adipose infiltration has been documented in a significant proportion of normal hearts[17]. However, ARVC diagnosis by endomyocardial biopsy has a lower sensitivity (67%) due to the segmental and progressive nature of ARVC, and because the intraventricular septum area that is usually biopsied (for safety reason), is rarely involved in the disease.

Non-invasive clinical assessment is preferred owing to frequent need for serial studies to monitor disease progression, and the growing cohort of asymptomatic relatives requiring evaluation. A recommended work-up would involve:

- Full-history is performed with particular focus on cardiac symptoms, compilation of detailed pedigree highlighting instances of sudden cardiac death and unexplained heart failure.
- A twelve-lead ECG examining non-specific abnormalities including intraventricular conduction delay in the right precordial or inferior leads, incomplete RBBB, and complete RBBB, and specific abnormalities such as QRS dispersion and inverted T waves in V1 to V3 (left-sided ARVC may be associated with T wave inversion in V4 toV6).
- Two-dimensional echocardiography with administration of intravenous contrast if required is performed to improve endocardial definition, to visualise structural and functional abnormalities.
- Exercise testing to unmask ventricular arrhythmia.
- Ambulatory ECG monitoring, performed usually for 24-48 hours, to detect spontaneous arrhythmia. Longer term monitoring may be required in asymptomatic patients to capture an event.
- Cardiovascular magnetic resonance imaging (MRI) is a non-invasive tissue characterization technique. MRI has been shown to be an important non-invasive technique of diagnosing ARVD/C because its ability to detect both morphological and structural abnormalities of the right ventricular wall[30], however, the diagnostic utility needs to be defined due to interobserver interpretation[31]. Over-reliance on presence of intramyocardial fat/wall thinning demonstrated by MRI without complete evaluation by Task Force criteria (see Figure 1,) causes a high rate of ARVD/C mis-diagnosis[32]. Thus, no single test can confirm diagnosis of ARVC[1,23].

The diagnosis of ARVC in index cases is established after evaluation of structural, histologic, electrocardiographic, arrhythmic, and genetic criteria that were proposed by a working group on ARVD/C[23]. These diagnostic criteria (Figure 1.1, adapted from Paul[33] *et al*) are subdivided into several major and minor criteria in each group. Diagnosis of ARVC requires that two major criteria, or one major and two minor criteria, or four minor criteria are satisfied from different groups. These criteria developed from tertiary centre experience with symptomatic index cases and SD victims were from the severe end of the disease spectrum. These guidelines are widely recognised to be highly specific, but lack sensitivity for early familial forms of the disease. The Task force guidelines nevertheless, continue to provide an outline of the main clinical findings in ARVC and are pivotal in confirming diagnosis in index cases. However, for patients that do not fulfil Task Force criteria, they cannot necessarily be reassured that they are unaffected. Since clinical features may develop or progress over time[34], continued clinical follow-up may ultimately elicit an ARVC diagnosis.

Familial ARVC with autosomal dominant mode of transmission implies a 50% probability of first-degree relatives carrying the disease-causing mutation. In these patients, isolated cardiac abnormalities are much more likely to represent disease expression. Accordingly, modifications were suggested to enhance the sensitivity of the Task force criteria within the context of familial ARVC. The modified criteria target detection of milder forms of the disease and facilitate cascade screening of relatives.

SD is often the first manifestation of disease in over 50% of index cases. For this reason, surveillance of family members is critical. A periodic evaluation on a 6-12 monthly basis from early adolescence to adulthood and beyond is advised. The full clinical assessment with the recommended work-up should be repeated on each occasion as many patients will have abnormalities in a single test but not in others, and certain abnormalities may only develop in later life.

Hamid and colleagues[6] proposed an extended set of modified ARVC clinical criteria (Table 1.1) that increased the diagnostic sensitivity in evaluation of asymptomatic relatives of affected patients. The clinical diagnosis of the concealed phase of ARVD/C is often more difficult than that of the overt phase of the disease based on

the Task Force criteria. Two international ARVD/C registries (European and American) have been set up to assess diagnostic criteria prospectively from a large population, and to integrate the genetic information.

Figure 1.1 Task Force criteria for diagnosing ARVC

Description of the standardized diagnostic criteria for ARVC as proposed by the "Study Group on Arrhythmogenic Right Ventricular Dysplasia/Cardiomyopathy of the Working Groups on Myocardial and Pericardial Disease and Arrhythmias of the European Society of Cardiology and of the Scientific Council on Cardiomyopathies of the World Health Organization" in 1994[23]. The diagnosis of ARVC is fulfilled if two major criteria, or one major plus two minor criterion, or four minor criteria from different groups (i.e., imaging, ECG, etc.) are present. *ECG* electrocardiogram; *LBBB* left bundle branch block; *LV* left ventricle; *RBBB* right bundle branch block; *RV* right ventricle. *= Detected by echocardiography, angiography, magnetic resonance imaging, or radionuclide scintigraphy. Figure obtained from Paul[33] *et al.*

Table 1.1 Proposed modification of Task Force Criteria

These modified criteria were devised for the clinical diagnosis of familial ARVC. Reproduced from Hamid[6] *et al.*

* Previously >1,000/24-hr period in task force criteria.

ARVC =arrhythmogenic right ventricular cardiomyopathy; ECG = electrocardiogram; EF = ejection fraction; LBBB = left bundle branch block; RV = right ventricle; SAECG = signal averaged electrocardiography; VT = ventricular tachycardia.

ARVC in First-Degree Relative Plus One of the Following:

1. ECG	T-wave inversion in right precordial leads (V_2 and V_3)
2. SAECG	Late Potentials seen on signal-averaged ECG
3. Arrhythmia	LBBB type VT on ECG, Holter monitoring or during exercise
	Extrasystoles >200 over an 24-hour period*
4. Structural or functional abnormality of the RV	Mild global RV dilatation and/or EF reduction with normal LV
	Mild segmental dilatation of the RV
	Regional RV hypokinesia

There is no curative treatment of ARVD/C patients. Avoidance of athletics or intense physical exercise is recommended as these activities hasten the progression of the disease. Thus, anti-arrhythmic drug therapy[35-37] with or without class I or class IIIβ-blockers is the first and frequently used approach directed at patient ventricular arrhythmias with a goal to prevent sudden cardiac death and other sustained arrhythmias which can cause syncope. The non-pharmacological therapy, including catheter ablation and implantable cardioverter-defibrillator (ICD) use is reserved for patients with life-threatening ventricular arrhythmias in whom drug therapy is ineffective or is associated with serious side effect. ICD is recommended for all ARVC patients who have experienced aborted sudden cardiac death or sustained ventricular arrhythmias. In ARVD/C patients who have progressed to severe right ventricular or biventricular dysfunction, treatment consists of therapy for heart failure including diuretics, ACE inhibitors, and digitalis as well as anticoagulant therapy. Heart transplantation may become necessary in these patients.

1.1.2 Mechanisms of ARVC

1.1.2.1 Overview of genetic defects in ARVC

Linkage analysis showed substantial genetic heterogeneity in ARVC with the identification of nine chromosomal loci associated with ARVC (section 1.2 and Table 1.2). Plakoglobin and desmoplakin gene mutations were previously identified[38,39] as causative for a fully penetrant autosomal recessive form of ARVC (PG mutation, Naxos disease) characterized by cutaneous and follicular abnormalities, and in Caravajal syndrome (desmoplakin mutation), a cardiocutaneous syndrome characterized by palmoplantar keratoderma, woolly hair, and diffuse cardiomyopathy distinct from ARVC. These two mutations both in desmosomal proteins implicated possible involvement of other desmosomal proteins or their binding partners in ARVC. Desmoplakin mutations associated with autosomal dominantly inherited ARVC and with left ventricular cardiomyopathy were subsequently identified in a subset of ARVC cases (section 1.5 and Table 1.4). Studies in PKP-2 null mice (-/-PKP2 and -/+PKP2) provided vital clues about the role of this Armadillo protein suggesting early embryonic death at E11 with profound cardiac abnormalities resulting from a failure of formation of normal cardiac desmosomes due to dissociation of desmoplakin from the abnormal junctions (section 1.7.3). Observations from these mice studies established an important role of PKP-2 in heart morphogenesis providing a rationale for a study leading to the discovery of twenty-five dominant heterozygous PKP-2 gene mutations in a cohort of one hundred and twenty ARVC patients[40]. This discovery highlighted possibility of further mutations in genes encoding other major desmosomal proteins to be involved in ARVC (sections 1.8.1 to 1.8.5 and Tables 1.5 to 1.7). Genetic screening of a cohort of British Caucasian ARVC patients undertaken in the present studies identified further four novel plakophilin-2 mutations[41] and three novel DP mutations (section 3.5.2 Part 1.3). Confirmation of the importance of predominant plakophilin-2 mutations in ARVC was provided by numerous subsequent studies examining different ARVC cohorts (section 1.8.3 and Table 1.5). Following the discovery of plakophilin-2 mutations, other mutations were discovered in ARVC that affected genes encoding desmoglein-2 and desmocollin-2 (sections 1.8.4 to 1.8.5 respectively) emphasizing the

predominance of abnormalities in desmosomal proteins to pathophysiological mechanisms of ARVC.

1.1.2.2 Pathogenic effects of ARVC gene mutations

Mutations in genes encoding the major proteins of cardiac desmosomes (plakophilin-2, desmoplakin, desmogelin-2, desmocollin-2 and plakoglobin,) are believed to exert pathogenic effects at three different levels involving desmosome composition and function, organisation of junction assemblies in the intercalated disc, and perturbation in the Wnt/β-catenin signalling pathway. The observation that plakoglobin fails to localise to intercalated discs of myocardial tissue of patients with mutation in plakoglobin[42], as well as in those with mutation in desmoplakin[43] and plakophilin-2[44,45] suggests a "final common pathway" role for plakoglobin in the pathogenesis of ARVC[45] regardless of the underlying gene mutation. The notion of PG being involved in a common pathway in ARVC pathogenesis is discussed further in section 1.1.2.2c. The general effect of different types of gene mutations on protein formation, function, and cellular consequences are discussed in sections 1.1.4 to 1.1.6. The possible pathogenic effects of ARVC gene mutations at the level of the desmosome and ID are discussed in sections 1.1.2.2a and 1.1.2.2b respectively

1.1.2.2a Pathogenic effects at level of desmosomes

At the level of the desmosome (section 1.3.3), pathogenic effects of gene mutations may result from haploinsufficiency (section 1.1.5) causing insufficient incorporation of a normal protein, or abolish essential inter-protein (protein-protein) interactions, or in the incorporation of mutant protein disturbing formation/function of normal desmosomes (dominant negative effects, section 1.1.4), or in reduction of the numbers of functional desmosomes. A recent study of myocardial biopsy ID ultrastructure examination of ARVC probands carrier of gene mutations encoding desmosomal proteins supported this contention by showing a reduction in the number of desmosomes and increased desmosomal length[46]. Desmosomal impairment might induce disruption of these structures resulting in reduced mechanical contacts mediated either directly by reduced desmosomal contacts, or indirectly by reduced gap junction and adherens junction contacts.

1.1.2.2b Pathogenic effects at level of intercalated disc

At the level of the intercalated disc, desmosomes arguably protect other junctional complexes from mechanical stress, the pathogenic effects of mutant desmosomal proteins may result in the structural re-organisation at the ID, as exemplified by abnormal small junctions and widening of the intercellular gap in the absence of convolution in myocardial tissue of mutation carriers[46]. Perturbation in gap junction turnover may result from destabilisation of cell adhesion complexes at the ID, resulting in heterogeneous conduction and a substrate for arrhythmogenesis in ARVC[42,43,47-49]. This mechanical junction remodelling in cardiomyopathies has been hypothesized by Saffitz[50] and colleagues to disrupt gap junction assembly (remodelling of gap junctions). Support for this hypothesis came from EM examination of ID and immuno-histochemical staining of ventricular biopsies obtained from Naxos disease[42] (2bp PG gene deletion), Caravajal syndrome[43] (1bp DP gene deletion), and autosomal dominant ARVC[51] (3bp in-frame PG gene insertion). In all three cases disruption of ID junctions with a reduction in the immuno-histochemical staining signal of membrane localised Cx-43 protein involving reduction in the P2 isoform of CX-43 localising in the junctional pool of Cx-43[50] (discussed in section 1.2.5) occurred. ID remodelling may result in remodelling at the ID and under abnormal mechanical stress, for e.g. during intense physical exercise, this may cause cardiomyocyte detachment, degeneration, fatty tissue replacement and fibrosis.

1.1.2.2c Pathogenic effects arising from Wnt signalling

Certain proteins involved in cell-cell adhesion (section 1.3) such as β-catenin and plakoglobin also participate in intercellular signalling via the Wnt/β-catenin pathway. This is an evolutionary conserved pathway in metazoan animals that is involved in a variety of cellular processes, including cell fate, cell proliferation, differentiation, cell survival, apoptosis, cell behaviour and migration during development of tissues and organs[52]. In the canonical Wnt/β-catenin pathway, the hallmark of the pathway is the stabilization and nuclear localization of β-catenin. In the absence of Wnt signalling, the free cytoplasmic level of β-catenin is tightly regulated by multiple ligands by formation of a multi-molecular complex that targets β-catenin for degradation via the

ubiquitin-proteasome complex (see Figure 1.2A). Active Wnt signalling (from soluble Wnt proteins) results in stabilization and cytoplasmic accumulation of β-catenin leading to its nuclear translocation and association with Tcf/Lef family of transcription factors involved in regulating gene expression[53]. The binding of β-catenin to an N-terminal domain of Tcf/Lef facilitates the assembly of multimeric complexes containing transcription co-activators such a CBP/p300, BCL9/LGS, and pygo, which activates transcription of target genes[54]. Wnt signalling is a dynamic and complex process that hinges on four complexes, the first is the Wnt receptor complex in the membrane, the second is the β-catenin destruction complex, the third is the nuclear TCF/LEF/β-catenin transcriptional activator complex, and the fourth is the nuclear TCF/LEF transcriptional repressor complex. A simplified view of canonical Wnt/β-catenin signalling is that in the absence of Wnt signalling, the β-catenin destruction complex assembles and consequently, Tcf/Lef assembles repressor complexes at target genes. Binding of Wnt ligands assembles receptor complexes with the disruption of β-catenin destruction complex; as a consequence β-catenin is able to form transcription activation complexes with Tcf/Lef in the nucleus[54].

PG competes with β-catenin in the canonical Wnt/β-catenin pathway[55] by reduction of the signalling through Tcf/Lef transcription factors (see illustration in Figure 1.2B). Plakoglobin and β-catenin can interact antagonistically at multiple levels including nuclear localisation, binding to Tcf/Lef transcription factors, ubiquitination, phosphorylation, binding to axin and adenomatous polyposis coli, incorporation into adherens junctions and desmosome assembly.

Figure 1.2 Wnt pathway and influence of PG signalling

Influence of β-catenin and plakoglobin in the Wnt signalling pathway. (A) β-Catenin (b) and plakoglobin (Pg) can bind, independently, to the cytoplasmic tail of cadherin adhesion receptors in adherens junctions (AJ). Via α-catenin (a), they mediate cadherin association with the actin cytoskeleton. When Wnt signaling is inactive, free β-catenin is degraded by a multi-molecular complex including the tumor suppressor APC, axin and glycogen synthase kinase (GSK), which phosphorylates β-catenin (PP). This complex associates with the ubiquitin-proteasome system via the Ubiquitin Lygase β-TRCP, which, together with Cul1 and Skp1, mediates the ubiquitination (Ub) of β-catenin and targets it for degradation by the proteasome. The binding of Wnt to the Frizzled (Frz) receptor activates Wnt signaling, and disheveled (Dsh) inhibits β-catenin turnover by suppressing GSK activity. This results in the accumulation of β-catenin in the nucleus, complex formation with TCF family transcription factors, and activation of target gene expression. (B) Plakoglobin can interact with the same proteins as β-catenin but, in addition, binds to the desmosomal cadherins desmocollin and desmoglein in desmosomes (DES), mediating their interaction, via desmoplakin (Dsp) and plakophilin (Plp), with intermediate filaments (IF). Plakoglobin is believed to result in a reduction in the trans-activation of target genes in complex with TCF (shown by ↓ in Figure 1.2B). Figure modified from Zhurinsky[55].

An atrial myocyte cell line (HL-1) siRNA inhibition of desmoplakin expression resulting in desmosome dysfunction in this cell line was accompanied by the delocalisation and nuclear translocation of plakoglobin. This resulted in competition between plakoglobin and β-catenin leading to suppression of canonical Wnt/β-catenin signalling through Tcf/Lef transcription factors and upregulation of genes implicated in adipogenesis and generation of new collagen and accumulation of fat droplets[56]. Using Cre recombinase driven by α-MHC gene promoter with a floxed desmoplakin allele, cardiac-restricted desmoplakin deletion resulted in the elimination of desmoplakin expression in homozygous mice showing embryonic lethality at E11[56]. Heterozygous cardiac DP null mice developed age-dependent multichamber cardiac enlargement and dystrophic myocardium with excess adipocytes and fibrosis, increased myocyte apoptosis and cardiac dysfunction. Increased cardiomyocyte nuclear plakoglobin localisation and ventricular arrhythmias were observed in heterozygous cardiac DP null mice[56]. Thus, cardiac desmoplakin deficiency results in inhibition of canonical Wntβ-catenin signalling switching cellular fate away from myogenesis and towards adipogenesis/fibrosis. In conclusion, current insight in ARVC pathogenesis suggests a common final pathway with plakoglobin delocalisation proposed as a key event[57]. Delocalisation and nuclear translocation of plakoglobin occurs with suppression of Wnt/β-catenin signalling. The specific interactions between plakoglobin and β-catenin that lead to suppression of canonical Wnt/β-catenin in ARVC are presently unknown. Additional transcriptional regulators of adipogenesis such as the Rho family of small GTPases and GATA transcription factors may also be involved in pathogenesis of ARVC.

Direct effects of mutations in genes encoding desmosomal proteins is probably one of the mechanisms involved in ARVC pathogenesis. Alternative or parallel mechanisms of ARVC may involve the effects of modifier gene mutations encoding other non-desmosomal proteins. Mutations present in the 5' and 3' UTR regulatory regions of TGFβ gene[58] and recently described missense mutation in the gene encoding transmembrane protein 43[59] emphasize the potential role of these other gene mutations in ARVC. Comparison of cardiac biopsies of genotype positive individuals for ARVC gene mutations (including those encoding the five major desmosomal protein components) and of individuals with confirmed ARVC clinical diagnosis albeit genotype negative (lacking mutations in any of the five major cardiac desmosomal proteins) showed that abnormalities at the ID were present in both

genotype positive and negative individuals. This strongly suggested that other still unknown disease-causing genes are likely to be involved in ARVC pathogenesis[46] and that a broad spectrum of ARVC forms would be required to be considered as intercellular junction cardiomyopathies arising from predominance of cell junction abnormalities at the ID.

A naturally occurring canine model of ARVC with autosomal dominant mode of inheritance arising in Boxer dogs shares similarities with human ARVC2 including presentation of concealed phase, overt, and myocardial dysfunctional phases of the disease, sudden cardiac death, ventricular tachyarrhythmias of RV origin, syncope, RV myocyte loss, fibro-fatty infiltrate found predominantly in the RV, myocarditis, and apoptosis[60]. This canine model of ARVC showed substantial loss of Cx-43 protein gap junctions as well as remodelling of other intercalated disc structures[61] and examination of DP, DSG-2, PKP-2, PG, and Cx-43 genes did not reveal causative mutations in the coding and flanking regions of these genes[61,62]. However, of the "big five" genes encoding desmosomal proteins it still remains to determine whether mutations in DSC-2 gene could account for ARVC in this animal model[61].

1.1.3 ARVC apoptosis and replacement fibrosis

Other basic mechanisms of ARVC include apoptotic cell death[63,64] and inflammation ranging from acute myocarditis to fibrous healing which in severe form of ARVC may affect both ventricles leading to congestive heart failure mimicking DCM[7,15].

ARVC was initially suggested to be a milder form of Uhl's anomaly, a congenital hypoplasia of the right ventricular myocardium where incessant apoptosis was believed to cause a partial or complete loss of the myocardium[65]. ARVC pathogenesis is thought to differ from that of Uhl's anomaly by episodic focal apoptosis occurring at any time in life, resulting in myocyte cell death and islands of residual conducting myocytes interspersed with fibro-fatty areas. This provides the arrhythmogenic substrate accounting for the delay in intraventricular impulse transmission, persistence of electrical depolarization during diastole (late potentials) and onset of re-entrant circuits with premature ventricular beats and ventricular tachycardia of left bundle-branch block morphology. Thus, cardiomyocyte apoptosis may be involved in

arrhythmias and sudden cardiac death. Apoptosis would culminate in replacement fibrosis superimposed on fatty replacement during repair as terminally differentiated cardiomyocytes have a limited capacity for cellular proliferation.

Various studies have shown apoptotic cell death in ARVC associated with cardiomyocyte loss in the myocardium[63,64,66-71], but it remains unresolved whether apoptosis in ARVC is a cause or effect of the disease. The study of Mallat[63] *et al* showed that myocyte apoptosis was frequently found in areas which have not undergone fibro-fatty replacement and very rarely in areas already affected. This suggested that apoptosis might be a primary process preceding fibro-fatty replacement. Recent EM examination of ARVC patient cardiac biopsies provided evidence of early expression of myocyte apoptosis[46] indicated by the presence of convoluted nuclei previously described[72].

1.1.4 Cellular consequences of gene mutations

Gene mutations are predicted to lead to either **loss of function** (proteins have reduced or no function) or result in **gain of function** (proteins may do something positively abnormal). For heterozygous autosomal dominant mutations, 50% of normal level of the protein may not be sufficient for normal function, and **haploinsufficiency** produces an abnormal phenotype from an autosomal dominant inheritance. Sometimes also, a non-functional mutant polypeptide interferes with the function of the normal allele in a heterozygous individual, giving a **dominant negative** effect. Gain of function mutations usually cause dominant phenotypes, because the presence of a normal allele does not prevent the mutant allele from behaving abnormally. This may often involve a control signalling system behaving inappropriately – signalling when it should not, or failing to switch off a process when it should.

Mutations at the gene level arise from a wide variety of sequence variations; they may be missense/nonsense mutations resulting in a single nucleotide change causing a codon to encode for a different amino acid from the one encoded in the normal wild type sequence, or for a codon to result in unscheduled termination (TAA, TAG, or TGA). Missense mutations could be disruptive to protein structure (exerting affect on folding of secondary structures) if the amino acid replacement results in a change of

character (hydrophobic: non-polar, polar: hydrophilic, charged: negative, charged: positive) of the substituted amino acid compared to the amino acid normally found. Missense mutation may also disrupt a site involved in inter protein-protein interactions (for example, desmoplakin missense mutation R2834H disrupts the interaction between DP and desmin intermediate filament). Missense mutations could also result in gain of function if it affects potential phosphorylation sites on serine, threonine, and tyrosine amino acid residues modified post-translationally, which may be involved in signalling function of the protein. Missense gene mutations disrupting an exonic spicing enhancer may also cause frameshift resulting in premature termination codon; that would lead to nonsense mediated mRNA decay (discussed further in sections 1.1.5 and 1.5.3) motif. Splice site mutations resulting in single nucleotide change affecting a donor splice (ds) site or an acceptor splice (as) located within introns may cause aberrant splicing with the retention of an intron sequence in pre-mRNA, exon skipping, or activation of cryptic splice site on an exon resulting in incorporation of a truncated exon. For examples of the effects of these splice site mutations in PKP-2, DSG-2, and DSC-2 see Table 1.5 (section 1.5.3), Table 1.6 (section 1.5.4), and Table 1.7 (section 1.5.5) respectively. The nomenclature for assigning splice site mutations are covered in chapter three (section 3.4.1 Part 1.1 and Figure 3.1) Mutations affecting 5' UTR or 3'UTR gene sequence could affect regulation at the level of gene expression. These UTRs may contain regulatory elements important in determining the level of gene expression, and mutations found in the regulatory regions of TGFβ[58] underline the effects of such mutations in ARVC. Small deletions (microdeletion $\leq$ 20 bp) or small insertions (microinsertion $\leq$ 20 bp) may result in out of frame (frameshift) mutations leading to insertion of aberrant amino acids followed by PTC or sometimes in the extension of translation frame resulting in the addition of novel additional amino acids at the end of the normal protein sequence. Gross deletions may result in deletion of an entire exon, deletion of several exons, or even deletion of an entire gene. Gross insertions may result in duplication of single exon, multiple exons or even duplication of an entire gene. A vast majority of mutations affecting genes encoding for desmosomal proteins result in frameshift or nonsense mutations – these cause premature termination codons (PTCs) which would result in formation of truncated protein or polypeptides with deleterious functions. Specific mechanism exists to eliminate mRNA containing PTCs as a means of preventing formation of these deleterious proteins. These mechanisms are discussed in the next section.

1.1.5 Nonsense-mediated mRNA surveillance

Nonsense-mediated mRNA decay (NMD) is an evolutionary conserved quality control pathway existing in all eukaryotes examined[73]. This pathway selectively targets the degradation of mRNAs harbouring PTCs more than 50-55 nucleotides upstream of a splicing generated exon-exon junction[74-78], however there are exceptions to this rule. Approximately 33% of inherited and acquired diseases are attributable to PTCs that truncate the open reading frame (ORF) and precludes the synthesis of full-length protein[79]. NMD blocks the translation of these mRNAs thereby preventing truncated proteins with dominant-negative or deleterious gain-of-function activities from forming.

PTCs arise in variety of ways including alteration to germ-line or somatic DNA resulting in random frameshift and nonsense mutations that are subsequently transcribed into mRNA. Frameshift mutations that are insertions or deletions not of multiple-of-three base pairs within an ORF can result in PTCs. Single base mutation that converts a sense codon into a nonsense codon also generates a PTC. Mutations at intron and exon boundaries that result in inefficient or inaccurate intron removal from pre-mRNA can create an intron-derived PTC or a shift in the ORF and a PTC downstream of the shift[80,81]. Another common source of PTCs is errors in RNA splicing, including aberrant alternative splicing[73,79,82,83].

Mechanistically, NMD is a complex process with the initial signal marking mRNA transcript for rapid decay requiring an intron downstream of a PTC for mRNA degradation to occur by the NMD machinery. The second signal targeting the transcript for NMD results from the deposition of a dynamic multi-protein complex (containing at least ten proteins, with the core NMD components consisting of three *trans*-acting factors, called upframeshift proteins (UPF)) 20-24 nucleotides upstream of exon-exon junctions on mammalian mRNAs during splicing, which defines a stop codon as a PTC. Interaction between this exon-junction complex (EJC) and NMD factors assembled at the upstream stop codon triggers a series of steps that ultimately lead to rapid mRNA decay.

Most mammalian mRNAs are down regulated by NMD in the nucleus or soon after entering the cytoplasm. Normal transcripts escape NMD because all EJCs are

deposited upstream of the stop codon, permitting the ribosomes to displace them. Aberrant transcripts harbouring PTCs, in contrast, have at least one EJC downstream of the PTC, thereby triggering NMD. Figure 1.3 illustrates the mechanism of NMD of transcript harbouring PTC and explains how mRNA transcripts containing genuine termination codons escape NMD. Figures 1.4-1.5 illustrates the downstream molecular processes involved in NMD. PTC-harbouring mRNA decay is elicited if factors that constitute the second signal (such as the EJC) are allowed to interact with factors bound at the stop codon. This does not occur in normal transcripts because the second signal factors are probably all stripped off by the ribosome. NMD is a highly conserved pathway that exists in all eukaryotes examined[73].

Recent studies have shown the existence of three alternative branches of the NMD pathways. The first that is independent of UPF2, the second that is independent of EJC core proteins instead depending on alternative RNA-binding proteins and a third that is independent of the UPF3a and UPF3b EJC factors. Some novel NMD second signals may exist as in some mammalian transcripts, such as human β-hexosaminidase and mouse Ig-μ, NMD occurs efficiently even when an exon-exon junction does not follow the PTC.

1.1.6 Nonsense-associated altered splicing

In addition to triggering NMD, premature termination codons are also found to alter the splicing pattern often leading to skipping of the PTC-containing exon The term "nonsense-associated altered splicing" (NAS) is used to describe such changes in splicing caused by PTCs. In many cases, NAS is induced because of the destruction of an exonic splicing enhancer (ESE, discussed further in section 1.5.3) by the PTC-generating nonsense or frame-shift mutation. However, for a few genes, NAS appears to be PTC specific indicating that premature termination of the translational reading frame affects splicing.

Figure 1.3 Recognition of mRNA transcript destined for NMD

Mammalian nonsense-mediated mRNA decay (NMD) occurs because of PTC recognition during a unique "pioneer" round of translation. NMD is specifically triggered when up-frameshift protein 1 (UPF1, labelled 1) is allowed to interact with UPF2 (2), which is bound to UPF3b (3b). UPF2 and UPF3b are both part of the EJC, which is recruited to exon-exon junctions (not shown) during mRNA splicing. In an aberrant transcript (*left panels*), there is typically at least one EJC deposited downstream of the premature stop codon, allowing it to interact with UPF1 recruited by cap-binding complex (CBC) and the eukaryotic release factors eRF1 and eRF3 (eRF). The interaction between UPF1 and UPF2 is enhanced by CBC, which is bound to the 5' cap of mRNAs undergoing the pioneer round of translation. In contrast, a normal transcript (*right panels*) avoids NMD because all of the EJCs (only one is shown) are upstream of the stop codon and are thus displaced by the ribosome before UPF1 is recruited. After surviving this proofreading step, normal transcripts exchange proteins at both their 5' and 3' ends and proceed to bulk translation. Reproduced from Chang[74] *et al.*

Figure 1.4 Early molecular events initiating NMD

Early molecular events preparing an mRNA to be degraded by nonsense-mediated mRNA decay (NMD). Translation of an mRNA during the pioneer round of translation (step 1; also see Figure 1.3) leads to recognition of the stop codon by the eukaryotic release factors eRF1 and eRF3, which recruit the NMD factor UPF1 (labelled 1; step 2). UPF1, in turn, recruits the protein kinase SMG-1 (S1), which together with the eRFs forms a transient complex called SURF (step 3). In an aberrant mRNA like the one shown, the SURF complex interacts with an EJC downstream (step 4). This interaction may be an obligate requirement for SMG-1 phosphorylation of UPF1 (step 5), which then probably triggers subsequent steps that ultimately degrade the mRNA (see Figure 4) and recycles release factors and the 40S and 60S ribosomal subunits (step 6). Abbreviations: CBC, cap-binding complex; EJC, exon-junction complex; S1, protein kinase SMG-1; SMG-1, suppressor with morphogenetic effect on genitalia-1; SURF complex, the SMG-1, UPF1, eRF complex; UPF1 (labelled 1), UPF2 (labelled 2), UPF3b (labelled 3b), up-frameshift proteins. Reproduced from Chang[74] *et al.*

Figure 1.5 Late molecular events culminating NMD

Late molecular events in nonsense-mediated mRNA decay (NMD) that ultimately degrade the mRNA. The phosphorylation of UPF1 recruits the SMG-5/SMG-7 heterodimers (labelled S5 and S7, respectively) and the phosphatase PP2A (steps 1 and 2). It is uncertain whether PP2A is initially associated with SMG-5/SMG-7 (as shown) or recruited at a later stage. Unknown events (perhaps P-body recruitment) trigger PP2A de-phosphorylation of UPF1 (step 3), which is likely to lead to the dissociation of PP2A and SMG-5/SMG-7 from the mRNP (step 4). Also unknown is what specific event leads to loss of the mRNA 5' cap by Decapping enzymes (Dcp, step 3). Decapping may be triggered by the recruitment of SMG-7, which is sufficient to elicit mRNA decay when artificially tethered to an mRNA. Alternatively, Decapping may be triggered by UPF1 de-phosphorylation. Regardless, once Decapping occurs, the mRNA body is susceptible to rapid decay by 5'-to-3' exonucleases (Xrn, step 4). Abbreviations used were CBC, cap-binding complex; EJC, exon-junction complex; S1, protein kinase SMG-1; UPF1 (labelled 1), UPF2 (labelled 2), UPF3b (labelled 3b), up-frameshift proteins. Reproduced from Chang[74] *et al.*

1.2 Genetics of ARVC

This section provides an overview of the genetics of ARVC; gene mutations affecting desmosomal proteins are covered in section 1.3. Several chromosomal locations were recognized by linkage studies in various kindreds with ARVC. Thus, nine separate chromosomal loci [57,84] were identified on chromosomes 1, 2, 3, 6, 10, 12 and 14, with two separate loci found each on chromosomes 10 and 14. These resulted in classification of eight ARVC subtypes (ARVC 1 to 8) and an associated recessively inherited condition called Naxos disease (Table 1.2, modified from Paul[33] *et al*).

In ARVC1, most frequently found in Northern Italy region, fourteen families were diagnosed with this disorder. Rampazzo [85] and Colleagues screened four candidate genes within the ARVC1 locus, including TGFβ3, but did not find mutations within the coding regions of the four genes examined. Beffagna[58] and colleagues, however reported mutations in the 5' and 3' untranslated regulatory sequences of TGFβ3 purportedly causing an over-expression of TGFβ3. The lack of TGFβ3 mutations in two kindreds with ARVC1 linkage and absence of confirmation of TGFβ3 over-expression in cardiac biopsy samples from affected patients in this study makes significance of the molecular role of TGFβ3 mutations in ARVD1 uncertain. This gene mutation was not directly associated with adherens or desmosomal cell junction (discussed in section 1.2) components; a possible link between TGFβ3 over-expression and TGFβ3-induced fibrosis in vivo in ARVC however, was made in this study. It was also speculated that TGFβ3 over-expression may indirectly affect cell-cell junction stability via a possible modulation of cell adhesion molecules, known to occur in the case of TGFβ1 exposed cardiac fibroblasts[86] and brochial epithelial[87] cells where increased levels of plakoglobin gene expression and of desmoplakin I and II protein occurred respectively.

The cardiac ryanodine receptor gene RyR2 has been shown to be involved in the pathogenesis of familial ARVC2[88] which is now known to have features typical of stress-induced catecholamine-dependent ventricular tachyarrhythmia syndrome rather than ARVD. The RyR2 gene product encodes a 565 KD monomer that interacts with four 12 KD FK–506 binding proteins (FKBP12.6) playing a crucial role in calcium regulation and excitation-contraction coupling[88]. RyR2 induces Ca^{2+} release from the

sarcoplasmic reticulum into the cytoplasm, and has been shown to be responsible for catecholamine induced ventricular tachycardia[89,90].

In 13 out of 37 members of three unrelated families of Italian, Slovenian and Belgian descent examined by Severini[91] *et al*, ARVC3 (provisionally referred to as ARVC2 by the authors) was mapped to the 14q12-q22 on chromosome 14. In three Italian families examined[92] a new ARVD4 locus was mapped to 2q32.1-q32.3. Linkage analysis in an extended eight generation family from a genetically isolated population of the island of Newfoundland, Canada[93] identified ARVD5 on 3p23. The laminin receptor-1 gene (LAMR1) was implicated in a mouse model for AVRD[94]. The LAMR1 gene mapped to 3p21.3 was implicated as a possible candidate gene in ARVD5. However, the gene responsible for ARVD5 mapped at 3p25 in fifteen unrelated families from a genetically isolated population of the island of Newfoundland, Canada was identified to encode a transmembrane protein 43 (TMEM43 protein)[59]. In a North American family spanning 5 generations and having 12 affected individuals with early-onset ARVC (≥ 10years age) and high penetrance, an ARVD6 locus was mapped to 10p12-p14[95]. In a linkage study of 12 patients from a Swedish family[96] with desmin-related myopathy and ARVC, an ARVD7 locus was mapped to 10q23.3. Several of these patients had episodes of chest pain or palpitations, and three affected males showed ARVC with non-sustained ventricular tachycardia, atrial flutter, and dilatation mainly of the right ventricle. A recent study[97] has shown mutations in the ZASP gene (LDB3) in patients with myofibrillar myopathy, some of whom had cardiac involvement. This study raises the possibility that the ZASP gene located on 10q22.3 might be a candidate gene in the Swedish family studied by Melberg[96] *et al.* In an Italian family study[39], the ARVD8 locus was mapped to 6p24 and a causative mutation (S299R) identified in exon 7 of the gene encoding desmoplakin.

A similar phenotypic expression occurs in all ARVC subtypes (with the exception of ARVC7) with left bundle branch block, T wave inversion in the right precordial leads, and presence of late potentials in signal averaged electrocardiography[23,98].

In the late nineties, positional cloning identified mutations in genes encoding DP in ARVC8, RyR2 in ARVC2, and PG in Naxos. Thus, at the start of the work described in this thesis (January 2004), the above two aforementioned genes encoding

desmosomal proteins were known to be involved in dominant ARVC8 and recessive Naxos disease. This raised the possibility that further desmosomal gene mutations may be involved in ARVC. In September 2004, Gerull[40] *et al* described twenty five novel PKP-2 mutations in one hundred and twenty unrelated Caucasian ARVC patients. TGF-β mutations affecting the untranslated region of the gene discovered in ARVC1 were reported in the year 2005[58] showing involvement of a second non-desmosomal protein in ARVC . In the following two years after discovery of PKP-2 mutations further mutations in genes encoding DSG-2 and DSC-2 were identified independently in different ARVC cohorts[46,99-104]. All three mutations affecting PKP-2, DSG-2, and DSC-2 genes were thus, identified by DNA screening approach. The genetic screening work described in this dissertation supports the involvement of DP and PKP-2 genes in familial ARVC with the discovery of further four novel mutations in plakophilin-2 and another three novel mutations in desmoplakin (section 3.4.1 Part1). Mutations in genes encoding all five cardiac desmosomal proteins (PKP-2, DP, DSG-2, DSC-2, and PG) indicate that ARVC is a multigenic disorder caused by abnormal cell-cell adhesion resulting from defects in desmosomes (section. Identification of genes at other ARVC loci may be hampered by difficulties in accurate ARVC clinical diagnosis and incomplete penetrance of the disease even between members of the same family. The discovery of a mutation (c.1073C>T) in the TMEM43 gene causing a missense protein sequence change (p.S358L TMEM43) in ARVC5 in March 2008[59] supports the suggestion that other non-desmosomal proteins may be involved in the pathogenesis of ARVC. Although little is known about the function of the TMEM43 gene it contains a responsive element for PPARγ, an adipogenic transcription factor, which may explain the characteristic fibro-fatty replacement of the myocardium seen in ARVC.

Table 1.2 ARVC chromosomal loci and identification of causative genes

? = not determined or not known. Table modified from Paul[33] et al. Highlighted in yellow are causative genes (PKP2, DSG-2 and DSC-2 and PG) identified by DNA screening of various ARVC cohorts.

Type	Chromosomal Loci	LOD score	Mode of inheritance	Penetrance	Gene	Author/Reference
ARVC1	14q23-q24	5.4	Autosomal dominant	High	5'& 3' UTR mutations TGFβ3	Rampazzo[105] Beffagna[58]
ARVC2	1q42-q43	4.0	Autosomal dominant	High	RyR2	Rampazzo[106]
ARVC3	14q12-q22	4.7	Autosomal dominant	?	?	Severini [91]
ARVC4	2q32.1-q32.3	3.5	Autosomal dominant	?	?	Rampazzo[92]
ARVC5	3p23	6.9	Autosomal dominant	Fully penetrant	TMEM43	Ahmad[93], Merner[59]
ARVC6	10p12-p14	3.9	Autosomal dominant	High	?	Li[95]
ARVC7	10q22.3	3.1	Autosomal dominant	?	?	Melberg[96]
ARVC8	6p24	4.32	Autosomal dominant	~50%	Desmoplakin	Rampazzo[39]
ARVC/PKP2	12p11		Autosomal dominant Autosomal recessive	Incomplete	Plakophilin-2	Gerull[40], Syriss[41], Van Tintelen[107], Dalal[108], Nagaoka [109], Antoniades[110], Kannankeril[111], Lahtinen[112] Awad[113]
ARVC/DSG-2			Autosomal dominant	High	Desmoglein-2	Pilichou[104], Syrris[101], Awad[100],Basso[46]
ARVC/DSC-2			Autosomal dominant	Incomplete	Desmocollin-2	Syrris[102] Heuser[103]
ARVC/PG			Autosomal dominant		Plakoglobin	Asimaki[51]
Naxos disease	17q21	3.6	Autosomal recessive	100%	Plakoglobin	Coonar[114], McKoy[38]

1.3 Cell-Cell Adhesion

1.3.1 Intercellular Junctions overview

Intercellular junctions include morphologically distinct types mediating cell-cell interactions. Adhering junctions are cadherin-containing intercellular junctions, which contribute to the mechanical strength of tissues and enable morphogenetic changes during development. They are characterised by a 10-30nm thick dense cytoplasmic plaque where bundles of cytoskeletal filaments are inserted. Two different types of junctions can be distinguished based on morphology and molecular composition: the ***d*esmosomes** (DS, *maculae adherentes*) and the **adhaerens junctions** (AJ, *zonula adhaerens*, *fascia adhaerens*, *punctum adhaerens*) are found in variety of tissues, including epithelia. The molecular assemblies in these two types of junctions are illustrated schematically in Figure 1.6b-c. Other types of specialized adhaerens junction forms occur in certain vascular and lymphatic endothelia (*cinctus adhaerens* and *complexus adhaerens*), in lens cells (*cortex adhaerens*) granule cells of the cerebellar glomerulli (*contactus adhaerens*). DS and AJ are clearly distinguished by the type of inserting cytoskeletal filament and the cadherin molecules participating in these junctions (Table 1.3 & illustration in Figure 1.6). Cadherins are single-pass transmembrane proteins that mediate Ca^{2+}-dependent adhesion. The extracellular domains of cadherins on opposing cell surfaces interact with one another, while their cytoplasmic domains are linked to the cytoskeleton, thereby mechanically coupling the cytoskeleton of adjacent cells. Classical cadherins such as E-, N-, P-, M- and VE participate mainly in homophilic interactions in AJ's, whereas in DS two different cadherins, the desmogleins (four subtypes DSG1-4) and desmocollins (three subtypes DSC1-3) participate in homophilic (DSG-DSG or DSC-DSC) or heterophilic (DSG-DSC) interactions. Desmocollin 1-3 additionally exists in two splice variant isoforms referred to as a-form and b-form, resulting in a shorter cytoplasmic cadherin domain for the b-form, which lacks the PG-binding site. Desmosomal cadherin subtype or isoform expression is tissue-type specific and is tightly regulated during morphogenesis and differentiation.

Table 1.3 Molecular distinction between Adhering Intercellular Junctions

Cell-Cell junction	Transmembrane linker	Extracellular connection	Intracellular connection	Intermediate binding molecules
Adherens Junctions	'Classical' Cadherins, Type I or Type II	Cadherin on the other cell Mostly homophilic interactions	Microfilaments, e.g. Actin	α & β-catenin, α-actinin, vinculin, plakoglobin, p120 catenin
Desmosomes	Desmosomal Cadherins, Desmoglein and Desmocollin	Cadherin on the other cell. Heterophilic interactions	Intermediate filaments e.g. Desmin, Vimentin, Keratin	Desmoplakin, plakoglobin, plakophilins & other 'minor' components, e.g. Desmocalmin, Pinin, etc

1.3.2 Adherens Junction

The adherens junctions found near the apical surface of polarized epithelial cells contain Type I or II cadherins (type I distinguished by histidine, alanine, valine, (HAV) tripeptide present in EC1 repeat region), which promote mainly, but not exclusively homophilic interactions. At the cytoplasmic face of the junction, β-catenin or plakoglobin interacts directly with the core region of 30 amino acids within the C-terminus of the cadherin cytoplasmic domain[115,116]. Both proteins are part of the ARM repeat family of proteins, sharing 65% homology and are thought to directly substitute for one another as structural components of AJ [117-119]. Both proteins consist of N- and C- terminal tails flanking a central twelve ARM repeat domain consisting of approximately 42 amino acids per ARM domain that mediates binding to the cadherin cytoplasmic domain. Huber[120] et al showed that the 3-D structure of β-catenin consisted of three alpha helices per ARM repeat that are packed against one another to form a super helix featuring a positively charged grove, that interacts with the C-terminal 100 amino acid residue of the cadherin cytoplasmic domain[121].

α-catenin, a protein structurally related to vinculin, provides a direct link to the actin filament cytoskeleton by binding to the N-terminal region of either β-catenin or plakoglobin[122]. Both the N- and C- terminus of α-catenin participate in connecting the cadherin complex to the cytoskeleton[123]. α-catenin interacts with actin filaments both

indirectly through actin-binding proteins such as α-actinin, vinculin, VASP and ZO1, and directly through interactions with actin filaments. In addition to β-catenin and plakoglobin, p120 catenin, another member of the armadillo protein family has been shown to bind the highly conserved juxtamembrane domain of cadherin[124]. Catenin p120 does not participate structurally in the junctional complex, but it is thought to participate in regulating cadherin adhesive activity. Numerous splice variants of p120 catenin exist and homologues of p120 catenin, including ARVCF (armadillo repeat gene-deleted in Velo-Cardio-Facial Syndrome), δ-catenin and p0071 (plakophilin 4) are also localised to adherens junctions and may function in a similar manner to p120 catenin.

1.3.3 Desmosomes

Desmosomes are intercellular junctions that are particularly prominent in tissues experiencing mechanical stress, such as the heart and epidermis. Desmosomes link IF to desmosomal cadherins and by tethering these stress-bearing cytoskeleton filaments to the plasma membrane, they serve as integrators of the IF cytoskeleton throughout the tissue, resulting in the formation of a supracellular network, which is critical for imparting mechanical integrity to tissues. Disease and animal models targeting desmosomal components underline the importance of desmosomes in development and tissue integrity, while down regulation of individual protein components in cancer metastasis and wound healing suggests their importance in cell homeostasis.

The desmosome is a symmetrical structure comprising two adjacent plasma membranes that sandwich a 30-nm intercellular space bisected by a central dense stratum or midline and are flanked by mirror-image tripartite electron-dense plaques[124]. Each half plaque comprises a total width of up to 50 nm. The core of the desmosome, containing the plasma membrane and intervening material, contains transmembrane and extracellular domains of desmosomal cadherins. The outer dense plaque (ODP), a 15- to 20-nm thick electron-dense region adjacent to the plasma membrane, is separated by less than 10nm from a 20 nm thick inner dense plaque (IDP), the later of which is intimately associated with a meshwork of intermediate filaments (Figure 1.6d-e). The ODP and IDP contain the cytoplasmic tails of the transmembrane cadherins and associated cytoplasmic proteins[125].

Figure 1.6 Adherens junction & desmosome structure

Electron micrograph (a) showing desmosome (asterisk) and adherens junction (arrow) in keratinocytes and the schematic illustration of association of molecular components in AJ (b) and DS (c). In the lower figure, (d) shows protein composition (standard abbreviations used) in various regions identified in electron micrograph of a typical desmosome (e). Reproduced from review articles[126,127].

Figure 1.7 Schematic Illustration of heart muscle and the intercalated disc

Illustration on the left is a schematic diagram of the ultrastructure of the heart muscle in the region of an intercalated disk. Contact between cells is accomplished by interdigitation in the vertical region and is smooth in the horizontal plane (HP). On the right the intercalated disc: Two regions can be identified in the stepwise junctions: A transverse portion which runs across the fibres at right angles and a lateral portion running parallel to the myofilaments. The junctional specializations making up the intercalated disk comprises fascia (A) adherens in the transverse portion of the disk, which serves to anchor actin filaments of the terminal sarcomeres to the plasma lemma. The desmosomes (B) found primarily in the transverse portion of the disk, binds cells together, preventing their separation during contraction cycles. The gap junction (C) restricted to the lateral portion of the disk (that area subjected to least stress) ionically couples cells and provides for spread of contractile depolarization. The significance of ionic coupling is that chains of individual cells behave as a syncytium, allowing the signal to pass from one cell to the other. Reproduced from Marshall[128]

DS are present in epithelia of many tissues, within the intercalated disks of the heart, follicular dendritic cells of the lymph nodes, and in the arachnoid plexus of the meninges[129]. DS can be associated with keratins (in epidermal keratinocytes), vimentin (in mesenchymal cells, for e.g., dendritic reticulum) or desmin (in cardiomyocytes) IF's, demonstrating their versatility in IF-binding. The molecular composition of desmosomal plaque and core components varies among tissues and within complex stratified epithelial tissues. A related structure, the *complexus adhaerentes*, is found in the lymphatic endothelium and in the sinus of lymph nodes. This structure is unique, containing a classical cadherin and the desmosome components desmoplakin and plakoglobin[130].

The extracellular domains of both types of desmosomal cadherins, desmogleins, and desmocollins are necessary for initiating Ca^{2+}-dependent cell-cell adhesion through their heterophilic interactions. Their cytoplasmic tails associate with proteins belonging to the armadillo family of proteins: plakoglobin and plakophilin, which link to desmoplakin. Desmoplakin in turn binds to the IF cytoskeleton[131,132], affording strength to the desmosomal junction. Different IF proteins interact with desmoplakin via distinct sequences in different IF domains[133]. Besides desmoplakin, other proteins found in the inner dense plaque include plectin, envoplakin and periplakin, all part of the plakin family of proteins[134,135]. Little is known about the spatial organisation of other minor protein components of desmosomes such as desmocalmin, pinin, keratocalmin[134], desmoyokin and erbin[136].

1.3.4 Intercellular junctions in cardiomyocytes – the intercalated disc

Large intercellular junction complexes known as intercalated discs (ID) that play a critical role in both electrical and contractile functions of the heart connect individual ventricular cardiomyocytes. Cardiomyocytes are highly differentiated bipolar cells that are almost completely filled with contractile elements, the myofibrils. Two classes of junctions are believed to assemble in the ID, the first are the plaque bearing adhering junctions and the second type is the gap junctions. Until very recently, it was assumed that two quite distinct and separate types of adhering junctions were assembled in the ID. The first type consisted of *fasciae adherentes* (or adherens junction, AJ) which anchor the contractile myofibrils with N cadherin enabling

transmission of contractile force, and the second type are the desmosomes (DS) which provides anchoring sites for desmin intermediate-filament to the desmosomal cadherins (DSG2 and DSC2) imparting the cohesiveness, resilience and integrity to the tissue. Finally, the gap junctions (GJ, discussed in the following section) constituting the non-plaque bearing intercellular junction found in the ID are responsible for the electrical coupling and transfer of small molecules between myocytes. All three types of junctions, AJ, DS, and GJ are believed to assemble as shown in Figure 1.7. The schematic structures of the adhering type of cell-cell junctions are shown in Figure 1.6.

However, the assumption that two discrete adhering type junctions are present in the ID was challenged in recent studies[137,138]. Examination of mammalian (human, bovine, rat and mouse) and non-mammalian (chicken, amphibia and fish) cardiac tissue by immunoelectron microscopy suggested that desmosomal proteins (desmoplakin, plakophilin-2, plakoglobin, desmocollin-2, and desmoglein-2) were not restricted to desmosome-like structures, but they also occurred in many, perhaps all, of the other adhering junctions of ID, thus occupying a very large proportion of the ID membrane. Furthermore, immunofluorescence and immunoelectron microscopic examination of myocardia of diverse mammalian species (human, cow, rat and mouse) established desmoplakin and other desmosomal proteins to occur in these adhering junctions in close proximity or even co-localise with N-cadherin, cadherin-11, α-catenin, β-catenin, vinculin, afadin, p120ctn, ARVCF, p0071, and ZO-1. Thus, it was concluded that the predominant type of adhering junctions present in ID is a unique 'hybrid' junction type termed ***area composita*** that is characterized by an unusually high molecular complexity with an intimate association of molecules of both ensembles, the desmosomal one and of the*fascia adhaerens* category[137].

1.4 Cardiac gap junctions and connexin-43

Gap junctions (GJ) are intercellular channels 1.5–2 nm in diameter. These permit the free passage of ions and small molecules between the cells, up to a molecular weight of about 1KD and allow the conduction of action potentials between cardiac myocytes leading to synchronized electrical propagation ensuring the rhythmic pumping of the

heart. Gap junctions are also involved in metabolic coupling between cells and are important in intercellular communication during organogenesis.

Figure 1.8 Ultrastructure of rat ventricular myocyte ID

Thin-section electron micrograph of rat ventricular myocytes intercalated disk illustrating the organization of desmosomes (d)), fascia adherentes junctions (fa), and the gap junctions (gj). Fasciae adherentes junctions mechanically couple the myofibrils (contractile apparatus) of the adjacent cells; desmosomes serve as anchor points for the desmin cytoskeleton. Gap junctions are situated in the membrane segments between the fasciae adherentes. Scale bar = 1 μm. Reproduced from Severs[139].

Gap junctions, adhaerens junctions, and desmosomes are spatially organized at the intercalated disks. The disks join abutting myocytes in a step-like structure so that the myofibrils of consecutive cells are mechanically joined in series at the fasciae adherentes junctions, i.e., in the vertical segments of disk steps. The gap junctions are located predominantly in the longitudinal segments of the steps. Desmosomes, which link to the desmin intermediate filament cytoskeleton, are found in association with

both the gap junctions and the adhaerens junctions. The organization of these cell-cell junctions in the ID of rat ventricular cardiomyocytes is illustrated in Figure 1.8 in a thin section of ventricular tissue.

The connexon (hemi-channel) is the functional unit of a gap junction; it is composed of six copies of membrane spanning connexins. A gap junction is composed of two juxtaposed connexons assembled by docking of two separate connexons derived from adjacent cells. The GJ encompass a central continuous pore providing permeability for ions and small molecules. There are at least 21 connexin isoforms expressed in humans[140] that are encoded by a large gene family representing structurally conserved proteins varying in size between 25 to 62 KD resulting from variation in length of the carboxy terminal region.

Multiple Connexin subtypes are expressed in the heart such as connexin-43, connexin-40 and connexin-45 that are found in distinctive combinations and relative quantities in different, functionally specialized subsets of cardiomyocyte[141-143]. Connexin-43 is the main connexin isoform expressed in ventricular cardiomyocytes at the intercalated disc[144]. An alteration in gap junction organization and Connexin subtype expression is a consistent feature of acquired human heart disease, which can give rise to conduction disturbances that may contribute to arrhythmogenesis.

Two overlapping forms of remodelling occur in heart disease including structural remodelling, which involves changes in the arrangement or organization of gap junctions (redistribution of gap junctions), and remodelling of Connexin expression, in which the amount or subtype of Connexin expression is altered. These forms of remodelling are now a well documented feature of human cell-cell junction cardiomyopathies associated with a high incidence of syncope, ventricular arrhythmias and sudden death, and heart disease of other aetiologies [50,144-146]. In the diseased ventricles, the most consistent quantitative alteration involves heterogeneous reduction in connexin-43 expression. Remodelling of myocyte gap junctions and alteration in expression of connexin-43 protein have been demonstrated in Caravajal syndrome, Naxos disease a cardiocutaneous syndrome of ARVC[42,43], and in a dominant ARVC caused by an in-frame insertion mutation in plakoglobin[51].

Gap junctions are dynamic structures with connexons being continually added to the edges of existing gap junctions, while channels are removed by endocytosis from the centre of the gap junction[147]. Connexins usually have a high turnover rate, with a half-life of between 1.5–5h[148]. During endocytosis of gap junctions, both membranes of the junction are internalised into one of the adjacent cells forming a double-membrane vacuole called an annular gap junction or connexosome. Endocytosis of gap junctions is thought to involve Clathrin. Internalization of gap junctions requires proteasomal activity[147]. However, the precise role of the proteasome in gap junction endocytosis is not clear. Following internalization of gap junctions, connexins are degraded in lysosomes.

Connexin 43 is phosphorylated at multiple different serine residues during its life cycle[149]. Phosphorylation of connexins regulates multiple steps in the life cycle of gap junctions, including connexin trafficking to the plasma membrane, assembly of connexons into gap junctions and gating of gap junction channels. There is also significant evidence that de-phosphorylation of connexins is important in regulating the internalization and degradation of gap junctions. Phosphorylation of connexins occurs primarily in the C-terminal tail. Protein kinases are involved in connexin phosphorylation include Mitogen-Activated Protein Kinase (MAPK), Protein Kinase C (PKC), Protein Kinase A (PKA), cdc2/cyclinB, Casein Kinase 1, v-src, and c-src. Connexin-43 is phosphorylated soon after synthesis and its phosphorylation pattern changes as it traffics through the endoplasmic reticulum and Golgi to the plasma membrane, ultimately forming a gap junction structure. Cx-43 migrates as multiple isoforms when analyzed by sodium dodecyl sulphate polyacrylamide gel electrophoresis (SDS-PAGE), including a faster-migrating form that includes non-phosphorylated (P0 or NP) Cx-43 and at least two slower-migrating forms, commonly termed P1 (phosphorylated forms at serine residues: S364/S365) and P2 (phosphorylated at serine residues: S325/S328/S330). Pulse-chase labelling analysis indicates that the Cx-43 isoforms progress from P0 to P1 to P2 and that the P2 isoform is associated with junctional gap junctions. When cardiac tissue is analysed for Cx-43 by WB analysis, only the low mobility ''phosphorylated'' isoforms are observed. Myocardial ischemia leads to Cx-43 ''de-phosphorylation'' (i.e., loss of P1 and P2, and gain of P0) and loss of localization from the intercalated disk, which probably contributes to contractile failure and arrhythmias. Thus, the membrane

localization of Cx-43 in gap junctions in disease states appears to be affected by its level of phosphorylation.

Modulation in gap junction turnover has been suggested to be an important mechanism for regulating GJIC[148] and increasing evidence suggests that ubiquitination is important in regulating gap junction degradation[147].

1.5 Diseases of the desmosomes

The desmosome is a target for autoimmune, infectious, and genetic disorders, resulting in common features such as skin blistering and hyperkeratosis. Some genetic disorders of the desmosomes, while apparent in infancy, usually become manifest in late teens and early adulthood, and are linked with cardiomyopathies (section 1.5.0). A summary of diseases of the desmosomes is shown in Table 1.4, adapted from review article[150].

Table 1.4 Diseases of the Desmosomes

Adapted from review article[150].* Human genome mutation (HGMD) online database: www.hgmd.cf.ac.uk/ac/index.php. Table 1.5 lists fifty-four novel plakophilin-2 mutations reported to the present date (March 2008).

	Mutated gene/target Antigen	Phenotype	References
Genetic Diseases	Desmoglein 1	Striate palmoplantar keratoderma (SPK) Lesions of the palms & soles exacerbated by mechanical trauma	Hunt[151] Rickman[152]
	Desmoglein 2 (Table 1.6)	Autosomal dominant right ventricular cardiomyopathy	Pilichou[104], Basso[46] Syrris[101], Awad[100]
	Desmoglein 4	Autosomal recessive hypotrichosis (LAH). Follicular abnormality Loss of hair on scalp, chest, arms, legs and sparse facial hair	Kljuic[153]
	Desmocollin-2 (Table 1.7)	Autosomal dominant ARVC	Syrris[102], Heuser[103], Beffagna[99]
	Desmoplakin (haploinsufficiency) (939+G>A, IVS7+1G>A)	Striate palmoplantar keratoderma (SPK) Acantholysis with keratin retraction	Armstrong[154] Whittock[155]
	Desmoplakin (C897G, S299R)	Autosomal dominant ARVC	Rampazzo[39]
	(I608_609insQSQFT DARKI)	Autosomal dominant biventricular cardiomyopathy Keratoderma, wooly hair	Norgett[156]
	Desmoplakin (G7402C, G2375R)	Autosomal recessive ARVC	Alcalai[157]
	(C3799T, R1267X)	Autosomal recessive ARVC, Naxos like syndrome	Uzumcu[158]
	Desmoplakin (C-term truncation, (7901delG, R2541fsX2559)	Autosomal recessive Carvajal Syndrome DCM, SPPK, wooly hair	Norgett[159]
	Desmoplakin (compound heterozygosity)	Palmoplanter keratoderma combination of nonsense/missense mutations	Whittock[160]
	[T2427A, C809X/T861G, N287K],	Alopecia, hyperkeratosis, acantholysis, keratin retraction	Whittock[160]
	[C1990T, Q664X/C7096T, R2366C], & [C5799T, R1934X/ & 6090delTT, S2030fsX2059]	Lethal acantholysis epidermolysis bullosa	Jonkman[161]

Table 1.4 (continued)

	Mutated gene/target Antigen	Phenotype	References
	Desmoplakin (2034insA, T586fsX594) (K470E, A566T, K1583R, c.542+5G>A) (G88A, V30M; A269G, Q90R; G699A, W233X; G8501A, R2834H (G3764A, R1225K; G5324T, R1775I; c.423-G>A, IVS3-1G>A) Various mutations (13 frameshift/nonsense and 4 missense mutations)	Autosomal dominant left ventricular ARVC	Norman[162] Basso[46] Yang[163] Bauce[164] Sen-Chowdhry[165]
	Plakoglobin	Naxos disease (Autosomal recessive ARVC, with PPK & wooly hair) Autosomal dominant arrhythmogenic right ventricular	McKoy[38] Asimaki[51]
	Plakophilin 1	Autosomal recessive ectodermal dysplasia, skin fragility Syndrome, hair loss & nail dystrophy	McGrath[135], McGrath[166] Whittock[167]
	Plakophilin 2 See HGMD website* Table 1.5 lists 54 PKP-2 mutations to date	Autosomal dominant ARVC	Gerull[40] , Syrris[41], Van Tintelen[107], Dalal[108], Nagaoka[109], Antoniades[110] Kannankeril[111], Lahtinen[112]
Autoimmune Diseases	Desmoglein 1	*Pemphigus foliaceus* Blistering of the superficial epidermis Circulating autoantibodies directed against DSG1	Amagai[168] Nousari[169]
	Desmoglein 1	Paraneoplastic pemphigus	Amagai[168]
	Desmoglein 3	Pemphigus vulgaris Autoantibodies against DSG3 cause blisters in oral cavity Antibodies against DSG3 & DSG1 cause blisters in the oral Cavity & the deep dermis	Amagai[168] Nousar[169]
	Multiple plakin	Mucous membrane & skin blistering, variable & severe in PV Bronchial epithelial lesions in subset of individuals Disease associated with a number of neoplasms	Hashimoto[170]
Infectious Disease	Desmoglein 1	*Staphylococcus aureus* scalded skin syndrome (SSSS) *Staphylococcus aureus* exfoliative toxin A or B cleaves DSG1 Superficial blister formation Also known as Ritter disease	Amagai[171,172] Hanakawa[173,174]

1.6 Role of cell-cell adhesion proteins in cellular signalling

Besides their role in providing adhesion at intercellular junctions, the armadillo catenins: β-catenins, plakoglobin, and plakophilins may also have signalling role in the nucleus, whereby they allow the cells to modulate their behaviour in response to changes in cell adhesion. Wheelock and colleagues[175] were the first to suggest that plakoglobin may play a role in signalling apart from their role in desmosome and adherens junction assembly.

1.6.1 Beta-catenin signalling

As discussed in section 1.1.2c, beta-catenin plays a pivotal role in mediating the Wnt signaling pathway responsible for regulation of differentiation in development[176]. It regulates cellular proliferation via its interaction with TCF/LEF transcription factors mediated through its Armadillo repeats. The association of β-catenin-TCF/LEF translocates the complex into the nucleus where it activates genes involved in cellular proliferation[177]. The carboxy terminus of β-catenin was essential for fully activating the transcription of target genes[178].

1.6.2 Plakoglobin signalling

A study using cell line lacking functional β-catenin showed that exogenous plakoglobin expression caused nuclear accumulation of plakoglobin and binding of plakoglobin to TCF-4 or LEF-3, suggesting that plakoglobin can directly activate Wnt signalling cascade without interacting with β-catenin[179]. This suggested that plakoglobin could have multiple functions as a transcriptional activator and as a cell adhesion molecule. In comparison with β-catenin, plakoglobin is a relatively weak transcriptional activator and this was ascribed to the difference in the carboxy termini of the two molecules[55] (<15% homology present)[180]. Plakoglobin can also act as a signalling molecule by the induction of anti-apoptotic protein Bcl-2[55], however further

studies are needed to establish a link between cell-cell junction and intracellular signalling pathways.

1.6.3 Plakophilin-2 signalling in ARVC

Precisely how plakophilin-2 might be involved in signalling in ARVC is not presently clear. Missense mutations may cause gain-of-function protein activity related to signal transduction via post-translational phosphorylation modification of serine, threonine, or tyrosine residues. Putative phosphorylation at several of these three amino acid residues are predicted by phosphorylation site prediction program (such as NetPhos protein phosphorylation site prediction program), to occur in various domains of plakophilin-2 protein molecule. One such phosphorylation modification site has been identified on serine residue number eighty-two[181] of PKP-2 protein which is phosphorylated by C-TAK1 (discussed further in the next section). Other types of post-translational modification such as ubiquitination and O-glycosylation occur in PG, these types of modifications may potentially regulate the activity of PKP-2.

1.6.4 Nuclear functions of PKP-2

In addition to the role of plakophilin-2 in the desmosomes, it also has, in common with other armadillo family proteins, a dual localisation in cell nucleus. The nuclear localization of plakophilin-2 was elucidated by Mertens and colleagues[182] using sucrose density gradient centrifugation showing that PKP-2 associated with RNA polymerase III holoenzyme (RPC155 protein, 155kD). The specific association of these two proteins was confirmed by *in vitro* solid-phase binding assay and co-localisation experiments. In addition to RPC155, RPC39 and RPC82 were also identified as binding partners implicating an association of plakophilin-2 with the Polymerase III holoenzyme, but not with the core Polymerase III complex. How precisely the dual localization of plakophilin-2 is regulated in the desmosomes and the nucleus is not well understood. Plakophilin-2 was identified as a substrate for Cdc26C-associated kinase 1 (C-TAK1) implicated in cell cycle regulation and Ras signalling[181]. Phosphorylation of plakophilin-2 by C-TAK1 generates a binding site

for σ14-3-3 proteins, which contributes to the specific localisation of plakophilin-2 in the cell. Engineered mutations introduced at serine residue number 82 in plakophilin-2 (S82A or V82A), around which a putative σ14.3.3 protein-binding site resides, exhibits increased nuclear accumulation of the plakophilin-2[181]. Since the C-TAK1 generated 14.3.3 binding site was not conserved among the plakophilins, this may explain why reduced nuclear localisation of over-expressed plakophilin-2 compared to that of plakophilin-1 was found in the study of Chen[183] *et al.* The precise role(s) of nuclear PKP2 is currently unknown[184].

1.7 Mice models of knockout genes encoding DS proteins

The crucial roles of desmosomal proteins in cardiac morphogenesis were elucidated in gene-knockout mice studies. Observations in these mice provided important clues about the role of these cell-cell adhesion proteins in the heart, and which provided a rationale for the screening of PKP-2, DSG-2, and DSC-2 genes leading to identification of mutations in these three genes in human ARVC.

1.7.1 Plakoglobin ablated transgenic mice

Plakoglobin-null mutant mice (plako$^{-/-}$) died from embryonic day 10.5 onwards, due to severe heart defects coinciding with the onset of heart contraction and mechanical stress. Some mutant embryos developed further, especially on a C57BL/6 genetic background, and died around birth, presumably due to cardiac dysfunction, and with skin blistering (reminiscent of human epidermolytic hyperkeratosis) and subcorneal acantholysis. Ultrastructural analysis in these mice embryos, revealed that desmosomes were greatly reduced in numbers, and structurally altered with a less dense plaque and atypical appearance of their desmoglea[185]. A related independent study of plakoglobin-null mice showed that they die of ventricular rupture and consequent pericardial tamponade. The tissue instability correlated with absence of desmosomes in the heart (desmosomes were unaffected elsewhere in developing epidermis or the gut), but instead extended adherens junctions or 'mixed type'

junctions were formed containing desmosomal protein components. This study concluded that plakoglobin is indispensable for both the formation of cardiac desmosomes and the proper segregation of desmosome & adherens junction components to determining the architectural stability of the intercalated disc in embryonic mouse heart[186].

1.7.2 Desmoplakin ablated transgenic mice

Desmoplakin is a ubiquitous protein molecule expressed in all desmosomes. Desmoplakin-null mice showed early embryonic lethality dying beyond embryonic day 6.5 due a loss or instability of desmosomes in extra embryonic tissue[187]. Tetraploid rescue in desmoplakin function increased embryonic survival by several days, allowing inspection of developing somatic tissues[188]. Marked abnormalities in the heart muscle, neuroepithelium, and skin epidermis were observed, as well as abnormalities in the complexus adherens junction in the microvasculature, consistent with the widespread importance of DP in tissue integrity during development. Fragile skin and cell-cell adhesion defects were apparent and were restricted to cells that would normally express desmoplakin. Few desmosomes were observed and those present were not linked to keratin filaments. DP-null mutant mice showed greater severity in phenotype compared with the PG-null mutant mice suggesting a possible functional redundancy of plakoglobin with members of other armadillo proteins, such as β-catenin or plakophilins. Plakophilins, plakoglobin and desmoplakin appear to play different roles in the desmosome, with desmoplakin performing a dual function in linking intermediate filaments (IF) and in providing stability to desmosomes; the known interactions of plakophilins and plakoglobin with desmosomal cadherins and IF's alone, it seems not to be sufficient to anchor IF to desmosomes in the absence of desmoplakin. Comparison of DP-null mice embryos with that of PG-null mice indicated presence of 'mixed type' of adhering junctions in the later with DSG2 diffusely spread over the cell surface, whereas DSG2, DSC2 and PKP2 still appeared clustered and co localised, albeit significantly reduced in DP-null mice. In addition, the sizes of adherens junctions were increased in PG-null mice, but these junctions were unaffected in DP-null mice.

Conditional ablation of DP in the developing mouse epidermis[189] using a Cre/LoxP system under control of keratin 14 promoter showed extreme skin fragility and pronounced intercellular separations in the basal and spinous layers of the skin in these animals. DS were only slightly reduced in number or size, but they lacked an inner plaque and IF attachment. Areas of intercellular separation showed that the complete desmosome was linked to one of the two cells, suggesting desmosomal cadherin-mediated adhesion was not affected, but rather the entire junction was torn out of adjacent cells owing to the lack of cytoskeletal attachment to the plaque. Maturation of adherens junctions and associated cortical actin filament network was impaired in keratinocytes from these DP-null mice, and exhibited defects in sealing of intercellular membranes. Culture of keratinocytes from these DP-null mice showed very few DS, but reintroduction of DP N-terminus at least partially rescued effects on membrane sealing. Thus, adherens junction maturation appears to require certain desmosomal functions, which are dependent on desmoplakin.

1.7.3 PKP-2 ablated transgenic mice

Plakophilin 2-null mice[190] died around mid-gestation (E10.5-11) due to lethal alterations in heart morphogenesis and stability characterised by reduced trabeculation, disarrayed cytoskeleton, ruptures of cardiac walls, and blood leakage into pericardiac cavity. Structures resembling desmosomes seen in cardiac tissue of wild type mice were absent in PKP-2-deficient mouse embryos, however adherens junction gross morphology was unaffected in this tissue. Immunogold electron microscopy examination in PKP-2 mutant mice revealed that desmoplakin had dissociated from plaques of adhering junctions connecting cardiomyocytes, instead forming granular cytoplasmic aggregates located between myofibrils and desmin intermediate filaments, away from the intercalated disc. Absence of PKP-2 caused the cytolinker DP to dissociate from plaques of adhering junctions. Double-immunofluorescence staining revealed that whereas in wild type developing heart desmoplakin co-localised with various adhering junctional components such as plakoglobin, β-catenin, plakophilin-2, N-cadherin, desmoglein-2, α-catenin, and $p120^{ctn}$, it did not associate significantly with any of these junctional proteins in the PKP-2-deficient mouse embryos, but instead it was dispersed in the cytoplasm away

from the intercalated disc. Desmoglein 2 could not be localised at significant levels in developing heart of PKP2-deficient mice, indicating that PKP-2 is an essential stabilising binding partner of desmosomal cadherins. Absence of desmosomes in cardiac tissue of PKP2 mutant embryos was tissue-specific as other epithelial tissues, such as the developing epidermis and stomach mucosa showed normal AJ and DS ultrastructure when compared with PKP-2 wild type mice. Whilst Plakoglobin and PKP-2 ablation showed a similar temporal (E10.5-E12) pathological alteration in desmosomes in cardiac tissues, an important difference was the firm association of desmoplakin in plaques of adhering junctions in the former, but not in the later case.

1.7.4 DSG-2 ablated transgenic mice

While knockout mice data for PG, DP and PKP-2 are available, no data are available on cardiac abnormalities in the DSG-2 knockout mice because loss of DSG-2 results in early embryonic lethality[191]. However, the crucial role of desmogleins generally in maintaining desmosome ultrastructure is supported by various studies showing decreased desmosomal plaque number associated with asymmetry and detachment[192-194]. Examination of myocardial biopsies of three individuals with ARVC carriers of DSG-2 gene mutation showed decreased desmosome numbers and widening of the intercalated disc gap[104].

1.7.5 DSC-2 ablation

There is presently no transgenic mouse study examining the impact of DSC2 ablation during embryonic development. However, the role of DSC2 in the heart of a Zebra fish model was examined using antisense morpholino oligonucleotides to DSC-2, which resulted in marked reduction in the levels of DSC*2* mRNA in the morphant embryos. The phenotype in these DSC2-targetted fish revealed significant dose-dependent bradycardia, chamber dilatation, and abnormal cardiac contractility with progressive pericardial oedema[103].

1.8 ARVC Gene mutations encoding desmosomal proteins

Several studies have implied that ARVC may be a disease of the desmosome[39,40,114,157]. Five major molecular components are found in cardiac desmosomes; these include the desmosomal cadherins (desmoglein-2 and desmocollin-2), the ARM-repeat proteins (plakoglobin and plakophilin-2), and the plakin family of proteins (desmoplakin). Since the discovery of desmoplakin and plakoglobin mutations in ARVC8 and Naxos disease in the late nineties, considerable progress was made since 2004 in identifying other causative mutations in ARVC with plakophilin-2 mutations shown to be associated with ARVC. Mutations affecting major desmosomal proteins have now been reported (Table 1.4) in several diseases, but specifically in the context of ARVC, disease causing mutations have now been found in all five major cardiac desmosomal components (DP, PG, DSG-2, DSC-2 and PKP-2); these findings suggests that ARVD/C is a multigenic disease of cellular adhesion[195] affecting the desmosome. A detailed analysis of mutations found in these cell adhesion molecules now follows.

1.8.1 Desmoplakin mutations in ARVC

The desmoplakin gene is located on chromosome 6 consisting of 24 exons. Alternative mRNA splicing forms two transcripts (DPI 2871 amino acid and DPII 2271 amino acid). DPI is the larger of the two proteins as it contains an additional 600 amino acid sequence within the coiled coil rod region that is alternatively spliced out in DPII isoform; DPI and DPII are abundantly expressed in all types of epithelia, while cardiac muscle contains only DPI [196]. Desmoplakin belongs to the plakin family of proteins in which plectin, envoplakin periplakin, epiplakin, and bullous pemphigoid antigen 1 (BPAG1) are structural homologues. Plectin the prototype protein of this family consists of a modular organization consisting of four sub domains referred to as the actin-binding domain (ABD) consisting of two calponin homology domains, a plakin domain found near the N terminus, a central rod domain and a C-terminus plakin repeat domain (PRD). The plakin domain of plectin was predicted to form six anti-parallel α-helices referred to as NN, Z, Y, X, W, and V based on

amino acid sequence. The crystal structure of the plakin domain of plectin recently determined at 2.05 angstrom resolution showed a tandem pair of spectrin repeats (SR) connected by an α-helical linker spanning these two repeats[197]. Protein structure prediction analysis of the plakin domain of plectin revealed nine consecutive SR organized in an array of tandem modules, with a Src-homology 3 domain inserted in the central spectrin repeat[197]. Homology search in other proteins belonging to the plakin family showed that a similar SR modular organization occur in other representative members of these protein family[197,198]. Thus, plakins are evolutionarily related to spectrins (spectraplakins), but have diverged to perform specialized functions. The modular structure of spectrin repeats found in plakin domain of plectin resembles that of β-spectrin and α-spectrin found in erythrocytes (Figure 1.9).

Desmoplakin is a spectraplakin with a modular plakin structure similar to that found in plectin, but it lacks the ABD and SR 1-2 and 7 (Figure 1.9) repeats. Other domains in desmoplakin consist of a central coiled–coil rod dimerization domain and a modular PRD consisting of A, B, and C sub-domains involved in binding to desmin and vimentin intermediate filament proteins[199]. The composition of the plakin domain as an array of tandem spectrin repeats has profound implications for its function in terms of the flexibility, and extensibility of the domain. The elastic properties of tandem SR are essential for the function of the proteins that contain such arrays.

All DP mutations discussed here are listed in Table 1.4 these are also represented in the illustration in Figure 1.10. A desmoplakin mutation (S299R) in ARVC8 was reported[39] to modify a putative phosphorylation site in the N-terminal domain involved in the binding of plakoglobin. In a study of Muslim-Arab family of twelve individuals from Jerusalem, with clinical syndrome of sudden death (8/12 family members), woolly hair, and a pemphigus-like skin disorder (keratoderma), a homozygous missense mutation (G2375R) in exon 24 of desmoplakin was found[157]. The Glycine residue at position 2375 is a highly conserved residue within the plakin repeat domain (PRD3) of the B segment of desmoplakin C terminus. The PRDs form a positively charged grove predicted to bind the intermediate filament. Hence, this mutation destabilized the PRD disrupting desmoplakin-intermediate filament binding. In another study of three Ecuadorian families[159] another homozygous desmoplakin mutation (c.7901delG, p.S2542fsX2560) truncated the desmoplakin protein molecule in the C-terminus which resulted in disruption of the IF network;

Figure 1.9 Modular organization of plakin domains

(a) Schematic representation of the domain organization of full-length plectin. The C-terminal region contains five type B and one type C plakin repeat domains. (b) Detail module organization of the N-terminal region of plectin and other representative plakins including BPAG1a/b/n, BPAG1e, desmoplakin and periplakin. Spectrin repeats (SR) are numbered according to plectin. The repeats of plectin and BPAG1 whose crystal structure is known are shown in dark gray. The ABD is formed by two calponin homology (CH) domains. The position of the six α-helical-rich regions (NN, Z, Y, X, W, and V) described in the plakin domain14 is indicated above the plectin structure. (c) The domain organization of the erythrocyte isoforms of α and β-spectrin is shown to illustrate the similarities with the plakin domain architecture, noticeably the array organization of tandem SR's, the localization of the ABD preceding the SR1 of β-spectrin, and the insertion of an SH3 domain within the ninth SR of α-spectrin. Reproduced from Sonenberg[197] *et al.*

resulting in a phenotype of palmoplantar keratoderma with woolly hair and DCM. Another autosomal dominant mutation caused by a heterozygous insertion (c.2034_insA) in desmoplakin resulted in DP truncation (p.T586fsX594) causing a predominantly left-sided ARVC[162]. A 30 base pair insertion in DP exon 14 resulted in the insertion of ten amino acids (c.608-609_insQSQFTDARKI) causing autosomal dominant biventricular cardiomyopathy with SPK and Woolly hair[156]. A homozygous stop codon mutation in DP exon 23 (c.C3799T) caused a truncation in DP (p.R1267X) resulting in a DPI isoform specific loss of protein expression. This nonsense DP mutation caused recessive biventricular cardiomyopathy with palmoplantar keratoderma and woolly hair[158]. Three novel DP mutations (p.R1255K and p.R1775I and a splice site mutation c.423-1G>A) were identified in four families with ARVC[164] with the missense mutations affected highly conserved arginine residues in different species. Both missense mutations were predicted to destabilize the rod domain preventing the formation of the coiled-coil region in DPI. The c.423-1G>A mutation altered an acceptor splicing site of intron 3 causing aberrant alternative splicing with skipping of exon 4 resulting in a PTC truncating the DP to a polypeptide of 200 amino acids. Analysis of sixty-six patients in a North American ARVC[163] cohort identified four DP variants (p.V30M, p.Q90R, p.W233X and p.R2834H). The effects of two missense mutations were examined functionally in SCC9 cell line by transient transfection of plasmid vectors encoding a small portion of DP N-terminus (DPNTP, first 584 amino acids) as well as full-length desmoplakin that incorporated these two missense mutations. These studies highlighted a failure of membrane localization of p.V30M and p.Q90R DP variants and their inability to bind to plakoglobin[163]; embryonic lethality of cardiac restricted expression of these missense DPs in mice corroborated these *in vitro* finding[163]. The nonsense p.W233X DP mutation examined by transient transfection in SSC9 cells failed to localize at cell-cell junctions and analysis of patient mRNA suggested that transcript with this PTC was probably degraded by NMD. An elegant demonstration of the effects of over-expression of R2834H DP protein in a cardiac restricted transgenic mouse showed increased cardiomyocyte apoptosis, cardiac fibrosis, lipid accumulation, and defects in cardiac development. R2834H DP in transgenic mice resulted in aberrant desmin localization and dissociation of plakoglobin, plakophilin-2, and beta-catenin from cell-cell junctions[163]. Mutation screening of twenty-one unrelated probands[46] revealed four novel desmoplakin mutations (p.K470E, p.A566T, p.K1583R and a

splice site c.542+5G>A), all three missense mutations occurred in amino acid residues highly conserved among species that were located in different domains (p.K470E in spectrin repeat SR5, p.A566T in SR6, and p.K1583R in the coiled-coil rod) of DP. The splice site mutation altered a donor-splicing site in intron 2, which probably affected the normal splicing of exons 2 and 3. Patient mRNA analysis showed no aberrant transcripts resulting from this mutation indicating that these transcripts were probably degraded by NMD surveillance[46].

1.8.1.1 Representative DP mutations illustrated

A schematic representation of location of all mutations affecting the desmoplakin protein molecule is shown in Figure 1.10. Two different orientations of the DP protein molecule is depicted: the first structure is based on the classical alpha helical structures of the amino terminus plakin domain deduced by Kathleen Green's group more than a decade ago (depicted by five boxes in blue, Z, Y, X, W, and V). The amino acid residues start positions of these five alpha helical domains identified by numbering in orange numbers have been derived relative to the reference DP sequence (Ensemble transcript ID: ENST00000211979, transcript size 2871 amino acid long) and 5' sequence of these helices identified by Virata[200] et al. This was followed by a central coiled coil dimerization region (box depicted in orange, numbering in orange according to Alcalai[157] et al and Yang[163] et al), and a plakin repeat domain consisting of three repeat units (depicted by boxes labelled A, B, and C in gold, numbering in orange according to Green[201] et al) which are important in mediating interactions with intermediate filament proteins (vimentin, desmin and keratin). The second protein structure of DP is depicted directly below the first to contrast the modular organization of the plakin N-terminal domain only based on the spectrin repeats identified (Figure 1.9). In this modular plakin domain structure, six spectrin repeats are identified (SR 3, 4, 5, 7, 8, and 9) with an insertion of an SH3 domain in between the SR5 repeat. The numbering of the spectraplakin repeat structures in the plakin domain of DP (marked in orange and purple numbers) are derived from the work of Sonnenberg[197] *et al.* Figure 1.10 shows the locations of twenty-four DP mutations reported in the literature to date (section 1.5, Table 1.4). These mutations are identified with an arrow and text (same colour used for both for

ease of identifying the location of a given mutation). Figure 1.10 also shows the locations of three additional novel desmoplakin mutations: Q273fsX288, M316fsX324 (both of these disrupt spectrin repeat SR4), and S442F (alters a highly conserved serine residue in SR5) identified in the genetic screening studies (Chapter 3, section 3.4.1 Part1). These three novel mutations are shown underlined (Figure 1.10).

Figure 1.10 Locations of DP mutations

Desmosomal targeting — **Dimerization** — **Desmin/vimentin/keratin**

N-terminal — **Rod** — **IF-binding**

Plakin Domain | **Coiled-Coil** | **Plakin Repeat Domain**

S2542fsX2560: recessive Naxos-like ARVC, Norgett[159]

G2375R: recessive Naxos-like ARVC, Alcalai[157]

1267X: DSP I nonsense mediated mRNA decay → haploinsufficiency, recessive Naxos-like ARVC, Uzumcu[158]

c.423-1G>A: R1255K: R17751: autosomal dominant ARVC, Bauce[164]

I608_Q609ins_QSQFTDARKI: autosomal dominant Naxos-like ARVC, Norgett[156]

T586fsX594 ARVC with left ventricular manifestations, Norman[162]

c.542+5G>A K470E: A556T K1583R autosomal dominant ARVC, Basso[46]

S442F: autosomal dominant ARVC, this study

Q331X: autosomal dominant striate palmoplanter keratoderma (SPK) → haploinsufficiency, Armstrong[154]

M316fsX324: autosomal dominant ARVC, this study

S299R: autosomal dominant ARVC, highly conserved PKC phosphorylation site lost by the mutation, Rampazzo[39]

Q273fsX288: autosomal dominant ARVC, this study

W233X: autosomal dominant ARVC, nonsense mediated mRNA decay → haploinsufficiency, failure of desmosomal localisation *in vitro*, perinuclear aggregation *in vitro*, Yang [163]

Q90R: autosomal dominant ARVC, embryonic lethal in mice, failure of desmosomal localisation *in vitro*, Yang[163]

V30M: autosomal dominant ARVC, embryonic lethal in mice, failure of desmosomal localisation *in vitro*, Yang[163]

R2834H autosomal dominant ARVC, Yang[163]

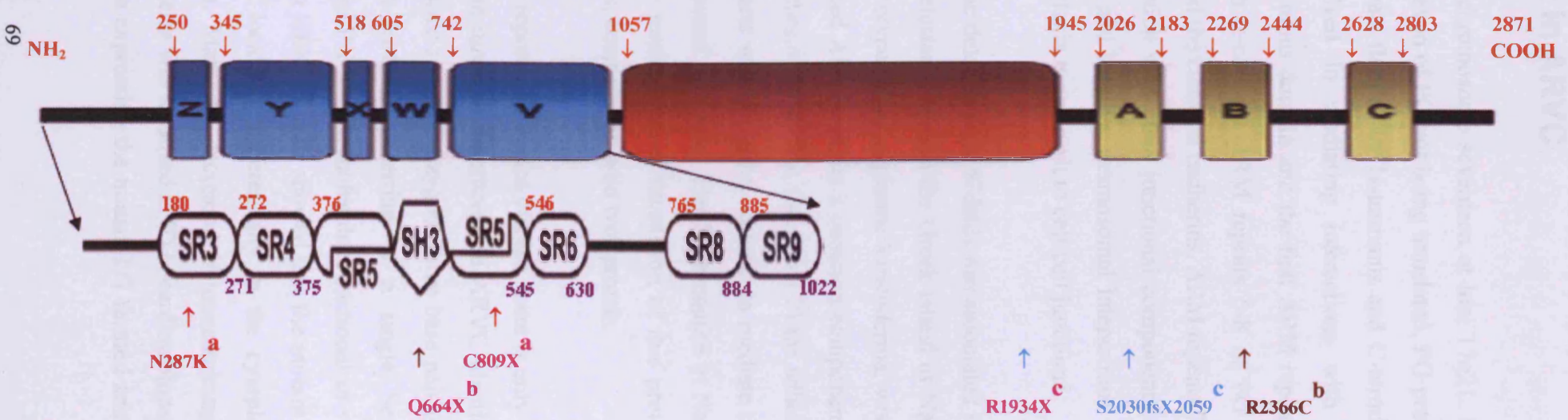

a, a = compound heterozygous missense/nonsense mutations, recessive skin fragility/wooly hair syndrome, Whittock[160]

b, b = compound heterozygous missense/nonsense mutations, recessive skin fragility/wooly hair syndrome, Whittock[160]

c, c = compound heterozygous frame-shift/nonsense mutations, neonatal lethal acantholytic epidermolysis bullosa, → presence of 1933aa nonsense DSPI and 2058aa truncated tDP protein, Jonkman[161]

1.8.2 Plakoglobin mutation in ARVC

The gene for plakoglobin is located on chromosome seventeen at loci 17q21. It is encoded by fourteen exons with the first exon of PG not being translated. PG protein consists of thirteen imperfect ARM repeats flanked by N-terminus and C-terminus domains. ARM repeats 1-3 are involved in mediating interactions with the desmosomal cadherins. Part of the N-terminus domain and the first ARM repeat of PG are required for its interaction with α-catenin. ARM repeats 6-8 of PG are involved in the interaction between PG and the classical cadherins. ARM repeats 7-11 are thought not to be involved in interaction with other junctional components, but appear to target PG to cell-cell contacts and stabilise desmosomal interactions. PG binds to the N-terminal domain of desmoplakin targeting it to cell-cell junctions.

A two-base homozygous mutation PG gene deletion (c.2157del2) was associated with Naxos disease[38]. This disease originally clustered around the Greek island of Naxos showing complete penetrance with a phenotype of palmoplantar keratoderma, woolly hair association with a recessively inherited ARVC. PG is a common component of two different types of intercellular cell adhesion junctions, (section 1.2) the adherens junction (AJ) and desmosomes. PG interacts with β- and α- catenin to mediate cell-cell adhesion in cardiac and dermal-epidermal junctions. The PG mutation in Naxos disease resulted in C-terminal premature termination of translation of this protein, which is shorter by 56 amino acid residues, compared to wild type protein.

Apart from the homozygous PG mutation reported in Naxos disease, there is only one reported PG mutation showing a dominant mode of inheritance in ARVC identified recently in a German family [51]. This resulted in a heterozygous three base pair gene insertion (118_119insGCA) causing an in-frame insertion of a single Serine (p.S39_K40insS) amino acid residue in the PG protein molecule. Functional *in vitro* expression of S39_K40insS PG protein in HEK293 cells showed that the mutant PG protein was apparently ubiquinated and localised preferentially in the cytoplasm targeting it for proteosomal degradation. Markedly decreased immunostaining of plakoglobin, desmoplakin, and Cx-43 proteins was localised at ID in cardiac biopsy of a patient with this PG mutation. Cell lines expressing the mutant PG formed smaller

and fewer desmosomes; these data suggests that expression of mutant PG protein accompanies alteration of the structure and distribution of mechanical and electrical junctions.

1.8.3 Plakophilin-2 mutations in ARVC

The PKP-2 gene is located on chromosome four and encoded by fourteen exons (Figure 1.11). Two PKP-2 protein isoforms are translated from two alternatively spliced mRNA transcripts, transcript 2b (long form consists of all fourteen exons being translated, 881 amino acid long) and transcript 2a (short form, with exon six not being translated, 837 amino acid long) respectively. Although several additional isotypes of plakophilin exist (PKP-1, PKP-3 and p007) in humans, PKP-2 is the predominant protein isotype expressed in heart[183] where both the short and long form of the proteins are present. The structure of PKP-2 protein is composed of a head domain of 348 amino acids where the vast majority of inter protein-protein interactions are known to take place[183], followed by ten imperfect ARM repeats, and a short C-terminus (Figure 1.11). Although the ARM repeats found in plakoglobin are known to mediate binding activity, the precise function of ARM repeats found in plakophilin-2 remains unclear.

Since the work of Gerull[40] and colleagues published in 2004 describing twenty-six PKP-2 mutations there are fifty-four novel plakophilin-2 mutations reported to date (March 2008) providing compelling evidence for a major role of PKP-2 in pathogenesis of ARVC with a divergent role of these mutations in distinct ethnic population. Plakophilin-2 occupies a central position as a stabiliser of myocardial desmosomes supported by studies performed in plakophilin-2 ablated transgenic mice (section 1.4.3).

Figure 1.11 Structure of PKP-2 gene & protein

Structure of the plakophilin-2 gene and protein illustrated schematically. For the gene structure, the clear boxes represent the 5' and 3' UTR of the gene, the black boxes represent each of the fourteen exons, ATG represents the initiation codon, and TGA represents the stop codon. The protein structure shown for the 2b isoform (transcribed from long form of the mRNA transcript) contains a head domain of 348 amino acid followed by ten imperfect ARM repeats (~42 amino acids/repeat). The C terminus domain of PKP-2 is quite short

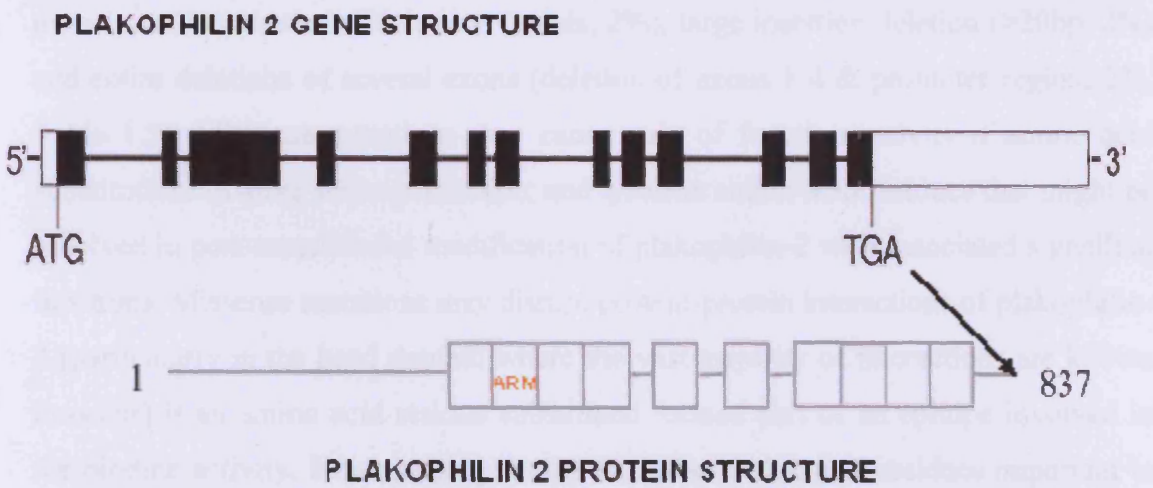

A chronological compilation of all plakophilin-2 mutations discovered to date is listed in Table 1.5. All PKP-2 mutations are transmitted in an autosomal dominant mode, except for a single mutation (c.2484C>T/c.2484C>T, p G828G, Table 1.5) that is transmitted in an autosomal recessive manner. Although PKP2 mutations appear to be common in ARVC and affects all three domains of the protein molecule, precisely how these mutations could cause ARVC is unknown. This section will explore possible mechanisms by which plakophilin-2 mutations might cause ARVC. The vast majority of plakophilin-2 mutations fall in the category of small insertion/deletions (<20 bp, Table 1.5, 37%) that are predicted to cause a frameshift (when the insertion/deletion are not a multiple of three bases) followed by a PTC. Many of these mRNA transcripts containing PTC would undergo degradation by NMD; however, if

some mRNA transcripts containing PTCs were to evade NMD surveillance then expression of truncated plakophilin-2 would lead to dominant negative effects if incorporated into desmosomes. Nonsense mutations account for nearly 24% of all plakophilin-2 mutations (Table 1.5), many of the mRNA transcripts with these PTCs would be expected to undergo NMD resulting in haploinsufficiency, or in exon skipping if NAS (see section 1.1.6) occurs. However, if NMD is bypassed then dominant negative effect will ensue if truncated plakophilin-2 polypeptide or protein were formed.

The missense mutations in plakophilin-2 comprise nearly 24% of all mutations whereas a smaller proportion of mutations arise from splice donor/acceptor site mutations (9%), insertion/deletions (indels, 2%), large insertion/deletion (>20bp, 2%) and entire deletions of several exons (deletion of exons 1-4 & promoter region, 2%, Table 1.5). Missense mutations may cause gain of function activity if amino acid substitutions involve serine, threonine, and tyrosine amino acid residues that might be involved in post-translational modification of plakophilin-2 with associated signalling functions. Missense mutations may disrupt protein-protein interactions of plakophilin-2 (particularly in the head domain where the vast majority of interactions are known to occur) if an amino acid residue substituted formed part of an epitope involved in the binding activity. Fine mapping studies to define amino acid residues important in the binding domains of plakophilin-2 to its diverse protein partners are currently unavailable, but the impact of certain highly conserved missense amino acid residue substitutions in plakophilin-2 head domain are predicted to be disruptive for this reason. The deleterious effects of missense mutations are commonly attributed to their impact on primary amino acid sequence and effect on protein secondary structure. However, several recent studies have shown that some missense mutations are deleterious because they disturb *cis*-acting splicing elements called exonic splicing enhancers (ESEs) that positively encourage the selection of flanking splice sites compensating for weak splice sites. Examples of pathogenic missense mutations affecting ESEs are well illustrated in other genes encoding hMLH1, hMLH2 and BRCA1 which leads to higher propensity for splicing defects[202,203].

ESEs are discrete, degenerate motifs of 6–8 nucleotides located inside exons. The study of normal splicing suggests that most exons contain at least one functional ESE

site. ESEs are target sequences for the family of conserved essential splicing factors - the serine- and arginine-rich (SR) proteins. ESEs play an important role in exon recognition. Missense nucleotide substitutions in ESEs can result in failure of SR proteins to bind to the ESE, which leads to failure of splisosome machinery to recognize the sequence as exonic causing exon skipping. Each SR protein recognizes specific, albeit degenerate and partially redundant, sequence motifs. ESE motifs of five members of the SR family (SF2/ASF, SF2/ASF (IgM-BRCA1), SRp40, SRp55, and SC35) have been identified. Apart from missense mutations, ESEs can also be disrupted by nonsense as well translationally silent point mutations (synonymous mutations). Aberrant exon skipping resulting from missense, nonsense, or translationally silent single-base substitutions is frequently, if not always, caused by disruption of a critical ESE. Disruption of an ESE may result in the pre-mRNA transcript to splice incorrectly, effectively deleting an entire exon-encoded segment of the protein. Mutations in one exon sometimes could cause skipping of multiple consecutive exons. If the length of the skipped exon(s) is not a multiple of three nucleotides, a frameshift may cause down regulation of the aberrantly spliced mRNA by NMD.

In addition to ESEs there are exonic splicing silencer (ESS), these are *cis*-regulatory elements that inhibit the use of adjacent splice sites, often contributing to alternative splicing (AS). ESSs often act through interactions with members of the heterogeneous nuclear ribo-nucleoprotein (hnRNP) family[204]. The molecular mechanisms by which ESSs inhibit splicing are just beginning to be uncovered. Presence of a higher density of ESEs in authentic exons than in pseudoexons may contribute to recognition of the correct exons, while presence of ESSs in pseudoexons may suppress their splicing[205]. Although ESSs are prevalent in the human genome they are a relatively less studied aspect of splicing compared to ESEs.

Table 1.5 Plakophilin-2 mutations in ARVC

PKP-2 mutations in autosomal dominant ARVC reported in various cohorts. * = mutations seen in previous studies. * = only PKP2 homozygous mutation documented causing a recessively inherited ARVC. Highlighted in yellow are the mutations discovered in genetic screening work described in section 3.5.4 Part 1 that have since been published[41]. Mutations listed are as reported until March 2008.

Nucleotide alteration	Amino Acid alteration	Type of mutation	References /No. probands
145_148delCAGA	S50fsX110	Small deletion → frameshift	Gerull[40]/120
216insG	Q74fsX85	Small insertion → frameshift	
235C>T	R79X	Nonsense	
534_535insCT	C179fsX190	Small insertion → frameshift	
419C>T	S140F	Missense	
1369_1372delCAAA	Q457X	Small deletion → nonsense	
1631_1632insTT	L544fsX563	Small insertion → frameshift	
1642delG	V548fsX562	Small deletion → frameshift	
1844C>T	S615F	Missense	
1912C>T	Q638X	Nonsense	
1948delA	V650fsX655	Small deletion → frameshift	
1951C>T	R651X	Nonsense	
1960A>C	K654Q	Missense	
2076_2077delAA	C693fsX741	Small deletion → frameshift	
2088insA	K696fsX742	Small insertion → frameshift	
2095C>T	Q699X	Nonsense	
2146-1G>C (IVS10 acceptor site)	N/A	Aberrant splicing	
2176C>T	Q726X	Missense	
2203C>T	R735X	Missense	
2386T>C	C796R	Missense	
2393_2401delCATTGAACA	N798fsX879	Small deletion → frameshift	
2424insA	E809fsX826	Small insertion → frameshift	
2489+1G>A (IVS12 donor site)	N/A	Aberrant splicing, retention 56bp of intron12 or skipping exon 12	
2490-1G>C (IVS12 acceptor site)	N/A	Aberrant splicing, retention 146bp of intron 12 or part skipping exon 13	
2509delA	V837fsX930	Small deletion → frameshift	

Nucleotide alteration	Amino Acid alteration	Type of mutation	References /No. probands
145_148delCAGA*	S50fsX110	Small deletion → frameshift	Syrris[41]/100
C419T*	S140F	Missense	
C1237T	R413X	Nonsense	
1597_1600delATCC	P533fsX561	Small deletion → frameshift	
1755_1756insTTGACTCA	L586fsX658	Small insertion → frameshift	
1709delC	V570fsX576	Small deletion → frameshift	
C1844T*	S615F	Missense	
2146-1G>C (IVS10 acceptor site)*	N/A	Aberrant splicing	
2197_2202delCACACCinsG	A733fsX740	Indel → frameshift	
235C>T*	R79X	Nonsense	Dalal[108]/58
145_148delCAGA*	S50fsX110	Small deletion → frameshift	
C419T*	S140F	Missense	
1171-2A>G		Aberrant splicing	
1271T>C	F424S	Missense	
13688delA	N456fsX458	Small deletion → frameshift	
1613G>A	W538X	Nonsense	
1642delG*	V548fsX562	Small deletion → frameshift	
2011delC	P671fsX683	Small deletion → frameshift	
2146-1G>C (IVS10 acceptor site)*	N/A	Aberrant splicing	
2197_2202delCACACCinsG*	A733fsX740	Indel → frameshift	
2489+1G>A (IVS12 donor site)*	N/A	Aberrant splicing	
2509delA*	V837fsX930	Small deletion → frameshift	

Nucleotide alteration	Amino Acid alteration	Type of mutation	References /No. probands
76G>A	D26N	Missense	Van Tintelen[107]/96
148_151delACAG	T50fsx60	Small deletion → frameshift	
184C>A	Q62K	Missense	
235C>T*	R79X	Nonsense	
258G>T	Y86X	Nonsense	
397C>T	Q133X	Nonsense	
1211_1212insT	V406fsX409	Small insertion → frameshift	
1848C>A	Y616X	Nonsense	
2028G>A	W676X	Nonsense	
2062T>C	S688P	Missense	
2386T>C	C796R	Missense	
2421C>A	Y807X	Nonsense	
2544G>A	W848X	Nonsense	
2489+1G>A (IVS12 donor site) *	N/A	Aberrant splicing	
C1237T*	R413X	Nonsense	Unsold[206]/1
145_148delCAGA*	S50fsX110	Small deletion → frameshift	Dalal[207]/9
1271T>C*	F424S	Missense	
1613G>A*	W538X	Nonsense	
1642delG*	V548fsX562	Small deletion → frameshift	
2011delC*	P671fsX683	Small deletion → frameshift	
2146-1G>C (IVS10 acceptor site) *	N/A	Aberrant splicing	
2489+1G>A (IVS12 donor site) *	N/A	Aberrant splicing	
2509delA*	V837fsX930	Small deletion → frameshift	

Nucleotide alteration	Amino Acid alteration	Type of mutation	References /No. probands
2196ins28bp	A733fsX740	Large insertion → frameshift	Kannankeril[111]/1
	V587I	Missense	Basso[46]/80
	N670fsX683		
	Q707X	Nonsense	
c.2484C>T/c.2484C>T*	G828G	Aberrant splicing	Awad[113]/1
1728_1729insGATG	R577fsX582	Small insertion → frameshift	Nagaoka[109]/1
971_980del10bp	G324fsX348	Small deletion → frameshift	Antoniades[110]/23
2509delA*	V837fsX930	Small deletion → frameshift	
2568del50bp	R857fsX858	Large deletion → frameshift	
176A>T	Q59L	Missense	Lahtinen[112]/29
184C>A*	Q62K	Missense	
1839C>G	N613X	Nonsense	
2421C>A*	Y807X	Nonsense	Otterspoor[208]/1
Deletion of exons 1-4 & promoter	functional null PKP-2 allele	large genomic rearrangement	Smagt[209]/82
Various mutations*	Various mutations	Seven frameshift/nonsense, three missense	Sen-Chowdhry[165]
Unique small insertions/deletions: 20/54	**37%**	**Unique splice site defects: 5/54**	**9%**
Unique Missense mutations: 13/54	**24.0%**	**Unique indels: 1/54**	**2%**
Unique Nonsense mutations: 13/54	**24.0%**	**Unique large insertion/deletions: 1/54**	**2%**
Large genomic deletion 1/54	**2.0%**		

1.8.4 Desmoglein-2 mutations in ARVC

Desmoglein-2 is expressed in many tissue including the myocardium[210]. DSG-2 is a type I integral membrane glycoprotein participating in Ca^{2+}-dependent cell-cell adhesion at desmosomal junctions, it is composed of a small signal domain (S) and a preprotein (P) domain followed by four highly conserved extracellular subdomains (EC1-EC4), a variable extracellular anchor (EA) domain, a single transmembrane domain(TM), and an intracellular anchor domain (IA). The DSG-2 cytoplasmic subdomains are composed of an intracellular cadherin-typical segment (ICS) a linker domain (LD) a repeat unit domain (RUD) containing six repeats and a terminal domain (TD). DSG-2 mediates calcium-dependent intercellular adhesion and in cardiac tissue it interacts laterally and transcellularly with desmocollin-2.

Following the discovery of plakophilin-2 mutations in ARVC, rapid progress during 2006-2007 resulted in the identification of DSG-2 mutations that were causative for autosomal dominant ARVC. Four separate reports[46,100,101,104] identified twenty-one (Table 1.6) unique mutations in DSG-2. These mutations are listed in chronological order in Table 1.6. The vast majority (67%) of these DSG-2 mutations are missense mutation that disrupts highly conserved amino acid residues involved in various functional domains of DSG-2. Some of these missense substitutions (p.R45Q & p.R48H) disrupt the Furin-recognition motif (RXXR) that is involved in cleavage (by subtilisin-like proprotein convertase) of inactive DSG-2 propeptide to mature active DSG-2 protein. Other missense amino acid substitutions (p.V56M, p.D154E, p.V1588G, p.Y87C, p.G100R, p.N266S, p.K294E, p.E331K, & p.V392I) appear to disrupt EC1, EC2, EC3, and EC4 domains. Small insertions/deletions comprise 19% of all DSG-2 mutations that can lead to a variety of outcomes resulting in frameshift, abnormal splicing, and a nonsense mutation (Table 1.6). Nonsense mutations comprise about 9% of DSG-2 mutations, some nonsense mutations (p.Q558X, p.Q591X) appear to truncate DSG-2 with loss of transmembrane and cytoplasmic sites (ICS) where binding sites for plakoglobin and plakophilin-2 are located. So far only one splice site mutation in DSG-2 has been reported in ARVC, this causes activation of an alternative cryptic splicing in exon 13 resulting in an aberrant mRNA lacking 38 bases of exon 13 that truncated DSG-2 protein to 646 amino acids[104].

Table 1.6 Desmoglein-2 in ARVC

Data was derived from genetic screening of various cohorts. * = mutations seen in previous studies or previously described.

Nucleotide alteration	Amino Acid alteration	Type of mutation	References /No. probands
260A>G	Y87C	Missense	Pilichou[104]/80
298G>C	G100R	Missense	
797A>G	N266S	Missense	
877A>G	K294E	Missense	
991G>A	E331K	Missense	
1881-2A>G	X646	Aberrant splicing in acceptor site of intron 12 activating alternative splicing in exon 13, 38bp downstream → frameshift	
1672C>T	Q588X	Nonsense	
1253_1257insATGA	E418fsX419	Small insertion → frameshift	
2036delG	G678fsX681	Small deletion → frameshift	
134G>A	R46Q	Missense	Awad[100]/33
143G>A	R49H	Missense	
915 G>A	W306X	Nonsense	
1517G>A	C507Y	Missense	
2431G>T	G812C	Missense	
298G>C*	G100R	Missense	Basso[46]/21
1253_1257insATGA*	E418fsX419	Small insertion → frameshift	
	Q558X	Nonsense	
3G>C	M1(start codon affected)	Start codon mutation→ abolishing translation?	Syrris[101]/86
165G>A	V56M	Missense	
473T>G	V158G	Missense	
829_840delCTTGAAGGGATG	227_280delLEGM	Small deletion → Abnormal splicing	
1174G>A	V392I	Missense	
1773_1774delTG	C591fsX591	Small deletion → frameshift with	
2759T>G	V920G	Missense	
Various mutations*	Various mutations	Nine frameshift/nonsense and one missense	Sen-Chowdhry[165]
missense 14/21 = 67%	**splice sites 1/21 = 5%**	**small inserts/deletions 4/21 = 19%**	**nonsense 2/21 = 9%**

1.8.5 Desmocollin-2 mutations in ARVC

Desmocollins are type I membrane glycoproteins mediating Ca^{2+}-dependent cell-cell adhesion at desmosomal junctions. Three desmocollin isoforms (DSC1-3) exists that are encoded by separate genes clustered on chromosome 18 in humans. Desmocollin-2 is ubiquitously expressed in tissues forming desmosomes and it appears to be the only isoform expressed in cardiac tissue[211]. Similar to Desmoglein-2 protein domain structure, desmocollin-2 is composed of a signal domain (S), a preprotein (P) domain followed by four highly conserved extracellular subdomains (EC1-EC4) and an extracellular anchor domain (EA) at its amino terminus. This is followed by a single transmembrane domain (TM) and a cytoplasmic tail at its carboxy terminus which consists of an intracellular anchor domain (IA) and an intracellular cadherin specific domain (ICS) that is present in desmocollin-2a isoform (long form of protein), but not in the desmocollin-2b (short form of protein) isoform.

Three independent studies have examined DSC-2 mutations in ARVC. In the first study, seventy-seven Caucasian ARVC probands not carrying gene mutations in desmoplakin, plakoglobin, plakophilin-2, or desmoglein-2 showed four affected individuals with two heterozygous frameshift DSC-2 gene mutations, c.1430del_C and c.2687_2688ins_GA (Table 1.7), resulting in DSC-2 protein truncations p.M477fsX480 and p.E896fsX900 respectively; with mutation carriers showing incomplete ARVC penetrance[102]. Mutation p.M477fsX480 is located in the fourth extracellular cadherin repeat unit (EC4) of desmocollin-2 and this mutation would be pathogenic as it truncates desmocollin-2 with the loss of transmembrane and cytoplasmic domains. The p.E896fsX900 mutation truncates desmocollin-2 protein in the ICS domain, which displays a high degree of sequence homology with desmosomal and non-desmosomal cadherins where a putative binding site for plakoglobin is located. How precisely these desmocollin-2 mutations might disrupt desmosome function remains speculative, but this may involve either NMD causing haploinsufficiency, or if NMD mechanisms are escaped then incorporation of truncated desmocollin proteins may cause dominant negative effects. A second study examined eighty-eight Caucasian probands for mutations in desmoglein-2 and desmocollin-2 genes. A single heterozygous mutation disrupting a highly conserved

3' splice-acceptor site in intron 5 (c.613-2A>G) of the DSC2 gene (Table 1.7) caused cryptic splicing resulting in skipping of the first 25 base pairs of exon 6 resulting in a frameshift and PTC after insertion of ten novel amino acid residues[103]. In a third study, a cohort of fifty-four Italian ARVC patients who were negative for mutations in DP, PKP-2, DSG-2, and TGFβ were examined by dHPLC and DNA sequencing analysis of the DSC-2 gene[99]. Two heterozygous mutations were found c.304G>A and c.1034T>C (Table 1.7) resulting in missense amino acid substitutions (p.E102K located in propeptide domain and p.I1345T located in the EC2 domain respectively). Both amino acid substitutions altered the physicochemical properties compared to the wild type amino acid residue found. *In vitro* expression studies of p.E102K and p.I1345T DSC-2 proteins in rat neonatal cardiomyocytes and HL1 cells showed that these two N-terminal missense DSC-2 mutant proteins affected the normal localisation of desmocollin-2 at the cell-cell junction.

Table 1.7 Desmocollin-2 mutations in ARVC

Found by the genetic screening of various cohorts. Two-hundred and nineteen probands in three independent studies were examined between these studies. Desmocollin-2 mutations appear to contribute a very small percentage of mutations in ARVC compared to all other gene mutations encoding other desmosomal proteins. * = Mutations previously described.

Nucleotide alteration	Amino Acid alteration	Type of mutation	References /No. probands
1430del_C	M477fsX480	Small deletion → frameshift	Syriss[102]/77
2687_2688ins_GA	E896fsX900	Small insertion→ frameshift	
613-2A>G	M211fsX221	Aberrant splicing resulting from splice-acceptor site intron 5 mutation that activates alternative cryptic splice causing skipping of first 25 bases of exon6 resulting in a frameshift and PTC after insertion of ten novel amino acids	Heuser[103]/88
304G>A	E102K	Missense	Beffagna[99]/54
1034T>C	I345T	Missense	
Two mutations*	Two mutations	One frameshift and one missense mutation	Sen-Chowdhry

1.9 Experimental Aims

A literature review at the beginning of the year 2004 on ARVC genetic studies showed that linkage analysis approach was used in identifying loci associated with ARVC; this resulted in the identification of three gene mutations by positional cloning responsible for ARVC2, ARVC4 and a recessive form of ARVC (Naxos disease) with manifestations of palmoplantar keratoderma and woolly hair. Two of genes involved, DP in ARVC4 and PG in Naxos disease were desmosomal constituents, whereas RyR2, a non-desmosomal component (cardiac sarcoplasmic reticulum calcium release channel) involved in regulating the intracellular Ca^{2+} levels was the gene involved in ARVC2. This led to a hypothesis that mutations in genes encoding other cell-cell adhesion proteins may be associated with ARVC. This formed the basis for carrying out the genetic screening work in Chapter 3.

The aim of the first part of the genetic screening work (Chapter 3, part 1) was to examine a cohort of one-hundred ARVC patients. Peripheral blood samples obtained from these patients were extracted to obtain genomic DNA. Template DNA was used for exon specific PCR amplification from the genes encoding for plakoglobin, desmoplakin, and plakophilin-2, followed by bidirectional DNA sequencing analysis. This approach identified mutations covering the entire coding and exon flanking regions in each of the three genes examined. The aim in the second part of the genetic screening work (Chapter 3, part 2) was to examine mutations identified in individual probands to determine the inheritance of the genetic defect in family members. In these family studies, genetic screening was performed by DNA sequencing, this allowed identification of family members of the probands inheriting a known genetic defect; and evaluations were performed applying both Task Force and modified ARVC criteria to determine clinical expression of the disease in family members. These pedigree studies provided supporting evidence for pathogenicity of sequence changes identified at the DNA level.

In the following three parts of this thesis (Chapters 4 to 6), the aims were to examine the *in vitro* functional effects of expression of three separate mutations found. Two separate plakophilin-2 gene mutations were analysed by functional studies (Chapters 4-5) involving mutations resulting in truncated and missense PKP-2 proteins respectively. A desmoplakin mutation was also analysed by functional studies

(Chapter 6) this involved a mutation resulting in truncated DP polypeptide. All three gene mutations identified in the genetic screening analysis were likely to be pathogenic as they associated with ARVC disease in family studies (Chapter 3, section 3.5.4 Parts 2.1, 2.5. and 2.7 respectively). Functional studies were performed to determine the consequence of expression of these mutant proteins *in vitro*, this was done using a cell line derivative of the HEK 293 lineage that is widely used to study the expression of both soluble and membrane bound proteins. This cell line was selected for expression studies of plakophilin-2 and desmoplakin full-length or their truncated and missense protein variants because of the high level of transfection of the cell line with vectors used. This resulted in a high level of expression and appropriate processing of these proteins for membrane targeting in HEK 293 cell system.

In Chapter 4, a mutation found causing an insertion/deletion within exon 11 of the plakophilin-2 gene resulted in a truncated protein (A733fsX740 PKP2, nucleotide change 2197_2202delCACACCinsG) and the expression of this protein was examined by functional studies in Flp-In T-Rex HEK293 stable cell lines to determine the effect of expression of this truncated plakophilin *in vitro*. Cloning of DNA encoding full-length and the truncated plakophilin-2 were performed in pcDNA4 and pcDNA5 plasmid vectors. These plasmids allowed expression of full-length and truncated PKP-2 proteins in cell culture experiments. Using pcDNA5 plasmid transfection, stable cell lines were established in Flp-In T-Rex HEK293 that expressed full-length and the truncated plakophilin proteins. Using induced cell lines expressing these plakophilin-2 proteins, the cellular proliferation, initial cell adherence and spreading, cell-cell adhesion assay and mechanical stretch was examined. The cellular localization and expression of plakophilin-2 and of connexin-43 proteins was examined in stable cells as remodelling of the later has been postulated to play a possible role in arrhythmogenesis in ARVC. Furthermore, the cell-cell electrical coupling in cell lines expressing full-length or truncated plakophilin-2 proteins was examined by electrophysiology to assess the measured cell input resistances, a measure of how well connected these cells are electrically. Non-transfected cell line and stable cells expressing full-length or truncated plakophilin-2 were analyzed by transmission electron microscopy to determine the effect on the formation of desmosomes *in vitro*. Using pcDNA4 plasmid transfection experiments in HEK 293T cells the interactions of truncated plakophilin-2 with desmosomal and adherens junction proteins was examined by immunoprecipitation.

In Chapter 5, a missense mutation causing a single serine to phenylalanine amino acid substitution in plakophilin-2 (S140F PKP-2, nucleotide change C419T) was encoded into cDNA that were cloned into pcDNA5 and pcDNA4 plasmid vectors. These plasmid vectors allowed expression of full-length and missense PKP-2 proteins in cell culture experiments. Stable cell line expressing S140F PKP-2 was established in Flp-In T-Rex HEK 293 cells using pcDNA5 plasmid transfection. Using induced stable cell line expressing missense and full-length PKP-2 proteins the cellular proliferation, initial cell adherence and spreading, cell-cell adhesion, and cellular mechanical stretch was examined. The cellular expression and cellular localization of missense plakophilin-2 and Cx-43 was examined in stable cell line to assess the localisation of Cx-43 protein to cell plaques. Non-transfected cell line and stable cells expressing either full-length or missense plakophilin-2 were analyzed by transmission electron microscopy to determine the effect on the formation of desmosomes *in vitro*. Using pcDNA4 plasmid transiently transfected in HEK 293T cells the interactions of missense plakophilin-2 with desmosomal and adherens junction proteins was examined by immunoprecipitation.

In Chapter 6, a heterozygous insertion of a single Adenosine nucleotide residue in exon 7 of desmoplakin (Q273fsX288 DP, nucleotide change 818_819_insA) resulted in truncation of desmoplakin to a polypeptide of 287 amino acids in length. A cDNA encoding the above insertion sequence and of a full-length desmoplakin control sequence were each cloned into pcDNA5 vector. Plasmid vectors encoding these sequences allowed expression of full-length or truncated DP proteins in cell culture experiments. Stable cell lines expressing full-length or truncated DP were established in Flp-In T-Rex HEK293 cells using pcDNA5 plasmids transfection. Using induced stable cell line expressing full-length or truncated DP proteins the cellular proliferation, monolayer cell-cell adhesion, and cellular mechanical stretch response to apoptosis was examined in these cell lines. The co-localization of truncated or full-length DP with either PKP-2 or PG at cell-cell junctions was examined by immunofluorescence in cell lines stably expressing full-length or truncated DP proteins. The Vimentin intermediate filament network was examined by immunofluorescence staining of stable cells expressing full-length or truncated DP proteins. Using stable cell lines the interaction of full-length or truncated DP with plakophilin-2 or plakoglobin proteins were examined by immunoprecipitation.

Chapter 2 –Materials and methods

2.1 Genetic analysis of an ARVC cohort

Blood samples were obtained from one hundred index ARVC patients (probands) who were diagnosed by Task Force criteria at the London Heart Hospital, in collaboration with Professor William McKenna and a consultant led clinical team after approval by the local ethics committee in University College London Hospital and obtaining informed patient consent. For Pedigree analysis, further blood samples were obtained with consent, from family members of the affected probands and both Task Force and modified criteria were applied in clinical assessments of these individuals.

2.1.1 DNA extraction from whole blood samples

QIAamp Mini Kit (QIAGEN) was used to extract DNA from EDTA preserved human blood samples. Archived blood samples were thawed to room temperature prior to DNA extraction. Protease enzyme supplied was added (20µl, 15µg/µl) to 1.5 ml Eppendorf micro-centrifuge tubes. Blood sample (200µl) was added followed by 200µl AL lysis buffer to each micro centrifuge tube and pulse-vortexing followed by incubation at 56°C for 10 minutes. Following the incubation and a brief centrifugation of the tubes, 200µl absolute ethanol was added to the samples. Samples were pulse-vortexed and the mixture was transferred to spin columns assembled in 2ml collection tubes. These were spun at 8000rpm for 1 minute. The filtrate was discarded and the spin column assembled in a new 2 ml collection tube. 500µl of AW1 buffer was added to the spin column followed by centrifugation at 8000 rpm for 1 minute. The filtrate was discarded and the spin column was placed in a clean 1.5ml Eppendorf tube. Sterile water 200µl was placed in the spin tube and after standing for 1 minute, the DNA was eluted by centrifugation at 8000 rpm for one minute. This procedure typically yielded 6µg of pure genomic DNA from 200µl of blood DNA samples were stored at 4°C.

2.1.2 Polymerase chain reaction

All PCR reactions were performed in the Gene Amp PCR System 9700 (Applied Biosystems) using Thermo-Fast 96-well (ABgene) plates. Optimum primer annealing

temperature and the number of cycles employed for PCR amplification varied with PCR fragments amplified. These were determined separately in experiments to work out the best conditions to achieve a high specificity of the PCR reaction. Individual exons for sequencing were <600bp and were obtained by PCR using AmpliTaq Gold polymerase (Applied Biosystems, UK), otherwise EXL DNA polymerase (Stratagene, UK) and AccuTaq LA (Sigma Aldrich, UK) polymerases were used for PCR of amplimers between 1000bp – 9,000bp in length. These enzymes were especially formulated for amplification of cloned DNA targets up to 48kb with a low error rate of mis-incorporated nucleotides (<1bp change per 10,000bp amplified product).

AmpliTaq Gold PCR

AmpliTaq PCR reaction was set up as follows:

2.5 µl	10x PCR buffer containing 1.5mM $MgCl_2$ (Applied Biosystems)
50-100 ng	Template DNA
1.0 µl	Forward primer* (10 picomoles, Invitrogen)
1.0 µl	Reverse primer* (10 picomoles, Invitrogen)
1.0 µl	dNTP mix, (2.5mM each dATP, dGTP, dCTP and dTTP (Invitrogen)
1.0 µl	25mM $MgCl_2$ (Applied Biosystems), omitted where appropriate
0.1 µl	AmpliTaq Gold DNA polymerase (Applied Biosystems, 0.5Units)

PCR grade H_2O was added to a final volume of 25µl. The following PCR program was used:

Segment	**Cycles**	**Temperature**	**Time**
1		96°C	10 minutes
2	X35-40	96°C	30 seconds
		45 - 68°C (as appropriate)	30 seconds
		72°C	1 minute
3		72°C	7 minutes
4		4°C	hold/∞

* Primer sequences are listed in Chapters 4-6.

EXL Polymerase PCR

EXL PCR was assembled as follows

5.0 µl	10x EXL buffer (Stratagene)
2.5 µl	dNTP mix, (10mM each dATP, dGTP, dCTP and dTTP, Invitrogen)
2.0 µl	Forward primer* (100ng/µl, Invitrogen)
2.0 µl	Reverse primer* (100µl ng/, Invitrogen)
0.5 µl	DMSO (Stratagene)
1.0 µl	Stabilising Solution (Stratagene)
15-60 ng	Vector template DNA (non-linearized)
1.0 µl	EXL DNA polymerase (Stratagene, 5 Units/µl)

PCR grade H_2O was added to a final volume of 50µl. The following PCR program was used:

Segment	Cycles	Temperature	Time
1		92°C	2 minutes
2	X10	92°C	20 seconds
		55°C	45 seconds
		68°C	x min, variable (1min/kbp length)
3	X15	92°C	20 seconds
		55°C	45 seconds
		68°C	x min + 10 seconds additional /cycle
4		68°C	20 minutes
5		4°C	hold /∞

* Primer sequences are listed in Chapters 4-6.

AmpliTaq LA (Long & Accurate) polymerase PCR

AmpliTaq LA PCR was assembled as follows:

5.0 µl	10x AccuTaq LA buffer (Sigma Aldrich)
2.5 µl	dNTP mix, (10mM each dATP, dGTP, dCTP and dTTP, Invitrogen)
1.0 µl	Forward primer* (100ng/µl, Invitrogen)
1.0 µl	Reverse primer* (100µl ng/, Invitrogen)
1.0 µl	DMSO (Sigma Aldrich)

5-50 ng	Vector DNA templates (non-linearized)
0.5 µl	AccuTaq LA DNA polymerase (Sigma Aldrich, 0.05 Units/µl)

PCR grade H_2O was added to a final volume of 50µl. The following PCR program was used:

Segment	Cycles	Temperature	Time
1		98°C	1 minute
2	X15	94°C	20 seconds
		55°C	45 seconds
		68°C	x min, variable (1min/kbp length)
3	X15	94°C	20 seconds
		55°C	45 seconds
		68°C	x min + 15 seconds additional /cycle
4		68°C	10 minutes
5		4°C	hold /∞

* Primer sequences are listed in Chapters 4-6.

GC-rich PCR

GC-rich PCR system (Roche) was used for amplifying genomic targets from a region of high G-C content and the PCR reaction was assembled as follows:

5.0 µl	GC-rich 10x PCR buffer with DMSO (Roche)
1.0 µl	dNTP mix, (2.5mM each dATP, dGTP, dCTP and dTTP, Invitrogen)
10 pmoles	Forward primer* (Invitrogen)
10 pmoles	Reverse primer* (Invitrogen)
2.5 µl	GC-rich resolution solution (Roche)
0.5 ul	GC-rich system enzyme mixture (2 Units/µl, Roche)
75 ng	Genomic DNA template

PCR grade H_2O was added to a final volume of 25µl. The following PCR program was used:

Segment	Cycles	Temperature	Time
1		95°C	3 minutes
2	X35	95°C	30 seconds
		60 – 68°C (as appropriate)	30 seconds
		72°C	45 seconds

3	72°C	7 minutes
4	4°C	hold/∞

* Primer sequences are listed in Chapters 4-6.

2.1.3 Restriction enzyme digests, agarose gel electrophoresis and gel DNA extraction

Plasmids obtained in cloning reactions or from SDM, were characterised by analytical scale restriction endonuclease digest. This involved either single or double-digest of super-coiled plasmid DNA with appropriate restriction enzymes. Restriction fragment-length analysis was performed in 2% (500-1000bp) or 0.8% (500-10,000bp) agarose gel electrophoresis allowing screening of large number of plasmid clones to verify positive clones containing the expected insert DNA sequence. Single or double restriction enzyme digests were performed using manufacturer's recommended protocol (Fermentas UK, New England Biolabs, Invitrogen UK,) employing appropriate buffer systems optimized for double-digest reactions. One enzyme unit of restriction enzyme in a total volume of ten microliters in x1 restriction enzyme buffer was used with a maximum amount of plasmid DNA in the digest not exceeding one microgram. Restriction digests were incubated for a minimum of four hours at 37°C or overnight at the same temperature.

For agarose gel electrophoresis of PCR and digests, liquefied gel solution was mixed with ethidium bromide (2.5μg/ml) prior to casting the gel. Loading dye containing bromophenol blue and orange G (x6 concentration, Fermentas) was diluted into PCR product or digest to x1 final concentration and samples were loaded into wells of a gel immersed in x1 TBE running buffer. The gel was electrophoresed in x1 TBE buffer at 150V until sufficient migration and resolution was achieved. Reference DNA size markers (10kb DNA ladder, Fermentas, UK) were loaded alongside to allow verification of the expected size specificity of samples analyzed. A permanent photographic record of the gel was obtained under ultraviolet light transillumination using a BioRad gel imaging system (Gel documentation system, BioRad, UK).
Specific PCR DNA band was excised from agarose gel exposed under preparative ultraviolet transillumination using a sterile scalpel blade. The gel sample containing

DNA band was weighed prior to performing a DNA gel extraction using the QIAquick gel extraction kit (Qiagen, UK). In a 1.5 ml Eppendorf tube for every 100 mg of agarose gel slice, 0.3 ml of QG was added and solubilisation of the gel in this buffer was achieved by incubation at 50°C for 10-15 minutes until the entire gel sample was completely dissolved (aided by periodic pulse-vortexing during the incubation) in this buffer. The mixture was transferred into a spin column assembled on top of a collection tube. The spin column was centrifuged at room temperature at 13,200 rpm for 1 minute and the flow-through was discarded. The spin column was assembled on the collection tube and 0.75 ml wash buffer PE was added followed by centrifugation at 13,200 rpm for 1 minute. The flow-through was discarded and the spin column was centrifuged again at 13,200 rpm for 1 minute to remove traces of ethanol residue. Finally, the spin column was assembled on a new sterile 1.5 ml Eppendorf tube and 50 µl of EB elution buffer was added, incubated at room temperature for 1 minute prior to centrifugation at 13,200 rpm for 1 minute to obtain the purified DNA fragment. Gel purified DNA sample was stored at –20°C.

2.1.4 DNA sequencing and data analysis

Removal of unincorporated nucleotides, primers, buffer, and enzyme from the PCR reaction was performed prior to bi-directional sequencing using the forward and reverse primer respectively.

2.1.4.1 Purification of PCR products

GFX-96 (96-well plate) purification

A GFX-96 plate purification system was used to purify simultaneously ninety-six PCR products according to the suggested manufacturer's protocol (GE Healthcare, UK). A GFX plate was assembled on top of a 96-well wash plate and 0.3 ml of binding buffer was added to each well. PCR reaction products were checked on an agarose gel and the remaining samples were transferred and mixed with binding buffer into individual wells of the GFX-96 plate. The plate was centrifuged at room temperature at 1800 rpm for 2 minutes and the flow-through was discarded. The GFX plate was re-assembled on a 96-well wash plate and ethanol containing wash buffer

(0.4 ml) was added to each well. The plate was centrifuged at 1800 rpm for exactly 5 minutes. The flow-through was discarded and the wash plate re-assembled on the 96-well wash plate. Following centrifugation at 1800 rpm for 1 minute to remove traces of residual ethanol, the GFX-96 plate was assembled on a 96-well collection plate and 20 µl of PCR grade water was added to each well. Following incubation of the plate for 1 minute at room temperature, it was centrifuged at 1800 rpm for 2 minutes. The purified PCR products in the collection plate were sealed with a clear plastic adhesive sheet to prevent sample evaporation Purified PCR products were stored at 4°C (short-term) or at –20°C (long-term).

Individual PCR purification

When small numbers of individual PCR products were purified, this was done using the QIAquick PCR (Qiagen, UK) purification kit according to manufacturer's protocol. Five times the volume of PB binding buffer was added to one volume of each PCR sample. The QIAquick spin column was assembled on a 2 ml collection tube and the sample mixture was transferred into the spin column and centrifuged at 13,200 rpm for one minute. The flow-through was discarded and the spin column was re-assembled on the collection tube. Wash buffer PE (0.75 ml) was added to the column and centrifugation was carried out at 13,200 rpm for another 1 minute and the flow through was discarded. Residual ethanol from the wash buffer in the column was removed after a final centrifugation at 13,200 rpm for 1 minute. Finally, the spin column was placed on clean 1.5 ml Eppendorf tube and 20 µl EB elution buffer was added and incubated at room temperature for one minute prior to centrifugation at 13,200 rpm for 1 minute. Purified PCR products were stored at 4°C.

2.1.4.2 PCR reaction for cycle sequencing

The BigDye Terminator v3.1 cycle sequencing kit (Applied Biosystems) was used according to the manufacturer's protocol. Briefly, for each DNA sample to be sequenced the following were added:

1.0 µl	Either forward* sequencing or reverse* sequencing primer (3ng/µl)
1.0 µl	BigDye Terminator cycle sequencing mixture
1-5µl	200 – 600 ng Purified PCR or plasmid DNA template

PCR grade H_2O was added to a final volume of 10µl. The following PCR program was used:

Segment	Cycles	Temperature	Time
1		96°C	2 minutes
2	X25	96°C	10 seconds
		50°C	5 seconds
		60°C	4 minutes
3		4°C	hold/∞

* Primer sequences are listed in Chapters 4-6.

2.1.4.3 Cycle sequencing reaction clean up and automated DNA sequencing

The DyeEx 96 kit (Qiagen, UK) was used according to the manufacturer's suggested protocol to remove unincorporated fluorescently labelled deoxynucleotides prior to DNA sequencing. A DyeEx 96 plate placed on a 96-well collection plate was centrifuged at room temperature for 3 minutes at 2600 rpm. The flow-through was discarded and the DyeEx 96 plate was placed on top of a Thermo-Fast 96-well plate (ABgene). Each sequencing reaction (10 µl) was carefully transferred into the centre of the resin of each well of the DyeEx 96 plate followed by centrifugation at 2600 rpm for 3 minutes. DyeEx purified samples collected in the Thermo-Fast 96-well plate were dried down at 70°C for 45 minutes in a thermal cycler block. Formamide (12 µl/well, Applied Biosystems) was added to each sample well and the plate was then sealed with an adhesive clear plastic sheet, briefly vortexed to mix and denatured at 96°C for 5 minutes followed by rapid cooling to 4°C on a thermal cycler block. DNA sequencing was performed in an automated sequencer (ABI 3130XL Genetic Analyzer) using DT3100POP6BDv3v1.mob, RapidSeq36_POP6DefaultModule, and BC3100POP6RR_SeqOffFtOff.saz as mobility, run, and analysis modules respectively. Sequencing data aligned with a synthetic trace generated from a reference file was analyzed by Seqscape program (Applied Biosystems, UK). Mutations were confirmed by bi-directional sequencing using forward and reverse primers complimentary to the fragment being analysed.

2.2 Cloning PCR amplified fragments

PCR amplified fragments were cloned into the following vectors:

pcDNA5/FRT/TO/TOPO/TA (Invitrogen)

pcDNA4/XPress/TOPO/TA (Invitrogen)

For cloning of PCR amplimer into plasmid vectors, the amplimers were either gel-purified or unpurified. The vector and PCR fragments were mixed in varying molar ratios ranging from 1:1 to 1:4 (vector:amplimer) and ligation was achieved by a vector mediated catalysis.

2.2.1 Cloning in pcDNA5/FRT/TO/TOPO/TA

The cloning in pcDNA5/FRT/TO/TOPO/TA (kit from Invitrogen, UK) was mediated by topoisomerase enzyme covalently associated with the vector at the cloning sites ("activated" vector) in which the energy conserved in phospho-tyrosyl bond between the DNA and the tyrosyl residue (Tyr274) of the topoisomerase drives the ligation of a PCR product. The EXL or AccuTaq derived PCR product contained 3' Adenosine residue overhangs on complementary DNA strands allowing annealing and ligation to the linearized vector containing complementary T residue overhangs at the cloning site. PCR product anneals in two possible orientations in either the sense orientation or anti-sense incorrect orientation. Cloning in plasmid pcDNA5/FRT/TO/TOPO/TA was performed according to manufacturer's recommended protocol:

1-4 µl Gel purified or unpurified PCR (molar ratio range: 1:1 to 1:4 (vector: insert)

1.0 µl Salt solution (Invitrogen, UK)

Sterile water was added to make the final volume to 5 µl, and then TOPO vector was added.

1.0 µl pcDNA5/FRT/TO/TOPO/TA (10ng, Invitrogen, UK)

The reaction was incubated at room temperature (22-23°C) for 5 minutes to 1 hour dependent on the size of the PCR amplimer cloned. Two microliters of the cloning reaction was transformed in TOP10 E *coli* cells (section 2.2.3) and single clones were selected and screened for correct orientation of the insert in the plasmid (section 2.2.4).

2.2.2 Cloning in pcDNA4/XPress/TOPO/TA

EXL PCR products encoding full-length PKP2, S140F PKP2, and A733fsX740 PKP-2 DNA were amplified using XPress primers using +2301A pcDNA5, S140F pcDNA5, and A733fsX740 pcDNA5 plasmid template DNA in separate reactions to obtain respective amplimers that were cloned into pcDNA4/XPress/TOPO/TA as follows:

1-4 µl Gel purified or unpurified PCR (molar ratio range: 1:1 to 1:4 vector: insert)

1.0 µl Salt solution

Sterile water was added to a final volume to 5 µl, and then TOPO vector was added

1.0 µl pCDNA4/XPress/TOPO/TA (10ng, Invitrogen)

The reaction was incubated at room temperature (22-23°C) for 1 hour. Two microliters of the cloning reaction was transformed into TOP10 cells (section 2.2.3) and single clones were selected and screened for correct orientation of the insert in the plasmid (section 2.2.4).

2.2.3 Transformation of cloned plasmids into competent TOP10 cells

Chemically competent TOP10 E *coli* cells (Invitrogen, 50 µl aliquots) were thawed from –80°C on ice for 10 minutes. Cloning reactions (5 µl reaction volume) from pcDNA5 or pcDNA4 was added to the competent cells. The transformation reaction mixture was mixed gently with the chemically competent cells. After 30 minutes incubation on ice, the cells were heat-shocked at 42°C for 30 seconds and transferred onto ice for two minutes. Sterile LB broth (1 ml) was added to the transformation reaction and this was left in a shaking incubator at 37°C for 1 hr. The bacterial cells were centrifuged at 10,000 rpm for 1 min and pellet was re-suspended in 150 µl of sterile LB before plating onto LB agar plates containing the appropriate selecting antibiotic (ampicillin 100µg/ml or kanamycin 50µg/ml. The plates were incubated overnight at 37°C. Single bacterial colonies were picked with a sterile 10 µl pipette tip and inoculated into 5 ml of LB broth containing the appropriate antibiotic and incubated in a shaker overnight at 37°C prior to performing a mini-plasmid DNA preparation (section 2.4.1). Plasmid obtained from mini-plasmid preparation was

checked for the presence of recombinant plasmid containing the cloned PCR fragment (section 2.24). For midi-plasmid DNA preparation, a single TOP10 bacterial clone, previously characterised, was cultured in 0.5 ml of SOC medium (Invitrogen, UK) for one hour and then plated on an LB agar plate containing the appropriate antibiotic and incubated overnight at 37°C. A sterile inoculation loop was used to streak across the plate to transfer an inoculum of this sample into a 0.5 litre bottle containing 250 ml of LB broth with the appropriate antibiotic followed by incubation overnight in a shaker at 37°C. The culture supernatant was processed for midi-plasmid preparation as described in the second paragraph of section 2.4.2.

2.2.4 Checking plasmids obtained in cloning reactions

Recombinant plasmid (1 μl) was digested with appropriate restriction endonuclease enzyme as described in section 2.1.3. This allows identification of recombinant plasmids containing the cloned PCR. Direct sequencing using BigDye terminator, sequencing primer, and 600 ng of plasmid DNA was performed to further confirm the orientation of the PCR fragment in the recombinant plasmid following the procedures described in sections 2.1.4.2 and 2.1.4.3.

2.3 PCR mediated site-directed mutagenesis

PCR mediated SDM was used to create specific change in a triplet codon to obtain a desired amino acid substitution. SDM allowed a single nucleotide substitution to be introduced into plasmid vector encoding a full-length normal protein sequence with missense mutation expression. Truncation mutations arising from insertion/deletion of specific nucleotide residues were similarly achieved by SDM using primers spanning the mutation site that allowed the insertion or deletion nucleotide residues to 'hairpin loop out' when annealed to full-length normal nucleotide sequence encoded on a plasmid vector. The Quick Change II SDM kit (Stratagene, UK) was used to generate mutant plasmid of interest from a large double-stranded plasmid.

Three steps were required to obtain the plasmid with a mutated cDNA of interest:

1. Thermal cycling was performed to denature super-coiled plasmid DNA template, annealing of specific mutagenic primers, and extension of PCR product using Pfu Ultra high fidelity DNA polymerase.
2. Addition of Dpn I restriction endonuclease digested the parental methylated and hemi-methylated plasmid double stranded DNA resulting in parental plasmid DNA degradation.
3. Transformation of the mutant plasmid into competent E *coli* cells for nick repair and amplification.

SDM PCR reaction was assembled as follows:

5.0 µl	10x Pfu Ultra HF reaction buffer
10 ng	double stranded plasmid DNA template
125 ng	Forward primer*
125 ng	Reverse primer*
1.0 µl	dNTP mix
3.0 µl	Quick Solution (Stratagene, UK)
1.0 µl	*PfuUltra* HF DNA polymerase (2.5U/µl, Stratagene, UK)

PCR grade water was added to a final volume of 50 µl. PCR was performed under the following conditions:

Segment	Cycles	Temperature	Time
1		95°C	1 min
2	X18	95°C	50s
		60°C	50s
		68°C	1 min/kb of plasmid length
3		68°C	10 min
4		4°C	hold/∞

* Mutagenic primer sequences are listed in Chapters 4-6.

2.4 Plasmid amplification in chemically competent TOP10 cells

Plasmid generated from cloning reaction or by SDM was first cultured up in a small volume to obtain mini-plasmid (section 2.4.1) preparation. This plasmid DNA

preparation was characterised by restriction endonuclease digest (section 2.1.3) and by DNA sequencing (sections 2.1.4.2 and 2.1.4.2) to identify the orientation of the cloned DNA insert and to confirm the expected insert sequence of full-length insert sequence, or to confirm presence of a desired mutation introduced by site directed mutagenesis. The selected plasmid was transfected into TOP10 cells and a bulk preparation of the desired plasmid was obtained after purification of culture medium using a midi-plasmid (section 2.4.2) preparation.

2.4.1 Mini-plasmid DNA preparation

An individual colony of transformed E. *coli* (TOP10) bacterium picked from an antibiotic selective plate was inoculated in a 10 ml polypropylene culture tube containing 5 ml of LB broth supplemented with the appropriate antibiotic (50-100 μg/μl). The tube was shaken overnight at 37°C at 225 rpm. Culture tube was centrifuged at 3,000 rpm at 4°C for 10 minutes. The bacterial pellet was extracted using a QIAprep spin plasmid MiniPrep Kit (QIAGEN, UK) according to the manufacturer's recommended protocol. Buffer P1 (0.25 ml containing ribonuclease A 100 μg/μl) was added to each pellet and mixed by pulse-vortexing. The resuspended pellet was transferred into 1.5 ml Eppendorf centrifugation tube, 0.25 ml of P2 lysis buffer was added, and the tubes inverted gently four to six times. Neutralization buffer N3 (0.35 ml) was added and the tubes inverted gently four to six times. After centrifugation at 13200 rpm for 10 minutes at 4°C, the supernatant was carefully transferred into a spin column assembled on a 2 ml collection tube. The spin column was centrifuged at 13200 rpm for 1 min at 4°C and the flow-through was discarded. Wash buffer PB (0.5 ml) was added to the spin column and the flow-through obtained after centrifugation at 13,200 rpm for 1 minute at 4°C was discarded. Wash buffer PE (0.75 ml) reconstituted in ethanol was added to the spin column and the column was centrifuged at 13,200 rpm for 1 minute at 4°C. The flow-through was discarded and the column was centrifuged again at 13200 rpm for 1 min to remove residual ethanol. The column was placed on a sterile 1.5 ml micro-centrifuge tubes and 50 μl of EB elution buffer was added, followed by incubation for 1 minute at room temperature, and centrifugation at 13200 rpm for 1 minute to elute the plasmid mini-preparation. The absorbance at 260nm of each DNA sample was measured in a spectrophotometer

(Libra S12, Biochrom Ltd, UK) to calculate the DNA concentration in μg/ml assuming a concentration of 50μg/ml for double stranded plasmid DNA at an absorbance value of 1.0 at 260nm. DNA from plasmid mini-preparation was stored at -20°C.

2.4.2 Midi-plasmid DNA preparation

Plasmid DNA (100-1000 ng) containing cloned cDNA of interest was added to 50 μl of TOP10 chemically competent E. *coli* cells in a 1.5 ml Eppendorf micro centrifuge tube, mixed gently and incubated on ice for 30 minutes. The mixture was heat-shocked in a water bath at 42°C for 30 seconds and transferred into ice for 2 minutes followed by the addition of 0.8 ml LB or SOC (Invitrogen) medium without antibiotic and the micro-centrifuge tube was shaken in a 37°C incubator at 225 rpm for 1 hour. The entire sample was transferred into a 0.5 litre flask containing 250 ml of LB broth with the appropriate selective antibiotic (50-100 μg/μl). The culture was shaken in an incubator at 250 rpm at 37°C for 24 hrs. The content of the flask were centrifuged at 3200 rpm at 4°C for 60 minutes in several Falcon 50 ml tubes.

The pooled bacterial pellet obtained was processed using a QIAGEN midi-plasmid purification kit according to the manufacturer's recommended protocol. Bacterial pellets re-suspended in a total of 4 ml of P1 re-suspension buffer were transferred in a single 50 ml falcon tube to which lysis buffer P2 (4 ml) was added, this was gently mixed by inverting four to six times, and the lysate was incubated at room temperature for 5 minutes. Chilled neutralization buffer P3 (4 ml) was added to the lysate and mixed gently by inverting four to six times and the mixture was immediately poured in a QIAfilter cartridge (QIAGEN, UK) and incubated at room temperature for exactly 10 minutes. A QIAGEN-tip 100 column pre-assembled in a 50 ml falcon tube and was equilibrated in QBT buffer (4 ml) under gravity flow. Following a ten-minute incubation of the lysate in the QIAfilter, the cap was removed from the cartridge and with the aid of a syringe plunger; the cell lysate in the QIAfilter was filtered into the pre-equilibrated QIAGEN-tip 100. The lysate was allowed to enter the resin under gravity flow and the flow-through was discarded. The QIAGEN-tip 100 was washed twice; each time with 10 ml of QC wash buffer and the

column was allowed to empty under gravity flow with the flow-through being discarded. The QIAGEN-tip 100 was assembled on top of sterile 15 ml falcon tube and 5 ml of elution buffer QF was added to the column, which was allowed to empty under gravity flow. To the eluted plasmid DNA, isopropanol (3.5 ml) was added and after mixing this was centrifuged at 3200 rpm at 4°C for 1 hr to obtain a plasmid DNA pellet. The pellet was carefully transferred in a 1.5 ml Eppendorf micro centrifuge tube in one ml 70% ethanol followed by centrifugation at 13,200 rpm at 4°C for 15 minutes. Traces of ethanol were removed from the plasmid pellet and the pellet was air-dried at room temperature for 5-10 minutes prior to resuspension in 30-50 µl of endotoxin-free Tris/EDTA buffer. The DNA concentration was calculated using measured absorbance at 260 nm. Plasmids were stored at -20°C.

2.5 Cell culture

All cell culture media, supplements including penicillin, streptomycin, zeocin, hygromycin, and blasticidin, foetal calf serum, and trypsin/EDTA were purchased from Invitrogen, UK.

2.5.1 Human embryonic kidney HEK 293T cell culture

HEK 293T cells were cultured in Dulbecco's modified Eagle medium (DMEM) supplemented with 10% foetal calf serum, 50 U/ml penicillin, 50 U/ml streptomycin, and glutamine (4 mM). The medium supplemented as above was referred to as complete DMEM. The medium was changed every 72 hours until the cells became 80-90% confluent when they were passaged into fresh complete DMEM. Confluent culture flasks or dishes were trypsinized by addition of Trypsin/EDTA solution (0.067 ml/cm^2 area of the culture dish/flask, e.g. 5 ml/T75 or 0.12 ml/well of 24-well plate) and incubating at 37°C for two-five minutes until all the cells had detached. Complete DMEM (0.06 ml/cm^2) was added to neutralise the action of trypsin and the cells resuspended uniformly. 1/10th – 1/5th of this was transferred into a fresh culture dish/flask with appropriate amount of complete DMEM medium and the dish/flask was incubated at 37°C, 5% CO_2 in a humidified incubator. Fresh medium was added

after 72 hours until cell became 80-90% confluent, when they were sub-passaged as above.

2.5.2 Transient plasmid transfection of HEK 293T cells

HEK 293T cell line was transfected to test the transient (24 to 48 hours post-transfection) protein expression from cloned cDNA of interest in various plasmids. low passage number HEK 293T cells (P1-10) were plated in complete DMEM in various plate formats 6-well (5 x 10^5 cells/well), 24-well (3 x 10^3 cells/well) or 48 well plates (1.5 x 10^3 cells/well), P_{90} (2 x 10^6) twenty-four hours before the start of the transfection experiment. The protocol described is for the 6-well format, but can be scaled up for other plate or flask formats. Twenty-four hours after incubation of 5 x 10^6 cells in 3 ml of complete DMEM per well at 37°C in 5% CO_2, plasmid DNA sample (4 μg in endotoxin-free TE buffer) was added to 0.1 ml of incomplete DMEM in a 1.5 ml sterile Eppendorf tube. Sterile Polyfect reagent (40 μg, Qiagen) was added and pulse-vortexed for 10 seconds and the mixture was incubated at room temperature (20-25°C) for 20 minutes for complex formation. During this incubation, 3 ml of complete medium from each well was replaced with fresh 1.5 ml of complete DMEM. After plasmid-Polyfect complex formation had taken place, 0.6 ml of complete DMEM was added to the Eppendorf tube and the content was transferred immediately into the well containing cultured HEK 293T cells and mixed by swirling to ensure uniform distribution. Transfection controls included vector plasmid DNA without a cDNA insert of interest or a no transfection control in which the entire procedure was carried out except for the omission of both plasmid DNA and Polyfect reagent was performed. Control wells and those containing transfection with the test plasmid were incubated for 24-48 hours at 37°C in 5% CO_2. For transient transfected cell expression of full-length or mutant protein of interest by confocal immunofluorescence microscopy, the entire procedure was performed with cells cultured on coverslips (Sarsdtedt, 25 mm plastic coverslip) in 6-well plate. Following twenty-four to forty-eight hours after transfection, the medium was removed from each coverslip and with the coverslip left *in situ* in the 6-well plate; they were immediately processed for immunofluorescence staining as described (section 2.7.2). Where expression of wild type or mutant proteins in transiently transfected HEK 293T cells were examined by

Western immunoblotting technique the cells were processed as described (section 2.6.2).

2.5.3 Flp-In T-Rex HEK 293 cell culture

The Flp-In T-Rex HEK 293 cell line (Invitrogen, UK) was supplied at a density of 3 x 10^6 cells/vial in cell freezing medium containing 90% foetal calf serum and 10% dimethylsulfoxide mixture. A vial of Flp-In T-Rex HEK 293 removed from liquid nitrogen was rapidly thawed in water bath at 37°C, and just before the entire vial content had fully thawed, the contents were transferred (under sterile conditions) into a T75 flask containing 10 ml of complete DMEM (section 2.5.1) and gently swirled to mix the contents. The flask was incubated at 37°C in 5% CO_2 for 48hrs to allow cells to adhere to the culture flask. Thereafter, the medium was removed and 10 ml of fresh complete DMEM supplemented with 15 μg/ml blasticidin (Invitrogen, UK) and 100 μg/ml zeocin was added to the cells to maintain a selective pressure for retaining a stably integrated FRT site present in the genome of this cell line. This growth medium was replaced every 72 hours until the cells became 80% confluent. The spent medium was aspirated and cells were washed in 8 ml sterile PBS to remove excess foetal calf serum. Five millilitres endotoxin-free Trypsin/EDTA solution (Invitrogen, UK) was added to the flask followed by incubation at 37°C, 5% CO_2 for exactly 5 minutes. The flask was gently agitated to dislodge the cell clumps from the flask and complete DMEM (5 ml) was added to neutralize the action of trypsin followed by uniform dispersal by trituration. Cell viability and counts were performed (section 2.7.1). For passaging the cell line, $1/10^{th}$ –$1/5^{th}$ of the resuspended cells were transferred into a new T75 flask containing 10 ml of complete DMEM and blasticidin and zeocin added to a final concentrations of 15 μg/ml and 100 μg/ml respectively.

2.5.4 Transfection of Flp-In T-Rex HEK 293 cells to establish stable cell line

Flp-In T-Rex HEK293 cell line allowed rapid generation of a stable cell line expressing a protein of interest from a Flp-In expression vector (pcDNA5/FRT). Targeted integration of pcDNA5/FRT expression vector containing a cloned cDNA of

interest into this cell line allowed high-level protein expression of the cloned cDNA of interest upon induction. Co-transfection of the pcDNA5 expression vector containing the cDNA of interest, and a Flp recombinase vector (pOG44) into the Flp-In HEK 293 cell line was required for targeted integration of the expression vector into a stably integrated FRT site at a transcriptionally active genomic locus in every cell. This ensured homogenous level of gene expression (Flp-In T-Rex system handbook, Invitrogen, UK) in every cell.

The Flp-In T-Rex HEK 293 cells were harvested as described (section 2.5.3) and 1/20 of the cell suspension was transferred in a (100 mm P_{90} petridish, Sarsdtedt), containing 10 ml of selective complete medium. The plate was incubated in a 37°C, 5% CO_2 humidified incubator until the cells became 30-40% confluent. Plasmid pcDNA5/FRT/TO vector containing cloned DNA of interest (4μg) and plasmid pOG44 (4μg, Invitrogen) which expressed the Flp recombinase gene were added to a 0.3 ml incomplete DMEM in a 1.5 ml Eppendorf tube. Polyfect transfection reagent (80 μl, QIAGEN, UK) was also added followed by pulse-vortexing of the mixture and incubation at room temperature for 20 minutes to allow complex formation. Culture medium in P_{90} dish was replaced with fresh complete medium (7 ml) containing only blasticidin (because targeted integration of pcDNA5/FRT vector containing a cloned DNA into the genome of Flp-In T-Rex HEK 293 cell line resulted in loss of zeocin resistance). One ml of complete medium supplemented with blasticidin was added to the Eppendorf tube and the mixture was triturated and transferred into the P_{90} dish. The P90 dish was incubated in a 37°C, 5% CO_2 in a humidified incubator for 24 hours.

Twenty-four after transfection culture medium in P_{90} plate was replaced with complete medium supplemented with blasticidin (15 μg/ml) and hygromycin (100 μg/ml). Cells acquired hygromycin resistance following targeted integration of the pcDNA5/FRT plasmid. Selective medium containing hygromycin and blasticidin was replaced every 72 hours providing a continuous selective pressure for clone of cells containing a stably integrated pcDNA5 with a cDNA of interest. Non-recombinant cell clones were hygromycin sensitive and therefore did not survive the selection process. When well-separated individual clones of surviving cells were visible (1-2 mm), individual clones were transferred into separate wells of a twenty-four well

plate. The growth medium was aspirated from the P_{90} plate and the cells washed with 5 ml of incomplete DMEM to wash out the foetal calf serum. Cloning disc (Sigma-Aldrich, UK, product Z374431) previously immersed in Trypsin/EDTA solution (Invitrogen, UK) was placed gently over each separate clone of cells and the plate was incubated for 5 minutes at 37°C. After the cells had detached from the surface of the P_{90} plate onto the disc, each cloning disc was individually transferred (using a sterile pair of tweezers) into separate well of a 24-well plate containing 750 µl of selective complete medium. The plate was incubated at 37°C, 5% CO_2 in a humidified incubator. This growth medium was aspirated and replaced with fresh selective complete medium every 72 hours until the cells became confluent. Cells in each well were washed with 0.75 ml sterile PBS and then trypsinized in 0.1 ml Trypsin/EDTA incubated at 37°C for two minutes. Thereafter, 1 ml of complete DMEM was added and the entire contents of the well was transferred into a well of a six well plate containing 3 ml selective complete DMEM followed by further incubation. Fresh selective complete medium was replaced every 72 hrs until cells became confluent. Medium was aspirated and cells washed with one ml sterile PBS followed by trypsinization in 0.5 ml Trypsin/EDTA at 37°C for 3 minutes. One ml complete medium was added and the entire suspension was aspirated and transferred to a T-25 flask containing 5 ml selective complete medium. T25 flasks were further incubated with fresh selective complete medium replaced every 72 hours until cells become confluent when they were washed in 2 ml sterile PBS and trypsinized in one ml Trypsin/EDTA at 37°C for 3 minutes. Selective complete medium (4 ml) was added, and the entire cell suspension was transferred into a T75 flask containing 5 ml selective complete medium and T75 flasks were further incubated with medium replacement every 72 hours until cells became confluent.

2.5.5 Long-term storage of stable cell lines

Stocks of various stable cells were prepared from T75 flasks reaching 80% confluence. Cells were trypsinized in 4ml Trypsin/EDTA for five minutes, resuspended in 6 ml complete medium, and a cell pellet obtained after centrifugation at x1000rpm for 3 minutes. To the cell pellet, 10 ml freezing solution (90% foetal calf serum and 10% cell culture grade DMSO) was added and after gentle trituration, aliquots of 1 ml were transferred into cryovials. Vials wrapped in polystyrene bubble

wrap were frozen for 48 hours at –80°C and then transferred into liquid nitrogen for long-term storage.

2.5.6 Inducing wild type or mutant protein expression in stable cell lines

Induction of proteins of interest (by Western immunoblotting & Immunofluorescence staining) in stable cell lines was performed six well plate format. Wells of a six well plate were seeded with 4 x 10^5 stably transfected cells (for analysis by WIB) or onto 25 mm coverslips (for analysis by immunofluorescence confocal microscopy) in a total volume of 3 ml complete DMEM supplemented with Blasticidin and Hygromycin (15 μg/ml and 100 μg/ml respectively). One set of wells in triplicate were designated non-induced stable cells (3 μl of 70% ethanol was added/well to each well) used as assay controls. A second set of triplicate wells were designated induced stable cells (3 μl of 100 μg/ml sterile tetracycline in 70% ethanol was added per well to give a final tetracycline concentration: 0.1 μg/ml). Both sets of stable cells were cultured for 24-72 hours after which cells were processed for either western immunoblotting analysis (section 2.6.2) or immunofluorescence staining and confocal microscopy (section 2.7.2) examination.

2.5.7 Sub-cellular protein fractionation using the Qproteome cell compartment kit

The Qproteome cell compartment kit (Qiagen, UK) was used to obtain sub-cellular protein fractions from stable cells. After trypsinization of cells from a T75 flask, they were centrifuged at x1000rpm for 3 minutes to obtain a cell pellet. The pellet was resuspended uniformly in 5 ml complete DMEM and a cell count and viability were determined as described in section 2.7.1. For comparison of cellular fractionation between different cells, the same numbers of cells (5 x 10^6) were used in each determination. An aliquot of cells in a 15 ml conical tube was pelleted by centrifugation at 1000 rpm for 3 minutes. The cell pellet was resuspended in 2 ml ice-cold PBS by trituration. The cell suspension was transferred into a 2 ml Eppendorf micro-centrifuge tube and a cell pellet was obtained by centrifugation at x 500g for ten minutes at 4°C. The cell pellet was washed again in 2 ml ice cold PBS and a cell

pellet was obtained by repeated centrifugation. To the pellet fraction, one ml of ice-cold extraction buffer CE1 (containing 10µl x100 protease inhibitor) was added and cells were resuspended by trituration through one ml pipette tip. The micro-centrifuge tube was put on a rotator for at 4°C for 10 minutes. The sample was centrifuged at x 1000g at 4°C for ten minutes and the supernatant fraction (cytosol fraction) was stored at 4°C. To the pellet fraction one ml extraction buffer CE2 (containing 10µl x100 protease inhibitor was added and the cells were resuspended by trituration and then placed in a rotator at 4°C for 30 minutes. The micro-centrifuge tube was centrifuged at x6000g at 4°C for 10 minutes and the supernatant fraction (membrane fraction) was stored at 4°C. To the pellet fraction 7 µl of Benzonase nuclease was added followed by addition of 13 µl of distilled water and the pellet was resuspended by flicking the tube. The pellet was left to incubate at room temperature for 15 minutes. To the pellet 0.5 ml of extraction buffer CE3 (containing 5µl x100 protease buffer) was added and the pellet was resuspended by trituration and then incubated at 4°C for 10 minutes on a rotator. The sample was centrifuged at x 6800g for 10 minutes at 4°C. The supernatant (nuclear protein fraction) was stored at 4°C. The pellet fraction was resuspended in 0.5 mls of extraction buffer CE4 (cytoskeletal fraction). All four protein fractions were desalted and concentrated by the addition of four volumes of ice-cold acetone and centrifugation of the samples at x 12000g for 10 minutes at 4°C to obtain the protein pellet fraction of each fraction. Each protein fraction was resuspended in 100 µl of RIPA buffer containing protease inhibitors. $1/5^{th}$ of each protein fraction was analyzed by western immunoblotting analysis (section 2.6.2).

2.6 Protein expression and protein-protein interaction analysis

2.6.1 Total cellular protein assay in cellular lysates

Adherent cells were trypsinized from well plates, T25, and T75 flasks and cell pellets were obtained as described before. To cell pellets obtained 0.15, 5, and 10 ml respectively of ice-cold RIPA buffer (50 mM Tris-HCl pH 7.4, 1% NP-40, 0.25% Na-deoxycholate, 150 mM NaCl, 1 mM EDTA, 1 mM Na_3VO_4, 1 mM NaF and Roche

protease inhibitor cocktail: 1 tablet per 7 ml of buffer) was added followed by trituration through a P1000 or P200 pipette tip. The lysates were sonicated twice on ice for 10 seconds with cooling on ice to prevent excessive sample warm-up. Cell lysates were centrifuged at 13,200 rpm for 10 minutes at 4°C to obtain the supernatant fraction. Protein concentration was measured in the supernatant using a Biuret protein assay reagent (Sigma Aldrich, UK) according to the manufacturer's instructions.

2.6.2 Western immunoblotting (WB) analysis

Sodium dodecyl sulphate polyacrylamide gel electrophoresis was performed as follows: for comparison of samples (for e.g. non-induced & induced or between two different samples), the same relative amount of total cell protein lysate (50-100 μg protein) was used for each sample. The protein was added into a 1.5 ml Eppendorf tube containing 5 μl of reducing and denaturing Laemmli SDS-PAGE sample buffer (x5 concentrated, BioRad, UK) and an appropriate volume of distilled water to a final volume of twenty-five microliters. Samples were denatured at 95°C for 5 minutes and then centrifuging at 13,200 rpm for 30 seconds. Precast Tris-glycine Novex gels (Invitrogen, UK) 10% (25 KD-150 KD protein resolution) or 8% (37 KD-250 KD protein resolution) of 1.5mm thickness were assembled in a Sure Lock electrophoresis gel tank (Invitrogen, UK) with 200ml x1 Tris-Glycine-SDS (Invitrogen, UK) placed in the upper buffer reservoir and 600 ml in the bottom buffer tank. 25 μl of denatured sample was loaded and 20 μl of precision plus protein dual-colour markers (Bio-Rad laboratories, UK) were loaded into an adjacent lane for size estimation (KD). The gel was run at 125 Volts for approximately two hours until a bromophenol blue tracking dye had reached the bottom of the gel.

For western blotting six Whatman 3M sheets (6 x 8 cm) and one Hybond nylon ECL membrane of the same size (Amersham) were pre-soaked in Tris-glycine methanol transfer buffer (TGM, final concentrations: 25 mM Tris base pH 8.3, 192 mM glycine, 10% (v/v) methanol). On a semi-dry transfer apparatus (Semi-phor, Hoefer Scientific, UK) three pre-soaked Whatman sheets were placed on the bottom anode plate followed by the nylon membrane, the gel, and further three pre-soaked Whatman sheets to complete the assembly. The cathode electrode lid of the semi-phor apparatus

completed the circuit using a power supply set at 60mA constant current for 90 minutes.

The blot was removed and placed in a tray containing 25 ml TBST/5% skimmed dried milk (5% wt/vol non-fat milk powder, 0.05 M Tris, 0.15 M NaCl, 0.05% Tween-20, pH 8.0) and placed on a rocking platform for one hour at room temperature. Blot was sealed in a sample bag (GE Healthcare) with 5 ml TBST/milk containing final dilution of primary antibody (mouse monoclonal, or rabbit polyclonal or goat polyclonal antibodies) at between 1:500 and 1:10,000 as recommended in the supplier's antibody data sheet. The blot was placed at 4°C overnight with the primary antibody. The following day the blot was equilibrated at room temperature for one hour and the primary antibody solution was removed followed by washing the blot three times (20 minutes/wash) in 150 ml TBST. Blot was resealed in sample bag with 5 ml TBST/milk containing 1.0 μg/ml horseradish peroxidase conjugated secondary antibodies (anti-mouse, anti-rabbit, or anti-goat specificities) and was placed on a rocking platform for 1 hour at room temperature. Three further TBST washes were performed as before after removal of blot from secondary antibody. The blot was placed in a sample bag and 0.5 ml ECL reagent 1 followed by ECL reagent 2 (GE Healthcare, UK) was added and the bag was sealed and placed in an autoradiography cassette with ECL Hyperfilm (GE Healthcare, UK) to obtain exposure for between one to twenty minutes. Hyperfilm was developed manually in developer followed by incubation in fixer (Kodak reagents, supplied by Sigma Aldrich, UK) for the recommended time.

2.6.3 Immunoprecipitation assays

Stable cells cultured in P_{90} culture dishes were harvested and washed in ice cold PBS. All subsequent steps were performed on ice and in a walk-in cold room. Forty eight hours after transfection cells were scrapped off the P_{90} dish using a plastic cell scraper into 500 μl of immunoprecipitation (x1 IP) buffer (10mM Tris HCl pH 7.6, 145mM NaCl, 1 mM Na_3VO_4, and 1% triton X-100 and one tablet of Roche protease inhibitor/10ml solution). Lysate was triturated six times through a 21-gauge needle on ice followed by centrifugation at 14,000 rpm for 30 minutes in a refrigerated

Eppendorf centrifuge to obtain a soluble whole cell lysate fraction. Protein concentration in the soluble lysate was determined by spectrophotometry (section 2.6.1. Soluble cell lysates (3 mg) were transferred into a sterile Eppendorf tube and pre-cleared by addition of 25 microliters of Protein G-Sepharose (Sigma Aldrich, UK) followed by incubation at 4°C for 30 minutes on rotator. Protein G-Sepharose was pelleted by centrifugation at 10,000g for 0.5 minute at 4°C and supernatant fraction was carefully transferred into a new Eppendorf tube making sure not to disturb the Protein G-Sepharose pellet. Three microgram of anti-XPress or six micrograms anti-DP (mouse monoclonal anti-XPress antibody, Invitrogen, UK, or goat anti-DP, sc-18082, Insight Biotechnology, UK, respectively) was added to pre-cleared supernatant followed by incubation on a rotator at 4°C for three hours. Control samples used an irrelevant antibody (anti-C myc) added to pre-cleared lysate or a no antibody control where addition of IP antibody to pre-cleared lysate was omitted. Fifty microliters of Protein G-Sepharose was added and the incubation at 4°C was continued overnight. Immuno-complexes were pelleted at x10000 g for 30 seconds and washed thrice in low stringency PBS/inhibitor followed by a single wash in x1 IP buffer. Immuno-complexes were denatured in x3 reducing Laemmli sample buffer at 100°C for ten minutes. Following centrifugation at x13000 g for 1 minute at room temperature, the denatured protein samples were electrophoresed on a 10% SDS PAGE gel (Invitrogen, UK) and Western immunoblotting analysis was performed as described in section 2.6.2.

2.7 Microscopy techniques

Light microscopy was performed in a standard Nikon microscope fitted with stage holding six- or twenty-four well tissue culture plates.

Confocal microscopy was performed in a Nikon Eclipse TE300 inverted microscope equipped with a motorized focus unit. The microscope was fitted with x10 eyepiece and x10, x20, x40 (oil immersion) and x100 (oil immersion) objective Nikon lenses. The microscope was equipped with a laser scanning system Radiance 2100 scan head (BioRad Laboratories, UK). The lasers used in the confocal microscope consisted of Red diode (637 nm), Green Helium/Neon (543 nm), Argon (456, 478, 488, and 514 nm) and a blue diode (405 nm). The lasers controller unit was a Radiance laser scanning system 2000 (BioRad Laboratories, UK). A Nikon super high-pressure

mercury-lamp power supply used located initial fluorescence of sample. The thickness of the section examined equalled a stack of six. After initial observation of the fluorescence image through the microscope unit the image was analysed using BioRad Zeiss laser sharp 2000 software that allowed acquisition of confocal images from the microscope. Scale size bar on images were fitted using Laserpix software (BioRad Laboratories, UK).

A Philips 201 transmission electron microscope equipped with a digital camera examined ultra-thin sections of Flp-In T-Rex HEK 293 stable cells over-expressing various desmosomal full-length or mutated proteins.

2.7.1 Cell number and viability determination

Trypsinized stable or transiently transfected cell lines were resuspended in complete DMEM. A Neubaur haemocytometer was assembled with a coverslip in place. A uniformly resuspended cell sample 10 µl was mixed with 10 µl sterile Trypan blue solution (Sigma Aldrich, UK). Ten microliters of this mixture was transferred between the coverslip on the Neubaur counting chamber and viewing under a light microscope (Nikon) with x40 objective lens in place, the number of cells in the centre twenty-five squares flanked by triple lines was counted. This number was multiplied by 2 x 10^4 to give the number of cells per ml in the original cell sample. Visual Trypan blue exclusion showed the percentage cell viability (number of cells not taking up Trypan blue/total number of cells counted in the field x 100). Trypsinization routinely gave >95% cell viabilities.

2.7.2 Immunofluorescence staining and confocal microscopy

Cells cultured in 6-well plates (section 2.5.2 & 2.5.6) were prepared for immunofluorescence staining and confocal microscopy examination. The medium was gently aspirated and with coverslips *in situ,* they were washed once in sterile PBS. Cells on coverslips were fixed *in situ* with 4% formaldehyde for 5 minutes at room temperature and after washing twice in PBS, they were permeabilised in

PBS/0.1% Triton X-100 for 5 minutes. Cells were washed twice with PBS and blocked in PBS/10% foetal calf serum for 30 min at room temperature. The primary antibody was diluted in PBS/1 % foetal calf serum and cells were left covered in this solution for one hour at room temperature. Following three PBS washes, secondary antibody conjugated with Alexa fluor-546 (red fluorescence, Invitrogen, UK) was diluted at the recommended dilution factor in PBS/10% foetal calf serum. This solution was left covering the cells in the dark for one hour at room temperature. Following three PBS washes, the cells were incubated in DAPI (4', 6 diamidino-2-phenylindole, nuclei fluoresce blue) solution for 5 min. After a brief wash in PBS, the coverslips were mounted on to microscope slides in 95%glycerol/PBS solution with cells face down in contact with the glass slide. Slides were stored at 4°C in the dark until visualised by confocal microscopy. Alexa conjugated-fluorochromes have enhanced stability in the dark at 4°C, and therefore do not require the use of anti-fading reagents.

For triple staining with FM 1-43 FX membrane dye (Invitrogen, UK, emitting a green fluorescence), coverslips were first exposed to this reagent 5μg/ml in Ca^{2+} and Mg^{2+} free HBSS medium for exactly 1 minute, prior to fixing in 4% paraformaldehyde. The rest of the staining procedure was essentially performed as previously described.

2.7.3 Gap junction intercellular communication (GJIC) measurement using Lucifer Yellow

Gap junction intercellular communication was assessed by confocal microscope following scrape loading of Lucifer Yellow dye and transfer of the fluorescent dye into adjacent cell layers. Tetracycline-induced confluent monolayer of stable cells cultured in a P_{30} dishes was gently rinsed in PBS. A fine linear incision was made in the monolayer using a 0.25mm thin silver wire. A solution of Lucifer Yellow (final concentration 5% dissolved in incomplete DMEM) was incubated with the scraped monolayer for exactly 5 minutes to allow uptake and transfer of the dye. Excess dye was washed off in PBS solution and the monolayer was then fixed in 5% formaldehyde. The uptake and extent of transfer of Lucifer Yellow from the scrape line was assessed by fluorescence microscopy using the Helium/Neon laser at 534nm

(green fluorescence) using the dark non-fluorescing nuclei as a count to asses the number of layers through which the dye was transferred.

2.7.4 Electron microscopy to determine desmosomal morphology

Stable cells cultured on Thermanox plastic coverslips (BD Bioscience, UK) were used, as they are specially adapted for ease of processing for examination by transmission-electron microscopy. Coverslips supplied were treated on one side to allow adherence of cultured cells. Stable cells were cultured under tetracycline-induced condition for 48-72 hours to allow expression of respective cell adhesion protein or mutant protein. For comparison with non-transformed Flp-In T-Rex HEK 293 cells, these were cultured similarly as stable cells. Culture medium was carefully removed from the coverslip in a twenty-four well tissue culture plate (BD Bioscience UK) and this was replaced with a standard Karnosky-style fixative and left *in situ* to fix the cells overnight at 4°C. The cells were processed further by a series of incubations involving three washes in PBS for 5 minutes each, fixation in osmium tetroxide for 20 minutes and three washes in purified water for 5 minutes. Stepwise dehydration was achieved in 10% IMS for 5 minutes, 30% IMS for 5 minutes, 50% IMS for 5 minutes, two washes in 70% IMS for 15 minutes each, two washes in 90% alcohol for 15 minutes each, two washes in 100% IMS for 15 minutes each, and a final wash in 100% IMS for 20 minutes. Samples were processed overnight in 50: 50 alcohol: Lemix™ on a rotator, followed by processing in Lemix™ on a rotator the following day. Pieces were cut out of the coverslips, small enough to fit the base of individual polythene embedding moulds (TAAB). These were placed in the TAAB moulds, orientated cells down (now visibly blackened by the osmium tetroxide). After the pieces had sunk to the bottom, they were with GREAT CARE pressed to the bottom (flush for cutting an insubstantial monolayer). Semi thin sections (Reichart Ultracut ultramicrotome at a nominal thickness of 0.5μm) mounted on glass slides were stained with Toluidine Blue for examination by light microscopy to confirm presence and quality of preparation, and then the Reichart Ultracut™ ultramicrotome was used to cut ultra thin sections. (nominally 70nm) directly onto water in the trough of a Diatome™ diamond knife. These were picked up on copper EM grids (300 mesh, high transmission, Gilder™). Sections were stained consecutively with saturated

Uranyl Acetate (50% ethanolic), then alkaline lead citrate (5 minutes each), with a good drop wise purified water wash after of each staining. A Philips 201 electron microscope equipped with a digital camera was used to examine desmosomes in different random fields. Electron micrographs were interpreted by an electron microscopist unaware of the identity of cell adhesion molecule expressed in desmosomes examined. Morphometric analysis of desmosomal widths and length were performed from electron micrographs (at x70000 magnification) and measurements in nm were derived from scale bars obtained from microscope internal size calibration at different magnifications.

2.8 Cellular adhesion, proliferation, and apoptosis analysis

2.8.1 Measuring initial cell-cell contact adhesion

The initial cell contact adhesion of stable cells was determined using a Vybrant Cell Adhesion Assay kit (Molecular Probes, UK) that is widely used in assessing cell-cell adhesion *in vitro*. A non-fluorogenic dye, calcein acetoxymethyl ester (calcein AM) produces Calcein a fluorescent product after the substrate is cleaved by esterase enzymes in live cells. Calcein absorbance (494 nm) was detected in a confocal microscope. Stable cells lines were cultured under tetracycline-induced conditions on 25 mm coverslips (2.0×10^3) until they were fully confluent. Sable cells (cultured separately under tetracycline-induced conditions) were harvested and re-suspended in pre-warmed DMEM at 3.6×10^6 cell/ml and 5 µl of calcein AM stock dye solution (final calcein AM concentration of 5 µM) was added to the cells. After 30 min incubation at 37°C/5% CO_2 in a humidified incubator, excess calcein AM was removed from these cells by washing thrice in sterile PBS and cells were resuspended to a density of 3.6×10^6 cells/ml in DMEM. An aliquot of labelled cells (100 µl) were layered on top of the fully confluent adherent cells on the coverslips. After incubation in 5% CO_2 humidified incubator at 37°C for five hours, all non-adherent labelled cells were carefully removed by washing with pre-warmed DMEM. Cells on the coverslips were fixed in 4% formaldehyde for ten minutes, washed once with PBS,

permeabilised in 0.1% Triton X-100/PBS, stained with DAPI (300 nM) solution and mounted in PBS/95% glycerol upside down on a glass microscope slides. Labelled cells were observed in a confocal microscope where the calcein-labelled cells appeared green (emission at 523 nm) versus a background of total cells labelled blue with DAPI (emission at 461 nm). The number of green cells relative to the blue cells in a given field of view were quantified and expressed as a percentage to indicate initial cell contact adhesion (% = no of green fluorescing cells/no of blue fluorescing cells x 100). The percentage of initial cell contact adhesion is a measure of initial cell-cell adherence, and the mean values obtained using stable cells expressing full-length cell adhesion proteins were compared with the value obtained in stable cells expressing mutant cell adhesion proteins. The % initial cell adhesion values obtained from six independent experiments were averaged to obtain a mean value and a student's t-test was used to make a statistical comparison of mean initial cell adhesion of stable cells expressing full-length and mutant cell adhesion molecules.

2.8.2 Dispase-based monolayer dissociation adhesion assay

This assay measures the adhesive strength of a highly confluent monolayer of cells *in vitro* subjected to controlled mechanical stress. The protocol is widely used to assess cell-cell adhesion in confluent monolayer of cells and was essentially carried out as described by Huen[212] *et al.* Stable cells were cultured in P_{60} mm Nunc plastic culture dishes in penicillin, streptomycin, foetal bovine serum, blasticidin and hygromycin supplemented DMEM (Invitrogen 19308-025) in the presence of 0.1 μg/ml tetracycline until cells were highly confluent. Cells were carefully washed in PBS and one ml of 2.4 U/ml Dispase II (Roche, Cat No 10295835001) was added to the dishes followed by incubation at 37°C for 30 minutes. Dispase II released the entire monolayer intact from the plastic tissue culture surface without dissociating individual cells. The monolayer was carefully rinsed twice in PBS without agitation and finally resuspended (one to five ml) in PBS. Gentle shearing (using predetermined and a controlled number of rotations on a tabletop rocker platform) or relatively more vigorous shearing (by triturating six times) through a P1000 pipette tip was applied to the monolayer. The sheared monolayer was photographed under Epi-white light

illumination using a BioRad Gel Documentation system (gel doc XR) and the image was captured using Quantity One version 4.6 image analysis program (BioRad Laboratories, UK). Cluster size of the sheared fragments provided a visual measure of the adhesive strength of the monolayer sheet of cells, wherein a large cluster size indicated an increased resistance to disruption by shearing force. A quantitative measurement of Dispase-based cell dissociation adhesion was carried out by counting under a light microscope the number of cluster of a predefined size (e.g. cluster size of $\geq$ 100) following disruption of cell monolayers.

2.8.3 Cellular proliferation assay

Cellular proliferation was measured using the CellTiter 96 AQueous One Solution reagent (Promega Corporation, UK) according to manufacturer's suggested protocol. This assay is an inexpensive non-radioactive alternative method widely used to assess cellular proliferation. The assay reagent contains Owen's compound, which is bio-reduced by live cells into a coloured formazan product. The amount of formazan produced was measured spectrophotometrically and was directly proportional to the number of surviving cells.

Cell proliferation assays were performed in a 6-well plate with an initial seeding density of 30,000 cells per well. Cell Titre AQueous One Solution reagent (80µl) was added to the medium in each well and plates were incubated for exactly 1 hour in the tissue culture incubator. The entire medium from each individual wells assayed was transferred into separate wells of a fresh plate and the absorbance at 490 nm was read in a Libra S12 spectrophotometer (Biochrom Ltd, UK). A plot of absorbance versus time elapsed after plating the cells was done on a single graph depicting stable cell lines over-expressing full-length or mutant cell adhesion proteins under induced or non-induced conditions for direct comparison of the cellular proliferation.

2.8.4 Cellular apoptosis assay

Caspase-3 activity is an index of cellular apoptosis and was measured using a colorimetric CaspACE Assay System (Promega Corporation, UK). A substrate (Ac-

DEVD-pNA) containing the chromophore *p*-nitroaniline (pNA) is cleaved by DVEDase in cells undergoing apoptosis, the action of which releases pNA. Free pNA produces a yellow colour detected spectrophotometrically at 405 nm. The amount of yellow colour produced was proportional to the amount of DVEDase activity in the sample.

Stable cells seeded at 400,000 cells/well in a 6-well plate were cultured in 3 ml complete DMEM supplemented with 15 μg/ml blasticidin, 100 μg/mg hygromycin, 3 μl 70% ethanol (triplicate wells, non-induced condition) or 0.1 μg/ml tetracycline (triplicate wells, induced conditions) until cells were nearly confluent. Stable cells were subjected to mechanical stretch (section 2.9.1) and were harvested to obtain a cell pellet by centrifugation at x1000 rpm for 2 minutes. The cell pellet lysis was performed using sonication for 10 seconds in lysis buffer. The supernatant obtained after centrifugation at 13,200 rpm for 5 minutes was assayed for total cell protein (section 2.6.1). The assay was performed in 96-well plate by adding the following to each well for every sample analysed: 64 μl assay buffer, 4 μl dimethylsulfoxide, 20 μl 100 mM dithiothreitol 60 μl protein lysate (148-480 μg protein), 48 μl sterile water and 4 μl DVED-pNA substrate. A blank was prepared as above except protein sample was omitted and total volume made up to 200μl with sterile water. The 96-well plate covered in foil was incubated for four hours at 37°C. Standards of pNA in the range 0-400 μM were prepared by diluting from a stock solution (supplied in the kit) in a 200 μl final volume containing a 10^{th} dilution of DMSO. After four hours, the absorbance of each sample was read at 405 nm against a blank tube, and using the standard curve generated from the absorbance readings of pNA standards (0-400 μM); the μM pNA released per μg protein lysate was calculated for each sample so that direct comparison between the samples could be made. Values of specific DVEDase activity (μM pNA/μg protein) for each of the triplicate samples in non-induced and induced conditions were plotted on a single graph depicting cell lines expressing full-length and mutant proteins.

2.9 Exposure of stable cell lines to mechanical cell-stretch

The effects of induced expression of full-length or mutant cell adhesion proteins in stable Flp-In T-Rex HEK 293 cell lines on programmed cell death following exposure to mechanical cell stretch was determined using the FlexerCell apparatus (FlexCell International Corporation). Each cell line was cultured on FlexerCell 6-well plates either in non-induced (without over-expression of protein of interest) or tetracycline-induced (resulting in induced over-expression of proteins of interest) conditions and they were subjected to controlled cyclical stretch in the FlexerCell apparatus for a defined time of exposure and magnitude of cell stretch. This was followed by recovery of the cells subjected to stretch prior to performing apoptosis assay on cell lysate obtained.

2.9.1 Mechanical cell-stretch of stable cells

To allow for observed difference in growth characteristic of stable cell line cultured on gelatine-coated silicon membrane insert and those cultured on tissue culture plastic, 0.5-1.5 x 10^6 cells were seeded per well in the FlexerCell 6-well plate. As before, the medium was 3 ml complete DMEM with blasticidin and hygromycin supplementation at 15 μg/ml and 100 μg/ml respectively, and either 3 μl 70% ethanol (control non-induced wells) or 3 μl tetracycline (0.1 μg/ml final concentration, induced wells) was added to the appropriate wells. Tetracycline induction was for the full duration of cell culture until they were nearly confluent. The FlexerCell 6-well plate was coated with type I gelatine, which allowed stable cell lines to adhere to the silicon membrane support. When cells were nearly confluent, plates were placed in a tissue culture incubator (humidified and set at 37°C with 5% CO_2) in a FlexerCell loading platform allowing assembly of four separate FlexerCell 6-well plates. Each plate was sealed in place on the platform with special silicon grease supplied, so that an airtight seal was made between the FlexerCell 6-well plate and a rubber gasket on the platform. The loading platform was linked to a computer-controlled vacuum pump so that precision suction at the desired strength (amplitude) and rate (frequency in Hz) could be applied to the FlexerCell 6-well plates assembled on the platform. Cyclical stretch at between 4-6% amplitude and 1 Hz frequency was applied to the plates for varying time between three to four hours. Cells were allowed recovery in the incubator for three hours after application of mechanical stretch. Plates were carefully disassembled from the platform and cellular pellets were obtained from each well

using standard trypsinization procedure, but all washings were pooled to retain any cells that had detached off the membrane insert. Cell pellets were stored at –80°C until processed for cellular apoptosis assay using the CaspACE assay system. FlexerCell 6-well plates were reused by washing in mild detergent followed by UV irradiation sterilisation, and silicone membranes of plates reused were recoated with sterile gelatine (Sigma, 0.2 mg/ml in complete DMEM, overnight incubation) and rewashing of wells in complete DMEM prior to plating stable cell lines for further stretch experiments.

2.9.2 Measuring apoptotic response of stable cell lines to mechanical cell-stretch

Cell pellets were processed for the CaspACE assay as described in section 2.8.4.

Chapter 3 – Genetic screening of ARVC patient DNA

3.1 Introduction

When studies in this chapter commenced in 2004, three gene mutations were identified in ARVC and its variant: the first was RyR2 in ARVC2, the second was desmoplakin in ARVC4, and the third was plakoglobin in Naxos disease. Apart from mutations reported in the untranslated regions of TGFβ in ARVC1 (discovered in August 2004) no other gene mutations were known until then in the remaining five ARVC loci (TMEM43 gene responsible for ARVC5 was reported in March 2008) as identification of causative genes were hampered by incomplete penetrance and by a lack of accurate ARVC clinical diagnosis.

3.2 Hypothesis and Experimental Aims

As two of the mutations identified previously were in genes encoding proteins involved in cell-cell adhesion it was hypothesized that further mutations in genes encoding other cell-cell adhesion proteins could be present in this disease. This formed the basis for performing the genetic screening work.

The working hypothesis was that mutations in genes encoding desmosomal proteins involved in cell-cell adhesion would disrupt various domains or sub-domains associated with these proteins and abnormalities manifested clinically may be determined by the location of mutations within the same protein or by mutations in different proteins resulting in structural or functional abnormalities.

Two experimental aims were set in these studies

1) The aim in the first part of the study was to screen one hundred index cases (probands) for mutations using a DNA screening approach to examine genes involved in desmosomal cell-cell adhesion. Three genes encoding desmosomal proteins were examined; these were derived from different families of proteins: one of these belongs to a member of the plakin family (desmoplakin), a second belongs to an Armadillo (ARM) family of proteins related to β-catenin (plakoglobin), and the third belongs to an ARM family of proteins related to the $p120^{ctn}$ sub-family of proteins (plakophilin-2). Both DP and PG

genes were known candidates involved in ARVC, but this was not the case for the PKP-2 gene. However, as plakophilins are associated with desmosomes, and PKP-2 is a predominant isotype expressed in the cardiac tissue, it was included as one of the genes in genetic screening studies.

2) The aim in the second part of the study was to perform pedigree analysis, this is a family study where the transmission of the inherited genetic defect (identified in a proband) is investigated in siblings, offspring, and relatives of the proband and the clinical expression of ARVC symptoms are evaluated in family members using modified & Task Force criteria. Seven out of the eleven mutations identified in the first part of the study were selected for pedigree analysis to determine transmission of the disease causing allele and clinical expression across the spectrum of ARVC disease phenotype manifestations.

3.3 Materials and methods

A consultant lead clinical team at the London Heart Hospital in collaboration with Professor William J McKenna performed the clinical evaluation of patients referred at the ARVC clinic, and which formed part of the British ARVC registry. Blood samples were collected (preserved in EDTA) after local ethics committee approval by the UCL Hospitals NHS trust and obtaining informed consent from one hundred patients who fulfilled ARVC clinical diagnostic criteria assessed under the Task Force guidelines. Blood samples were stored at -20°C prior to analysis and were thawed to room temperature prior to use. Blood samples were also collected after obtaining informed consent from first, second, third, etc. generation relatives of each proband for performing pedigree analysis when this was permitted. Both the Task Force and modified clinical ARVC diagnostic criteria were applied for evaluating family members of the proband.

DNA was extracted from preserved peripheral whole blood samples as described previously (section 2.11). Primers flanking the coding region and the immediate adjacent intron flanking sequence in each of these three genes (DP, PG, and PKP-2) were used in PCR reactions (section 2.1.2) to amplify overlapping DNA fragments

covering all exons and the immediate flanking intron regions of each of these three genes. Each amplified DNA fragment was sequenced bi-directionally using Big Dye chain-terminating chemistry (Applied Biosystems, UK) in an ABI 3100XL genetic analyser (sections 2.1.3 to 2.1.3.3). DNA sequence data was analysed using Seqscape software (Applied Biosystems, UK) that aligned sequences against a synthetic trace generated by the software using the appropriate reference sequence (Accession numbers: plakophilin-2, NM_004572.2; plakoglobin, NM_002230; desmoplakin, NM_004415) obtained from the Genebank database. This allowed identification of mutations in the coding regions and immediate flanking intron regions of each gene analysed. Nucleotide sequence variants identified were checked in public domain databases (for example, ensemble genome browser and NCBI SNP database) to ascertain whether the sequence variant had been previously reported. Reference sequences used were for the long-form transcripts of plakophin-2, plakoglobin, and desmoplakin. The numbering of all mutations, polymorphisms, and other unknown sequence changes (not falling in the previous two categories) were relative to the nucleotide numbering in the reference sequence for each transcript with the first Adenine nucleotide in the ATG initiation codon designated as nucleotide number 1.

PCR primers designed manually with reference to the published gene sequences, utilised intron flanking regions (whenever possible) so that primer pairs amplified overlapping PCR fragments allowing complete sequence read through to be obtained. Amplimers were restricted to less than 600bp in size, primers contained 50-60% total GC content and were checked to exclude significant self complementarity or inter-primer complementarity (< four consecutive nucleotide runs). The theoretical melting temperature of each oligonucleotide primer was calculated using an established formula:

$Tm = 81.5^{\circ}C + 16.6^{\circ}C \times (\text{Log}_{10}[Na^{+}] + [K^{+}]) + 0.41^{\circ}C \times (\%GC) - 75/N$

Where $[Na^{+}]$ = sodium ion molar concentration, percentage GC = total percentage of G and C residues, N = length of the oligonucleotide primer, $[K^{+}]$ = potassium ion molar concentration.

The AmpliTaq enzyme PCR buffer used in the PCR reactions contained 50mM Na^{+}, but it did not contain any KCL and therefore the $[K^{+}]$ did not feature in the formula

used for calculating the theoretical melting temperature. The PCR annealing temperature was varied ± 5-10°C on either side of the calculated Tm, and/or $MgCl_2$ concentration (2-2.5 mM) was varied in the PCR optimization reactions to work out the best conditions for obtaining a single amplimer of the expected size. The primer sequences and PCR conditions optimised for PG, PKP-2, and DP are listed in Tables 3.1 – 3.3. Amplification of targets in G-C rich region was performed using a G-C rich PCR kit (Roche, UK) according to the manufacturer's instructions (GC rich PCR, section 2.1.2).

The desmoplakin gene is encoded in twenty-four separate exons. Although each of the individual exons 1 to 22 was amplified in its entirety in a single PCR reaction, this was not feasible with exons 1, 23, and 24 as these exons were quite large. Therefore, overlapping fragments (two fragments for exon 1, seven fragments for exon 23 and nine fragments for exon 24) were amplified for these exons. Overlapping fragments allowed the entire sequence of exons 1, 23, and 24 to be assembled and their sequence confirmed by Seqscape analysis. For plakophilin-2 exon 3 was also quite large therefore, this particular exon was amplified in two overlapping fragments (3A and 3B). Exon 12 of PKP-2 was amplified using two sets of primers pairs as upstream of exon 12 a sequence of ten consecutive thymidine residues cannot be amplified intact by AmpliTaq enzyme resulting in double peaks during sequencing of the PCR fragment with PKPex12F primer. Downstream of the exon there is a naturally occurring deletion in many samples which makes the PKPex12R primer useless too. Therefore, to overcome these problems the two internal primers (see Table 3.2) were used for sequencing.

3.4 Results

3.4.1 Part 1: Screening of ARVC cohort for mutations in Desmoplakin, Plakoglobin and Plakophilin-2 genes

Table 3.1, 3.2, and 3.3 lists the PCR primer sequences and the conditions used for PG, PKP-2, and DP PCR respectively. In each table primer sequences in 5' to 3' orientation are listed in pairs indicated by gene name, exon number, and an F or R suffix to indicate the forward and reverse primers respectively. Where multiple primer pairs were used to cover the PCR of a large exon (for example DP exon 23) then these primer pairs were further identified by additional numbering of the fragments after the exon amplified (for e.g. for the seven fragments of DP exon 23 these are labelled as DPex23.1 to DPex23.7). The sizes in base pairs of each exon and of the PCR product obtained are stated in the next column. The optimal primer annealing temperature (deduced from preliminary experiments) and special conditions required (such the use of a GC-rich system or a employing a non-standard concentration of $MgCl_2$) are stated in the next column. The sequencing primer used to obtain an initial sequence read-out was indicated in each table, this could be either the forward or the reverse primer. Mutations, polymorphisms or other unknown sequence changes identified were confirmed by bi-directional sequencing using the complementary PCR primer to confirm the suspected sequence alteration.

3.4.1 Part 1.1 Classification of mutations

For the purpose of this study, mutations were classified based on nucleotide sequence changes that led to the following:

1) Truncation of protein during translation of mRNA transcript compared to the wild type resulting from frame-shift nucleotide sequence change (either short sequence insertions, short deletions or combination of insertion and deletions referred to as 'indels') causing a PTC to be encountered further downstream of the insertion or deletion. Alternative to protein truncation is rare, but sometimes insertion/deletions can cause addition of extra residues extending the overall reading frame, this can happen, when insertion or deletions occur in the last exon

of the gene. Frame-shift mutations identified in these studies resulted only in protein truncation.

2) Splice junction variants (affecting the donor splice site or the acceptor splice present in the flanking intervening intron sequence) may result in exon skipping, or in aberrant splicing causing retention of only a part of an exon or the retention of an of intron. The nomenclature for assigning splice site sequence changes (Figure 3.1) are illustrated using two hypothetical mutations in donor and acceptor splice sites respectively. The first ten nucleotides in the donor and splice sites were considered essential for normal splicing to occur.
3) Single nucleotide changes that cause a nonsense sequence change (TAA, TAG, and TGA) leading to a PTC.
4) A single nucleotide change causing a missense sequence variant not listed as a known SNP and not detected in 400 normal control DNA samples. This missense sequence variant was assumed a mutation if it was associated with the clinical expression of ARVC in family studies. These missense mutations identified were analysed using web based programs such as SIFT (sorting in-tolerant from tolerant amino acids), POLYPHEN (*Poly*morphism *Pheno*typing), and RUSSEL analysis to determine the severity of missense amino acid substitutions on protein structure and function. This results in classifying missense protein variants as benign, most likely benign, most likely pathogenic, or certainly pathogenic. SIFT predicts whether a naturally occurring non-synonymous amino acid substitution affects protein function based on homology and the physical properties of amino acids. SIFT returns predictions for what amino acid substitutions will affect protein function. SIFT is a multi-step analysis which searches for and chooses similar sequences, makes an alignment of these sequences, and calculates scores based on the amino acids appearing at each position. Polyphen is another tool, which predicts possible impact of an amino acid substitution on the structure and function of human proteins using both physical and comparative considerations of an amino acid change. SIFT and Polyphen analysis of missense mutations found in the genetic screening of the ARVC cohort are described in a later section (section 3.4.1 Part 1.7). Russel allows comparison of substituted amino acid residue with the wild-type amino acid residue based on their physicochemical properties. Another tool used for analysis of missense mutations affecting substitutions of serine, threonine, and tyrosine residues is a phosphorylation

prediction program called NetPhos. NetPhos predicts potential phosphorylation sites in serine and threonine residues based on homology search of conserved motifs found in these amino acid residues at known phosphorylation sites found in other proteins. NetPhos examines protein of interest and predicts putative phosphorylation sites based on conserved motifs used by various phosphorylation enzymes. Another tool used in the analysis of missense amino acid substitutions is a program called ESE finder. ESE finder predicts the effect of a nucleotide variant (encoding a missense mutation) on exon splicing enhancer sequence (discussed in section 1.8.3) found within an exon.

Figure 3.1 Nomenclature of donor and acceptor splice site mutation explained using a hypothetical example

Illustrated below is a hypothetical example of two different splice site mutations. The last nucleotide of exon 10 and first nucleotide in exon 11 are numbered 2145 and 2146 respectively (according to the numbering relative to a reference sequence). The horizontal line identifies intron 10 with twelve consecutive nucleotides shown for simplicity. The donor site is close to the intron sequence adjacent to exon 10 while the acceptor site is close to intron sequence adjacent to exon 11. The numbering of the nucleotide residues in intron 10 is as shown with even number of residues closest to exon 10 being numbered with + sign while those closest to exon 11 are numbered with – sign. The red arrow marks an acceptor site mutation (c.2146-1G>C) while the blue arrow marks a donor site mutation (c.2145+5C>T).

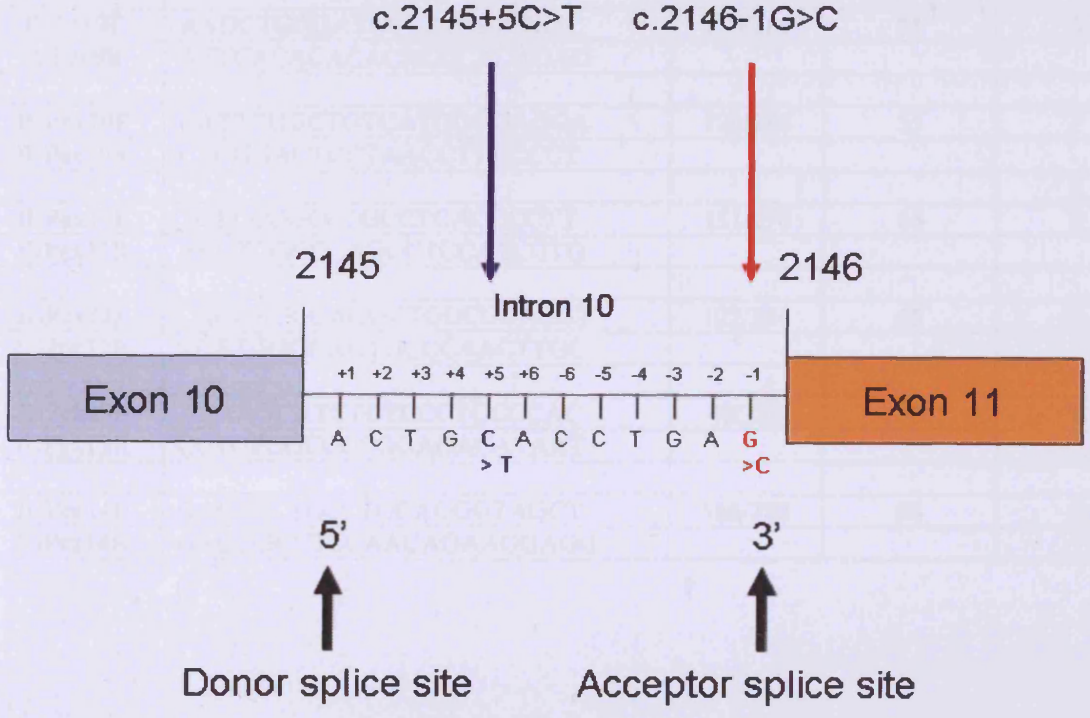

Table 3.1 PG primers and conditions used for PCR

Plakoglobin PCR primer sequences, annealing temperatures, and the expected sizes of the PCR amplimers. All PCR were performed between 35-40 cycles using a final concentration of 2 mM MgCl2 in the buffer supplied with AmpliTaq Gold DNA (Applied Biosystems) polymerase enzyme.

Primer	Sequence (5'-3')	Exon/PCR size (bp)	PCR-Annealing temperature ^{0}C	Sequencing primer
JUPex1F	CTTGGCTGTCAGGTCTCTTCGC	111/201	-	-
JUPex1R	TCTGTCCCCAACGATACCTGCG			
JUPex2F	CTGGGCCAGGTGACTTCCTGCT	216/323	65	R
JUPex2R	TCTCTCCAGGACCCAGGCAGGT			
JUPex3F	AGTGTCTGCCCAGCCCACTGC	260/392	67	F
JUPex3R	ACAATGTCCCTCCCCTGAGGACATCT			
JUPex4F	GCCTCTCCTTAGTGCTCACGTC	239/344	58	R
JUPex4R	AGGGGAGAGGCCCAAGTGAGAG			
JUPex5F	GCTCACATGTATGCCAGGCCTC	202/323	60	F
JUPex5R	GCAGGATAGAAGATGGCGCAAG			
JUPex6F	CCCGCGCTTCCTTGTTCCTGTCA	145/295	62	F
JUPex6R	CATCAGCCACGGGGAGCATGGCT			
JUPex7F	CCATTGTGGAGGCTGGTGAGTATG	104/310	65	F
JUPex7R	AGATGCCCAGACAGGAGGCTGGAT			
JUPex8F	TGGAGTTGGCTGCTCCCTGAC	339/434	62	R
JUPex8R	ACCTAAGCCTGCTGCAGGGTG			
JUPex9F	AAGCTGGGATCCTTCAGATGTC	156/289	55	R
JUPex9R	ATTCACACACACACCCACAGAG			
JUPex10F	CATTCGGCTGTCATGGGGAGGA	120/266	55	F
JUPex10R	CTGGGACTCCTAACCTTGCCCT			
JUPex11F	TGTCCGGCCTGCCTCACCCCTT	151/276	65	F
JUPex11R	ACGTCGGCCAGCCTCCATCGTG			
JUPex12F	CACGATGGAGGCTGGCCGACGT	122/234	65	R
JUPex12R	CCATGGGCAGTGCCCAACTTGC			
JUPex13F	AGAAGCATCTCTCCCTGCCCAC	40/223	55	F
JUPex13R	CCTCTGGCCCCGGAGACATAAT			
JUPex14F	GACTGCTCCCTGCAGGGTAGCT	166/288	58	R
JUPex14R	GAGGGCCTCCAACAGAAGGAGG			

Table 3.2 PKP-2 Primers and conditions used for PCR

PKP-2 PCR primer sequences, annealing temperatures, and the expected sizes of the PCR amplimers. All PCR were performed between 35-40 cycles using a final concentration of 2 mM $MgCl_2$ in the buffer supplied with AmpliTaq Gold (Applied Biosystems, UK) enzyme, unless otherwise indicated.

Primer	Sequence (5'-3')	Exon/PCR size (bp)	PCR-Annealing temperature ^0C	Sequencing primer
PKP2ex1F	ACTCGAGCGGGGCGGGGCTCG	248/414	68, GC rich kit	F
PKP2ex1R	ACTCCCAGCACGCGGGGTGAG		0.5mM GC resol sol	
PKP2ex2F	TACTTGTTCTTGGCCTTCATTAC	113/332	55	F
PKP2ex2R	ACTTGGGAAAAGTAAACACTC			
PKP2ex3AF	AGTCCTCAGCAAAGTTGAAATTTG	698/423	53	F
PKP2ex3AR	GTCAAAAACGGTGTCGCTAACAGA			
PKP2ex3BF	CACATACCACAGACAGTACCAG	698/443	58	R
PKP2ex3BR	TGTGCTGGCAATGACTGAACTG			
PKP2ex4F	AGTATTCGCTGAGTCGTCTCT	136/291	55	F
PKP2ex4R	GCAAAGTCACCATAATAGAAG			
PKP2ex5F	GAAAGGTTATAGTCAGCATCAG	208/413	55	F
PKP2ex5R	CATCAATCATTTGCTCCAGGA			
PKP2ex6F	TTGCTGTGTTCATAAAGGAGCC	132/258	55	F
PKP2ex6R	ATTACAGGCGCAGACCACGACA			
PKP2ex7F	TTCAGCGGTCATTTTGGTCCCA	178/305	55	F
PKP2ex7R	TGACTTCCTTGGGGCTACCTAA			
PKP2ex8F	CAAAGACCTGTTGGATACACA	118/250	55	F
PKP2ex8R	CCAAGCGGCTATCTTAAGAAT			
PKP2ex9F	TATCACACCTGCAAGGATATC	165/324	58	F
PKP2ex9R	GCCGATATATACCAAGTACTT			
PKP2ex10F	GTGAAATTATAGCCATCACCTG	174/303	55	F
PKP2ex10R	CTGAATTGAATGTAGGTAAGTC			
PKP2ex11F	CATCTTCATCAACCTCTGGTA	154/322	58	F
PKP2ex11R	GGTGATACAGACAACATTTCA			
PKP2ex12F	TGGGATCTTGGGATTAAGAAAC	190/259	65	R
PKP2ex12	TTACGCATCGCCTGCACTAATG			
PKP2ex12	AAGAAACTCTCCCTGATTTGGT	190/274	62 (1.5mM $MgCl_2$)	F
PKP2ex12R	CATGACCGCACATTCACAACCGG			
PKP2ex13F	AGGCCGCATCCAGAAGCCTCA	88/224	55	F
PKP2ex13R	TTCCCAGGGTCAAGTCAAGTGG			
PKP2ex14F	CCACTTGACTTGACCCTGGGAA	1639/246	58	F
PKP2ex14R	GGTTTCTTGGGCTGGGTAGTAG			

Table 3.3 DP Primers and conditions used for PCR

Desmoplakin PCR primer sequences, annealing temperatures, and the expected sizes of the PCR amplimers. All PCR were performed between 35-40 cycles using a final concentration of 2 mM $MgCl_2$ in the buffer supplied with AmpliTaq Gold DNA (Applied Biosystems) polymerase enzyme.

Primer	Sequence (5'-3')	Exon/PCR size (bp)	PCR-Annealing temperature ^0C	Sequencing primer
DPex1.1F	AAGAAACCGGCCAGGTGTGG	449/393	-	-
DPex1.1R	TCATGCGGCCCAGAGTGTTGATC			
DPex1F	AGGTAGCGAGCAGCGACCTCG	449/361	65	R
DPex1R	AGTCGTCCAGAGGAGGACGGT			
DPex2F	GGTAAAGGGTCTCACAGGAGTGGT	103/325	55	R
DPex2R	GTGAAAGAGGTCAGTGAATAGGCC			
DPex3F	CTTGCTTCCATTAATGCCCATGAA	149/291	60	F
DPex3R	AGTGTAACTGGTTATGAGGAGTTC			
DPex4F	CCAGAACGGGTTTTCATAGGC	175/314	55	R
DPex4R	CACACAAACACATGGGCTGAC			
DPex5F	GGTGTGCGTAAGTGAAACAGGT	129/260	55	R
DPex5R	GTAATTACACGATCCTTCGGTAG			
DPex6F	AGGAGGCTTAGAAGGGCCACTC	51/218	55	F
DPex6R	TCCCCGCCAGGATGTGCTTGAT			
DPex7F	CAGAGAACACCAGTCACTGCA	162/282	60	F
DPex7R	CCAGCTCTTCAAGGCAACAGG			
DPex8F	AACAGCGTGATTCTTTGGCA	105/386	50	F
DPex8R	CCAACCCCTGGTGTAGGGTA			
DPex9F	TGGTGTTCATGCATCTGTACAA	96/214	50	F
DPex9R	CAAAAGATTAGGTATTAAGACC			
DPex10F	CTACTAGATGAAATTGCTCAT	126/254	55	F
DPex10R	TCCAAGGCATGTGTTTTATCT			
DPex11F	TGCAGGTTGAAAATCTCCTCT	153/302	55	F
DPex11R	AATGTTGCTTTCTTGATGGAC			
DPex12F	CATCTCTGTTTCCATCATTGAG	155/313	55	F
DPex12R	TATAAACACCTGCCCTCTTCCT			
DPex13F	TCCCATTTGGGATGAAGTGTG	127/263	60	F
DPex13R	AACTGTTGGACACAGGCACTG			
DPex14F	CTCTTCTTGATTGCATTGTGG	202/340	55	F
DPex14R	AGTTTTATGCAAACTCCCTTC			
DPex15F	TAGCACCTTGATACCTAGGTAT	227/377	60	R

DPex15R	GCCTACAAACATTTAAACCAGG			
DPex16F	CAGCATATTGTACACCTTAAAT	167/340	55	R
DPex16R	AGAAACTGTAAGGCAAGCATCT			
DPex16F	CAGCATATTGTACACCTTAAAT	167/340	55	R
DPex16R	AGAAACTGTAAGGCAAGCATCT			
DPex17F	GTGAGAGGCAAATCTTCACAGA	139/270	55	F
DPex17R	TGGGAGCTCAGATCTGAATTAG			
DPex18F	AGTGTAGCATACAATGGGAGAA	194/319	55	R
DPex18R	GACATTATCTTGTGAACAACCA			
DPex19F	TCAAGTGAATTTCTGGGTGA	163/386	55	F
DPex19R	AAGCCTTCACAAAATGGGTT			
DPex20F	AAGGGTACAAATAACAGTGGTA	84/246	52	F
Dpex20R	ATCAGCAAGTCATGCAGTTAAT			
DPex21F	GTGGAACTGTAGCTGTTAGTGA	108/265	55	F
DPex21R	GAAAAGGGAAGAGGCAGGAGAC			
DPex22F	ATCGGTCAAATTACATAGGACT	99/257	48	F
DPex22R	CCAAATCCATGTTATAATGTGG			
DPex23.1F	CTTCTTTCTTGGAATGTGAGGT	2295/420	55	F
DPex23.1R	ACATTGCCTTGCTTTCTGCAGT			
DPex23.2F	GACCAACAGAAGAATGACTATG	2295/381	60	F
DPex23.2R	CTGCTCAGTGGCCTGCAAGAT			
DPex23.3F	GGATGAAATTGTCAGGCTCAA	2295/415	58	F
DPex23.3R	TATCCTCTTCCTTCTGCATGG			
DPex23.4F	ACCAAGACCACCATCCACCAG	2295/416	55	F
DPex23.4R	TGGACCCTTTGTAATCTCGCG			
DPex23.5F	ACCGGAAATGCCTGGAAGATG	2295/397	55	F
DPex23.5R	CTCTTCTTAACAATGGATGCC			
DPex23.6F	ATCACCAACCTGACCCAGCAG	2295/351	55	F
DPex23.6R	CCTCAGGTTCCGCAGTTCTTC			
DPex23.7F	CTCACAGAGAACCTGACCAAG	2295/333	58	R
DPex23.7R	GAGCACAGTTCAGATGAGATA			
DPex24.1F	GTTAAGTCGTGATAGTAATATG	3931/420	55	F
DPex24.1R	CTTGATCTCTGCTTGGAGTCTT			
DPex24.2F	GAAGAACAGTCTTAGGAGTGA	3931/409	55	F
DPex24.2R	TCCTTAGGAGAAGCAGATGCT			
DPex24.3F	CCTTCTGGGTGCAGGATCTAT	3931/466	60	F
DPex24.3R	TCGGGGATCATTCAGGGATCG			
DPex24.4F	GTAGACCCTGTGAACAGTGTC	3931/417	65	F
DPex24.4R	CGGAAGCTTCTGTTTTGTGGT			

DPex24.5F	CAAGCTGCATAGCAGGCATAT	3931/410	55	F
DPex24.5R	CTTATATGCTATGTCAACTGG			
DPex24.6F	ATTGACCCAAAGGAGAGCCAT	3931/406	55	F
DPex24.6R	CATCTGATCCCGTGATGGTTA			
DPex24.7F	TGTGAGCAGGAATGTGAATGG	3931/413	55	F
DPex24.7R	GTAATGGAGATTTTCTCCAGG			
DPex24.8F	TTGCAGCCATCTTTGACACAG	3931/416	60	F
DPex24.8R	ATCTATGAACCCCTTCCGGAT			
DPex24.9F	AGGATAAGCACCGAAGAAGC	3931/480	60	R
DPex24.9R	CTGCAAGCACCGGGATTTTCT			

3.4.1 Part 1.2 Classification of Polymorphisms

A given single nucleotide sequence change was considered a potential polymorphism under the following criteria:

1) A single nucleotide was reported to occur at a defined position (in the SNP database, Single Nucleotide Polymorphism, these are referred to as listed polymorphisms and usually have a SNP number, for example, I305F in the DP gene is a known SNP with an assigned SNP number of rs17604693.
2) If a similar sequence change was found present in 400 healthy control subjects, but the polymorphism was not listed in the literature then this could be regarded as an unreported polymorphism.
3) If the single nucleotide sequence change resulted in a third-base change that did not cause an amino-acid change (synonymous amino acid substitution) and therefore, this was a silent polymorphism.

3.4.1 Part 1.3 Desmoplakin mutations found

Desmoplakin mutations found are summarised in Table 3.4. All three mutations found were novel, as they were not reported in the literature. Two of these desmoplakin mutations resulted in sequence insertions within exon 7 (c.818-819insA) and exon 8 (c.946_947insATACGCA) of the desmoplakin gene, causing a PTC to be encountered in both mRNA transcripts formed that would result in truncation in the translated

proteins (p.Q273fsX288 and p.M316fsX324 DP). The third DP mutation resulted in single nucleotide substitution in exon 11 of desmoplakin (c.C1604T) causing a missense mutation (p.S442F). An analysis of the effect of p.S442F DP mutation on protein structure and function using SIFT, Polyphen was performed, and results of these analyses can be found in section 3.4.1 Part 1.7.

3.4.1 Part 1.4 Plakophilin-2 mutations found

Plakophilin-2 mutations found are summarised in Table 3.4. They consist of eight mutations, of which four (p.413X, p.P533fsX561, p.L586fsX658, and p.A733fsX740) were novel as they were not previously described in the literature. These four mutations resulting from gene insertion, c.1755_1756insTTGACTCA (p.L586fsX658)); deletion, c.1597_1600delATCC (p.P533fsX561); and an indel, c.2197_2202delCACACCinsG (p.A733fsX740) caused reading frameshift resulting in PTCs in mRNA transcripts formed, and a nonsense mutation, c.C1237T, p.R413X resulted in a PTC in the mRNA transcript formed. Four other PKP-2 mutations found were previously reported by Gerull and colleagues[40]. These included a frameshift mutation c.145_148delCAGA (pS50fsX110), two missense mutations c.C419T (p.S140F) and c.C1844T (p.S615F), and an intervening sequence splice acceptor site mutation c.2146-1G>C causing abnormal splicing. The splice site mutation was reported to result in the activation of cryptic splice acceptor site in intron 12 with retention of 160bp of the intron, or alternatively the activation of another cryptic splice acceptor site in exon 13 resulting in the loss of 17bp in exon 13 (see supplementary information[40]). All eight plakophilin-2 mutations discovered in the present genetic screening are illustrated in Figure 3.2 to define changes at the nucleotide and protein level.

3.4.1 Part 1.5 Identification of families for pedigree analysis

Table 3.4 also identified nine families (families A to I) in which pedigree analysis investigating mutations: p.A733fsX740 PKP-2 (families A, B, and C), p.L586fsX658 PKP-2 (family D), p.R413X PKP-2 (family E), p.S615F PKP-2 (family F), p.S140F

PKP-2 (family G), p.S50fsX110 (family H) and p.Q273fsX288 DP (family I) were performed (section 3.4.1 Part 2).

3.4.1 Part 1.6 Identification of Polymorphisms

Several polymorphisms found in the genes encoding plakoglobin, plakophilin-2, and desmoplakin are listed in Table 3.5. Some of these are listed polymorphisms, whereas others are presumed to be polymorphisms as they were also present in about 4 in 200 DNA samples obtained from normal individuals. One variant (c.C1577T, p.T526M in PKP-2) found in proband A116 has been included as a probable polymorphism as SIFT and Polyphen analysis predicted that this missense amino acid was tolerant and predicted to be benign (data not shown). The consequence of this presumed PKP-2 polymorphism in A116 on desmosomes is expected to be of minimal functional importance as an insertion desmoplakin mutation was additionally presented in this proband (Table 3.4).

Table 3.4 Mutations found in genes for DP and PKP-2

Mutations found in desmosomal genes encoding desmoplakin (DP) and plakophilin-2 (PKP-2) in a cohort of 100 ARVC cases. Families A to I identified here were examined in the second part of this study (section 3.4.2 Part 2). Highlighted in blue identifies the seven novel mutations found in DP and PKP2 genes. The asterisks denote mutations that were already reported in the literature. HGVS nomenclature was followed for assigning mutations.

Gene	Exon	Proband & (family	Mutation at nucleotide level	Mutation at protein level	Predicted Effect on Protein
DP	7	A116 (I)	c.818-819insA	**p.Q273fsX288**	Disruption of SR4 Spectrin repeat, loss off rod & C-terminus. Loss of IF aggregation
	8	A53	c.946_947insATACGCA	**p.M316fsX324**	Disruption of SR4 Spectrin repeat, loss off rod & C-terminus. Loss of IF aggregation
	11	A27 & A58	c.C1604T	**p.S442F**	Conserved Serine residue altered in SR5 Spectrin repeat
PKP-2	1	A165 (H)	c.145_148delCAGA	* p.S50fsX110	Severe N-terminus truncation with loss of all ARM repeats & C-terminus
	3	A104 (G)	c.C419T	* p.S140F	Conserved Serine residue altered in N-terminus
	5	A144 (E)	c.C1237T	**p.R413X**	ARM repeat 2 disrupted, loss of C-terminus
	7	A150	c.1597_1600delATCC	**p.P533fsX561**	ARM repeat 4 disrupted, loss of C-terminus
	8	A9 (D)	c.1755_1756insTTGACTCA	**p.L586fsX658**	ARM repeat 5 disrupted, loss of C-terminus
	9	A18 (F)	c.C1844T	* p.S615F	Conserved Serine residue altered in ARM repeat 6
	11	A48 (A), A145 (B) & A39 (C)	c.2197_2202delCACACCinsG	**p.A733fsX740**	ARM repeat 8 disrupted, loss of C-terminus
	11	A108	c.2146-1G>C, abnormal splicing	* Activated cryptic splicing in exon 13	ARM repeat 8 disrupted, truncation in the C-terminus

Table 3.5 Polymorphisms in PG, PKP-2 & DP genes

Polymorphisms found in Plakoglobin (PG), Plakophilin-2 (PKP-2) and Desmoplakin (DP) in a cohort of 100 ARVC patients. The nomenclature for splice site polymorphisms uses the + sign to describe donor splice site and the – sign to describe acceptor splice site polymorphisms. Abbreviation: dup = duplicated nucleotide and IVS = intron or intervening non-coding sequence flanking two exon sequences (for example, IVS 11 is the intervening sequence immediately following exon 11 and located between exons 11 and 12.

Gene	Exon/ Intron	Proband	Sequence altered at the nucleotide level/Protein level	Comments
PG	3	A3, A32, A58, A62, A128 & A152	c.C425A/p.R142H	Variant present in six probands
PKP-2	7	A116	c.C1577T/p.T526M	Variant predicted tolerant and benign by SIFT & Polyphen
	8	A22	c.G1772T/p.R591I	Seen in ~ 4/200 normal control samples
	IVS7	A142	c.1689-8dupT	Seen in ~ 4/200 normal control samples
	9	A145	c.T1941G/p.C647W	Seen in ~ 4/200 normal control samples
	IVS11	A103	c.2299+14A>C	Seen in ~ 4/200 normal control samples
	IVS11	A144	c.2299+7C>T	Seen in ~ 4/200 normal control samples
DP	1	A138, A11, A144	c.G384A/p.G35G	Synonymous polymorphism
		A32, A11, A152, A19.3	c.T405C /p.Y42Y	Known SNP: rs36087964
	7	A35.6, A32, A137, A109, A19	c.A1192T/p.I305F	Known SNP: rs17604693

Figure 3.2 Schematic illustration of PKP-2 mutations

The PKP-2 gene structure shows open boxes representing untranslated 3' and 5' regions of the gene, the filled boxes representing fourteen exons, and the horizontal line between two exons representing an intron. The vertical lines mark the positions of eight gene mutations found with affected nucleotide numbering indicated by text in black. Corresponding protein changes are shown in green with underlining indicating the four novel mutations identified. The protein structure of plakophilin-2 was previously discussed (section 1.8.3, Figure 1.11), the location of c.C419T and c.2179_2201delCACACCinsG gene mutations on the PKP-2 protein (p.S140F and p.A733fsX740 PKP-2) are identified in blue, and the predicted effect of these mutations on the protein are shown in Table 3.4. A733fsX740 and S140F PKP-2 proteins expressions obtained in cellular systems determined their functional consequences (Chapters 4, and 5) *in vitro*.

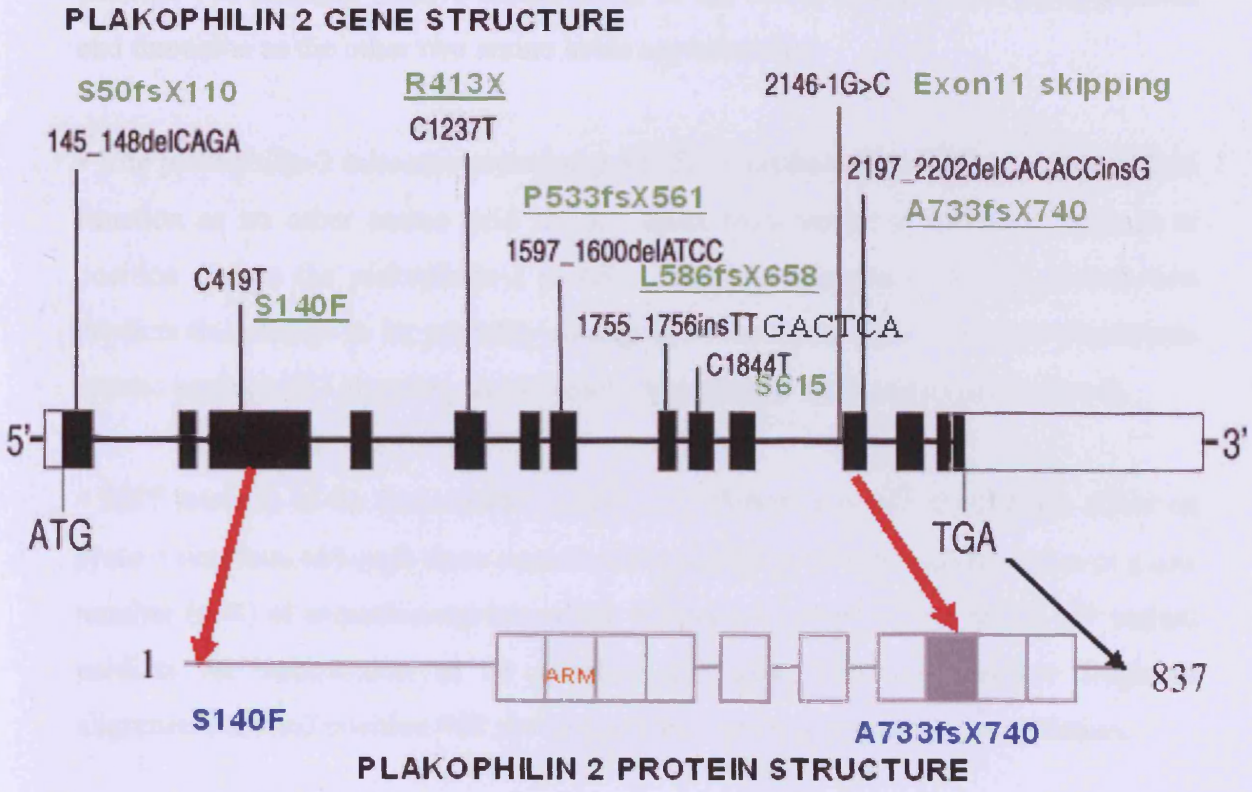

3.4.1 Part 1.7 Russel, SIFT, AND POLYPHEN analysis of missense PKP-2 and DP mutations found

Out of the eleven mutations found in the genetic screening of the ARVC cohort (Table 3.4), three of these were missense mutations: p.S140F PKP-2 (c.C419T), p.S615F PKP-2 (c.C1844T), and p.S442F DP (c.C1604T). In all three mutations, a serine amino acid residue substitution with a phenylalanine amino acid residue

occurred. Russell analysis (http://www.russell.embl-heidelberg.de/aas/) of a serine to phenylalanine change indicates that this results in substitution of a polar sulphur containing amino acid with an aromatic hydrophobic amino acid; hence, the substituted phenylalanine residue has a different physicochemical property from the serine residue and this is predicted to be a disfavoured substitution. The predicted effects of these three missense mutations were analysed using SIFT and Polyphen analysis (pages 140-146)

- For the plakophilin-2 missense mutation p.S140F, SIFT predicts that this amino acid substitution should be tolerant with a score of 0.13. Polyphen analysis of S140F PKP-2 substitution predicts this to be benign, with the multiple fragment alignments around position 140 showing relative conservation of the serine residue (with phenylalanine and threonine as the other two amino acids represented).

- The plakophilin-2 missense mutation p.S615F is predicted by SIFT to affect protein function as no other amino acid residue apart from serine is predicted tolerant at position 615 in the plakophilin-2 protein. Polyphen analysis of S615F substitution predicts this change to be probably damaging, with the multiple fragment alignments around position 615 showing an extremely high degree of sequence conservation.

- SIFT analysis of the desmoplakin missense mutation, p.S442F predicts an affect on protein function, although there was a lower confidence in this prediction due to a low number (n=4) of sequence representation. Polyphen analysis of the S442F DP variant predicts the substitution to be possibly damaging with the multiple fragment alignments around position 442 showing a high degree of sequence conservation.

SIFT & Polyphen predictions for S140F PKP-2, S615PKP-2 and S442F DP

Analysis to determine whether plakophilin-2 missense mutations S140F and S615F and desmoplakin mutation S442F are tolerated or not tolerated according to the protein prediction algorithm SIFT (Sorting Intolerant From Tolerant)

Web-site link: http://blocks.fhcrc.org/sift/SIFT.html

SIFT results

Predictions for S140F PKP-2

Substitution at position 140 from S to F is predicted TOLERANT with a score of 0.13.
Median sequence conservation: 3.42
Sequences represented at this position: 11

Predict Not Tolerated	Position	Seq Rep	Predict Tolerated
w	140S	0.61	c m h y i F l p v r g q n k e D A T S

Predictions for S615F PKP-2

Substitution at position 615 from S to F is predicted to AFFECT PROTEIN FUNCTION with a score of 0.00.
Median sequence conservation: 3.02
Sequences represented at this position:17

Predict Not Tolerated	Position	Seq Rep	Predict Tolerated
y w v t r q p n m l k i h g f e d c a	615S	0.94	S

Predictions for S442F DP

Substitution at position 442 from S to F is predicted to AFFECT PROTEIN FUNCTION with a score of 0.00.
Median sequence conservation: 4.32
Sequences represented at this position: 4
WARNING!! This substitution may have been predicted to affect function just because the sequences used were not diverse enough. **There is LOW CONFIDENCE in this prediction.**

Predict Not Tolerated	Position	Seq Rep	Predict Tolerated
y w v t r q p n m l k i h g f e d c a	442S	0.67	S

POLYPHEN prediction for S140F PKP-2

Acc number	Position	AA 1	AA 2	Description
148664226	140	S	F	plakophilin 2 isoform 2b [Homo sapiens]

This variant is predicted to be benign

Prediction	Available data	Prediction basis	Substitution effect	Prediction data
benign	alignment	alignment	N/A	PSIC score difference: 0.045

PSIC profile scores for two amino acid variants

Score1	Score2	|Score1-Score2|	Observations	Diagnostics
+0.801	+0.756	**0.045**	9	calculated

Multiple alignment around substitution position

Sequences: all Flanks: 25 Show alignment

Mapping of the substitution site to known protein 3D structures

Database	Initial number of structures	Number of structures
PQS	56	0

Fragment of multiple alignments around PKP-2 position 140:

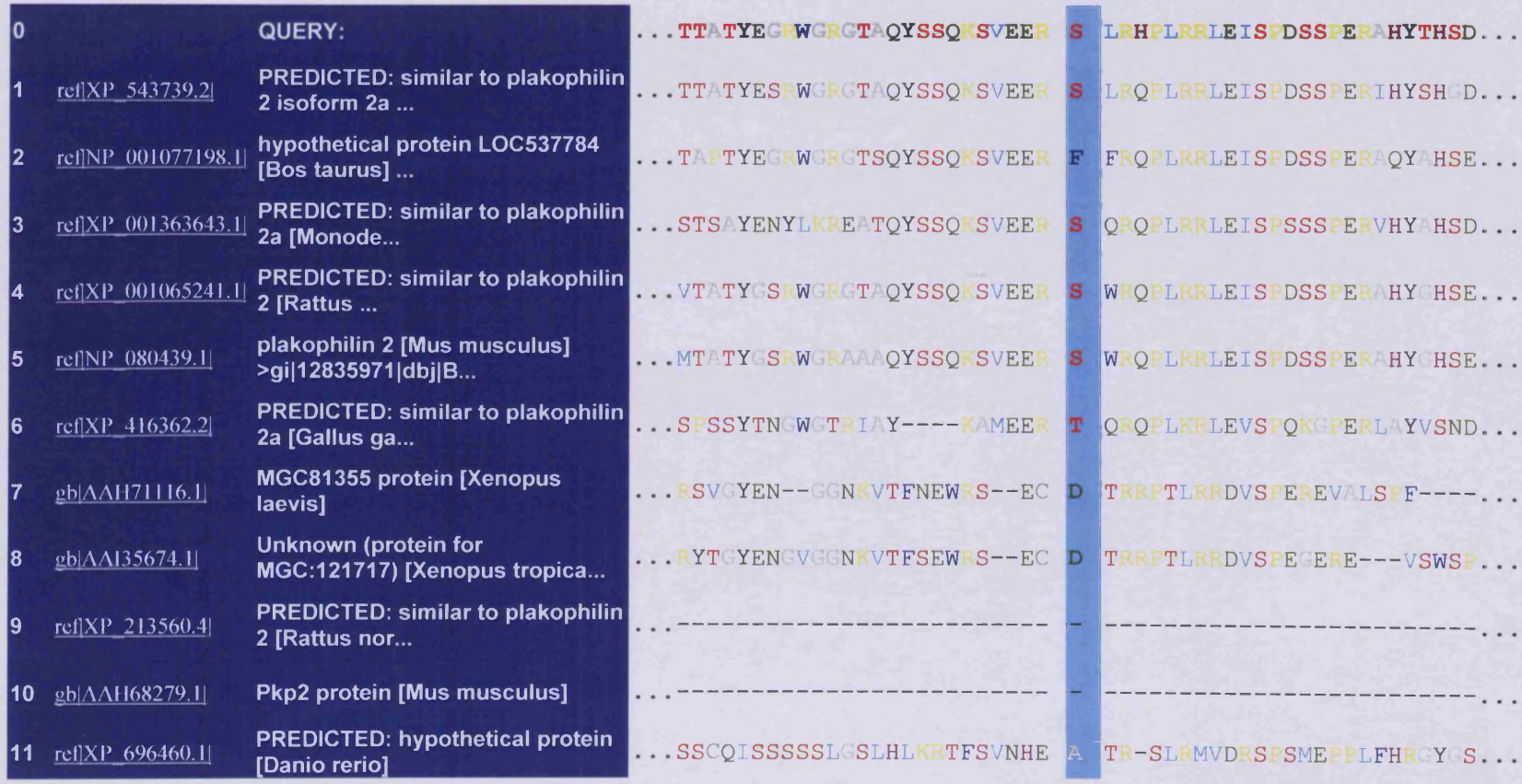

POLYPHEN prediction for S615F PKP-2

Acc number	Position	AA 1	AA 2	Description
148664226	615	S	F	plakophilin 2 isoform 2b [Homo sapiens]

Prediction

This variant is predicted to be probably damaging

Prediction	Available data	Prediction basis	Substitution effect	Prediction data
probably damaging	alignment	alignment	N/A	PSIC score difference: 2.149

PSIC profile scores for two amino acid variants

Score1	Score2	|Score1-Score2|	Observations	Diagnostics
+1.525	-0.624	**2.149**	11	calculated

Multiple alignment around substitution position

Sequences: all Flanks: 25 Show alignment

Mapping of the substitution site to known protein 3D structures

Database	Initial number of structures	Number of structures
PQS	56	0

Fragment of multiple alignments around PKP-2 position 615:

POLYPHEN prediction for S442F DP

Acc number	Position	AA 1	AA 2	Description
P15924	442	S	F	Desmoplakin (DP) (250/210 KD paraneoplastic pemphigus antigen). LENGTH: 2871 AA

Prediction

This variant is predicted to be possibly damaging

Details

Sequence features of the substitution site

Region	Site	Feature table	Critical sites
N/A	N/A	show FT fields for P15924	2480

Prediction	Available data	Prediction basis	Substitution effect	Prediction data
possibly damaging	FT alignment	alignment	N/A	PSIC score difference: 1.773

PSIC profile scores for two amino acid variants

Score1	Score2	|Score1-Score2|	Observations	Diagnostics
+1.245	-0.528	1.773	9	Pre-computed

Multiple alignment around substitution position

Sequences: all Flanks: 25 Show alignment

Mapping of the substitution site to known protein 3D structures

Database	Initial number of structures	Number of structures
PQS	56	0

Fragment of multiple alignments around DP position 442:

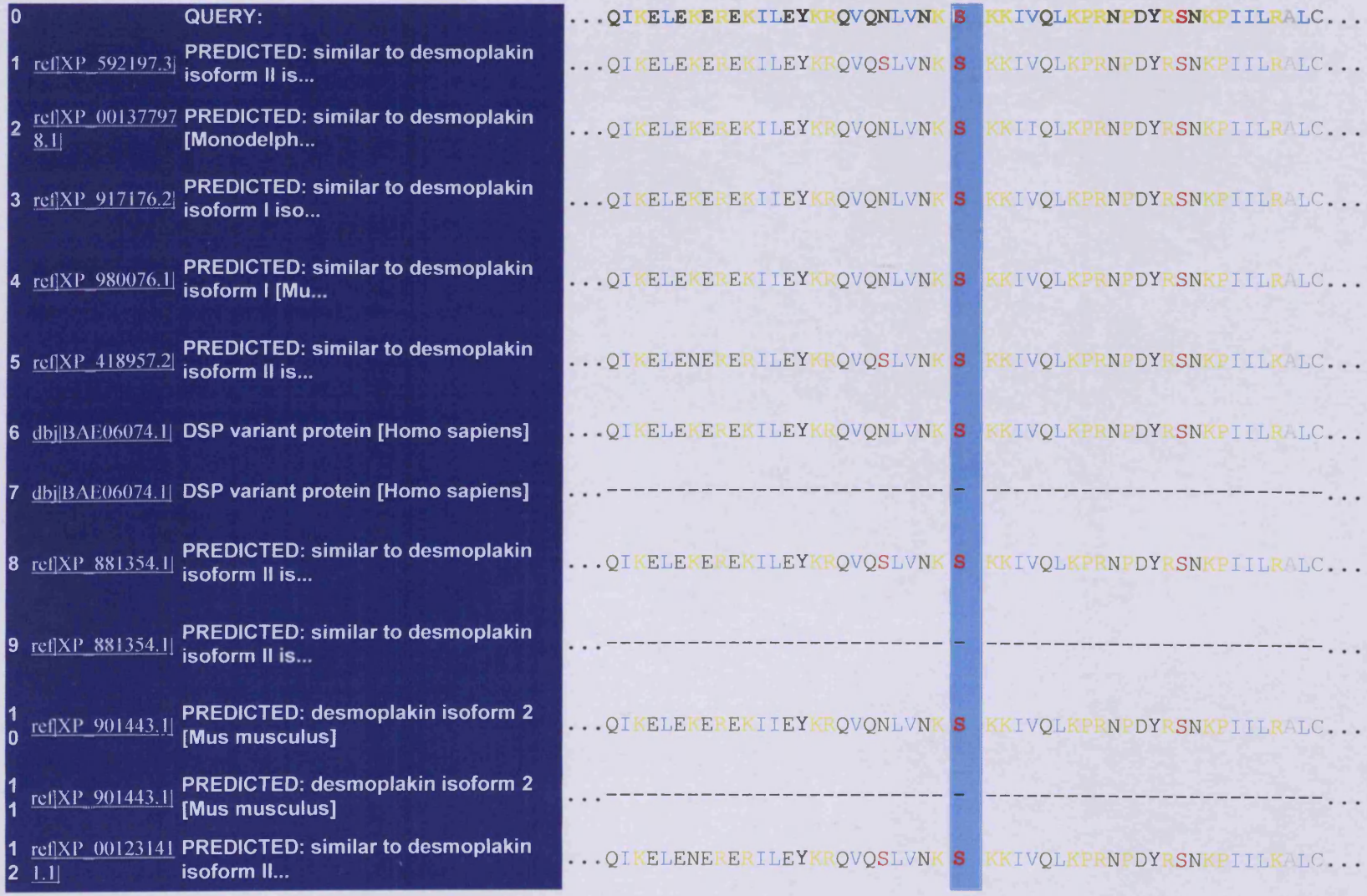

3.4.1 Part 1.8a Effect of S140F PKP2 on predicted binding of SR protein (SC35) to ESE motif

Accurate removal of introns from pre-mRNA requires multiple cis-elements, including the splice sites, poly pyrimidine tract, branch site, and other intronic and exonic sequences that have a positive or negative effect on splicing. Positive-acting sequences termed exonic splicing elements (ESE) are identified in exons associated with regulated splicing. These exons are typically adjacent to introns with weak intronic splicing signals and require ESEs for their inclusion. Deletion of an ESE often causes exon skipping, or in the case of terminal exon, suppresses removal of the last intron.

The effect of the missense plakophilin-2 mutation (p.S140F, c.C419T in exon 3) was checked to establish whether this mutation affected a potential exonic splicing enhancer-binding site. The entire wild type PKP-2 exon 3 and that of the mutant nucleotide sequences (WT: TCC, mutant: TTC) were analysed using a web-based program, (http://rulai.cshl.edu/cgi-bin/tools/ESE3/esefinder.cgi?process=home), ESE finder which predicts ESE motifs recognised by five known SR proteins (SF2/ASF, SF2/ASF (IgMBRCA1), SC35, SRp40 and SRp55). The program assigns a threshold matrix score for each motif that is recognised by a single SR protein and the predicted recognition score of each motif in the submitted sequence. The threshold is a value above which a score for a given sequence is considered to significant (high score motifs). A high score value implies recognition by an ESE element by the respective SR protein, but the presence of a high score motif in a sequence does not necessarily identify that sequence as an ESE in the native context as a nearby silencer element may prevent the SR protein from binding. Using the ESE finder program, the wild type nucleotide sequence around Serine residue number 140 was predicted to contain a high score motif (value = 4.15371) recognised by human SC35 protein under normal splicing condition based on the consensus sequence GRYYcSYR (see next page). The exon 3 nucleotide sequence encoding the S140F mutation site was also assigned a high score value of 3.92287 for recognition by human SC35 protein.

ESE finder prediction of SC35 protein motif at the site of S140F PKP-2 mutation

Wild type nucleotide sequence of exon 3 and mutant exon 3 sequence encoding the S140F mutation were analysed using a web-based program, ESE finder. The URL for this program is http://rulai.cshl.edu/cgi-bin/tools/ESE3/esefinder.cgi?process=home

Data shown below were obtained from ESE finder using input sequences as above.

Human SC35 protein binding to consensus motif threshold value = 2.383

Wild Type exon 3 sequence

Position*/Motif recognition Site/Score

80 (-619)/GG**TCC**TTG /4.15371 (TCC is the codon for Serine residue no. 140).

Mutant S140F exon 3 sequence

Position*/Motif recognition Site/Score

80 (-619)/GG**TTC**TTG/3.92287 (TTC is the codon for Phenylalanine residue)

The current weighted matrix values (release 3.0) and the consensus motifs obtained with sc35 SR protein is shown below; the height of each letter reflects the frequency of each nucleotide at a given position, after adjusting for background nucleotide composition. At each position, the nucleotides are shown from top to bottom in order of decreasing frequency; orange letters indicate above-background frequencies.

* Both positions from 5'end (through 1) and 3'end (through -1) are given

Protein

SC35

Matrix

	[1]	[2]	[3]	[4]	[5]	[6]	[7]	[8]
A	-0.88	0.09	-0.06	-1.58	0.09	-0.41	-0.06	0.23
C	-1.16	-1.58	0.95	1.11	0.56	0.86	0.32	-1.58
G	0.87	0.45	-1.36	-1.58	-0.33	-0.05	-1.36	0.68
T	-1.18	-0.2	0.38	0.88	-0.2	-0.86	0.96	-1.58

Logo

CONCENSUS sequence:

GRYYcSYR

Threshold

2.383

3.4.1 Part 1.8b Effect of S140F PKP2 on predicted phosphorylation of serine residues

The prediction of potential phosphorylation sites on serine, threonine and tyrosine amino acid residues in plakophilin-2 protein was performed using a bioinformatics approach using a program, NetPhos2 (http://www.cbs.dtu.dk/services/NetPhos/). Phosphorylation prediction sites only on serine residues were examined as PKP-2 mutations in genetic screening affecting only serine residues (p.S140F and p.S615F) were encountered. The result of NetPhos analysis shown in Table 3.6 lists all serine residues (with a score >0.85) which are predicted as putative phosphorylation sites. NetPhos predictions in Table 3.6 shows that there is a clustering of putative phosphorylation sites around residue 140 highlighted in red. Serine residue 140 in PKP-2 protein is predicted a potential phosphorylation site with a score of 0.873. Other Serine residues in close proximity of serine 140 were also predicted to be potentially phosphorylated (for example serine residues 132, 135 and 151 and 154 are all high score putative phosphorylation site predictions). Serine residue at position 615 was not predicted by NetPhos to be a potential phosphorylation site, whilst a serine residue at position 82 reported to be phosphorylated was correctly identified as a potential phosphorylation site by NetPhos.

3.4.1 Part 1.9 Electropherograms of mutations found

The wild type and mutant DNA sequence electropherograms of three DP mutations and eight PKP-2 mutations are depicted in Figures 3.3-3.13. In each figure, the relevant part of the electropherogram shows in the top part the normal sequence derived from unaffected normal controls and the bottom part identifies the probands displaying genetic defect with the arrowhead underneath each mutant sequence marking the point where nucleotide sequence change begins. All sequences shown are obtained from the forward sequencing direction and nucleotide numbering are derived relative to the numbering in the reference sequences in accession numbers: plakophilin-2, NM_004572.2; plakoglobin, NM_002230; and desmoplakin, NM_004415 with the first Adenine residue in the ATG initiation codon designated position.

Table 3.6 NetPhos predictions for phosphorylation of Serine residues in PKP-2

All serine residue that are predicted to be putative phosphorylation sites with a score of >0.85 are included. Serine residue number 615 in plakophilin-2 substituted by phenylalanine in a PKP-2 mutation studied in family F (Figure 3.15) was not predicted to be a putative phosphorylation site. Serine residue number 140 was predicted to be a potential phosphorylation site, shown highlighted in red.

Sequence	Serine residue No	Context	Score	Prediction *S* = putative phosphorylation
gi_14866422	44	LAGSSGRGG	0.866	*S*
gi_14866422	53	QTVKSLRIQ	0.929	*S*
gi_14866422	71	KGRSSVGNG	0.996	*S*
gi_14866422	82	HRTSSVPEY	0.981	*S*
gi_14866422	132	AQYSSQKSV	0.982	*S*
gi_14866422	135	SSQKSVEER	0.997	*S*
gi_14866422	140	VEERSLRHP	0.873	*S*
gi_14866422	151	RLEISPDSS	0.981	*S*
gi_14866422	154	ISPDSSPER	0.964	*S*
gi_14866422	155	SPDSSPERA	0.997	*S*
gi_14866422	225	YQHGSVSDT	0.980	*S*
gi_14866422	286	QNRASRSSW	0.992	*S*
gi_14866422	289	ASRSSWHQS	0.997	*S*
gi_14866422	297	SSFHSTRTL	0.923	*S*
gi_14866422	313	AVDSSGRRA	0.935	*S*
gi_14866422	358	ERAVSMLEA	0.995	*S*
gi_14866422	693	LIAKSVRNY	0.968	*S*
gi_14866422	744	VGDPSVKKT	0.973	*S*
gi_14866422	826	IMAISAGDA	0.968	*S*
gi_14866422	833	DAYASNKAS	0.967	*S*
gi_14866422	878	KAYHSLKD-	0.997	*S*

3.4.1 Part 1.9a Desmoplakin mutations

Figure 3.3 Desmoplakin Mutation: p.Q273fsX288

Wild Type DP Exon 7 sequence

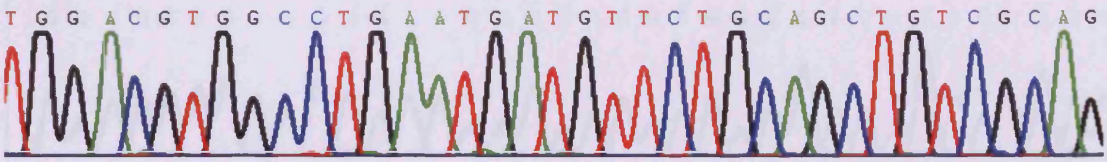

A116 Mutant DP exon 7 sequence: c.818-819het_insA,

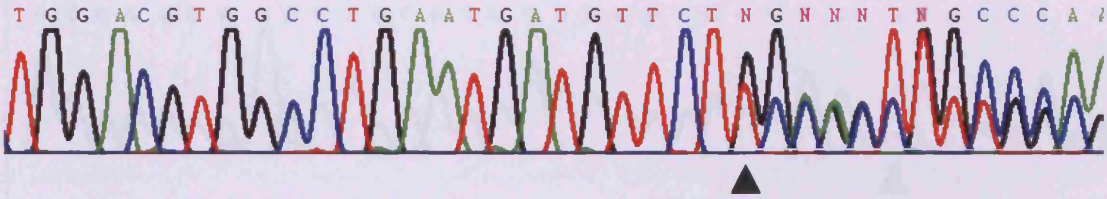

Figure 3.4 Desmoplakin Mutation: p.M316fsX324

Wild type DP Exon 8 sequence

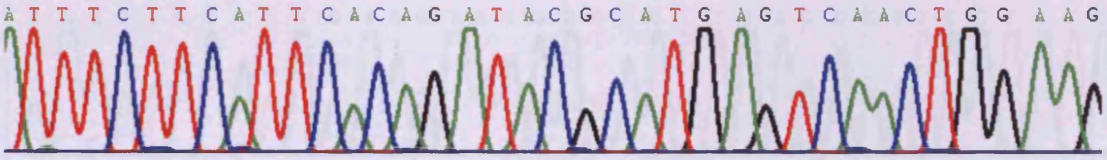

A53 Mutant DP Exon 8 sequence: c.946_947het_insATACGCA

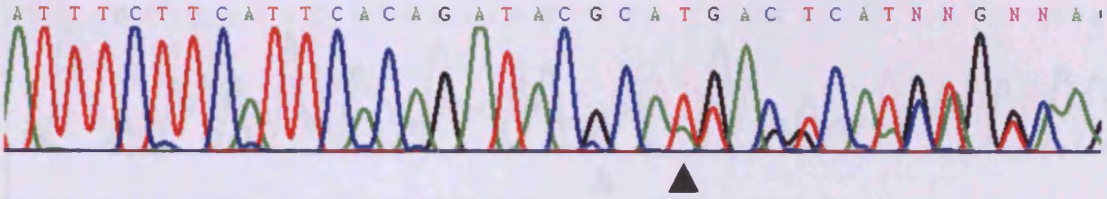

Figure 3.5 Desmoplakin Mutation: p.S442F

Wild Type DP Exon 11 sequence

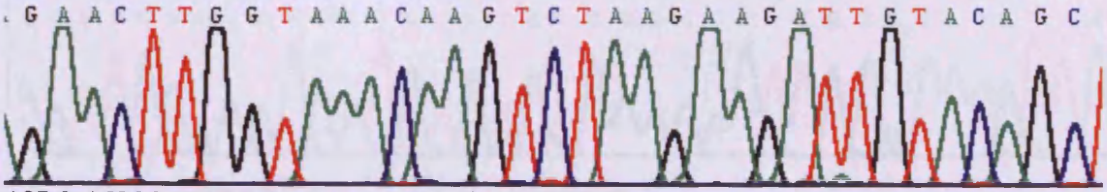

A27 & A58 Mutant DP Exon 11 sequence: het _c.C1604T

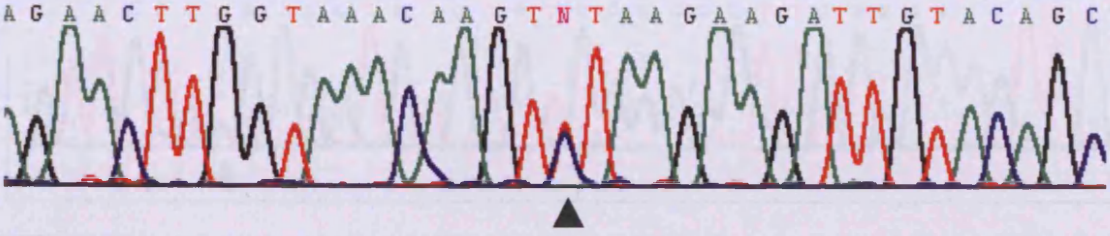

3.4.1 Part 1.9b Plakophilin-2 mutations

Figure 3.6 Plakophilin-2 Mutation: p.S50fsX110

Wild type PKP2 Exon 1 sequence

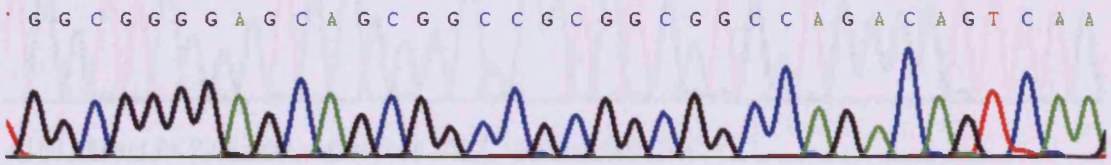

A165 Mutant PKP2 Exon 1 sequence: c.145_148het_delCAGA

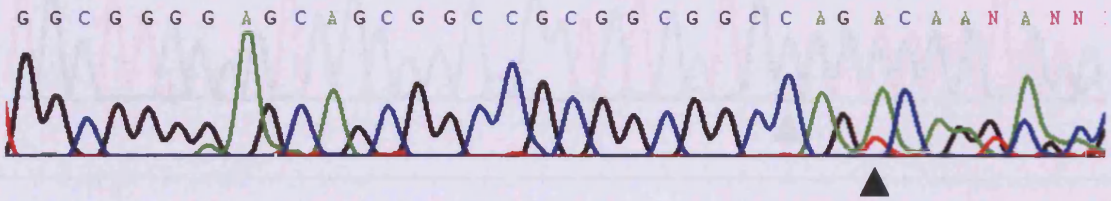

Figure 3.7 Plakophilin-2 Mutation: p.S140F

Wild Type PKP2 Exon 3 sequence

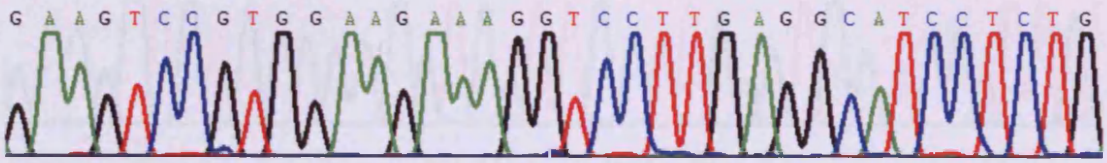

A104 Mutant PKP2 Exon 3 sequence: het_c.C419T

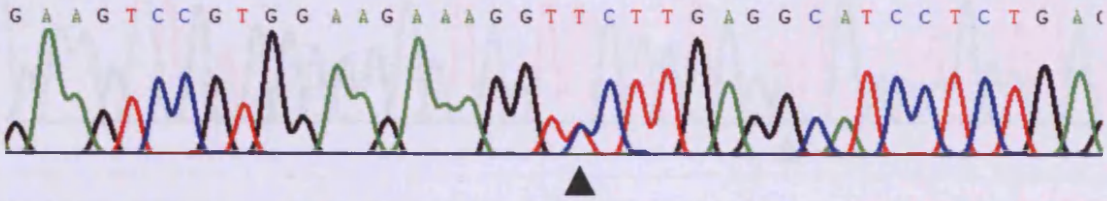

Figure 3.8 Plakophilin-2 Mutation: p.R413X

Wild Type PKP2 Exon 5 sequence

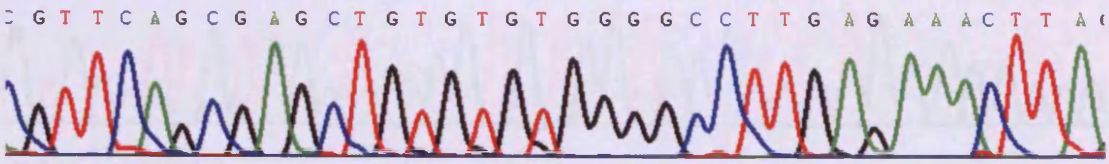

A144 Mutant PKP2 Exon 5 sequence: het_c.C1237T

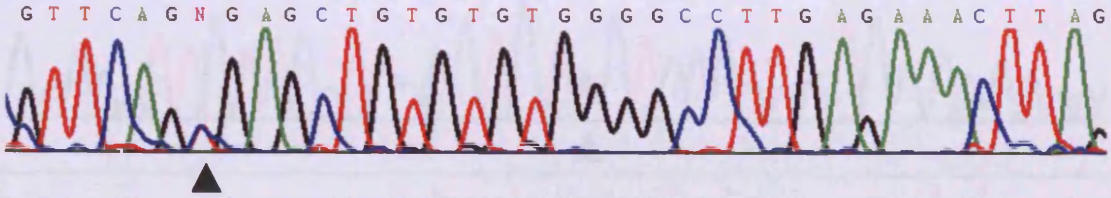

Figure 3.9 Plakophilin-2 Mutation: p.P533fsX561

Wild Type PKP2 Exon7 sequence

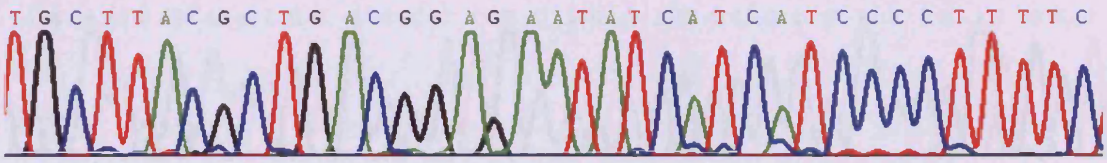

A150 Mutant PKP2 Exon7 sequence: c.1597_1600het_delATCC

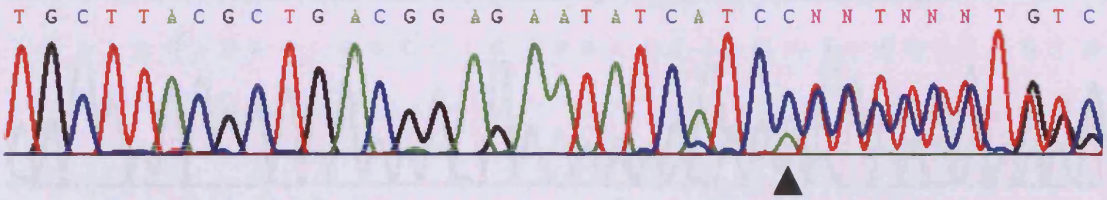

Figure 3.10 Plakophilin-2 Mutation: pL586fsX658

Wild Type PKP2 Exon8 sequence

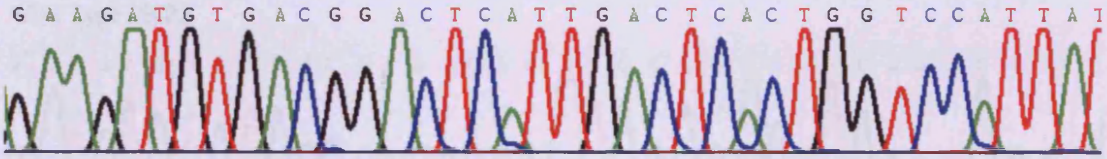

A9 Mutant PKP2 Exon 8 sequence: c.1755_1756het_insTTGACTCA

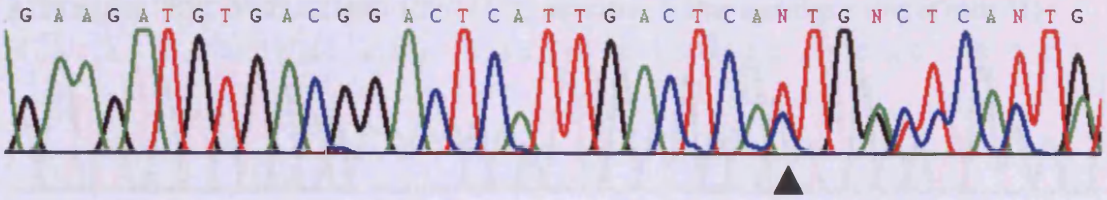

Figure 3.11 Plakophilin-2 Mutation: p.S615F

Wild Type PKP2 Exon 9 sequence

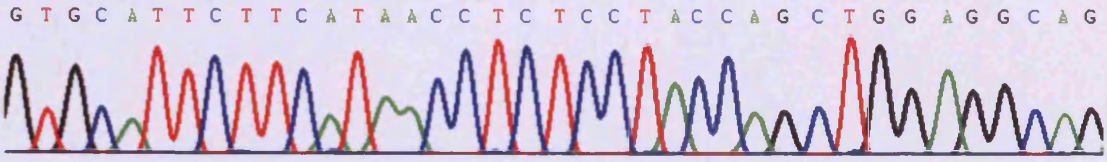

A18 Mutant PKP2 Exon 9 sequence: het_c.C1844T

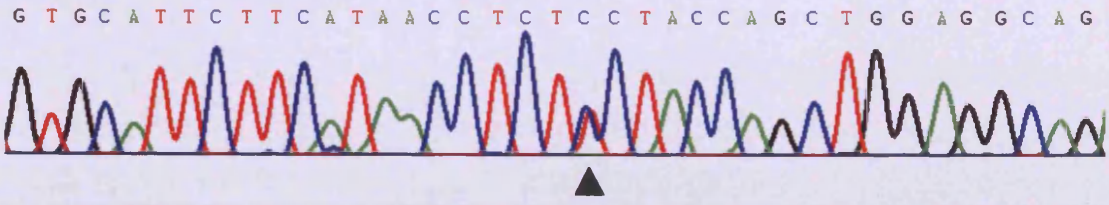

Figure 3.12 Plakophilin-2 Mutation: p.A733fsX740

Wild Type PKP2 Exon 11 sequence

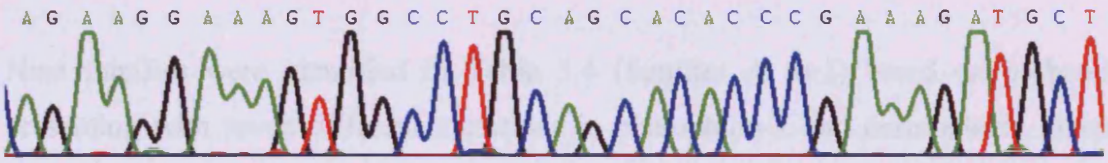

A48, A145 & A39 Mutant PKP2 Exon 11 sequence: c.2197_2202het_delCACACCinsG

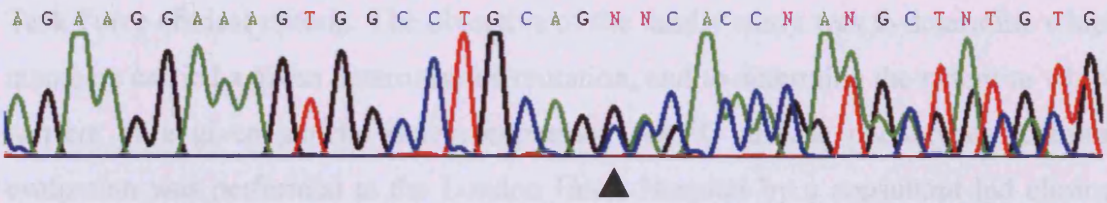

Figure 3.13 Plakophilin-2 Mutation: Abnormal splice acceptor site (Exon 11 skipping)

Wild Type PKP2

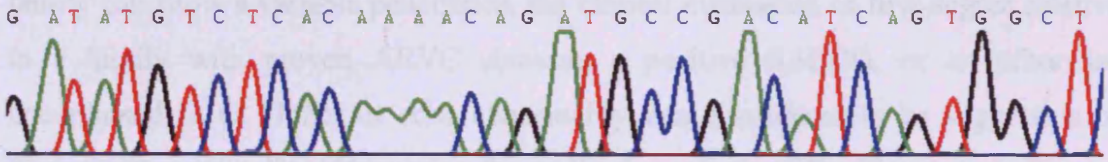

A108 mutant PKP2 IVS10 c.2146G-1G>C (ATG immediately after mutation = start of exon 11)

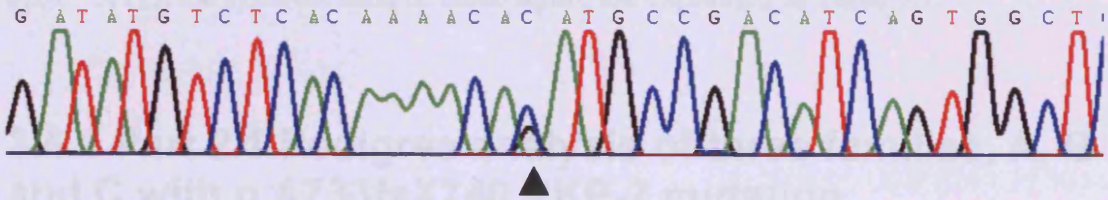

3.4.1 Part 2: Pedigree Analysis (Single family genetic and clinical analysis)

Nine families were identified in Table 3.4 (families A to I) based on probands presenting with seven different mutations in plakophilin-2 and desmoplakin genes. These families consented for pedigree analysis and individuals in each family were evaluated by genetic screening (which was performed by myself) and by modified and Task Force clinical criteria. The objective of the family study was to determine which members carried a given heterozygous mutation, and to determine the extent to which carriers of a given genetic defect expressed ARVC disease phenotypes. Clinical evaluation was performed at the London Heart Hospital by a consultant led clinical team, this included family history, SAECG with a 40Hz filter, transthoracic echo, contrast echo (where appropriate), 12-lead ECG, 24-hour ambulatory ECG, and in some cases cardiac magnetic resonance imaging. As the disease expression within a family can show a variable penetrance, the clinical evaluation of first-degree relative in a family with proven ARVC showing a positive SAECG, or an otherwise unexplained ECG, Holter or echo abnormality was considered to be suggestive of disease expression. For interpreting the pedigree analysis of families A to I (Figures 3.14 – 3.17), the symbols used in those figure are explained in Table 3.7.

3.4.1 Part 2.1 Pedigree analysis of three families, A, B and C with p.A733fsX740 PKP-2 mutation

The Plakophilin-2 mutation, p.A733fsX740 was found in three unrelated families (families A, B, and C, Figure 3.14):

• Family A was a very large Scottish family consisting of one hundred and forty five individuals, only the relevant part of the pedigree is illustrated (family A, Figure 3.14). This shows that the genetic defect was detected in five individuals, showing an autosomal dominant inheritance pattern through three generations with six individuals clinically affected by ARVC. The proband III:2 died suddenly with no previous cardiac history; ARVC was only confirmed on post-mortem. The proband's brother III:1 presented with recurrent ventricular tachycardia but ARVC was only confirmed

after the proband's death. Out of a possible thirteen immediate family members consenting to evaluation, three (III:4, III:6 and IV:3) fulfilled clinical diagnostic criteria and were confirmed to carry the mutation. Three family members (III:3, III:9 & III:10) did not fulfil Task Force Criteria, but aroused suspicion of incomplete ARVC penetration based on the following observations: precordial T-wave inversion (III:3), mild RV enlargement on echo (III:9), and >1000 ectopic beats on 24-hour Holter monitoring (III:10). All of these three individuals fulfilled modified criteria, but only III:3 carried the c.2197_2202delCACACCinsG genetic defect.

- In family B, the p.A733fsX740 PKP-2 mutation was detected in the proband III:1 who died suddenly at twenty-one years of age. With six of the immediate family consenting to genetic screening, only his mother, II:2 carried the heterozygous c.2197_2202delCACACCinsG genetic defect, but she only fulfilled the modified ARVC criteria with an abnormal T-wave inversion in V1-V3 on ECG.

- In family C, the p.A733fsX740 PKP2 mutation was detected in the proband III:1 who died suddenly at fifteen years of age, he had previously presented with syncope at seven years of age and a clinical diagnosis of ARVC was confirmed at eight years. Out of the ten possible immediate family members spanning through three generations, only three (II:1, II:2 and II:2) were available and gave consent to evaluation. None had evidence of clinical ARVC disease expression. However, a first-degree relative of the proband, III:3 had previously died suddenly and she was found to have fibroelastosis on post-mortem examination. DNA sample was available only from the proband, which was found to carry the c.2197_2202delCACACCinsG genetic defect in PKP-2.

Table 3.7 – Explanation of symbols used in Pedigree Analysis

Symbols used in pedigree analysis of families A to I (Figures 3.14 – 3.17) are explained below

Symbol	Explanation
Square	Males
Circle	Females
Solid symbol	Meeting Task Force Criteria or confirmed affected at Post-Mortem
Grey symbol	Deceased individual who did not undergo clinical evaluation and was considered probably affected due to sudden death (<40yrs), or by their position in the pedigree as an obligate gene carrier
Shaded symbol	Meeting only the Modified Criteria
Dotted symbol	Mutation Carrier not fulfilling ARVC diagnostic Criteria
Open symbol	Unaffected by ARVC
Underlined Roman numeral	Individual undergoing clinical evaluation
Slanted bar symbol	Deceased individual
+ symbol	Carrier of the gene mutation
- symbol	Individual free of the gene mutation
Arrow symbol	Index case or Proband

Figure 3.14 Pedigree analysis examining p. A733fsX740 PKP-2 (families A, B, & C)

Transmission of PKP-2 gene mutation c.2197_2202_delCACACC_insG was examined in three separate families A, B, and C. Symbols are explained in Table 3.7.

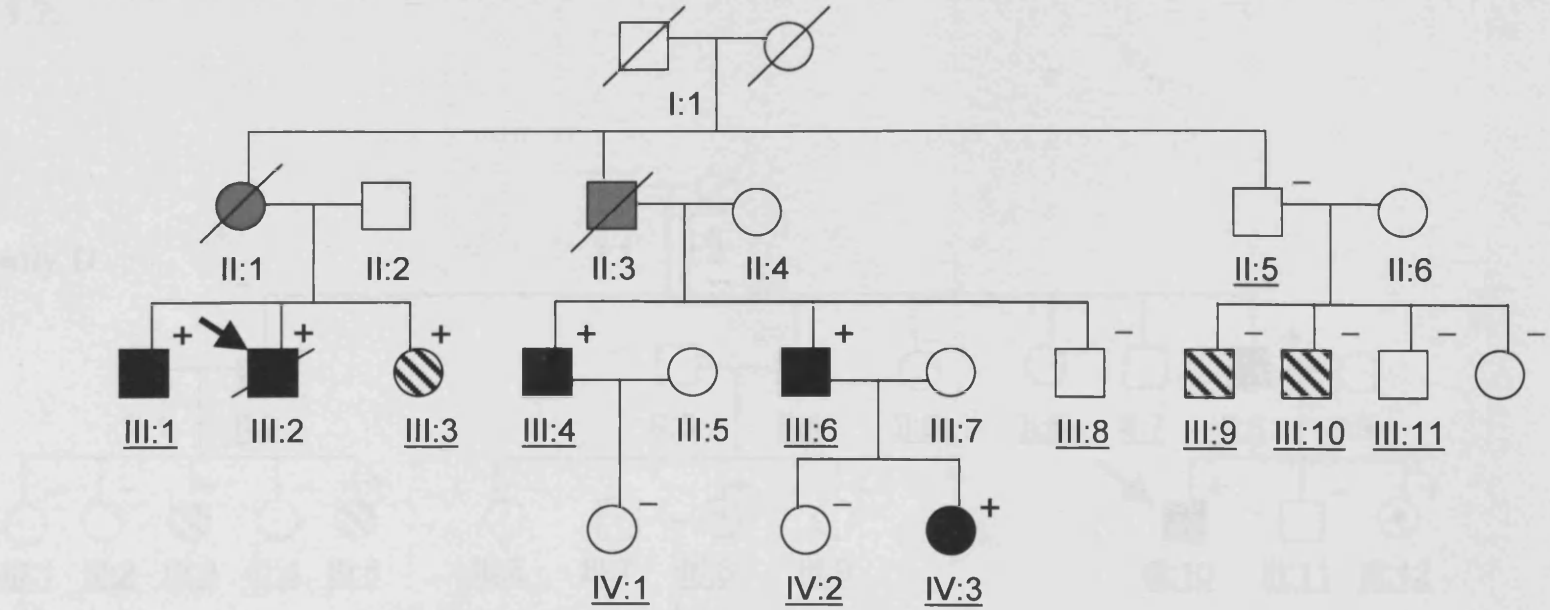

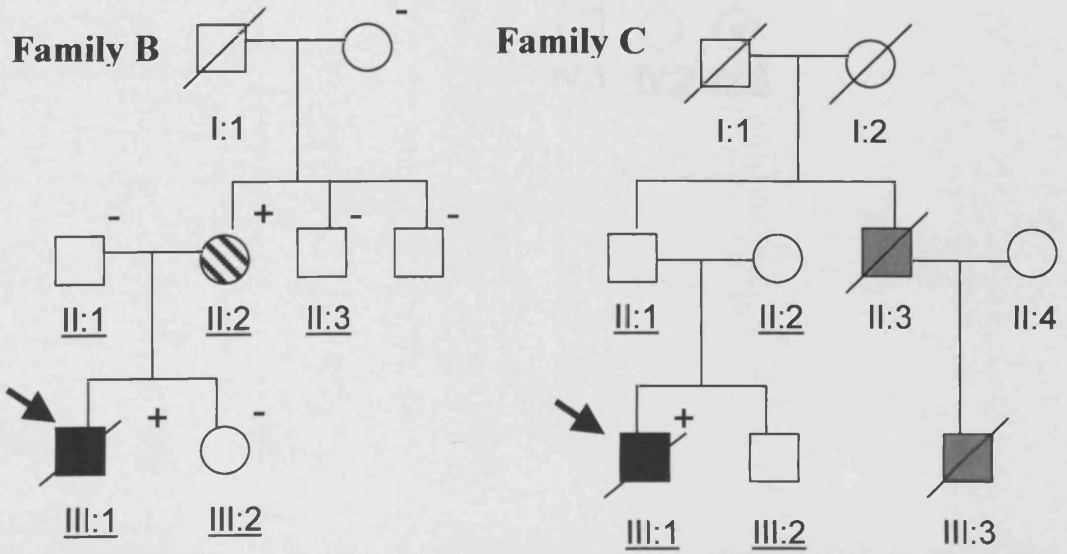

Figure 3.15 Pedigree analysis examining p.L586fsX658 PKP-2 (family D)

Transmission of PKP-2 gene mutation c.1755_1756_insTTGACTCA was examined in family D. Symbols are explained in Table 3.7.

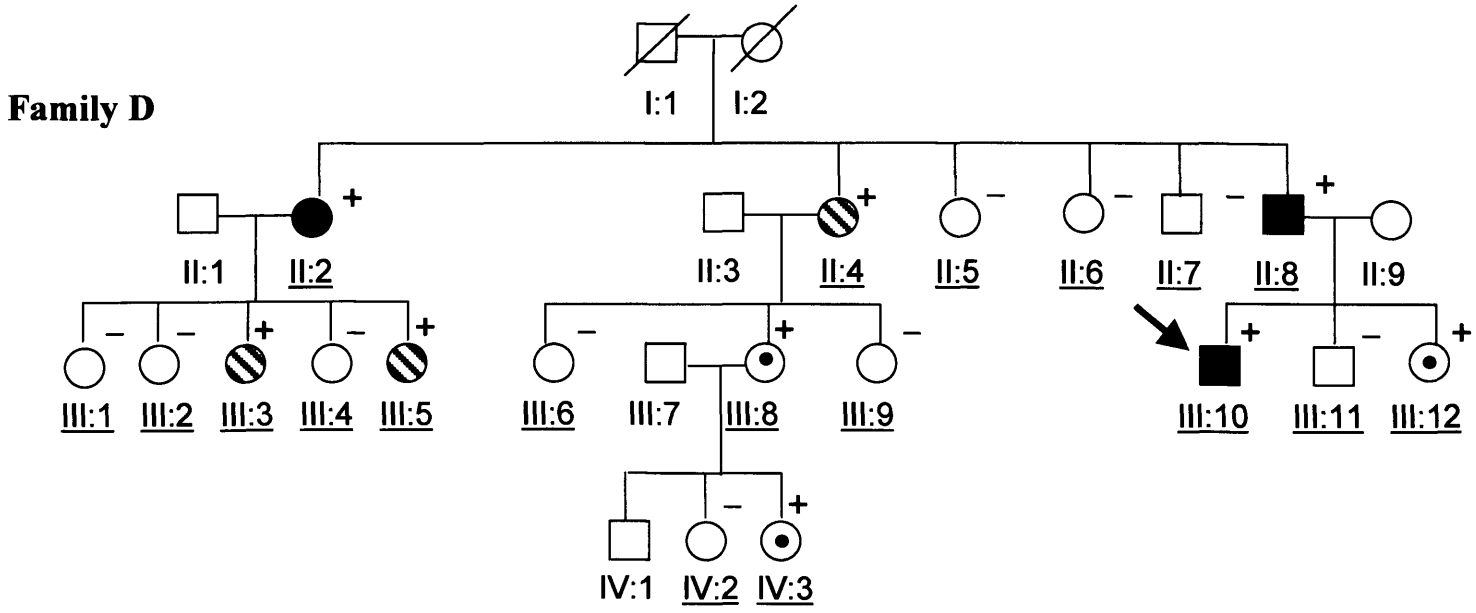

Figure 3.16 Pedigree analysis examining p.R413X, p.S615F, p.S140F, and p.S50fsX110 PKP-2 (families E, F, G, and H respectively)

Transmission of PKP-2 gene mutations: c.C1237T, c.C1844T, c.C419T, c.145_148delCAGA were examined in families E, F, G, and H respectively. Symbols are explained in Table 3.7

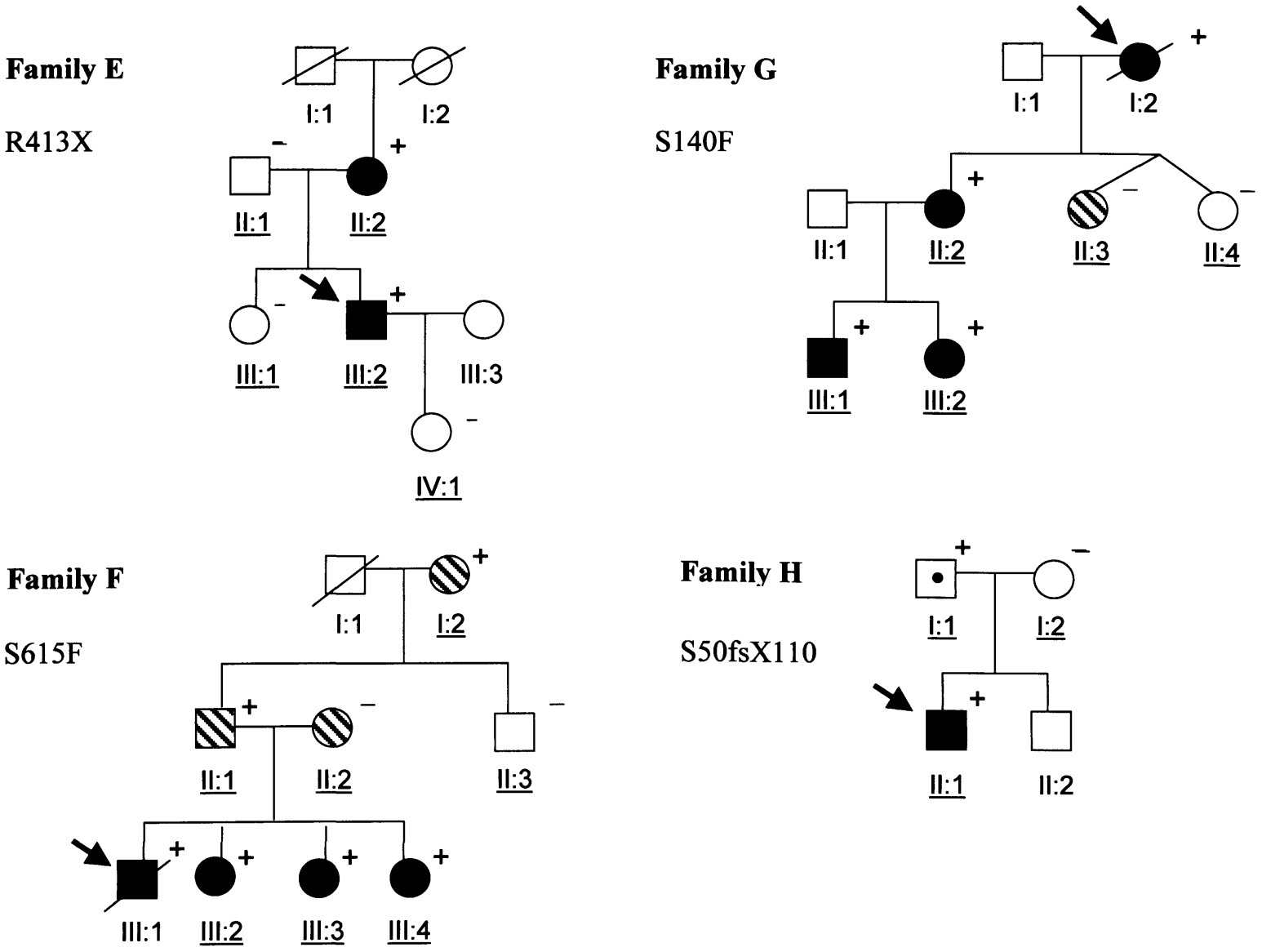

Figure 3.17 Pedigree analysis examining p.Q273fsX288 DP (family I)

Transmission of DP gene mutation c.818_819insA was examined in family I. Symbols are explained in Table 3.7.

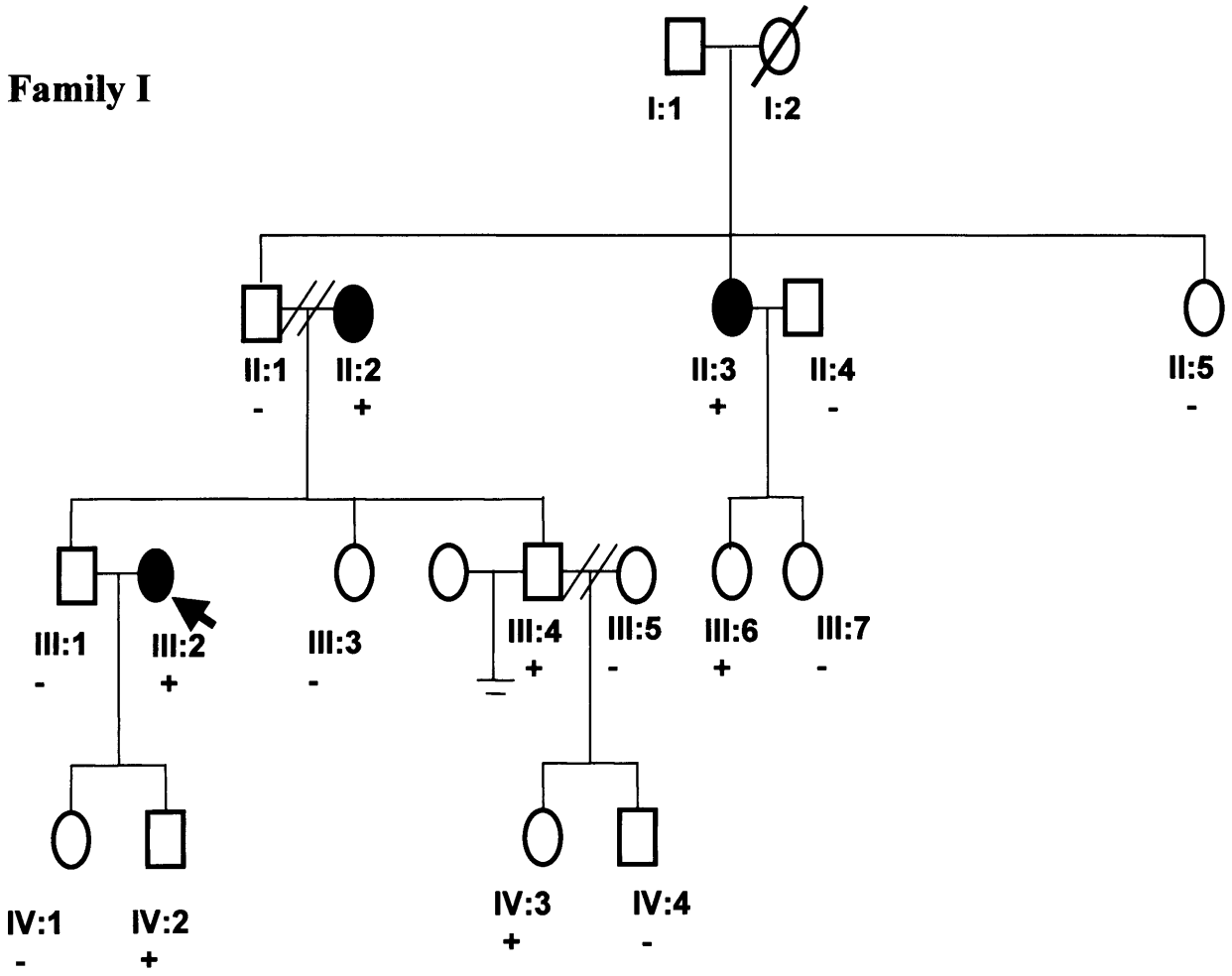

3.4.1 Part 2.2 Pedigree analysis of family D carrying p.L586fsX658 PKP-2 mutation

The plakophilin-2 mutation p.L586fsX658 was examined in family D. This was a family with forty-three members spanning through three generations. Part of the pedigree reproduced (Figure 3.15) illustrates twenty-six of these individuals, and in out of nineteen of these family members consenting to evaluation, five individuals met either the Task Force (II:2, II:8) or the modified ARVC clinical criteria (II:4, III:3 & III:5) and all five of these individuals carried the c.1755_1756insTTGACTCA PKP-2 genetic defect. The proband's sister (III:12) and a further two individuals of first (III:8) or second (IV:3) degree relative of the proband were found to carry the genetic defect, but none of them fulfilled ARVC diagnostic criteria, demonstrating that inheriting the mutant gene alone is not sufficient for phenotypic ARVC disease expression. This is an important point to note as it shows evidence of incomplete disease penetrance. Possible mechanisms for the incomplete penetrance are discussed in section 3.5.4.

3.4.1 Part 2.3 Pedigree analysis of family E carrying p.R413X PKP-2 mutation

The plakophilin-2 mutation p.R413X PKP-2 was examined (Figure 3.16) in family E. The proband (III:2) aged forty had an episode of cardiac arrested while playing hockey, but he was successfully resuscitated. The proband had precordial T-wave inversion, an enlarged hypokinetic right ventricle, and a positive SAECG. He had inherited the c.C1237T gene mutation from his mother (II:2); she had normal ECG and no evidence of arrhythmia, but had an aneurysmal segment in the right ventricular outflow tract on echocardiography. Three other additional individuals who consented to testing (II:1, III:1 & IV:1) were asymptomatic and found not to carry the c.C1237T gene mutation.

3.4.1 Part 2.4 Pedigree analysis of family F carrying p.S615F PKP-2 mutation

The plakophilin-2 mutation, p.S615F was examined in family F. In out of forty-one immediate members spanning four generations, nineteen consented for evaluation (only a part of the pedigree is illustrated in Figure 3.16). The proband died suddenly at 15 years of age. The proband's three sisters (II:2, III:3 & III:4) met Task Force criteria and together with the proband all four individuals carried the c.C1844T gene mutation. Both of the proband's parents met the modified criteria, but only his father (II:1) carried the c.1844T gene mutation, which he inherited from his mother (I:2). None of the proband's maternal lineage carried this PKP-2 genetic defect.

3.4.1 Part 2.5 Pedigree analysis of family G carrying p.S140F PKP-2 mutation

The plakophilin-2 mutation, p.S140F was examined in family G (Figure 3.16). The proband (1:2) died suddenly at the age of 36 years and ARVC diagnosis was confirmed at post-mortem. Out of seventeen family members spanning through three generations, five consented for evaluation. Three individuals (II:2, III:1 & III:2) met Task Force criteria and carried the c.419T gene mutation, whilst a relative (II:3) satisfying the modified criteria, did not carry the genetic defect.

3.4.1 Part 2.6 Pedigree analysis of family H carrying p.S50fsX110 PKP-2 mutation

The plakophilin-2 mutation, p.S50fsX110 was examined in family H (Figure 3.16). The proband (II:1) carried the c.145_148delCAGA gene mutation. Whilst sixteen family members spanning four generations were present in the family only the proband's parents consented to evaluation, and although his father (I:1) carried the gene mutation, he did not fulfil ARVC diagnostic criteria. The proband's mother was asymptomatic and she did not carry the genetic defect.

3.4.1 Part 2.7 Pedigree analysis of family I carrying p.Q273fsX288 DP mutation

The desmoplakin mutation, Q2733fsX288 was evaluated in family I (Figure 3.17). Seven members were evaluated clinically and in genetic screening. The proband (III.2) aged 43 years had incurred two episodes of aborted sudden death presumably related to ARVC. Although the proband did not meet Task force Criteria (only two minor criteria satisfied: non-sustained VT plus 1000 ectopics/24hr period and LV and RV enlargement with preserved systolic function on echo), genetic screening was carried out taking into consideration her arrhythmia far exceeded what would be expected in DCM with her cardiac function. She was found to carry the desmoplakin p.Q273fsX280 mutation. The proband's mother (II:2) had no cardiac symptoms (no arrhythmia on exercise testing or Holter monitoring, and SAECG was negative, but she showed an abnormal ECG with QRS dispersion (major criterion) and a contrast echo with RV and LV wall motion abnormality (minor criterion); she carried the desmoplakin c.818_819insA gene mutation. The proband's brother III:4 also carried the genetic defect, he had syncopal episodes in childhood and clinical evaluation at the age of 35 years showed an abnormal ECG pattern and conventional echo showed borderline LV enlargement with normal systolic function and right ventricle. SAECG was negative and there was no arrhythmia on exercise testing. Further evaluation (contrast echo and Holter monitoring) was pending on III:4 and in his daughter, IV:3 aged 6 years. The proband's son (IV:2) carried the genetic defect, but his lack of clinical findings (normal ECG, no evidence of arrhythmia) at age 7 years were not surprising; his sister (IV:1) did not have ARVC and was genotype negative for the desmoplakin mutation. The proband's maternal aunt II:3 lived abroad and available clinical details suggests a history of palpitations. She satisfied ARVC diagnostic criteria based on repolarization and right ventricular structural abnormalities and she carried the c.818_819insA desmoplakin genetic defect. II:3's daughter, III:6, who also lived abroad inherited the desmoplakin gene mutation and had a history of palpitations, but her clinical details were not available.

Two other mutations found in proband A108 (c.2146-1G>C mutation affecting consensus splice acceptor site in plakophilin-2) and in proband A150 (p.P533fsX561, c.1597_1600delATCC in PKP-2) in Table 3.4 could not be characterised by pedigree analysis, as additional family members of both probands declined further clinical investigations.

3.5 Discussion

3.5.1 Genetic screening of ARVC cohort

Genetic screening of a cohort of one-hundred ARVC probands identified fourteen probands carrying mutations in the genes encoding for DP and PKP-2 (Table 3.4). Eleven different mutations were identified; three of these were in desmoplakin and eight were in plakophilin-2. No mutations were found in the gene for plakoglobin in the ARVC cohort examined and this appears to be consistent with observations indicating the presence of only two mutations in plakoglobin have been found to date, one causing a recessively inherited Naxos disease[38] and the second causing an autosomal dominant ARVC[51].

3.5.1a Desmoplakin mutations

Desmoplakin is an obligatory cytolinker protein essential in desmosome formation where it is involved in linking the outer dense plaque region of desmosomes to sites of intermediate filament attachment within the inner dense plaque. Desmoplakin protein (SDS PAGE apparent migration sizes of 210 or 220 KD) exists in two alternatively spliced isoforms. The protein forms a homo-dimer within desmosomes by self association within the coiled coil rod region and the N-terminal head domains interacts with plakoglobin and plakophilins within the outer dense plaque of desmosome. The plakin repeat domains within the C-terminus region of desmoplakin establish association with keratin, desmin, or vimentin intermediate filament within the inner dense plaque of desmosome. Desmoplakin tethers desmosomes to intercellular intermediate filament networks between two adjacent cells, and by this

mechanism, it imparts adhesive strength to a structure formed by condensation of DSG2 and DSC2 desmosomal cadherin proteins.

Three desmoplakin gene mutations were found in the cohort examined that were absent in 400 control DNA samples. Two of these mutations arise from nucleotide sequence insertions in exon 7 (c.818_819insA, p.Q273fsX288) and exon 8 (c.946_947insATACGCA, p.M316fsX324) causing reading frame shift that were both predicted to disrupt within spectrin repeat, SR4 in the plakin domain of desmoplakin protein molecule. A third mutation seen in two unrelated probands was a nucleotide change encoding a missense change in exon 11 (c.C1640T, p.S442F) resulting in alteration of a serine residue in SR5 of desmoplakin (Table 3.4). The two DP gene mutations resulting in the formation of truncated DP proteins was speculated to compromise desmosomal function by disrupting sites of intermediate filament attachment within the inner dense plaque. The S442F mutation affected a serine residue highly conserved in chimpanzee, monkey, dog, mouse, rat, cattle and fowl desmoplakin. Pedigree analysis of the S442 missense mutation was not possible as family members declined consent for genetic and clinical evaluations.

None of three DP mutations found in the genetic screening work were previously reported in the literature. The location of these three mutations on DPI isoform of the protein is illustrated (Figure 1.10) where it is evident, the two truncating mutations disrupt modular assembly of the plakin domain of desmoplakin with the loss of the rod and the plakin repeat domains. The missense desmoplakin mutation causes the substitution of a highly conserved serine residue within the SR5 spectrin repeat in the plakin domain. The effect of the missense desmoplakin mutation on protein structure and function analysed by SIFT and Polyphen predicted that this mutation affected protein function with damaging consequences based on physical and comparative considerations of the amino acid change.

All three DP gene mutations found in the present screening work affected the N-terminus domain of the protein. However, there does not appear to be mutational hot spots in the DP gene, as generally in ARVC, gene mutations affecting the N-terminus, rod and the C-terminus functional domains of DP protein are equally represented (Figure 1.10). Furthermore, in a recent study of two-hundred ARVC patients (conducted between January 2003 to June 2007) in which forty-three families with

two or more affected individuals were examined found seventeen different DP gene mutations, with fourteen resulting in chain termination and four causing primarily missense amino acid substitutions (see online-only data supplement [165]).

3.5.1b Plakophilin-2 mutations

Eight plakopophilin-2 mutations were found by genetic screening of the ARVC cohort. These were predicted to disrupt different domains in the plakophilin-2 protein (Table 3.4). Plakophilin-2 is an essential protein in cardiac tissue localising both in desmosomes as well as in the nuclei playing an essential role in cell signalling[134,183]. In the desmosomes, plakophilin-2 appears to function by stabilising the lateral connections between the desmosomal plaque proteins in the outer dense plaque. It is closely related to an Armadillo p120^{ctn} family of proteins and structurally it contains a globular N-terminal head domain followed by ten imperfect amino acid repeats (ARM repeats) and a short C-terminal tail[134].

Genetic screening of the ARVC cohort identified 8/100 or 8% of probands who were carriers of PKP-2 mutations. This was a relatively small cohort of ARVC patients examined to arrive at an accurate figure for the prevalence of PKP-2 mutations in the population studied. Examination of several other ARVC cohorts from different geographic locations have shown that PKP-2 mutation carriers could account 14% in an Italian cohort of eighty patients[104], 27% in a Western European cohort of one-hundred and twenty patients[40] and 43% in a North American cohort of fifty-eight patients[108]. The most striking finding was in a Dutch study in which 70% of a cohort of twenty-three patients[107] with demonstrable familial disease had PKP-2 mutations, suggesting that plakophilin-2 is the major determinant of familial ARVC in the Netherlands[107]. The varying prevalence of PKP-2 mutation carriers may be due to small sample size of the cohorts, varying ethnicities of the population, and patient selection bias. In most referral centres individuals with asymptomatic arrhythmia of right ventricular origin account for majority of index cases, while in the UK a greater proportion of cases were identified by familial evaluation after death of the proband from pathologically proven ARVC probably resulting in a selection bias. A wide spectrum of plakophilin-2 mutations were identified in the present genetic screening

work including missense, insertions, deletions, indel and splice sites mutations; this was consistent with observations in other cohorts examined[40,107,108,207].

Of the eight plakophilin-2 mutations found, four of these were previously described[40]. Two of these mutations resulted in a single nucleotide substitution in exon 3 (c.C419T) and exon 9 (c.C1844T) resulting in the substitution of a serine residue with a phenylalanine residue in both cases (p.S140F and p.S615F respectively). The third mutation involved nucleotide sequence deletion in exon 1 (c.145_148delCAGA) of the PKP-2 gene causing a PTC in the mRNA transcript formed with a potentially severely truncated protein (p.S50fsX110) translation. The fourth mutation was an intervening sequence splice acceptor site mutation c.2146-1G>C causing an abnormal splicing with retention of 160bp of the intron 12, or the loss of a 17bp sequence of exon 13 due to activation of a cryptic splice site[40]. This splice site PKP-2 mutation is an example of a recurrent mutation[108,207].

The p.S50fsX110 plakophilin-2 mutation reported in other studies[40,108,207] is a second example of a recurrent mutation in ARVC. The nucleotide change (c.145_148delCAGA) encoding this change leads to the formation of an mRNA transcript containing a PTC. This mRNA transcript probably was degraded via the NMD machinery causing PKP-2 haploinsufficiency. Plakophilin-2 mutations p.S615F and c.2146-1G>C, previously described[40], lead to disruption of a conserved serine amino acid residue within Arm repeat 6, and an abnormal splicing disrupting ARM repeat 8 respectively[40]. The p.S615F mutation resulted in substitution of a serine residue highly conserved in dog, mouse, rat and fowl plakophilin-2 All eight plakophilin-2 mutations described in Table 3.4 were absent in 400 control DNA samples examined.

The p.S140F is a third example of a recurrent mutation that is found in other cohorts examined[40,108] this disrupted a conserved serine amino acid residue. Although this mutation was predicted to be tolerant and probably benign by SIFT and Polyphen analysis respectively, family study (Figure 3.16, family G) showed that transmission of this mutation was associated with the clinical expression of ARVC in three other family members (individuals II:2, III:1 and III:2). DNA sequence analysis program, ESE finder indicated that a potential exon splicing enhancer sequence was present at the site of the p.S140F missense substitution. However, the c.C419T nucleotide

change did not result in the abolishment of an ESE element in exon 3 of plakophilin-2 recognised by SC35 protein, as a high score motif was still recognised after the nucleotide change. This suggested that it was unlikely that this nucleotide could affect the normal splicing involving exon 3. However, bioinformatics analysis of the PKP-2 protein using NetPhos phosphorylation algorithms predicted several putative serine residue phosphorylation sites (Table 3.6) indicating that there was a clustering of putative phosphorylation sites around the serine residue at position 140. Although there is no literature evidence supporting the functional relevance of phosphorylation at any of these serine residues including serine 140, some of these serine residues may conceivably partake in signalling activity of PKP-2. One such serine residue at position number 82 in PKP-2 protein was reported to be phosphorylated by CTAK1 *in vitro*[181] that generated a binding site for σ14-3-3 proteins affecting the nuclear localization of PKP-2 was correctly identified by NetPhos as a phosphorylation site (score of 0.981, Table 3.6). Expression of S140F PKP-2 protein in Flp-In T-Rex HEK 293 cells was achieved to determine functional consequence of its expression (Chapter 5).

Four PKP-2 mutations found were novel having not been described in the literature before. The mRNA transcript resulting from one of these mutations (c.C1237T, p.R413X PKP-2) might have been predicted to undergo NMD and cause PKP-2 haploinsufficiency, this mutation was subsequently identified in a large German family[206], and using mRNA expression analysis and sequencing transcription of the defective allele leading to a presumed truncated PKP-2 was indicated. Family members of the proband in this study were reported to display a severe ARVC phenotype with frequent occurrence of SD at young age (5 cases at age 14-29) occurring mostly during physical exercise. The age of onset of arrhythmia in the family was significantly lower compared to patients with ARVC due to other PKP-2 mutations, and the penetrance was strongly sex-dependent with all carrier males developing the disease, but only 30% of carrier females developed ARVC. Clinically affected patients LV biopsy showed pathological nuclei, hypertrophied cardiomyocytes, reduced myofibers, and fibrosis. EM examination showed abnormal mitochondria and dilated ID. A mouse model over-expressing R413X PKP-2 was reportedly established, but functional studies using this animal model has not appeared in the literature to date. Although a definitive demonstration of the truncated protein in cardiac tissue of affected individual was not reported in this study, the

structural changes in the ID reported by EM examination suggests the truncated R413X PKP-2 protein could be inserted causing dominant negative effect.

Three of the other novel plakophiln-2 mutations p.P533fsX561, p.L586fsX658 and p.A733fsX740 were localised within conserved ARM repeat domains causing protein truncations resulting in plakophilin-2 proteins lacking seven, six or three out of the ten ARM repeats respectively; it is possible that some of these three mutations might result in PKP-2 haploinsufficiency as mRNA transcripts containing PTCs may undergo NMD. However, if small amounts of these transcripts escaped NMD then the formation of these truncated plakophilin-2 proteins lacking these ARM repeat structures may compromise PKP-2 protein function via a dominant negative effect if these proteins were inserted into desmosomes.

3.5.2 Family studies of PKP-2 mutation carriers

Studies of plakophilin-2 pedigree analysis represent for the first time a systematic analysis of genotype-phenotype correlation in families carrying plakophilin-2 genetic defects which were not examined in detail in a previously reported study[40]. Heterogeneous phenotypic expression (variable expressivity) was observed among individuals carrying the same mutation in a given family. The Task Force criteria facilitated ARVC diagnosis, but lacked sensitivity for early diagnosis of disease when clinical findings are often subtle. The modified ARVC criteria[6] applied to relatives of the probands, in the context of family screening because of incomplete disease expression, increased the diagnostic yield, but this reduced the specificity. This was shown by several examples: III:9 & III:10 (Figure 3.14, family A), II:2 (Figure 3.16, family F), and II:3 (Figure 3.16, family G) where these individuals were found to be genotype negative for the respective PKP-2 mutation identified in the proband in each family, but all of them fulfilled some of the modified ARVC diagnostic criteria. Pedigree analysis allowed the identification of asymptomatic family members who had inherited a particular genetic defect identified in the index case patient. This information was relevant for clinical management and continued surveillance of these individuals who were at risk of developing overt ARVC at some point during their lifetime, or who were at an increased risk of sudden cardiac death as a first clinical symptom of the disease. Conversely, family members of the proband who do not have demonstrable cardiological abnormalities and who do not carry the genetic defect

identified in the proband can be reassured and dismissed from lifelong periodic follow-up cardiological screening allowing scarce clinical resources to be targeted to proven gene-positive mutation carriers. Pedigree analysis is also useful for cascade screening of relatives who are at risk of developing ARVC for identifying transmission of a genetic defect identified in the proband. Pedigree analysis may result in reclassification of sequence variant of unknown clinical significance as a mutation if the transmission of the identified genetic defect (resulting in a missense amino acid substitution) is associated with expression of clinical symptoms, but this approach may not always be successful due to variable expressivity of ARVC clinical symptoms and reduced penetrance of the disease. The p.S140F PKP-2 mutation is a good example of a missense sequence change being classified as a mutation following pedigree analysis.

Haplotype analysis of index cases with four apparently recurrent PKP-2 mutations (c.C235T; p.R79X, c.C397T; p.Q133X, c.T2386C; p.C796R, and c.2489+1G>A) in a Dutch cohort revealed allele sharing which was consistent with founder effects. However, in other studies of Western European[40] and North American[108] ARVC cohorts no evidence of founder effects were found for recurrent mutations. In the absence of founder effects, however, the proportion of common or recurrent mutations in the ARVC population is too limited to be useful as a first-line genetic screening approach. The vast majority of PKP-2 mutations found in the present screening study and in other studies are 'private' mutations that are associated in specific families. Thus although as many as fifty-four PKP-2 mutations are known to be associated with familial ARVC (Table 1.5), the vast majority of these may be specific only in certain populations or present in single families, thereby limiting their usefulness in genetic testing in the general population. The implication of frequent private mutations is that some of these may be novel mutations for which limited information is available regarding their pathogenicity. For deletions, insertions, and splice site mutations involving frame shift and nonsense mutation resulting in PTC, a causative role in ARVC may be assumed. However, for missense mutations involving single amino acid substitution its absence from ethnically matched control subjects must be verified followed by the screening of other family members to establish causality through correlation of clinical and genetic findings. A detailed search of the effect of a missense mutation using literature search, public and diagnostic mutation databases, SIFT, Polyphen, Russell and splice site analysis are required to determine whether the

unclassified variant could be tolerant and benign or intolerant and probably pathogenic.

An important observation from examination of other PKP-2 mutation carriers is that an important minority of ARVC patients are homozygous for PKP2 mutations[113] or double heterozygous. For example, screening the parents of a proband of sixteen years of age who died from SD, found that the mother carried a nonsense mutation in exon 5 of PKP-2 gene while the father carried a pathogenic missense mutation in exon 15 of the desmoglein-2 gene[165].

3.5.3 Importance of missense mutations in ARVC

Generally, missense mutations are difficult to prove as causative for a disease unless supportive evidence indicates a functional or structural change in the protein concerned. In other non cardiac diseases, such as hereditary non-polyposis colon cancer (HNPCC), missense mutations can be found that affect the levels of the expression of proteins involved in DNA mismatch repair (MMR, proteins: hMLH1, hMSH2, and hMSH6). Supportive evidence for pathogenicity of these gene mutations resulting in missense protein formation can be derived by examining the levels of proteins by immuno-histochemical staining of tumour tissue where they can be associated with knockdown in the expression levels of MMR proteins. Three missense mutations were found in the cohort of ARVC patients examined. All three missense mutations affected serine residues in desmoplakin (p.S442F DP) and plakophilin-2 (p.S140F & p.S615F PKP-2) substituted by phenylalanine residues. Using pooled data derived from all ARVC gene mutations (DP mutations: Table 1.4, PG mutations: section 1.8.2, PKP-2 mutations: Table 1.5, DSG2 mutations: Table 1.6, and DSC2 mutations: Table 1.7), ninety-six novel mutations were identified in ARVC. Out of these, thirty-six (38.0%) were missense mutations indicating that single amino acid substitutions constitute an important class of mutations involved in the pathogenesis of ARVC. DSG-2 had the greatest proportion of missense mutations with 66.7% (14/21), followed by desmoplakin with 57% (8/14) and PKP2 with 24.0% (13/54).

Precisely how missense mutations might cause ARVC is not fully understood, but for some missense mutations, such as in desmoplakin (p.V30M & p.Q90R), the head

domain of DP protein was affected by the missense substitution disrupting the binding of DP to PG and affecting its membrane localization. Similarly, in the case of desmoglein-2 missense mutations (p.V56M, p.D154E, p.V1588G, p.Y87C, p.G100R, p.N266S, p.K294E, p.E331K, & p.V392I) these appear to disrupt specific extracellular domains in DSG-2 (EC1, EC2, EC3, and EC4) protein. One identified PKP-2 missense mutation (p.S140F PKP-2) was examined in a stable Flp-In T-Rex HEK 293 cell line to determine the functional consequence of cellular expression of this protein.

3.5.4 Incomplete penetrance and variable disease expression in pedigree analysis

Pedigree analysis of families A – I in section 3.4.1 Part 2 showed evidence of variable phenotypic expression and incomplete penetrance of ARVC in families examined. Variable phenotypic expression in ARVC implies that family members carrying a given gene mutation encoding a desmosomal protein will always express clinical symptoms of the disease, but the severity of clinical presentation will vary (mild to severely affected) amongst family members inheriting that genetic defect. Some of these individuals may fulfil Task Force ARVC diagnostic criteria; others may not achieve diagnostic scores to fulfil Task Force criteria, while others may only fulfil some of the modified set of ARVC diagnostic criteria. Incomplete penetrance (or reduced penetrance) implies that although the genetic defect has been characterised in a given family, the transmission of this genetic defect alone will not always accompany the expression of ARVC clinical symptoms in all family members. A good example of incomplete penetrance was seen in pedigree analysis of family D where three individuals (III:12, III:8, and IV:3, Figure 3.15) related to the proband inherited the c.1755_1756_insTTGACTCA genetic defect, but none of these three individuals fulfilled any of the ARVC diagnostic criteria (modified or Task Force ARVC criteria). Hence, in a family based investigation only a percentage of individuals carrying a genetic defect will express ARVC disease. Dominant ARVC with PKP-2 mutations in this study showed a reduced penetrance in about 47%[41] of cases examined. Incomplete penetrance in ARVC results from the following factors:

• Age-related reduced penetrance seen in pedigrees with PKP-2 mutations carriers demonstrates normal or mild disease phenotypes even at the age of beyond seventy. Dalal[207] *et al* performed the clinical screening of twenty six PKP-2 mutation carriers related to nine probands with pathogenic PKP-2 mutation and found 31% of these individuals fully fulfilled Task Force ARVC criteria while 35% had at least some Task Force criteria apart from a family history of ARVC. The penetrance of symptoms, diagnosis of ARVC (meeting Task Force criteria), occurrence of ventricular tachycardia and death in these individuals were all shown to be age-dependent[207]. Due to age-related penetrance of ARVC estimates of penetrance must be linked to the age of the target population studied, acknowledging that younger individuals without phenotypic expression may later develop this condition. The accurate analysis of penetrance of ARVC mutations based on age is important in order to allow proper counselling for mutation carriers at young ages to estimate their lifetime risk.

• Gender-related penetrance in ARVC is higher in men than women, with an approximate ratio of 3:1[213]. The penetrance of ARVC has been reported to be between 62-67% in men[6,207,214]. Analysis of measures of severity of disease between the two genders indicated an influence of the male gender on phenotypic manifestations of ARVC with men more likely to have late potentials on SAECG, frequent ventricular extrasystoles on a 24-Holter monitor, and right ventricular dilatation on imaging[207]. The lower penetrance of ARVC among women may be due to lesser exposure to environmental factors such as viral agents causing inflammation or sustained vigorous athletic activity.

• Reduced penetrance may result from biological differences, for example, myocyte apoptosis is believed to play a role in the pathogenesis of ARVC, and myocardial cell apoptosis was inhibited by the effects of oestrogen *in vitro* and *in vivo* via the activation of phopho-inositol-3 kinase/AKT signalling. This may explain the lower incidence of ARVC in women.

• Other environmental factors such as viral triggers and aerobic activity may predispose men to the effects of these on ARVC. Men may also be at a higher risk to environmental factors influencing disease outcomes. The importance of environmental factors influencing the rates of ventricular arrhythmia and severity of structural right ventricular dysfunction was emphasized in the work of Dalal and colleagues[207] who examined two sets of monozygotic twins with ARVC and showed discordant severity of disease.

3.5.5 Limitations of genetic screening and future studies

The limitation of the present study are five-fold: firstly, that only a very small sample of ARVC probands (one-hundred index cases) was studied to gather enough information about how different mutations affecting plakophilin-2 or desmoplakin may be involved in the pathogenesis of ARVC. Secondly, the number of individuals consenting to participate in the clinical and genetic screening limits the pedigree information that is available from each family study. Thirdly, only the coding regions and immediate flanking intron regions of the three genes encoding desmosomal proteins were examined by DNA sequencing, therefore any sequence variants in the 5' or 3' UTR regions of these genes will not be identified using this approach. Fourthly, DNA sequencing will not detect the deletion/duplication of single or multiple exons or of an entire gene. Detection of such large deletions requires alternative methods such as multiplex ligation probe dependent amplification (MLPA) analysis. However, a recent report examining one-hundred and twenty ARVC patients in a Dutch cohort who were referred for PKP-2 mutation testing, and who had tested negative by denaturing gradient gel electrophoresis and sequencing, found only one patient by MLPA analysis with deletion affecting the promoter region and exons 1-4 of the PKP-2 gene resulting in a functional null allele[209]. Thus, the frequency of large genomic deletion in PKP2 gene, which goes unnoticed with sequencing, appears to be very low. Lastly, mutation identification studies in the present ARVC cohort examined only three of the genes encoding desmosomal protein (DP, PG, and PKP-2). Other genes encoding desmosomal cadherin proteins expressed in the heart (DSG-2 and DSC-2) were not examined in the present studies. In addition, future work may involve the identification of other ARVC-related novel genes not yet been screened. This may involve examination of additional components such as, for example, plectin, other components such as alpha T-catenin, and intermediate filament protein such as desmin for encoded gene mutations.

3.5.6 Advent of Genetic Testing in ARVC

The discovery of large number of mutations in the "big three genes" (plakophilin-2 desmoplakin and desmoglein-2, Tables 1.5 – 1.6 and Figure 1.10) encoding

desmosomal proteins has opened up the possibility of genetic testing for ARVC in the clinical setting. Three scenarios seem amenable to genetic testing in ARVC:

1) Confirmatory and predictive testing in relatives with or without clinical features of ARVC is a relatively straightforward relying on bi-directional DNA sequencing of all known genes and DNA sequencing of the affected exon containing the genetic defect being. Confirmatory testing is defined as the use of genetic testing to corroborate clinical suspicion of ARVC in an index case. In line with most other cardiovascular diseases, ARVC is genetically heterogenous and therefore, would appear to be less amenable to genetic testing. However, confirmatory genetic testing may play an increasing role in ARVC due to the unique challenges of establishing a clinical diagnosis. Predictive testing is defined as the genetic testing to exclude or verify the presence of a known mutation in relatives of a family.
2) Pre-symptomatic diagnosis of ARVC, particularly in the setting of sudden cardiac death in >50% of index cases provides the strongest argument in favour of adapting a proactive approach to familial evaluations[6,214]. This approach emphasizes the need for a timely diagnosis of the concealed phase of ARVC, during which a dearth of symptoms may belie significant arrhythmic risk.
3) Cascade Screening where the presence or absence of an identified genetic defect is investigated by DNA sequencing in extended relatives of an index case. This type of genetic testing has an upshot of reassuring gene-negative relatives constituting 50% of individuals tested, and allowing targeted use of scarce clinical resources on gene-positive individuals.

However, there are several obstacles affecting the utility of genetic testing of ARVC in the general population:

- The major obstacle of using a sequencing approach in genetic testing is that despite its reliability, this is a labour-intensive and cost-intensive process. The comprehensive screening of all known five genes (PKP-2, DP, DSG-2, DSC-2, and PG) and flanking intron regions of each exon involves the coverage of a large genomic region of approximately 40Kb. Nevertheless, as emerging techniques such as whole genome amplification (WGA) overcome problem of reliability and prohibitive present costs

come down, then it is foreseeable that clinical benefits of a genetic analysis in ARVC may eventually outweigh the technical limitations.

- Since an important minority of ARVC patients are homozygous[113], double heterozygous[165] or compound heterozygous[100], digenic inheritance with a gene-dose effect in ARVC underscores the importance of screening every coding region of all known disease-causing genes, even after isolation of a putative pathogenic mutation.
- Allelic heterogeneity precludes the use of genetic probes in genetic diagnosis. Thus, DNA sequencing appears to be the mainstay of genetic screening or testing in ARVC.
- Although PCR restriction fragment-length polymorphism analysis approach is amenable as a relatively inexpensive approach, its utility is limited to mutations that fall within restriction sites.
- It has been suggested that some of the numerous missense sequence changes found in ARVC may be pathogenic only when accompanied by additional genetic polymorphism[165].
- Results of genotype-phenotype correlation studies[104,165] examining the "big three genes" in ARVC estimate a pick-up rate of between 30-40% of successful genotyping of all ARVC patients[215]. Since ARVC is a familial disease in 50% of cases, it implies that the remainder of the cases will not show mutations in the known genes, but they may possibly harbour mutations in genes not yet implicated.
- Silent gene mutation carriers are individuals who, at any point in time, lack evidence of clinically penetrant disease, but retain the capacity to transmit the disease to their children. Silent carriers are frequent in ARVC and may give a false impression in small families of a sporadic disease.

3.5.7 Impact of p.S140F PKP-2, p.A733fsX740 PKP-2 and p.Q273fsX288 DP mutations

Two plakophilin-2 mutations (p.S140F and p.A733fsX740) and one desmoplakin mutation (p.Q273fsX280) were selected for further functional studies. The p.S140F PKP-2 mutation was examined by functional studies because it resulted in the substitution of a relatively conserved serine residue in human PKP-2 with an aromatic phenylalanine amino acid residue within the N-terminus head domain of PKP2. The head domain of plakophilin is involved in the vast majority of the protein-protein interactions previously reported[183]. This serine residue is highly conserved in several

species (human, cat and mouse plakophilin-2) and is only replaced by an analogous threonine residue at this position in chicken plakophilin-2 or a phenylalanine in bovine plakophilin-2. Although SIFT and Polyphen analysis predicted the p.S140F missense change to be tolerant and benign, pedigree analysis of family G showed that this genetic defect was clearly pathogenic as the transmission of this single nucleotide change (c.C419T) was associated with clinical expression of ARVC. Since c.C419T PKP-2 mutation did not appear to cause loss of an ESE within exon 3 of PKP-2 recognised by the SC35 splicing protein, no effect on the normal splicing of PKP-2 was predicted. Examination of putative phosphorylation sites within the PKP-2 protein, however, indicated that serine residue at position 140 may be potentially phosphorylated clustering around other adjacent serine residues also with high likelihood of being phosphorylated.

Functional study of A733fsX740 PKP-2 protein expression was performed as this truncated protein was the largest of all PKP-2 protein truncations found in this genetic screening work, this protein molecule retained the N-terminus head domain and seven ARM repeat units with loss of the final three ARM units and C-terminus region. Study of this mutation was considered important because Chen[183] and colleagues examining functional properties of different domains of PKP2a isoform *in vitro* did not attribute any inter-protein interaction of the C-terminus portion of PKP-2a, although the elimination of all ten ARM repeat units in PKP-2a reportedly led to a reduction in the amount of plakoglobin binding in immunoprecipitation analysis[183].

Expression of A733fsX740 protein was examined in functional study (Chapter 4) as compelling evidence was established for the pathogenic nature of this indel nucleotide sequence change in three independent families (Figure 3.13, families A, B, and C) probably indicating alteration of some property of desmosomes.

The desmoplakin mutation p.Q273fsX280 was examined by functional studies as a predicted truncated (33 KD) N-terminus head-domain DP polypeptide formed might compete with full-length desmoplakin for insertion into desmosomes. The amino-terminus of desmoplakin domain is important for association with the desmosomal junctional plaque through interactions with plakoglobin and plakophilin[216]. A study supporting a role of desmoplakin in intermediate filament attachment in desmosomes was provided by protein expression work in A431 epithelial cells in which an N-

terminus 70KD desmoplakin peptide, referred to as the DNTP peptide[217] was over-expressed. This truncated desmoplakin polypeptide was recruited to the desmosomal plaque region; however, it displaced endogenous full-length desmoplakin from cell-cell contacts and disrupted intermediate filament attachment to the cell surface.

The Q273fsX280 DP polypeptide truncates within the SR4 spectrin repeat in the plakin domain and this may disrupt interactions with PG and PKP-2. This truncated DP polypeptide lacks the coiled coil rod region and the C-terminus essential for DP self-dimerization and interaction with the intermediate filament network respectively. Thus, expression of induced Q273fsX288 DP polypeptide achieved *in vitro* in Flp-In T-Rex HEK 293 stable cells established its functional consequence.

Chapter 4

Functional Studies of A733fsX740 Plakophilin-2 protein expression in tPKP2 cells

4.1 Introduction

Genetic screening of an ARVC cohort and pedigree analysis of three unrelated families A-C (Figure 3.14) showed an autosomal dominant mode of transmission of ARVC with incomplete penetrance caused by an insertion/deletion (c2197-2202_delCACACC_insG) sequence within exon 11 of the PKP-2 gene. This resulted in PKP-2 protein truncation (p.A733fsX740 PKP-2). The p.A733fsX740 PKP-2 mutation was reported in a total of six unrelated probands; three of these were from probands in the present cohort examined[41] and subsequently another three unrelated probands were identified in a North American ARVC cohort[108] suggesting that this mutation could be a possible recurrent mutation. Another novel mutation involving a 28 nucleotide insertion (at position 2196, reference sequence NM_004572.2) within exon 11 of the plakophilin-2 gene [111] resulted in a frame shift causing truncation of PKP-2 with an identical effect on the protein (p.A733fsX740) as the c.2197_2202delCACACC_insG mutation found in the present genetic screening. Given the prevalence of p.A733fsX PKP-2 mutation and lack of literature data on functional significance of the region implicated by this PKP-2 mutation, the truncated PKP-2 protein was expressed in Flp-In T-Rex HEK 293 stable cells to examine its effect on cellular characteristics compared to a control cell line expressing full-length PKP-2 protein.

Plakophilin-2 mutation p.A733fsX740 resulted in premature protein translation termination within the eighth Armadillo repeat unit. However, the truncated PKP-2 protein retains nearly 85% of the full-length sequence of the plakophilin-2a isoform; nonetheless, this truncated protein undoubtedly affected structural or functional properties of PKP-2 protein as pedigree analysis of three unrelated families showed expression of ARVC clinical symptoms with the inheritance of the genetic (c.2197_2202_delCACACC_insG) defect.

4.2 Experimental approach to investigate functional effects of A733fsX740 PKP-2 protein expression

The mRNA transcript formed during transcription from the PKP-2 gene encoding the indel mutation (c.2197_2202delCACACCinsG) contains a PTC and therefore the

transcript should undergo NMD resulting in PKP-2 haploinsufficiency. The problem with frame shift mutations is that the protein product might be expressed, and if so, this could be dominant negative. Thus even if NMD occurs, small amounts of the transcript might escape NMD mechanism and protein translation would result in formation of a truncated PKP-2 that could act in a dominant negative fashion if inserted into desmosomes. Two stable cell lines expressing full-length and truncated PKP-2 proteins were generated to investigate this proposition.

Cloning of full-length and A733fsX740 PKP-2 DNA was performed in pcDNA5 and pcDNA4 vectors that permit stable cells to be established and inter-protein interaction to be examined using an anti-XPress immunoprecipitation approach using these two vectors respectively. Using pcDNA5 plasmids, Polyfect-mediated cationic transfection allowed selection of stable clones expressing either full length or truncated PKP-2 proteins in an established tet-on system in Flp-In T-Rex HEK 293 cells. Several studies were performed using stable cells expressing full-length (designated **wPKP2 cells**) and truncated PKP-2 (designated **tPKP2 cells**) proteins:

1) Expressions of full-length or truncated PKP-2 proteins were confirmed by confocal microscopy and western immunoblotting in wPKP2 and tPKP2 cells. The distribution of full-length and truncated PKP-2 proteins expressed in wPKP2 and tPKP2 cells were examined in different cellular compartments (in cytosol, membrane, nuclear, and cytoskeletal fractions) using a commercial cell fractionation kit.
2) Properties of wPKP2 and tPKP2 cells were examined to compare cellular proliferation rate and initial cell-cell contact adhesion using commercial kits measuring cell growth characteristics and intercellular adhesion using a colorimetric (bio-reduction of substrate to produce a coloured formazan product) and a fluorescence assay (cellular esterase enzyme cleavage of substrate to release calcein, a fluorescent product) respectively. Another assay measured adhesive strength of monolayer to compare wPKP2 and tPKP2 cells using an enzyme-based adhesion assay that releases confluent monolayers followed by controlled exposure to shear stress and visualization of the monolayer fragments formed[212]. In this monolayer adhesion assay, Dispase II enzyme released monolayer from the plastic culture surface without disrupting intercellular adhesion (cell-cell contacts preserved), and then the released monolayer was subjected to controlled shear stress. Fragments formed were

assessed with larger monolayer fragments indicating better cell-cell adhesion (resistance to fragmentation) while smaller fragments indicate weaker cell-cell adhesion (increased susceptibility to fragmentation).

3) Stable cells exposed to controlled mechanical cell stretch were allowed to recover for a short time. Non-induced and tetracycline-induced wPKP2 and tPKP2 cells treated in this manner were compared for their response to specific apoptosis activity measured using a commercial CaspACE assay kit that measured colorimetric release of a yellow product from a colourless substrate cleaved by caspases enzymes (caspases were activated by cleavage during induced apoptosis following mechanical stretch) in these stable cells. This procedure measured the extent of apoptosis in wPKP2 and tPKP2 cells subjected to cellular stretch to determine whether expression of truncated PKP-2 influenced the degree of apoptosis.
4) Cx-43 protein was examined in stable cells as this gap junction protein is the major connexin expressed in the heart ventricles, and it has been recently implicated as a possible mechanism for arrhythmogenesis in heart diseases. The level of Cx-43 protein in soluble cell lysates and cell membrane localized Cx-43 protein was compared in non-induced and induced wPKP2 and tPKP2 cells using western immunoblotting and confocal microscopy analysis respectively.
5) Electrophysiology performed using a single electrode recording changes in potential differences of induced wPKP2 and tPKP2 cells to injected step pulses of electrical current enabled the cell input resistance (ri) of each stable cell line to be determined. The ri values obtained provide a measure of how well each stable cell line is connected to one another in a cluster. The ri value in stable cells without cell surfaced localized Cx-43 protein is expected to be greater than the ri value in stable cells that express Cx-43 in their gap junctions, as presence of Cx-43 gap junctions would facilitate the flow of current through the cell cluster. The cell input resistance values obtained from wPKP2 and tPKP2 stable cells were compared by student's t-test. An independent measure of the extent of functional coupling between induced wPKP2 and tPKP2 cells was assessed using Lucifer Yellow dye transfer providing a measure of gap junction intercellular communication (GJIC)[218].
6) Desmosomes formed *in vitro* in induced wPKP2 and tPKP2 cells examined by electron microscopy were compared with desmosomes formed in non-

transfected Flp-In T-Rex HEK 293 cells to determine the effect of truncated PKP-2 protein expression on the morphology of desmosomes.

Lastly, using pcDNA4 vectors HEK 293 T cells were transfected to obtain transient expressions of full-length and A733fsX740 PKP-2 N-terminally XPress epitope tagged proteins. These PKP-2 proteins were immunoprecipitated using a mouse monoclonal antibody reactive to the XPress epitope allowing the extent of interaction of these two PKP-2 proteins with other endogenous desmosomal proteins to be determined.

4.3 Experimental Aims

Seven overall objectives were set in this part of the study. The first was to clone wild type PKP-2a DNA into an expression vector pcDNA5/FRT/TO/TOPO/TA. The second was to construct expression mutant c.2197_2202_delCACACC_insG PKP2 in pcDNA5/FRT/TO/TOPO/TA using site directed mutagenesis. The third was to make stable cell lines in Flp-In TRex HEK 293 and verify expressions of PKP2 and A733fsX740 PKP2 in these stable cells. The fourth was to examine the proliferation rates, cell adhesion, and the effect of mechanical cell stretch to measured apoptosis following recovery of wPKP-2 and tPKP-2 stable cells to an exposure to mechanical cell stretch. The fifth was to examine connexin-43 protein levels in wPKP-2 and tPKP-2 stable cell lines, and to ascertain whether electrical conduction properties (ri values) were affected and the extent of gap junction intracellular communication occurring in a stable cell line. The sixth was to examine desmosomes formed in induced wPKP-2 and t-PKP-2 stable cell lines and to compare them with desmosomes formed in non-transfected control Flp-In T-Rex HEK 293 cells. The seventh was to clone DNA encoding full-length PKP-2 and A733fsX740 PKP-2 into pcDNA4/XPress/TOPO/TA expression vector to achieve transient transfection in HEK 293T cells for examining protein-protein interaction of these expressed PKP-2 proteins using anti-XPress antibody immunoprecipitation (IP) analysis.

4.4 Materials and Methods

All plasmid vectors were purchased from Invitrogen (Invitrogen, UK). Antibodies were purchased from various suppliers such as Invitrogen, Becton Dickinson (BD

Bioscience), Abcam (Abcam Plc, UK), Sigma Aldrich (Sigma Aldrich, UK), and Santa Cruz antibodies were purchased from Insight Biotechnologies, UK. Cell culture media and supplements such as penicillin, streptomycin, Zeocin, blasticidin, hygromycin, and bovine foetal calf serum were purchased from Invitrogen.

4.4.1 Cloning of PKP-2 in pcDNA5/FRT/TO/TOPO/TA

Both plakophilin-2a and plakophilin-2b isoforms are expressed in the human heart. The 2a isoform lacks a 46 amino acid ARM repeat unit encoded by exon 6 in the PKP-2 gene, which is alternatively spliced out. Mutation screening (Chapter 3) of an ARVC cohort did not reveal any mutations within the sequence encoded by exon 6 of plakophilin-2, and other studies examining PKP-2 mutations in various other ARVC cohorts did not find any mutations within this spliced out region. Hence, a pakophilin-2a DNA sequence obtained by PCR amplification was cloned in a plasmid vector pcDNA5/FRT/TO/TOPO/TA, the cloned plasmid permitted PKP-2a protein expression in mammalian cell systems *in vitro*.

An IMAGE plasmid clone of plakophilin-2 (product TC117285, Origene, USA) encoding a PKP-2a DNA sequence was the template DNA used for amplifying a 2662bp PCR fragment of PKP2a using EXL DNA polymerase (section 2.1.2). PCR was carried out using primers spanning an ATG start and TAG stop codons and containing a Kozak recognition sequence (for correct protein translation in HEK 293 cell) preceding the ATG start site. EcoR V restriction sites flanked the 5' and 3' ends respectively. The restriction sites incorporated in the amplified PCR fragment provided an alternative cloning strategy within the multiple cloning site of the plasmid vector. However, pcDNA/FRT/TO/TOPO/TA topoisomerase catalyzed ligation successfully cloned the PKP2a PCR fragment in this study. The primer sequences (Table 4.1) were used to amplify a 2662bp PCR product that was cloned into pcDNA/FRT/TO/TOPO/TA using the method described (section 2.2.1). The map of pcDNA5 plasmid (Figure 4.1) shows the T-A overhang positional cloning of a PCR amplified DNA insert (encoding a gene of interest) using vector-mediated topoisomerase catalysed reaction to obtain a plasmid containing a cloned gene of interest. Using this cloning strategy the 2662bp PCR product encoding PKP2a was cloned in pcDNA5 to obtain a plasmid designated –2301A pcDNA5 (Table 4.1).

Plasmid -2301A pcDNA5 would fortuitously express a truncated plakophilin-2a (p.S747fsX753) in Flp-In T-Rex HEK 293 cell transfection. A single Adenosine residue was missing at nucleotide position 2301 (numbering relative to PKP2b reference sequence in accession number NM_004572.2) in the cloned PKP2a DNA. Hence, PCR mediated site-directed (section 4.4.2) mutagenesis was used to re-introduce the missing Adenosine residue at position 2301 to obtain a pcDNA5 plasmid correctly encoding full-length PKP-2a.

Table 4.1 PCR Cloning of PKP-2a in pcDNA5 using an IMAGE clone of plakophilin-2

Cloning of a PCR fragment amplified from a PKP-2a IMAGE clone (Origene technologies, Inc., USA Cat No TC300868) in pcDNA5/FRT/TO/TOPO/TA plasmid. PCR primers PKP2 for and PKP2 rev generated a 2662bp fragment using the IMAGE clone as template DNA. The PKP2a PCR amplified fragment contained a Kozak recognition sequence preceding an ATG translation start site. A termination stop codon, TGA, was incorporated in the reverse primer. The resulting plasmid designated –2301A pcDNA5 was sequenced to confirm nucleotide-coding sequence of the cloned PKP 2a DNA. Sequencing verified a missing Adenosine nucleotide residue at position 2301 (reference sequence: NM_004572.2). The missing Adenosine nucleotide residue was not a PCR-mediated amplification artefact, but occurred in the PKP2a Origene IMAGE clone purchased. The manufacturer of the IMAGE clone (Origene, USA) independently verified the missing Adenosine residue in the plasmid supplied.

Primer Pairs	Sequence (5'-3')	PCR size (bp) / Enzyme used/ Template	Destination vector containing cloned PCR product	Plasmid obtained
PKP2 for	AAAGATATCGAAATGGCAGCCCCCGGCGCCCCAGCT	2662/EXL/Origene IMAGE PKP-2a DNA	pcDNA5/FRT/TO/TOPO/TA	-2301A pcDNA5
PKP2 rev	AAAGATATCTCAGTCTTTAAGGGAGTGGTAGGC			

Figure 4.1 pcDNA5 plasmid map for cloning PKP-2

Cloning of full-length PKP2a and A733fsX740 PKP2a polymerase chain reaction DNA amplified fragments into pcDNA5/FRT/TO/TOPO/TA vector used in stable (inducible) protein expressions of these PKP2a proteins in Flp-In T-Rex HEK 293 cells. The map shows the strategy for cloning a PCR product into the pcDNA5/FRT/TO/TOPO/TA vector; the T/A site cloning approach was used which relied on vector catalyzed Topoisomerase reaction. The vector map is reproduced from the vector handbook (Invitrogen, UK).

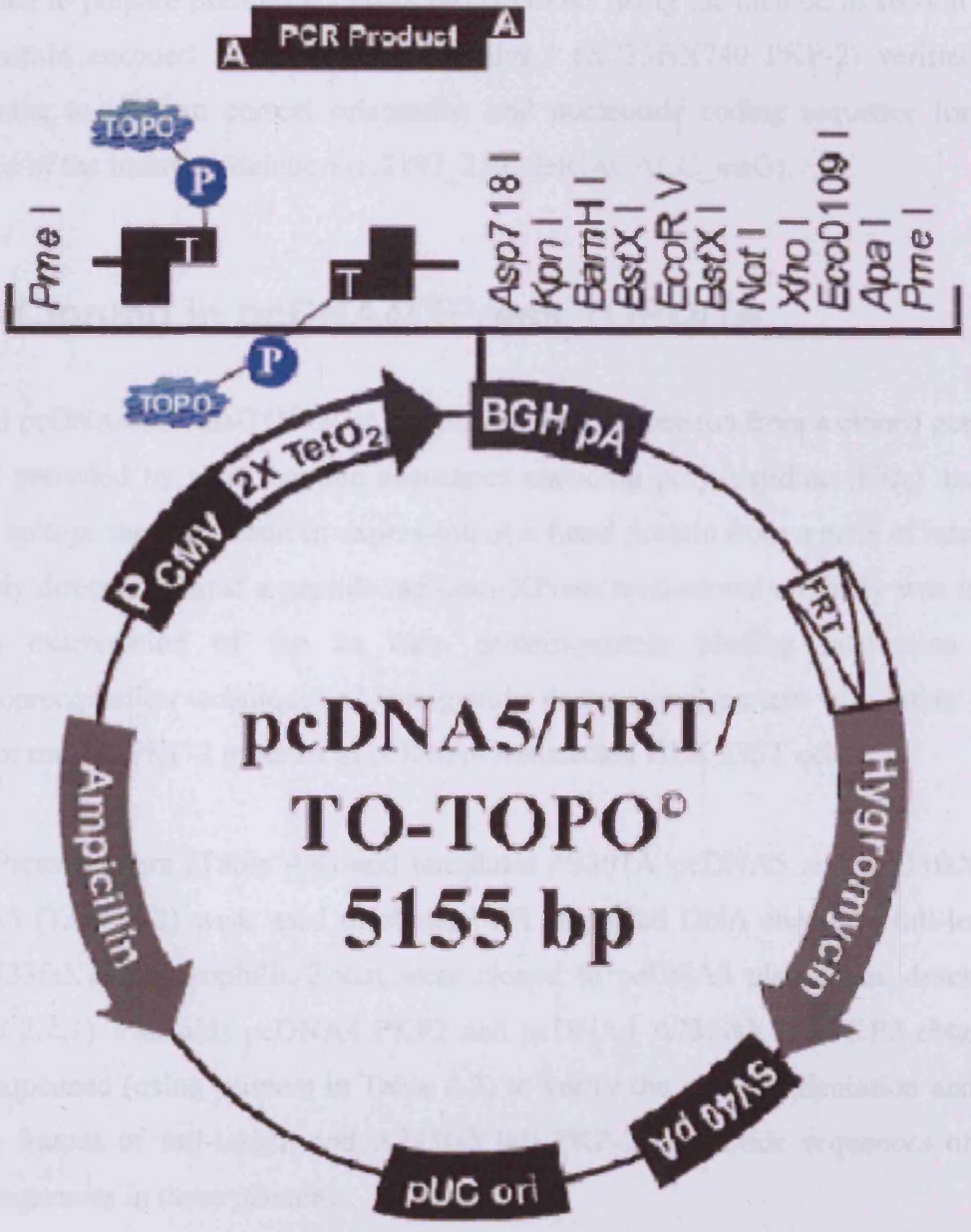

4.4.2 Site Directed Mutagenesis to obtain full-length and A733fsX740 plakophilin-2 encoded in pcDNA5 vector

Plasmid –2301A pcDNA5 DNA was used in SDM (section 2.3) PCR to obtain plasmid +2301A pcDNA5 that encodes full-length PKP2a (mutagenic primers listed in Table 4.2,). +2301A pcDNA5 maintained the correct reading frame for expression of full-length PKP-2a protein in Flp-In T-Rex HEK 293 cells. Both plasmids –2301A pcDNA5 and +2301A pcDNA5 were sequenced to verify entire nucleotide sequences of the cloned DNA. The sequencing primers (Table 4.3,) verified the insert nucleotide sequences of the above two plasmids. Site-directed mutagenic primers (Table 4.2) were used to prepare plasmid A733fsX740 pcDNA5 using the method in section 2.3; this plasmid encoded a truncated plakophilin-2 (A733fsX740 PKP-2) verified by sequencing to confirm correct orientation and nucleotide coding sequence for the presence of the insertion/deletion (c.2197_2202delCACACC_insG).

4.4.3 Cloning in pcDNA4/XPress TOPO/TA

Plasmid pcDNA4/XPress/TOPO/TA enables protein expression from a cloned gene of interest preceded by short peptide sequences encoding poly-histidine (His_6) and an XPress epitope tag, this result in expression of a fused protein from a gene of interest. Antibody directed against a peptide tag (anti-XPress monoclonal antibody was used) enables examination of the *in vitro* protein-protein binding interaction (by immunoprecipitation technique) of endogenous desmosomal protein with either full-length or mutant PKP-2 proteins in pcDNA4 transfected HEK 293T cells.

The XPress primers (Table 4.4) and templates +2301A pcDNA5 and A733fsX740 pcDNA5 (Table 4.2) were used to obtain PCR amplified DNA encoding full-length and A733fsX740 plakophilin-2 that were cloned in pcDNA4 plasmid as described (section 2.2.2). Plasmids pcDNA4 PKP2 and pcDNA4 A733fsX740 PKP2 obtained were sequenced (using primers in Table 4.3) to verify the correct orientation and the reading frames of full-length and A733fsX740 PKP-2 nucleotide sequences of the insert sequences in these plasmids.

Table 4.2 SDM to obtain pcDNA5 encoding full-length and truncated A733fsX740 PKP-2

Site-directed PCR mutagenesis to obtain +2301A pcDNA5 and A733fsX740 pcDNA5 plasmids which are suitable for *in vitro* transfection studies in Flp-In T-Rex HEK 293 cells to obtain tetracycline-induced expressions of full-length PKP-2 and A733fsX740 PKP-2 proteins respectively. The Plasmid -2301A pcDNA5 containing an out of frame coding sequence of PKP2a (Table 4.1) was mutated by site directed mutagenesis to obtain +2301A pcDNA5 plasmid that correctly encoded the full-length PKP2a coding sequence. Plasmid A733fsX740 pcDNA5 containing the nucleotide coding sequence for the mutant A733fsX740 PKP2a was generated from +2301A pcDNA5 by site directed mutagenesis using the primers shown. Resulting plasmids obtained were sequenced to verify the entire protein encoding nucleotide sequences in these plasmids.

Purpose of Site Directed Mutagenesis	Forward primer Sequence (5'-3')	Reverse primer Sequence (5'-3')	Plasmid Mutated	Resulting plasmid Obtained
Create a plasmid encoding full-length PKP2a in pcDNA5	PKP2 Mut2301A for TTGGTGACCCAAGTGTGAAAAAGACA GCCATCTCGCTGCTGAG	PKP2 Mut2301A rev CTCAGCAGCCAGATGGCTGTCTTTTT CACACTTGGGTCACCAA	-2301A pcDNA5	+2301A pcDNA5
Create a plasmid encoding A733fsX740 PKP2a in pcDNA5	PKP2 A733fsX740 for CAGAAGGAAAGTGGCCTGCAGGCGAA AGATGCTGCATGTTGGT	PKP2 A733fsX740 rev ACCAACATGCAGCATCTTTCGCCTGC AGGCCACTTTCCTTCTG	+2301A pcDNA5	A733fsX740 pcDNA5

Table 4.3 PKP-2 primers for verifying sequence of cloned PKP-2

Sequencing primers for verifying the full-length PKP-2 and A733fsX740 PKP-2 DNA cloned into pcDNA5/FRT/TO/TOPO/TA vector. These primers were used to amplify either a PCR from each of the cloned inserts followed by sequencing using the respective forward or reverse, or they could be used directly in cycle sequencing reactions with plasmid templates containing the above inserts. For PCR amplification, an annealing temperature of 55°C was used with 1.5mM $MgCl_2$ concentration and 35cycles using 10ng plasmid preparation. PCR product sizes referred to amplification of wild type plakophilin-2 insert cloned into pcDNA5/FRT/TO/TOPO/TA. For the A733fsX740 plakophilin-2 insert cloned into pcDNA5/FRT/TO/TOPO/TA, the PCR product obtained using the primer pair Y forward/Y reverse is shorter by five bases because of the deletion/insertion. The P forward and Z reverse lie upstream and downstream of the insert cloned within the pcDNA5/FRT/TO/TOPO/TA vector.

Primer Pair	Sequence (5'-3')	PCR size (bp)
P forward	TTAGTGAACCGTCAGATCGCC	395
P reverse	AGGTTGTAGACATACTCAGGA	
Q forward	AGATCCTGGGACAACTGGACA	450
Q reverse	CACGGACTTCTGGGAGCTGTA	
R forward	TGACATGCTAAAGGCTGGCAC	340
R reverse	GTACTGTCTGTGGTATGTGTC	
S forward	TATGCTCGTTCCGAGATCGTG	359
S reverse	CTGGAATCCACGGCGACACTG	
T forward	CACTCAGAACAGGGCTTCCAG	271
T reverse	TTCTGGAAGCACTCGTGCTGT	
U forward	ACAGCACGAGTGCTTCCAGAA	320
U reverse	TCAGCGTAAGCAATGCTTCTG	
V forward	AGCAAACCAGAGACTTGGAGA	295
V reverse	TTTGGGTAGTCTCCTTCAGGC	
W forward	CAGAAGCATTGCTTACGCTGA	357
W reverse	CTTTTGTTGTTGTCAGTCTGG	
X forward	TAACCTCTCCTACCAGCTGGA	418
X reverse	CGAGATGGCTGYCTTTTTCAC	
Y forward	TCAGTGGCTCAGACAGTTGTC	350
Y reverse	TTGTTGGAGGCATAGGCATCG	
Z forward	ACCAGAATGCACGCGACCTTC	367
Z reverse	AGGCACAGTCGAGGCTGATCA	

Table 4.4 Cloning of PCR amplified DNA encoding either full length or truncated PKP-2 into pcDNA4

Cloning of PKP-2 and A733fsX740 PKP-2 into pcDNA4/XPress/TOPO/TA vector suitable for *in vitro* transfection studies to obtained XPress-tagged expression of full-length and A733fsX740 PKP-2 protein expression in HEK 293T cells. Transient expression of these XPress-tagged PKP-2 proteins in HEK 293T transfected cells can be immunoprecipitated using an anti-XPress antibody. Plasmids +2301A pcDNA5 and A733fsX740 pcDNA5 (Table 4.2) were used as PCR templates with EXL DNA polymerase to obtain amplimers that were cloned in pcDNA4/XPress/TOPO/TA. Primer pairs PKP2 XPress for and PKP2 XPress rev amplified PCR fragments encoding either full-length PKP-2 or A733fsX740 PKP-2 DNA that was cloned in pcDNA4/XPress/TOPO/TA preceded by vector encoded sequences for poly-histidine and an XPress tag (amino acid sequence: DLYDDDK). The cloned PKP-2 DNA maintained the proper reading frame for protein translation with an ATG translation start site used from the host vector. A stop codon for protein translation termination was contained in the amplified cloned DNA inserts. PKP-2 or A733fsX740 PKP-2 proteins expressed in HEK 293T transfected cells contained N-terminal fused 6XHis tag and an XPress epitope adding 3.9 KD to the size of each PKP2 expressed.

Primer Pairs	Sequence (5'-3')	PCR size (bp) / Enzyme used/ Template	Destination vector PCR product cloned into	Plasmids obtained
PKP2 XPress for	ATGGCAGCCCCCGGCGCCCCAGCT	2517 & 2522* /EXL/ **	pcDNA4/XPress/TOPO	pcDNA4 A733fsX740 PKP2 or pcDNA PKP2
PKP2 XPress rev	GCTCTAGATCAGTCTTTAAGGGAGTGGTAGGC			

* PCR fragment sizes 2522 and 2517bp were for full-length PKP-2, and A733fsX740 PKP-2 amplimers respectively.

** Templates used A733fsX740 pCDNA5 and +2301A pcDNA5 respectively.

4.4.4 Preparation of stable transfected cell lines

Stable cell lines were established in Flp-In T-Rex HEK293 cells using pcDNA5 PKP2 and pcDNA5 A733fsX740 PKP2 plasmids as per procedure described previously (section 2.5.4) to obtain full-length PKP-2 and A733fsX740 PKP2 protein expressions upon tetracycline-induction. At least five different clones of each stable cell line established were selected and clonally expanded, and a best clone showing strong stable tetracycline-induced protein expression by western blotting (section 2.6.2) and immunofluorescence staining (section 2.7.2) were selected for functional studies based on the above criteria: clone **wPKP2** expressed full-length PKP-2 and clone **tPKP2** expressed A733fsX740 PKP-2 under tetracycline-induction respectively.

4.5 Results

4.5.1 Characterization of plakophilin-2 expressions in wPKP2 and tPKP2 stable cells

Full-length PKP-2a was expressed in tetracycline-induced wPKP2 stable cells that localised as punctate staining at cell-cell junctions (Figure 4.2A) and this was detected as a strongly induced 98.7 KD band (Figure 4.3A) by SDS PAGE/western immunoblotting analysis, which correlated with the predicted size of PKP-2a. Using confocal microscopy examination of PKP-2 staining procedure (protocol omitting detergent treatment step) that preserved nuclear PKP-2 staining, but not of membrane PKP-2[182], induced PKP-2a was shown to be present in the nucleus (Figure 4.4A) of tetracycline-induced wPKP2 cells. Sub-cellular fractionation of tetracycline-induced wPKP2 cells (Figure 4.5A) confirmed nuclear presence of PKP-2a protein. The antibody used in these localization studies was a mouse anti-plakophilin-2 recognising an epitope located within the N-terminus between amino acid residues 19 to 183. A predominant localisation of full-length PKP-2a occurred in the cytoplasm, membrane, and cytoskeletal fractions of tetracycline-induced wPKP2 cells, whereas a smaller amount of this protein was associated with the nuclear fraction examined by sub-cellular fractionation and distribution studies (Figure 4.5A). A human heart ventricular lysate (100μg protein) was analysed by SDS PAGE and western

immunoblotting analysis that showed expressions of both PKP-2a and PKP2b proteins in the lysate (Figure 4.2C).

Truncated plakophilin-2 (A733fsX740 PKP-2) expressed in tetracycline-induced tPKP2 cells was localised by confocal microscopy in punctate staining at the cell-cell contacts (Figure 4.2B). The truncated PKP-2 was detected as a 77.1 KD band by SDS PAGE and western immunoblotting analysis (Figure 4.3B) that correlated with the predicted size of this truncated PKP-2 protein. Endogenous full-length PKP2 was also present in tKPK2 cells, which migrated at an expected position on the SDS PAGE gel. Using confocal microscopy examination of PKP-2 staining procedure (protocol omitting detergent treatment) that preserved nuclear PKP-2 staining, but not of membrane PKP-2[182], induced A733fsX740 PKP-2 was shown to be present in the nucleus (Figure 4.4B) of tetracycline-induced tPKP2 cells. Sub-cellular distribution studies of induced tPKP2 cells (Figure 4.5B) showed strong expression of a truncated PKP-2 in cytoplasm and cytoskeletal fractions with roughly equal amount of an endogenous PKP-2 and truncated PKP-2 compartmentalizing in the cytoskeletal fraction. Both truncated and endogenous PKP2 appeared in the membrane compartment, but with more endogenous PKP-2 localising in this fraction. In the nuclear fraction, roughly equal amounts of endogenous and truncated PKP-2 were present. The sub-cellular fractionation Qproteome cell compartment kit is used to fractionate proteins specific for the cytosol, membrane, nuclear and the cytoskeletal compartments of HEK 293 and other cells [219,220]. However, the validity of this kit has been verified by examining specific protein marker distribution in the four protein fractions obtained from a different stable cell line expressing truncated DP protein (fractionation of tDP stable cells verified in Figure 6.5).

Figure 4.2 Immuno-localisation of full-length and A733fsX740 PKP-2 in wPKP2 and tPKP2 cells by confocal microscopy

Localization of expressions of full-length PKP-2 and A733fsX740 PKP-2 to the cell membranes of tetracycline-induced wPKP2 and tPKP2 stable cell lines respectively. Immunofluorescence images showing blue fluorescence signal resulting from DAPI nuclear staining, green fluorescence resulting from FM 1–43FX membrane dye staining, red fluorescence resulting from full-length PKP2 or A733fsX740 PKP2 staining with anti-PKP2 antibody (610788, BD Bioscience) followed by anti-mouse Alexa 546 and merge representing composite staining (all panels on the far right) with all signals superimposed. A punctate staining of each plakophilin indicates a staining reminiscent of desmosomal reactivity. The size bar on each image in the green channel represents 8μm.

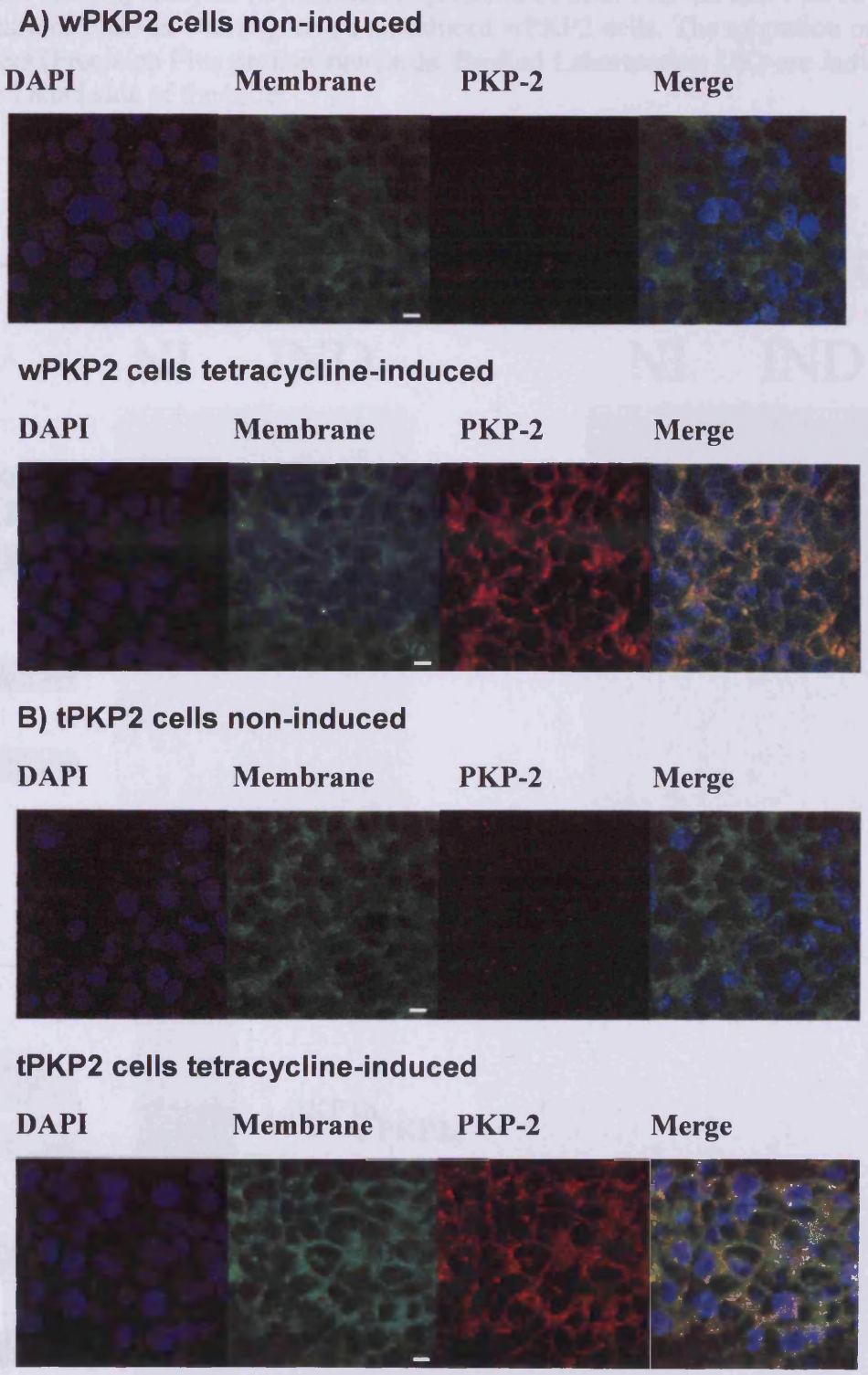

Figure 4.3 Western blot analysis of the expressions of PKP-2 & A733fsX740 PKP-2 in wPKP2 & tPKP2 cells and of PKP-2s in human heart ventricular lysate

Analysis of expressions of full-length PKP-2 and A733fsX740 PKP-2 in non-induced (NI) or tetracycline-induced (IND) wPKP2 (A) and tPKP2 (B) stable cells determined by western blotting technique. A mouse monoclonal antibody to human PKP-2 (1:500, BD Bioscience, product 610788) was used followed by a goat anti-mouse HRP conjugate (1:5000 dilution, Abcam). Blots were exposed to ECL reagents (GE Healthcare) and developed using Kodak reagents. Human heart ventricular lysate western blotting analysis (C) showed expression of both PKP-2a and PKP2b isoform expression; PKP-2a was expressed in induced wPKP2 cells. The migration of protein markers (Precision Plus protein standards, BioRad Laboratories, UK) are indicated on the left hand side of the blots

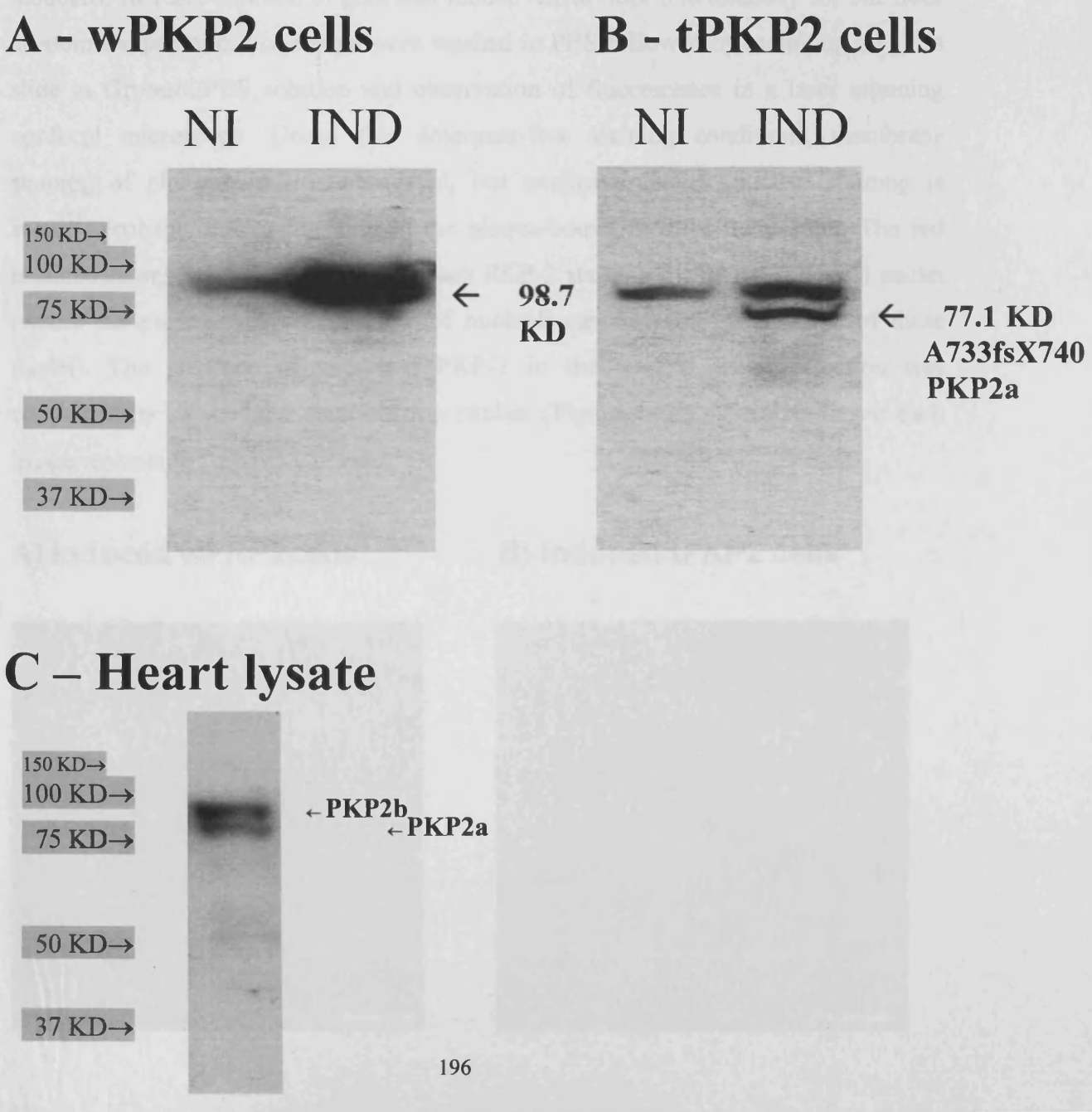

Figure 4.4 Demonstration of nuclear presence of full-length and truncated PKP-2 in wKPP2 and tPKP2 induced cells

Nuclear staining of full-length PKP-2 and A733fsX740 PKP-2 demonstrated in tetracycline-induced wPKP2 and tPKP2 stable cells respectively using confocal microscopy. Cells were cultured on glass coverslips in the presence of 0.1μg/ml tetracycline to induce the expressions of the respective PKP2 isoforms in each stable cell line. Seventy-two hours after induction, cells were fixed in –20°C methanol for five minutes followed by incubation in acetone for 30 seconds. After rinsing the cells in PBS, they were incubated in 10% FBS/PBS solution for thirty minutes, followed by incubation in 1:200 dilution of mouse anti-plakophilin-2 (BD Bioscience, 610788) for thirty minutes at room temperature. Coverslips were washed gently twice in PBS and incubated in 1:200 dilution of goat anti-mouse Alexa fluor-546 antibody for one hour at room temperature. Coverslips were washed in PBS followed by mounting on glass slide in Glycerol/PBS solution and observation of fluorescence in a laser scanning confocal microscope. Under this detergent-free staining conditions, membrane staining of plakophilin-2 is abrogated, but exclusive intense nuclear staining is seen[221], probably due to masking of the plaque-bound form of the protein. The red immunofluorescence signal localized each PKP-2 staining inside the spherical nuclei (where the presence of dark outline of nucleoli can be seen inside some of these nuclei). The presence of truncated PKP-2 in the nuclear protein fraction was confirmed by sub-cellular fractionation studies (Figure 4.5B). The size bar on each image represents 5μm.

A) Induced wPKP2cells

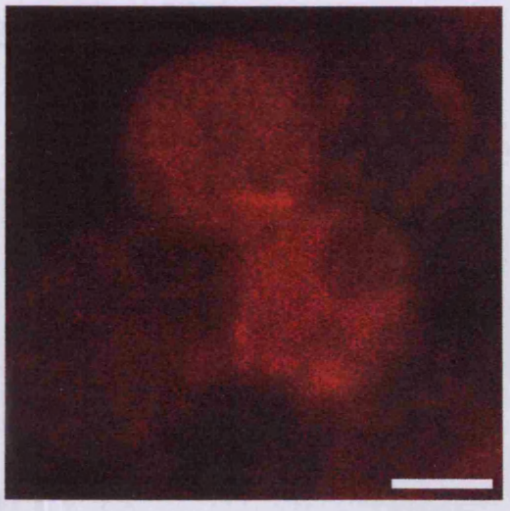

B) Induced tPKP2 cells

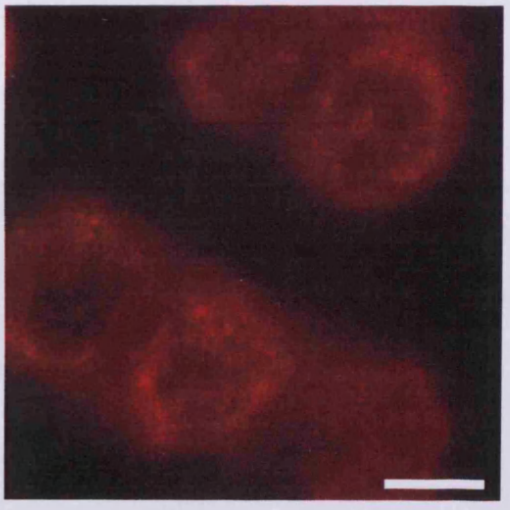

Figure 4.5 sub-cellular localization of full length & truncated PKP2 in wPKP2 and tPKP2 stable cells

Sub-cellular distribution of A) full-length PKP-2, or B) A733fsX740 PKP-2 in cytosolic (CYT), membrane (MEM), nuclear (NUC) and cytoskeletal (CSK) protein fractions obtained from tetracycline-induced (48hrs) wPKP2 or tPKP2 stable cells respectively. Sub-cellular protein fractions were obtained from $5x10^6$ cells from each cell line using the Qproteome cell compartment kit (Qiagen, UK). Each protein fraction obtained was precipitated in four volumes of ice-cold acetone and the pellet was resuspended in 100µl RIPA buffer containing protease inhibitor cocktail (Roche). $1/5^{th}$ of each protein fraction was electrophoresed in a 10% SDS PAGE gel and transferred onto a Hybond ECL membrane. Following blocking of blot in TBST/5% milk, it was incubated with 1:500 mouse monoclonal anti-plakophilin-2 (610788, BD Bioscience) for one hour in TBST/5% milk at room temperature. Following washing of the blots in TBST, they were exposed to 1:3500 dilution of anti-mouse HRP conjugate in TBST/5% milk for one hour at room temperature. After washing the blots in TBST, they were incubated in ECL reagents (GE Healthcare) followed by exposure to ECL Hyperfilm (GE Healthcare).

A) Induced wPKP2 cells

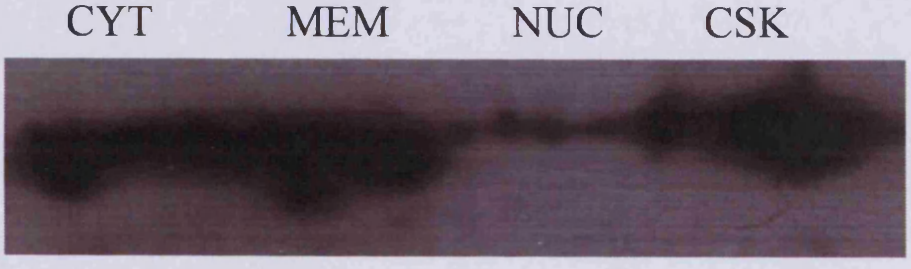

← **98.7 KD full-length PKP2a and endogenous PKP2**

B) Induced tPKP2 cells

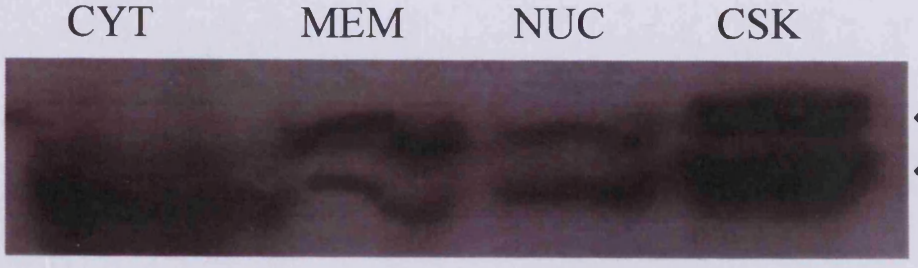

← **98.7 KD PKP2a**

← **77.1 KD A733fsX740 PKP2a**

4.5.2 Properties of wPKP2 and tPKP2 stable cells

Cellular proliferation of wPKP2 and tPKP2 cells did not alter substantially as the values of the slopes obtained by regression analysis were similar in these cells upon tetracycline induction to obtain expressions of full-length or truncated PKP-2 respectively (Figure 4.6). The initial cell-cell adhesion of induced calcein-labelled wPKP2 or tPKP2 cells plated onto homologous confluent monolayers of induced wPKP2 and tPKP2 cells cultured on plastic coverslips showed that there was significantly increased adherence of tPKP2 cells compared to wPKP2 cells (Figure 4.7). A Dispase-based cell dissociation assay measuring the adhesive strengths of highly confluent induced monolayers of wPKP2 and tPKP2 cells showed an increased resistance to fragmentation of tPKP2 monolayer versus those of wPKP2 (larger fragments seen in tPKP2) monolayer when these were subjected to shear stress (Figure 4.8). The increased adhesive strength of tPKP2 monolayer was reflected during trypsinization procedure as confluent induced tPKP2 monolayer took a consistently longer time (five minutes, data not shown) to come off the culture flask compared to confluent induced wPKP2 monolayers that came off earlier (three minutes, data not shown). Stable wPKP2 and tPKP2 cells subjected to mechanical cell-stretch and then allowed to recover for a short while showed that there was approximately a two-fold increased apoptosis measured in tPKP2 cells compared to wPKP2 cells (Figure 4.9). During the mechanical cell stretch experiments, cells were cultured on gelatine-coated silicon membranes, which did not permit immuno-staining *in situ* to demonstrate apoptosis. However, analysis of whole cell lysates of mechanically stretched and non-stretched wPKP2 and tPKP2 cells by western immunoblotting showed that cells exposed to mechanical stretch expressed increased 17KD active caspase-3 protein band (formed by activation of caspases-3), which appeared more intense in induced stretched tPKP2 cells (Figure 4.10).

Figure 4.6 Proliferation of wPKP2 and tPKP2 cells

Cellular proliferation of stable wPKP2 and tPKP2 cells expressing full-length PKP-2 and A733fsX740 PKP-2 respectively. 15,000 cells per well were plated in a twenty-four well plate and allowed to attach overnight. Cell proliferation was measured spectrophotometrically at 490nm by measuring the reduction of Cell Titer AQ One solution (Promega, UK) after incubation of substrate with cells for exactly one hour. The seven data points obtained in each treatment were fitted to a linear tread line using Microsoft Excel software. The values of the slopes were: 0.0216, 0.0231, 0.0231, 0.0236 for wPKP2NI, wPKP2 IND, tPKP2 NI and tPKP2 IND cells respectively.

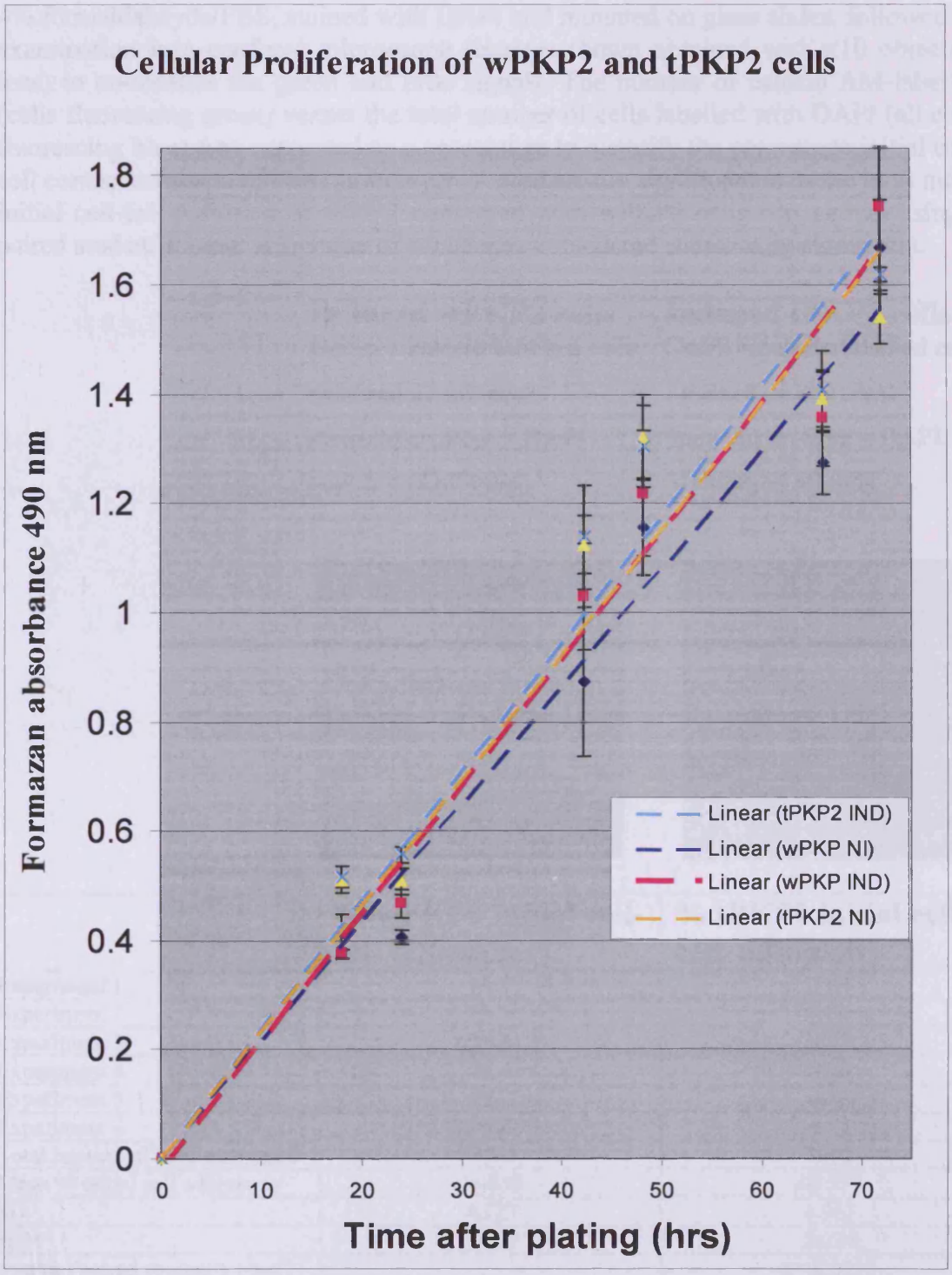

Figure 4.7 Initial cell-cell contact adhesion assay of wPKP2 and tPKP2 cells

Initial cell-cell contact adhesion measured in wPKP2 and tPKP2 stable cell lines expressing full-length PKP-2 and A733fsX740 PKP-2 respectively. Both cell lines were cultured under tetracycline-induced conditions on 13 mm plastic coverslips to obtain a uniform highly confluent monolayer of cells. Separate suspension aliquots (1 x 10^6) of each tetracycline-induced cells previously pre-incubated in 10μM Calcein AM dye were allowed to adhere to the homologous unlabelled confluent monolayer of cells growing on coverslips conditions for five hours at 37°C/5%CO_2. Coverslips were carefully washed four times in complete DMEM medium. Coverslips were fixed in 4% formaldeheyde/PBS, stained with DAPI and mounted on glass slides, followed by examination in a confocal microscope (images shown obtained with x10 objective lens) to co-localise the green and blue signals. The number of calcein AM-labelled (cells fluorescing green) versus the total number of cells labelled with DAPI (all cells fluorescing blue) was expressed as a percentage to quantify the percentage initial cell-cell contact adhesion of each monolayer. A statistically significant increase in % mean initial cell-cell adhesion of tPKP2 compared with wPKP2 cells was shown using a paired student's t-test. A p-value of <0.05 was considered statistically significant.

Induced wPKP2 cells
Green = calcein labelled cells retained on adherent monolayer, Blue = DAPI staining of all cells

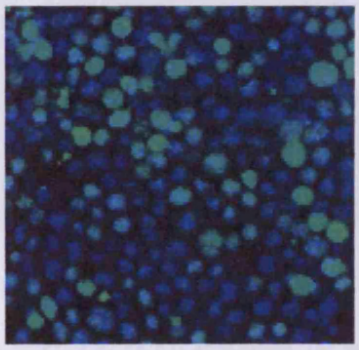

Induced tPKP2 cells
Green = calcein labelled cells retained on adherent monolayer, Blue = DAPI staining of all cells

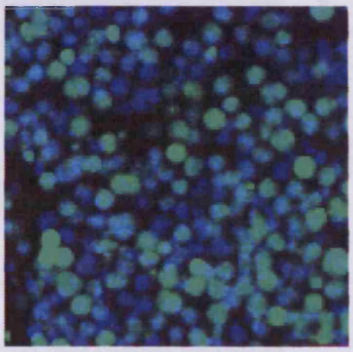

	% wPKP2 initial cell-cell adhesion	% tPKP2 initial cell-cell adhesion
Experiment 1	20.7	39.8
Experiment 2	23.3	41.4
Experiment 3	24.4	37.3
Experiment 4	25.4	33.0
Experiment 5	29.3	46.6
Experiment 6	35.4	44.9
Total number of cells examined	3000	3000
Mean % initial cell adherence	26.050	40.517
SD	4.723	4.957
SEM	1.928	2.024
p value (paired student's t-test)		p= 0.0036

Figure 4.8 Dispase-based induced wPKP2 and tPKP2 monolayer dissociation adhesion assay

Monolayer adhesive strength of tetracycline-induced wPKP2 and tPKP2 confluent monolayers measured using a Dispase-based cell dissociation assay[212]. Each cell line was cultured in 60 mm Nunc brand plastic culture dishes in penicillin, streptomycin, foetal bovine serum, blasticidin and hygromycin supplemented DMEM (Invitrogen 19308-025) in the continued presence of 0.1μg/ml tetracycline until cells were highly confluent. Medium was decanted from each dish and the cell monolayer was carefully washed in PBS. One ml of 2.4U/ml Dispase II (Roche, Cat No 10295835001) was added to the dishes followed by incubation at 37°C for 30 minutes. The entire intact monolayer lifted off the plastic cell culture dish by Dispase treatment was carefully rinsed in PBS and resuspended in five ml of PBS. The cell monolayer was subjected to shearing for exactly ten rotations on a rocking tabletop platform. Sheared monolayer was photographed under Epi-white light illumination in BioRad Gel Documentation system (gel doc XR) using quantity one version 4.6 software for image analysis. This adhesion assay showed visually that tPKP2 cells resisted fragmentation, resulting in larger fragments after ten rotations compared to control wPKP2 cells forming comparatively smaller fragments under the same conditions.

Control wPKP2 stable cells expressing full-length PKP-2

Small monolayer fragments formed in wPKP2 cells by shearing

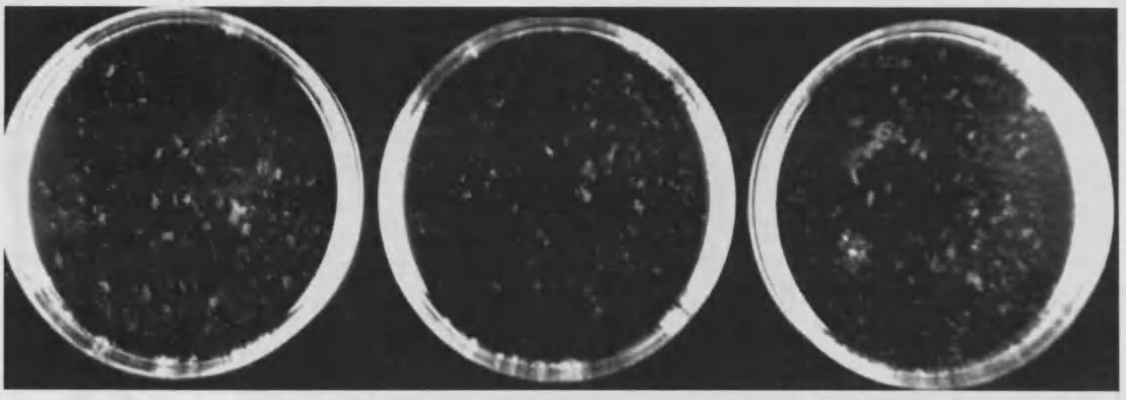

tPKP2 stable cells expressing A733fsX740 PKP-2

Larger monolayer fragments in tPKP2 cells by shearing → increased monolayer adhesion
Arrows indicate presence of large fragments in tPKP2 cells that are not present in wPKP2 cells

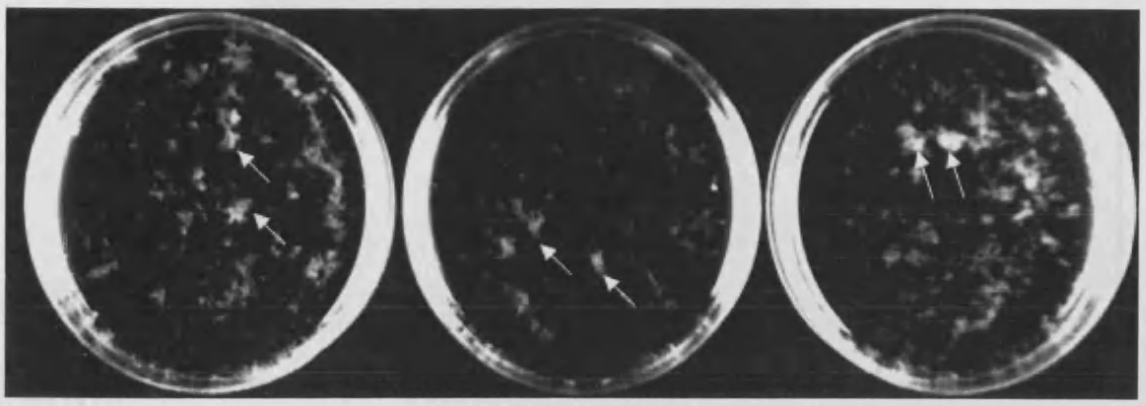

Figure 4.9 Effect of mechanical cell-stretch on apoptosis of wPKP2 and tPKP2 stable cells

Effect of mechanical cell stretch on the measured apoptosis determined in wPKP2 and tPKP2 stable cells. Student's paired t-test statistical p value = 0.1448 (wPKP2 NI versus wPKP2 Ind) and $p < 0.0001$ (tPKP2 Ind versus either tPKP2 NI or wPKP2 Ind). Apoptosis levels are mean values of n = 6 experiments $\pm$ standard deviations. The CaspACE assay system (Promega, UK) was used to measure the specific activity of caspase-3 in cell lysates of cells subjected to mechanical stretch using the Flexer cell-stretch apparatus with 4% cell-stretch applied at a frequency of 1Hz for 3.5 hours followed by recovery of cells for 3 hours prior to assessing apoptosis. Cell plating density was 0.5×10^6 cells/six well plate and these were cultured for 48 hours prior to exposure to mechanical stretch. Induced cells were cultured in presence of 0.1μg/ml tetracycline.

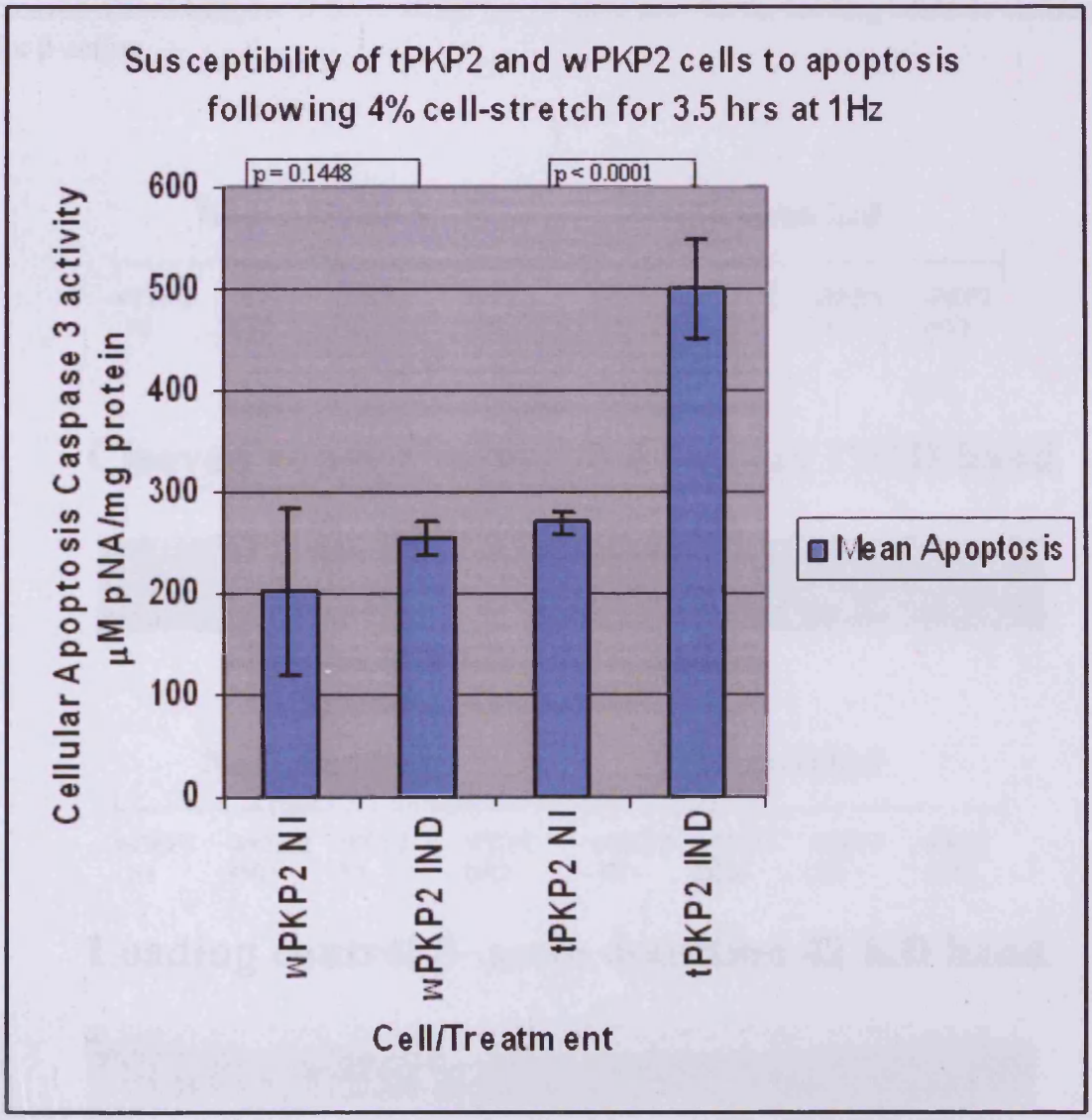

Figure 4.10 Western blot analysis of active caspase-3 in wPKP2 and tPKP2 cells not exposed or exposed to 4% mechanical cell-stretch at 1 Hz for 3.5 hrs

Western blot analysis to detect cleaved Caspase-3 in cell lysates of non-stretched and mechanically stretched wPKP2 and tPKP2 cells. Cells were subjected to 4% mechanical stretch at 1Hz for 3.5hours in the Flexer cell-stretch system. Non-stretched cells were cultured in a FlexerCell six well plate and handled in an identical manner as cells exposed to mechanical cell-stretch except that these cells were spared exposure to mechanical cell-stretch. Cell lysates were prepared in RIPA buffer from cells that had undergone 4% mechanical stretch or from cells that were not subjected to stretch. 100µg of cell lysates were electrophoresed on a 15% SDS PAGE gel and blotted on ECL Hybond membrane. Following blocking of blots in TBST/5%milk they were incubated either in 1:500 rabbit anti-active caspase3 antibody (antibody detects a band of 17 KD, Abcam Plc, UK) or in 1:2000 rabbit anti β-actin antibody (Abcam, ab-8227) for one hour. Blot were washed in TBST and incubated in 1:3500 mouse anti-rabbit HRP conjugate (Abcam) for one hour. Blot were washed in TBST and incubated in ECL reagents followed by exposure to ECL Hyperfilm and development using Kodak photographic reagents. Top part of the figure shows cleaved active Caspase-3 band while the bottom part shows loading controls staining for β-actin.

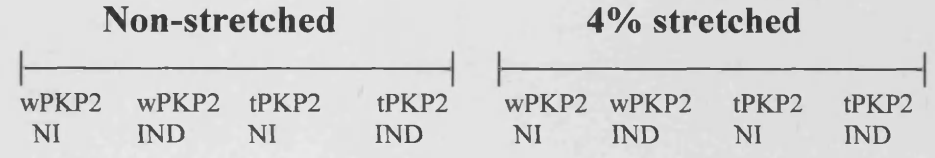

Cleaved active Caspase-3 detection 17KD band

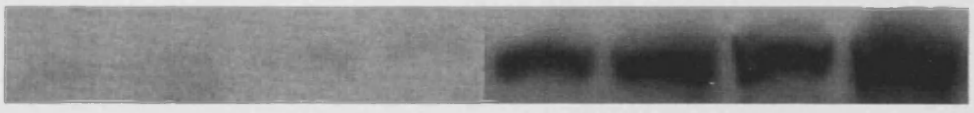

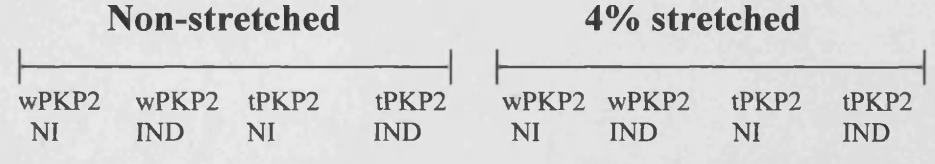

Loading control β–actin detection 42 KD band

4.5.3 Connexin-43 protein expression in wPKP2 and tPKP2 stable cells

Analysis of non-induced and induced wPKP2 and tPKP2 highly confluent monolayer soluble cell lysates by western immunoblotting showed strong Connexin-43 protein bands in both cells (Figure 4.11). However, examination of these induced cells by confocal microscopy confirmed Connexin-43 protein localization to cell membranes of wPKP2 cell membranes (Figures 4.12A and Figure 4.13), but this was consistently absent in tPKP2 cell membranes as shown by a representative staining (Figure 4.12B).

Figure 4.11 Western blot analysis of whole cell lysates of wPKP2 and tPKP2 cells to measure Cx-43 and plakophilins

Connexin-43 levels in wPKP2 and tPKP2 cells analyzed by western blotting analysis. The top panel shows the levels of Cx43, middle panel shows PKP-2 and A733fsx740 PKP-2 levels and bottom panel shows β-actin as loading control. Stable wPKP2 and tPKP2 cells were cultured in the absence (NI) or presences of 0.1μg/ml tetracycline (IND) for 72 hrs until cells were fully confluent. Cell lysates were prepared in RIPA buffer and equal amounts of cell lysates (100 microgram protein) were separated in a 10% SDS PAGE system. Gels were blotted onto ECL Hybond membrane and blots were blocked in TBST/milk followed by incubation in 1: 2000 rabbit anti-connexin-43 (GJA1, Abcam ab-113700), or 1:500 mouse anti-human PKP2 (610788, BD Bioscience), or 1:2000 rabbit anti-β-actin (loading control, Abcam, ab-8227). Following washing of blots in TBST they were incubated in either 1:5000 anti-mouse HRP or 1:5000 anti-rabbit HRP. Blots were washed in TBST and incubated in ECL reagents (GE Healthcare) followed by exposure to ECL Hyperfilm and development with Kodak photographic reagents.

Detection of Connexin-43 using antibody GJA1 43KD band

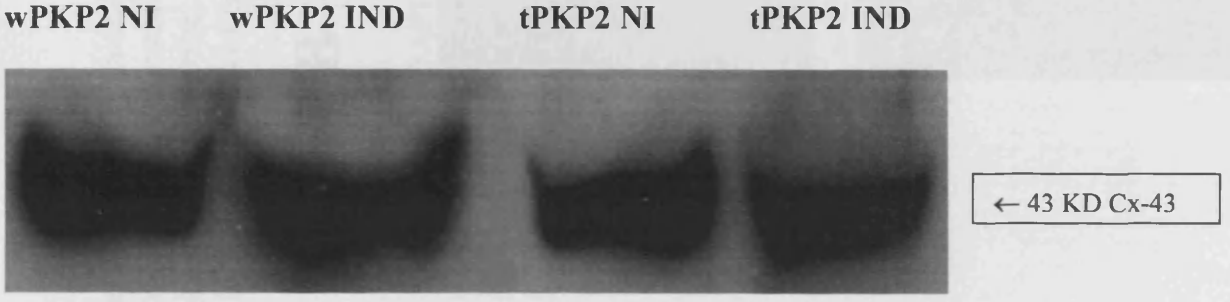

Detection of PKP2a (97 KD) and A733fsX740 PKP-2 (81KD)

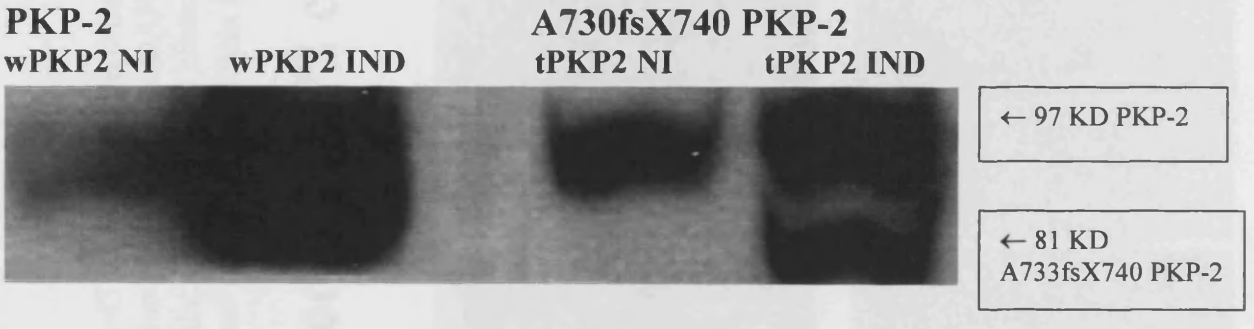

Detection of loading control β-actin 42KD band

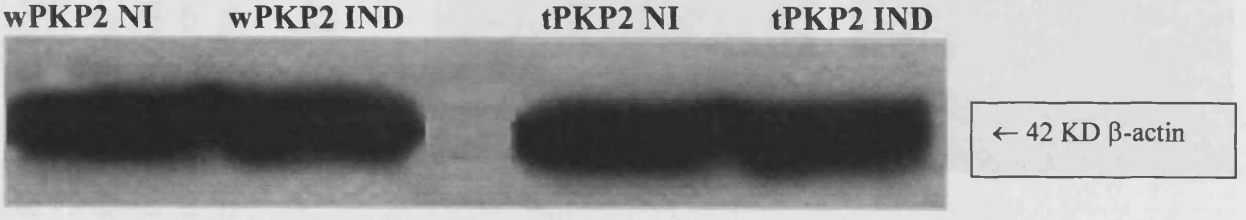

Figure 4.12 High Magnification immuno-localisation of Cx-43 expression in wPKP2 and tPKP2 stable cells

Localization of Connexin-43 expression determined by immunofluorescence staining and confocal microscopy examination of induced wPKP2 and tPKP2 stable cell lines. Blue channel records DAPI nuclear staining, green channel records cell membrane staining with FM 1-43FX dye, red channel records connexin-43 staining, and composite channel shows all three signals together. Images were obtained using x100 objective lens. The size bar in the green channel represents 10μm. Cx-43 protein localization in cell membranes of wPKP2 cells occurs, but this is absent in tPKP2 cells.

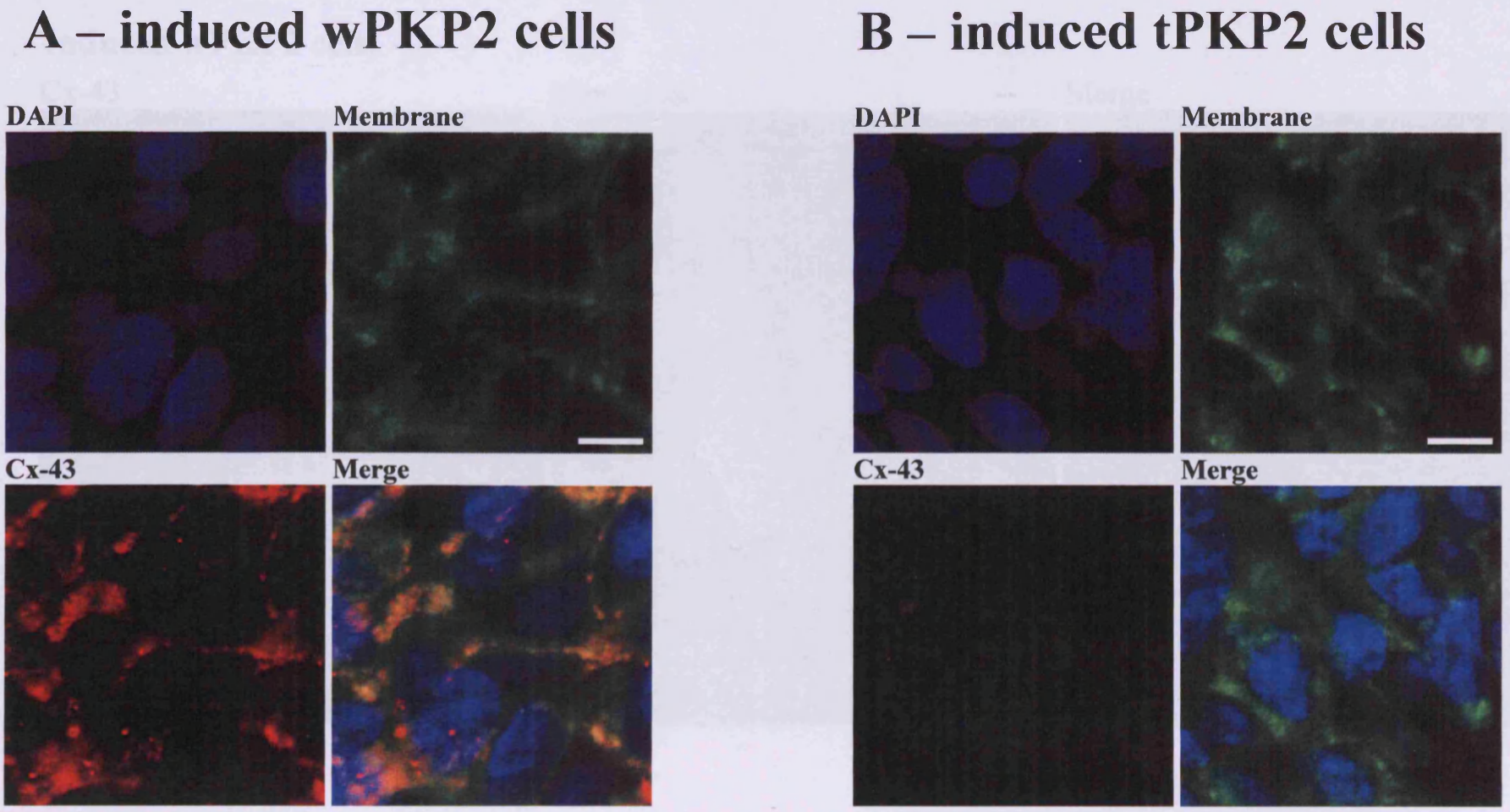

Figure 4.13 Low magnification immuno-localisation of Cx-43 to cellular membrane of tetracycline-induced wPKP2 stable cells

Confocal microscopy localization of connexin-43 expression to cell membranes of induced wPKP2 cells. Red channel shows connexin-43 protein staining, green channel shows cell membrane staining with FM 1-43FX dye and merge channel shows both signals superimposed. These images were obtained using x40 oil immersion objective lens. Cx-43 protein is present abundantly in these cells and localizes within the cellular membrane of induced wPKP2 cells. The size bar in the green channel represents 7 μm.

Induced wPKP2 cells

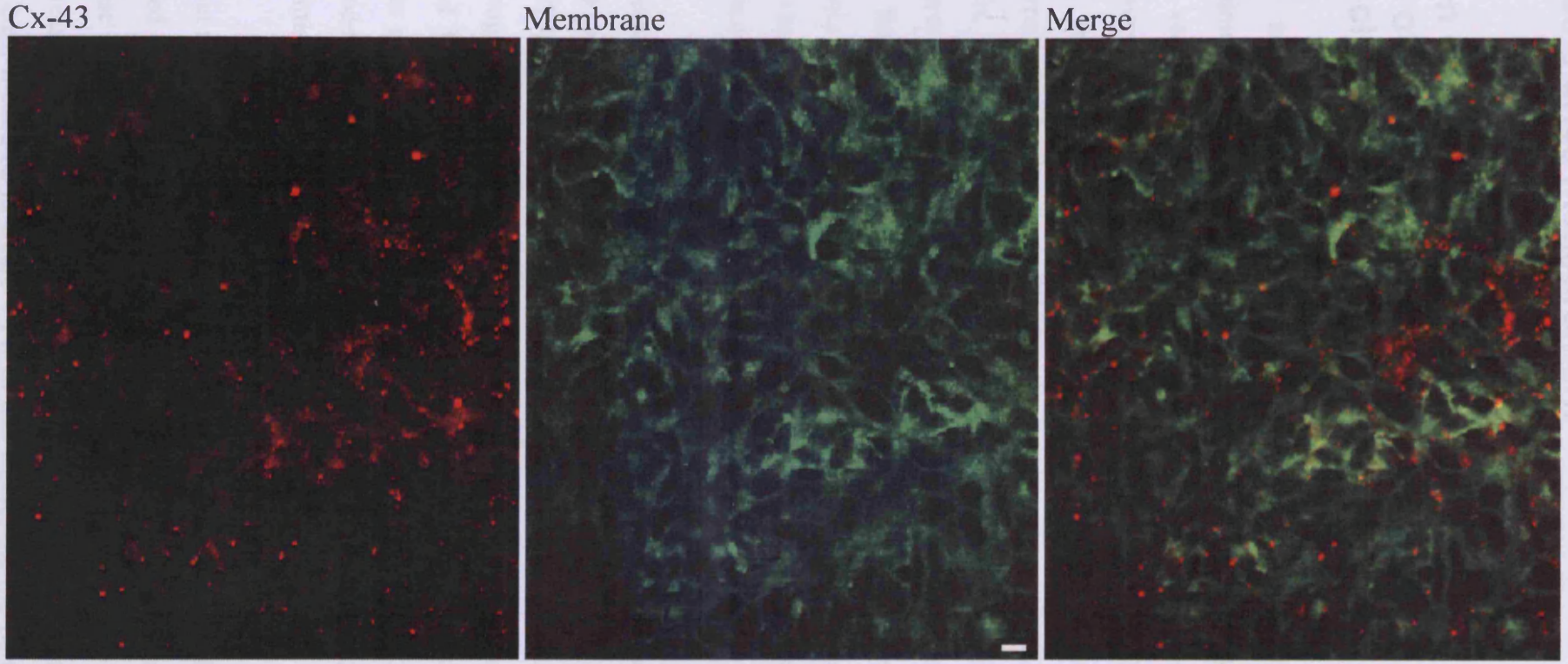

4.5.4 Cell Input Resistance measurement

4.5.4.1 Description of the measurement of the cell input resistances of tetracycline-induced wPKP2 and tPKP2 stable cell clusters

This electrophysiological technique compares two different monolayer cell preparations to determine how well cells in the monolayer connect to each other by measuring the flow of an electric current through cell clusters. The rationale for employing this technique was to determine whether the difference in connexin-43 protein localising at cell membranes of induced wPKP2 versus tPKP2 cells accompanied a better current conduction in wPKP2 cells compared to tPKP2 monolayers: the later cells, which did not express connexin-43 protein at cell membranes. Cell lines were cultured in 35mm diameter culture dishes in the presence of tetracycline (0.1μg/ml) for expression of respective plakophilins (full-length or truncated PKP-2). Both cells were highly confluent prior to performing cell input resistance measurements. These experiments were performed in collaboration with Professor Chris Fry; Dr Rosaire Gray performed the measurements and data analysis.

The cell input resistance measurements were carried out using a single 3M KCl-filled borosilicate microelectrode pulled using an automated micropipette puller (P-87, Sutton Instruments Co, USA) designed to construct uniform microelectrodes of similar resistance. The voltage measured by the microelectrode was compared to a reference electrode (a liquid 3M KCl junction) in contact with the extracellular (cell culture medium) fluid. The membrane potential of an individual cell was recorded against the reference electrode after inserting the microelectrode into a single cell and ensuring a steady state potential difference (p.d) was obtained.

Prior to performing cell input resistance measurements, a steady state value of the cell membrane potential recorded on an oscilloscope was rescaled to allow simultaneous recording of an injected pulse of electrical current and the elicited potential difference. For cell input resistance measurement of each cell preparation, a single experiment consisted of two measurements, illustrated in figure 4.14. In this figure, the top part shows a schematic diagram of the microelectrode setup for each of the two

measurements, the middle part shows electrical circuits in each situation, and the bottom part showed the p.d. change recorded in each case upon injection of a step pulse of an electric current. In Figure 4.14A, the microelectrode was placed in contact with culture medium alone that surrounded the cell monolayer. The p.d. measured in response to injecting step pulses of varying magnitude of electrical current through the microelectrode and into the medium determined the microelectrode resistance r_{el} (following Ohm's law). The time constant of the microelectrode, $\tau_{el} = r_{el}\, c_{el}$, where c_{el} = the capacitance of the microelectrode, was extrapolated from p.d. traces recorded on a fast time scales (see section 4.5.4.2). The time constant τ was the time required for the voltage to reach (1 – 1/e) of its maximum plateau (i.e. about 63%). In Figure 4.14B, a microelectrode was inserted into a single cell and the change of p.d. was recorded following injection of varying step pulses (14 ms duration) of current. The voltage recordings in Figure 4.14A and Figure 4.14B were monitored on a slow and on a fast time scale to determine the resistance of the cellular preparation, r_{prep} (Figure 4.14B) or that of the electrode alone r_{el} (Figure 4.14A). The respective time constants τ_{el} and τ_{prep} were extrapolated from the fast voltage response traces using curve-fitting software of the stored transients. The resistance of the cell was given by the equation $r_{cell} = r_{prep} - r_{el} \simeq r_i$, where r_{cell} = cell input resistance, r_{prep} was the measured resistance of the preparation (using Ohm's law, R=V/I) and r_{el} = resistance of the microelectrode. It was assumed that r_{cell} was predominantly determined by r_i (the intracellular resistivity). r_i was in series with the membrane resistance, r_m, but $r_m << r_i$. The rise in p.d. in response to injection of current in the preparation was given by a time constant, $\tau_{prep} = r_{prep}c_{prep}$, where c_{prep} = capacitance of the preparation. The time constant of the cell, $\tau_{cell} = \tau_{prep} - \tau_{el}$, where τ_{prep}= time constant of the preparation and τ_{el} = time constant of the electrode. The τ_{cell} value was a measure of cellular mass of each preparation as it was assumed that cell mass was proportional to cell membrane area of unit specific capacitance.

r_i values were plotted as a function of τ_{cell} when a linear relationship was generally observed for each monolayer. The slope of the line was a measure of resistance of the preparation (dominated by r_i) as a function of unit cell mass. A decrease of slope would indicate a unit reduction of r_i. r_i itself was assumed a sum of cytoplasm resistance, r_c, and intercellular coupling resistance, r_j. An increase of Connexin-43 expression would reduce r_j, and hence r_i, per unit change of τ_{cell} – i.e. the slope of the plot would be reduced.

Figure 4.14 Principles of cell input resistance measurement

Cell input resistance measurements were made using measurements in two situations: A) electrode in solution and B) electrode inserted inside a cell.

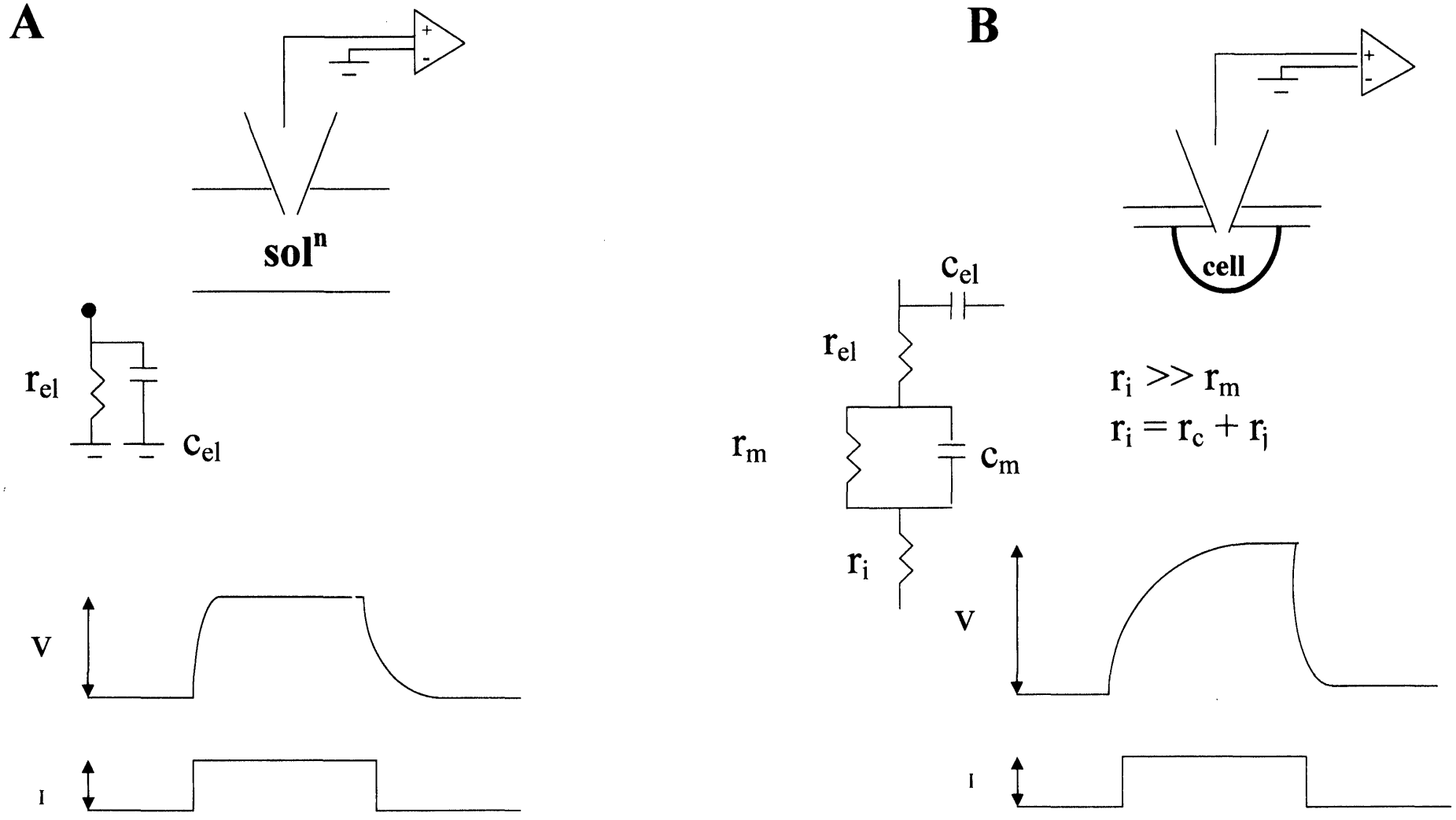

$v = Ir_{el}$, $r_{el} = v/I$

$\tau_{el} = r_{el}c_{el}$

$v = Ir_{prep}$, $r_{prep} = v/I$

$r_{cell} = r_{prep} - r_{el} \simeq r_i$

$\tau_{prep} = r_{prep}c_{prep}$.

$\tau_{cell} = \tau_{prep} - \tau_{el}$

4.5.4.2 Results: measurement of the cell input resistances of induced wPKP2 and tPKP2 cell clusters

Representative intracellular and extracellular p.d. recordings obtained from individual cell input resistance measurements of wPKP2 and tPKP2 monolayers are shown in Figures 4.15 and 4.16 respectively. The fast p.d. change recordings were analyzed using Kaleidograph^{TR} software to obtain r_{fast} (representing cell input resistances, see Tables 4.5 and 4.6) values, and the τ_{cell} values were calculated after estimating τ_{prep} and τ_{el} values with the aid of this software.

Analysis of clusters of individual wPKP2 and tPKP2 monolayers recordings suggested a small difference in coupling between these two cell monolayers as shown by sample data in Figure 4.17. However, statistical analysis of pooled data obtained from five separate experiments measuring cell input resistances in wPKP2 and tPKP2 monolayers (Tables 4.5 and 4.6 respectively) showed no statistically significant difference between the average r_{fast}/ι values of wPKP2 and tPKP2 monolayers (mean values derived at end of sixth columns in Tables 4.5 and 4.6 compared by paired student's t-test, $p = 0.234$). The values of average r_{fast} plotted versus average τ (derived from fourth and fifth columns respectively in Tables 4.5 and 4.6) plotted graphically for wPKP2 and tPKP2 cells (Figure 4.18) shows that two separate regression lines fit each data set. However, the value of the slopes of these two lines ($y = 103.7x$ for wPKP2 cells and $y = 105.4x$ for tPKP2 cells) showed only a modestly small reduction in value for wPKP2 cells expressing connexin-43 at cell membranes, suggesting there was little difference in the cell input resistances, and the degree of electrical coupling between wPKP2 and tPKP2 cell clusters.

Another technique measuring how well cell clusters are connected to each other involves assessing the extent of transfer of Lucifer Yellow in confluent monolayers of cells. This measure of GJIC performed in tetracycline-induced wPKP-2 cell clusters (Figure 4.19) showed that induced wPKP2 cells were not particularly well coupled to each other as dye transferred poorly across a maximum of eight adjacent cell layers from the scrape line. Efficient gap junction intracellular coupling (GJIC) in wPKP2 cells would result in more than twenty adjacent cells transferring the dye (personal communications with Professor Chris Fry). Similar data were obtained in tPKP2 cell GJIC with a maximum transfer across 4-7 cell layers (data not shown).

Figure 4.15 Potential difference recordings in wPKP2 cells

Traces of p.d. changes recorded in wPKP2 cells in response to injecting a step pulse of current intracellularly and of the extracellular electrode p.d. response with a comparable step pulse of current. In A) trace of an intracellular recording of a wPKP2 monolayer performed on a slow time-base, in B) trace of intracellular recording of a wPKP2 monolayer performed on a fast time-base, and in C) extracellular electrode recording performed on a slow time-base.

A) wPKP2
Intracellular slow time-base

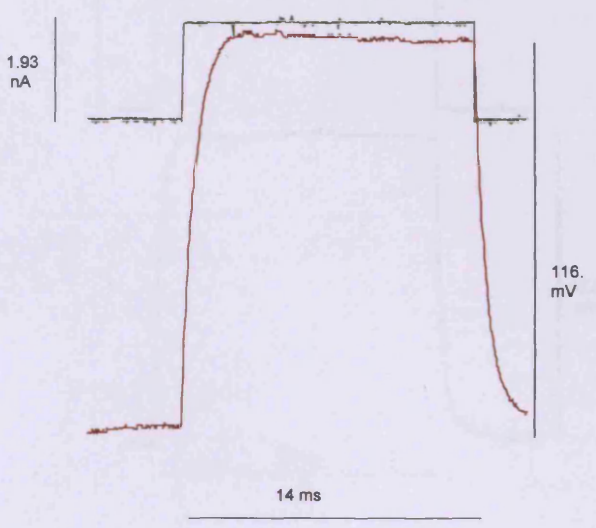

B) wPKP2
Intracellular fast-time base

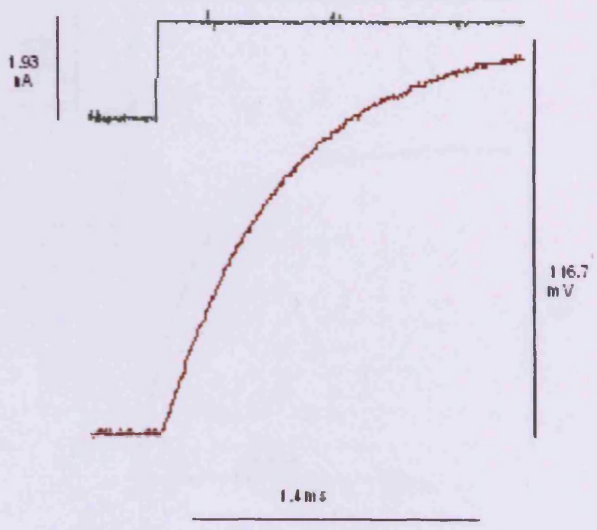

C) wPKP2
Extracellular

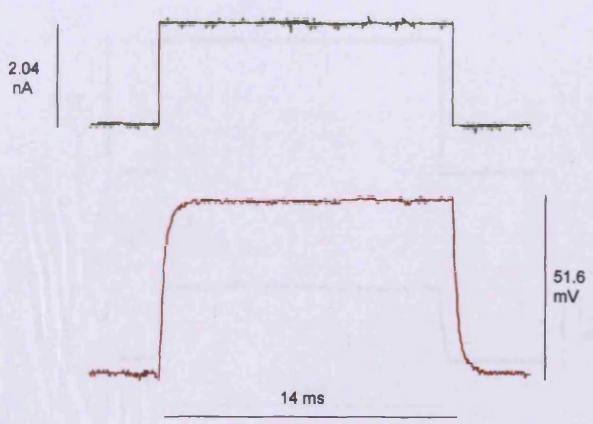

Figure 4.16 Potential difference recordings in tPKP2 cells

Traces of p.d. changes recorded in tPKP2 cells in response to injecting a step pulse of current intracellularly and of the extracellular electrode p.d. response with a comparable step pulse of current. In A) trace of an intracellular recording of tPKP2 monolayer performed with a slow time-base, in B) trace of intracellular recording of tPKP2 monolayer performed with a fast time-base, and in C) extracellular electrode recording performed with a slow time-base.

A) tPKP2
Intracellular slow time-base

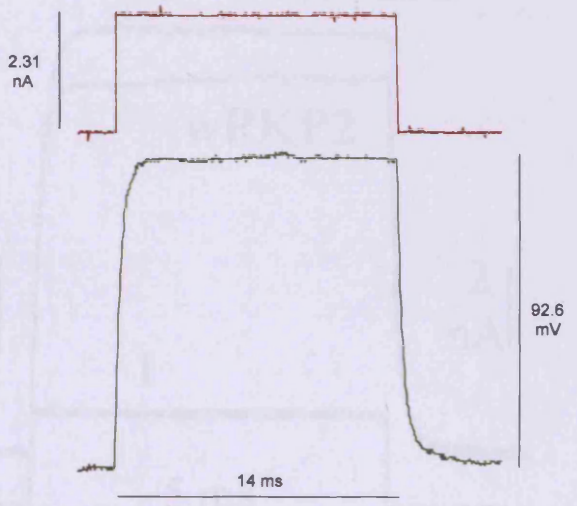

B) tPKP2
Intracellular fast-time base

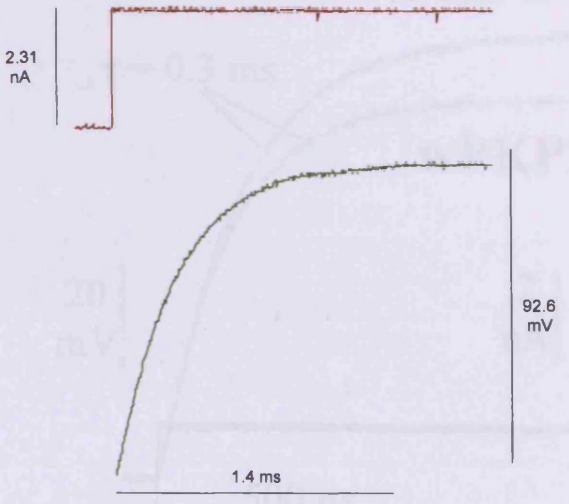

C) tPKP2
Extracellular

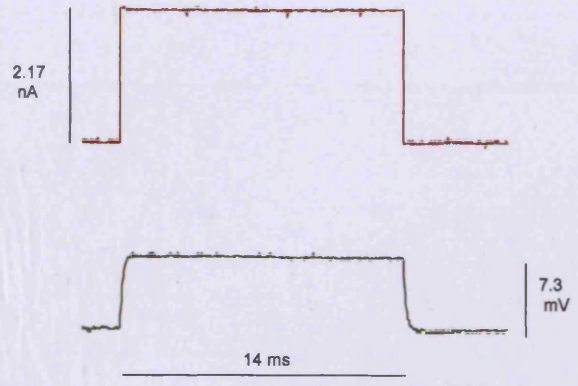

Figure 4.17 Individual cell input resistance measurements in wPKP2 and tPKP2 cells

Representative cell input resistance measurements showing a small difference in the measured cell input resistance of wPKP2 cell clusters compared to that of tPKP2 cell clusters. A smaller value of ri per unit time constant (ri = [V/I]/τ), ri wPKP2 cells = 34.1[68.2 x10^{-3}/2 x10^{-9}] and ri tPKP2 cells = 40.9 [81.8 x10^{-3}/2 x10^{-9}] megaΩ) as in wPKP2 versus tPKP2 cells here, suggests a marginally better coupling between wPKP2 cell clusters

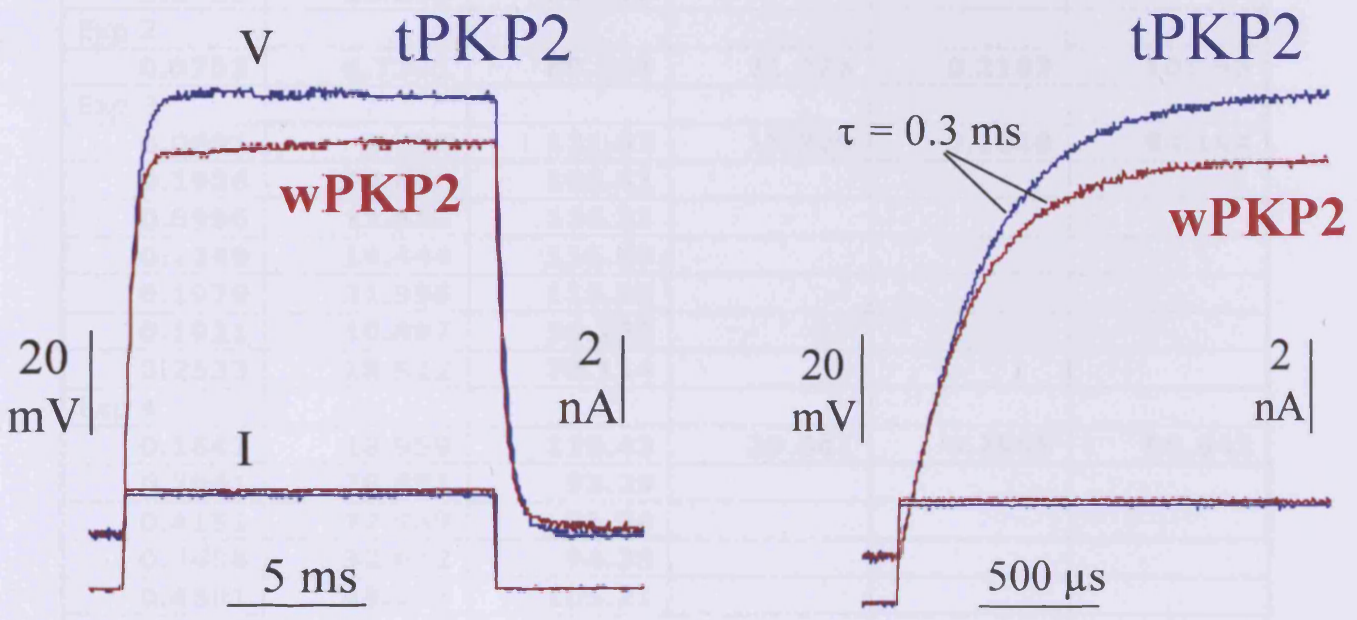

Table 4.5 Cell input resistance measurements from five separate experiments of wPKP2 cell monolayers

Cell input resistance measurements in wPKP2 cell monolayers from twenty-six individual cell recordings obtained in five separate experiments.

wPKP2 Cells			Average	Average	Average
τ value	rfast	rfast/τ	rfast	τ value	rfast/τ
Exp 1					
0.1304	**12.984**	**99.571**	**19.653**	**0.1783**	**110.2**
0.1317	**13.301**	**100.97**			
0.0833	**9.3748**	**112.54**			
0.1131	**13.033**	**115.37**			
0.1671	**18.651**	**111.71**			
0.3035	**33.541**	**110.52**			
0.3253	**36.076**	**110.91**			
0.1726	**20.265**	**117.39**			
Exp 2					
0.0753	**6.7301**	**89.338**	**21.376**	**0.2103**	**101.65**
Exp 3					
0.0691	**8.392**	**121.63**	**15.229**	**0.1618**	**94.144**
0.1956	**20.809**	**106.41**			
0.0996	**11.582**	**116.31**			
0.1249	**14.444**	**115.63**			
0.1979	**21.956**	**110.93**			
0.1921	**10.897**	**56.755**			
0.2533	**18.522**	**73.114**			
Exp 4					
0.1643	**18.959**	**115.43**	**29.841**	**0.2998**	**99.542**
0.2861	**26.681**	**93.29**			
0.4151	**37.989**	**91.54**			
0.3458	**32.632**	**94.38**			
0.4591	**48.286**	**105.21**			
0.1287	**14.496**	**112.66**			
Exp 5					
0.2467	**27.902**	**113.09**	**29.069**	**0.2617**	**111.08**
0.1269	**15.423**	**121.52**			
0.3164	**35.201**	**111.27**			
0.3568	**37.751**	**105.82**			
				Mean n=5	**103.32**
				SD	**7.2248**
				SEM	**3.6124**

Table 4.6 Cell input resistance measurements from five separate experiments of tPKP2 cell monolayers

Cell input resistance measurements in tPKP2 cell monolayers from twenty-four individual cell recordings obtained in five separate experiments.

tPKP2 Cells			Average	Average	Average
τ value	rfast	rfast/τ	rfast	τ value	rfast/τ
Exp 1					
0.0941	**11.145**	**118.42**	**11.145**	**0.0941**	**118.44**
Exp 2					
0.2498	**37.409**	**149.77**	**15.511**	**0.1399**	**110.87**
0.1031	**10.884**	**105.57**			
0.1518	**17.331**	**114.19**			
0.0824	**7.4428**	**90.361**			
0.1273	**12.205**	**95.898**			
0.1191	**11.258**	**94.526**			
0.1521	**14.599**	**95.989**			
0.1341	**12.955**	**96.607**			
Exp 3					
0.1348	**15.253**	**113.18**	**12.449**	**0.1069**	**116.45**
0.1198	**13.953**	**116.5**			
0.0991	**12.432**	**125.45**			
0.0741	**8.1568**	**110.08**			
Exp 4					
0.3911	**36.965**	**94.54**	**24.545**	**0.2641**	**92.938**
0.1622	**14.658**	**90.37**			
0.2373	**22.024**	**92.83**			
0.2735	**22.051**	**80.622**			
0.2461	**21.113**	**85.825**			
0.1937	**19.009**	**98.151**			
0.3187	**33.326**	**104.58**			
0.2907	**27.214**	**93.625**			
Exp 5					
0.3101	**33.357**	**107.6**	**27.934**	**0.2449**	**114.06**
0.2471	**28.947**	**117.19**			
0.1777	**21.499**	**121.01**			
				Mean n=5	**110.55**
				SD	**10.243**
				SEM	**5.1184**

Figure 4.18 Comparative plot of average rfast versus average τ values extrapolated from measurements using five different experiments each of wPKP2 and tPKP2 stable cell monolayers

Graphical plot of rfast values versus τ values obtained from five separate experiments of cell input resistance measurements in wPKP2 and tPKP2 monolayers (average rfast versus average τ values plotted from Tables 4.5 and 4.6 respectively). Five data points in wPKP2 cells fit a regression line (y = 103.7x) while five data points in tPKP2 cells fit a regression line (y = 105.4x). Since only a modestly small reduction in the value of the slope was found in wPKP2 cells expressing Cx-43 gap junctions, this indicated there was little difference in the cell-cell coupling between wPKP2 cell clusters with cell membrane localized Cx-43 and tPKP2 cell clusters lacking cell membrane Cx-43.

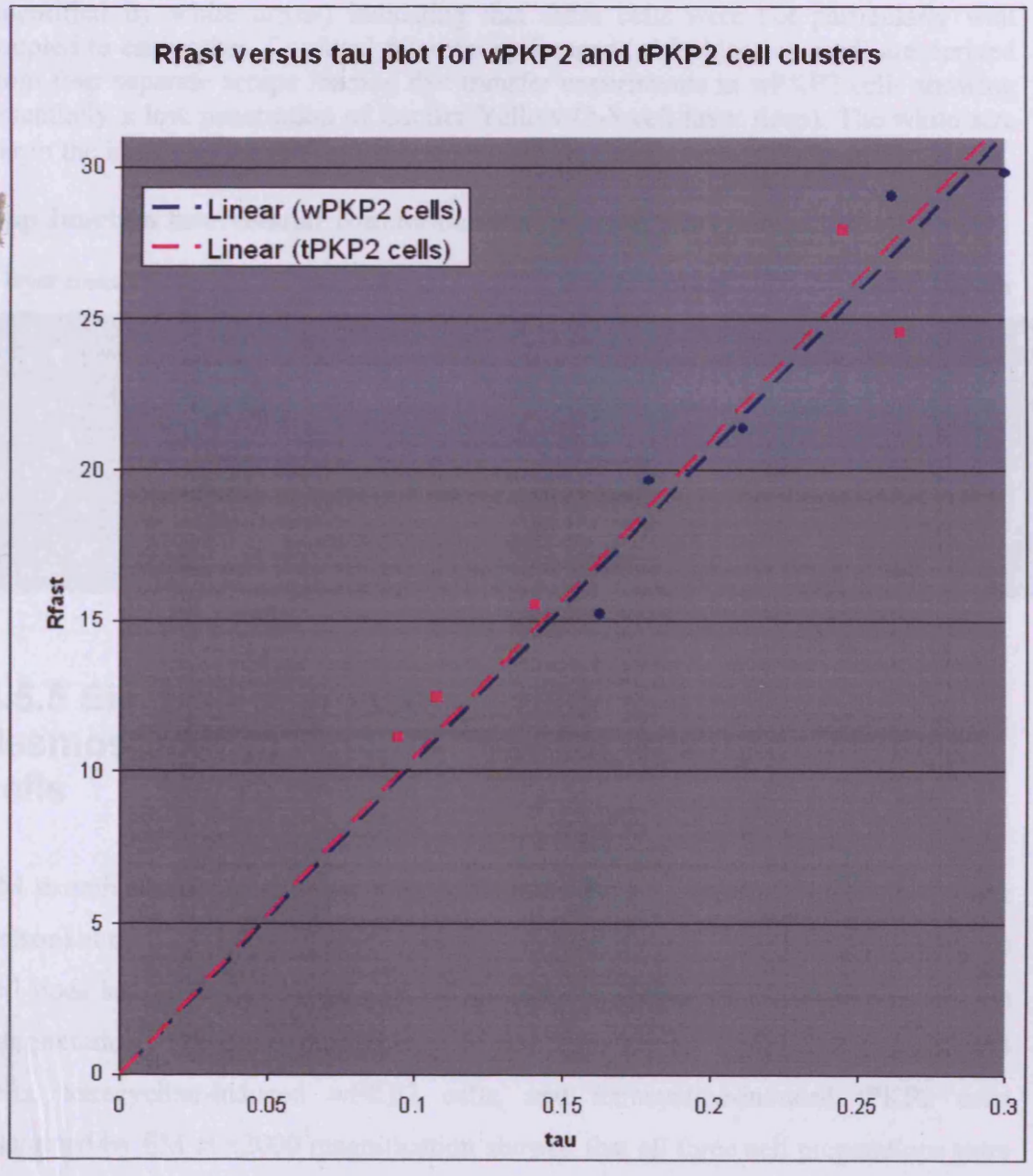

Figure 4.19 Confocal microscopy determination of GJIC in tetracycline induced wPKP2 cells

Gap junction intercellular communication (GJIC) determined in tetracycline-induced wPKP2 following scrape loading of Lucifer yellow dye and determination of the extent of dye transfer by confocal microscopy. Stable cells (wPKP2) were cultured in P_{30} dishes in complete DMEM containing blasticidin, hygromycin and tetracycline to obtain induction of full-length PKP-2 for the full duration of culture until cells were highly confluent. A fine incision was made in a wPKP2 monolayer of cells followed by the addition of 5% Lucifer yellow dye for exactly 5 minutes. Following washing of excess dye in PBS the extent of Lucifer yellow dye transfer was assessed by confocal microscopy. Lucifer Yellow penetrated through a maximum of eight adjacent cell layers (each cell layer is identified relative to the positions of the nuclei indicated by the dark non-fluorescing area around the cytoplasm with a red bar in the image on the right hand side of the image on the left) measured relative from the scrape line (identified by white arrow) indicating that these cells were not particularly well coupled to each other. Confocal microscopy images (x10 objective used) are derived from four separate scrape loading dye transfer experiments in wPKP2 cells showing essentially a low penetration of Lucifer Yellow (3-8 cell layer deep). The white size bar in the image on the left (at the bottom right hand side) represents 8 μm.

Gap Junction Intercellular communication in tetracycline induced wPKP2 cells

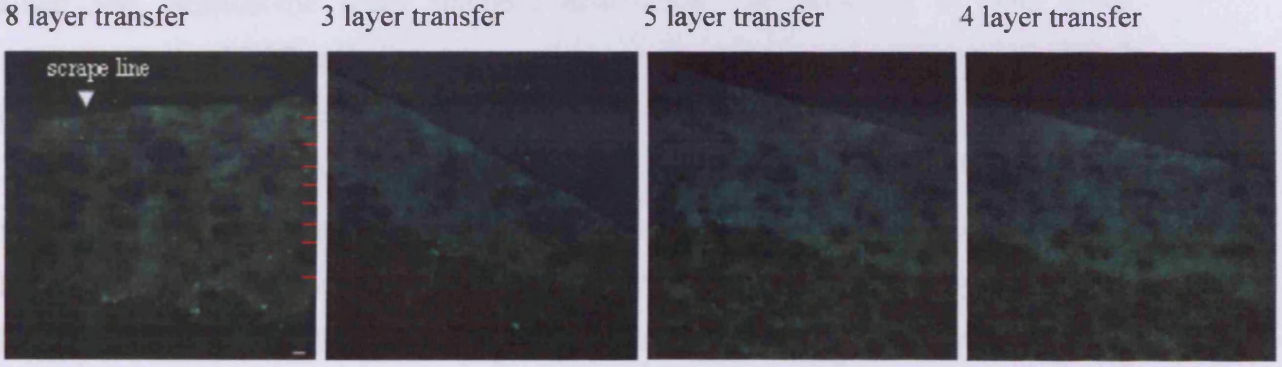

4.5.5 Electron microscopy examination of desmosomes in Flp-In T-Rex 293, wPKP2 and tPKP2 cells

EM examinations of cell lines were performed by an electron microscopist (Peter Balson) at the Royal Free Hospital electron microscopy unit. The identities of all three cell lines analyzed by EM were revealed after completion of EM analysis and data interpretation. The gross morphology of non-transformed Flp-In T-Rex HEK 293 cells, tetracycline-induced wPKP2 cells, and tetracycline-induced tPKP2 cells examined by EM at x2000 magnification showed that all three cell preparations were

viable with a good preservation of cellular ultrastructure (Figure 4.20). Examination of desmosomes at x70000 magnification (Figure 4.21) showed that desmosomes in Flp-In T-Rex 293 cells were not well developed. Desmosomes in wPKP2 cells were undoubtedly more prominent showing electron dense plaques with dense filament associations. Desmosomes in tPKP2 cells, in contrast appeared to form intermittent DS coupling with pale plaques. Some desmosomes in induced tPKP2 cells had less prominent filament association (dashed arrow, Figure 4.21C) while other desmosomes present in these cells were devoid of any filaments (marked by asterisks, Figure 4.21C). In some tPKP2 desmosomes in which filaments could be localized their organization was in a plane perpendicular with the length of the desmosome (two arrows in Figure 4.22B) while in wPKP2 desmosomes the filaments were organised in a plane parallel with the length of desmosomes (Figure 4.22A). Electron micrographs of tPKP2 and wPKP2 cellular junctions illustrated at lower magnification of x30000 (Figure 4.23) further emphasize the observed difference between these two desmosomes. The arrows in figure 4.23 indicate the intermittent DS coupling with pale ODP whilst a desmosome with electron dense ODP is marked by an asterisk, albeit this desmosome lacks filament association; the presence of both types desmosomes in tPKP2 cells is not unexpected as over-expressed A733fsX740 PKP-2 is present in conjunction with endogenous full length PKP-2 protein (Figure 4.5B). Although there was a visual suggestion on examination of serial section that the intermittent DS coupling in induced tPKP-2 cells may be shorter than found in control induced wPKP2 desmosomes, statistical analysis of mean desmosomal lengths in Flp-In T-Rex 293 cells, induced wPKP2 cells and induced tPKP2 cells did not show a statistical difference in mean desmosomal length as pair-wise comparisons between the three groups showed that the p values were all >0.05 (Figure 4.24). All electron micrographs are representative of images analyzed in all three cell lines.

Figure 4.20 Gross morphology of non-transformed Flp-In T-Rex HEK 293 cells, tetracycline-induced wPKP2 cells, and tetracycline-induced tPKP2 cells

Gross morphology of non-transfected Flp-In T-Rex 293 control cells and of wPKP2 and tPKP2 cells expressing full-length and A733fsX740 PKP2 respectively. Cells cultured on Thermanox plastic coverslips in complete DMEM were induced where required, with 0.1μg/ml tetracycline for 72 hours until they were confluent. Coverslips processed for electron microscopy (see section 2.7.4) were examined in a Philips 201 electron microscope at x 2000 magnification to examine the gross morphology of these cells. All there preparations showed cell viability with good preservation of ultrastructure. The size bar in each electron micrograph represents 10μm

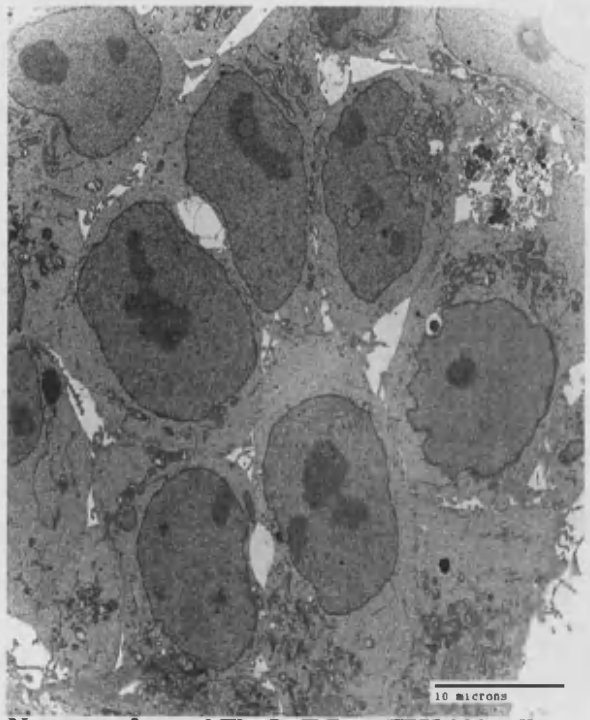

Non-transformed Flp-In T-Rex HEK 293 cells

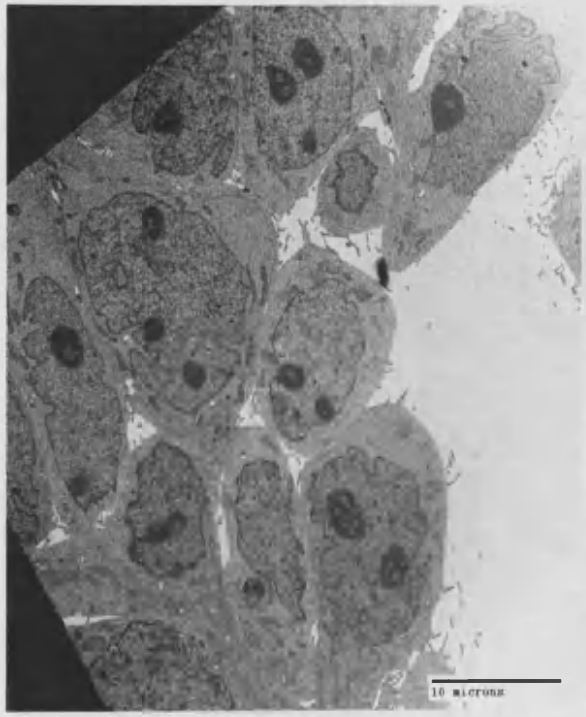

Tetracycline-induced wPKP2 cells

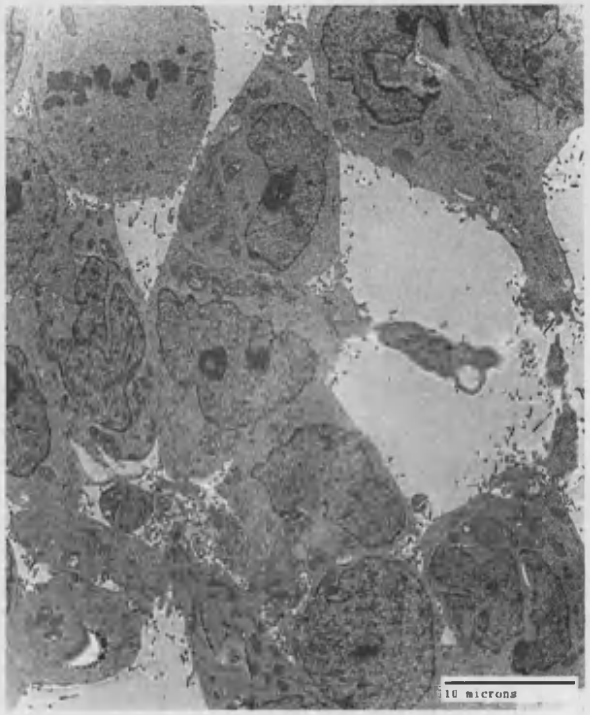

Tetracycline-induced tPKP2 cells

Figure 4.21 Morphology of desmosomes formed in Flp-In T-Rex HEK 293, wPKP2 and tPKP2 cells

Desmosome morphology in Flp-In T-Rex 293 non-transfected control cell and in induced wPKP2 and tPKP2 cells expressing full-length and A733fsX740 PKP-2 respectively. Cells cultured on Thermanox plastic cover slips in complete DMEM were induced where required in 0.1μg/ml tetracycline for 72 hours until they were highly confluent. Coverslips processed for electron microscopy (see section 2.7.4) were examined in a Philips EM microscope at x 70000 magnification to examine desmosome morphology. Full-length PKP-2 expression resulted in formation of electron dense desmosomes with prominent filaments (arrows, B) in wPKP2 cells, while A733fsX740 PKP-2 expression resulted in the formation of pale repeated desmosomal couplings (asterisks, in C) with less prominent filament association (dashed arrow, C) or with absence of filament association (desmosomes marked by asterisks, C). Flp-In T-Rex HEK 293 cells formed less prominent desmosomes (A) compared to wPKP2 cell desmosomes presumably due to low level of recruitment of endogenous desmosomal plaque proteins. The size bar in each electron micrograph represents 100 nm.

A) Flp-In T-Rex 293 cells **B) wPKP2 cells** **C) tPKP2 cells**

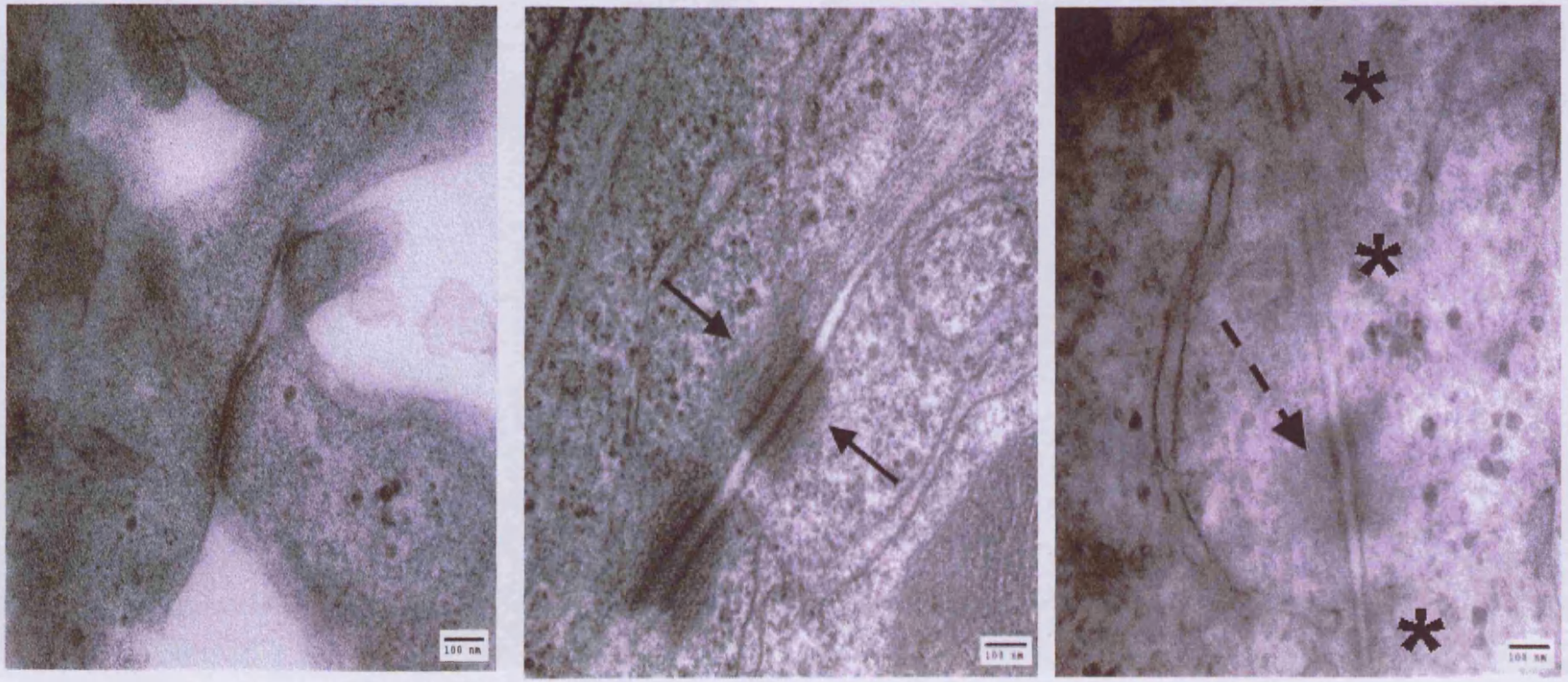

Figure 4.22 Filament organization of desmosomes in induced wPKP2 and tPKP2 cells

Cells cultured on Thermanox plastic cover slips in complete DMEM were induced where required in 0.1μg/ml tetracycline for 72 hours until they were highly confluent. Coverslips processed for electron microscopy (see section 2.7.4) were examined in a Philips EM microscope at x 70000 magnification to examine desmosome morphology. The filaments are organised in induced wPKP2 desmosomes running parallel with the length of the desmosomes, whereas in induced tPKP2 cells the two intermittent desmosomal couplings have filaments running perpendicular to the length of the desmosomes. The asterisk identifies a desmosome lacking filaments as seen in previous electron micrographs. The scale bars represent 100 nm.

A) Induced wPKP2 cells

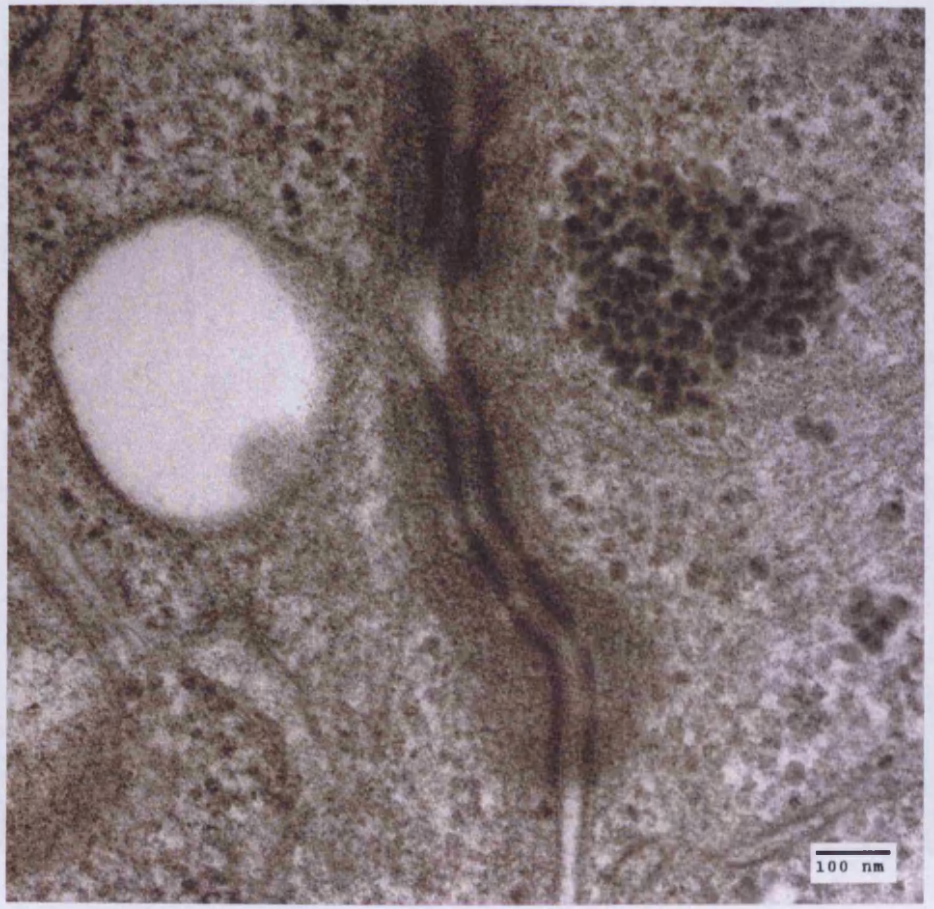

B) Induced tPKP2 cells

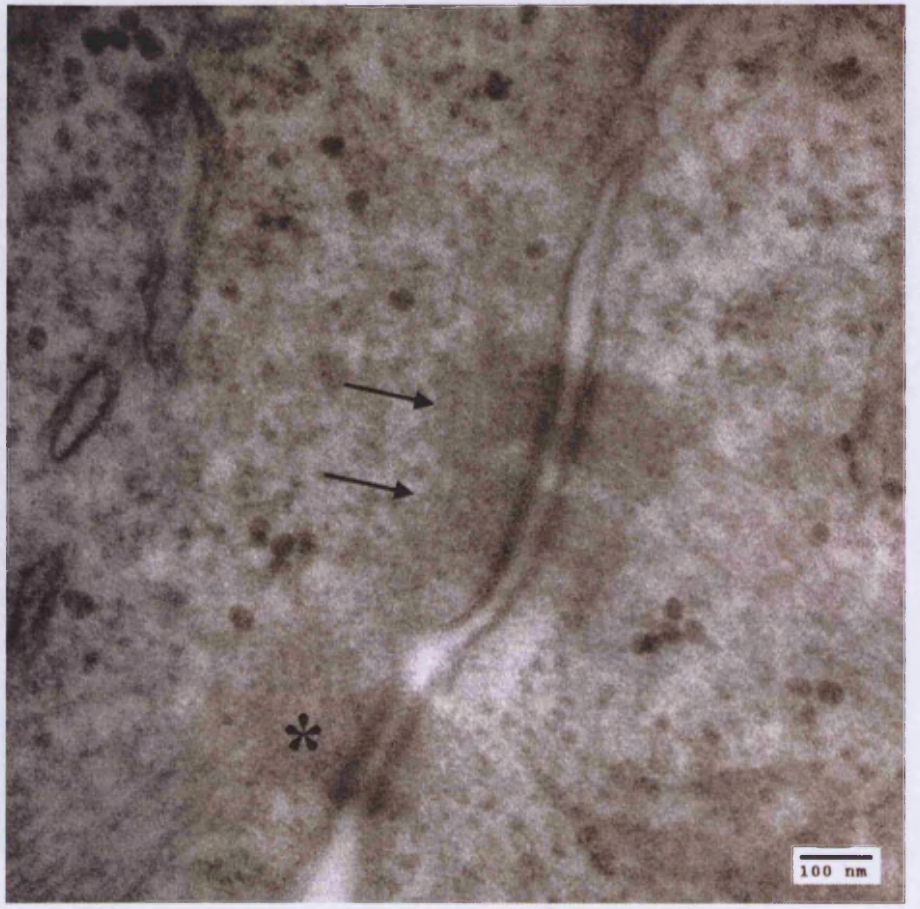

Figure 4.23 Lower magnification EM micrograph contrasting the differences of desmosomes formed in tPKP2 and wPKP2 cells

Examination of desmosomes in induced tPKP2 cells. This is a representative electron micrograph of desmosomes found in tPKP2 cells showing intermittent DS linkages with pale plaques. Inset shows desmosomes from induced wPKP2 cells at the same magnification for comparison. Tetracycline-induced tPKP2 and wPKP2 cells cultured on Thermanox coverslips for 72 hours were processed *in situ* for electron microscopy. Desmosomes were examined by transmission electron microscopy in a Philips 201 electron microscope at x 30000 magnification. Arrows indicate short repeated DS linkages with a pale outer dense plaque. Asterisk indicates a DS with 'normal' electron dense outer dense plaque, desmosomes of induced tPKP-2 cells were largely devoid of filaments compared to those in induced wPKP-2 desmosomes, which showed electron dense plaques with prominent filaments (marked by two arrows, inset). The size bar represents 500 nm.

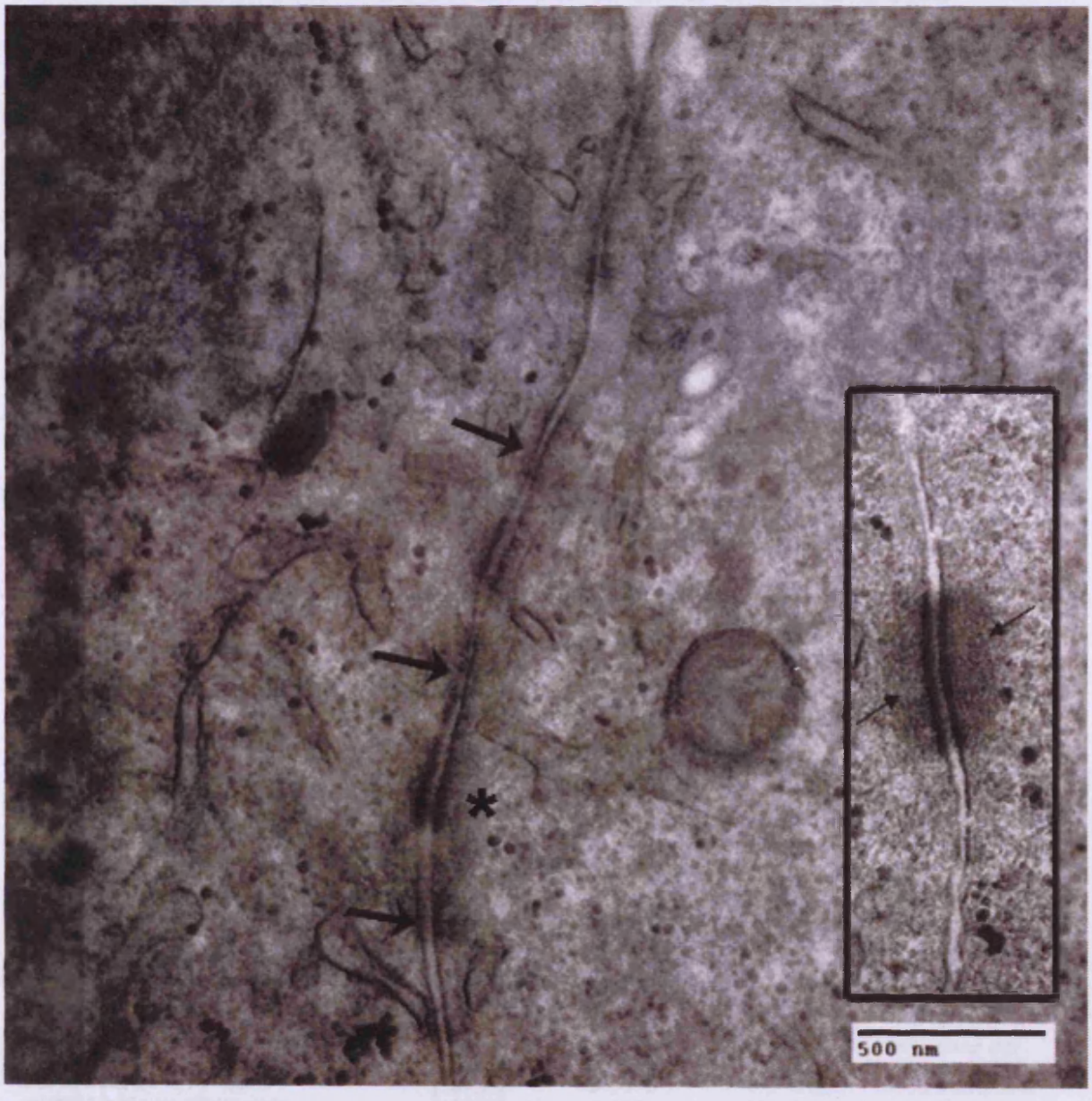

Figure 4.24 Statistical analysis of desmosomal length in Flp-In T-Rex HEK 293, wPKP2 and tPKP2 cells

Statistical analysis of the lengths of desmosomes found in Flp-In 293, wPKP2 and tPKP2 stable cells. A minimum of fourteen measurements of desmosomal lengths (nm) were taken from electron micrographs of desmosomes obtained from each of the three cell types. Data were analyzed using Graph Pad Prism software using ANOVA analysis followed by Bonferroni post-test computation of significance. The graph shows plots of individual values in each group of cells and the table below shows results of the Bonferroni multiple comparison statistical test parameters between the three data sets from Graph Pad. Pair-wise analysis did not show statistically significant difference ($p>0.05$) in desmosomal length comparing either control Flp-In or control wPKP2 desmosomes with tPKP2 desmosomes. Flp-In desmosomal length were also not significantly different to those of wPKP2 desmosomes ($p>0.05$)

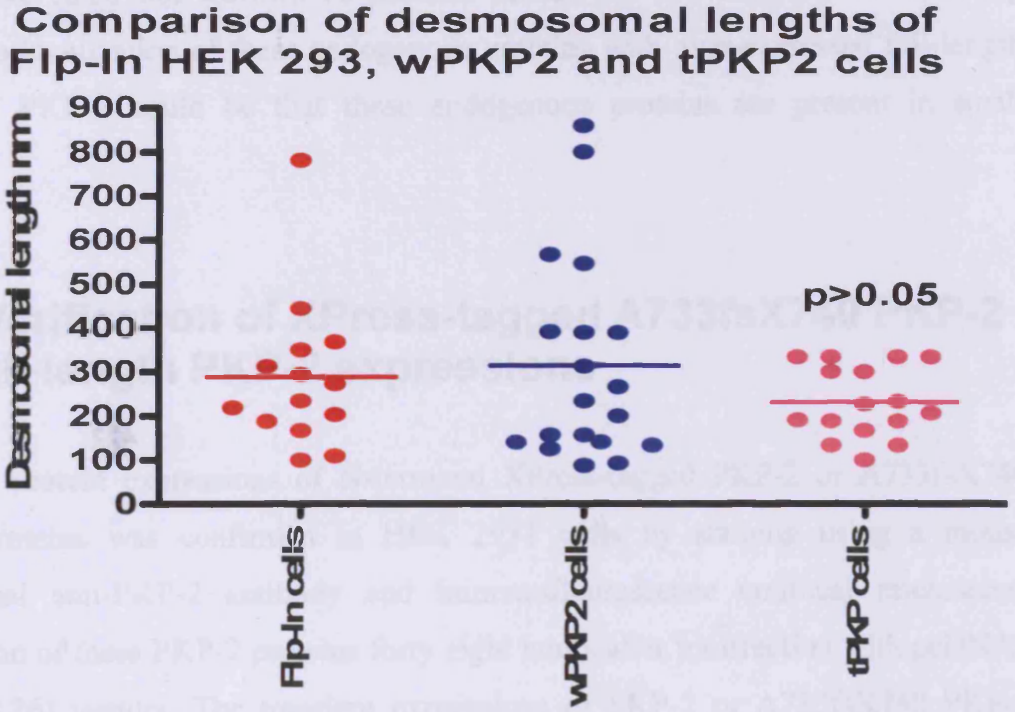

Parameter	Flp-In cells	wPKP2 cells	tPKP cells	Data Set-D
Table Analyzed				
Data 2				
One-way analysis of variance				
P value	0.3782			
P value summary	ns			
Are means signif. different? (P < 0.05)	No			
Number of groups	3			
F	0.9932			
R squared	0.04139			
Bartlett's test for equal variances				
Bartlett's statistic (corrected)	14.46			
P value	0.0007			
P value summary	***			
Do the variances differ signif. (P < 0.05)	Yes			
ANOVA Table	SS	df	MS	
Treatment (between columns)	62730	2	31360	
Residual (within columns)	1453000	46	31580	
Total	1515000	48		
Bonferroni's Multiple Comparison Test	Mean Diff.	t	P value	95% CI of diff
Flp-In cells vs wPKP2 cells	-26.24	0.4192	P > 0.05	-181.8 to 129.3
Flp-In cells vs tPKP cells	57.74	0.8878	P > 0.05	-103.9 to 219.3
wPKP2 cells vs tPKP cells	83.98	1.393	P > 0.05	-65.84 to 233.8

4.5.6 Endogenous plakoglobin co-localization with full-length and truncated PKP-2 in wPKP2 and tPKP2 cells

Examination of immunofluorescence co-localized endogenous PG staining with truncated PKP-2 appeared weaker (Figure 4.25B) in cell-cell contacts of induced tKP2 cells compared to the co-localized endogenous PG staining with full-length PKP-2 in cell-cell contacts of induced wPKP2 cells (Figure 4.25A, representative of triplicate staining). Co-localization studies of endogenous β-catenin, DP, DSG-2 and DSC-2 with either full-length or truncated PKP-2 were not reproducible and therefore inconclusive (data not shown). A possible reason for the difficulty in obtaining reliable co-localization of these endogenous proteins with over-expressed full-length or S140F PKP-2 could be that these endogenous proteins are present in small amounts.

4.5.7 Verification of XPress-tagged A733fsX740 PKP-2 and full-length PKP-2 expressions

Transient protein expressions of N-terminal XPress-tagged PKP-2 or A733fsX740 PKP-2 proteins was confirmed in HEK 293T cells by staining using a mouse monoclonal anti-PKP-2 antibody and immunofluorescence confocal microscopy localization of these PKP-2 proteins forty eight hours after transfection with pcDNA4 (Figure 4.26) vectors. The transient expressions of PKP-2 or A733fsX740 PKP-2 proteins localized by immunofluorescence confocal microscopy in HEK 293T cells were also verified using a mouse monoclonal anti-XPress antibody, which gave an identical result (data not shown) as obtained using anti-PKP2 antibody staining. SDS PAGE/western blotting analysis using anti-XPress and anti-PKP-2 antibodies verified expressions of PKP-2 proteins in soluble cell lysates. This revealed a full-length PKP-2 band (predicted and apparent SDS PAGE size 103.6 KD) and a truncated plakophilin-2 band (predicted and apparent SDS PAGE size 81 KD) in transfected HEK 293T cells forty-eight hours after transfection with pcDNA4 vectors (Figure 4.27).

4.5.8 Interaction of endogenous PG, β-catenin, DP, DSC-2 and DSG-2 with full-length or truncated PKP-2

Co-immunoprecipitation assays in transiently transfected HEK 293T cells showed reduced association of endogenous plakoglobin with truncated PKP-2 compared to its interaction with full-length PKP-2 (Figure 4.28, representative of triplicate assays). However, no differences were found in the levels of endogenous beta-catenin associating with either truncated or full-length PKP-2 (Figure 4.29, representative data of triplicate assays performed). Attempts to co-IP endogenous desmoplakin, desmocollin-2, and desmoglein-2 with either truncated or full-length PKP2 were unreliable resulting in variable immunoprecipitation of all three endogenous proteins (data not shown). This was probably because of insufficient extraction of these membrane-associated or cytoskeletal-associated proteins under the conditions employed.

Figure 4.25 Co-localization of PKP-2s and PG in wPKP2 and tPKP2 cells

Confocal microscopy immunofluorescence co-localization of endogenous plakoglobin with either full-length PKP-2 or A733fsX740 PKP-2 in tetracycline-induced wPKP2 and tPKP2 cells respectively. DAPI nuclear staining produces a blue signal, rabbit anti-human PG followed by anti-rabbit Alexa-488 produces green signal localizing PG staining, mouse anti human PKP-2 followed by anti-mouse Alexa 546 produces red signal localizing PKP-2 and A733fsX740 PKP-2 in wPKP2 and tPKP2 cells respectively. Merged signals are obtained with all three composite signals superimposed. Images were obtained using x40 oil immersion objective. The size bar in each green channel represents 5 μm. This is a representative result of triplicate staining performed.

A) Endogenous PG/PKP-2 co-localization in wPKP2 cells

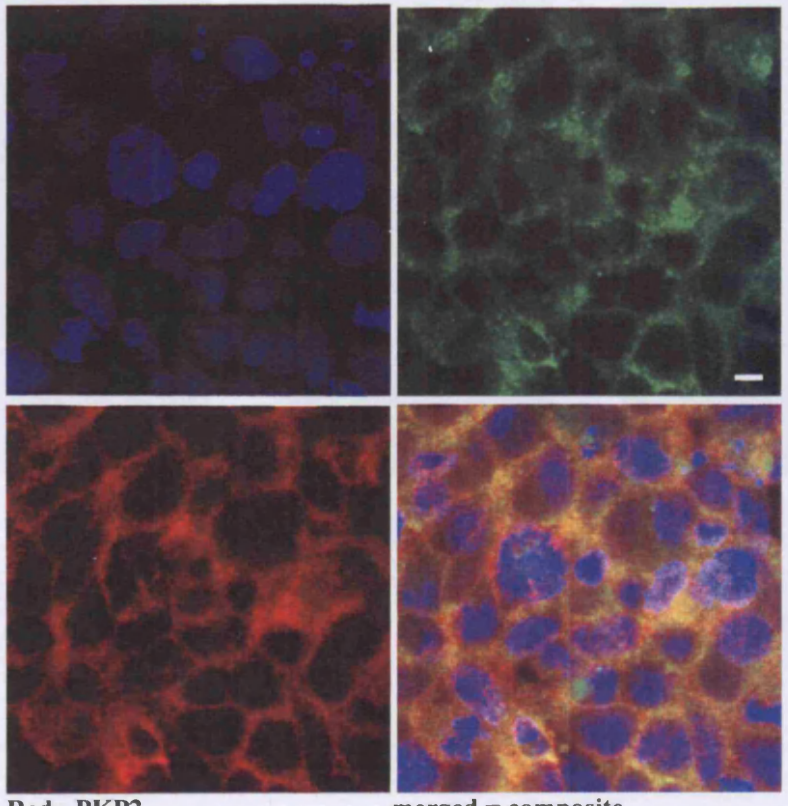

B) Endogenous PG/A730fsX740 PKP-2 co-localization in tPKP2 cells

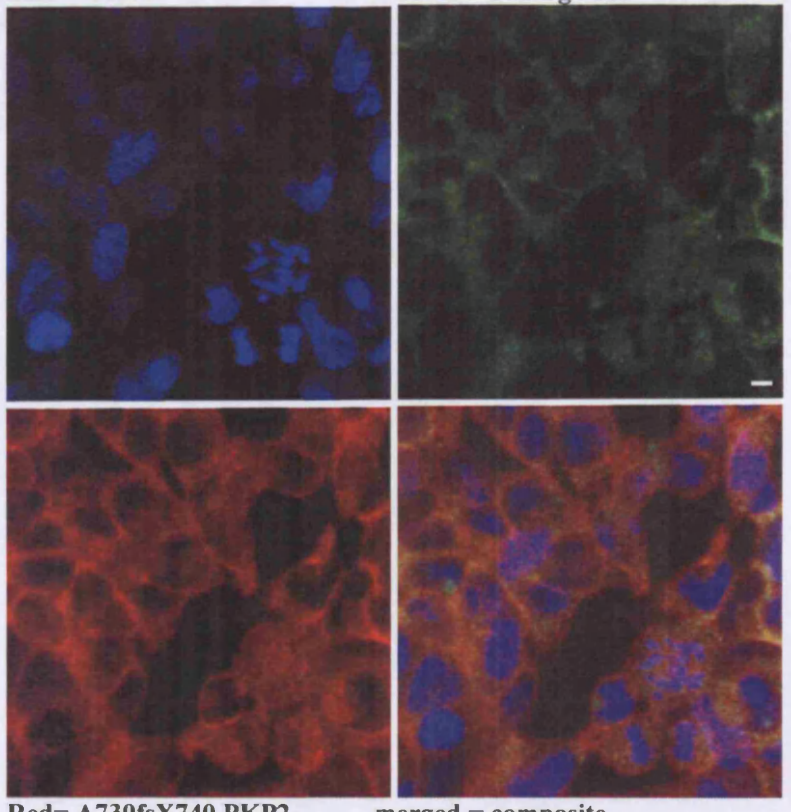

Figure 4.26 Confocal microscopy localization of PKP-2 and truncated PKP-2 in HEK293T cells transfected with pcDNA4 vectors encoding these plakophilins

Verification of the expressions of either full-length PKP-2 or A733fsX740 PKP-2 in $1x10^5$ HEK 293T cells cultured on 13mm plastic coverslips transfected with 1μg pcDNA4 PKP2 or pcDNA4 A733fsX740 PKP2 plasmids for forty-eight hours using 10μl Polyfect reagent. Following fixation of cells in 4% formaldehyde, permeabilization in 0.1% triton X-100 and blocking in 10%FBS, they were incubated with 1:200 dilution of mouse monoclonal anti-PKP2 (610788, BD Bioscience) for 1hr at room temperature. Cells were washed in PBS and incubated with 1:200 Alexa fluor 546 goat anti-mouse (Invitrogen) for 1hr at room temperature. Following PBS washes cells were incubated with DAPI nuclear stain (Invitrogen) and mounted on glass slide. Control cells transfected with pcDNA4 (without an insert, A); pcDNA4 PKP2 transfected cells (B) and pcDNA4 A733fsX740 PKP2 transfected cells (C). Blue fluorescence shows DAPI nuclear staining, red fluorescence shows PKP-2 or A733fsX740 PKP-2 staining (B and C respectively), and merged fluorescence shows composite signals. The size bar in each DAPI stained image on the left panels represents 10 μm.

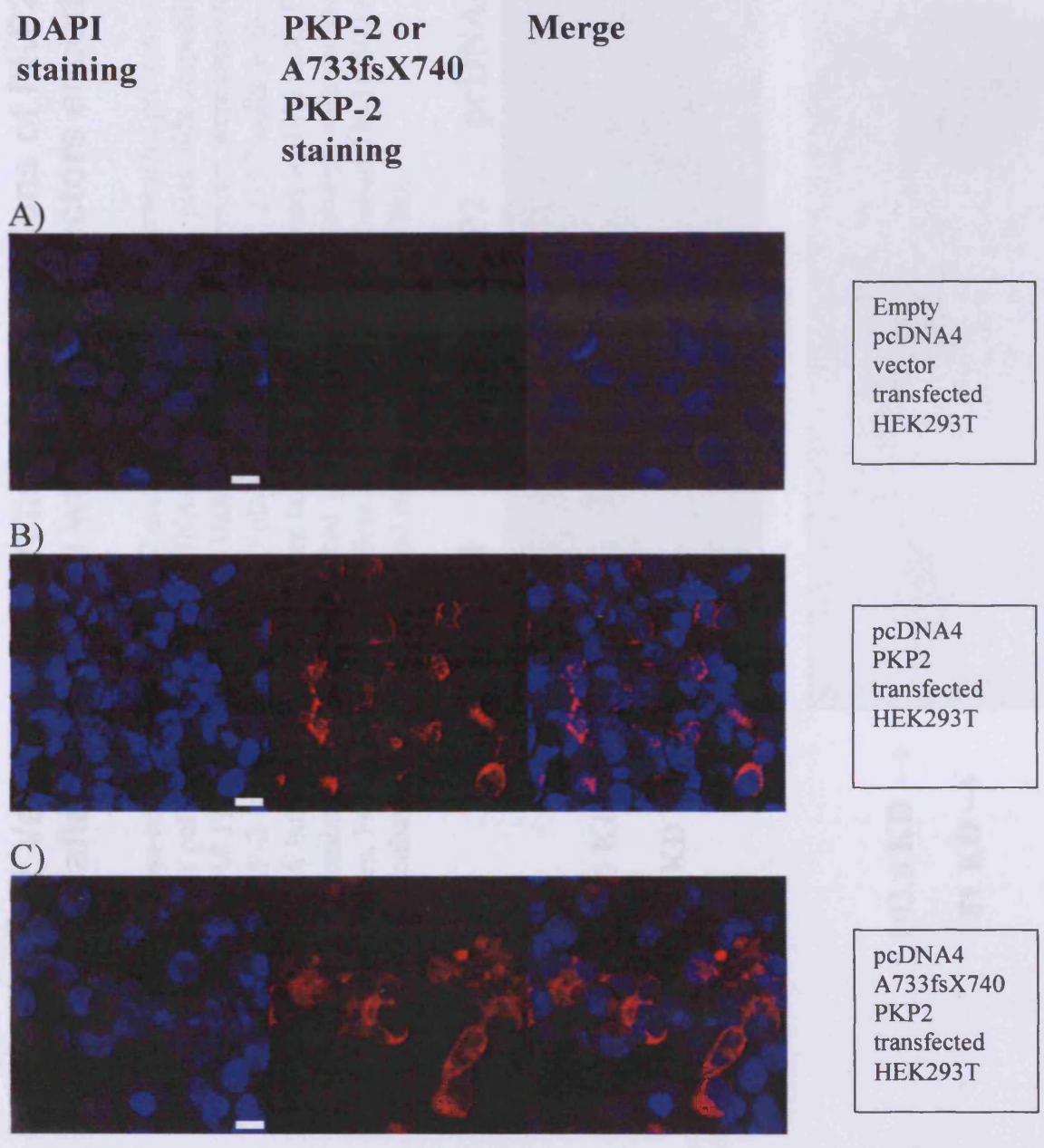

Figure 4.27 Verification of transient expressions of PKP2 and truncated PKP2 in HEK 293T cells after transfection with pcDNA4 vectors encoding these plakophilins

N-terminal XPress-tagged full-length PKP2 and A733fsX740 PKP2 transient protein expressions obtained in HEK 293T cells following transfection with pcDNA4 PKP2 and pcDNA4 A733fsX740 PKP2 plasmids respectively. HEK 293T cell lysates of non-transfected (control), pcDNA4 PKP2 or pcDNA4 A733fsX740 transfected cell lysates were analyzed by Western blotting probed using anti-XPress (top) or anti-PKP-2 antibodies (bottom). Following transfection of 293T cells with 1μg of each plasmid for 48 hours, cell lysates prepared in RIPA buffer (100μg protein per lane) were electrophoresed in 10% SDS PAGE and transferred using semi-dry transfer on Hybond ECL membrane. Blots were blocked in TBST/milk and incubated with mouse monoclonal (1:5000 anti-XPress or 1:500 anti-PKP-2) antibodies. Following washing of blots in TBST they were incubated in 1:3500 rabbit-anti-mouse HRP. Following TBST washes, the blots were incubated in ECL reagents and exposed to ECL Hyperfilm.

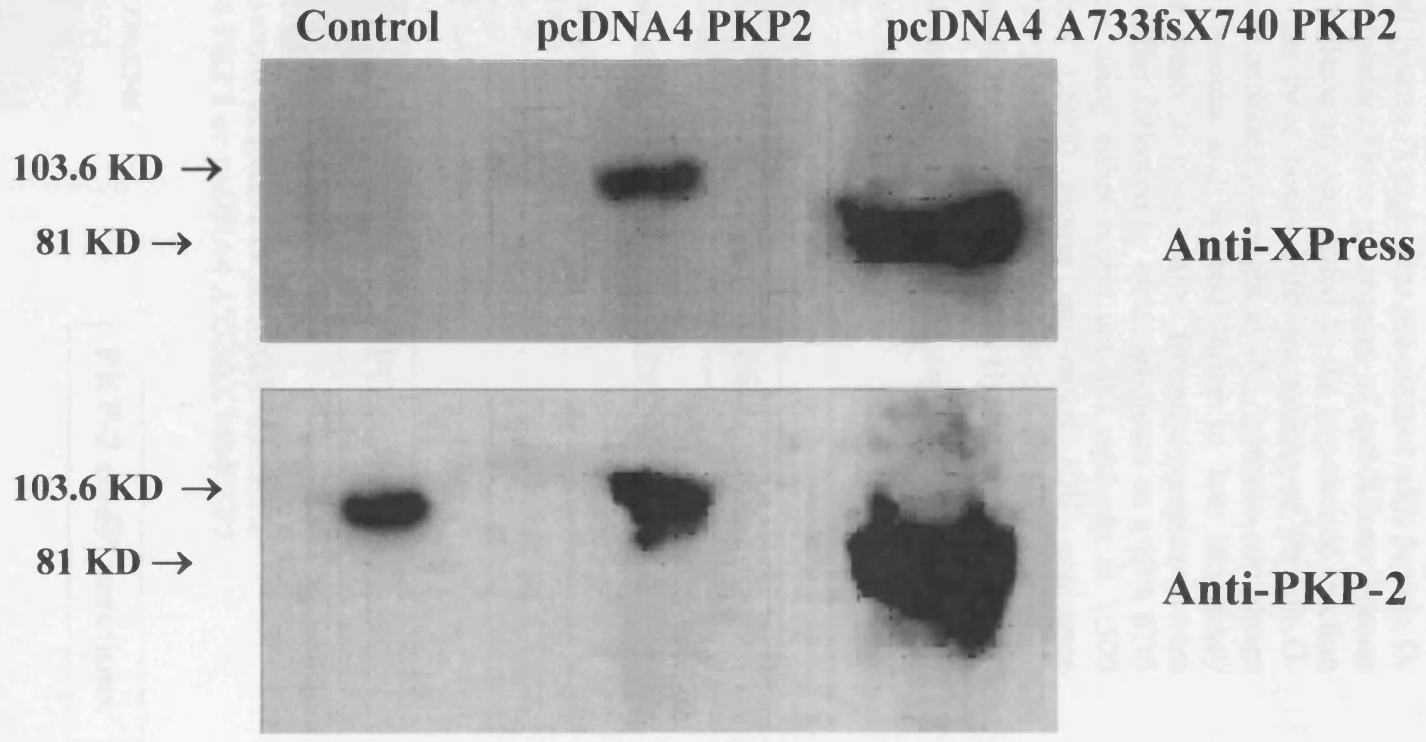

Figure 4.28 Co-IP analysis using anti-XPress binding of PKP-2 or truncated PKP-2 to endogenous PG

Co-immunoprecipitation of XPress-tagged full-length or A733fsX740 PKP-2 with endogenous plakoglobin performed in transfected HEK 293T cells. Forty-eight hours after transfection of 293T cells with pcDNA4 PKP2 or pcDNA4 A733fsX740 PKP2 plasmids (4μg/P90 dish), cells were scrapped off P90 dishes in lysis buffer (10 mM Tris HCl pH 7.6, 145 mM NaCl, 1 mM Na_3VO_4, and 1% triton X-100 + protease inhibitors). Triton X-100 soluble cell lysates (3 mg) were pre-cleared with Protein G-Sepharose at 4°C for 30 minutes on rotator. Three microgram of anti-XPress (mouse monoclonal anti-XPress antibody, Invitrogen) was added to the pre-cleared fraction and incubated on a rotator at 4°C for three hours. Fifty microliters of Protein G-Sepharose was added and incubation continued overnight at 4°C. Immuno-complexes were pelleted at 10000g for 0.5 minute and washed thrice in low stringency PBS/inhibitor followed by a single wash in lysis buffer. Immuno-complexes were denatured in 3x reducing Laemmli buffer followed by electrophoreses on a 10% SDS PAGE and immunoblotting analysis using either rabbit anti-PG antibody at 1:500 dilution (Santa Cruz sc7900) and 1:5000 mouse anti-rabbit HRP conjugate (Invitrogen) or 1:500 mouse anti-PKP2 and 1:5000 goat anti-mouse HRP conjugate followed by incubation in ECL reagents and exposure to ECL Hyperfilm.

A) Triton X-100 cell lysates (equal amount, 100μg) loaded on 10% SDS PAGE

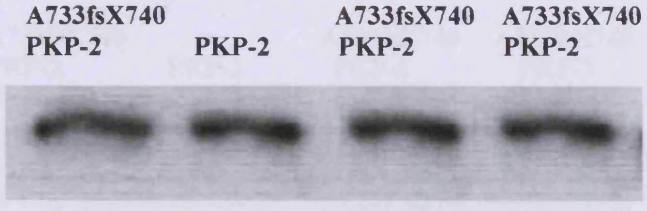

B) IP Probed for plakoglobin association with PKP-2 or A733fsX740 PKP-2

C) Probe to determine relative amounts of PKP-2 or A733fsX740 PKP2 Co-IP in cell lysates of pcDNA4 PKP2 or pcDNA4 A733fsX740 PKP2 transfected HEK 293T cells

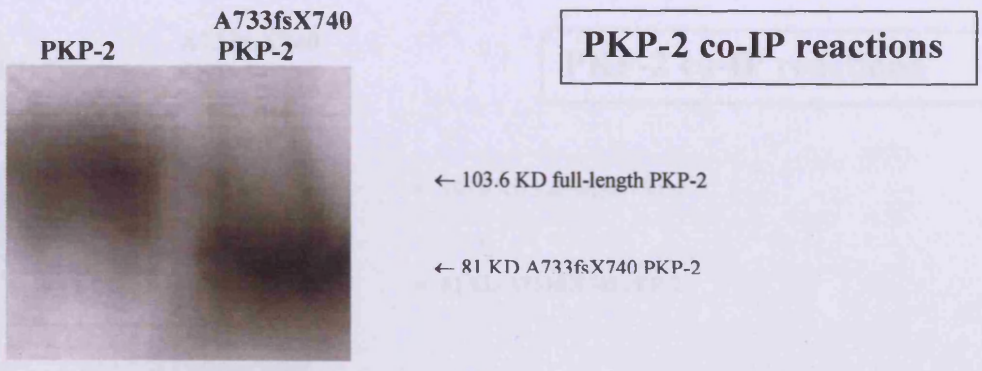

Figure 4.29 Co-IP analysis using anti-XPress binding of PKP-2 or truncated PKP-2 to endogenous β-catenin

Co-immunoprecipitation of XPress-tagged full-length or A733fsX740 PKP-2 with endogenous β-catenin performed in transfected HEK 293T cells. Forty-eight hours after transfection of 293T cells with pcDNA4 PKP2 or pcDNA4 A733fsX740 PKP2 plasmids (4μg/P90 dish), cells were scrapped off P90 dishes in lysis buffer (10 mM Tris HCl pH 7.6, 145 mM NaCl, 1 mM Na_3VO_4, and 1% triton X-100 + protease inhibitors). Triton X-100 soluble cell lysates (3mg) were pre-cleared with Protein G-Sepharose at 4°C for 30 minutes on rotator. Three microgram of anti-XPress (mouse monoclonal anti-XPress antibody, Invitrogen) added to the pre-cleared fraction was incubated on a rotator at 4°C for three hours. Fifty microliters of Protein G-Sepharose was added and incubation continued overnight at 4°C. Immuno-complexes were pelleted at 10,000g for 0.5 minute and washed thrice in low stringency PBS/inhibitor followed by a single wash in lysis buffer. Immuno-complexes were denatured in 3x Laemmli buffer followed by electrophoresis on a 10% SDS PAGE and immunoblotting analysis using either 1:500 rabbit anti-β-catenin antibody (Abcam, ab2982) and 1:5000 mouse anti-rabbit-HRP conjugate (Invitrogen) and 1:500 anti-mouse PKP-2 and 1:5000 goat anti mouse HRP conjugate followed by incubation in ECL reagents and exposure to ECL Hyperfilm.

A) Triton X-100 cell lysates (equal amount, 50μg) loaded on 10% SDS PAGE

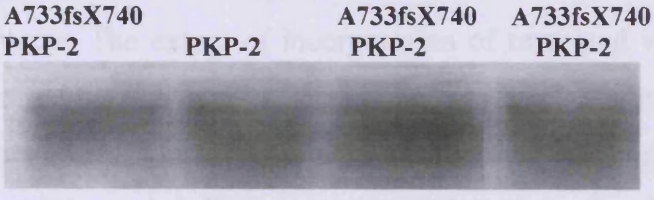

B) IP Probed for β-catenin association with PKP-2 & A733fsX740 PKP-2

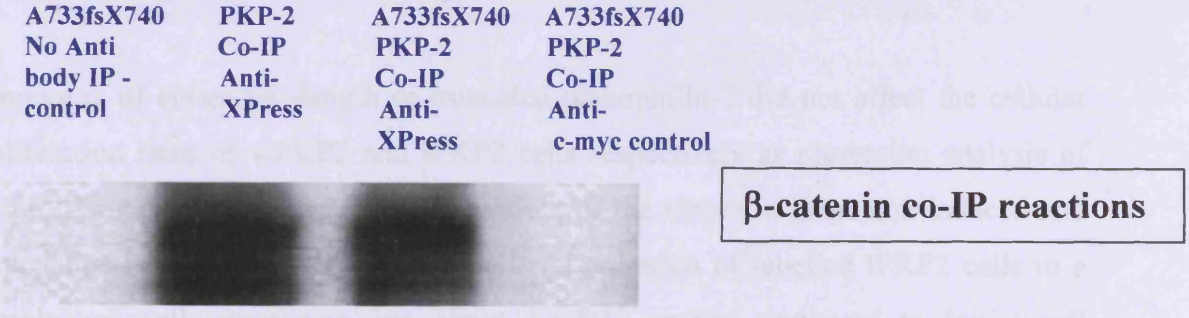

C) Probe to determine relative amounts of PKP-2 or A733fsX740 PKP2 Co-IP in cell lysates of pcDNA4 PKP2 or pcDNA4 A733fsX740 PKP2 transfected HEK 293T cells

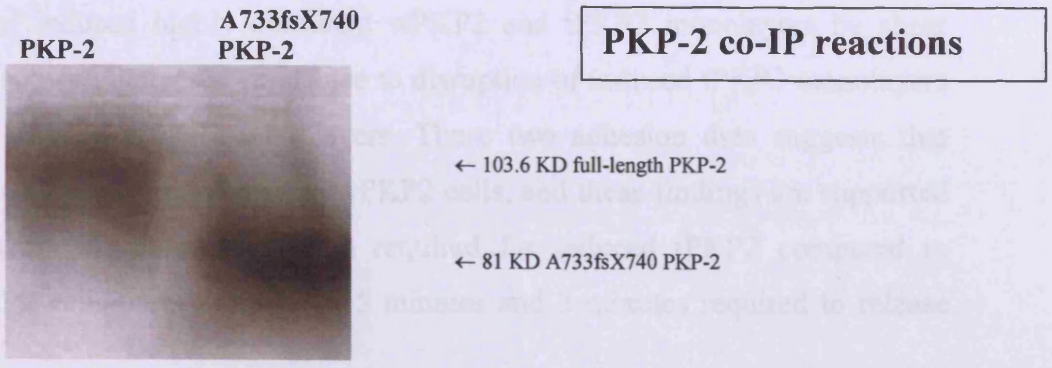

4.6 Discussion

Two stable cell lines were generated to examine the functional effect of expression of full-length and A733fsX740 PKP-2 proteins at a cellular level in Flp-In T-Rex HEK 293 cells. Reduced level of A733fsX740 PKP-2 protein relative to the endogenous PKP-2 protein observed in the membrane fraction of sub-cellular fractionated induced tPKP2 cells, suggested that A733fsX740 PKP-2 protein might incorporate less efficiently into cell-cell contacts. Localization studies of a different plakophilin (PKP-1) using transfection experiments in a PKP-1 null A431D derivative of a cervical squamous carcinoma cell line showed that over-expression of a PKP-1 protein lacking the final forty-one amino acid residues in the carboxy-terminus failed to localize this protein at cell-cell contacts in these transfected cells[222], implying that the last 41 residues of PKP-1 are important for its insertion into cell-cell contacts. It is speculative whether an analogous region present in full-length PKP-2, but lacking in A733fsX740 PKP2 might affect the localization of the truncated PKP-2 at cell-cell contacts. The extent of incorporation of truncated versus full-length PKP-2 proteins into cell-cell contacts could be assessed using double cell line transfection experiments expressing a GFP-conjugated full-length PKP-2 protein and a FLAG-tagged truncated PKP-2 protein followed by localization of dual-colour immuno-fluorescence signals in cultured cells.

Expression of either full-length or truncated plakophilin-2 did not affect the cellular proliferation rates of wPKP2 and tPKP2 cells respectively as regression analysis of the proliferation data gave comparable values of the slopes in these non-induced and tetracycline-induced cells. The initial cell-cell adhesion of labelled tPKP2 cells to a homologous cell monolayer was about 1.5-fold greater compared to initial cell adhesion of labelled wPKP2 cells to a homologous cell monolayer. The increased initial tPKP2 cell-cell adhesion was investigated by a different assay measuring the dissociation of induced highly confluent wPKP2 and tPKP2 monolayers by shear stress, which showed increased resistance to disruption of induced tPKP2 monolayers compared to induced wPKP2 monolayers. These two adhesion data suggests that tPKP2 are more adherent compared to wPKP2 cells, and these findings are supported by a consistently longer trypsinization required for induced tPKP2 compared to induced wPKP2 cells (data not shown, 5 minutes and 3 minutes required to release

clusters of tPKP2 and wPKP2 cells respectively). The increased cell-cell adhesion of tPKP2 cells is an anomaly in regards to electron microscopy data, which showed abnormal cell-cell contacts in these cells compared to control wPKP2 cells. The mechanism responsible for increased cell-cell adhesion is not obvious. As far as the direct binding of plakophilins to intermediate filament proteins is concerned, both PKP-1a as well as PKP-2a are known to strongly interact *in vitro* with cytokeratin IF proteins such as CK5, CK14 & CK18, and less so with CK8 and vimentin examined by blot overlay assays[223]. An over-expressed head fragment of PKP-1a was reported to decorate and disrupt keratin filament network organization in certain transfected cells[224]. Although the interaction of A733fsX740 PKP-2 with IF proteins is unknown, it is speculated that insertion of this protein into cell-cell contacts may cause a dominant negative effect in tPKP2 cells resulting in intermittent DS coupling largely lacking filaments indicating inappropriate desmosomal coupling.

In vivo specific mechanisms are postulated to regulate binding of PKP-2 or PKP-1 to desmoplakin and intermediate filaments, where plakophilins are generally excluded from interacting directly with IF proteins[223]. Desmoplakin is the main protein directly involved in the interaction with IF proteins. The evidence supporting this is firstly, an N-terminal truncated desmoplakin peptide transiently expressed in simple epithelial cells and fibroblasts show co-localization with IF fibrils resulting in gradual disruption of endogenous IF network[132]. Secondly, the last 68 amino acids of desmoplakin C-terminus are essential for its binding to IF proteins[131], and this binding can be modulated indirectly, for instance, by site-specific phosphorylation of a specific serine residue[225].

Cell-cell adhesion in epithelial cells such as primary keratinocytes has been shown to depend on PG where it accomplishes this role through the regulation of desmosome assembly and function[226], however very little is known about the mechanisms of cell-cell adhesion in HEK 293T cells. Although HEK 293 cells adopt epithelial cell type of morphology, they are believed to be closely related to early differentiating neuronal cell lineages such as PC12 and Ntera-2 cells as they express an array of different intermediate filament proteins resembling expression patterns in these cell types. HEK 293 cells express large amounts of neurofilaments -M and -L (type IV IF proteins), smaller amounts of α-internexin and neurofilaments -H (type IV IF proteins). HEK

293 cells do not express desmin, GFAP and nestin, but they express vimentin (type III IF protein), keratin 8, and keratin18 (type I IF proteins) in a heterogenous staining pattern[227]. Given this complex expression pattern of IF proteins in HEK 293 cells, it is plausible that the A733fsX740 PKP-2 might differentially affect these IF networks and tPKP2 cell-cell adhesion. The relevance of increased tPKP2 cell-cell adhesion is dubious in a cardiac context as desmin is the only IF protein expressed in cardiomyocytes. Irrespective of the underlying mechanism of increased cell-cell adhesion in tPKP2 cells, A733fsx740 PKP-2 protein insertion into tPKP2 desmosomal cell-cell contacts appears to exert a dominant negative effect in these cells. Similarly, in the nucleus where A733fsX740 PKP-2 also localises, it may exert a dominant negative effect by interfering with presumed nuclear signalling function(s) of endogenous PKP-2. In contrast with other junctional plaque proteins such as β-catenin and plakoglobin, there is limited data available about the signalling pathways in which PKP-2 might integrate. One possible interaction of PKP-2 described was with endogenous β-catenin in transfected SW40 cells over-expressing PKP-2a causing the activation of β-catenin/T cell factor-signalling activity[183].

Various studies have examined apoptotic cell death in ARVC shown to be associated with cardiomyocyte loss[63,64,66-71], however, it was not clear from these studies whether apoptosis was causative for ARVC. One hypothesis is that weakened cell-cell adhesion between cardiomyocytes in ARVC arise presumably from dominant negative mutant cell adhesion protein insertion, and this may under inappropriate mechanical stress (for example during intense physical exercise), cause myocyte detachment with consequent replacement with fibrous and/or fatty tissue as myocytes have a limited capacity for cellular proliferation. Expression of truncated and full-length PKP-2 proteins in HEK 293 cells provided an opportunity to examine the response of tPKP2 and wPKP2 cell to mechanical cell-stretch and induced apoptosis. Caspase-3 activity measured in cells recovering from an exposure to mechanical cell-stretch showed presence of its activity in both wPKP2 and tPKP2 cells, but this was approximately two-fold higher in mechanical cell-stretched induced tPKP2 cells compared to mechanical cell-stretched tetracycline-induced wPKP2 cells. The intensities of active caspase-3 bands detected by SDS PAGE and western immunoblotting analysis in control wPKP2 or tPKP2 cells not exposed to cell-stretch was weak, but exposure to cell-stretch showed a dramatic increase in the intensities of

active caspase-3 bands in both types of cells. This increase, however appeared to be greater in induced tPKP2 cells compared to induced wPKP2 cells. Taken together with the EM data showing abnormal cell-cell contacts in tPKP2 cells the mechanical cell-stretch data indicates that incorporation of A733fsX740 PKP2 into cell-cell contacts probably weaken these contacts, and therefore, tPKP2 cells presumably sustain increased cellular injury with marked activation of cellular apoptosis. The signalling pathways responsible for this response in tPKP2 cells was not investigated, but in the following paragraphs discussion relating to mechanical cell-stretch of cardiomyocytes provide some insight of the responses of these cells to mechanical cell-stretch Based on a proposed framework of mechanism linking contractile and electrical dysfunction in cell-cell junction cardiomyopathies[50,228], A733fsX740 PKP-2 protein expression in tPKP2 cell-cell junctions is envisaged to cause abnormal mechanical cell-cell coupling due to desmosomal instability resulting in cellular injury probably manifesting in enhanced apoptosis from intolerance to the applied mechanical cell stretch. In the following two paragraphs, a brief overview of apoptosis and current knowledge about effect of stretch on cardiomyocytes *in vitro* is described.

Apoptosis, generally is a tightly controlled programmed cell death process, which is characterized by cytomembrane overturn, DNA fragmentation, nuclear condensation and cell shrinkage[229]. Two types of apoptosis pathways are recognised the mitochondria-dependent (intrinsic) pathway and a death receptor-dependent (extrinsic) pathway. Both types have been found in cardiomyocyte apoptosis[230]. In the intrinsic pathway various apoptotic factors such as cytochrome c, apoptosis inducing factor (AIF), Smac/DIABLO and endonuclease G are released into the cytoplasm when stimulated by intrinsic death signals. Once cytochrome c is released it rapidly activates caspase-9, which leads to activation of caspase-3 and execution of apoptosis[231,232]. Bcl-2 family of proteins are involved in regulating this process[233]. In the extrinsic pathway, apoptosis is initiated after binding of various ligands to their death receptors (DR) such as FasL to Fas, TNF-alpha to tumour necrosis factor receptor1 (TNFR1), Apo3L to DR3, and TNF-related apoptosis-inducing ligand (TRAIL) to DR4 and DR5. Binding of ligands results in trimerization of DR, recruitment and activation of procaspase-8 through adaptor molecules such as Fas-associated protein with death domain (FADD). Active caspase-8 subsequently cleaves

downstream caspases as well as other pro-apoptotic factors to initiate intracellular amplification of the apoptotic response.

Mechanical stretch activates multiple signalling pathways (MAPK, JAK/STAT & PKC) which in rat cardiomyocytes may be responsible for a hypertrophic or apoptosis response, depending on the system used and degree of stretch applied[234]. Based on in vitro studies, prolonged mechanical cell-stretch was reported to induce apoptosis in adult cardiomyocytes via enhancement of autosecretion of angiotensin II, which led to Bax expression and apoptosis in a p53 dependent manner[235,236], although this view was challenged[237]. Another report attributed mechanical cell-stretch induced apoptosis in cardiomyocytes to production of reactive oxygen species (ROS) during periodic stretch[238]. Both Bax and ROS can influence in mitochondria, hence supporting the roles of mitochondria-dependent pathway in stretch-induced cardiomyocyte apoptosis. Further support for this pathway came from neonatal rat cardiomyocytes exposed to sustained stretch that undergo mitochondria-dependent apoptosis via cytochrome c and Smac/DIABLO release from mitochondria into cytosol accompanied by loss of mitochondrial membrane potential[239]. A report describing the involvement of FADD-linked death receptor signalling in apoptosis of rat neonatal cardiomyocytes exposed to sustained stretch has been described[240]. Ventricular cardiomyocytes *in vivo* are exposed to continual mechanical cell-stretch due to the rhythmic contraction and cardiomyocytes must be able to endure normal level of mechanical cell-stretch, however, in ARVC it is believed that exposure to abnormal level of mechanical cell-stretch (degree and frequency of mechanical cell-stretch, for example during intense physical exertion) superimposed with abnormal mechanical junctions (weakened cell-cell contact between cardiomyocytes caused either by insertion of dominant negative proteins or by a lack of sufficient wild-type protein insertion due to haploinsufficiency) may result in cardiomyocytes sustaining cellular injury and increased programmed cell death. Although mechanical stretch activated pathways in cardiomyocyte apoptosis are described *in vitro*, no direct evidence in the literature exists to suggest that defective cell-cell mechanical coupling resulting from abnormal desmosomal protein insertion *in vitro* could enhance cardiomyocyte apoptosis in response to mechanical cell-stretch exposure. A recent study examining the expression of a defective PG protein (S39_40KinsS PG) in Flp-In T-Rex HEK 293 stable cells not only demonstrated enhanced cellular proliferation

but also reduced apoptosis levels in these cells compared to stable cells expressing wild type PG protein, however, the effect of mechanical cell stretch in these stable cells was not examined[51]. A cardiac restricted transgenic mice study expressing a mutant missense desmoplakin protein (R2834H DP transgenic mice) compared with control wild type transgenic mice expressing full-length DP showed evidence of ID remodelling (irregularly shaped ID with marked widening of gaps between adjacent anchoring sarcomeres affecting both AJ and DS junctions), increased cardiomyocyte apoptosis cardiac fibrosis, neutral lipid accumulation and aberrant desmin intermediate filament localization *in vivo* [163]. These data therefore appear to be the first evidence linking defective cardiomyocyte mechanical junctions arising from an expressed mutant DP protein in the heart with apoptosis of these cardiomyocytes from exposure to normal mechanical cell-cell stretch (from rhythmic contraction) *in vivo*. HEK 293 stable cells cannot tolerate the high level of cellular stretch (up to 20%) that cardiomyocytes are able to endure *in vitro*, but the increased apoptosis of tPKP2 cells in response to mechanical stretch demonstrate that these cells can respond in a similar fashion to R2834H transgenic mice cardiomyocytes *in vivo*.

Although the loss of desmosomal integrity is known to disrupt mechanical junctions in hearts afflicted with ARVC, this does not directly explain the highly arrhythmogenic nature of the disease, particularly in cases in which life-threatening arrhythmias can occur in the absence of severely displaced fatty or fibro-fatty myocardium. Saffitz and colleagues [50,228,242] recently proposed that disruption of mechanical coupling may lead to a loss of gap junction-mediated electrical coupling. Connexin-43 is the main cardiac gap junction protein important in ventricular conduction. This protein was examined in stable tPKP2 and wPKP2 cells. A strong expression of Cx-43 protein was found in soluble cell lysates of highly confluent non-induced as well as tetracycline-induced wPKP2 and tPKP-2 cells. However, examination of Cx43 protein by confocal microscopy showed Cx-43 protein localization in cell-cell contacts of induced wPKP2 cells, but this Cx-43 protein localization pattern was consistently absent in induced tPKP2 cells. The absence of Cx-43 protein localizing at tPKP2 cell-cell contacts despite Cx-43 protein being present in the cytosol suggests a failure of incorporation of Cx-43 into cellular membrane of tPKP2 cells. It is possible that low amounts of Cx-43 protein incorporated into tPKP2 cell membrane will result in a diffuse staining pattern that is

not detected by confocal microscopy. HEK 293 cells are excellent cells for plasmid vector transfection studies resulting in high expression of membrane bound proteins, however these cells suffer a drawback for localization of expression as nuclei of HEK 293 cells occupy a significant proportion of the cell space and they lack a cubical geometry found in other epithelial cells (such as MDCK or A431). These factors might further hinder detection of small amounts of immuno-localized Cx-43 signals in induced tPKP2 cells due to the poor discrimination of weak signals by confocal microscopy. A likely explanation for the lack of detectable Cx-43 at cell-cell contacts of tPKP2 cells might be that Cx-43 protein assembly into gap junctions is disrupted because of destabilized abnormal tPKP2 cell-cell contacts formed by the insertion of A733fsX740 PKP-2; both the incorporation of A733fsX740 PKP-2 protein into cellular membrane and disruption of cell-cell contacts of induced tPKP2 cells were confirmed by sub-cellular fractionation/immunostaining and by electron microscopy examination respectively. Gap junctions in the cardiomyocyte ID are known to be located close to desmosomal contacts, which suggest that these mechanical junctions provide the stability at the plasma membrane for incorporation of these rigid gap junction assemblies. Precisely why Cx-43 protein expressed in tPKP2 cells fails to incorporate into functional gap junctions is not known, but the stability and turnover of this protein could be affected by multiple mechanisms (section 1.4).

Supportive data for a role of PKP-2 in the proper function and distribution of Cx-43 gap junction protein was recently obtained in cultured rat neonatal ventricular cardiomyocytes transfected with adenoviral vector containing a specific silencer sequence construct for PKP-2. Transfection achieved loss of cell-cell contact immuno-localized PKP-2, a significant redistribution of Cx-43 (with fewer Cx-43 gap junctions being detected, instead Cx-43 was found mostly in the intracellular space), and reduction in Lucifer Yellow dye transfer (GJIC) between cardiomyocytes[218]. The data from these PKP-2 inhibition studies emphasize the importance of PKP-2 in proper assembly of Cx-43 gap junctions, and suggests a crosstalk between Cx-43 and PKP-2 proteins in which the presence of PKP-2 was essential for regulating and coordinating the formation of and interactions between mechanical and electrical junctional complexes. Immuno "pull-down" experiments showed Cx-43 and PKP-2 to be part of a common macromolecular complex in these studies. The data obtained from tPKP2 cells suggests that abnormal cell-cell contacts disrupt mechanical

linkages affecting the assembly of Cx-43 protein into functional gap junctions. Additional supporting evidence suggesting the mechanism of arrhythmogenesis in ARVC might be linked by a crosstalk between structures involved in mechanical coupling with those that maintain electrical communication was obtained from a study in a spontaneous animal model of ARVC in Boxer dogs. Although the presumed gene mutations involved in this animal model of ARVC are still pending identification (mutations were not present in the coding regions of genes for DP, PG, PKP-2, DSC-2 and Cx-43[61,62]), examination of ID in cardiac biopsy of afflicted dogs showed significant loss of Cx-43 gap junction protein in cardiac ID associated with severe remodelling of other intercalated disc structures[61]. Similarly, in human heart conditions myocyte gap junction remodelling was reported to cause alterations in the amount and distribution of Cx-43 protein in gap junctions seen in Caravajal syndrome[43], Naxos disease[42], and more recently in autosomal dominant ARVC caused by an in-frame insertion mutation in plakoglobin[51]. Thus, there is now an increasing body of evidence pointing to the disruption of Cx-43 gap junctions resulting from abnormal mechanical coupling. Furthermore, a recent study accentuated the critical function of PKP-2 in the formation, architectural organization, and stability of the junctions within the area composita of the ID of rat neonatal cardiomyocyte culture. In these studies, the prolonged siRNA-mediated reduction of cardiomyocyte content of PKP-2 showed progressive disintegration and the loss of the area composita with significant reduction in the number of cell-cell contacts between cardiomyocytes[243].

Electrophysiological studies determining cell input resistances in induced tPKP2 cells and wPKP2 cells established the extent of current conduction in these cells. However, statistical analysis of calculated cell input resistance values indicated no significant statistical differences in these cells. This might probably be due to compensatory up-regulation of other connexin proteins in tPKP2 cells. This phenomenon can be observed *in vitro* during modulation of the expression of one connexin subtype[244] resulting in the upregulation of another connexin subtype. Analysis of wPKP2 and tPKP2 cell gap junction intracellular communication indicated that both cells were poorly coupled (maximum dye transfer across eight cell layers, but highly efficient cell-cell coupling would result in transfer of dye across twenty or more layers) to each other as a limited dye transfer was observed in these cells. Stable cell functional studies in wPKP2 and tPKP2 cells showed the limitations of HEK 293 cell system in

performing complex analysis of the inter-relationship of expression of defective cell-cell adhesion protein and the effect on mechanical junction stability and influence on gap junction protein functionality. Although Cx-43 was demonstrated in wPKP2 cell-cell contacts, this does not demonstrate the state of functionality of these gap junctions in these cells as the gating properties of these gap junctions can be modulated *in vivo*. Other cellular systems such as isolated rat neonatal ventricular cardiomyocytes are probably a more relevant system for examining the effect of abnormal cell-cell junction protein on electrical and mechanical dysfunction in a cardiac context. Recent studies examining the area composita in the ID of cardiomyocytes *in vitro* demonstrated the utility of this culture system[137,138,245,246] in evaluating the functional contributions of various cell-cell adhesion proteins in the ID.

The antibody reactive to PKP-2 (BD Bioscience, P63420) was used for confirming the expression of A733fsX740 PKP-2 expression by SDS PAGE and western immunoblotting and confocal microscopy immuno-localization analysis of tPKP2 cells, but this antibody was not suitable for immuno-localizing truncated PKP-2 into desmosomes by electron microscopy as the antibody recognizing an N-terminal epitope reacts with all PKP-2 proteins (endogenous PKP-2 and over-expressed PKP-2a as well as A733fsX740 PKP-2). Tagged-truncated PKP-2 expression in stable cells is necessary for a definitive localization of truncated PKP2 into desmosomes.

Although the localization studies of truncated PKP2 into desmosomes are not available, desmosomes in control non-transfected Flp-In, induced wPKP2 and tPKP2 cells showed marked differences in morphology with wPKP2 cells forming prominent desmosomes with electron dense plaques and filament association while tPKP2 cells formed intermittent DS coupling with pale plaque region, and which largely appeared to lack extensive filament association; when filaments could be localized in tPKP2 desmosomes their morphological organization appeared to be different from filaments found in induced wPKP2 desmosomes. Low level of recruitment of desmosomal plaque proteins or their reduced expressions in non-transformed Flp-In T-Rex HEK 293 cells might be responsible for the lack of conspicuous desmosomes.

There could be two reasons for prominent desmosomes in wPKP2 cells, firstly over-expressed PKP-2a could bind to endogenous desmosomal proteins, targeting them to

the plasma membrane, and thereby dramatically increase their stability. Secondly, over-expressed PKP-2a may directly be involved in regulating the synthesis of other desmosomal proteins in the nucleus; the induction of desmosomes would then depend on a putative signalling function of PKP2a. However, since PKP2a localised in the membrane as well as in the nucleus, both of these mechanisms might contribute to the recruitment of endogenous desmosomal proteins. If indeed there was an upregulation of desmosomal components by over-expressed PKP-2a then this could be tested by examining the expression of mRNA encoding other desmosomal proteins by RT-PCR or by examining the endogenous proteins levels in these cells by western immunoblotting analysis.

In common with mutations in the gene encoding human PKP-1 that lead to impaired association of keratin intermediate filaments with the plasma membrane in keratinocytes, lack of PKP-2 in mouse cardiomyocytes also causes intermediate filaments to retract from the membranes[190]. Thus, both PKP-1 and PKP-2 play essential roles in mediating desmoplakin association with desmosomes in the epidermis and heart respectively. In contrast with mouse cardiomyocytes lacking PG where DP remains firmly associated with the plaques of adhering junctions[186], DP was no longer associated with cardiomyocyte junctions in the absence of PKP-2, suggesting that PKP-2, possibly together with PG might be essential for fixing DP to the junctional plaques of cardiomyocytes[190]. It is believed that PKP-2 is important in recruiting DP to the plaque and for stabilizing lateral connections in the desmosomes through its interactions with other plaque proteins via its head domain[183,184], while PG is thought to be important for clustering DP to desmosomal cadherins. Precisely why tPKP2 cell desmosomes possess little or no filaments might be explained by recent studies examining the role of PKP-2 in DP assembly dynamics. The functional requirement of PKP-2 in the formation and translocation of DP particles to cell-cell contacts was demonstrated in a study tracking fluorescent DP-GFP in SCC9 cells in which PKP-2 was found to co-localize with assembly competent DP-GFP particles in the cytoplasm and into nascent desmosomes at sites of cell-cell contacts[216]. Furthermore, it is now known that PKP-2 affects DP assembly by scaffolding a DP-PKP-2-PKCα protein complex[247]. In this study siRNA mediated reduction of PKP-2 protein expression in SCC9 and A431 cells showed an impaired DP localization at sites of cell-cell contacts. In SCC9 cells PKP-2 was shown to regulate PKC signalling

by recruiting it to DP. PKP-2 deficient SCC9 cells showed increased phosphorylation of myristolylated alanine rich PKC substrates, and a reduction in the amount of DP co-immunoprecipitated in complex with PKCα[247]. The association of PKCα with the assembly competent DP particle regulates DP assembly into desmosomes possibly through modulation of serine phosphorylation at position 2849 which regulates the association of DP with intermediate filaments[199,225]. As previously discussed, DP is essential for recruiting IF filament into desmosomes, and it is speculative whether A733fsX740 PKP-2 might alter assembly dynamics of DP by affecting the availability of PKCα required for the appropriate assembly of intermediate filament binding. Additionally, since reduced amounts of endogenous PG associates with A733fsX740 PKP-2 this may also affect the clustering of desmoplakin into cell-cell junctions as PG serves as a linker between cadherins and DP via its binding to the N-terminal domain of DP.

A suitable antibody facilitating the immunoprecipitation of full-length PKP-2 as well as A733fsX740 PKP-2 in wPKP2 and tPKP2 cells was not commercially available. Thus, DNA encoding full-length or truncated PKP-2 was cloned in pcDNA4 plasmid vector and this was used to transfect HEK 293T cells for obtaining transient protein expressions of N-terminally XPress-tagged full-length or truncated PKP-2 proteins. The reduced interaction of A733fsX740 PKP-2 (three ARM repeats missing) with PG was unexpected as previous studies had shown that the head domain of PKP2 was primarily involved in its interaction with PG[183]. However, the relative importance of the PKP-2 ARM repeats in binding to PG was emphasized in that study where a reduced association of a PKP-2 protein fragment lacking all ARM with PG was shown, however comparatively, the association of PG with a PKP-2 protein fragment including all ARM repeats but lacking the head domain was even more reduced [183]. These domain specific studies of PKP-2a expression *in vitro* suggests that the head domain as well as the ARM repeats of PKP-2 may co-operatively modulate the binding of PG. The binding of endogenous β-catenin with truncated PKP-2 in IP assays occurred at a level comparable to the interaction of β-catenin with full-length PKP-2, and this was consistent with a previous finding confirming that PKP-2a interacted with β-catenin mainly through its N-terminus head domain[183].

Both isoform of endogenous DP proteins were expressed in wPKP2 and tPKP2 stable cells (data not shown), however the immunoprecipitation of full-length PKP-2 and truncated PKP-2 proteins using anti-XPress antibody co-immunoprecipitated variable amounts of DP, as well as DSG-2 and DSC-2 in wPKP2 and tPKP2 Triton X-100 soluble cell lysates (data not shown). It is arguable that the location of the epitope tag in the expressed PKP-2 might be important for obtaining successful immunoprecipitation of endogenous DP, DSG-2, and DSC-2 proteins that were poorly immunoprecipitated in this study. The XPress tag on PKP-2 in this study was N-terminally located, however, in a study examining over-expressed C-terminus FLAG tagged PKP-2a in SCC9 cells it was reported that endogenous desmoplakin was variably immunoprecipitated using an anti-FLAG antibody[183]. Thus, poor cellular extraction of these protein complexes rather than the location of the tag seem plausible explanation for the difficulty of obtaining reliable immunoprecipitation of these proteins and the inefficient transfer of large proteins by semi-dry transfer method might be an additional factor contributing to the variable amounts of co-IP of these endogenous proteins. The immunoprecipitation of Desmoglein-2 was reported to be problematic in SCC9 cells expressing C-terminal FLAG-tagged PKP-2a which failed to immuno-precipitate endogenous DSG-2 using an anti-FLAG antibody, however, DSG-3 also expressed in these cells was successful immunoprecipitated[183]. The immunoprecipitation of endogenous DSC-2 with C-terminal FLAG-tagged PKP-2a in SSC9 cells has not been reported in a previous study[183]. Cell membrane and cytoskeleton localized DP, DSG-2, and DSC-2 proteins may inefficiently extract into solution and other buffer systems (for example, RIPA buffer, and using a different detergent such as NP40) may be required to obtain sufficient amounts of complexes of these endogenous proteins with either full-length or truncated PKP-2 proteins. Although the precise amino-acid residues responsible for the interaction of PKP-2 with PG, DP, DSG-2, β-catenin, and DSC-2 are unknown all these inter-protein interactions are believed to occur via the head domain of PKP-2[183].

It is not known whether A733fsX740 PKP-2 protein is indeed expressed or incorporated into cardiac desmosomes of patients affected with the c.2197_2202_delCACACCinG PKP-2 gene mutation, as it was not possible to obtain heart tissue sample from any individuals in the three families examined by pedigree studies. Availability of tissue sample would allow verification of the presence of

mRNA encoding a truncated protein by reverse transcription polymerase chain reaction, or by examining the presence of A733fsX740 PKP-2 truncated protein in diseased heart lysates by western immunoblotting analysis, or by immuno-electron microscopy to localize expression of a truncated PKP-2 protein in cardiac ID.

4.7 Summary of the main findings of the study

DNA encoding full-length and c.2197_2202_delCACACC_insG PKP-2 was cloned in pcDNA5 and pcDNA4 plasmid vectors. Using pcDNA5 vectors encoding full-length or truncated PKP-2 (p.A733fsX740 PKP-2), two stable cell lines were established using Flp-In T-Rex HEK 293, one of these cell lines, **wPKP2,** expressed full-length PKP2, and a second cell line, **tPKP2,** expressed truncated PKP-2.

A strong tetracycline-induced expression of full-length PKP2 (with a predicted and apparent SDS PAGE migration size of 98.7 KD) occurred in wPKP2 cells that was localised at cell-cell contacts and in the cell nuclei by confocal immunofluorescence staining. Sub-cellular protein fractionation of induced wPKP2 cells followed by Western immunoblotting analysis confirmed a predominant expression of PKP2 in the cytoplasm, membrane, and cytoskeletal protein fractions, while some PKP2 was associated with the nuclear protein fraction.

A strong tetracycline-induced expression of A733fsX740 plakophilin-2 (predicted and apparent SDS PAGE migration size of 77.1 KD) occurred in tPKP2 cells, which localized at cell-cell contacts and in the cell nuclei by confocal immunofluorescence staining. Sub-cellular protein fractionation of induced tPKP2 cells followed by western immunoblotting analysis indicated a strong expression of the truncated plakophilin-2 in the cytoplasm and cytoskeletal fractions, where roughly equal amount of both the endogenous plakophilin-2 and the mutant protein compartmentalized in the later fraction. The membrane fraction showed expression of both truncated and endogenous plakophilin-2, but the amount of endogenous plakophilin-2 protein appeared to be greater than that of the truncated PKP-2 protein. Both endogenous and truncated plakophilins were present in roughly equal amounts in the nuclear fraction.

Induced wPKP2 and tPKP2 cells proliferated at similar rates to non-induced wPKP2 and tPKP2 cells. The initial cell-cell contact adhesion of induced wPKP2 and tPKP2 cells showed statistically significant increased adherence of tPKP2 cells compared to wPKP2 cells when assessed by plating of these Calcein-labelled cells to homologous monolayer of cells cultured induced on coverslips. Adhesive strengths of confluent monolayers of induced wPKP2 and tPKP2 cells assessed by monolayer Dispase-based dissociation adhesion assays showed significantly increased resistance to fragmentation of sheared tPKP2 monolayer compared to those of wPKP2 monolayer. Tetracycline-induced wPKP2 and tPKP2 cells recovering from exposure to mechanical stretch showed statistically significant increased apoptosis (approximately two-fold) in tPKP2 cells compared to wPKP2 cells. Whole cell lysate western blot analysis of induced wPKP2 and tPKP2 cells showed that whilst Connexin-43 protein was strongly detected in both induced wPKP2 and tPKP2 cells only the localization of Cx-43 protein to cell-cell junctions of wPKP2, but not in tPKP2 cells was found by confocal microscopic examination of these induced cells. Cell input resistance measurements did not show significant differences to pulse current conduction within monolayer of induced wPKP2 and tPKP2 cells. Scrape-loading Lucifer Yellow dye transfer experiment indicated in wPKP2 cells that these did not couple particularly well to one another as dye transferred poorly in these cells. Examination of Flp-In T-Rex HEK 293, wPKP2, and tPKP2 cells showed that whilst desmosomes formed in Flp-In cells these were not as conspicuous as those formed in wPKP2 cells expressing full-length PKP-2 showing dense plaque and filament attachment. In contrast, however, desmosomes in tPKP2 cells compared to those in wPKP2 cells formed intermittent DS couplings with pale plaque region and largely lacking filaments; these filaments when present were observed to be organized differently compared to those found in induced wPKP2 cells. Overall, the measured desmosomal lengths in Flp-In, wPKP2 and tPKP2 cells were not statistically different from one another. Reduced localization of endogenous plakoglobin was observed at the cell-cell contacts of induced tPKP2 cells compared to wPKP2 cells.

N-terminally tagged transient protein expression of full-length (predicted and apparent SDS PAGE size 103.6 KD) and truncated (predicted and apparent SDS PAGE size 81 KD) plakophilin-2 obtained in HEK 293T cells obtained 48hour after transfection of pcDNA4 vectors showed reduced association of truncated PKP-2 with PG by

immunoprecipitation studies. Beta-catenin appeared to associate to the same extent with both truncated and full-length plakophilin-2

4.8 Future Studies

Flp-In T-Rex HEK 293 stable cells expressing truncated PKP2 and PKP2 provided a practical model system for assessing the functional impact of cell membrane incorporated PKP-2 proteins. However, these stable cells have obvious limitations in studying PKP-2 mutations in a cardiac setting. In this context, isolated rat neonatal ventricular cardiomyocytes is an appropriate model system to examine the effects of A733fsX740 PKP-2 protein expression. Isolated neonatal rat cardiomyocytes are widely used to examine transient protein expressions and mechanical cell-stretch studies; these primary cells are relatively easy to isolate and can be maintained in culture for up to twelve days duration in spite of having limited capacity for cellular proliferation[246]. Although a human cardiomyocyte cell line is available[248], it is not possible to examine the effect of A733fsX740 PKP-2 protein expression in this cell line using pcDNA5 A733fsX740 plasmid vector because of poor transfection/expression obtained using plasmid vectors (personal communications with the author). However, it might be possible to use human cardiomyocyte cell line for examining the effects of A733fsX740 PKP-2 protein expression using a different vector delivery system, such as an adenoviral vector. A mouse model describing a cardiac restricted expression of mutant cell-cell adhesion protein[163] is an elegant system allowing the role of mutant cell adhesion proteins to be evaluated in the ID *in vivo*, however it is by no means an easy system due to the high level of technical expertise required in establishing genetically engineered transgenic mice. It may be possible to determine the incorporation of A733fsX740 PKP-2 into tPKP2 cell desmosomes using an epitope-specific antibody raised against the last eight amino acids in A733fsX740 PKP-2 fragment, which are novel to the truncated PKP-2. The reduced filament association seen in tPKP2 cells must be examined by confocal immuno staining localization studies to demonstrate the disruption of intermediate filament protein network (for example, vimentin) in these cells. Immuno-localization studies also need to be performed to determine whether there is an altered localization of DP into tPKP2 cell-cell junctions, which might explain the reduced intermediate filament association in these cells. Examination of levels of PKCα in immuno

complex with A733fsX740 PKP-2-DP in induced tPKP2 cells compared to levels PKPCα in immuno-complex with PKP-2-DP in induced wPKP2 cells may shed light on a possible mechanism explaining the lack of filaments in induced tPKP2 cells. Although over-expressions of PKP-2 and A733fsX740 PKP-2 proteins in Flp-In T-Rex HEK 293 cells have shown an effect on desmosome morphology and endogenous PG localization, these studies must be confirmed in other cell systems such as MDCK or A431 cells that form robust desmosomes *in vitro* and permit better co-localization of desmosomal proteins to confirm observations from the present studies. Since p.A733fsX740 PKP-2 appears to be a recurrent mutation, it might be possible to obtain heart tissue from affected individuals in the future to verify the presence of A733fsX740 PKP-2 protein in cardiac tissue to support a possible dominant negative effect of the protein or to exclude this possibility because of NMD mechanisms causing haploinsufficiency. The reduced association of PG in desmosomes of tPKP2 cells may imply a possible signalling function of PG in tPKP2 cells, which requires investigation in future studies. The absence of cell membrane localized Cx-43 protein in induced tPKP2 cell-cell contacts requires further investigation particularly to examine the phosphorylation and ubiquitination status of Cx-43 protein as these are important in the targeting of Cx-43 to cell membranes and turnover of the protein. Optimization of co-IP reactions using different combination of buffers and detergents are required for obtaining sufficient cellular extraction of immuno-complexes containing endogenous DP, DSG-2, and DSC-2 formed with over-expressed either full-length or truncated PKP-2 proteins. The co-IP of full-length and truncated PKP-2 with endogenous Cx-43 protein need to be examined further because of the apparent lack of incorporation of Cx-43 protein in tPKP2 cells and evidence in the literature supporting the importance of PKP-2 in proper function and distribution of Cx-43 gap junctions and the coexistence of PKP-2 and Cx-43 as a macromolecular complex present at cell-cell contacts. The co-IP data has to be verified with confocal microscopy localization studies, the failure to obtain reliable co-localization of other endogenous proteins such as β-catenin, DP, DSG-2, and DSC-2 with either full-length or truncated PKP-2 may be a limitation of HEK 293 stable cells as they are not the best cell line for localization studies and some of these endogenous proteins may be expressed in small amounts, but it should be possible using double plasmid co-transfection transient expressions of either over-expressed tagged full-length PKP-2 or over-expressed tagged truncated PKP-2 together with each of these different epitope-tagged plasmids encoding β-catenin, DP, DSG-2 and DSC-2 to alleviate the problem of low amounts of endogenous protein co-localization.

Chapter 5

Functional Studies of S140F

Plakophilin-2 protein expression in mPKP2 cells

5.1 Introduction

Genetic screening of an ARVC cohort and pedigree analysis of family G (section 3.42 part 2.5) showed an autosomal dominant mode transmission of ARVC caused by PKP-2 gene mutation (c.C1604T) resulting in a missense sequence change p.S140F in the PKP-2 protein. (Table 3.4, Figure 3.2). This mutation described previously by Gerull[40] *et al*, results in the substitution of a serine residue relatively conserved in different species (human, cat and mouse PKP-2), but functional study of the missense PKP-2 protein was not performed in that study. The interactions of PKP-2 protein with other desmosomal proteins have been reported to depend critically on the head domain (first 348 amino acid residues) of PKP-2[183]. A novel association of PKP-2 with β-catenin demonstrated by yeast two-hybrid assay, IP analysis of transient transfected human tongue squamous cell carcinoma SCC9 cell line, and in co-IP analysis of transient transfected COS cells[183] showed that β-catenin specifically co-immuno precipitated with both PKP-2 and its head domain but only weakly with the ARM repeat domains of PKP-2. This novel association of PKP-2 with β-catenin raised the possibility that PKP-2 might participate in the cross-talk between adherens and desmosomal junctions and signal transduction pathways via Wnt-signalling[183].

5.2 Experimental approach to investigate functional effect of S140F PKP-2 protein expression

The S140F PKP-2 protein formed was predicted tolerant and benign by SIFT and Polyphen analysis (section 3.4.1 part1.7), however pedigree analysis established a clear association of the inheritance of the genetic defect (cC1604T) with expression of ARVC. The cC1604T gene mutation in exon 3 of PKP-2 was shown to reside on a SC35 protein recognition exon splice enhancer sequence, however, ESE finder computer program algorithm analysis of the wild type and mutant PKP-2 exon 3 sequences showed that the C>T nucleotide substitution does not abolish the splice enhancer sequence (section 3.4.1 part 1.8a), hence no effect on the splicing of PKP-2 protein was predicted. Serine residues phosphorylation site predictions in PKP-2 protein indicated that serine residue at position 140 might be a potential phosphorylation site involved in a putative signalling function of the protein (section

3.4.1 part 1.8b and Table 3.6). A stable cell line expressing missense PKP-2 protein was established to investigate its functional effect at a cellular level.

Cloning of DNA encoding S140F PKP-2 was performed in pcDNA5 and pcDNA4 vectors that permit stable cell line to be established and inter-protein interaction to be examined using an anti-XPress immunoprecipitation approach using these two vectors respectively. Using pcDNA5 PKP2 and pcDNA5 S140F PKP2 plasmids, Polyfect-mediated cationic transfection allowed selection of stable clones expressing either full length or missense PKP-2 proteins in an established tet-on system in Flp-In T-Rex HEK 293 cells. Several studies were performed using stable cells expressing full-length (designated **wPKP2 cells**) and missense PKP-2 (designated **mPKP2 cells**) proteins:

1) Expressions of full-length or truncated PKP-2 proteins were confirmed by confocal microscopy and western immunoblotting in wPKP2 and mPKP2 cells. The distribution of full-length and missense PKP-2 proteins expressed in wPKP2 and mPKP2 cells were examined in different cellular compartments (in cytosol, membrane, nuclear, and cytoskeletal fractions) using a Qiagen cell compartment fractionation kit.
2) Properties of wPKP2 and mPKP2 cells were examined to compare cellular proliferation rate and initial cell-cell contact adhesion with commercial kits described previously in chapter 4. Another assay measured confluent monolayer adhesive strengths of wPKP2 and mPKP2 cells using a Dispase-based monolayer dissociation assay.
3) Stable cells exposed to controlled mechanical cell stretch were allowed to recover for a short time. Non-induced and tetracycline-induced wPKP2 and mPKP2 cells treated in this manner were compared for their response to specific apoptosis activity measured using a CaspACE assay kit. This procedure measures the extent of apoptosis in wPKP2 and mPKP2 cells subjected to mechanical cell-stretch to determine whether expression of the missense PKP-2 influenced the degree of mPKP2 cell apoptosis.
4) Cx-43 protein a major connexin expressed in the heart ventricle was examined in triton X-100 soluble cell lysates of non-induced and tetracycline-induced wPKP2 and mPKP2 cells and the localization of cell membrane bound Cx-43 protein was compared in tetracycline-induced wPKP2 and

mPKP2 cells using western immunoblotting and confocal microscopy analysis respectively.

5) Desmosomes formed *in vitro* in tetracycline-induced wPKP2 and mPKP2 cells examined by electron microscopy were compared with desmosomes formed in control non-transfected Flp-In T-Rex HEK 293 cells to determine the effect of missense PKP-2 protein expression on the morphology of desmosomes.

Lastly, using pcDNA4 vectors HEK 293 T cells were transfected to obtain transient expressions of full-length and S140F PKP-2 N-terminally XPress epitope tagged proteins. These PKP-2 proteins were immunoprecipitated using a mouse monoclonal antibody reactive to the XPress epitope allowing the comparison of interaction of these two PKP-2 proteins with other endogenous desmosomal proteins.

5.3 Experimental Aims

Six overall objectives were set in this part of the study. The first was to make expression mutant S140F PKP2 plasmid in pcDNA5/FRT/TO/TOPO/TA using site directed mutagenesis of +2301ApcDNA5 plasmid. The second was to make a stable cell line in Flp-In TRex HEK 293 and verify the expression of S140F plakophilin-2 in this cell line. The third was to examine the proliferation rates, initial cell-cell contact adhesion, Dispase-based monolayer adhesion strength, and the effect of mechanical cell stretch on the measured apoptosis of mPKP2 stable cell line. The fourth was to examine Cx-43 protein expression at sites of cell-cell contacts in stable cell lines expressing PKP-2 and S140F PKP-2. The fifth was to examine desmosomes formed in non-transfected Flp-In T-Rex HEK293 and in tetracycline-induced wPKP2 cells and mPKP2 stable cells. The sixth was to clone S140F PKP-2 into pcDNA4/XPress/TOPO/TA expression vector for transient transfection expression of XPress-tagged S140F PKP-2 in HEK 293T cells to determine the degree of interaction of S140F PKP-2 protein with other desmosomal proteins using co-IP with an anti-XPress antibody and comparing with co-IP of XPress-tagged full-length PKP-2 with other desmosomal proteins.

5.4 Materials and Methods

Plasmid +2301 pcDNA5 was prepared as previously described in chapter 4. Flp-In-T-Rex HEK 293 cell line, all antibiotics, and media supplies were purchased from Invitrogen, UK. Quick-Change site directed mutagenesis kit was purchased from Stratagene, UK

5.4.1 SDM to obtain S140F PKP2 DNA encoded in pcDNA5/FRT/TO/TOPO/TA

Site-directed PCR mutagenesis (section 2.3) of +2301 pcDNA5 plasmid was performed using mutagenic primers (Table 5.1) to incorporate the c.C1604T nucleotide change in PKP-2 DNA encoded within +2301 pCDNA5 plasmid to obtain a plasmid (S140F pcDNA5) encoding the S140F PKP-2 mutation.

5.4.2 Cloning of S140F PKP2 in pcDNA4/XPress /TOPO/TA

An amplimer (2522bp) of S140F PKP-2 obtained by PCR using S140F pcDNA5 as template and XPress primers was cloned into pcDNA4 plasmid vector using vector-based topoisomerase cloning (Table 5.2).

5.4.3 Establishing stable transfected cell lines

Stable cell lines were established in Flp-In T-Rex HEK293 cells using pcDNA5 PKP2 and pcDNA5 S140F PKP2 plasmids according to procedure described previously (section 2.5.4) to obtain full-length PKP-2 and S140F PKP2 protein expression upon tetracycline-induction. Five separate clones of each stable cell line established were selected and clonally expanded, and the clone showing strong stable tetracycline-induced protein expression by western blotting (section 2.6.2) and immunofluorescence staining (section 2.7.2) was examined in functional study. Two stable cell line clones were selected for functional studies based on the above criteria: clone **wPKP2** expressed full-length PKP-2 (identical clone as the one that was used previously in Chapter 4) and clone **mPKP2** expressed S140F PKP-2 under tetracycline-induction.

Table 5.1 SDM to obtain pcDNA5 encoding full-length and missense S140F PKP-2

Site-directed PCR mutagenesis to obtain +2301A pcDNA5 and S140F pcDNA5 plasmids which are suitable for *in vitro* transfection in Flp-In T-Rex HEK 293 cells to obtain stable cell tetracycline-induced expression of either full-length PKP-2 or S140F PKP-2 proteins respectively. Plasmid -2301A pcDNA5 containing an out-of-frame coding sequence of PKP2a (Table 4.1) was mutated by site directed mutagenesis to obtain +2301A pcDNA5 plasmid (previously described, section 4.4.2) that correctly encoded the full-length PKP2a coding sequence. Plasmid S140F pcDNA5 containing the nucleotide coding sequence for the mutant S140F PKP-2a was generated from +2301A pcDNA5 by site directed mutagenesis using the primers shown. Resulting plasmids obtained were sequenced to verify the entire protein encoding nucleotide sequences in these plasmids.

Purpose of Site Directed Mutagenesis	Forward primer Sequence (5'-3')	Reverse primer Sequence (5'-3')	Plasmid Mutated	Resulting plasmid Obtained
Create a wild plasmid expressing full-length PKP-2a in pcDNA5	PKP2 Mut2301A for TTGGTGACCCAAGTGTGAAAAAGACA GCCATCTCGCTGCTGAG	PKP2 Mut2301A rev CTCAGCAGCCAGATGGCTGTCTTTTT CACACTTGGGTCACCAA	-2301A pcDNA5	+2301A pcDNA5
Create a plasmid expressing S140F plakophilin-2a in pcDNA5	PKP2 S140F for TCCGTGGAAGAAAGGTTCTTGAGGCAT CCTCTG	PKP2 S140F rev CAGAGGATGCCTCAAGAACCTTTCTT CCACGGA	+2301A pcDNA5	S140F pcDNA5

Table 5.2 Cloning of S140F PKP-2 in pcDNA4/XPress/TOPO/TA

Cloning of either full-length PKP-2 or S140F PKP-2 DNA in pcDNA4/XPress/TOPO/TA vector suitable for *in vitro* transfection studies to obtain XPress-tagged expressions of either full-length or S140F PKP-2 proteins in HEK 293T cells. S140F PKP-2 PCR fragment obtained using S140F pcDNA5 as template DNA and PKP2 XPress for and PKP XPress rev primers was cloned in pcDNA4 plasmid vector. Transient expression of these XPress-tagged PKP-2 proteins in HEK293T transfected cells were co-immunoprecipitated using an anti-XPress antibody. Plasmids +2301 pcDNA5 and S140F pcDNA5 (described in Table 5.1) were used as PCR templates with EXL DNA polymerase to obtain amplimers that were cloned in pcDNA4/XPress/TOPO/TA. The Primer pairs PKP2 XPress for and PKP2 XPress rev amplified PCR fragments encoding either full-length PKP-2 or S140F PKP-2 DNA that was cloned in pcDNA4/XPress/TOPO/TA preceded by vector encoded sequences for poly-histidine and an XPress tag (amino acid sequence: DLYDDDK). The cloned PKP-2s maintained the proper reading frame for protein translation with an ATG translation start site used from the host vector. A stop codon for protein translation termination was contained in the amplified cloned DNA inserts. PKP-2 or S140F PKP-2 proteins expressed in HEK 293T transfected cells contained N-terminal fused 6XHis tag and an XPress epitope adding 3.9 KD to the size of each PKP2 protein that was expressed.

Primer Pairs	**Sequence (5'-3')**	**PCR size (bp) / Enzyme used/ Template**	**Destination vector PCR product cloned into**	**Plasmid obtained**
PKP2 XPress for	ATGGCAGCCCCCGGCGCCCCAGCT	2522* /EXL/ **	pcDNA4/XPress/ TOPO/TA	pcDNA4 PKP2, pcDNA4 S140F PKP2
PKP2 XPress rev	GCTCTAGATCAGTCTTTAAGGGAGTGGTAGGC			

* Both full-length PKP2 and S140F PKP2 PCR fragment sizes were 2522bp long

** Templates used +2301A pcDNA5 and S140F pCDNA5 respectively.

5.5 Results

5.5.1 Characterization of S140F PKP-2 expression in mPKP2 stable cells

Missense PKP-2 was expressed in tetracycline-induced mPKP2 stable cells that localized as punctate staining at cell-cell contacts (Figure 5.1B), and this was detected as a strongly induced 98.7 KD band (Figure 5.2B) by SDS PAGE/ western immunoblotting analysis, which correlated with the predicted size of PKP-2a protein. Using confocal microscopy examination of PKP-2 staining (protocol omitting detergent treatment step) that preserved nuclear staining, but not of membrane PKP-2[182], induced S140F PKP-2 was found to be present in the nucleus (Figure 5.3B) of tetracycline-induced mPKP2 cells. Sub-cellular distribution in induced mPKP2 cells (Figure 5.4B) showed that missense plakophilin-2 localized predominantly in the cytoskeletal compartment, with some protein also present in the cytoplasm. Missense PKP-2 protein was found to be distributed in the membrane and nuclear compartments in equal amounts.

Figure 5.1 Immuno-localisation of full-length and S140F PKP-2 in wPKP2 and mPKP2 cells by confocal microscopy

Localization of expressions of full-length PKP-2 and S140F PKP-2 to the cell membranes of tetracycline-induced wPKP2 and mPKP2 stable cell lines respectively. Immunofluorescence images showing blue fluorescence signal resulting from DAPI nuclear staining, green fluorescence resulting from FM 1–43FX membrane dye staining, red fluorescence resulting from full-length PKP-2 or A733fsX740 PKP-2 staining with anti-PKP-2 antibody (610788, BD Bioscience) and merge representing composite staining (all panels on the far right) with all three signals superimposed. A punctate staining of each plakophilin examined indicates a staining reminiscent of desmosomal reactivity. The white size bar on each image in the green channel represents 8μm.

A) wPKP2 cells non-induced

DAPI **Membrane** **PKP-2** **Merge**

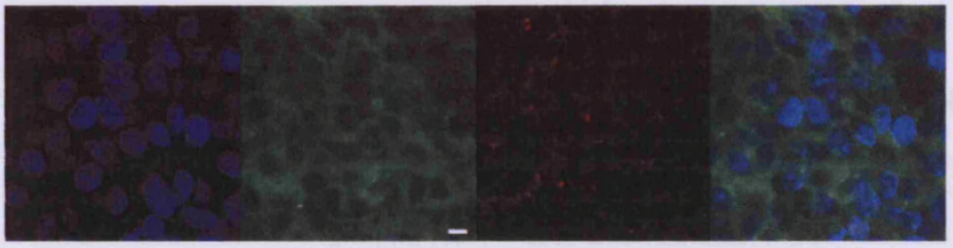

wPKP2 cells tetracycline-induced

DAPI **Membrane** **PKP-2** **Merge**

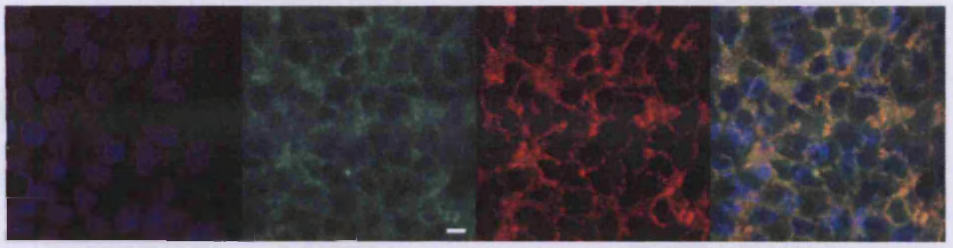

B) mPKP2 cells non-induced

DAPI **Membrane** **PKP-2** **Merge**

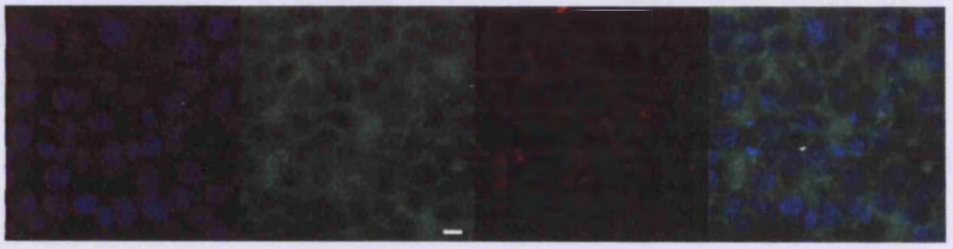

mPKP2 cells tetracycline-induced

DAPI **Membrane** **PKP-2** **Merge**

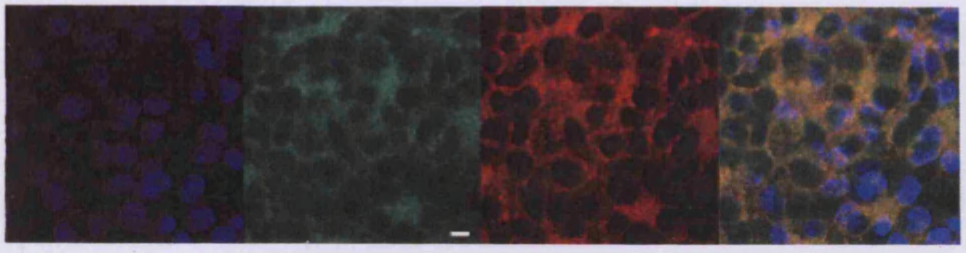

Figure 5.2 Western blot analysis of the expressions of PKP-2 & S140F PKP-2 in wPKP2 & mPKP2 cells

Analysis of expressions of full-length PKP-2 and S140F PKP-2 in non-induced (NI) or tetracycline-induced (IND) wPKP2 (A) and mPKP2 (B) stable cells determined by western blotting technique. A mouse monoclonal antibody to human PKP-2 (1:500 dilution, BD Bioscience, product 610788) was used followed by a goat anti-mouse HRP conjugate (1:5000, Abcam). Blots were exposed to ECL reagents (GE Healthcare) and developed using Kodak reagents. The migration of protein markers (Precision Plus protein standards, BioRad Laboratories, UK) are indicated on the left hand side of the blots

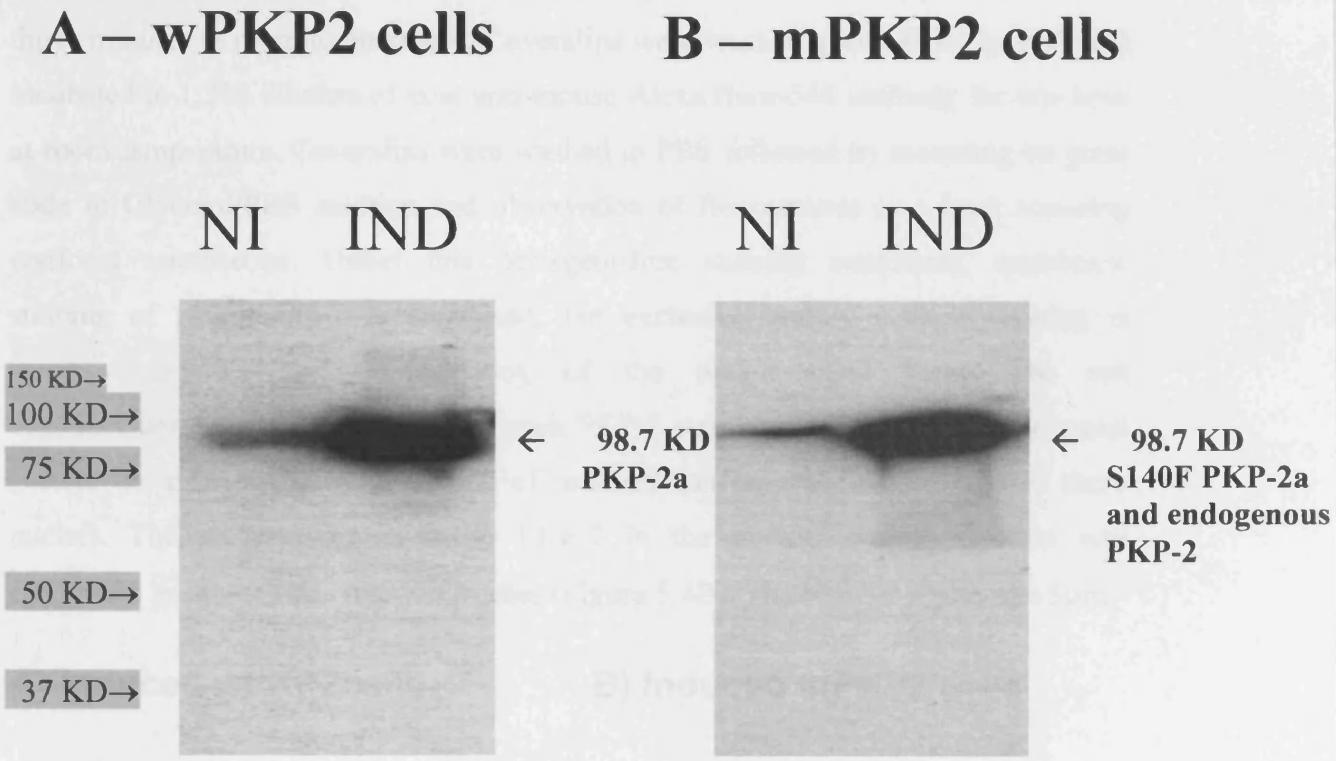

Figure 5.3 Demonstration of nuclear presence of full-length and missense PKP-2 in wPKP2 and mPKP2 induced cells

Nuclear staining of full-length PKP-2 and S140F PKP-2 demonstrated in tetracycline-induced wPKP2 and mPKP2 stable cells respectively using confocal microscopy. Cells were cultured on glass coverslips in the presence of 0.1μg/ml tetracycline to induce the expressions of the respective PKP-2 isoforms in each stable cell line. Seventy-two hours after induction, cells were fixed in –20°C methanol for five minutes followed by incubation in acetone for 30 seconds. After rinsing the cells in PBS, they were incubated in 10% FBS/PBS solution for thirty minutes, followed by incubation in 1:200 dilution of mouse anti-plakophilin-2 (BD Bioscience, 610788) for thirty minutes at room temperature. Coverslips were washed gently twice in PBS and incubated in 1:200 dilution of goat anti-mouse Alexa fluor-546 antibody for one hour at room temperature. Coverslips were washed in PBS followed by mounting on glass slide in Glycerol/PBS solution and observation of fluorescence in a laser scanning confocal microscope. Under this detergent-free staining conditions, membrane staining of plakophilin-2 is abrogated, but exclusive intense nuclear staining is seen[221], probably due to masking of the plaque-bound form. The red immunofluorescence signal localized each PKP-2 staining inside the spherical nuclei (where the presence of dark outline of nucleoli can be seen inside some of these nuclei). The presence of missense PKP-2 in the nuclear protein fraction was confirmed in sub-cellular fraction studies (Figure 5.4B). The size bar represents 5μm.

A) Induced wPKP2cells **B) Induced mPKP2 cells**

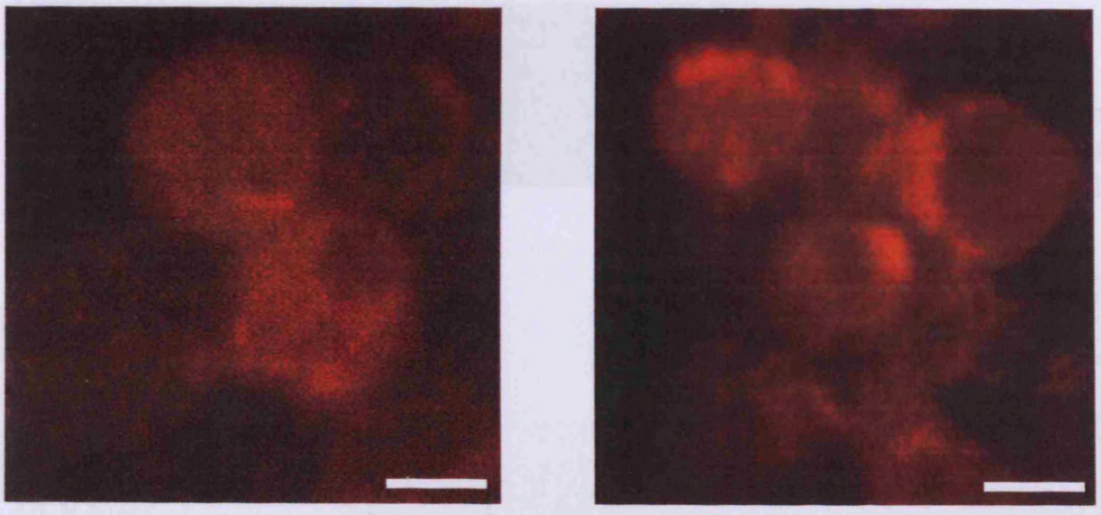

Figure 5.4 Sub-cellular localization of full-length and missense PKP-2 in wPKP2 and mPKP2 cells

Sub-cellular distribution of A) induced PKP2, or B) induced S140F PKP2 in cytosolic (CYT), membrane (MEM), nuclear (NUC) and cytoskeletal (CSK) protein fractions in tetracycline-induced (48 hrs) wPKP2 or mPKP2 stable cells respectively. Sub-cellular protein fractions were obtained from $5x10^6$ cells using the Qproteome cell compartment kit (Qiagen). Each protein fraction was precipitated in 4 volumes of ice-cold acetone and the pellet was resuspended in 100µl RIPA containing protease inhibitor cocktail (Roche). $1/5^{th}$ of each protein fraction was electrophoresed in a 10% SDS PAGE and transferred to a Hybond ECL membrane. Following blocking of blot in TBST/5% milk, blot was incubated with 1:500 mouse monoclonal anti-PKP-2 (610788, BD Bioscience) for one hour in TBST/5% milk at room temperature. Following washing of the blots in TBST, they were exposed to 1:3500 dilution of anti-mouse HRP conjugate in TBST/5% milk for one hour at room temperature. Following washing of the blots in TBST they were incubated in ECL reagents (GE Healthcare) and exposed to ECL Hyperfilm (GE Healthcare).

A –Induced wPKP2 cells

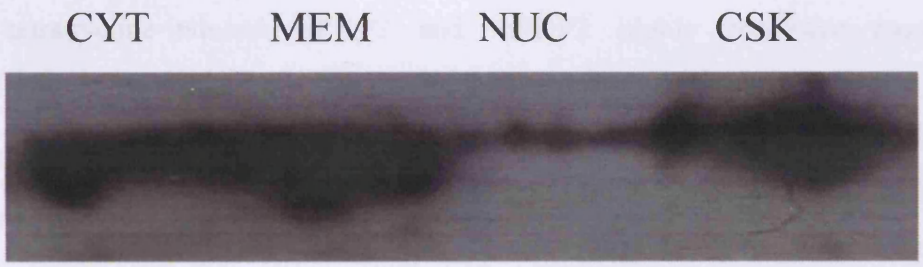

← **98.7 KD endogenous PKP-2 + over-expressed PKP-2a**

B – Induced mPKP2 cells

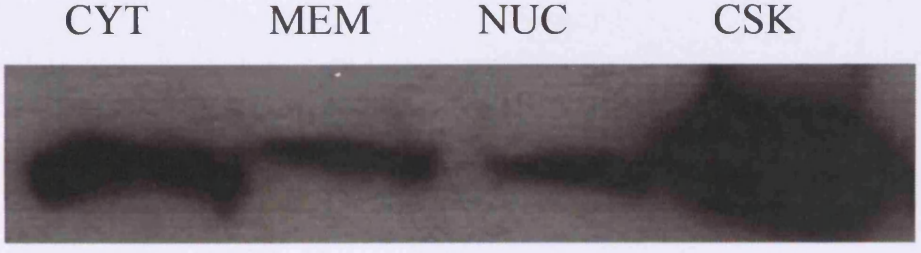

← **98.7 KD endogenous PKP-2 + S140F PKP2a**

5.5.2 Properties of mPKP2 stable cells

Cellular proliferation of wPKP2 and mPKP2 cells did not appear to be substantially altered by the expressions of full-length or truncated PKP-2 respectively as comparable values of the slopes were obtained by regression analysis of the data in tetracycline-induced cell lines (Figure 5.5). Calcein-AM labelled induced mPKP2 or wPKP2 cells did not show a statistically significant difference in initial cell-cell contact adherence of these two cell lines to homologous monolayer of cells established on coverslips (Figure 5.6). The adhesive strengths of induced mPKP2 and wPKP2 monolayers measured using a Dispase-based cell dissociation assay did not show any differences in resistances to shear stress-induced fragmentation as both monolayers formed comparable fragment sizes assessed visually (Figure 5.7) indicating that S140F PKP-2 probably did not affect the adhesive strength of mPKP2 monolayer. Stable wPKP2 and mPKP2 cells subjected to mechanical cell-stretch and then allowed to recover for a short while did not show statistical difference in the specific apoptosis activity in these cells (Figure 5.8). Analysis of non-induced and tetracycline-induced wPKP2 and mPKP2 highly confluent monolayer NP-40 detergent-soluble cell lysates by western immunoblotting showed strong Cx-43 protein bands under both conditions in each stable cell line (Figure 5.9 representative data of triplicate experiments). Examination of tetracycline-induced wPKP2 and mPKP2 cells by confocal microscopy confirmed strong Cx-43 protein localization to cell-cell contacts of both cells under tetracycline-induced conditions (Figure 5.10, representative of triplicate experiments).

Figure 5.5 Proliferation of wPKP2 and mPKP2 cells

Cellular proliferation of stable wPKP2 and mPKP2 cells expressing full-length PKP-2 and S140F PKP-2 respectively. 15,000 cells per well were plated in a twenty-four well plate and allowed to attach overnight. Cell proliferation was measured spectrophotometrically at 490nm by measuring the reduction of Cell Titer AQ One solution (Promega, UK) after incubation of substrate with cells for exactly one hour. The six data points obtained in each treatment were fitted to a linear tread line using Microsoft Excel software. The values of the slopes were: 0.0101, 0.0111, 0.0104, and 0.0108 for wPKP2NI, wPKP2 IND, mPKP2 NI and mPKP2 IND cells respectively.

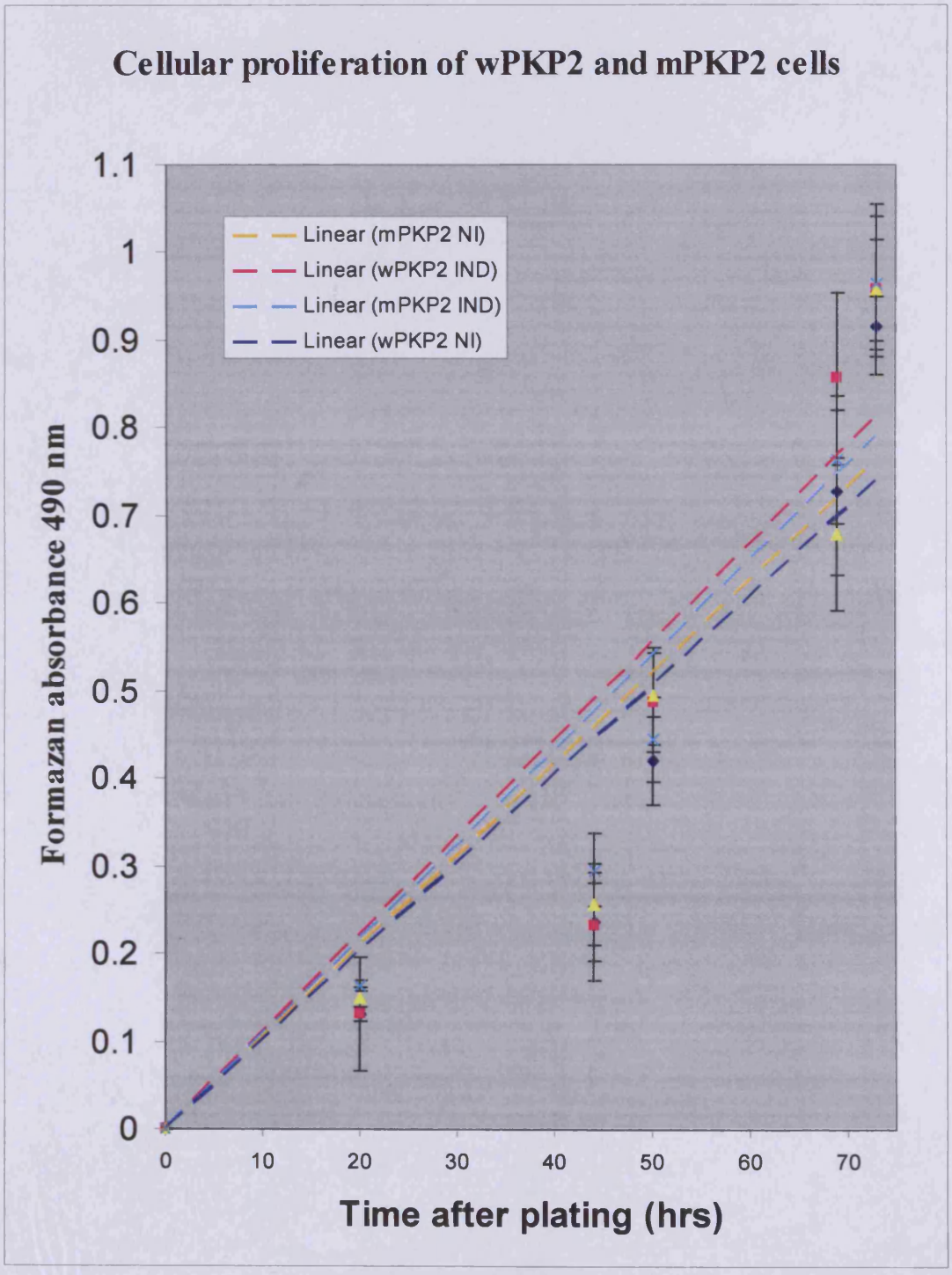

Figure 5.6 Initial cell-cell contact adhesion assay of wPKP2 and mPKP2 cells

Initial cell-cell contact adhesion measured in wPKP2 and mPKP2 stable cell lines expressing full-length PKP-2 and S140F PKP-2 respectively. Both cell lines were cultured under tetracycline-induced conditions on 13 mm plastic coverslips to obtain a uniform highly confluent monolayer of cells. Separate suspension aliquots (1 x 10^6) of each tetracycline-induced cells previously pre-incubated in 10μM Calcein AM dye were allowed to adhere to the homologous unlabelled confluent monolayer of cells growing on coverslips conditions for five hours at 37°C/5%CO_2. Coverslips were carefully washed four times in complete DMEM medium. Coverslips were fixed in 4% formaldeheyde/PBS, stained with DAPI, and mounted on glass slides, followed by examination in a confocal microscope (images shown using x10 objective lens) to co-localise the green and blue fluorescence. The number of calcein AM-labelled (cells fluorescing green) versus the total number of cells labelled with DAPI (all cells fluorescing blue) was expressed as a percentage to quantify the percentage initial cell-cell contact adhesion of each monolayer. No statistical difference (student's paired t-test p value = 0.5387) of % mean initial cell-cell contact adhesion between wPKP2 or mPKP2 cells was found. A p-value of <0.05 was considered statistically significant.

Induced wPKP2 cells
Green = calcein labelled cells retained on adherent monolayer, Blue = DAPI staining of all cells

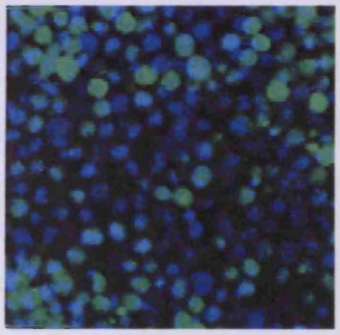

Induced mPKP2 cells
Green = calcein labelled cells retained on adherent monolayer, Blue = DAPI staining of all cells

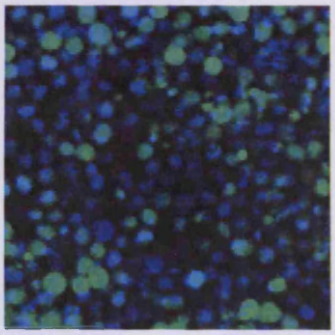

	% wPKP2 initial cell-cell adhesion	% mPKP2 initial cell-cell adhesion
Experiment 1	20.7	29.4
Experiment 2	23.3	29.7
Experiment 3	24.4	27.6
Experiment 4	25.4	24.1
Experiment 5	29.3	29.4
Experiment 6	35.4	27.9
Total number of cells examined	3000	3000
Mean	26.417	28.017
SD	5.225	2.107
SEM	2.133	0.860
p value (paired student's t-test)		p= 0.5387

Figure 5.7 Dispase-based induced wPKP2 and mPKP2 monolayer dissociation adhesion assay

Monolayer adhesive strength of tetracycline-induced wPKP2 and mPKP2 confluent monolayers measured using a Dispase-based cell dissociation assay[212]. Each cell line was cultured in P_{60} Nunc brand plastic culture dishes in penicillin, streptomycin, foetal calf serum, blasticidin and hygromycin supplemented DMEM (Invitrogen 19308-025) in the continued presence of 0.1μg/ml tetracycline until cells were highly confluent. Medium was decanted from each dish and the cell monolayer was carefully washed in PBS. One ml of 2.4U/ml Dispase II (Roche, Cat No 10295835001) was added to the dishes followed by incubation at 37°C for 30 minutes. The entire intact monolayer lifted off the plastic cell culture dish by enzyme treatment was carefully rinsed in PBS and resuspended in five ml of PBS. The cell monolayer was subjected to shearing for exactly ten rotations on a rocking tabletop platform. Sheared monolayer was photographed under Epi-white light illumination in BioRad Gel Documentation system (gel doc XR) using quantity one version 4.6 software for image analysis. Comparable level of monolayer fragmentation resulted in sheared mPKP2 and wPKP2 monolayers after ten rotations indicating that S140F PKP-2 expression does not influence cell-cell adhesion.

Control wPKP2 stable cells expressing full-length PKP-2

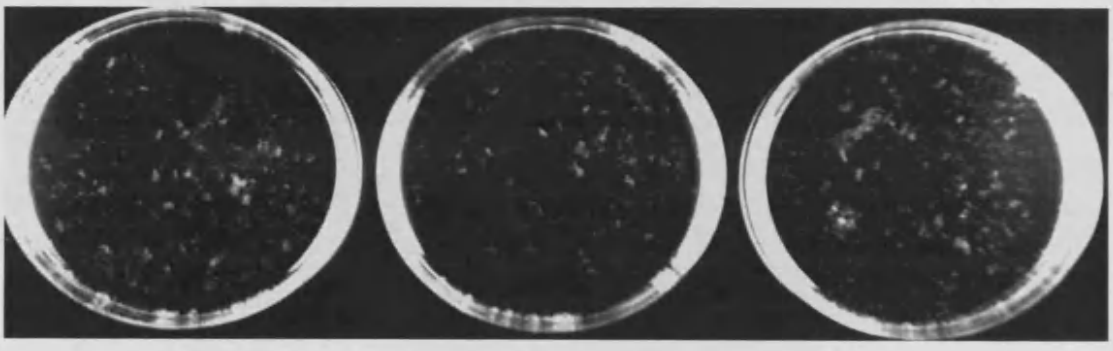

mPKP2 stable cells expressing S140F PKP-2

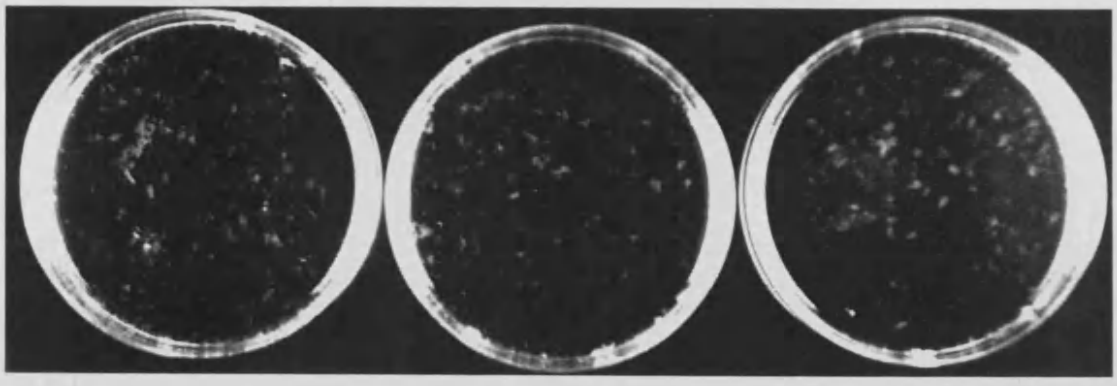

Figure 5.8 Effect of mechanical cell stretch on apoptosis of wPKP2 and mPKP2 stable cells

Effect of mechanical cell-stretch on the measured apoptosis determined in wPKP2 and mPKP2 stable cells. Apoptosis levels are mean values of n = 6 experiments ± standard deviations. The CaspACE assay system (Promega, UK) was used to measure the specific caspase-3 activity in cell lysates of cells subjected to mechanical stretch using the Flexer cell-stretch apparatus with 4% cell-stretch applied at a frequency of 1Hz for 4.0 hours followed by recovery of cells for 3 hours prior to assessing apoptosis. Cells were plated at a density of 0.5 x 10^6 cells/six well plate and cultured for 48 hours prior to exposure to mechanical stretch. Induced cells were cultured in presence of 0.1µg/ml tetracycline. Statistical analysis using paired student's t-test showed that there were no differences in the mean apoptosis of wPKP2 or mPKP2 cells with all p values >0.05.

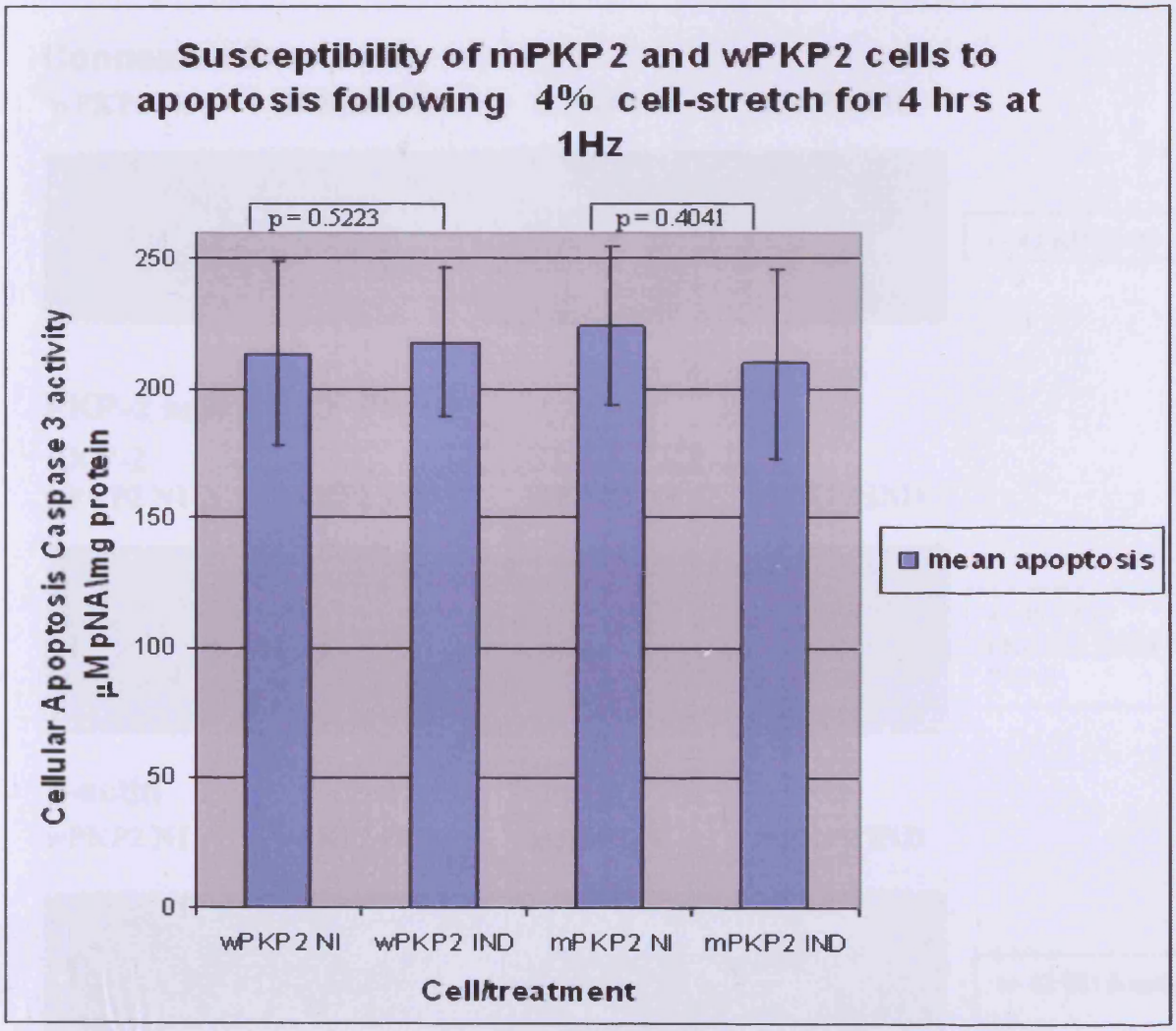

Figure 5.9 Western blot analysis of whole cell lysates of wPKP2 and mPKP2 cells to measure Cx-43 and plakophilins

Connexin-43 protein levels in wPKP2 and mPKP2 cells analyzed by western blotting analysis. The top panel shows the levels of Cx43 protein, middle panel shows PKP-2 and S140F PKP-2 protein induction and bottom panel shows β-actin protein levels as loading controls. Stable wPKP2 and mPKP2 cells were cultured in the absence (NI) or presence of 0.1μg/ml tetracycline (IND) for 72 hrs until cells were fully confluent. Detergent-soluble cell lysates were prepared in RIPA buffer and equal amounts of protein (100 microgram protein) were separated on a 10% SDS PAGE system. Gels were blotted onto ECL Hybond membrane and blots were blocked in TBST/milk followed by incubation in 1:2000 rabbit anti-connexin-43 (GJA1, Abcam ab-113700), or 1:500 mouse anti-human PKP2 (610788, BD Bioscience), or 1:2000 rabbit anti-β-actin (loading control, Abcam, ab-8227). Following washing of blots in TBST they were incubated in either 1:5000 anti-mouse HRP or 1:5000 anti-rabbit HRP. Blots were washed in TBST and incubated in ECL reagents (GE Healthcare) followed by exposure to ECL Hyperfilm and development with Kodak photographic reagents.

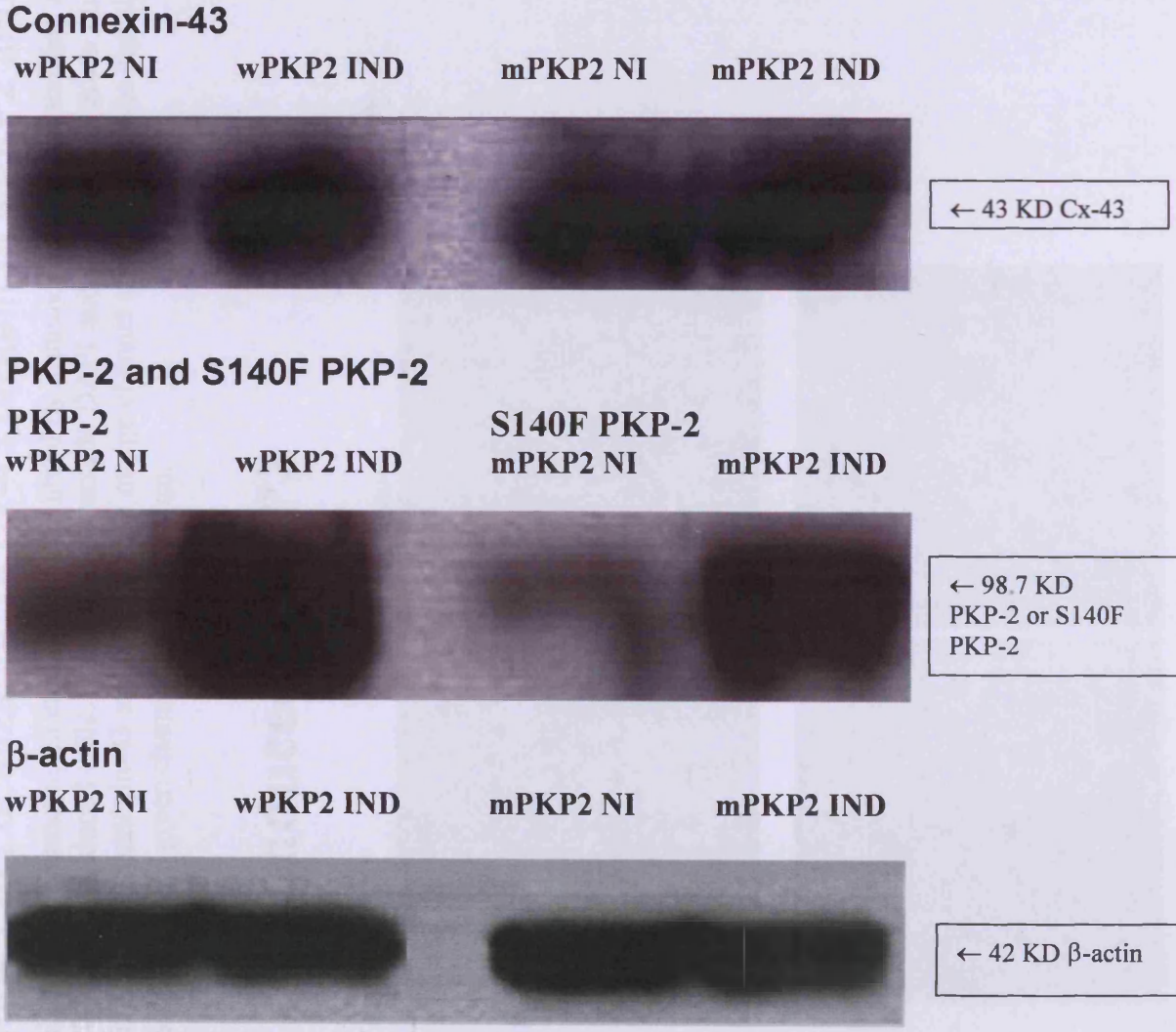

Figure 5.10 Localization of Cx-43 protein in wPKP2 and mPKP2 cells

Localization of Connexin-43 expression determined by immunofluorescence staining and confocal microscopy examination of wPKP2 (A) and mPKP2 (B) tetracycline-induced cells. Blue channel records DAPI nuclear staining, green channel records cell membrane staining with FM 1-43FX dye, red channel records connexin-43 staining, and the merge channel shows composite signals. Images were obtained using x40 objective oil immersion lens. The size bar in the green channel represents 5μm.

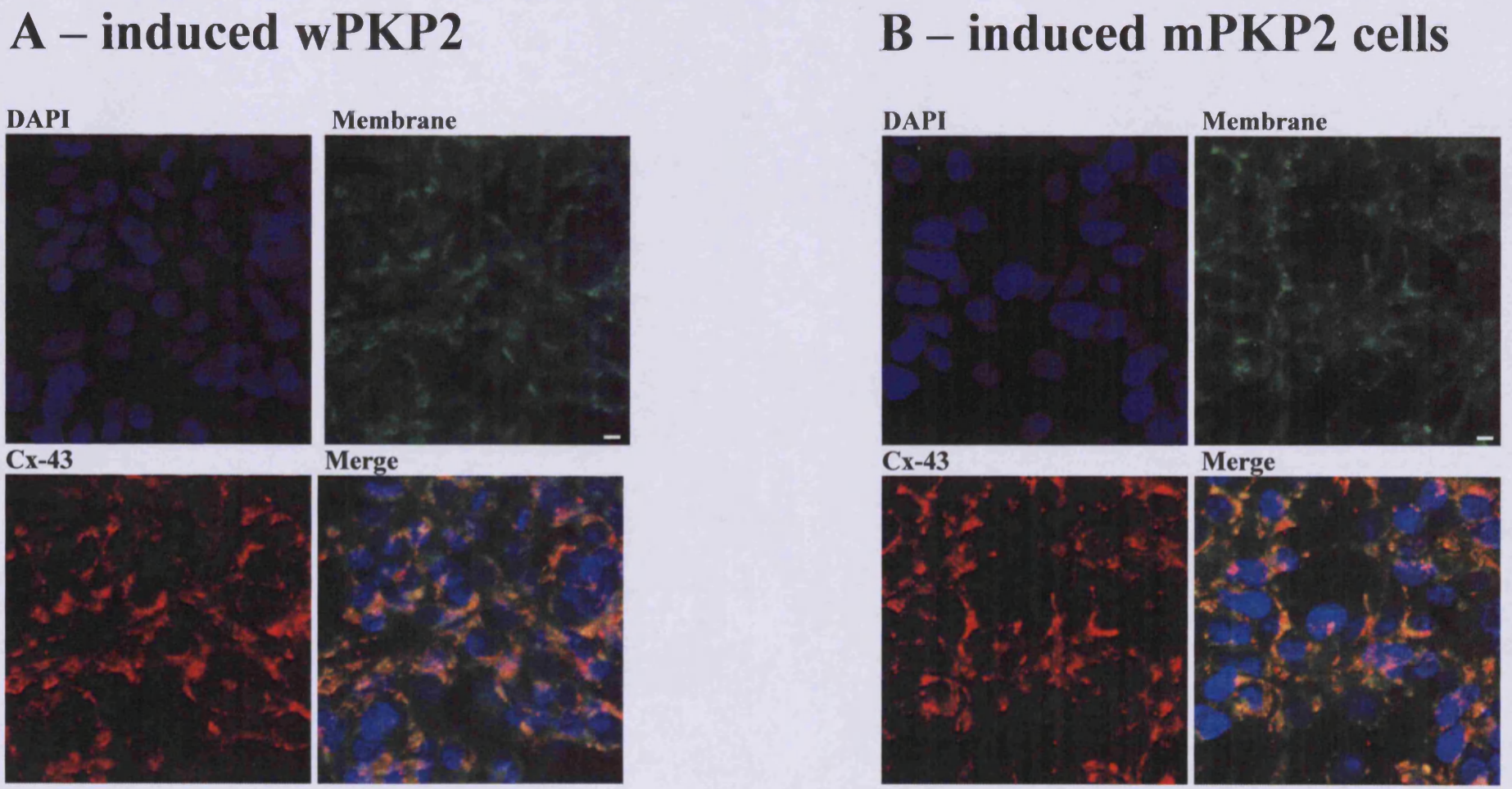

the co-localized staining intensity of full-length PKP-2 and endogenous PG p
wPKP2 cells (Figure 5.11, representative of triplicate staining). Results of co-loca
endogenous β-catenin, DP, DSG-2 and DSC-2 with either full-length or S140F PI
not reproducible and therefore these studies were inconclusive (data not shown). A
reason for the difficulty in obtaining reliable co-localization of these endogenou
with over-expressed full-length or S140F PKP-2 could be that these endogenou
might be present in small amounts.

5.5.4 Examination of desmosome morphology in mPK stable cells

The gross morphology of non-transformed Flp-In T-Rex HEK 293 cells, tetracyclin
wPKP2 cells, and tetracycline-induced mPKP2 cells were examined by electron m
at x2000 magnification in a Philips 201 transmission electron microscope. The ident
three cell lines were revealed after completion of data analysis. All of these cell pre
were viable with a good distribution of sub-cellular organelles (Figure 5.12). Induce
and mPKP2 cells and control non-transfected Flp-In T-Rex HEK 293 cells cu
Thermanox coverslips were examined by transmission electron microscopy to deter
desmosome morphology. Whilst desmosomes formed in non-transfected cells, they
particular well developed, presumably due low level of recruitment of endogenous de
plaque proteins, induced wPKP2 cells on the other hand showed very prominent des
with electron dense plaques (Figure 5.13 A and B respectively). Induced S140
expression resulted in considerably longer desmosomes in mPKP2 cells (Figure
Examination of serial EM sections suggested that the longer desmosomes formed i
cells might be due to fusion of adjacent desmosomes (Figure 5.13C, inset). Exceptio
desmosomes exist in tetracycline-induced mPKP2 cells as demonstrated by

desmosome measuring nearly 1300 nm in length present in serial sections (Figure 5.14) of these cells. Such large desmosomes were not present in either wPKP2 or Flp-In T-Rex HEK293 cells; the mean desmosomal length of wPKP2 cells was 325 nm. Thus, desmosomes in mPKP2 cells can be up to four-times longer compared to desmosomes found in control cells. Statistical analysis of desmosomal lengths in Flp-In T-Rex HEK 293, wPKP2 and mPKP2 cells by ANOVA analysis followed by Bonferroni post-test correction and multiple comparison between these three groups of desmosomes showed a significant difference ($p<0.001$) in desmosomal lengths between either Flp-In and mPKP2 or wPKP2 and mPKP2 desmosomes (Figure 5.15). Although a formal analysis of the % area of the cell membrane that desmosomes occupy was not performed, it was evident from electron micrographs that desmosomes in induced mPKP2 cells occupied a larger area of the cell membrane compared to those of induced wPKP2 cell desmosomes (compare Figures 5.13B and 5.13C), indicating there might be fewer desmosomes per unit length in induced mPKP2 cells.

5.5.5 Verification of XPress-tagged S140F PKP-2 and full-length PKP-2 expressions

Transient protein expressions of N-terminal XPress-tagged PKP-2 or S140F PKP2 proteins was confirmed in HEK 293T cells by immunofluorescence staining confocal microscopy localization of these PKP-2 proteins forty eight hours after transfection with pcDNA4 (Figure 5.16) vectors. The transient expressions of PKP-2 or S140 PKP-2 proteins (Figure 5.16) were verified using a mouse monoclonal anti-PKP-2 antibody (reactive near the N-terminus of PKP-2), however, an identical result was obtained using monoclonal anti-XPress antibody staining and confocal microscopy localization of these PKP-2 protein expressions in transfected HEK 293T cells (data not shown). SDS PAGE/western blotting analysis of soluble cell lysates from pcDNA4 PKP2 or pcDNA4 S140F PKP2 transfected HEK293T cells was performed to confirm full-length or S140F PKP-2 proteins using both anti-XPress and anti-PKP-2 (reactive near the N-terminus of PKP-2) antibodies which revealed identical bands for both full-length and missense PKP-2 proteins (predicted and apparent SDS PAGE size of 103.6 KD, Figure 5.17).

Figure 5.11 Co-localization of PKP-2s in induced mPKP2 and wPKP2 with endogenous PG

Confocal microscopy immunofluorescence co-localization of endogenous plakoglobin with either full-length PKP-2 or S140F PKP-2 in tetracycline-induced wPKP2 and mPKP2 cells respectively. DAPI nuclear staining produces a blue signal, rabbit anti-human PG followed by anti-rabbit Alexa-488 produces green signal localizing PG staining, mouse anti-human PKP-2 followed by anti-mouse Alexa 546 produces red signal localizing PKP-2 and S140F PKP-2 respectively. Merged signals represent composite signals superimposed. Images were obtained using x40 oil immersion objective. The size bar in each green channel represents 7μm.

A) Endogenous PG/PKP-2 co-localization in wPKP2 cells

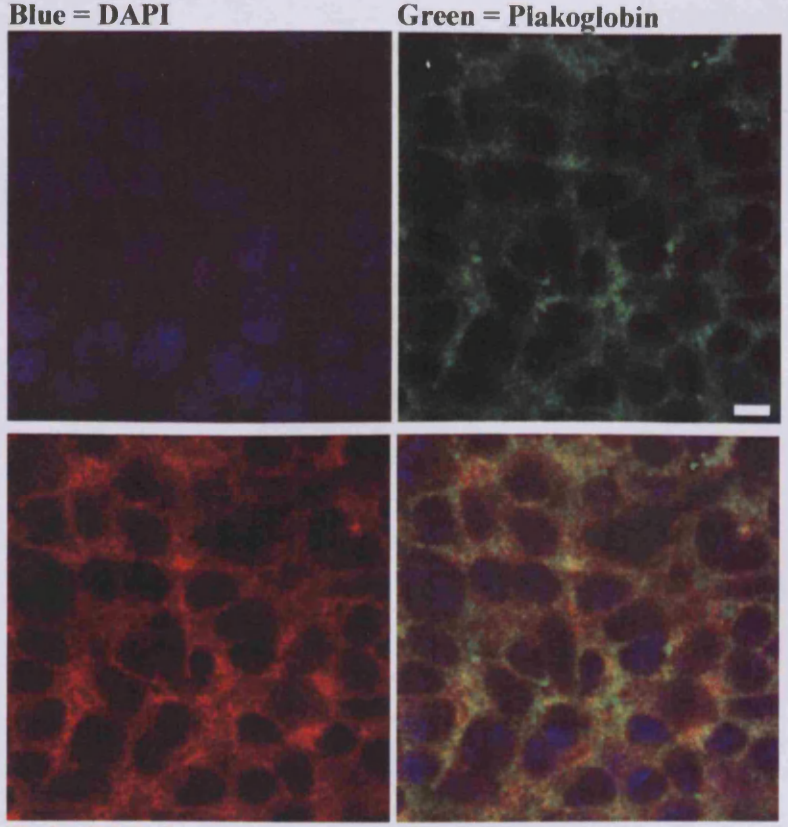

B) Endogenous PG/S140F PKP-2 co-localization in mPKP2 cells

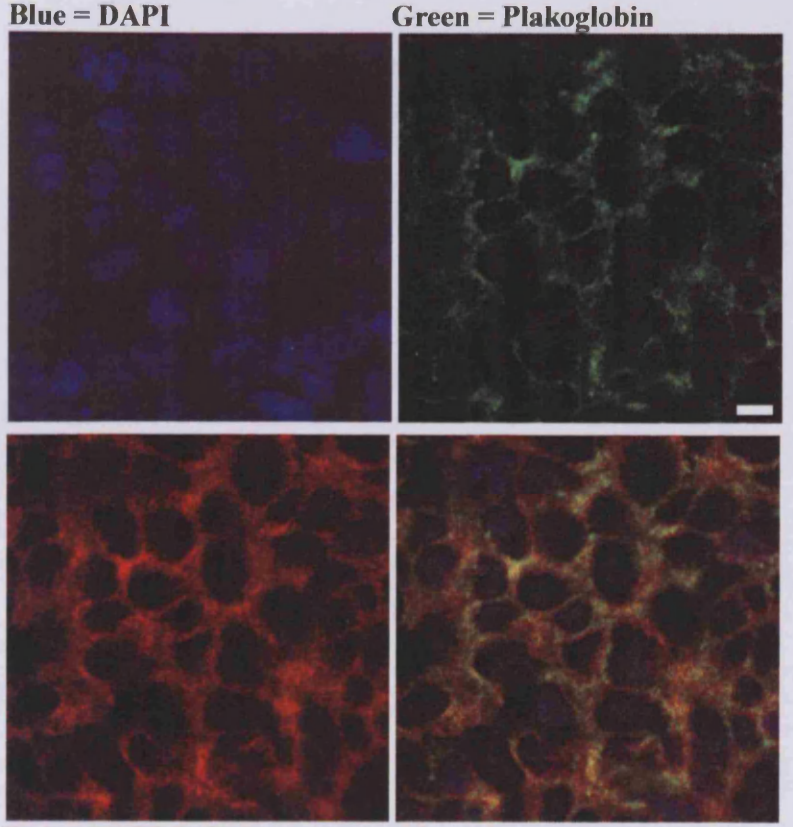

Figure 5.12 Gross morphology of non-transformed Flp-In T-Rex HEK 293 cells, tetracycline-induced wPKP2 cells, and tetracycline-induced mPKP2 cells

Gross morphology of non-transfected Flp-In T-Rex 293 control cells and of stable wPKP2 and mPKP2 cells expressing full-length and S140F PKP-2 respectively. Cells cultured on Thermanox plastic coverslips in complete DMEM were induced where required, with 0.1μg/ml tetracycline for 72 hours until they were confluent. Coverslips processed for electron microscopy (section 2.7.4) were examined in a Philips 201 electron microscope at x 2000 magnification to examine the gross morphology of these cells. The bar on each electron micrograph represents 10μm

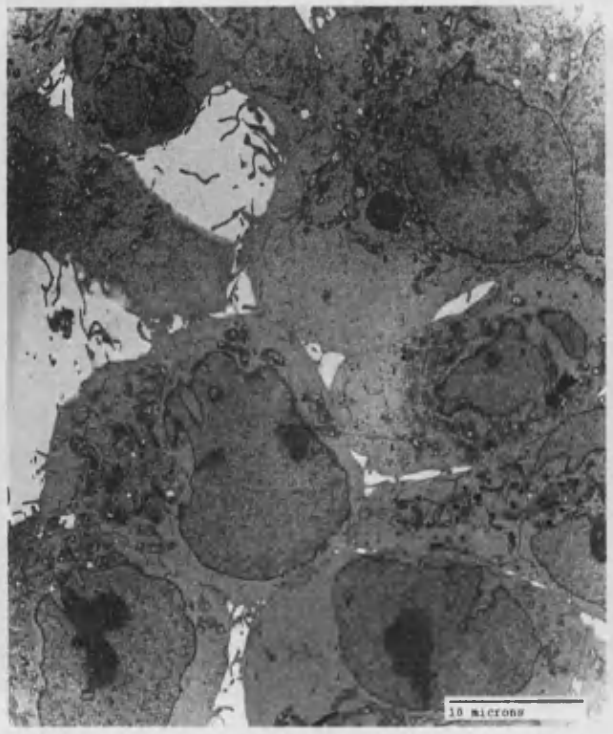

Non-transformed Flp-In T-Rex HEK 293 cells

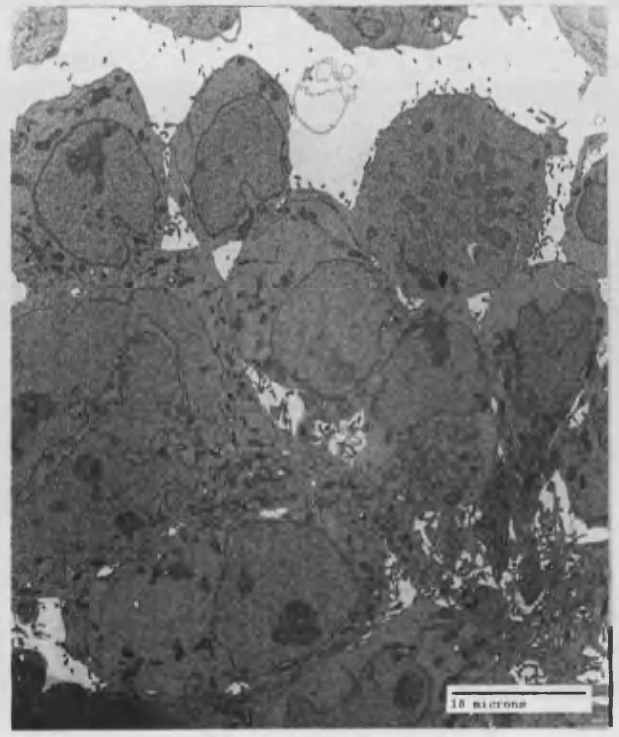

Tetracycline-induced wPKP2 cells

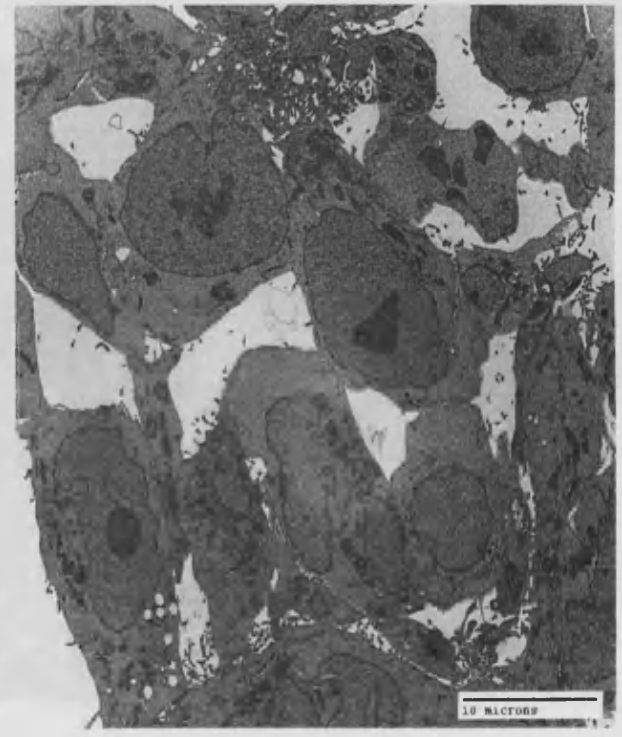

Tetracycline-induced mPKP2 cells

Figure 5.13 Morphology of desmosomes formed in Flp-In T-Rex HEK 293, wPKP2 and mPKP2 tetracycline-induced cells

Desmosome morphology in non-transformed Flp-In T-Rex 293 control cells and in stable tetracycline-induced wPKP2 and mPKP2 cells expressing full-length and S140F PKP-2 respectively. Cells cultured on Thermanox plastic cover slips in complete DMEM were induced in 0.1μg/ml tetracycline for 72 hours until they were confluent. Coverslips processed for electron microscopy (section 2.7.4) were examined in a Philips EM microscope at x 70000 magnification to examine desmosome morphology. The bar on each electron micrograph represents 100nm. Induced expression of full-length PKP-2 in wPKP2 cells resulted in formation of prominent electron dense desmosomes (B), while S140 PKP-2 expression in mPKP2 cells resulted in the formation of significantly longer desmosomes, which appeared to result from fusion of adjacent desmosomes (C, inset, top left corner).). Flp-In T-Rex HEK 293 cells formed less prominent desmosome (A) compared to wPKP2 cell desmosomes presumably due to low endogenous level of recruitment of endogenous desmosomal plaque proteins. Dense filament associations were present in both wPKP2 and mPKP2 cells.

A) Flp-In T-Rex 293 cells **B) wPKP2 cells** **C) mPKP2 cells**

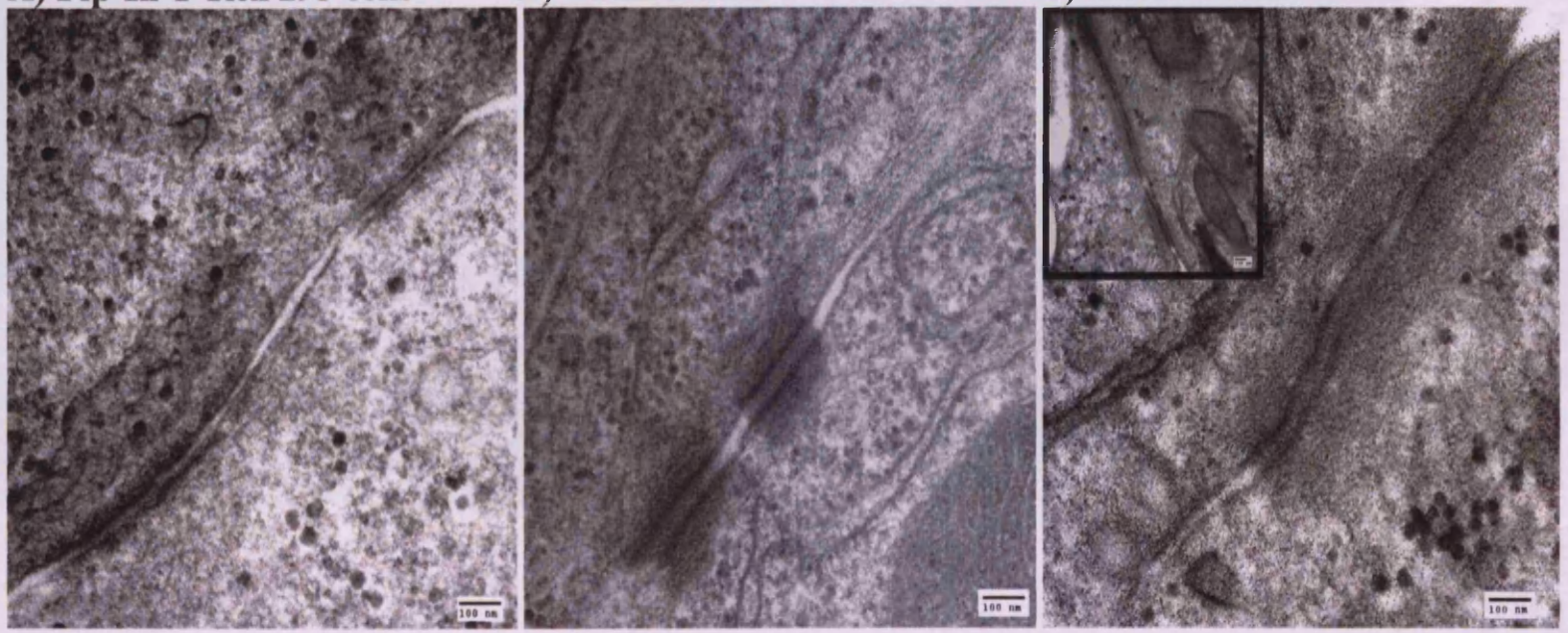

Figure 5.14 High magnification electron micrograph of a single desmosome in tetracycline-induced mPKP2 cell

Examination of a desmosome at a high magnification in induced mPKP2 cells. This is a representative electron micrograph of an exceptionally long desmosome obtained in induced mPKP2 cells. Tetracycline-induced mPKP2 cells cultured on Thermanox coverslips for 72 hours were processed *in situ* for electron microscopy. A single desmosome examined by transmission electron microscopy at x 70000 magnification shown here was nearly 1300 nm in length compared with a mean value of 325 nm for desmosomes found in wPKP2 cells. Examination of serial sections of mPKP2 cells showed presence of such long desmosomes with dense filament association.

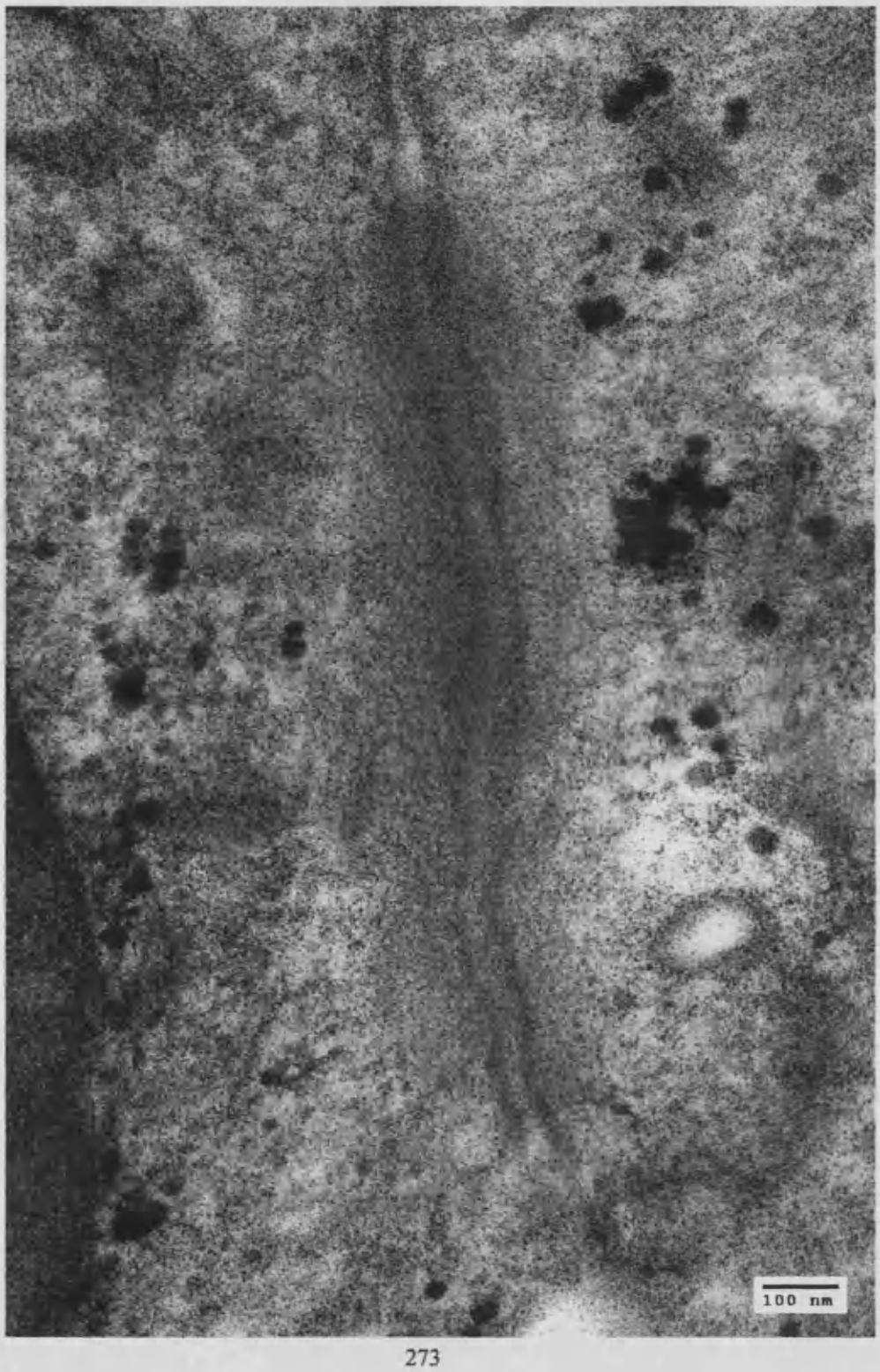

Figure 5.15 Statistical analysis of desmosomal length in Flp-In T-Rex HEK 293, wPKP2 and mPKP2 induced cells

Statistical analysis of desmosomal lengths in Flp-In 293, wPKP2 and mPKP2 stable cells (the later two were tetracycline-induced). A minimum of fourteen measurements of desmosomal lengths (nm) were taken from electron micrographs of desmosomes obtained from each of these three cells. Data were analyzed using Graph Pad Prism software using non-parametric ANOVA analysis followed by Bonferroni post-test computation of significance. The graph shows plots of individual values in each group of cells and the table below shows results of the Bonferroni multiple comparison statistical test parameters between the three data sets from Graph Pad. Pair-wise analysis showed a significant difference ($p<0.001$) in desmosomal length comparing either control Flp-In or control wPKP2 desmosomes with mPKP2 desmosomes. Flp-In desmosomal length were not significantly different from those of wPKP2 desmosomes ($p>0.05$).

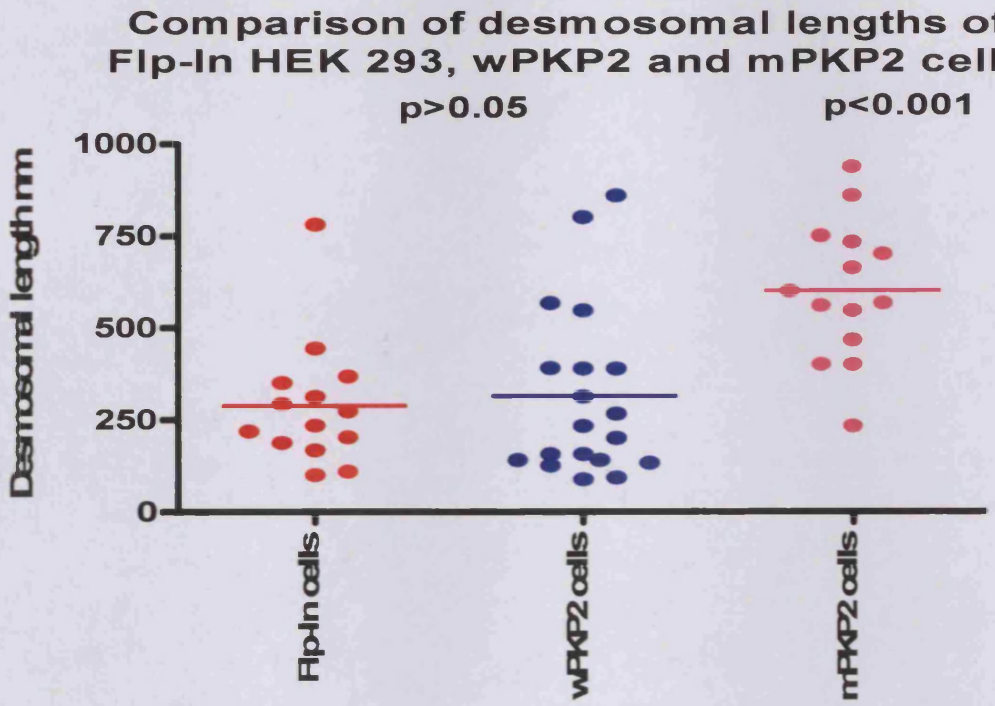

Parameter	Flp-In cells	wPKP2 cells	mPKP2 cells	Data Set-D
Table Analyzed				
Data 1				
One-way analysis of variance				
P value	0.0002			
P value summary	***			
Are means signif. different? (P < 0.05)	Yes			
Number of groups	3			
F	10.52			
R squared	0.3235			
Bartlett's test for equal variances				
Bartlett's statistic (corrected)	1.386			
P value	0.5000			
P value summary	ns			
Do the variances differ signif. (P < 0.05)	No			
ANOVA Table	SS	df	MS	
Treatment (between columns)	874300	2	437100	
Residual (within columns)	1828000	44	41550	
Total	2703000	46		
Bonferroni's Multiple Comparison Test	Mean Diff.	t	P value	95% CI of diff
Flp-In cells vs wPKP2 cells	-26.24	0.3655	P > 0.05	-204.9 to 152.5
Flp-In cells vs mPKP2 cells	-312.4	4.055	P < 0.001	-504.2 to -120.6
wPKP2 cells vs mPKP2 cells	-286.2	3.985	P < 0.001	-464.9 to -107.4

Figure 5.16 Confocal microscopy localization of PKP-2 and missense PKP-2 in HEK293T cells transfected with pcDNA4 vectors encoding these plakophilins

Verification PKP-2 and S140F PKP-2 protein expression in $1x10^5$ HEK 293T cells cultured on 13mm plastic coverslips and transfected with 1μg pcDNA4 PKP2 or pcDNA4 S140F PKP2 plasmids for forty eight hours using 10μl Polyfect reagent. Following fixation of cells in 4% formaldehyde, permeabilization in 0.1% triton X-100 and blocking in 10% FBS, they were incubated in 1:200 mouse monoclonal anti-PKP-2 (610788, BD Bioscience) for 1hr at room temperature. Cells were washed in PBS and incubated in 1:200 Alexa fluor 546 goat anti-mouse (Invitrogen) for 1hr at room temperature. Following PBS washes of coverslips, they were incubated in DAPI nuclear stain (Invitrogen) and mounted on glass slide. Control cells transfected with pcDNA4 (without an insert, A); pcDNA4 PKP2 transfected cells (B) and pcDNA4 S140F PKP2 transfected cells (C). Blue fluorescence shows DAPI nuclear staining, red fluorescence shows PKP-2 or S140F PKP-2 staining (B and C respectively), and merge shows composite signals. The size bar in each DAPI stained image on the left panels represents 10 μm.

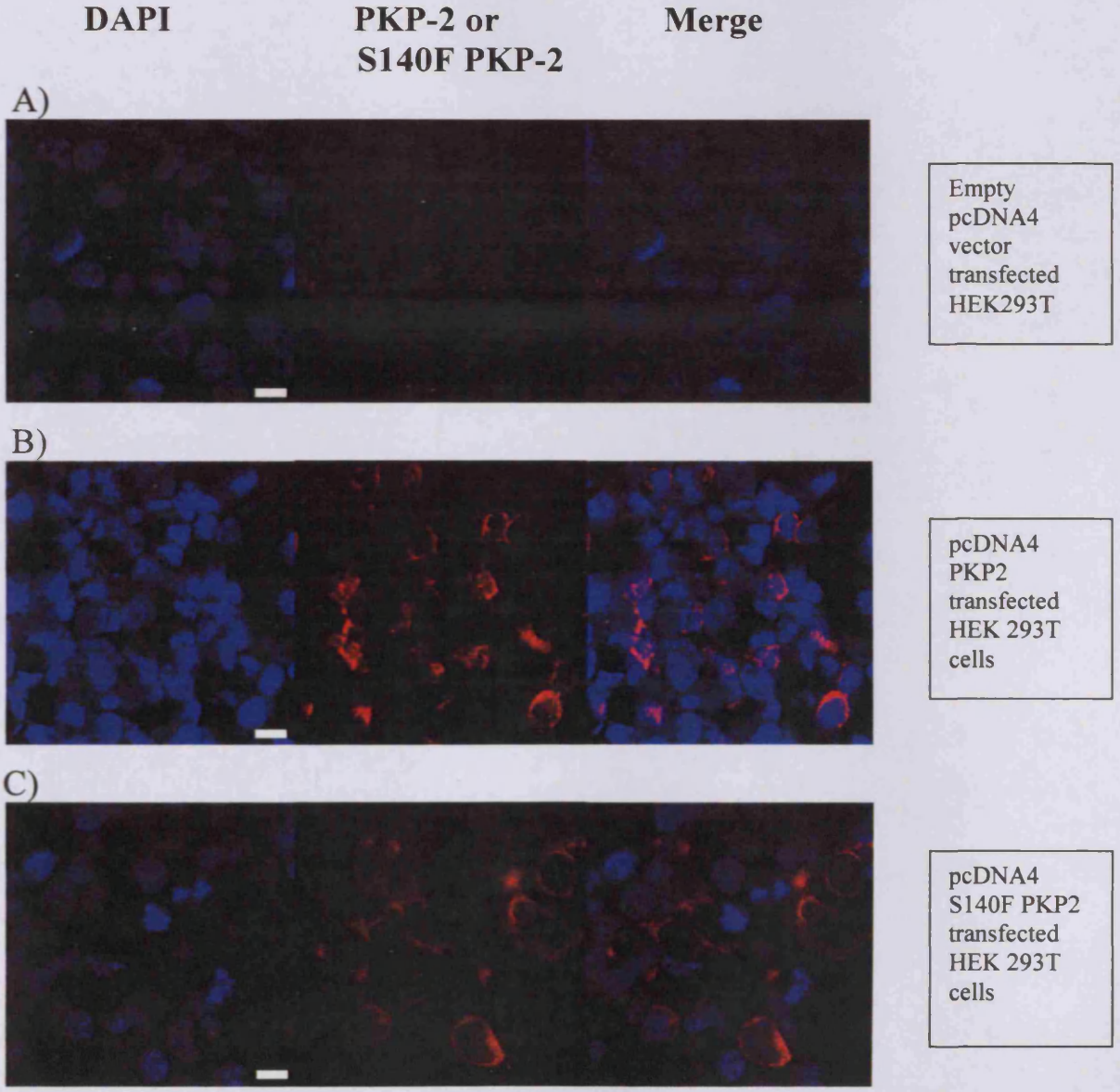

Figure 5.17 Verification of transient expressions of PKP-2 and missense PKP-2 in HEK 293T cells transfected with pcDNA4 vectors encoding these plakophilins

XPress-tagged full-length PKP-2 and S140F PKP-2 transient protein expressions obtained in HEK 293T cells following transfection with pcDNA4 PKP2 and pcDNA4 S140F PKP2 plasmids respectively. HEK 293T cell lysates of non-transfected (control), pcDNA4 PKP2 or pcDNA4 S140F PKP2 transfected cell lysates were analyzed by Western blotting probed using anti-XPress (top) or anti-PKP-2 antibodies (bottom). Following transfection of 293T cells with 1μg of each plasmid for forty eight hours, soluble cell lysates prepared in RIPA buffer (100μg protein per lane) were electrophoresed in 10% SDS PAGE and transferred using semi-dry transfer on Hybond ECL membrane. Blots were blocked in TBST/milk and incubated with mouse monoclonal (1:5000 anti-XPress, Invitrogen or 1:500 anti-PKP-2, BD Bioscience, 610788) antibodies. Following washing of blots in TBST they were incubated in 1:3500 rabbit-anti-mouse HRP. Following TBST washes, the blots were incubated in ECL reagents and exposed to ECL Hyperfilm.

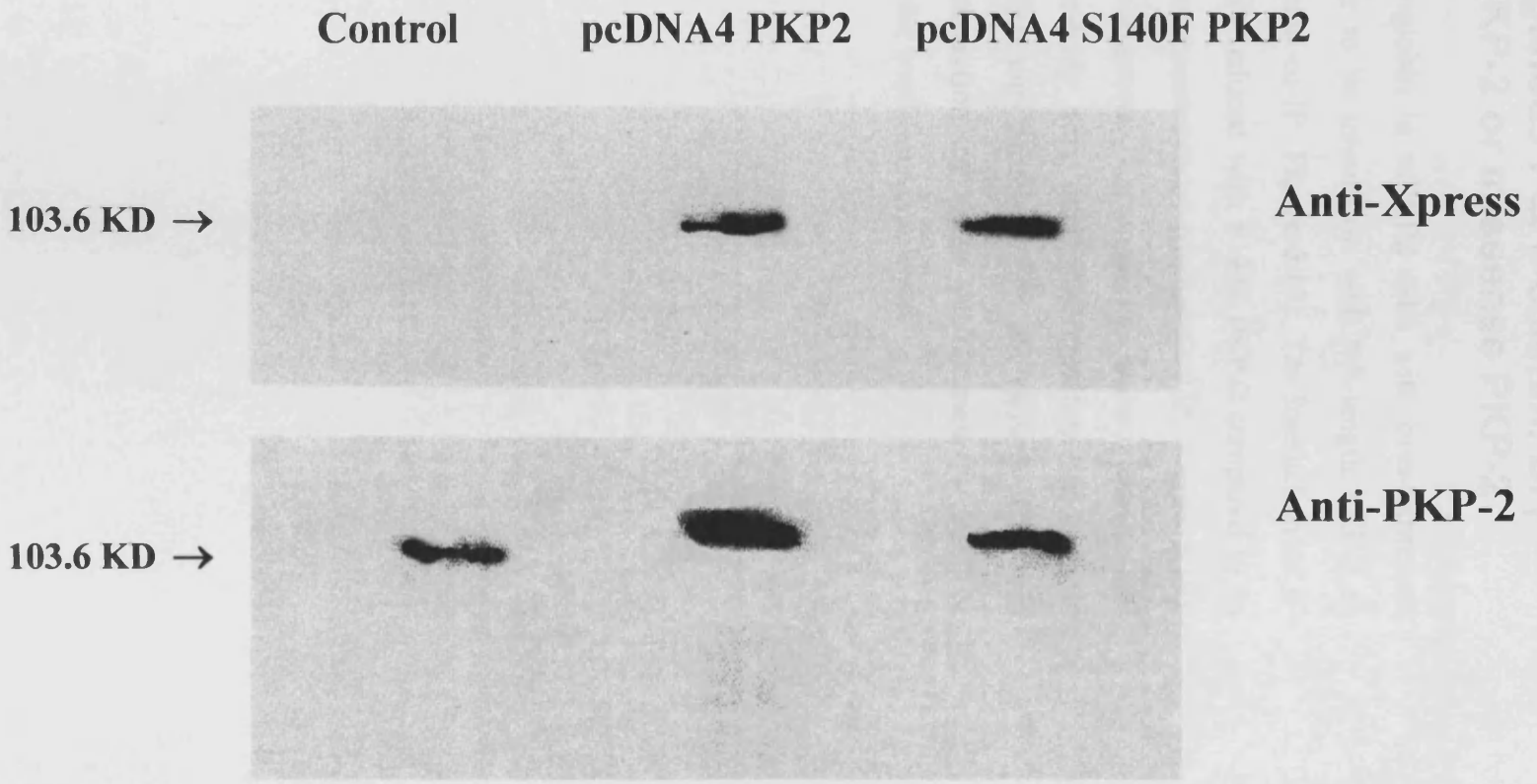

5.5.6 Interaction of endogenous PG, β-catenin, DP, DSC-2 and DSG-2 with PKP-2 or missense PKP-2

The interaction of endogenous plakoglobin in mPKP2 cells with over-expressed S140F PKP-2 appeared to be similar to its interaction with full-length PKP-2 in wPKP2 cells (representative of triplicate co-IP, Figure 5.18). The interaction of β-catenin however, appeared significantly reduced with S140F PKP-2 compared to its interaction with full-length PKP-2 (representative of triplicate co-IP, Figure 5.19). The co-immunoprecipitation of endogenous desmoplakin, desmoglein-2, and desmocollin-2 using anti-XPress antibody was unreliable resulting in variable immunoprecipitation of all three endogenous proteins (data not shown). This was probably because of insufficient extraction of these membrane-associated or cytoskeletal-associated proteins under the conditions employed.

Figure 5.18 Co-IP analysis using anti-XPress binding of PKP-2 or missense PKP-2 to endogenous PG

Co-immunoprecipitation of XPress-tagged full-length PKP-2 or S140F PKP-2 with endogenous plakoglobin performed in transfected HEK 293T cells. Following 48 hours after transfection of HEK 293T cells with pcDNA4 PKP2 or pcDNA4 S140F PKP2 plasmids (4μg/P90 dish), cells were scrapped off P90 dishes in lysis buffer (10mM Tris HCl pH 7.6, 145mM NaCl, 1 mM Na_3VO_4, and 1% triton X-100 + protease inhibitors). Soluble cell lysates (3mg) were taken for IP, with a prior pre-clearing with Protein G-Sepharose at 4°C for 30 minutes on rotator. Three microgram of anti-XPress (mouse monoclonal anti-XPress antibody, Invitrogen) was added to the pre-cleared fraction and incubated on a rotator at 4°C for three hours. Fifty microliters of Protein G-Sepharose was added and incubation continued overnight at 4°C. Immuno-complexes were pelleted at 10,000g for 0.5 minute and washed thrice in low stringency PBS/inhibitor followed by a single wash in lysis buffer. Immuno-complexes were denatured in 3x Laemmli buffer followed by electrophoreses on a 10% SDS PAGE and immunoblotting analysis using either 1:500 rabbit anti-plakoglobin antibody (Santa Cruz sc7900) and a 1:5000 mouse anti-rabbit-HRP conjugate (Invitrogen, UK) or 1:500 goat anti-human PKP-2 (reactive to a PKP-2 peptide near the C-terminus, Insight Biotechnology, sc-18976) and 1:5000 rabbit anti-goat HRP conjugate (Insight Biotechnology, BP5000) followed by incubation in ECL reagents and exposure to ECL Hyperfilm.

A) Triton X-100 cell lysates (equal amount, 100μg) loaded on 10% SDS PAGE

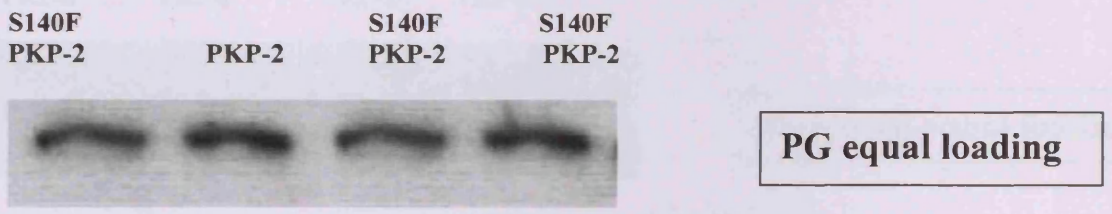

B) IP Probed for plakoglobin association with PKP-2 & S140F PKP-2

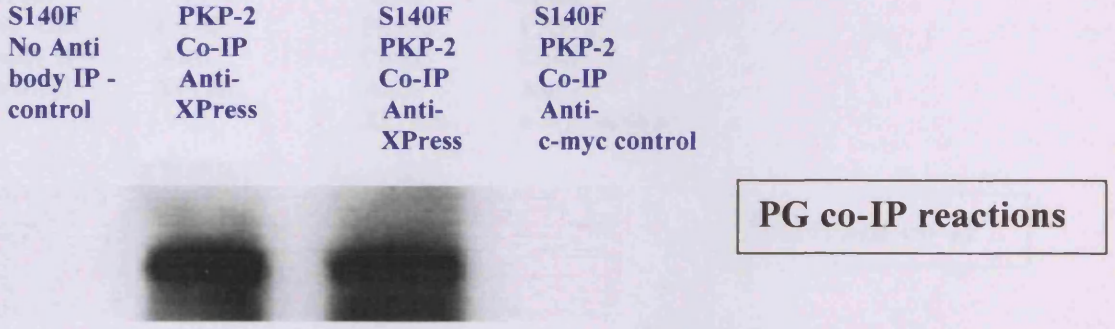

C) Probe to determine relative amounts of PKP-2 or S140F PKP-2 co-immunoprecipitated by anti-XPress antibody in cell lysates of pcDNA4 PKP2 and pcDNA4 S140F PKP2 transfected HEK 293T cells

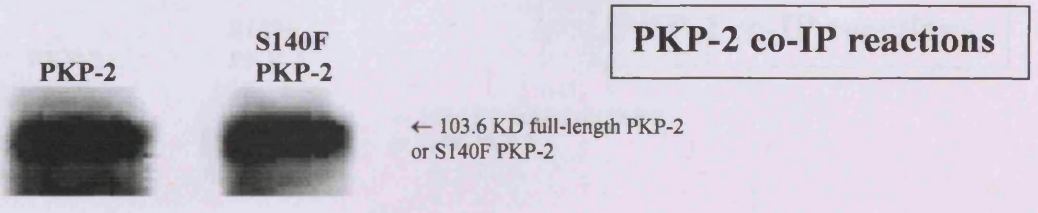

Figure 5.19 Co-IP analysis using anti-XPress binding of PKP-2 or missense PKP-2 to endogenous β-catenin

Co-immunoprecipitation of XPress-tagged full-length or S140F PKP-2 with endogenous β-catenin performed in transfected HEK 293T cells. Following 48 hours after transfection of 293T cells with pcDNA4 PKP2 or pcDNA4 S140F PKP2 plasmids (4μg/P90 dish), cells were scrapped off P90 dishes in lysis buffer (10mM Tris HCl pH 7.6, 145mM NaCl, 1 mM Na_3VO_4, and 1% triton X-100 + protease inhibitors). Soluble cell lysates (3mg) were taken for IP, with a prior pre-clearing with Protein G-Sepharose at 4°C for 30 minutes on rotator. Three microgram of anti-XPress (mouse monoclonal anti-XPress antibody, Invitrogen) was added to the pre-cleared fraction and incubated on a rotator at 4°C for three hours. Fifty microliters of Protein G-Sepharose was added and incubation continued overnight at 4°C. Immuno-complexes were pelleted at 10,000g for 0.5 minute and washed thrice in low stringency PBS/inhibitor followed by a single wash in lysis buffer. Immuno-complexes were denatured in 3x Laemmli buffer followed by electrophoreses on a 10% SDS PAGE and immunoblotting analysis using either 1:500 rabbit anti-β-catenin antibody (Abcam, ab2982) and 1:5000 mouse anti-rabbit-HRP conjugate (Invitrogen, UK) or 1:500 goat anti-human PKP-2 (reactive to a PKP-2 peptide near the C-terminus, Insight Biotechnology, sc-18976) and 1:5000 rabbit anti-goat HRP conjugate (Insight Biotechnology, BP5000) followed by incubation in ECL reagents and exposure to ECL Hyperfilm.

A) Triton X-100 cell lysates (equal amount, 100μg) loaded on 10% SDS PAGE

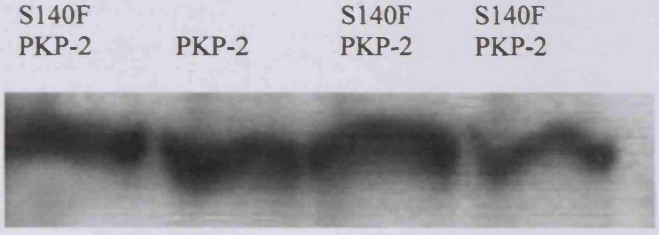

B) IP Probed for β-catenin association with PKP2 & S140F PKP2

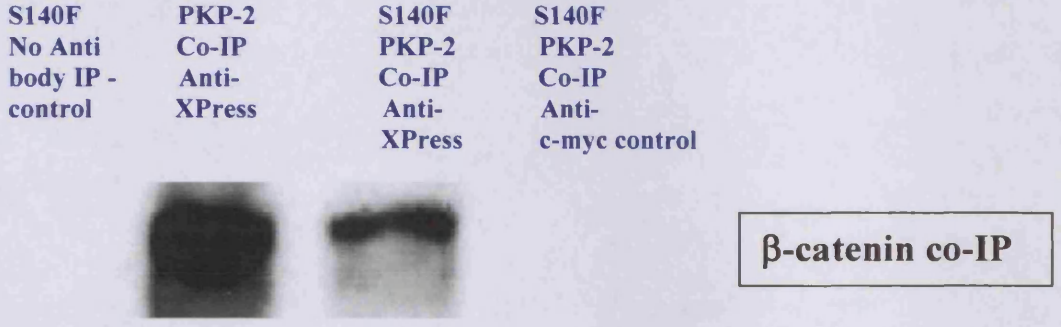

C) Probe to determine relative amounts of PKP-2 or S140F PKP-2 co-immunoprecipitated by anti-XPress antibody in cell lysates of pcDNA4 PKP2 and pcDNA4 S140F PKP2 transfected HEK 293T cells

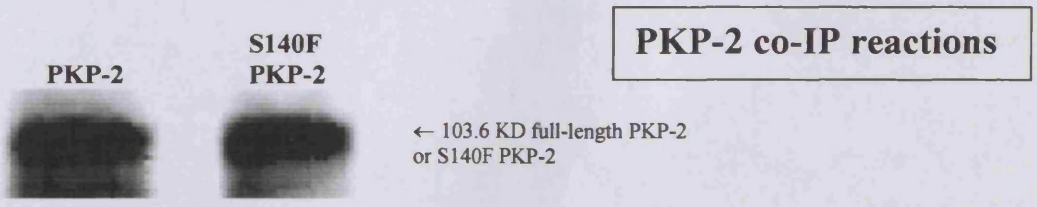

5.6 Discussion

Stable cell lines expressing S140F PKP-2 and full-length PKP-2 were analyzed by functional studies. Although the missense protein was expressed in tetracycline-induced mPKP2 cells, no significant differences were found in their proliferation, cell-cell adhesion, induced apoptosis to mechanical cell stretch and expression of connexin-43 gap junctions compared to tetracycline-induced wPKP2, indicating that these cellular functions/processes were not disrupted by the expression of S140F PKP-2.

S140F PKP-2 was expressed in tetracycline-induced mPKP2 cells localizing at both the cell-cell contacts and within the nucleus in a pattern that was similar to that of full-length PKP-2 in wPKP2 cells. The relative amounts of S140F PKP-2 and of endogenous PKP-2 in sub-cellular protein fractions of tetracycline-induced mPKP2 cells could not be distinguished based on size alone using a monoclonal antibody raised against a sequence near the N-terminus of PKP-2 (BD Bioscience, P63420) as this antibody recognized both proteins with an identical molecular weight. The epitope of this monoclonal antibody is located between amino acid residues 19 to 183 of PKP-2 (BD Bioscience technical information). It is not known whether the S140F PKP-2 substitution affected the epitope recognition of this antibody, as fine amino acid residue mapping studies were not available to define its epitope (technical information, BD Bioscience). It seems unlikely however, that S140F substitution in PKP-2 protein affects the recognition of this protein using the BD Bioscience anti-PKP-2 antibody as pcDNA4 S140F PKP2 vector transient transfection of HEK 293T cells and IP of this soluble cell lysate using anti-XPress antibody showed that the XPress-tagged S140F PKP-2 protein also reacted with an anti-PKP-2 polyclonal antibody (reactive to a human PKP-2 peptide near the C-terminus) correlating with the expected migration position of S140F PKP-2 in SDS PAGE immunoblotting analysis (Figures 5.18C and 5.19C).

A highly striking effect of S140F PKP-2 protein expression on desmosome morphology occurred in tetracycline induced mPKP2 cells with formation of extremely long desmosomes that ostensibly appeared to develop by fusion of neighbouring desmosome to form large intercellular junctions; such large intercellular junctions were absent in tetracycline-induced wPKP2 cells. Thus, S140F substitution

in PKP-2 appears to cause a **gain of function** as formation of these long desmosomal structures in tetracycline-induced mPKP2 cells would implicitly activate/disrupt a signalling pathway involving PKP-2. The mechanism of the formation of these large intercellular junctions in induced mPKP-2 cells has not been investigated in the present studies however; it seems probable that the loss of a putative phosphorylation site on serine residue number 140 in the PKP-2 protein may affect a signalling role of this protein. Evidence in the literature suggests that amongst the plakophilins, a strong expression of PKP-1 in the suprabasal layers of epidermal keratinocytes correlates with an increase in desmosome stability, number and size, this role of PKP-1 was highlighted by mutations in PKP-1 gene resulting in the loss of PKP-1 protein expression in ectodermal dysplasia/skin fragility where desmosome numbers and size are reduced compared to those in normal individuals. This suggests a function for PKP-1 in regulating desmosome size and functional integrity[222]; PKP-2 is not known to influence the size of desmosomes, and therefore, it is likely that the effect of S140F PKP-2 on desmosome size in induced mPKP2 cells is mediated by an effect of this protein via protein-protein interactions essential for assembly of the desmosomal plaque components; this probably involves disruption/activation of a signalling function of PKP-2. PG is also known to regulate the size of desmosomes as expression of a PG protein truncated in the final ninety-two amino acids of the C-terminus causes formation of extremely long junctions or groups of tandemly linked desmosomes in A431 cells[249], similar to those found in tetracycline-induced mPKP2 cells. The interaction between p0071/PKP-4 and the C-terminus of PG is thought to regulate the size of desmosomes[250]. Thus, the formation of long desmosomes may be linked with the interference of any of a number of different types of proteins involved in the assembly of the desmosomal plaque, resulting in the disruption of a common signalling pathway.

The question also arises whether the large intercellular junctions seen in tetracycline-induced mPKP2 cells might be "mixed-type" junctions as cross-talk between adherens junctions and desmosomes exists to ensure their appropriate assembly and segregation at sites of cell-cell contacts. Several lines of evidence suggests that formation of adherens junctions is functionally linked to desmosome assembly [126,134,175,251]. Blockade of adherens junction formation by an anti-E-cadherin antibody inhibits the formation of desmosomes in MDCK cells suggesting a cross-talk between adherens junctions and desmosomes[251]. A431D cells, a clonal variant of A431 epithelial cells,

express the requisite desmosomal protein components, but lack a classical cadherin or α-catenin and are unable to assemble desmosomes. Re-expression of E-cadherin in A431D cells was insufficient to trigger desmosome assembly, but reintroduction of PG or an E-cadherin-PG chimera led to desmosome formation in these cells, suggesting that E-cadherin-PG complex may be important in the assembly of these junctions[175]. Formation of desmosome-like structures in the skin of PG knockout mice, however suggests that other proteins besides PG might be involved in the cross-talk affecting the dynamics of desmosome assembly[185]. Other proteins such as p0071/PKP-4 (localized in the area composita of human ID[137]), β-catenin and PKP-2 may compensate for this function of PG as all of these proteins have been shown to associate with proteins present in both adherens and desmosomal junctions[183,249]. The regulated expression of p0071/PKP-4 is thought to important as this influences the size and number of the desmosomal and adherens junctions[249].

The marked reduction in the interaction of endogenous β-catenin with S140F PKP-2 in pcDNA4 S140F transfected HEK 293T soluble cell lysate raises the question whether β-catenin could be involved in signalling cross-talk between AJ and DS adhering junctions in induced mPKP-2 cells. Such a role for β-catenin was supported by a study showing that FLAG-tagged PKP-2a transiently expressed in SCC9 cells was associated with two of the endogenous adherens junction components, β-catenin and E-cadherin[183]. It is tempting to speculate that the reduced association of β-catenin with S140F PKP-2 might probably interrelate with the formation of long desmosomal junctions seen in tetracycline-induced mPKP2 cells, however further studies are needed to clarify this association in other cellular systems. The association between β-catenin and PKP-2 proteins seen in wPKP2 and mPKP2 induced cells seem especially pertinent in a cardiac context as large polar arrays of closely spaced or fused composite, plaque-bearing adhering junctions (the area composita) comprising of nearly 90% of the total ID area shows a strong co-localization of most protein components belonging to both assemblies of adhering junctions, as indeed, that which occurs between β-catenin and PKP-2[137]. The *in vitro* disruption of PKP-2 expression in the area composita of cardiomyocyte ID using siRNA-mediated reduction of PKP-2 cardiomyocyte content[242] highlights the central role of PKP-2 in the organization, formation, stabilization, and functions of the area composita, and of the ID, which

undergoes structural remodelling in human arrhythmogenic right ventricular cardiomyopathy[46].

Bioinformatics computer algorithms predict potential phosphorylation sites based on the consensus recognition sequence of known protein kinases, or based on the known phosphorylation sites in a homologous protein. The predicted sites are then verified by mutational analysis (genetic approach) or by immunological methods with antibodies that specifically recognise the predicted phosphorylation site. Unfortunately, the consensus recognition sites of most protein kinases are not stringent enough to be very useful in predicting phosphorylation sites. Since protein kinases most likely recognize three-dimensional structures instead of linear sequences in their substrates, a bioinformatics approach based on structural information is needed to accurately predict phosphorylation sites in proteins. NetPhos software predicted a potential phosphorylation site at serine residue number 140 in PKP-2 (section 3.4.1 part 1.8b) and although the relevance of this predicted post-translational modification of PKP-2 is not known because modification at this serine residue has not been reported in the literature, it seems highly likely that phosphorylation predicted at this site might be of functional significance based on data derived from a genetic approach showing significantly reduced binding of S140F PKP-2 with β-catenin by co-IP analysis, and the dramatic morphological change in desmosomes from tetracycline-induced mPKP2 stable cells.

The cell-cell adhesion data obtained by measuring contact adhesion of labelled mPKP2 cells with homologous non-labelled cells cultured on coverslip and using the Dispase-based monolayer dissociation assay of mPKP2 cells is an anomaly with respect to electron microscopy data, which showed presence of significantly longer desmosomes with dense filament association. As previously discussed (section 4.6), very little is known about cell-cell adhesion in HEK 293 cells and these cells express several different intermediate filament proteins resembling a cell line of an early neuronal lineage. The relevance of the apparent normal cell-cell adhesion of tetracycline-induced mPKP2 cells in the face of abnormally long desmosomes in a cardiac context seems dubious as unlike in cardiomyocytes where desmin intermediate filament protein is expressed this is not the case in HEK 293 cells.

It is not known whether the S140F PKP-2 protein is indeed expressed or incorporated into cardiac desmosomes of patients affected with the c.C1604T PKP-2 gene mutation as heart tissue sample was not available from affected individuals in family G (section 3.4.1 part 2.5). Based on the results of the analysis of the exon 3 nucleotide sequences of wild type and mutant PKP-2 by ESE finder (section 3.4.1 part 1.8a), it seems unlikely that an mRNA transcript encoding the S140F substitution would undergo NMD as an ESE element identified was not abolished by the sequence change. Hence, there was no predicted effect on the splicing of the mRNA transcript. Since c.C1604T PKP-2 gene mutation is a recurrent mutation it is possible that in future ARVC genetic screening heart tissue sample will become available from an affected individual. This will allow detection of mRNA encoding the missense protein by reverse transcription polymerase chain reaction and the presence of S140F PKP-2 protein in diseased heart lysate can be determined by western immunoblotting analysis. The incorporation of S140F PKP-2 into the ID structures can be examined and its effect on the ultrastructure of desmosomes can be determined. The co-localization and interaction of S140F PKP-2 with other desmosomal and adherens junction proteins, including β-catenin can be performed to determine the characteristics of cross-talk between these junctions.

5.7 Summary of main findings of the study

The cloning of S140F plakophilin-2 into pcDNA5 and pcDNA4 plasmid vectors is described utilizing the topoisomerase catalyzed reaction in the plasmid vector. Using S140F plakophilin cloned into a pcDNA5 vector, a stable cell line, **mPKP2**, was established in Flp-In T-Rex HEK 293 cells and the effect of expression of S140F plakophilin-2 in mPKP2 cells was characterized by the addition of tetracycline to overcome tet-repression.

Strong induction of full-length PKP2 (size 98.7 KD) was reported previously in wPKP2 cells (Chapter 4) with its expression localised to cell-cell contacts and in nucleus by confocal immunofluorescence staining. Sub-cellular protein fractionation of induced wPKP2 cells followed by Western immunoblotting analysis confirmed a predominant expression of PKP2 in the cytoplasm, membrane, and cytoskeletal fractions, while some PKP2 associated with the nuclear protein fraction (Chapter 4).

S140F PKP-2 (size 98.7 KD) was induced in mPKP2 cells and its expression localized to cell-cell contacts and in the nucleus by confocal immunofluorescence staining. Sub-cellular protein fractionation of induced mPKP2 cells followed by Western immunoblotting analysis indicated strong association of missense plakophilin-2 in the cytoskeletal fractions and presence of this protein in the cytoplasm fraction. Equal amounts of S140F PKP-2 compartmentalized in membrane and nuclear fractions.

Stable wPKP2 and mPKP2 cells proliferated to the same extent and expression of either full-length or missense plakophilin-2 did not affect their proliferation rates. The initial cell-cell adhesion of wPKP2 and mPKP2 cells showed no statistically significant difference when Calcein-labelled cells were allowed to adhere to homologous cell monolayer cultured on coverslips. Adhesive strengths of confluent monolayers of induced wPKP2 and mPKP2 cells assessed by Dispase-based cell dissociation assay did not show any difference in resistance to fragmentation based on visual assessment of fragment sizes produced in sheared mPKP2 monolayer compared to those of wPKP2 monolayer. Mechanically stretched tetracycline-induced wPKP2 and mPKP2 cells recovering from stretch exposure did not show a statistically significant difference in the induced apoptosis of these cell lines. Triton X-100 soluble cell lysate western blot analysis of wPKP2 and mPKP2 cells showed that Connexin-43 protein was strongly detected in non-induced and tetracycline-induced mPKP2 cells and wPKP2 cells. Confocal microscopy examination of these induced cells confirmed localization of Connexin-43 to cell-cell contacts of both tetracycline-induced wPKP2 cells and mPKP2 cells. Examination of Flp-In T-Rex HEK 293, tetracycline-induced wPKP2, and tetracycline-induced mPKP2 cells by transmission electron microscopy showed formation of desmosomes in Flp-In T-Rex HEK 293 cells, but these were not particularly robust. Desmosomes in tetracycline-induced wPKP2 were prominent (with dense plaque and filament association) however, whilst desmosomes in tetracycline-induced mPKP2 cells also appeared to be prominent and with dense filament association, the mean desmosomal length of these cells was statistically significantly longer compared to either Flp-In T-Rex HEK 293 or tetracycline-induced wPKP2 cells. Endogenous plakoglobin co-localization with S140F PKP-2 in cell-cell contacts of tetracycline-induced mPKP2 cells was not

significantly different to its co-localization with full-length PKP-2 in tetracycline-induced wPKP2 cells.

XPress-tagged transient protein expression of full-length (size 103.6 KD) and missense (size 103.6 KD) PKP-2 in HEK 293T cells was obtained 48 hour after transfection with pcDNA4 vectors. Immunoprecipitation studies showed no differences in the amounts of plakoglobin associating with either missense PKP-2 or PKP-2. β-catenin however, showed significantly reduced association with missense PKP-2 compared to its association with PKP-2. Other endogenous desmosomal proteins such as DP, DSG-2, and DSC-2 did not co-IP reproducibly with the anti-XPress antibody and therefore the effects of binding of these proteins to missense PKP-2 could not be determined.

5.8 Future Studies

Both the bioinformatics approach and a genetic approach strongly suggests that the S140F substitution probably affects a putative signalling function of PKP-2 hence a definitive confirmation of the phosphorylation of the affected serine residue needs to be obtained by phosphopeptide analysis and Edman degradation of the labelled protein. Although the cellular characteristics of mPKP2 cells appeared not to be altered relative to those of wPKP2 cells, the dramatic effect on desmosome formation in tetracycline-induced mPKP2 cells was unexpected. This effect of S140F PKP-2 must be examined in other cell systems, such as SSC9, MDCK, and A431 cells, which would permit better quality co-localization data to be obtained by immunofluorescence confocal microscopy, verify the effect of S140F PKP-2 on the ultrastructure of desmosomes robustly formed in these cell lines, and allow protein-protein interactions to be examined between S140F PKP-2 and proteins present in the adherens junction.

The significance of the reduced association of β-catenin with S140F PKP-2 needs to be examined in induced mPKP2 cell immunofluorescence staining confocal microscopy analysis to determine whether the co-localization of these two proteins is affected compared to the co-localization of β-catenin and full-length PKP-2 in induced wPKP2 cells. In order to overcome limitations of co-localizing missense and full-length PKP-2 proteins with potentially low endogenous amounts of β-catenin, co-

transfection with plasmids encoding PKP-2 proteins and β-catenin in HEK 293T cells may be required. The co-localization of S140F PKP-2 with other desmosomal proteins in induced mPKP2 cells as well as the co-IP of the missense PKP-2 protein with other desmosomal proteins requires optimization using modified staining and co-IP protocols incorporating different detergent and/or buffers.

Isolated neonatal rat ventricular cardiomyocytes maintained in culture for up to 12 days continue to synthesize myocardium-specific proteins, and remarkably most of the plaque proteins including DP, PG, PKP-2, p120, α-catenin, and β-catenin can still be localized at membrane structures showing a high degree of co-localization in the area composita of cardiomyocyte ID found *in situ*[246]. Transfection of rat cardiomyocyte cultures with plasmid or viral encoded S140F PKP-2 should allow the interaction of this protein with β-catenin and its consequence on the organization of the area composita at the ID to be determined in an *in vitro* relevant cardiac system.

A transgenic mouse model with a cardiac restricted expression of mutant desmosomal protein[163] would be a useful *in vivo* approach to examine of the effects of S140F PKP-2 protein within the ID of cardiomyocytes to determine the relevance of the *in vitro* data obtained from induced mPKP2 cells. Although the transgenic mouse model is a technically demanding system it offers several benefits allowing the effect of missense PKP-2 to be investigated within the area composita in a milieu of the molecular complexity of this unique structure, examination of the effect of the missense protein on the ultrastructure of area composita within the ID, and examination of the cross-talk between different junctional protein components.

Immunoelectron microscopy using gold-conjugated antibodies against proteins specific for desmosomes and adherens junctions would be required to determine whether the long intercellular junctions in induced mPKP2 cells might be "mixed-type" junctions.

A working hypothesis has emerged from functional studies undertaken in mPKP2 cells suggesting that substitution of serine amino acid residue at position 140 with the loss of a putative phosphorylation could be related to the formation of abnormal long desmosomes with prominent filament association. The weak association of missense PKP-2 protein with β-catenin may participate in a speculated cross-talk between

adherens junctions and desmosomes in mPKP2, which seems relevant in polar epithelial cells where AJ and desmosomes are present as discreet junctions however, in cardiomyocyte ID such a molecular cross-talk may be of a greater relevance because of the intimate association of these protein assemblies along the area composita[246]. Non-cadherin bound β-catenin can participate in the Wnt-signalling pathway through the interaction of TCF/Lef1 transcription factors[176] and since PKP-2 co-precipitates a non-cadherin pool of β-catenin, it raised the possibility that PKP-2 might be involved in regulating β-catenin/TCF signalling. Evidence for this role of PKP-2 was obtained in a human colon carcinoma cell line with constitutive β-catenin/TCF transcription activity in which over-expression of PKP-2 strongly elevated activation of TOPFLASH reporter compared to reporter plasmid only control; the activation of TOPFLASH was also shown to be competitively abolished with simultaneous over-expression of both PKP-2 and E-cadherin[183]. Future studies in mPKP-2 and w PKP-2 cells should include determination of the roles of over-expressed full-length and missense PKP-2 on Wnt-signalling.

Chapter 6

Functional Studies of Q273fsX288 Desmoplakin protein expression in tDP cells

6.1 Introduction

Genetic screening of the ARVC cohort identified two separate DP gene mutations that caused reading frame-shifts resulting in the truncation of translated DP proteins in the SR4 spectrin repeat of the plakin domain of DP (Table 3.4). One of these mutations c.818_819insA (p.Q273fsX288 DP) showed incomplete penetrance with variable clinical ARVC expression (family I, Chapter 3). Expression of a DP polypeptide with a predicted size of about 33KD might form in patient heart if an mRNA transcribed from the mutant DP gene was translated. Additionally, both full-length DP and Q273fsX288 may be present in patient tissue sample as only one allele was affected by the c.818_819insA mutation. The Q273fsX288 DP polypeptide encodes a small part of the N-terminal domain of DP while the rod region, intermediate filament-binding plakin repeats (A, B and C), and a glycine-serine-arginine rich domain (GSR) are missing.

An mRNA transcribed from a DP gene carrying the c.818_819insA mutation is rather likely to undergo NMD resulting in DP haploinsufficiency. Heterozygous mouse models with a cardiac-restricted over-expression of a mutated desmosomal gene would be especially suitable for studying frame-shift mutations that undergo NMD, but such a study was not feasible under this project proposal. However, as small amounts of the affected DP transcript might escape NMD surveillance this could result in the formation of a severely truncated DP polypeptide. The study described in this chapter examines the effect of truncated Q273fsX288 DP polypeptide expression on cellular characteristics of Flp-In HEK 293 stable cells.

6.2 Experimental approach to investigate functional effect of Q273fsX288 DP protein expression

Cloning of DNA fragment encoding a small fragment of the DP gene incorporating the final codon for W at position 358 and of a DNA encoding full-length DP was performed in pcDNA5 vector. SDM of pCDNA5 vector incorporating the small DP DNA fragment was performed to obtain pcDNA5 vector encoding the sequence for Q273fsX288 DP polypeptide. Polyfect-mediated cationic transfection of pcDNA5 plasmids allowed selection of stable cell clones to express either full length or truncated DP proteins under the control of an established tet-on system in Flp-In T-Rex HEK 293 cells.

Several studies were performed using stable cells expressing full-length (designated wDP cells) and truncated DP (designated tDP cells):

1) Expressions of full-length or truncated DP proteins were confirmed by confocal microscopy and western immunoblotting analysis in wDP and tDP cells. The distribution of full-length and truncated DP proteins were examined in different cellular compartments of induced wDP and tDP cells (in cytosol, membrane, nuclear, and cytoskeletal fractions) using a Qiagen cell compartment kit.
2) Properties of wDP and tDP cells were examined to compare cellular proliferation rates using a colorimetric assay and their response to induced apoptosis under mechanical cell-stretch using a CaspACE assay system.
3) The co-localizations of endogenous PKP-2 and PG with either full-length or truncated DP were examined by confocal microscopy analysis of tetracycline-induced wDP and tDP stable cells respectively.
4) The interaction of either full-length DP or truncated DP with endogenous PG and PKP-2 proteins was determined by immunoprecipitation analysis of detergent solubilised cell lysates of induced wDP and tDP stable cells using a polyclonal antibody directed against an N-terminus sequence of DP.
5) The sub-cellular distribution of endogenous PG and PKP-2 proteins were determined in tetracycline-induced wDP and tDP cells to establish whether these protein distributions in different fractions were altered by the expression of a truncated DP polypeptide.
6) Desmosomes in tetracycline-induced wDP and tDP cells were examined by transmission electron microscopy and compared with desmosomes in control non-transfected Flp-In T-Rex HEK 293 cells to determine whether DP polypeptide protein expression affected the morphology of these desmosomes
7) The strength of cell-cell adhesion in tetracycline-induced wDP and tDP monolayers were assessed using an established Dispase-based monolayer dissociation assay[212] to determine if this was altered by the expression of a DP polypeptide.
8) The vimentin intermediate filament network was examined in tetracycline-induced wDP and tDP stable cells by immunofluorescence staining and confocal microscopy analysis to determine if the organization of this cytoskeletal protein was altered by expression of DP polypeptide.

6.3 Experimental Aims

Eleven overall objectives were set in this part of the study. The first was to construct a pcDNA5/FRT/TO/TOPO/TA plasmid encoding a DP DNA fragment of Q273fsX288 DP using site directed mutagenesis of a cloned 1094 bp partial DP DNA fragment in pcDNA5 plasmid. The second was to clone a PCR fragment encoding full-length DP in pcDNA5 vector. The third was to establish stable cell lines in Flp-In TRex HEK 293 that express Q273fsX288 DP and full-length DP under the control of a tet-on system. The fourth was to verify the expressions of Q273fsX288 DP and full-length DP in these stable cell lines using immunofluorescence staining confocal microscopy analysis and to determine the distribution of full-length or truncated DP in sub-cellular fractions of these stable cells using a cell compartment kit. The fifth was to examine the proliferation rates of these stable cell lines and to determine their response to induced apoptosis upon mechanical cell-stretch. The sixth was to determine the immunofluorescence co-localization of endogenous PG and PKP-2 proteins with either full-length or truncated DP in stable cells. The seventh was to determine the interactions of either endogenous PG or PKP-2 with full-length or truncated DP proteins using co-immunoprecipitation analysis. The eighth was to determine the sub-cellular distributions of endogenous PG and PKP-2 proteins in induced wDP and tDP cells. The ninth was to examine desmosomes in non-transfected Flp-In T-Rex HEK293 and in induced wDP and tDP stable cells. The tenth was to determine the Dispase-based monolayer dissociation adhesion strengths of these induced stable cell lines. The eleventh was to examine the vimentin IF network in wDP and tDP stable cell lines.

6.4 Materials and Methods

A goat anti-human DP polyclonal antibody was purchased from Santa Cruz Biotechnology (product sc-18082). All other reagents including cell culture media, supplements, and antibiotics were purchased from Invitrogen, UK. Low melting point agarose was purchased from Sigma Aldrich, UK.

6.4.1 Cloning of DP and Q273fsX288 DP in pcDNA5/FRT/TO/TOPO/TA

A plasmid, P1140 (map shown in Figure 6.1), containing a cloned desmoplakin DNA with an 5' UTR (a gift kindly provided by Professor Kathleen Green, Department of Pathology, Dermatology and RH Lurie Cancer Centre, Northwestern University, USA) was used for obtaining DP DNA sequences by PCR. P1140 was used as a template DNA in EXL DNA polymerase reaction (primer sequences in Table 6.1) to generate a DP PCR fragment, 8.633kbp in length, which contained a Kozak recognition sequence before the ATG start site and a TGA stop codon. The amplified DP PCR fragment lacked the untranslated UTR sequence found in P1140. This DP PCR fragment was cloned into pcDNA5/FRT/TO/TOPO/TA (section 2.2.1) to generate plasmid pcDNA5 DP. An another DP PCR fragment was generated by EXL DNA polymerase using the plasmid P1140 as template, this PCR product incorporated the ATG start site preceded by the Kozak recognition sequence and flanked on the 3' site by a triplet nucleotide sequence completing the encoding of amino acid W at position 358 (Ensemble transcript ID: ENST0000021199). The PCR product (1094bp) also contained KpnI and Bam HI restriction nucleotide sequences incorporated at the 5' and 3' positions respectively. The 1094bp DP PCR product was cloned into pcDNA5/FRT/TO/TOPO/TA utilising the topoisomerase-catalyzed reaction to generate plasmid pcDNA5 1094 DP.

6.4.2 Site-directed mutagenesis to obtain Q273fsX288 DP encoded in pcDNA5/FRT/TO/TOPO/TA

Plasmid pcDNA5 1094 DP was used as a template in SDM (section 2.3) using mutagenic primers (Table 6.1) to generate plasmid pcDNA5 1094 mutA DP that contained an insertion of an Adenosine residue c.818_819 insA (accession number NM_004415) predicted to cause a reading frame-shift resulting in a predicted truncation of the translated DP polypeptide (Q273fsX288 DP). Plasmids pcDNA5 DP, pcDNA 1094 DP and pcDNA5 1094 mutA DP were sequenced to verify the cloned desmoplakin DNA sequence orientations and to confirm the reading frames in plasmids pcDNA5 DP and pcDNA5 1094 mutA DP.

6.4.3 Establishing stable cell lines expressing full-length DP and Q273fsX288 DP

Stable cell lines were established in Flp-In T-Rex HEK293 cells using pcDNA5 DP and pcDNA5 1094 mutA DP plasmids according to procedures described (section 2.5.4) to obtain full-length DP and Q273fsX288 DP protein expressions upon tetracycline-induction. At least five different clones of each stable cell line established were selected and clonally expanded, and a stable cell clone characterized with strong tetracycline-induced protein expression by immunofluorescence staining (section 2.7.2) and western blotting (section 2.6.2) was selected for functional studies. Based on these criteria two stable cell clones were selected: clone **wDP** expressed full-length DP and clone **tDP** expressed Q273fsX288 DP.

Figure 6.1 Map of plasmid P1140 encoding full-length DP

Plasmid P1140 was kindly supplied by Professor Kathleen Green (Northwestern University, Illinois, USA). It contained a full-length desmoplakin coding sequence preceded by a 5' UTR sequence of DP. A FLAG epitope was incorporated at the end of the C-terminus of desmoplakin. The plasmid DNA was sequenced to verify that the entire desmoplakin-coding region was free of nucleotide errors. The plasmid was utilized as a template in a PCR reaction to obtain an 8633 bp amplicon that was cloned into a pcDNA5 plasmid expression vector (Table 6.1), which was used for establishing stable cells expressing DP used as a control for functional studies of Q273fsX288 DP expression. Plasmid map was reproduced courtesy of Professor Kathleen Green (Northwestern University, Illinois, USA).

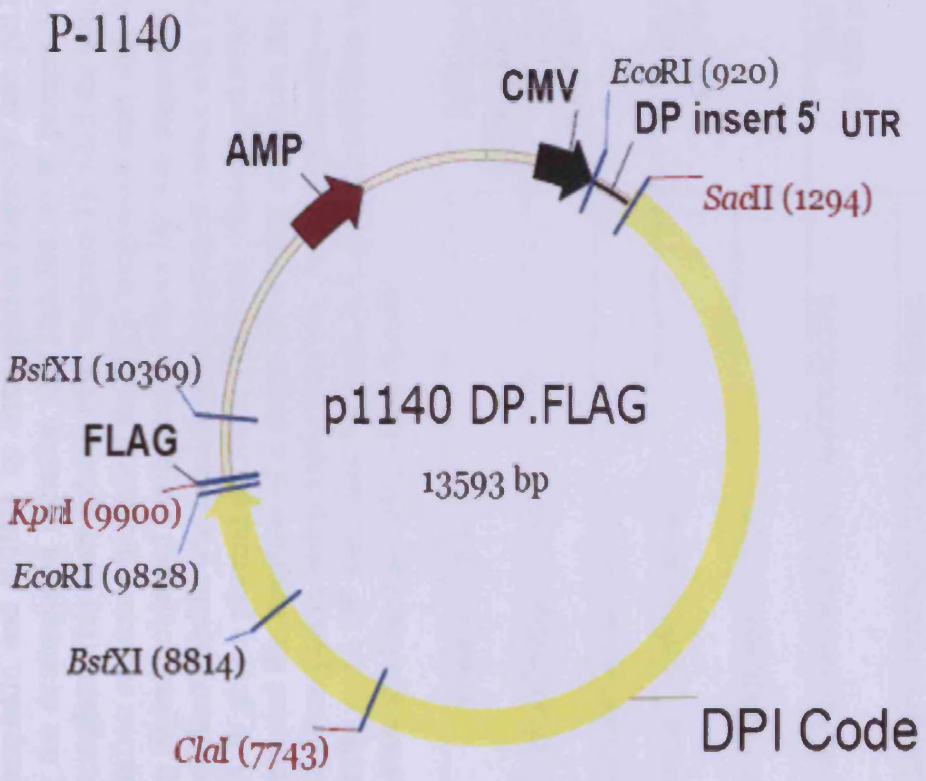

Table 6.1 Cloning in pcDNA5/FRT/TO/TOPO/TA of full-length DP and a fragment of 1094 bp DP to obtain pcDNA5 encoding Q273fsX288 DP by site-directed PCR mutagenesis

Cloning of full-length desmoplakin and a 1094 bp desmoplakin fragment into pcDNA5/FRT/TO/TOPO/TA vector and SDM to obtain a pcDNA5 plasmid encoding the desmoplakin mutation Q273fsX288. PCR primers DSP for and DSP rev were used to generate an 8633bp fragment using P1140 as a template. This desmoplakin PCR fragment encoded the entire full-length desmoplakin sequence lacking the 5' UTR. It contained a Kozak recognition sequence preceding the ATG translation start site. A termination stop codon, TGA, was incorporated in the reverse primer. The resulting plasmid obtained designated pcDNA5 DP was sequenced to confirm nucleotide sequence of the encoded DP DNA insert. A 1094 bp fragment of desmoplakin was amplified using primers shown with P1140 as a template. This 1094 bp fragment was cloned in pcDNA5/FRT/TO/TOPO/TA to give a plasmid pcDNA5 1094 DP. Plasmid pcDNA5 1094 DP was used a template in a SDM reaction using primers shown which incorporated the insertion of a single Adenosine residue in the plasmid obtained (pcDNA5 1094 mutA DP) encoding a frame-shift in the translated desmoplakin polypeptide resulting in the expression of a 33KD Q273fsX288 desmoplakin fragment. Plasmids pcDNA5 DP and pcDNA5 1094 mutA DP were used for establishing stable cell lines in Flp-In HEK 293 cells permitting the over-expression of DP and Q273fsX288 DP in a tetracycline-inducible culture system.

Primer Pairs	Sequence (5'-3')	PCR size (bp) / Enzyme used/ Template	Destination vector PCR product cloned into	Plasmid obtained
DSP for	GGTACCGAAATGGGCTGCAACGGAGGCTCC	8633/ ACCUTAQ/ P1140	pcDNA5/FRT/TO/TOPO/TA	pcDNA5 DP
DSP rev	GCGGCCGCCTAGTGCCCAATAGAACTACTGC			
1094 DSP for	CGGGGTACCGAAATGGGCTGCAACGGAGGCT	1094/ EXL/ P1140	pcDNA5/FRT/TO/TOPO/TA	pcDNA5 1094 DP
1094 DSP rev	CGCGGATCCCACTGCGTCTGCAGAGTGTCC			
1094 mutA DSP for	GGATCACCTGCGACAGCTGCAAGAACATCATTCAGGCCACGTC	1094/ EXL/ 1094 pcDNA5	pcDNA5/FRT/TO/TOPO/TA	pcDNA5 1094 mut A DP
1094 mutA DSP rev	GACGTGGCCTGAATGATGTTCTTGCAGCTGTCGCAGGTGATCC			

6.5 Results

6.5.1 Cloning of DP in pcDNA5/FRT/TO/TOPO/TA

Cloning of desmoplakin full-length PCR fragment into pcDNA5 was a particularly difficult procedure because the PCR fragment encoding full-length DP was a large amplimer (~8.7Kb) which easily fragmented during cloning. Multiple steps were followed for successfully cloning of full-length DP DNA. The PCR fragment obtained using high fidelity AmpliTaq LA DNA polymerase was electrophoresed in a low melting temperature agarose gel (Sigma Aldrich, UK) without the use of ethidium bromide staining and exposure to ultraviolet light to minimise photolysis of the amplified PCR fragment. The low melting point agarose facilitated the release of the PCR fragment into solution without the use of gel purifications kits ensuring that further handling of the PCR product was avoided. The solubilised PCR fragment obtained from a low melting point agarose gel slice was used directly in the pcDNA5 cloning reaction. The ratio of purified DP PCR fragment: plasmid vector was meticulously optimized for successful insertion of the full-length DP fragment into pcDNA5 T/A cloning site. Very large numbers of isolated recombinant plasmids had to be screened because partial DP PCR fragments cloned more efficiently and plasmid re-circularization without an insert occurred frequently. The sequence of the cloned full-length DP had to be checked to verify that this was free from PCR derived errors, a task that was not trivial given the large size of the nucleotide sequence encoding full-length DP.

6.5.2 Characterization of DP and Q273fsX288 DP expressions in stable cell lines

Stable wDP and tDP cells expressed endogenous DP I and II (DP II lacks most of the dimerization coiled-coil rod DP domain) proteins constitutively. However, upon tetracycline induction of wDP cells, full-length DP I was over-expressed localizing at a sub-membranous location (Figure 6.2A) within these cell-cell contacts by immunofluorescence staining confocal microscopy analysis (consistent with the location of DP at the juncture between intermediate filament network and the cytoplasmic tail of the transmembrane desmosomal cadherins, Figure 1.6d) and detected as a strongly induced band of 250 KD (predicted size based on protein sequence was 330KD) by SDS PAGE analysis (Figure 6.3A). The Plakin family of proteins are all known to run aberrantly on SDS PAGE gels with their size estimates

being significantly lower than the predicted molecular weight based on cDNA sequence data[131]. The DP I isoform was chosen to be over-expressed in wDP cells as only this isoform was able to form a DP protein dimer. In tetracycline-induced tDP cells, Q273fsX288 DP was over-expressed localizing as punctate staining by immunofluorescence staining confocal microscopy analysis suggesting a membrane localization of the induced DP polypeptide (Figure 6.2B). Q273fsX288 DP was detected as a strongly induced band of 33 KD by SDS PAGE immunoblotting analysis (Figure 6.3B), which correlated with the predicted size of the DP polypeptide. Tetracycline induction of tDP cells did not appear to significantly alter the amount of endogenous DP I and II proteins (Figure 6.3B).

6.5.3 Sub-cellular localization of DP and Q273fsX288 DP in induced wDP and tDP stable cell lines

Sub-cellular fractions obtained from induced wDP cells showed that over-expressed DP I was primarily found in the cytoskeletal protein fraction with presence of endogenous DP I and II proteins in the cytoplasm protein fraction; over-expressed DP I was not present in either the membrane (confirming the sub-membranous immuno-localization of DP 1 by IF, Figure 6.2A) or nuclear protein fractions of induced wDP cells (Figure 6.4A). In tetracycline-induced tDP cells endogenous DP I and DP II proteins constitutively expressed were present in the cytoplasm and the cytoskeletal protein fractions, but not in the membrane or nuclear protein fractions. Over-expressed Q273fsX288 DP (the band present in all four fractions on the bottom part of Figure 6.4B) however, was present in the cytoplasm, membrane, cytoskeletal, and surprisingly, also in the nuclear fraction of induced tDP cells. A bioinformatics program, Predict NLS online (http://cubic.bioc.columbia.edu/cgi/var/resonline.pl) analysis of the polypeptide sequence of Q273fsX288 DP did not reveal presence of known nuclear localization signals in this polypeptide (data not shown). However, the presence of this polypeptide in the nuclear protein fraction of induced tDP cells does not appear to be an artefact resulting from a significant cross-contamination with the membrane fraction because assessment of the purity of each of these four protein fractions using specific protein marker distribution showed minimal cross-contamination (Figure 6.5). The sub-cellular fractionation was carried out according to the Qproteome recommended protocol (section 2.5.7, Qproteome handbook available online), which was reportedly tested and shown to give reliable separation of protein fractions in cell compartments derived from a wide variety of cells including, HeLa, Jurkat, NIH-3T3, COS as well as HEK 293 cells (references to publications contained in Qiagen Qproteome handbook).

Figure 6.2 Immuno-localisation of full-length DP and Q273fsX288 DP in wDP and tDP cells by confocal microscopy

Localization of protein expression of full-length DP and Q273fsX288 in non-induced and tetracycline-induced wDP (A) and tDP (B) stable cell lines respectively. Immunofluorescence images showing blue fluorescence signal resulting from DAPI nuclear staining, green fluorescence resulting from FM 1–43FX membrane dye staining, red fluorescence resulting from Q273fsX288DP or full-length DP staining with 1:200 goat polyclonal antibody to human desmoplakin reactive to a region near the N-terminus of the molecule (Santa Cruz, sc-18082) and an Alexa fluor-546 conjugated donkey anti-goat antibody (Invitrogen) and merge representing composite signals. The white size bar on each image in the green channel represents 8μm.

A) wDP cells non-induced

DAPI **Membrane** **DP** **Merge**

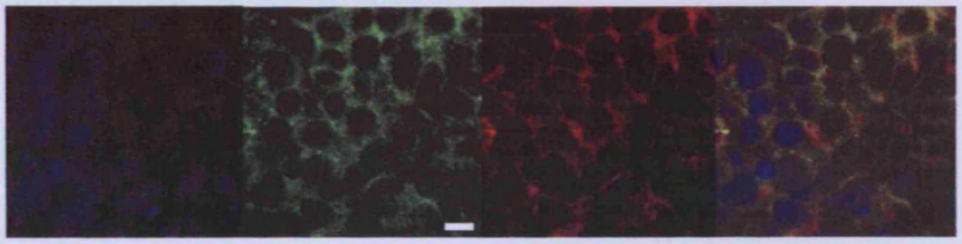

wDP cells tetracycline-induced

DAPI **Membrane** **DP** **Merge**

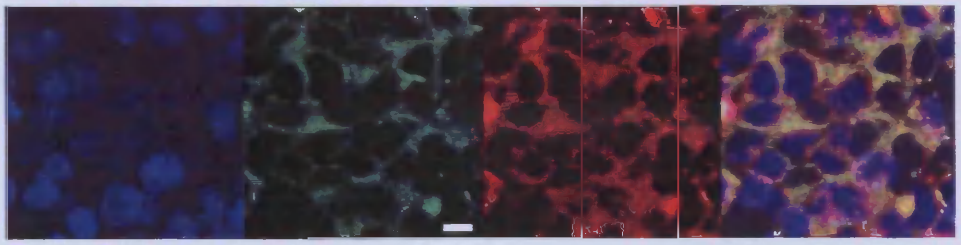

B) tDP cells non-induced

DAPI **Membrane** **DP** **Merge**

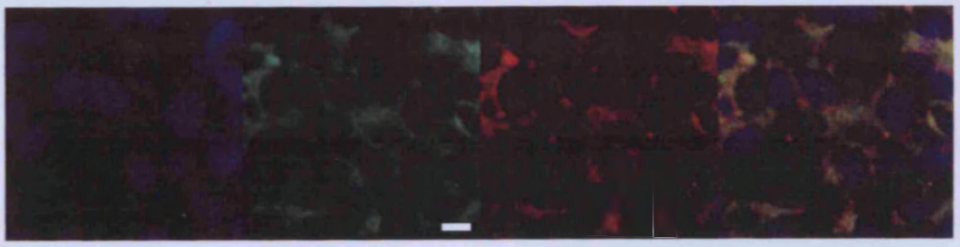

tDP cells tetracycline-induced

DAPI **Membrane** **DP** **Merge**

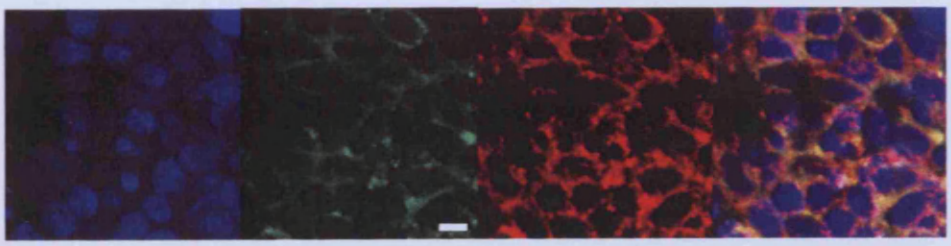

Figure 6.3 Western blot analysis of the expressions of full-length DP and Q273fsX288DP in wDP & tDP cells

Analysis of expressions of full-length DP and Q273fsX288 DP in non-induced (NI) or tetracycline-induced (IND) wDP (A) and tDP (B) triton X-100 soluble stable cell lysates determined by western blotting technique. A goat polyclonal antibody to human desmoplakin (1:500 dilution, Santa Cruz, sc-18082) was used followed by a rabbit anti-goat HRP conjugate (1:5000 dilution, Insight Biotechnology, BP5000). Blots were exposed to ECL reagents (GE Healthcare) and developed using Kodak reagents. The migration of protein markers (Precision Plus protein standards, BioRad Laboratories, UK) are indicated on the right hand side of the blots. The apparent SDS PAGE migration sizes of endogenous DP protein bands in non-induced wDP cells are smaller than the predicted protein sizes.

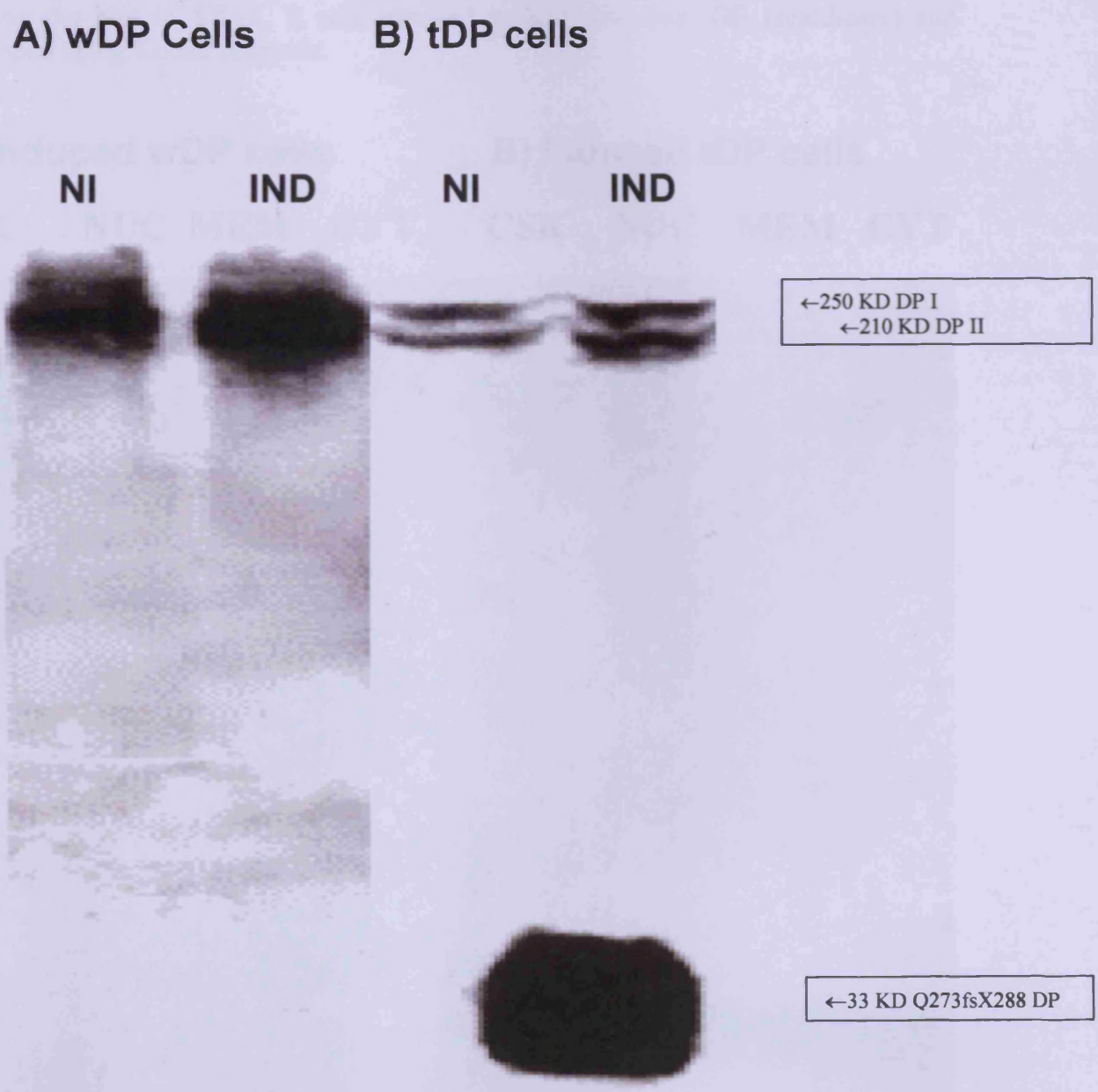

Figure 6.4 Sub-cellular localization of full-length and Q273fsX288 DP in wDP and tDP cells

Sub-cellular distribution of over-expressed full-length DP I and over-expressed Q273fsX288 DP in cytosolic (CYT), membrane (MEM), nuclear (NUC) and cytoskeletal (CSK) protein fractions determined by SDS PAGE and immunoblotting analysis these fractions derived from tetracycline-induced (0.1μg/ml, 72hrs) wDP (A) or tDP (B) stable cells respectively. Sub-cellular protein fractions were obtained from $5x10^6$ cells using the Qproteome cell compartment kit (Qiagen, UK). Each protein fraction was precipitated in 4 volumes of acetone (-20°C) and the pellet was resuspended in 100 μl RIPA containing cocktail of protease inhibitors (Roche). $1/5^{th}$ of each protein fraction was electrophoresed in a 10% SDS PAGE gel and transferred onto a Hybond ECL membrane. Following blocking of blot in TBST/5% milk, it was incubated with 1:500 goat anti-human Desmoplakin I/II (Santa Cruz Biotechnology, sc-18082) at 4°C overnight. Blot was washed in TBST followed by incubation in 1:5000 rabbit anti-goat HRP conjugate (Insight Biotechnology, BP5000). After washing the blot in TBST, it was exposed to ECL reagents (GE Healthcare) and developed using Kodak reagents.

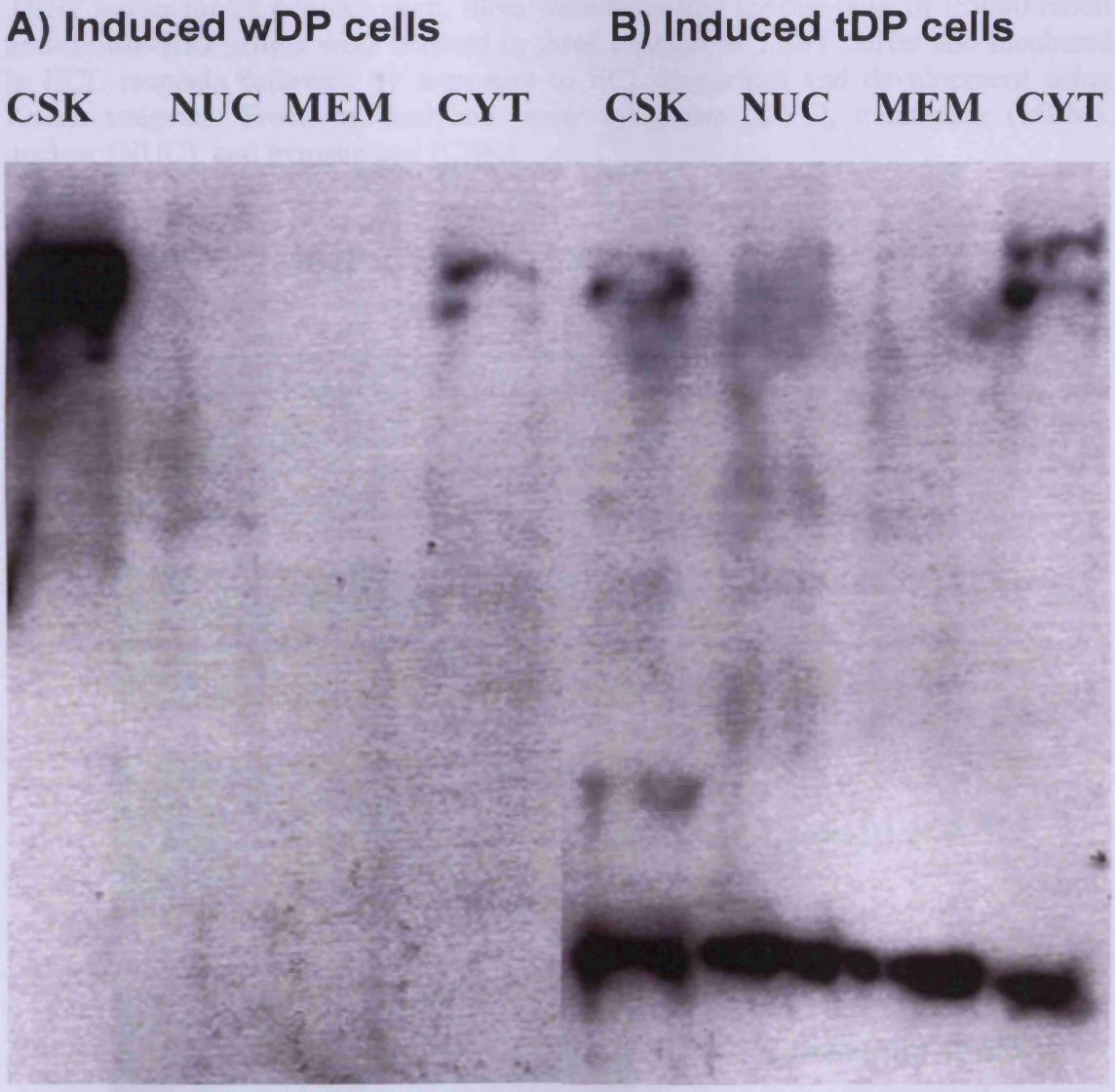

Figure 6.5 Assessment of purities of protein fractions of cytoplasmic, membrane, nuclear and cytoskeletal obtained from tetracycline-induced tDP cells using the Qproteome cell compartment kit

Assessment of purities of fractionated sub-cellular protein fractions obtained from tetracycline-induced tDP cells using the Qproteome cell compartment kit (Qiagen, UK). 5 x10^6 cells were fractionated according to the manufacturer's protocol. Each protein fraction was precipitated by the addition of four volumes of acetone (-20°C), and following precipitation the pellet was resuspended in an equal final volume of 100 µl in RIPA buffer. 1/5th of each protein fraction was separated under reducing and denaturing conditions in a 10% SDS PAGE system. Proteins were blotted from the gels onto ECL Hybond membranes using semi-dry transfer method in TGM transfer buffer. Blots were blocked in TBSTM buffer and incubated for one hour in 1:1000 mouse anti-human α-tubulin (Sigma Aldrich, T5168), or 1:500 dilution of the following antibodies: mouse anti-human N cadherin (Zymed, 33-3900), or mouse anti-human cyclin D1 (Abcam, ab6152), or mouse anti-human cytokeratin-18 (Santa Cruz Biotechnology, sc-6259). Following washing of the blots in three changes of TBST buffer for 20 minutes each, blots were incubated for one hour in 1:5000 rabbit anti-mouse-HRP. Blots were washed in three changes of TBST buffer and incubated in ECL reagents followed by exposure to ECL Hyperfilm and development using Kodak reagents. Fractions analyzed were: cytoplasm (CYT), membrane (MEM), nuclear (NUC), and cytoskeletal (CSK).

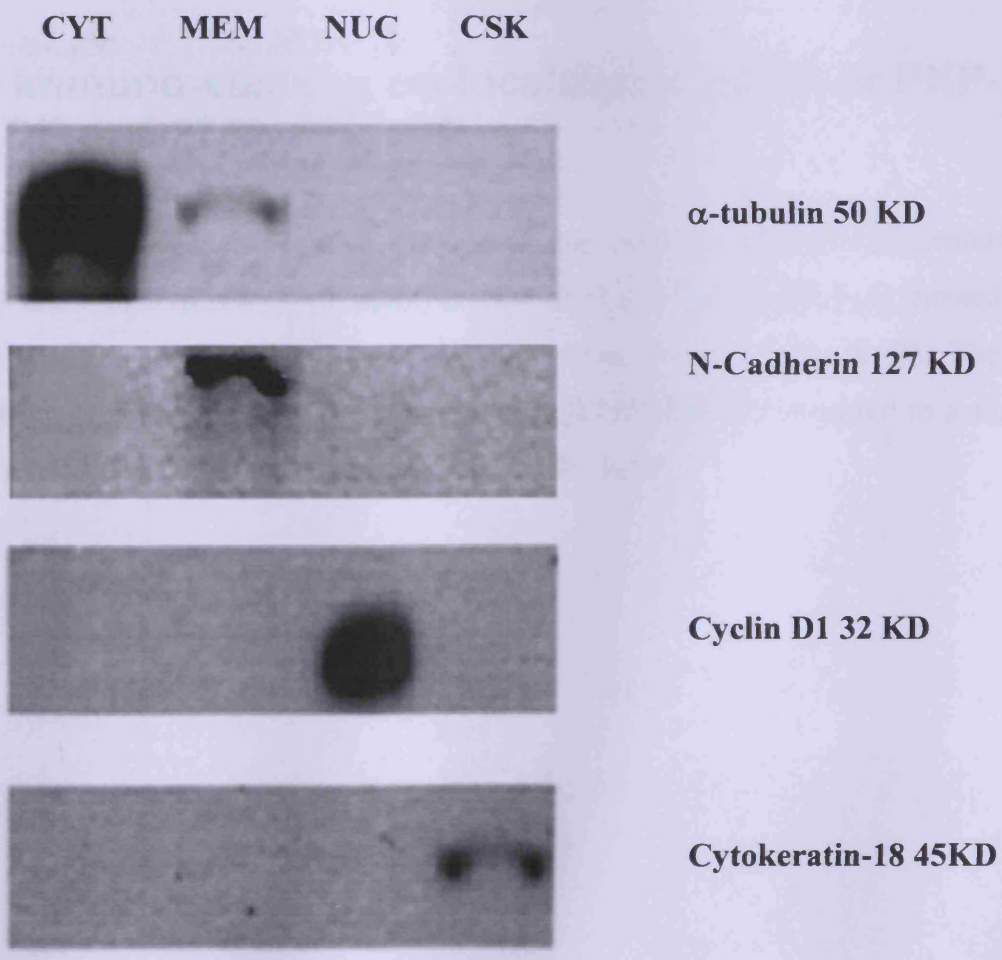

6.5.4 Cellular proliferation and effect of mechanical stretch on wDP and tDP cells

Cellular proliferation of wDP and tDP cells did not appear to be substantially altered by the expressions of full-length or Q273fsX288 DP respectively as comparable values of the slopes were obtained by regression analysis of the data in tetracycline-induced cell lines (Figure 6.6). Stable wDP and tDP cells subjected to mechanical cell-stretch and then allowed to recover for a short while did not show statistical differences in the induced specific apoptosis activity of these cells (Figure 6.7). The magnitude of applied mechanical cell stretch in wDP and tDP cells was slightly higher (5%) compared to 4% stretch used in mechanical stretch experiments chapters 4 and 5 because the Flexer cell apparatus relies on a tight vacuum seal being established, introducing a variation in the actual recorded mechanical stretch achieved. A marginally longer duration of stretch (four hours) and a higher cell plating density ($1.5x10^6$) of wDP and tDP cells was used in these stretch experiments compared to stretch experiments in chapters 4 and 5.

6.5.5 Immuno-staining co-localization of PG or PKP-2 with DP or Q273fsX288 DP

Immunofluorescence staining confocal microscopy co-localization of endogenous PG with DP and Q273fsX288 DP in induced wDP and tDP cells respectively showed that PG co-localized in these cells to a similar extent (Figure 6.8A & B). The co-localization of endogenous PKP2 with DP and Q273fsX288 DP occurred to a similar extent in induced wDP and tDP cells (Figures 6.8C & D).

Figure 6.6 Proliferation of wDP and tDP cells

Cellular proliferation of stable cell lines wDP and tDP over-expressing full-length and truncated DP proteins respectively. 60,000 cells were plated in a twenty-four well plate and allowed to attach overnight. Cell proliferation was measured spectrophotometrically at 490nm by measuring the reduction of Cell Titer AQ One solution (Promega Corporation, UK) after incubation with cells for exactly one hour. The measured cell growth indicated no significant differences in the proliferation rates of non-induced or induced wDP and tDP cells. The values of the slopes were: 0.0134, 0.0137, 0.0131, and 0.0139 for wDP NI, wDP IND, tDP NI and tDP IND cells respectively.

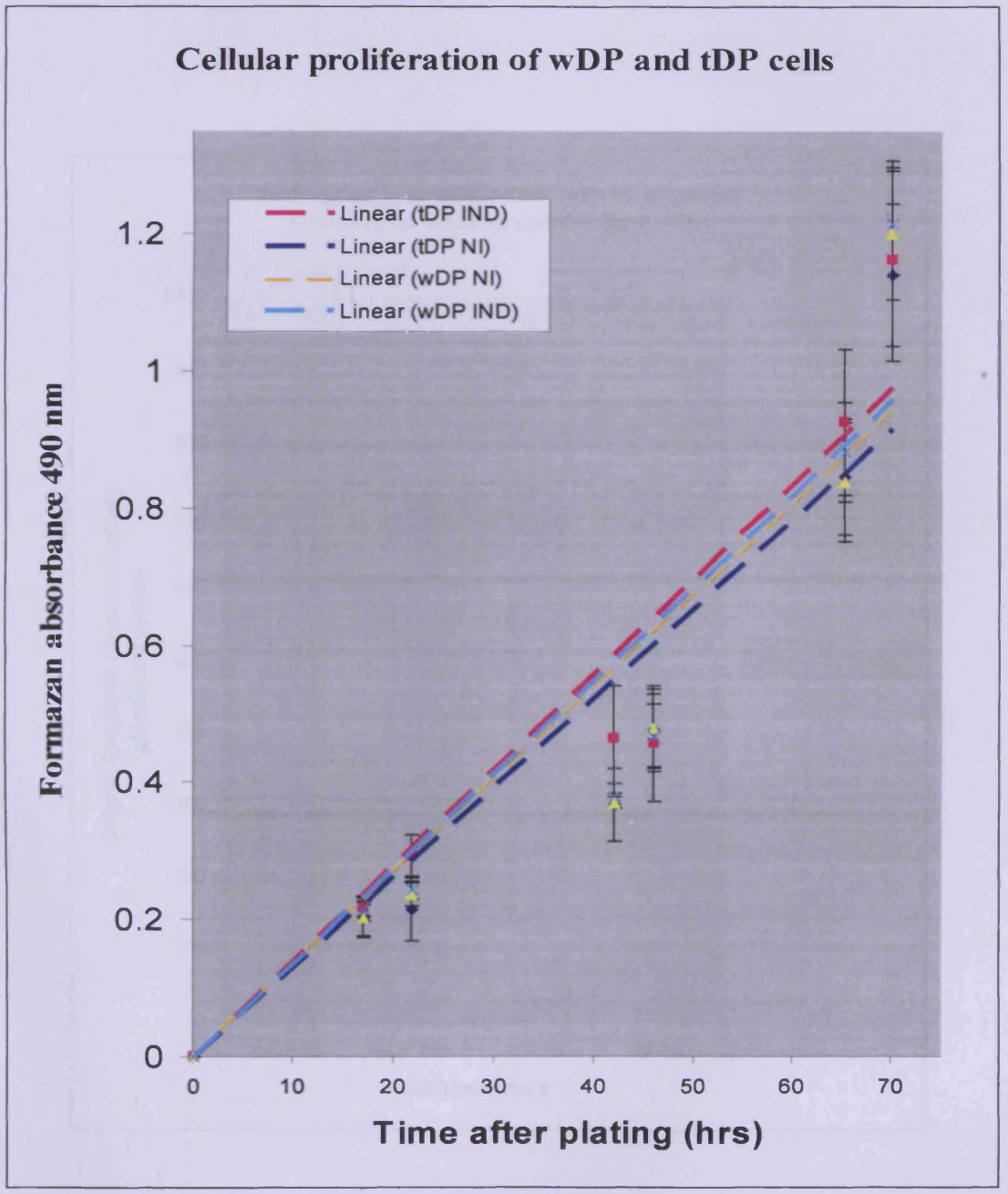

Figure 6.7 Effect of mechanical cell stretch on apoptosis of wDP and tDP stable cells

Effect of mechanical cell stretch on measured apoptosis of recovering wDP and tDP stable cells expressing DP or Q273fsX288 DP. Apoptosis levels are mean values of n = 6 experiments ± standard deviations. The CaspACE assay system (Promega, UK) was used to measure the specific caspase-3 activity in cell lysates of cells subjected to mechanical stretch using the Flexer cell-stretch system with 5% cell-stretch applied at a frequency of 1Hz for 4 hours. Paired student's t test p values comparing mean apoptosis were: wDP NI versus wDP IND, p=0.502; tDP NI versus tDP IND, p=0.826; wDP IND versus tDP IND, p=0.951. Cells were allowed to recover for 3 hours prior to measuring caspases-3 activity. Initial cell plating density was 1.5 x10^6 cells/six well plate and cells were cultured for 48 hours.

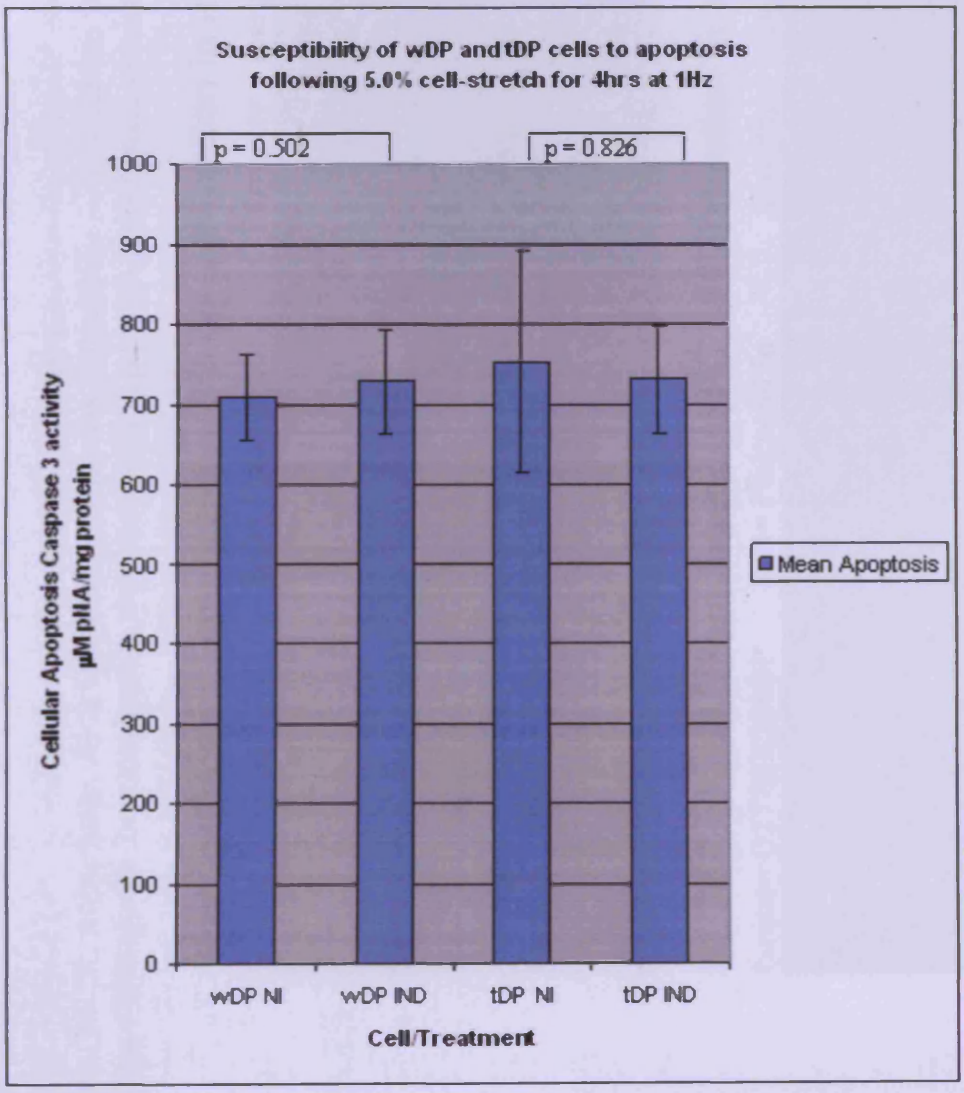

Figure 6.8 Co-localization of PG or PKP-2 with full-length DP and Q273fsX288 DP in induced wDP and tDP cells

Confocal microscopy co-localization of PG and PKP-2 in tetracycline-induced wDP and tDP cells over-expressing full-length DP and Q273fsX288 DP respectively. A) & B) shows endogenous plakoglobin co-localization with desmoplakin proteins while C) & D) shows endogenous plakophilin-2 co-localization with desmoplakin proteins. Images were obtained using x40 oil immersion objective lens.

A) Full-length DP/ endogenous PG co-localization in induced wDP cells

Green= full-length DP **Red= Plakoglobin** **Overlay = merged**

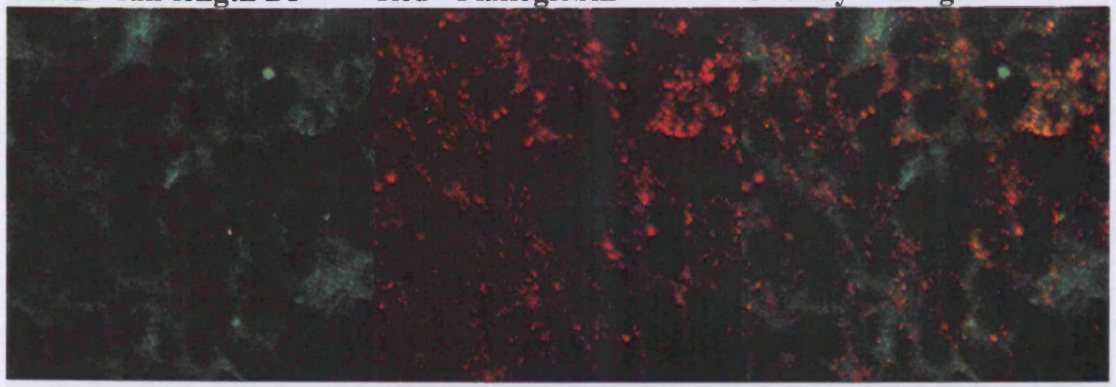

B) Q273fsX288 DP/endogenous PG co-localization in induced tDP cells

Green= Q277fsX288DP **Red= Plakoglobin** **Overlay = merged**

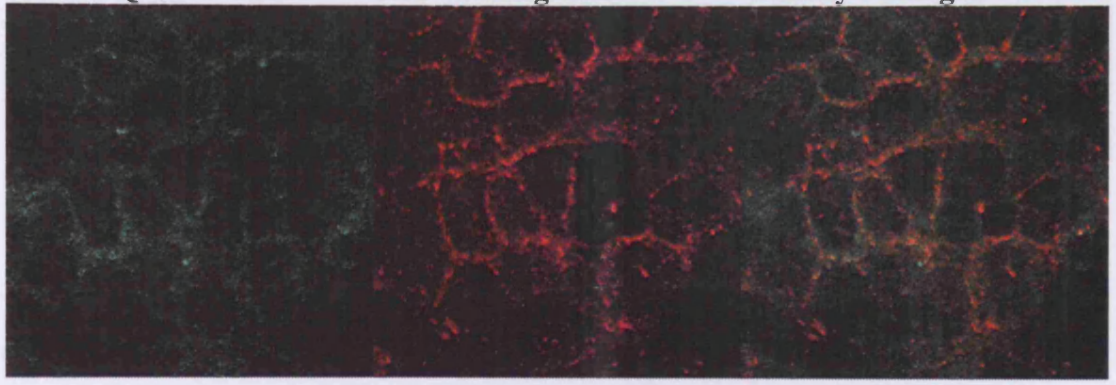

Figure 6.8 continued

C) Full-length DP/endogenous PKP-2 co-localization in induced wDP cells

Green= full-length DP Red= Plakophilin-2 Overlay = merged

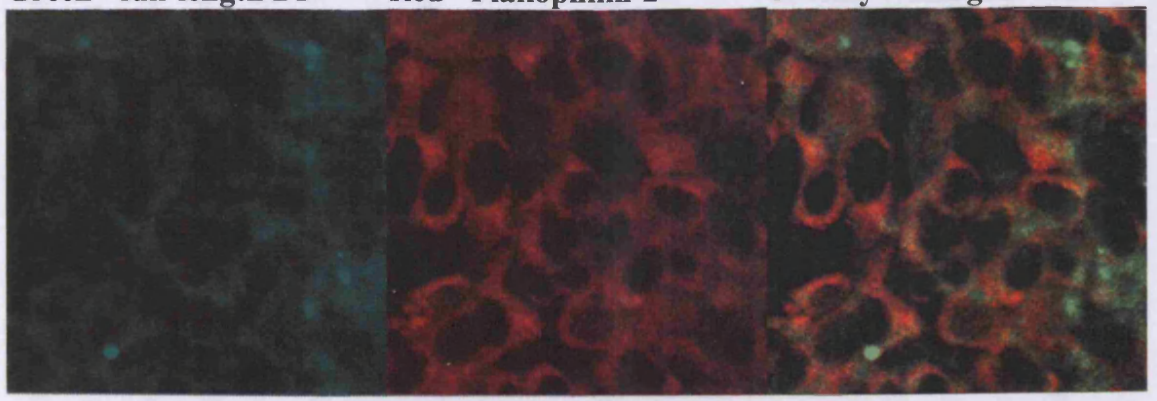

D) Q273fsX288 DP/endogenous PKP-2 co-localization in induced tDP cells

Green= Q273fsX288 DP Red= Plakophilin-2 Overlay = merged

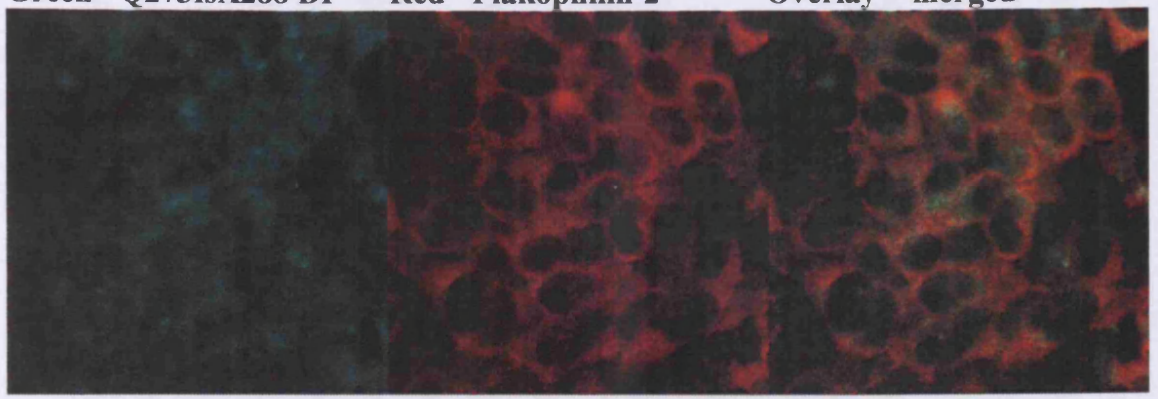

6.5.6 Interaction of endogenous PG or endogenous PKP-2 with DP or Q273fsX288 DP

The amount of endogenous plakoglobin interacting with full-length DP and Q273fsX288 DP did not appear to be significantly different in wDP and tDP cell lysates respectively (Figure 6.9) even though the amount of DP and Q273fsX288 DP that was immunoprecipitated by the goat-anti DP antibody from wDP and tDP cell lysates were comparable. The amount of endogenous PKP-2 interacting with full-length DP and Q273fsX288 DP did not seem to be significantly different in induced wDP and tDP cell lysates (Figure 6.10), albeit comparable amounts of full-length DP and Q273fsX288 DP were immunoprecipitated by the goat-anti DP antibody from wDP and tDP cell lysates. The lack of a difference in the binding of PG and PKP-2 with either DP or Q273fsX288 DP suggests that the truncated DP polypeptide retains the binding sites for both PG and PKP-2, which is in agreement with EM data (section 6.5.8) suggesting that Q273fsX288 DP is able to form normal ODP in desmosomes of induced tDP cells.

6.5.7 Distribution of PG and PKP-2 in sub-cellular fractions of induced wDP and tDP cells

Sub-cellular fractions of induced wDP and tDP cells obtained using the Qproteome cell compartment kit (Qiagen, UK) were analyzed by western immunoblotting analysis to determine the distribution of endogenous either PG or PKP2 in each of the four sub-cellular fractions obtained from these cells. Plakoglobin distribution (Figure 6.11) did not appear to be significantly different in any of the four sub-cellular fractions (cytoplasm, membrane, nuclear and cytoskeletal) derived from either induce wDP or induced tDP cells. The distribution of PKP-2 (Figure 6.12) also did not appear to be significantly different in any of the four sub-cellular fractions derived from either induced wDP or induced tDP cells

Figure 6.9 Co-IP analysis using goat anti-human DP binding of DP or truncated DP to endogenous PG

Co-immunoprecipitation of full-length DP or Q273fsX288 DP with endogenous PG performed in tetracycline-induced wDP and tDP cell lysates. Following induction of expression of respective desmoplakin protein over-expression, stable cells were scrapped off P90 dishes in lysis buffer (10mM Tris HCl pH 7.6, 145mM NaCl, and 1% triton X-100 + protease inhibitors). Soluble cell lysates (3mg) were taken for IP, with a prior pre-clearing with Protein G-Sepharose at 4°C for 30 minutes on rotator. Twelve microgram of sc 18082 (goat anti-human DP antibody) was added to the pre-cleared fraction and incubated on a rotator at 4°C for three hours. Fifty microliters of Protein G-Sepharose was added and incubation continued overnight at 4°C. Immuno-complexes were pelleted at 10,000g for 0.5 minute and washed thrice in low stringency PBS/inhibitor followed by a single wash in lysis buffer. Immuno-complexes were denatured in 3x Laemmli buffer followed by electrophoreses on a 10% SDS PAGE and immunoblotting analysis using an anti-plakoglobin antibody at 1:500 dilution (Santa Cruz sc7900) and a goat anti-rabbit-HRP conjugate at 1:5000 dilution (Invitrogen) followed by incubation in ECL reagents and exposure to ECL Hyperfilm.

A) Triton X-100 cell lysates (equal amount, 100μg) loaded on 10% SDS PAGE

tDP wDP tDP wDP

PG equal loading

B) IP Probed for plakoglobin association with DP & Q273fsX288 DP

tDP	wDP	tDP	wDP
No Anti-body IP control	Co-IP Anti-DP	Co-IP Anti-DP	Co-IP Anti-c-myc control

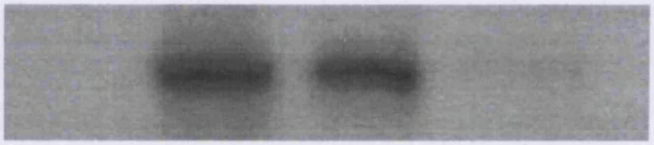

PG co-IP reactions

C) Probe to determine relative amounts of DP I/II or Q273fsX288 DP coimmunoprecipitated by sc18082 antibody in tetracycline-induced wDP or tDP cell lysates

wDP tDP

DP & Q273fsX288 DP co-IP reactions

←250 KD DP I
←210 KD DP II

← 33 KKD Q273 fsX288 DP

Figure 6.10 Co-IP analysis using goat anti-human DP binding of DP or truncated DP to endogenous PKP-2

Co-immunoprecipitation of full-length DP or Q273fsX288 DP with endogenous PKP-2 performed in tetracycline-induced wDP and tDP cell lysates. Following induction of expression of respective desmoplakin protein over-expression, stable cells were scrapped off P90 dishes in lysis buffer (10mM Tris HCl pH 7.6, 145mM NaCl, and 1% triton X-100 + protease inhibitors). Soluble cell lysates (3mg) were taken for IP, with a prior pre-clearing with Protein G-Sepharose at 4°C for 30 minutes on rotator. Twelve microgram of sc 18082 (goat anti-human DP antibody) was added to the pre-cleared fraction and incubated on a rotator at 4°C for three hours. Fifty microliters of Protein G-Sepharose was added and incubation continued overnight at 4°C. Immuno-complexes were pelleted at 10,000g for 0.5 minute and washed thrice in low stringency PBS/inhibitor followed by a single wash in lysis buffer. Immuno-complexes were denatured in 3x Laemmli buffer followed by electrophoreses on a 10% SDS PAGE and immunoblotting analysis using an anti-Plakophilin-2 antibody at 1:500 dilution (catalogue no. 610788, BD Bioscience,) and a rabbit anti-mouse-HRP conjugate at 1:5000 dilution (Invitrogen) followed by incubation in ECL reagents and exposure to ECL Hyperfilm.

A) Triton X-100 cell lysates (equal amount, 100μg) loaded on 10% SDS PAGE

tDP wDP tDP tDP

PKP-2 equal loading

B) IP Probed for plakophilin-2 association with DP & Q273fsX288 DP

tDP	wDP	tDP	tDP
No Anti-body IP control	Co-IP Anti-DP	Co-IP Anti-DP	Co-IP Anti-c-myc control

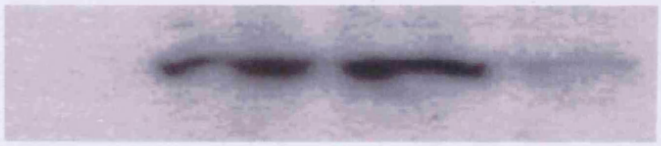

PKP-2 co-IP reactions

C) Probe to determine relative amounts of DP I/II or Q273fsX288 DP coimmunoprecipitated by sc18082 antibody in tetracycline-induced wDP or tDP cell lysates

wDP tDP

←250 KD DP I
←210 KD DP II

DP & Q273fsX288 DP co-IP reactions

← 33 KD Q273 fsX288 DP

Figure 6.11 Sub-cellular distribution of endogenous PG in induced wDP and tDP cells

Sub-cellular distribution of endogenous PG in tetracycline-induced wDP and tDP cells determined using the Qproteome cell compartment kit (Qiagen, UK). Cells were cultured in 0.1 μg/ml tetracycline for seventy-two hours in DMEM supplemented with 10% FBS, penicillin/streptomycin, blasticidin and hygromycin. Protein fractions enriched in cytoplasm, membrane, nuclear and cytoskeletal were obtained from 5 x 10^6 of each cell line using the Qproteome cell compartment according to the manufacturer's instruction. Each protein fraction was precipitated by the addition of four volumes of –20°C acetone and resuspended in a final equal volume of 100 μl in RIPA buffer. 1/5th of each protein fraction was separated in a 10% SDS PAGE gel under reducing condition. The semi-dry transfer in Tris-glycine methanol transfer buffer transferred proteins to ECL Hybond membrane. The blot was blocked in TBST/milk followed by incubation in 1:500 rabbit anti-human PG (Santa Cruz, sc-7900) at 4°C overnight. Blot was washed in TBST followed by incubation in 1:5000 goat anti-rabbit HRP conjugate (Invitrogen). Blot was exposed to ECL reagents (GE Healthcare) and developed using Kodak reagents. Key to sub-cellular fractions: CYT = cytosolic, MEM = membrane, NUC = nuclear, and CYK = cytoskeletal.

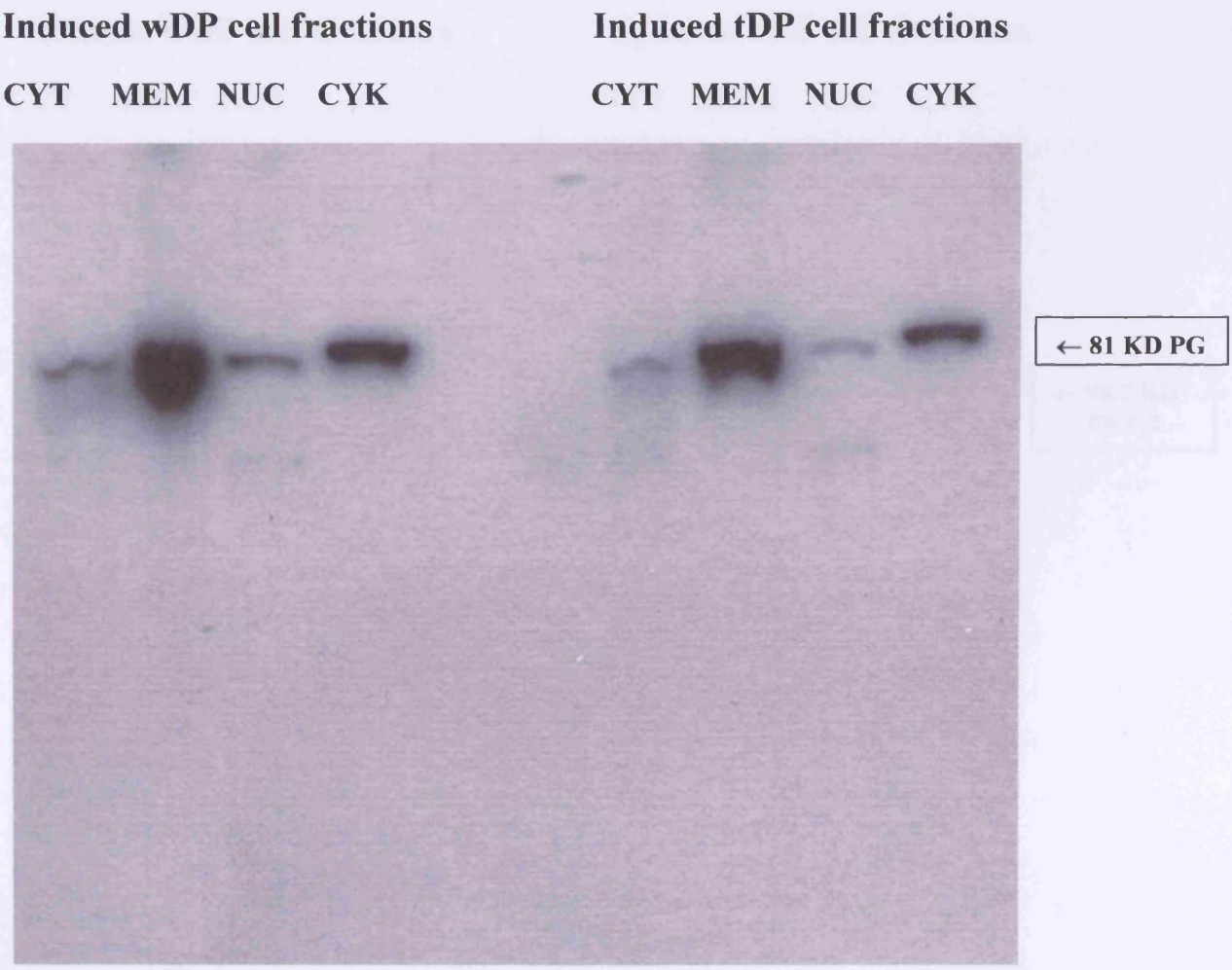

Figure 6.12 Sub-cellular distribution of endogenous PKP-2 in induced wDP and tDP cells

Sub-cellular distribution of endogenous PKP-2 in tetracycline-induced wDP and tDP cells determined using the Qproteome cell compartment kit (Qiagen, UK). Cells were cultured in 0.1 μg/ml tetracycline for seventy-two hours in DMEM supplemented with 10% FBS, penicillin/streptomycin, blasticidin and hygromycin. Protein fractions enriched in cytoplasm, membrane, nuclear and cytoskeletal were obtained from 5 x 10^6 of each cell line using the Qproteome cell compartment kit according to the manufacturer's instruction. Each protein fraction was precipitated by the addition of four volumes of –20°C acetone and resuspended in a final equal volume of 100 μl in RIPA buffer. 1/5th of each protein fraction was separated in a 10% SDS PAGE gel under reducing condition. The semi-dry transfer in Tris-glycine methanol transfer buffer transferred proteins to ECL Hybond membrane. The blot was blocked in TBST/milk followed by incubation in 1:500 mouse anti-human PKP-2 (BD Bioscience, 610788) at 4°C overnight. Blot was washed in TBST followed by incubation in 1:5000 rabbit anti-mouse HRP conjugate (Invitrogen). Blot was exposed to ECL reagents (GE Healthcare) and developed using Kodak reagents. Key to sub-cellular fractions: CYT = cytosolic MEM = membrane, NUC = nuclear, and CYK = cytoskeletal.

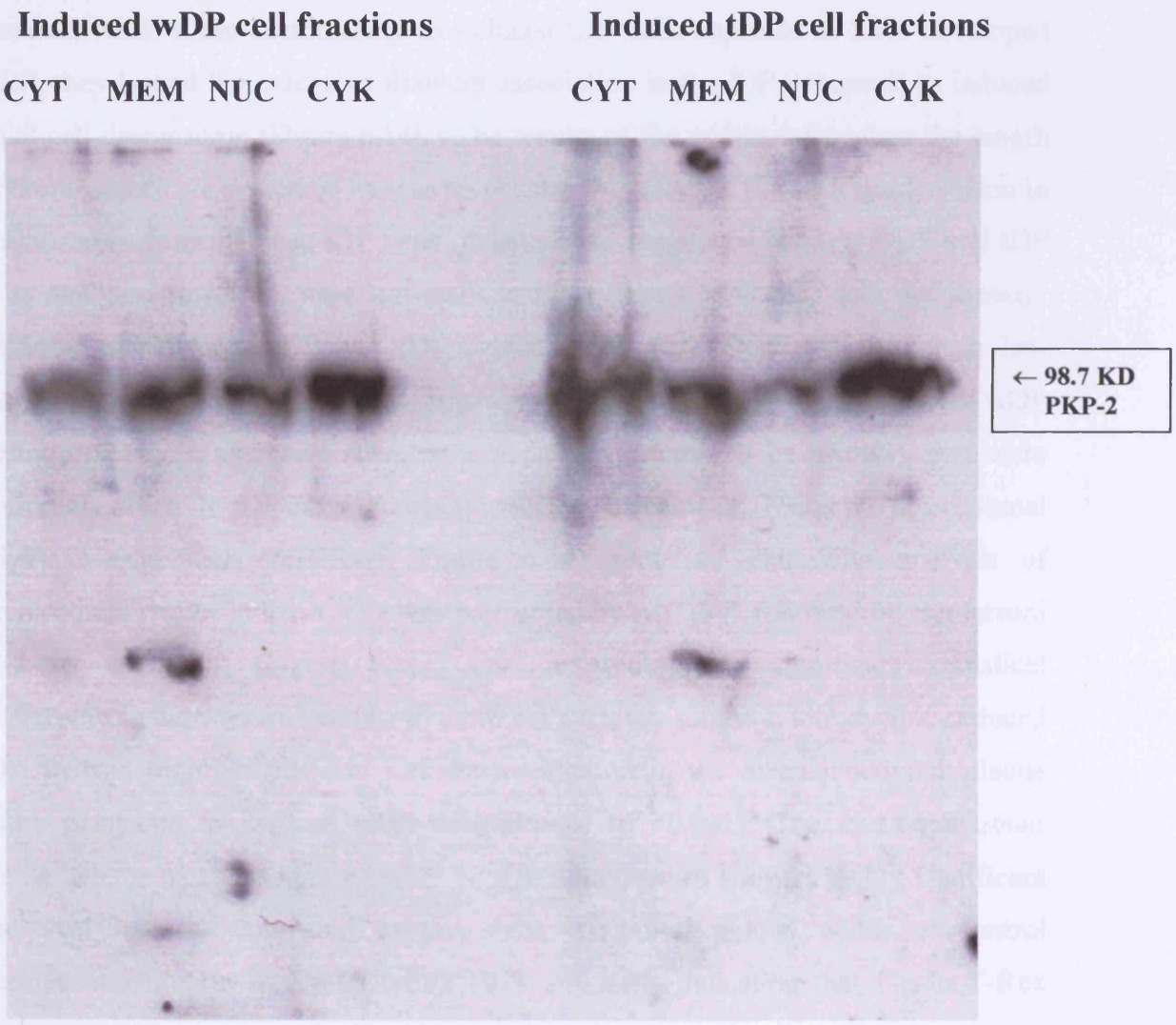

6.5.8 Examination of Desmosomes in tetracycline induced wDP and tDP cells

The gross morphology of non-transformed Flp-In T-Rex HEK 293 cells, tetracycline-induced wDP cells, and tetracycline-induced tDP cells were examined by electron microscopy at various magnifications in a Philips 201 transmission electron microscope. The identities of all three cell lines were revealed after completion of data analysis. All three cell preparations were viable with a good distribution of sub-cellular organelles (Figure 6.13). Non-transfected Flp-In T-Rex HEK 293, wDP, and tDP cell desmosomes were examined by transmission electron microscopy (Figure 6.14) at a magnification of x70000. Desmosomes in Flp-In T-Rex HEK 293 cells were not well developed as noted previously. Desmosomes in tetracycline-induced wDP cells (Figure 6.14B) showed electron dense plaques with highly extensive filament condensation in the IDP, which can extend beyond the length of the desmosome. In contrast, while some desmosomes in induced tDP cells appeared to have developed ODP, they lacked the extensive filament association in the IDP compared to induced wDP cell desmosome (Figure 6.14C) The results of the widths rather than the length of desmosomes are presented here to emphasize the effect of filament condensation in desmosomes from induced tDP cells (desmosomal lengths of induced wDP and tDP cells analyzed however, were not statistically different, $p>0.005$, data not shown). Differences between wDP and tDP desmosomes were illustrated further in low magnification (x 15000) electron micrograph (Figure 6.15) which showed wDP desmosomes with extensive filament associations (identified by arrows), that were noticeably absent in tDP desmosomes (identified by asterisks). Using the desmosomal width measurements described (Figure 6.14) statistical pair wise analysis of desmosomal widths in these cells was performed by ANOVA followed by Bonferroni post-test correction (Figure 6.16). This showed highly significant statistical differences in desmosomal widths in these cells. Desmosomes in tetracycline-induced tDP showed highly significant statistical reduction in the mean junctional plaque width compared to induced wDP desmosomes ($p <0.001$). The mean junctional plaque widths of either induced wDP or tDP desmosomes showed highly significant statistical increase compared to the mean junctional plaque width of control desmosomes present in Flp-In T-Rex HEK 293 cells indicating that Flp-In T-Rex

HEK 293 cell desmosomes are probably not efficient at recruiting filaments to their desmosomal plaques as these desmosomes are generally not well developed.

Comparisons of desmosomes in induced wPKP2 cells (Chapter 4, figure 4.21B) with those formed in induced wDP cells (Figure 6.14B) showed that whilst both desmosomes were prominent in terms of their ODP, the striking difference between wDP cell desmosomes and those in wPKP2 cells was that there was a much denser filament association in wDP desmosomes compared to those in wPKP2 cells. This was supported by desmosomal width measurements indicating a larger width of wDP desmosome (Figure 6.14B, measured width = 440nm, versus Figure 4.21B, desmosome in bottom left hand side width = 250nm). This suggests that DP over-expression probably increases the amount of DP protein recruited into the desmosomal plaque with increased condensation of intermediate filaments.

Figure 6.13 Gross morphology of non-transformed Flp-In T-Rex HEK 293 cells, tetracycline-induced wDP cells, and tetracycline-induced tDP cells

Examination of gross morphology of non-transfected Flp-In T-Rex HEK 293 control cells, and of stable wDP and tDP cells expressing full-length and Q273fsX288 DP respectively. Cells cultured on Thermanox plastic coverslips in complete DMEM were induced where required, with 0.1μg/ml tetracycline for 72 hours until they were confluent. Coverslips processed for electron microscopy (section 2.7.4) were examined in a Philips 201 electron microscope at x 2000 magnification to examine the gross morphology of these cells. The bar on each electron micrograph represents 10 μm

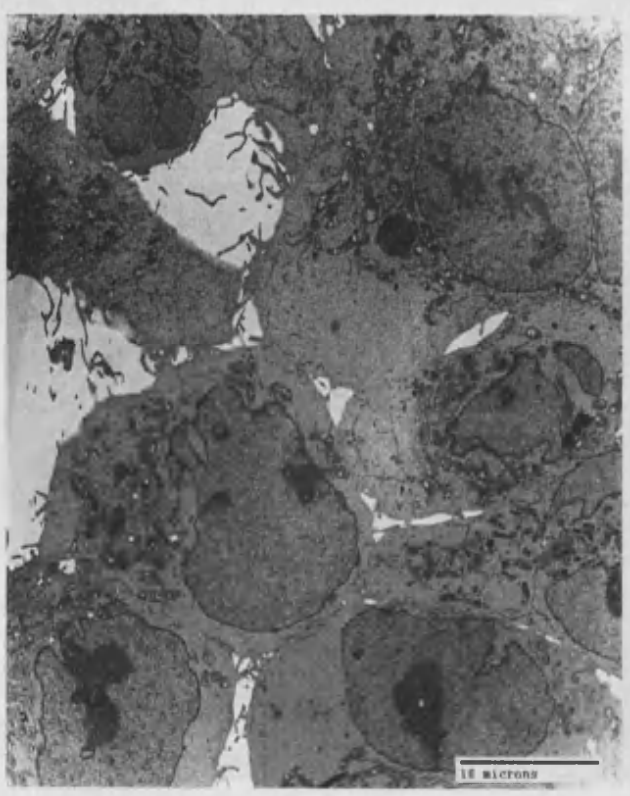

Non-transformed Flp-In T-Rex HEK 293 cells

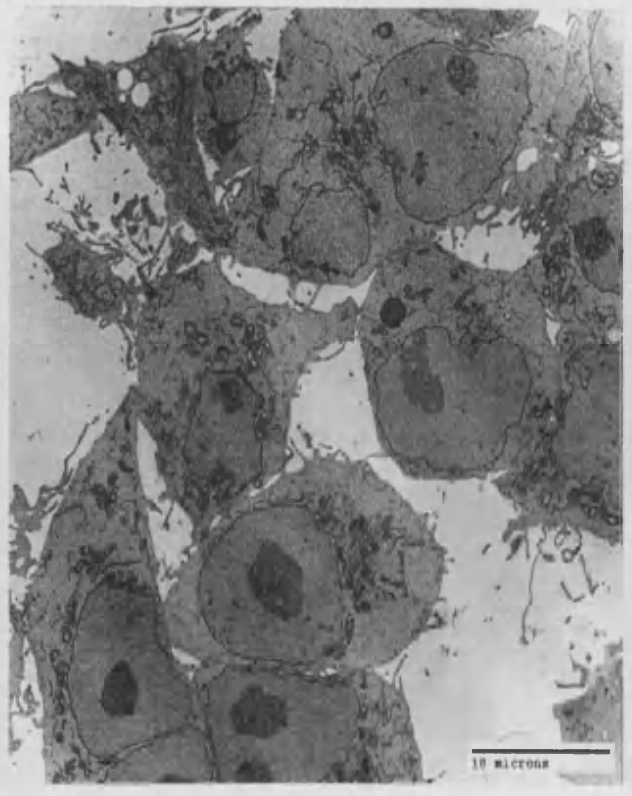

Tetracycline-induced wDP cells

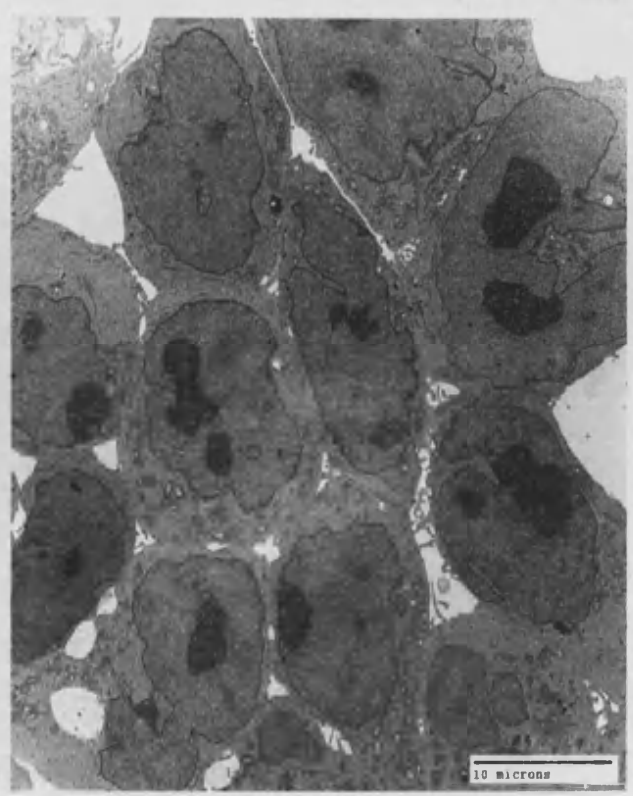

Tetracycline-induced tDP cells

Figure 6.14 Morphology of desmosomes formed in Flp-In T-Rex HEK 293, wDP and tDP cells

Electron micrographs of representative desmosomes found in highly confluent non-transfected Flp-In T-Rex HEK 293 and in tetracycline-induced wDP and tDP cells. Cells cultured on coverslips were fixed in Karnovsky style of fixative for twenty-four hours at room temperature. Ultra-thin sections (nominal 70 nm) were processed for electron microscopy (section 2.7.4) and were examined in a Philips electron microscope. All micrographs are at the same magnification (x 70000) and the size bar on each micrograph represents 100 nm. Desmosomes in induced wDP cells (B) were highly prominent with dense ODP and extensive filament association, while desmosomes in tDP cells (C) although these had developed ODP they showed less extensive filament association resulting in reduced desmosomal width. Non-transfected cells had less prominent desmosomes probably due to low level of desmosomal plaque protein recruitment. The desmosomal width measurements in Flp-In, wDP, and tDP cells is illustrated here with the widths between the two red dots in A, B, and C measured to give values of 118, 440, and 200 nm respectively. Statistical analysis of further desmosomal width measurements of these cells is shown in Figure 6.16.

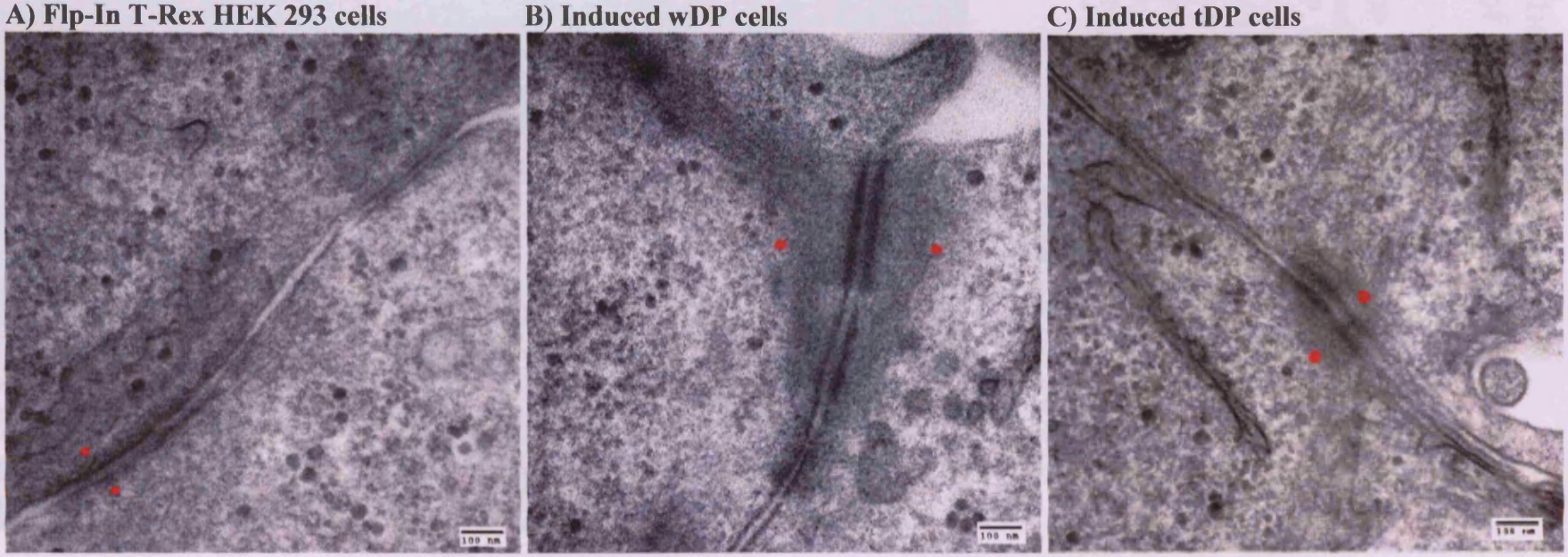

Figure 6.15 Lower magnification EM micrograph contrasting the differences of desmosomes formed in wDP and tDP cells

Examination of desmosomes in induced wDP cells. This is a representative electron micrograph of desmosomes found in wDP cells showing electron dense DS plaques with extensive filament associated in the IDP. Inset shows desmosomes from induced tDP cells at the same magnification for comparison, these desmosomes did not show the filament associations (marked by asterisks) seen in wDP desmosomes (indicated by the two arrows). Tetracycline-induced wDP and tDP cells were cultured on Thermanox coverslips for 48 to 72 hours and cells were processed *in situ* for electron microscopy. Desmosomes were examined by transmission electron microscopy in a Philips 201 electron microscope at x 15000 magnification.

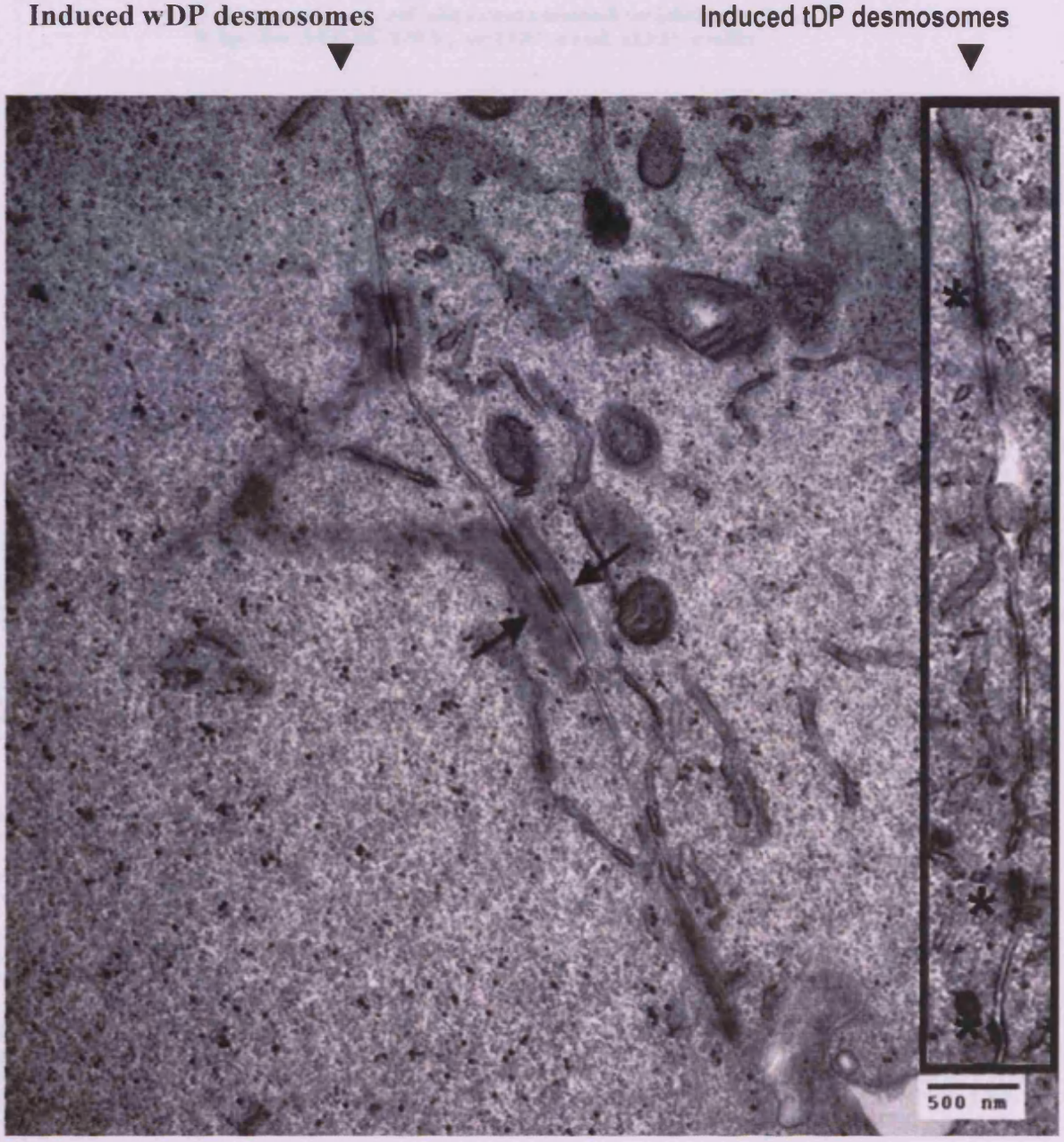

Figure 6.16 Statistical analysis of desmosomal widths in Flp-In T-Rex HEK 293 and induced wDP and tDP cells

Statistical analysis of desmosomal widths (plaque width) in Flp-In T-Rex HEK 293 and in induced wDP and induced tDP cells expressing DP and Q273fsX288 DP. Measurements of desmosomal widths (nm) were taken from electron micrographs of desmosomes obtained from each of these cells. Data were analyzed using Graph Pad Prism software using non-parametric ANOVA analysis followed by Bonferroni post-test computation of significance. The graph shows plots of individual values in each group of cells and the table below it shows results of the Bonferroni multiple comparison statistical test parameters between the three data sets obtained from Graph Pad. Pair-wise analysis showed significant differences in desmosomal widths comparing control Flp-In desmosomes with either induced wDP or induced tDP desmosomes. Desmosomal plaque width of tDP desmosomes was significantly reduced compared to wDP desmosomes. Pair wise significance levels were all at $p < 0.001$.

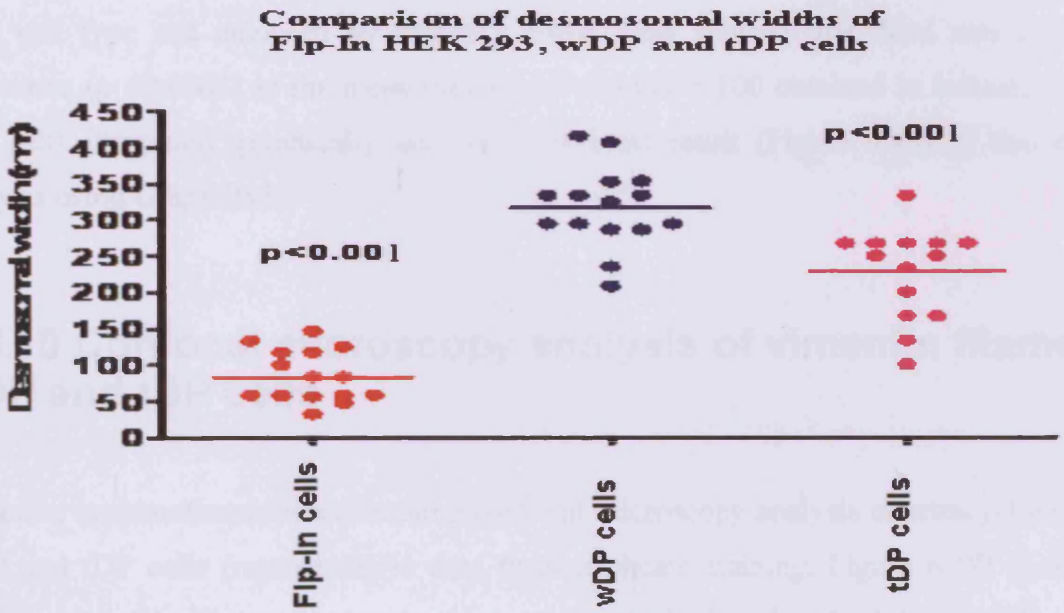

Parameter	Flp-In cells	wDP cells	tDP cells	Data Set-D
Table Analyzed				
Data 1				
One-way analysis of variance				
P value	P<0.0001			
P value summary	***			
Are means signif. different? (P < 0.05)	Yes			
Number of groups	3			
F	81.01			
R squared	0.7941			
Bartlett's test for equal variances				
Bartlett's statistic (corrected)	5.781			
P value	0.0555			
P value summary	ns			
Do the variances differ signif. (P < 0.05)	No			
ANOVA Table	SS	df	MS	
Treatment (between columns)	434700	2	217400	
Residual (within columns)	112700	42	2683	
Total	547400	44		
Bonferroni's Multiple Comparison Test	Mean Diff.	t	P value	95% CI of diff
Flp-In cells vs wDP cells	-238.0	12.58	P < 0.001	-285.2 to -190.8
Flp-In cells vs tDP cells	-150.5	7.955	P < 0.001	-197.6 to -103.3
wDP cells vs tDP cells	87.53	4.628	P < 0.001	40.37 to 134.7

6.5.9 Dispase-based cell dissociation assay of induced wDP and tDP monolayers

Highly confluent monolayers of tetracycline-induced wDP and tDP cells cultured in P_{60} culture dishes were enzymatically released from the plastic dish using Dispase II, which released intact monolayer without dissociating individual cells and these were then subjected to trituration for exactly six times. Using induced wDP and tDP monolayers handled in an identical manner described, clusters of cells in each cell line were examined photographically to assess the sizes of fragments obtained from the two groups of cell. Larger fragments were obtained in induced wDP monolayers than from induced tDP monolayers (Figure 6.17). The number of clusters with >100cells/fragment were counted (using a dissecting microscope) in each cell type and analysed by student's t-test. This showed that there was a statistical difference ($p < 0.0001$) in the mean number of clusters > 100 obtained in induced wDP and tDP cells illustrated graphically and with tabulated result (Figure 6.18) of the statistical analysis using Graph Pad.

6.5.10 Confocal microscopy analysis of vimentin filament in wDP and tDP cells

Vimentin immunofluorescence staining confocal microscopy analysis of tetracycline induced wDP and tDP cells (representative data from triplicate staining, Figure 6.19) showed that whereas vimentin filament networks were present in both induced wDP and tDP cells, the vimentin filaments localized extensively between induced wDP cells (Figure 6.19A). In induced tDP cells however, vimentin filaments appeared to be associated within individual cells, but did not appear to connect with adjacent tDP cells (Figure 6.19B).

Figure 6.17 Dispase-based induced wDP and tDP monolayer dissociation adhesion assay

Adhesive strength of tetracycline-induced wDP and tDP confluent monolayers measured using a Dispase-based cell dissociation assay[212]. Each cell line was cultured in 60 mm Nunc plastic culture dishes in penicillin, streptomycin, fetal bovine serum, blasticidin and hygromycin supplemented DMEM (Invitrogen 19308-025) in the presence of 0.1μg/ml tetracycline until cells were highly confluent. Medium was decanted from each dish and the monolayer was gently rinsed in 5 ml PBS. One ml of 2.4U/ml Dispase II (Roche, Cat No 10295835001) was added to the dishes followed by incubation at 37°C for 30 minutes. The released monolayer released was carefully rinsed in PBS without agitation and one ml of PBS was added. The monolayer was subjected to shear stress by trituration (six times) through a P1000 (one ml pipette tip). The triturated cell monolayer sample was photographed under Epi-white light illumination in BioRad Gel Documentation system (gel doc XR) using quantity one version 4.6 image analysis software. Triturated tDP monolayer resulted in significantly decreased number of cell clusters (>100 cells) compared to those obtained in triturated wDP cell monolayer indicating that tDP cells were prone to increased fragmentation resulting in smaller fragments after shearing compared to those seen in wDP cells.

A) Triturated tetracycline-induced wDP monolayer → forms larger fragments

No of cell clusters>100cells/0.15ml sample (triplicate counts/sample):

95, 93, 97 105, 109, 110 117, 113, 115

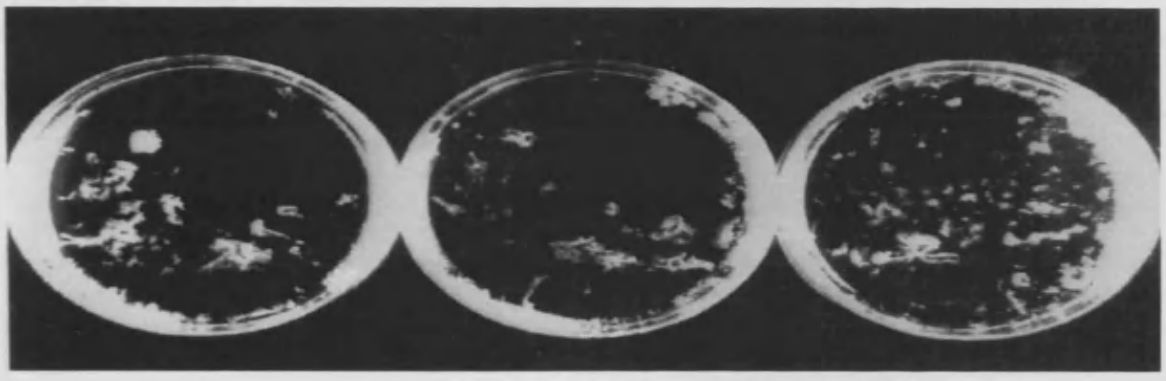

B) Triturated tetracycline-induced tDP monolayer → forms smaller fragments

No of cell clusters>100cells/0.15ml sample (triplicate counts/sample):

10, 11, 9 13, 15, 16 19, 19, 18

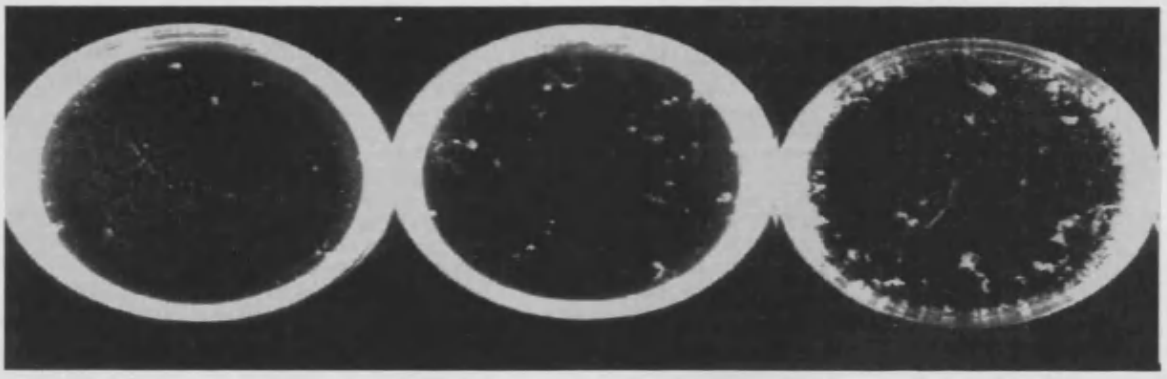

Figure 6.18 Analysis of Dispase-based wDP and tDP monolayer dissociation adhesion assay

Data obtained in figure 6.15 was analyzed using Graph Pad and is illustrated graphically (mean ± SD). Statistical student's t-test analysis showed significant reduction in the mean value of clusters >100 cells in induced tDP cells compared with the mean value obtained in induced wDP cells ($p<0.0001$) as shown in the table.

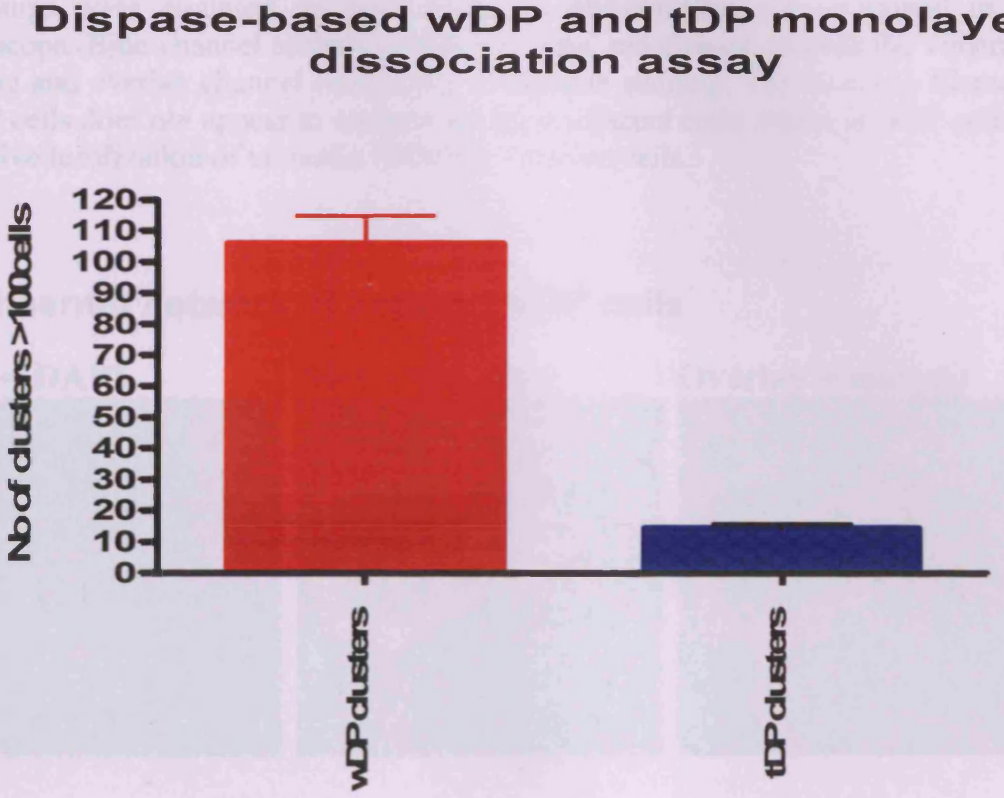

Parameter	Value
Table Analyzed	Data 1
Column A	wDP clusters
vs	vs
Column B	tDP clusters
Unpaired t test	
P value	P<0.0001
P value summary	***
Are means signif. different? (P < 0.05)	Yes
One- or two-tailed P value?	Two-tailed
t, df	t=28.03 df=16
How big is the difference?	
Mean ± SEM of column A	106.0 ± 3.000 N=9
Mean ± SEM of column B	14.44 ± 1.292 N=9
Difference between means	91.56 ± 3.266
95% confidence interval	84.63 to 98.48
R squared	0.9800
F test to compare variances	
F, DFn, Dfd	5.390, 8, 8
P value	0.0282
P value summary	*
Are variances significantly different?	Yes

Figure 6.19 Examination of Vimentin intermediate filament network in wDP and tDP cells by confocal microscopy

Confocal microscopy examination of tetracycline-induced wDP and tDP stable cells stained for vimentin. Cells were cultured on plastic coverslips in the presence of tetracycline (0.1μg/ml) to induce over-expression of full-length and Q273fsX288 DP. Cells were cultured for forty-eight hours and fixed in 4% formaldehyde/PBS for ten minutes. Following washing of the cells, they were permeabilised in 0.1 % triton X-100 for five minutes and then blocked in 10 % fetal bovine serum in PBS for thirty minutes. Cells were incubated in 1:200 mouse monoclonal anti-vimentin (Santa Cruz Biotechnology, sc-6260) for one hour. Following washing of cells in TBST buffer they were incubated in DAPI solution to stain nuclei. Coverslips were mounted on glass slides in glycerol/PBS and examined in a confocal microscope. Blue channel records nuclear staining, red channel records the vimentin network staining and overlay channel records the composite staining. The vimentin filament network in tDP cells does not appear to connect between adjacent cells, whilst in wDP cells there is an extensive localization of vimentin filaments between cells.

A) Vimentin network of induced wDP cells

B) Vimentin network of induced tDP cells

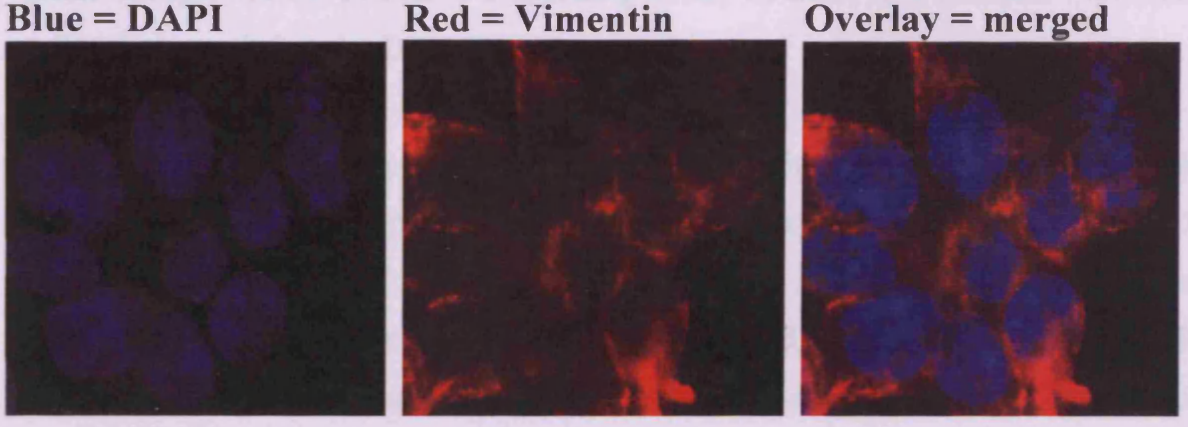

6.5 Discussion

Three lines of experimental evidence indicated that localization and interaction of either endogenous PG or PKP-2 with truncated DP was not adversely affected at the site of induced tDP cell-cell contacts. Firstly, the immunofluorescence staining co-localization of either endogenous PG or PKP-2 with either DP or Q273fsX288 DP in induced wDP or tDP cells did not appear to be significantly different in these cells. Secondly, IP analysis of detergent soluble cell lysates from wDP and tDP cells did not show significant differences in the amounts of either endogenous PG or PKP-2 interacting with either DP or Q273fsX288 DP, although it could be argued that endogenous DP I and DP II proteins expressed at basal levels in induced tDP might conceal differences in binding of endogenous PKP-2 or PG to Q273fsX288 DP alone. However, immunoprecipitation of induced wDP and tDP soluble cell lysate with goat anti-DP antibody showed that DP immunoprecipitated in lysates from induced wDP cells, but in induced tDP cell lysates the antibody predominantly immunoprecipitated Q273fsX288 DP rather than endogenous DP, suggesting that immuno-complexes formed between either PG or PKP-2 with Q273fsX288 DP might be present in a greater amount than the immuno-complexes formed by endogenous DP either because of reduced recruitment of endogenous DP into plaques of induced tDP cells (probably resulting from a dominant negative effect of Q273fsX288 DP) or less likely because of reduced solubility of larger complexes formed by endogenous DP proteins. Therefore, the immunoprecipitated endogenous PG and PKP-2 in induced tDP cell lysates probably represent interactions mainly with the DP polypeptide. Thirdly, in each of the four protein fractions enriched for cytoplasm, membrane, nuclear and cytoskeletal compartments obtained from induced wDP and tDP cells there were no significant differences in the amounts of either endogenous PG or PKP-2 associating in any of these four fractions from induced tDP cells relative to induced wDP cells.

Endogenous DP (DPI/II) proteins are expressed constitutively in wDP and tDP stable cells and these DP proteins are present together with over-expressed DP I and Q273fsX288 DP in tetracycline induced wDP and tDP cells respectively. It was not possible to determine the extent of incorporation of endogenous DP and truncated DP into desmosomes of tDP cells by immuno-electron microscopy using a goat polyclonal antibody (Santa Cruz Biotechnology, sc-18082) directed against a twenty amino acid sequence near the N-terminus of DP as the

antibody reacts with both endogenous DP and truncated DP. A tagged expression of DP polypeptide might discriminate the relative incorporation of this DP polypeptide and endogenous DP proteins present. The relative incorporation of DP polypeptide into cell-cell contacts of induced tDP cells should determine the extent of displacement of endogenous DP in induced tDP cells, however, although this was not examined in this study, it was evident that expression of truncated DP in induced tDP cells caused a **dominant negative** effect on desmosome morphology, as these desmosomes lacked the extensive filament association found in control induced wDP cell desmosomes. The smaller widths of induced tDP cell desmosomes relative to induced wDP desmosomes appear to reflect a varying degree of disruption of IF assembly in the IDP of desmosomes formed between induced tDP cells probably resulting from a displacement of endogenous DP assembly. The mechanism for the dominant negative effect of Q273fsX288 DP expression in induced tDP cells might involve the preferential recruitment of the small DP polypeptide, which might be present in molar excess in this induced cell expression system compared to endogenous DP protein (assuming Q273fsX288 DP does not affect the expression level of the endogenous DP proteins). The preferential recruitment of Q273fsX288 DP into desmosomes might also result from the loss of adjacent N-terminal sequence found in full-length DP, which might influence the insertion of the DP polypeptide into desmosomes. Q273fsX288 DP is deficient in the coiled-coil rod and the plakin repeat domains, and therefore, this polypeptide cannot directly support the assembly and attachment of intermediate filaments. The coiled-coil rod of DP is important for DP dimerization and also stabilizing interactions with vimentin intermediate filament proteins, whilst the plakin repeat domains of DP are important in determining the specificities of IF protein binding to desmoplakin in different cells.

As discussed in the previous two chapters, several different intermediate filament proteins are expressed in HEK 293 cells, but desmin a cardiac IF protein was absent. HEK 293 cells express abundant amount of vimentin IF protein[227]; this protein can be recruited into the IDP of desmosomes via its interaction with the C-terminus PRD in DP and robust alignment of DP with vimentin IF networks in transient transfection assays requires DP rod domain[131,132], suggesting that the interaction of full-length DP and vimentin may be strengthened considerably by the formation of DP coiled-coil dimer. Examination of vimentin IF protein network in induced wDP and tDP cells by immunofluorescence staining confocal microscopy revealed that whereas this IF network was present in both induced wDP and tDP cells, it was

extensively localized between induced wDP cells, but not between induced tDP cells. Although the clustering of desmosomal cadherins in induced tDP cell-cell contacts is assumed to occur normally in induced tDP cell-cell contacts (these are promoted by PG mediated interactions with the cytoplasmic tail of desmoglein-desmocollin heterodimers[252], Figure 1.6d), the incorporation and assembly of Q273fsX288 DP polypeptide into the cytoplasmic plaque appears to uncouple vimentin filament attachment at sites of induced tDP cell-cell contacts whilst maintaining apparently normal interactions between either PG or PKP-2 and this DP polypeptide.

The role of IF network assembly in regulating the cell-cell adhesive strength has been demonstrated in an inducible stable cell variant of A431 expressing a FLAG-tagged truncated N-terminus 584 amino acid DP polypeptide, which led to dissociation of Kertin8/18 IF from the junctional plaque[212]. These induced A431 cells readily dissociated in Dispase-based monolayer dissociation assays, suggesting that loss of proper IF assembly affects tissue integrity. The vimentin IF network in induced tDP cells may not be completely uncoupled (for example, in the electron micrograph of Figure 6.14C some filament association is seen in the IDP of an induced tDP desmosome). This could be because some endogenous DP present in these cells could either assemble in competition with Q273fsX288 DP into induced tDP desmosomes or other accessory proteins known to interact with IF proteins *in vitro*, such as PKP-2, might augment the recruitment of vimentin in the absence of full-length DP incorporation into desmosomes. Using the Dispase-based monolayer dissociation assays the fragmentation of tDP and wDP monolayers were examined after shearing. This resulted in formation of smaller fragments in induced tDP cells while larger fragments formed in induced wDP cells, this together with the data obtained from vimentin filament organization in induced tDP cells provides supportive evidence suggesting that disrupted vimentin-IF network in induced tDP cells compromise their adhesive strength.

The extent of interference from endogenous DP proteins in co-IP reactions of induced tDP cell lysates for determining interactions of Q273fsX288 DP with either endogenous PG or PKP-2 proteins appears to be small, but theoretically, this problem can be avoided by the use of tagged Q273fsX288 DP expression in cell lines. However, the cloning of DP into a tagged expression vector was not performed because of technical problems with cloning of full-length DP DNA. Plasmid P1140 contained nucleotide sequence encoding a FLAG epitope

located at the C-terminal end of the cloned DP gene and this plasmid could allow examination of FLAG-tagged DP pull down assays in HEK 293T cells using an anti-FLAG antibody. However, it was not possible to obtain a plasmid encoding truncated DP with a C-terminal FLAG tag directly from plasmid P1140 using SDM PCR as the nucleotide sequence for the FLAG tag is situated downstream of the nucleotide sequence encoding the frame-shift, which therefore, would not lead to the translation of Q273fsX288 DP containing a FLAG tag at the C-terminal end of the DP polypeptide. Other plasmid vectors with a C-terminal FLAG tag were not commercially available, however vectors containing a FLAG tag located at the N-terminus of a multiple cloning site were available and it would have been relatively easy to clone in a DNA fragment encoding Q273fsX288 DP, but this approach was impractical as a FLAG epitope located at the N-terminal end of desmoplakin or its fragments disrupt important protein-protein interactions (personal communication, Lisa Godsel, Northwestern University, USA) of these proteins. Therefore, for the purpose of this study, stable wDP and tDP cells were used for examining interactions of either full-length or truncated DP with either endogenous PG or PKP-2 with an antibody directed against DP suitable for immuno-precipitation studies.

Early studies using ectopic expression of DP I carboxy terminus alone or in combination with the rod domain showed that these DP polypeptides co-aligned with and disrupted the IF network in COS-7 and NIH 3T3 cells, but neither of these polypeptides appeared to incorporate into desmosomes suggesting that 1056 amino acid (90 KD) N-terminal globular head domain of DP (Figure 1.10) could be necessary for the localization of DP into the desmosomal plaque[132]. The role of the DP N-terminus in targeting DP to the desmosomal plaque was investigated by studies showing that the expression of the first 584 amino acid fragment of DP (DP-NTP, 70 KD) co-localized this DP polypeptide at A431 cell-cell contacts with PG, DSC-2 and DSG[217,252]; and in COS-7 cells DP-NTP was shown to co-localise with PKP-1 including its head domain wherein these interactions were confirmed by yeast two hybrid analysis[253]. Additionally, the ectopic expression of N-terminal DP polypeptides in COS-7 cells using plasmids encoding N-terminal deletions of DP demonstrated that the first 194 amino acids in DP N-terminus were essential for integrating DP into the desmosomal plaque[131]. Fine mapping studies of amino acid sequences within DP N-terminal subsequently revealed that amino acid residues between 86 to 176 are essential for efficient desmosomal recognition of DP in keratinocytes, with the first 29 residues being critical[254] for this function.

These studies support the contention that Q273fsX288 DP should contain the requisite sites for desmosomal targeting. The data obtained from studies with Q273fsX288 DP suggests that this DP polypeptide can co-localize with PG and PKP-2 plaque proteins in the ODP of induced tDP cell-cell desmosomal contacts and that the DP polypeptide can interact normally with these two plaque proteins as shown by co-IP studies. The recruitment and insertion of Q273fsX288 DP, however, appears to disrupt vimentin intermediate filament condensation within the inner plaque region of induced tDP desmosomes. This implies that Q273fsX288 DP acts in a dominant negative manner disrupting the assembly and linking of the intermediate filament network between neighbouring induced tDP cells.

Stable A431 epithelial cell lines fortuitously expressing DP-NTP showed this polypeptide assembled together with other desmosomal proteins into distinct junctions at cell-cell contacts, but severely dissociated endogenous DP binding to cell-cell contacts with associated loss of keratin intermediate filament attachment[217]. Ultrastructure of desmosomes in these cells showed that they possessed a central dense stratum and an ODP, but the associated filaments present in the IDP of normal desmosomes were absent. This study supported the proposal that DP-NTP acted in a dominant negative manner interfering with assembly of endogenous DP in A431 cell-cell contacts shown to be disrupted by cellular localization and biochemical analysis[217]. A range of junctional structures were reported to coexist in these A431 stable cells, ranging from oversized desmosomes containing large amounts of endogenous DP and associated IF bundles to structures containing DP-NTP but little endogenous DP and largely lacking IF coupling[217]. The data obtained from induced tDP stable cell line are in agreement with data from A431 cells in so far as showing disruption of the vimentin filament network in tDP cells (versus disruption of keratin filaments in A431), and desmosome ultrastructure of tDP cells suggesting that not only were some desmosomes deficient in filament association in the IDP, but also that some desmosomes appeared to incorporate filaments to a varying extent as indicated by the distribution of desmosomal widths in induced tDP cells and their differences with the desmosomal widths of induced wDP cells. Induced tDP desmosomes, however, appeared to differ from A431 desmosomes, as oversized desmosomes were not observed in induced tDP stable cells. Evidence supporting the displacement of endogenous DP in desmosomal plaque of tDP cells has not been obtained, but the disruptive effect on vimentin filament network with the associated effect on desmosomal widths in these cells is highly suggestive.

An association of DP-NTP with adherens junction proteins reported in A431 cells[217] suggested lateral co-assembly of DS and AJ junctions. The interaction of E-cadherin, α-catenin and β-catenin with Q273fsX288 DP was not examined in induced tDP cell lysates and therefore, it remains unknown whether the segregation of DS and AJ junctions of tDP cells could be affected; this however seems unlikely as "mixed-type" or oversized cell-cell junctions were not observed by transmission electron microscopy examination of induced tDP cells. In support of this observation in induced tDP cells, a study previously described using a Tet-On A431 inducible stable cell expression of FLAG-tagged DP-NTP [212] showed that "hybrid junctions" with the intermingling of AJ and DS junctions did not occur in these cells .

Interestingly another mutation 40 amino acids downstream of Q273fsX288 DP (i.e. p.W233X DP, c.699G>A DP) found in an ARVC patient from a North American ARVD registry showed that an mRNA encoding this truncation was not present in cDNA amplified from lymphocytes from the affected patient suggesting that the mRNA transcript probably undergoes NMD. Expression of W233X DP protein in a desmosome forming human tongue squamous carcinoma cell line showed the formation of perinuclear aggregates of this protein, but it neither localised at cell-cell contacts nor was it present diffusely in the cytoplasm[163]. Q273fsX288 DP also was associated with the nuclear protein fraction in induced tDP; this might suggest a probable localization of the DP polypeptide around the nuclei of induced tDP cells.

6.6 Summary of main findings of the study

Plasmids encoding full-length DP DNA and Q273fsX288 DP DNA were prepared in pcDNA5 vectors. Using pcDNA5 plasmids, two stable cell lines were established using Flp-In T-Rex HEK 293, one of these cell lines, **wDP,** expressed full-length DP, and a second cell line, **tDP,** expressed truncated DP.

A strong tetracycline-induced expression of full-length DP (with a predicted size of 331.8 KD and apparent SDS PAGE migration size of 250 KD) occurred in wDP cells that was localised at sub-membranous sites of cell-cell contacts by confocal immunofluorescence staining. Sub-cellular protein fractionation of induced wDP cells followed by western immunoblotting

analysis confirmed that full-length DP was primarily found in the cytoskeletal protein fractions.

A strong tetracycline-induced expression of Q273fsX288 DP (predicted and apparent SDS PAGE migration size of 33 KD) occurred in tDP cells, which localized in a punctate staining pattern at sites of cell-cell contacts by confocal immunofluorescence staining. Sub-cellular protein fractionation of induced tDP cells followed by western immunoblotting analysis indicated presence of Q273fsX288 DP in cytoplasm, membrane, nuclear and cytoskeletal protein fractions. The localization of Q273fsX288 DP differed from that of full-length DP as the former was associated in the cytoskeletal and the membrane, but the later was primarily found in the cytoskeletal fraction protein fraction. The presence of Q273fsX288DP in the nuclear protein fraction suggests that this DP polypeptide might be present in the perinuclear region.

Induced wDP and tDP cells proliferated at similar rates to non-induced wDP and tDP cells. Tetracycline-induced wDP and tDP cells recovering from exposure to mechanical stretch showed no statistically significant difference in induced apoptosis. These data indicated that cell proliferation and the apoptosis were not affected by the expression of the truncated DP polypeptide.

No apparent differences in the immunofluorescence staining co-localization of either endogenous PG or PKP-2 proteins with DP and Q273fsX288 DP were observed in induced wDP and induced tDP cells respectively. Immunoprecipitation analysis showed no significant differences in the interactions of either endogenous PG or PKP-2 proteins with DP and Q273fsX288 DP in cell lysates obtained from induced wDP and tDP cells respectively; and analysis of sub-cellular protein fractions obtained from induced wDP and tDP cells supported these findings as the distributions of either endogenous PG or PKP-2 did not appear to be altered significantly in the cytoplasm, membrane, nuclear and cytoskeletal compartments of these induced cells.

Examination of vimentin filament network in induced tDP and wDP cells showed that while these were developed in both cell types, vimentin filaments appeared to connect extensively neighbouring cells in induced wDP cells but this was not the case in induced tDP cells.

Examination of Flp-In T-Rex HEK 293, induced wDP and induced tDP cells showed that whilst desmosomes formed in Flp-In cells these were not prominent. Desmosomes in induced wDP were highly prominent with dense plaques and extensive filament localization affecting their plaque widths. The filament organization in desmosomes from induced wDP cells can extend beyond the length of the desmosomes. In contrast, however, desmosomes in tDP cells compared to those in wDP cells had varying desmosomal plaque widths including many desmosomes with little or no filament condensation; this affected their measured plaque widths. The measured desmosomal plaque widths of Flp-In T-Rex HEK 293, induced wDP, and induced tDP cells showed highly significant statistical differences (p value < 0.0001) with mean desmosomal width of wDP cells being greater than the mean value in tDP cells, while the mean widths of wDP and tDP desmosomes were each greater than the mean value in Flp-In T-Rex HEK 293 non-transformed cells.

Consistent with the observed disruption of vimentin filament network in induced tDP cells, a Dispase-based monolayer dissociation assay showed a statistically significant increased fragmentation of sheared induced tDP2 monolayer compared to those of induced wPKP2 monolayer.

6.7 Future Studies

The effects of Q273 fsX288 DP should be examined in other cell systems, such as SSC9, MDCK, and A431 cells, which allow better morphological co-localization data to be obtained by immunofluorescence confocal microscopy. These cells form robust desmosomes and comparison between non-transfected and transfected cells should allow the effect of Q273fsX288 DP on the ultrastructure of desmosomes to be verified in these cells. SSC9, MDCK and A431 cells express different intermediate filament protein from vimentin expressed in tDP cells, therefore examination of the effect of Q273fsX288 DP on other IF protein assembly (for example, keratin) in these cells may support the findings in tDP cells. Rat neonatal cardiomyocytes may be used to assess the significance of the findings from tDP cells in a cardiac relevant cell culture model; this may however, require expression of full-

length DP and truncated DP using viral vector expression systems to obtain optimum expression of these proteins.

Q273fsX288 DP appears to exert a dominant negative effect in induced tDP cells, sharing similarities with an inducible A431 cell line expressing a 70 KD fragment of DP-NTP. The apparently normal interaction of Q273fsX288 DP with PG and PKP-2 in induced tDP cells needs to be verified by yeast two hybrid studies. The assumed displacement of endogenous DP in desmosomal plaques of induced tDP cells should be examined by several approaches: firstly a biochemical approach should allow the relative amounts of Q273fsX288 DP and endogenous DP to be determined, and if needed this might be modulated by changing the concentration of tetracycline used during induction of tDP cells, secondly, an immunofluorescence staining confocal microscopy examination of the localization of endogenous DP and Q273fsX288 DP in induced tDP cells must be carried out using differential staining using anti-DP antibodies directed against the N-terminus, C-terminus and the rod domains (for example, antibodies NW161, NW6 and DP2.15 respectively can be used[217]) to determine the extent of endogenous DP displacement in these cells, thirdly, an immuno staining electron microscopy examination would verify the extent of redistribution of endogenous DP in these cells, with non-induced tDP cells serving as an appropriate control for immunoelectron microscopy studies. The final fourteen amino acid residues in truncated DP are unique (peptide sequence in Q273fsX288 DP: EHHSGHVQGDHVDQ, sequence in full-length DP: NIIQATSREIMWIN) and this might make it feasible to raise monoclonal antibodies allowing the differential recognition of truncated DP and endogenous DP binding. Using different sized gold particle-conjugated to these monoclonal antibodies specific for these peptide sequences the localization of Q273fsX288 DP by immunoelectron microscopy and determination of the relative extent of endogenous DP displacement within desmosomes of induced tDP cells might be possible. The staining for cortical actin using rhodamine-conjugated phalloidin needs to be performed in induced tDP cells and non-induced tDP cells as a control to determine whether there might be an alteration in the cortical actin microfilament system of cells expressing Q273fsX288 DP.

It is not known whether c.818_819insA DP gene mutation found in family I (section 3.4.1 part 2.7) causes haploinsufficiency resulting from nonsense mediated degradation of mRNA transcript encoding the truncated DP polypeptide, this seems quite likely as many mRNA

transcripts encoding frameshift are efficiently targeted by the NMD machinery. The c.818_819insA DP gene mutation has not been reported in further patients in different cohorts examined, however further cascade screening of family I, may in the future, provide sample of cardiac tissue from an affected individual that would allow protein and cDNA studies to examine whether NMD with haploinsufficiency is a plausible mechanism for the cardiomyopathy seen in affected patients. A heterozygous transgenic mouse model encoding the c818-819ins A DP would be a feasible *in vivo* model system to examine the effect of expression of mutant DP protein from one defective copy of the DP gene.

Chapter 7

Discussion and future direction

7.1 Compare and contrast molecular roles of PKP-1 and PKP-2 in desmosomes

PKP-2 is a predominant plakophilin isoform expressed in the human heart (p0071/PKP-4 is also present, but its role in the heart is not clear), however because of the similarities (structural homology and conserved functions) with PKP-1, the role of PKP-1 in desmosomes is first discussed. The general structure of PKP-1 and PKP-2 is identical consisting of a basic charged head domain, which is considerably larger in PKP-2, but shares only a 25% sequence identity apart from a bipartite HR2 element at the very end of the N-terminus[221,255]. This is followed by successive ARM repeats forming a superhelix of helices consisting of positively charged grove, and a very short carboxy-terminal extension. The ARM repeat domains are composed of ten repeat units one of which is a large insert producing a characteristic kink resulting in a sickle shape in these proteins[184]. PKP-1 and PKP-2 share 42% overall identity with each other however, the homology in their ARM domains is high (70%)[255].

The last 40 amino acids in the carboxyl terminus of PKP-1 are required for its localization in the plasma membrane while residues at the very beginning of the N-terminal are necessary for recruiting DP to the membrane and desmosome assembly[222]. PKP-1 is strongly expressed localizing in desmosomes found in the suprabasal layer of stratified epithelia, certain complex epithelia, and the urothelium. PKP-1 promotes lateral clustering[253] of desmosomal protein complex, provides stability to the structure[256] and controls desmosome size[257] by binding tightly to desmoplakin to augment desmoplakin recruitment to sites of cell contact[258]. Genetic defect in PKP-1 reduces desmosome stability and size in the skin and increased keratinocytes migration[259]. PKP-1 acts co-operatively with plakoglobin to promote clustering of desmosomal plaque complexes at cell-cell contacts[260]. A study examining the contribution of different domains of PKP-1 proteins binding to desmosomes in HaCaT cells showed that the head domain was essential for targeting it to desmosomes and enhancing recruitment of desmoplakin, desmoglein, desmocollin, and plakoglobin. While the ARM domain of PKP-1 can associate with actin microfilaments, full-length PKP-1 preferentially localizes to desmosomes[257].

PKP-2 is found in desmosomes of virtually all cell types, including simple one-layered epithelia and non-epithelial tissues such as the myocardium and Purkinje fibres of the heart

and the dendritic reticulum of lymphatic system. It is also present in basal proliferative cells of most multilayered epithelia such as the mucosal lining of stomach, oesophagus, and vagina and in cornifying stratified squamous epithelium of the skin. PKP-2 has a broad repertoire of binding partners of desmosomal as well as non-desmosomal origin. Proteins which have been reported to interact with PKP-2 include DSG-1, DSG-2, DSC2a, PG, DP, p0071/PKP-4, β-catenin, αT-catenin, and E-cadherin PKCα[183,246,249,260], but PKP-2 is less efficient than PKP-1 at recruiting DP and other desmosomal proteins to cell membranes[183,260]. PKP-2 is not known to increase DP content or affect desmosomal size, but it appears to be important in trafficking DP to the plasma membrane via non-membranous assembly-competent particles formed in close association with keratin filaments[216]. Although the ARM repeats of PKP-2 shares structural homology with the ARM repeats in $p120^{ctn}$ and PG no binding partners have been identified for these repeats in PKP-2. All the inter-protein interactions involving PKP-2 appears to occur via its globular head domain[184].

PKP-2 as well as PG, DP, DSC2 and DSG2 appear to co-localise at desmosomal and adherens junctions in the ID of cardiomyocytes as shown by recent immunoelectron microscopy studies revealing that, at ID, desmosomes and facia adherentes structures form a highly integrated system called the area composita. The exclusive localization of proteins specific only for desmosomes and adherens junctions is largely lost[137,138,244] in this structure. In the area composita cardiomyocytes form multiple interactions between protein assemblies belonging to classical desmosomal and adherens junction origins – resulting in a complex and interlinked association between different molecular components that is different and distinctive from polar epithelial cells that possess discrete and separate entities of these two adhering type of junctions. The complex intermolecular interactions in the area composita are believed to be superimposed by a unique interaction between PKP-2 and α-T-catenin which has been proposed to bridge the actin microfilaments and desmin intermediate filament networks[260]. PKP-2 also associates with β-catenin, a protein normally associated only in adherens junction, and this potentially might influence β-catenin signalling or the assembly of cell-cell junctions[183].

PKP-2 has a fundamental function in desmosome assembly and maintenance of tissue integrity. The importance of PKP-2 in heart morphogenesis was demonstrated in PKP-2 null-mice which showed lethal cardiac damage[190] at mid-gestation resulting in absence of

desmoplakin from virtually all cell-cell junctions, thus emphasizing that PKP-2 was important in the assembly of junctional proteins in the ID. PKP-1 mutations manifest in cutaneous defects, but PKP-2 mutations cause ARVC[40,41,46,107,108,110,112,207,262] associated with fibro-fatty replacement of cardiomyocytes, ventricular tachyarrhythmias and sudden cardiac death (section 1.1.1), but these mutations do not manifest cutaneous defects presumably due to redundant functions of these plakophilin proteins in the skin. Mutations in PKP-2 appear to be the most common amongst the five major desmosomal proteins (section 1.8.3 and Table 1.5) and are linked to ARVC with a propensity for early onset of symptoms and arrhythmias[108]. In the genetic screening of the ARVC cohort mutations were found in eight out of one hundred (8%, section 3.4.1 part 1.4) patients. It has been speculated that lack of PKP-2 resulting from haploinsufficiency and the insertion of a mutant PKP-2 protein into cardiac desmosomes could impair cell-cell adhesion by loss of function of PKP-2 protein, resulting in disruption of adjacent cardiomyocyte cell-cell junctions particularly in response to inappropriate mechanical stress (for e.g. during intense competitive sports). However, direct evidence supporting this concept is lacking and functional studies performed (Chapters 4, 5, and 5) have attempted to shed light on how expressions of three different mutant proteins could be linked with changes observed in desmosomes and cellular functions.

7.2 Lessons learned from plakophilin-2 mutant protein expression functional studies

PKP-2 gene mutations c.2197-2202_delCACACC_insG and c.C1604T resulting in protein truncation p.A733fsX740 PKP-2 and formation of a missense p.S140F PKP-2 protein each caused autosomal dominant ARVC in affected patients. These mutant PKP-2 proteins were expressed in stable HEK 293 cells under tetracycline-induced condition and the effect of each mutant protein expression was examined *in vitro* to provide functional evidence linking defects in these PKP-2 proteins with alteration in desmosomal structure and/or cell function. Both PKP-2 proteins affected desmosomes, but produced different structural changes as well as functional effects at a cellular level because of domain specific alterations in these mutant PKP-2 proteins (Table 3.4). Altered desmosomal structures and cellular characteristics seen in induced cell lines may offer possible mechanisms to explain the cardiomyopathy seen in affected individuals. Although A733fsx740 PKP-2 expression can exert dominant negative effects on desmosomes *in vitro*, it is possible that the c.2197-2202_delCACACC_insG PKP-2

gene mutation may cause haploinsufficiency due to NMD of the transcript formed by PKP-2 gene expression from the affected allele, and this might be a predominant mechanism for the cardiomyopathy in affected patients. The lack of Cx-43 gap junction protein localization within cell-cell contacts of induced tPKP2 cells provides a potential mechanism for the arrhythmia seen in ARVC and is supported by recent studies defining the roles of PKP-2 in maintaining the structures at the ID[242] and coordinating the assembly of Cx-43 gap junction protein at sites of cell-cell contacts[61,218].

Functional studies of tetracycline-induced tPKP2 cells showed that A733fsX740 PKP-2 protein appeared to be inserted competitively into cell membrane fraction together with endogenous PKP-2 and this caused dominant negative effects resulting in intermittent desmosomal linkages with pale plaques that largely lacked filaments. The lack of Cx-43 protein localized at the cell-cell contacts, enhanced apoptosis of induced tPKP2 cells subjected to mechanical cell stretch. Induced tPKP2 cells also showed increased cellular adhesion measured by two different assays, but the significance of this data is not clear, as it does not reconcile with the EM data showing abnormal DS linkages. Mechanical cell stretch of stable HEK 293 cells resulted in apoptosis of these cells, and although the mechanism was not investigated, it is possible that apoptosis in HEK 293 stable cells might occur by mechanisms similar to those in mechanical stretched rat neonatal cardiomyocytes *in vitro*[234,237,238]. The abnormal DS linkages in induced tPKP2 cells are believed to augment the level of cellular injury in these cells enhancing the apoptosis response of these cells compared to control induced wPKP2 cells expressing normal DS linkages. This assumption is in agreement with *in vivo* data obtained from cardiomyocytes of R2834H DP cardiac restricted transgenic mice showing increased apoptosis of these cells due to abnormalities in mechanical junctions assembled in these mice[163]. Strong adhesions are required in the ID of cardiomyocytes to prevent fragmentation as this structure, which is under continuous stress.

The lack of detectable signal by immuno-fluorescence staining confocal microscopy examination of Cx-43 protein localization at cell membranes of induced tPKP2 cells suggests that A733fsX740 PKP2 insertion into cell membranes might destabilise mechanical junctions preventing formation of Cx-43 gap junctions as a direct consequence of impaired cell-cell junctions found by EM examination of these cells. The dependence of mechanical junction stability in promoting gap junction formation is recognised[49,228,241] and supported by several

lines of evidence. For instance, gap junctions were known to associate into macromolecular complexes containing cell adhesion molecules[263,264] and interference with N-cadherin expression prevented gap junction formation[265]. Cardiac-specific loss of N-cadherin gene in mice also led to significant decrease in the amount of connexin found in gap junctions with ensuing slowing of ventricular conduction velocity[48]. Furthermore, in three cardiomyopathies (Carvajal Syndrome, Naxos disease and autosomal dominant ARVC) caused by defective linkage between adhesive junctions the remodelling of gap junctions was observed[42,43,51]. The absence of Cx-43 at plasma membranes of tPKP2 cells is an important finding as a reduction in Cx-43 protein immuno-histochemical staining at cell membrane is implicated as a possible mechanism for arrhythmogenesis. Expression of Connexin-43 protein alone appears not to be sufficient for the assembly of functional gap junctions as PKP-2 has been shown to play an essential role in regulating and coordinating the formation and interactions between mechanical junctions and electrical junctional complexes in cardiac cells using siRNA mediated inhibition studies of PKP-2 expression [218].

Comparison of cell input resistance measurements of induced wPKP2 cells (expressing Cx-43 at cell membranes) and in induced tPKP2 cells (not expressing Cx-43 at cell membranes) did not show a statistical difference in the conduction of pulsed current between these two cell types. Possible explanations for this might be that as a compensatory mechanism other Connexin subtypes might be expressed, or that although Cx-43 protein was not detected in induced tPKP2 cell membrane, this might be below the threshold detection level by confocal microscopy. If this was the case, then it could be possible that small amount of Cx-43 present at cell membrane would be sufficient to permit normal current conduction. It is known from transgenic mice models that the magnitude of Connexin 43 protein reduction required for ventricular arrhythmia is large (86-95%)[266]. Furthermore, computer modelling studies predict that reductions of up to 40% in gap junction content (without change in junction size) would be unlikely to have a major impact on conduction velocity[267]. Also, the total Connexin levels are shown to be indicators of potential capacity for cell-to-cell communication, but this does not provide information on the quantity of functional channels open[268].

The most striking feature of desmosomes in induced tPKP2 cells appear to be their intermittent coupling (indicating inappropriate assembly of the junction) with pale plaque (indicating reduced content of plaque proteins), predominant absence of filament association

in these desmosomes and altered alignment of filaments compared to induced wPKP2 cells. These dominant negative effects of A733fsX740 PKP-2 may be related to the reduced interaction of truncated PKP-2 with endogenous PG (this presumably result in reduced clustering of desmosomal proteins at the ODP); and the altered intermediate filament organization presumably result from disruption of the recruitment of endogenous DP by A733fsX740 PKP-2 into induced tPKP2 cell desmosomes. PKP-2 is important in recruiting DP to the desmosomal plaque[216,247] and reduced interaction of PG in immuno-complex with A733fsX740 PKP-2 may affect the intermediate filament organization in desmosomes as a recent study using electron tomography and immuno-labelling of keratinocytes from PG null mice (-/- PG) highlights an essential role of PG for the effective intermediate filament anchorage to desmosomes[269].

Functional studies examining the effects of S140F PKP-2 protein expression did not show substantial effects on cellular properties of induced mPKP2 cells. Expression of S140F PKP-2 appear to cause a gain of function in induced mPKP2 cells manifesting a striking effect on desmosome size and interaction of missense PKP-2 with β-catenin. The presence of extremely long desmosomes (seemingly formed by lateral fusion of adjacent desmosomes) in induced mPKP2 cells might not be caused by a direct effect of missense PKP-2 as PKP-2 *per se* is not known to control desmosome size. Either the loss of a serine residue and a putative phosphorylation site in S140F PKP-2 may directly affect the binding of PKP-2 to β-catenin by disrupting a domain important in this interaction or a signalling role of PKP-2 may be affected via altered protein-protein mediated interactions. The significantly reduced interaction of S140F PKP-2 with β-catenin may be one possible mechanism influencing the cross talk between adherens and desmosomal junctions, which seems particularly pertinent in the area composita of the ID in human cardiomyocytes where these proteins are intimately localized. This might explain the cardiomyopathy seen in patients carrying the c.C1604T PKP-2 gene mutation as the missense PKP-2 protein is quite likely to be incorporated into the area composita. Additionally it seems reasonable to suppose that PKP-4/p0071 might also mediate the cross-talk with PKP-2 in the area composita where these two proteins are intimately associated[137] and their interactions *in vitro*[250] can occur.

7.3 Insights into the role of desmoplakin in cell-cell adhesion

The desmosomal cadherin-plakoglobin complex is coupled to the IF network by desmoplakin, a member of the spectra-plakin family of proteins[197,270,271]. The amino terminus of DP binds to PG and plakophilins, whereas the carboxy-terminus interacts with IF[126,272]. Desmoplakin is expressed ubiquitously in all tissues possessing desmosomes. The importance of DP *in vivo* is supported by findings showing that DP-null mice die just after implantation at E6.5 owing to defects of the extraembryonic endoderm. These mice had significantly fewer desmosomes than wild-type mice[187], and the few desmosomes present were not attached to keratin intermediate filaments. These DP-null mice also revealed a role of DP in tissue morphogenesis as the embryos failed to undergo the massive cellular proliferation observed at E5-6. Furthermore, chimeric morulae expressing DP in extraembryonic tissues do not survive beyond E9.5 as a result of defects in the developing epidermis, neuroepithelium, and heart associated with disorganized desmosome assembly and severing of IF attachment[188,189].

7.4 Lessons learned from desmoplakin mutant protein expression functional study

Q273fsX288 DP polypeptide expression can exert a dominant negative effect on desmosomes of induced tDP cells; they lack the extensive filament association seen in desmosomes of induced wDP cells expressing full-length DP. This affects the adhesive strength of induced tDP monolayer, which is reduced compared to the adhesion of induced wDP monolayer; this might be caused by a lack of attachment of desmosomes to vimentin intermediate filaments resulting in a reduction in the width of the junctional plaques in induced tDP cells. Although expression of a truncated DP polypeptide showed an effect on desmosomes, it is quite likely that the c.818_819insA DP gene mutation may cause haploinsufficiency due to NMD of the transcript formed from the DP null allele. In humans, the recruitment of desmoplakin into desmosomes decreases when one of the allele is null, resulting in formation of rudimentary desmosomes with reduced IF attachment[154,155].

Previous mapping studies of amino acid residues in the N-terminal of DP[131,254] suggested that Q273fsX288 DP probably retains the sequence information important for desmosomal

targeting, but it lacks the domains essential for DP oligomerization and intermediate filament protein attachment. Functional study of Q273fsX288 DP expression showed that this protein was competitively inserted into induced tDP cell membranes, and possibly into induced tDP cell-cell contacts. Q273fsX288 DP appeared to interact normally with endogenous PG as well as PKP-2 and the content of these two armadillo proteins in various sub-cellular fractions or their cellular immuno co-localization with Q273fsX288 DP appeared not be significantly different when compared with induced wDP cells expressing full-length DP. However, although the extent of incorporation of endogenous DP into desmosomes of these cells was not examined, a striking absence of the extensive filament attachment to cell-cell junctions identified ultrastructurally suggested that the intermediate filament network was disrupted. Vimentin, one of several abundant IF proteins expressed in HEK 293 cells[227] was examined by immuno-staining localization in induced wDP and tDP cells as this protein together with desmin and keratin IF proteins are known to interact directly with desmoplakin in desmosomes. This showed that vimentin connected extensively with neighbouring cells in induced wDP cell clusters, but this was not the case in induced tDP cell clusters. Lack of an extensive vimentin network and ultrastructurally identifiable filaments in induced tDP cells was supported by examination of the adhesive strength of tDP monolayers, which showed that these fragmented readily when subjected to shearing. However, no effects on cellular proliferation or on the measured apoptosis following mechanical cell-stretch of these cells were observed. Induced tDP stable cells are similar in three respects with another inducible Tet-On system in A431 stable cell line expressing a 584 amino acid DP-NTP polypeptide. Firstly, as with to vimentin filament disruption in tDP cells, A431 cells dissociate Kertin8/18 intermediate filaments from their junctional plaques. Secondly, in induced A431 cells the total or cell surface distribution of desmosomal proteins was unaltered as was the case with the distribution of endogenous PG and PKP-2 in all cellular fractions and at the cell surface of induced tDP cells. Thirdly, both induced A431 cells and tDP cells were readily dissociated in Dispase-based monolayer dissociation assays.

7.5 Ultrastructure studies of cell-cell junctions in ARVC

In all three functional studies ultrastructurally identifiable changes in cell-cell junctions were observed, affecting desmosomes in induced tPKP2, mPKP2 and tDP cells in a different

manner. In induced tPKP2 cells, intermittent DS coupling with pale plaques and sparse filaments with abnormal orientations occurred. In induced mPKP2 significantly longer desmosomes were formed presumably by fusion of adjacent desmosomes, these had normal ODP and the expected association of filaments aligned normally as found in control induced wPKP2 cells. In induced tDP cells whilst desmsomes had apparently normal electron dense ODP, their filaments were localized to varying extent, affecting their desmosomal widths with many desmosomes lacking filament association altogether. Thus the effects of of these mutant desmosomal protein expression on desmosomes seem to be linked with separate functions of these desmosomal proteins explaining the differences in desmosomal lengths or widths; in the case of PKP-2 mutant protein expressions, distinct changes in desmosome morphology seem to be linked to domain specific effects caused by expression of PKP-2 mutant proteins, which might be modulated by disruption or activation of signalling functions of this molecule.

Literature review suggests that mutations in genes encoding DP, PKP-2 and DSG-2 can also lead to similar effects in desmosomes as found in induced tPKP2, mPKP2 and tDP cells. For example, a quantitative morphometric study of ARVC endomyocardial biopsies obtained from patients without any identified gene mutations and with some ten patients with mutations in DP, PKP-2 and DSG-2 genes analyzed by transmission electron microscopy[46] found that overall, mean desmosomal length and desmosomal percent length were both significantly higher in ARVC patients with these mutations. Desmosome number per unit length was significantly lower in ARVC patients with these mutations, whilst desmosomal gap was widened. In addition to these changes abnormally located long desmosomes, dissarranged filaments, abnormally small junction with intermitent DS couplings and pale plaques in the presence of a normal ID convolution index were observed. This study provided ultrastructural evidence of ID remodelling in ARVC patients in both genotype positive (carrying mutations in any of five known desmosomal genes) as well as genotype negative ARVC patients (lacking mutations in the coding regions of the five desmosomal genes), and confirmed earlier EM studies showing pale structures and flattened convolutions with rare or small desmosomes and decreased filaments[272,273]. Abnormal small junctions with series of intermittent repeated desmosomal couplings and elongated long desmosomes have been observed in ARVC, and these have similarly been observed in Carvajal syndrome caused by a recessive desmoplakin mutation[159]. Also PG-null mouse embryos showed decreased myofibril compliance and reduced cell-cell adhesion resulting from reduced desmosome numbers and

altered structure[185]. The ID of R2834H DP transgenic mice showed widening gaps and absence of desmsosmes[163]. Many of the ultrastructural features (such as intermittent desmosomal coupling, pale plaques, long desmosomes, and disruption to filaments) reported in the literature in ARVC[46,104] were also observed in EM analysis of cell-cell junctions in induced tPKP2, mPKP2, and tDP cells, this therefore raises the question whether the resulting desmosomal phenotypes are solely because of physical disruption of cell-cell adhesion or whether these are coupled with signalling mechanisms that influence additional cellular processes. The observed ultrastructural changes in HEK 293 cells would need to be examined in other cell systems to determine the relevance in a cardiac context.

7.6 Cardiomyocyte cell culture for investigating cell-cell adhesion

HEK 293 cells while being amenable to high plasmid transfection rates and offers ease of establishing stable cell constructs with an inducible system for mutant desmosomal protein expression, have an obvious limitation for studying the effects of these proteins in a cardiac context. In a recent study[246] rat neonatal cardiomyocytes were examined during 2 weeks in culture to assess their suitability as models cell systems for looking at perturbation at the ID. The ID is a very large, myocardium-specific and functionally sensitive structure. The importance of this structure is evident from a number of deletions or mutations in genes encoding ID proteins[40,41,45,100-104,107,109-111,113,162,163,190]. Cultures of rat neonatal cardiomyocytes when compared with cardiomyocytes *in situ* revealed that while these cell cultures are useful as limited models for myocardiac structure and function, they represent only incomplete albeit progressively deteriorating pathogenic copies of the natural cardiomyogenesis program. However, remarkably most of the plaque proteins examined (DP, PG PKP2, p120, α- and β-catenin) were localized at membrane structures in cardiomyocyte cultures. Neonatal rat ventricular cardiomyocytes cultures (NRVC) may therefore be a suitable *in vitro* model for assessing the loss of function of proteins involved in the adhering junctions at the area composita of the ID. NRVC can be problematic as low transfection efficiency could result in low expression of transfected gene products, but cloning into viral vectors should overcome this drawback.

7.7 Animal studies investigating mechanism of ARVC

As haploinsufficiency appears to be one of several mechanisms in cardiomyopathy seen in affected ARVC patients, animal models involving heterozygous gene expression (+/-) in a cardiac restricted pattern are especially suitable for examining frameshift mutations that undergo NMD to evaluate the *in vivo* effects of haploinsufficiency. NRVC obtained from transgenic mice expressing a mutant desmosomal protein (+/-) should also be a useful approach for future studies to examine the effects of a functional null allele. Several animal models have shed new light on the possible mechanisms of ARVC. A study in ten month old heterozygous PG deficient (PG +/-) mice examined the effect of a reduced PG expression in cardiac defects in these mice[275]. Isolated perfused plakoglobin (+/-) hearts had spontaneous ventricular tachycardia of right ventricular origin and prolonged right ventricular conduction times compared to wild-type hearts. Exercise training accelerated development of right ventricular dysfunction and arrhythmias in plakoglobin (+/-) mice. Histology and ultrastructure examination did not identify right ventricular abnormalities in affected animals. Thus, it was concluded that heterozygous plakoglobin deficiency provoked ARVC and accelerated manifestation of the phenotype in effort-induced training. The effect of effort induced studies in PKP-2 deficient (+/-)mice have not been reported, such a study may provide important clues about the loss of function of this protein *in vivo*, as PKP-2 gene mutations causing reading frame shift are by far the most predominant types of mutations in ARVC (Table 1.5)

In another study[56] using atrial myocyte cell lines expressing siRNA against DP, suppression of DP expression led to nuclear localization of plakoglobin, with a two-fold reduction in canonical Wnt/beta-catenin signalling through Tcf/Lef1 transcription factors. Increased expression of adipogenic and fibrogenic genes and accumulation of fat droplets were observed in these cell lines. Furthermore, a cardiac-restricted deletion of DP impaired cardiac morphogenesis with high embryonic lethality resulting in the homozygous (DP -/-) mice. Heterozygous (+/-) DP-deficient mice exhibited excess adipocytes and fibrosis in the myocardium, increased myocyte apoptosis, cardiac dysfunction, and ventricular arrhythmias[56], which seemed to recapitulate ARVC in human.

A transgenic mouse cardiac restricted over-expression model examining missense DP affecting the DP tail domain [163] showed that whereas mice over-expressing wild type DP had no detectable histologic, morphological, or functional cardiac changes, a transgenic mouse with R2834H DP over-expression showed increased cardiomyocyte apoptosis, cardiac fibrosis, and lipid accumulation, along with ventricular enlargement and cardiac dysfunction in both ventricles. Disruption of desmin-DP interactions were also seen in the ID of these mice and irregularly shaped ID with widening gaps affecting both AJ and desmosomes were identified ultrastructurally. Transgenic R2834H DP mice showed dissociation of a number of junctional proteins from cell-cell junctions (increased expression and redistribution of PG, PKP2 and β-catenin, and redistribution of Cx-43). The authors believed that these changes in various junctional complexes were probably secondary to DP-desmin disruption. The failure of desmin to localise with DP at ID of R2834H DP transgenic mice by IHC was a feature that was also noted in Carvajal syndrome[43]. Disruption in the desmin-DP interaction was suggested to lead to instability of desmosomes, resulting in a reduced resistance to the constant mechanical stress experienced by cardiomyocytes. Gross widening of junctions in the ID in R2834H transgenic mice reminiscent of human ARVC supported this contention.

The above genetically manipulated models of ARVC suggested that these animal models are important tools in assessing the molecular defects of cell-cell adhesion proteins providing insights on mechanisms of ARVC. However, there are also spontaneous models of ARVC described in the domestic cat[276] and boxer dogs[60], which might be useful for analyzing how genetic defects might cause ARVC. The canine model in this respects could be useful as it shows familial transmission of ARVC, and although screening of coding sequence of genes encoding desmosomal proteins have not as yet shown any defects in these genes[61,62], the model would appear to be useful in targeting the discovery of further unidentified genes involved in ARVC. The future studies from this work would be to test heterozygous mutations in cardiomyocyte cell cultures or in animal models where one affected allele (+/- system) encoding a mutant cell adhesion molecule is expressed in a cardiac restricted manner allowing the molecular defects of these proteins to be examined in the ID.

7.8 Genetic screening of ARVC cohort - Pitfalls

Although PKP-2 gene mutations result in missense, nonsense, frameshift, splice site mutations there are some apparently silent (synonymous) amino acid changes that can give rise to cryptic splicing in the PKP-2 mRNA, resulting from the loss of ESE elements or the creation of ESS elements in an exon sequence. One such change, involves a synonymous amino acid change (p.gly828) in an ARVC patient who had a homozygous mutation in PKP-2 (c.[2484C>T]+[2484C>T]), which caused predominantly cryptic splicing (resulting from creation of a novel splice donor site), with a 7 nucleotide deletion in exon 12 (r.[2483_2489del]). This caused a frame shift disrupting the last 54 amino acids of PKP2 resulting in extension of reading frame by 145 nucleotides (48 amino acids) into the 3'UTR[113]. A second alternatively spliced PKP2 form present in the proband and one of his children showed retention of intron 13-14 with proper splicing at other exon junctions, resulting in the addition of three additional nucleotide residues after exon 13 followed by premature termination with loss of 21 amino acids encoded by exon 14. Thus, the possibility of cryptic or alternative splicing should be considered in apparently synonymous amino acid substitutions found in ARVC. Other problems in genetic screening of ARVC cohorts include low frequencies of some ARVC mutations, some intronic nucleotide changes may be difficult to assign as mutations, and effect of modifier genes or presence of mutations in more than one gene can complicate the screening. An absence of mutation in any of the five known desmosomal genes[277] does not rule out ARVC, as mutations might be present in non-desmosomal genes[58,59] or in other unidentified genes. Rare polymorphisms may be difficult to distinguish from mutations, and assigning pathogenicity to missense sequence changes requires exhaustive literature searches, bioinformatics approach, and further genetic studies in an individual family to classify a sequence variant of unknown clinical significance. Screening of all five desmosomal genes implicated in ARVC is labour intensive and requires immense resources; some large genes, such as desmoplakin, pose a technical challenge for sequencing, but new sequencing technologies may alleviate these difficulties

7.9 Domain specific effects of DP mutations

Figure 1.10 shows the locations of twenty four DP mutations reported in the literature to date (June 2008) as well as the locations of three DP mutations identified from the present genetic

screening work. Why some missense mutations in the PRD of DP affect only the heart (p.R2834H DP) and others only the skin (p.R2336C DP) can be explained molecularly by the different binding sites for desmin (cardic IF) or keratin (skin IF) binding sites that are disrupted in the PRD by these mutations. Nonetheless, the effect of the vast majority of the missense and nonsense mutations in this region on the binding of desmin and keratin IFs to desmosomes is not different; they all produced both an abnormal skin and heart phenotype due to reduced attachment of desmosomes to IF proteins[157,161]. Missense mutations in the plakin domain that affect both the heart and the skin have also been found[160]. These defects are most likely associated with a failure of desmoplakin to bind to plakoglobin since mutations in plakoglobin cause a very similar disorder in both humans and mice, i.e. skin defects associated with developmental anomalies of the hair and cardiomyopathy[38,186]. Why some of the missense mutations in the plakin domain only affect the heart, while others affect both the heart and the skin is an open question, but it is clear that the different clinical manifestations cannot be explained by the failure of desmoplakin to bind to either plakoglobin or plakophillin-2.

7.10 Conclusions from studies undertaken

Inclusion of genetic screening of mutations in genes frequently mutated in ARVC would clearly improve the clinical criteria from a simply diagnostic standpoint; however, given that ARVC is a genetically heterogenous disease, with incomplete penetrance, with presence of frequent 'private family' mutations, and a disease where the possiblity of further unidentified gene mutations is high and existing screening already involves the coverage of a large genomic region of approximately 40Kb – these factors would weigh down on the cost benefit for population based screening/diagnosis of this disease using a genetic approach.

The confirmation of an abnormal genotype, particularly in family members, could identify carriers at risk for transmitting ARVC to offsprings and who might potentially develop clinical manifestations of ARVC. Conversely, the absence of a particular genotype identified in a family would greatly argue against ARVC, especially in asymptomatic individuals. The presence alone of an abnormal genotype may not predict high risk in an individual, but it should prompt vigilant care. In an individual with boderline clinical findings, an abnormal genotype may aid in securing an ARVC clinical diagnosis, although perhaps such an

individual may be at a lower risk than an individual with overt clinical manifestations. Recent studies have shown that the type of gene mutation in ARVC is also important. For example, patients with ARVC due to PKP-2 mutations were found to have propensity for earlier arrhythmias than patients who met Task Force criteria but did not carry PKP-2 mutations[108]. Genetic screening of human ARVC cohort showed mutations affecting various parts of the plakophilin-2 and desmoplakin protein domains, and by far, the most frequent mutations, were found to reside in the plakophilin-2 gene with all domains of the protein molecule appearing to be affected.

The Flp-In T-Rex HEK 293 cell line is a useful *in vitro* model system allowing the role of mutant PKP-2 and DP proteins to be investigated at the level of desmosomes and cellular functions. The Flp-In T-Rex HEK293 cell model has been used successfuly to examine the Ryanodine receptor2 protein mutations *in vitro* to determine the effect of C terminal mutations in storage-overload-induced Ca^{2+} release [278]. This showed the versatility of the Flp-In cell sytem as RyR2 is fairly large protein molecule to express and assemble appropriately in these cells for functional analysis.

The value of the work performed is to show that ARVC is a genetic disease of the desmosomes, affecting the genes encoding PKP-2 and DP, and in out of a total of eleven mutations found, seven were novel mutations, and with gene mutations being inherited in families in an autosomal dominant manner with incomplete pentrance due to age and sex of the individual. Three separate mutations affecting at the protein level: p.S140F PKP-2, p.A733fsX740 PKP-2 and p.Q2273fsX288 DP were examined in stable HEK 293 cells using protein expression studies, cellular assays and analysis of desmosomes in cell lines expressing these mutant proteins. S140F PKP-2 caused a gain of function with formation of long desmosomes and reduced interaction with β-catenin, suggesting that loss of a putative serine phosphorylation site in PKP-2 may possibly be involved in signal transduction and the changes observed ultrastructurally in desmosomes. Expression of A733fsX740 PKP-2 and Q273fsX288 DP proteins each caused distinct dominant negative effects on desmosome morphology and in cellular functions specific to the roles of these two proteins; the effect of A733fsX740 PKP-2 also revealed a dominant negative effect on Cx-43 protein localization at cell-cell contacts and enhanced apoptosis of cells expressing this truncated plakophilin-2; the dominant negative effects in cells expressing A733fsX740 PKP-2 may be caused by the

reduced interaction of expressed A733fsX740 PKP-2 protein with PG. Disparate effects on cell-cell adhesion and desmosome morphology were observed in stable cells expressing S140F PKP-2 and A733fsX740 PKP-2 proteins, but these effects may be due to a complex expression pattern of various IF proteins in HEK 293 cells that might modulate cell-cell adhesion in a different manner. These functional studies have provided important mechanisms to explain the cardiomyopathy and arrhythmogenesis seen in patients inheriting these gene mutations in PKP-2 and DP, and a framework for further future studies (see chapters 4, 5, and 6 under 'Future Studies') using cardiac relevant cell culture systems and mice models to investigate how gene mutations might be linked to the observed changes in ARVC *in vivo*. While many of the features of ARVC can be explained by functional studies in HEK 293 cells, recent studies have also postulated molecular mechanisms for adipogenesis[56,59] to explain the fatty or fibrofatty replacement of cardiomyocytes occurring in ARVC.

Bibliography

1. Richardson P, M.W., Bristow M, Maish B, Mautner B, O'Connell J, et al . Report of the 1995 World Health Organization/International Society and Federation of cardiology Task Force on Defination and Classification of Cardiomyopathies. *Circulation* **93**, 841-842 (1996).
2. Dalla Volta, S., Battaglia, G. & Zerbini, E. "Auricularization' of right ventricular pressure curve. *Am Heart J* **61**, 25-33 (1961).
3. Fontaine G, G.G., Frank R,. Stimulation studies and epicardial mapping in ventricular tachycardia: study of mechanisms and selection for surgery. *In: Kulbertus HE (ed). Reentrant arrhythmias: Mechanism and treatments Lancaster: MTP Press Limited*, 333-350 (1977).
4. Corrado, D. et al. Spectrum of clinicopathologic manifestations of arrhythmogenic right ventricular cardiomyopathy/dysplasia: a multicenter study. *J Am Coll Cardiol* **30**, 1512-20 (1997).
5. Fontaine, G., Fontaliran, F. & Frank, R. Arrhythmogenic right ventricular cardiomyopathies: clinical forms and main differential diagnoses. *Circulation* **97**, 1532-5 (1998).
6. Hamid, M.S. et al. Prospective evaluation of relatives for familial arrhythmogenic right ventricular cardiomyopathy/dysplasia reveals a need to broaden diagnostic criteria. *J Am Coll Cardiol* **40**, 1445-50 (2002).
7. Corrado, D. et al. Arrhythmogenic right ventricular dysplasia/cardiomyopathy: need for an international registry. Study Group on Arrhythmogenic Right Ventricular Dysplasia/Cardiomyopathy of the Working Groups on Myocardial and Pericardial Disease and Arrhythmias of the European Society of Cardiology and of the Scientific Council on Cardiomyopathies of the World Heart Federation. *Circulation* **101**, E101-6 (2000).
8. Yoshioka, N. et al. Electrocardiographic and echocardiographic abnormalities in patients with arrhythmogenic right ventricular cardiomyopathy and in their pedigrees. *Am J Cardiol* **85**, 885-9, A9 (2000).
9. De Pasquale, C.G. & Heddle, W.F. Left sided arrhythmogenic ventricular dysplasia in siblings. *Heart* **86**, 128-30 (2001).
10. Michalodimitrakis, M., Papadomanolakis, A., Stiakakis, J. & Kanaki, K. Left side right ventricular cardiomyopathy. *Med Sci Law* **42**, 313-7 (2002).
11. Okabe, M., Fukuda, K., Nakashima, Y., Arakawa, K. & Kikuchi, M. An isolated left ventricular lesion associated with left ventricular tachycardia-arrhythmogenic "left" ventricular dysplasia? *Jpn Circ J* **59**, 49-54 (1995).
12. Marcus, F.I. et al. Right ventricular dysplasia: a report of 24 adult cases. *Circulation* **65**, 384-98 (1982).
13. Thiene, G., Nava, A., Corrado, D., Rossi, L. & Pennelli, N. Right ventricular cardiomyopathy and sudden death in young people. *N Engl J Med* **318**, 129-33 (1988).
14. Burke, A.P., Farb, A., Tashko, G. & Virmani, R. Arrhythmogenic right ventricular cardiomyopathy and fatty replacement of the right ventricular myocardium: are they different diseases? *Circulation* **97**, 1571-80 (1998).
15. Basso, C. et al. Arrhythmogenic right ventricular cardiomyopathy. Dysplasia, dystrophy, or myocarditis? *Circulation* **94**, 983-91 (1996).
16. Sheppard, M.N. Arrhythmogenic right ventricular dysplasia and arrhythmogenic right ventricular cardiomyopathy: do these entities exist and are they the same disease? *Curr Diag Pathol* **5**, 150-156 (1998).
17. Fontaliran, F. et al. [Nosologic frontiers of arrhythmogenic dysplasia. Quantitative variations of normal adipose tissue of the right heart ventricle]. *Arch Mal Coeur Vaiss* **84**, 33-38 (1991).
18. Corrado, D., Basso, C., Rizzoli, G., Schiavon, M. & Thiene, G. Does sports activity enhance the risk of sudden death in adolescents and young adults? *J Am Coll Cardiol* **42**, 1959-1963 (2003).
19. Fontaine, G. et al. Arrhythmogenic right ventricular dysplasia. *Annu.Rev Med* **50**, 17-35 (1999).
20. Gemayel, C., Pelliccia, A. & Thompson, P.D. Arrhythmogenic right ventricular cardiomyopathy. *J Am Coll Cardiol* **38**, 1773-81 (2001).
21. Norman, M.W. & McKenna, W.J. Arrhythmogenic right ventricular cardiomyopathy: perspectives on disease. *Z Kardiol* **88**, 550-4 (1999).
22. Pawel, B.R. et al. Sudden death in childhood due to right ventricular dysplasia: report of two cases. *Pediatr Pathol* **14**, 987-95 (1994).

23. McKenna, W.J. et al. Diagnosis of arrhythmogenic right ventricular dysplasia/cardiomyopathy. Task Force of the Working Group Myocardial and Pericardial Disease of the European Society of Cardiology and of the Scientific Council on Cardiomyopathies of the International Society and Federation of Cardiology. *Br Heart J* **71**, 215-8 (1994).
24. Basso, C., Corrado, D. & Thiene, G. Cardiovascular causes of sudden death in young individuals including athletes. *Cardiol Rev* **7**, 127-35 (1999).
25. Corrado, D., Basso, C., Schiavon, M. & Thiene, G. Screening for hypertrophic cardiomyopathy in young athletes. *N Engl J Med* **339**, 364-9 (1998).
26. Corrado, D., Thiene, G., Nava, A., Rossi, L. & Pennelli, N. Sudden death in young competitive athletes: clinicopathologic correlations in 22 cases. *Am J Med* **89**, 588-96 (1990).
27. Cho, Y. et al. Arrhythmogenic right ventricular cardiomyopathy and sudden cardiac death in young Koreans. *Circ J* **67**, 925-8 (2003).
28. Tabib, A. et al. Circumstances of death and gross and microscopic observations in a series of 200 cases of sudden death associated with arrhythmogenic right ventricular cardiomyopathy and/or dysplasia. *Circulation* **108**, 3000-5 (2003).
29. Sen-Chowdhry, S., Syrris, P. & McKenna, W.J. Genetics of right ventricular cardiomyopathy. *J Cardiovasc Electrophysiol* **16**, 927-35 (2005).
30. Castillo, E. et al. Arrhythmogenic right ventricular dysplasia: ex vivo and in vivo fat detection with black-blood MR imaging. *Radiology* **232**, 38-48 (2004).
31. Bluemke, D.A. et al. MR Imaging of arrhythmogenic right ventricular cardiomyopathy: morphologic findings and interobserver reliability. *Cardiology* **99**, 153-62 (2003).
32. Bomma, C. et al. Misdiagnosis of arrhythmogenic right ventricular dysplasia/cardiomyopathy. *J Cardiovasc Electrophysiol* **15**, 300-6 (2004).
33. Paul, M., Schulze-Bahr, E., Breithardt, G. & Wichter, T. Genetics of arrhythmogenic right ventricular cardiomyopathy--status quo and future perspectives. *Z Kardiol* **92**, 128-36 (2003).
34. Jaoude, S.A., Leclercq, J.F. & Coumel, P. Progressive ECG changes in arrhythmogenic right ventricular disease. Evidence for an evolving disease. *Eur.Heart J* **17**, 1717-1722 (1996).
35. Fontaine, G. et al. Arrhythmogenic right ventricular dysplasia. *Annu Rev Med* **50**, 17-35 (1999).
36. Gear, K. & Marcus, F. Arrhythmogenic right ventricular dysplasia/cardiomyopathy. *Circulation* **107**, e31-3 (2003).
37. Leclercq, J.F. & Coumel, P. Characteristics, prognosis and treatment of the ventricular arrhythmias of right ventricular dysplasia. *Eur Heart J* **10 Suppl D**, 61-7 (1989).
38. McKoy, G. et al. Identification of a deletion in plakoglobin in arrhythmogenic right ventricular cardiomyopathy with palmoplantar keratoderma and woolly hair (Naxos disease). *Lancet* **355**, 2119-24 (2000).
39. Rampazzo, A. et al. Mutation in human desmoplakin domain binding to plakoglobin causes a dominant form of arrhythmogenic right ventricular cardiomyopathy. *Am J Hum Genet* **71**, 1200-6 (2002).
40. Gerull, B. et al. Mutations in the desmosomal protein plakophilin-2 are common in arrhythmogenic right ventricular cardiomyopathy. *Nat Genet* **36**, 1162-4 (2004).
41. Syrris, P. et al. Clinical expression of plakophilin-2 mutations in familial arrhythmogenic right ventricular cardiomyopathy. *Circulation* **113**, 356-64 (2006).
42. Kaplan, S.R. et al. Remodeling of myocyte gap junctions in arrhythmogenic right ventricular cardiomyopathy due to a deletion in plakoglobin (Naxos disease). *Heart Rhythm* **1**, 3-11 (2004).
43. Kaplan, S.R. et al. Structural and molecular pathology of the heart in Carvajal syndrome. *Cardiovasc Pathol* **13**, 26-32 (2004).
44. Vatta, M., Marcus, F. & Towbin, J.A. Arrhythmogenic right ventricular cardiomyopathy: a 'final common pathway' that defines clinical phenotype. *Eur Heart J* **28**, 529-530 (2007).
45. Tsatsopoulou, A.A., Protonotarios, N.I. & McKenna, W.J. Arrhythmogenic right ventricular dysplasia, a cell adhesion cardiomyopathy: insights into disease pathogenesis from preliminary genotype--phenotype assessment. *Heart* **92**, 1720-1723 (2006).
46. Basso, C. et al. Ultrastructural evidence of intercalated disc remodelling in arrhythmogenic right ventricular cardiomyopathy: an electron microscopy investigation on endomyocardial biopsies. *Eur Heart J* **27**, 1847-54 (2006).
47. Kostetskii, I. et al. Induced deletion of the N-cadherin gene in the heart leads to dissolution of the intercalated disc structure. *Circ Res* **96**, 346-354 (2005).

48. Li, J. et al. Cardiac-specific loss of N-cadherin leads to alteration in connexins with conduction slowing and arrhythmogenesis. *Circ Res* **97**, 474-481 (2005).
49. Li, J., Patel, V.V. & Radice, G.L. Dysregulation of cell adhesion proteins and cardiac arrhythmogenesis. *Clin Med Res* **4**, 42-52 (2006).
50. Saffitz, J.E., Hames, K.Y. & Kanno, S. Remodeling of gap junctions in ischemic and nonischemic forms of heart disease. *J Membr Biol* **218**, 65-71 (2007).
51. Asimaki, A. et al. A novel dominant mutation in plakoglobin causes arrhythmogenic right ventricular cardiomyopathy. *Am J Hum Genet.* **81**, 964-973 (2007).
52. Logan, C.Y. & Nusse, R. The Wnt signaling pathway in development and disease. *Annu Rev Cell Dev Biol* **20**, 781-810 (2004).
53. Willert, K. & Jones, K.A. Wnt signaling: is the party in the nucleus? *Genes Dev.* **20**, 1394-1404 (2006).
54. Hoppler, S. & Kavanagh, C.L. Wnt signalling: variety at the core. *J Cell Sci* **120**, 385-393 (2007).
55. Zhurinsky, J., Shtutman, M. & Ben Ze'ev, A. Plakoglobin and beta-catenin: protein interactions, regulation and biological roles. *J Cell Sci* **113**, 3127-3139 (2000).
56. Garcia-Gras, E. et al. Suppression of canonical Wnt/beta-catenin signaling by nuclear plakoglobin recapitulates phenotype of arrhythmogenic right ventricular cardiomyopathy. *J Clin Invest* **116**, 2012-2021 (2006).
57. MacRae, C.A., Birchmeier, W. & Thierfelder, L. Arrhythmogenic right ventricular cardiomyopathy: moving toward mechanism. *J Clin Invest* **116**, 1825-8 (2006).
58. Beffagna, G. et al. Regulatory mutations in transforming growth factor-beta3 gene cause arrhythmogenic right ventricular cardiomyopathy type 1. *Cardiovasc Res* **65**, 366-73 (2005).
59. Merner, N.D. et al. Arrhythmogenic Right Ventricular Cardiomyopathy Type 5 Is a Fully Penetrant, Lethal Arrhythmic Disorder Caused by a Missense Mutation in the TMEM43 Gene. *Am J Hum Genet* **In Press, Corrected Proof. Am J Hum Genet. (2008), doi:10.1016/j.ajhg.2008.01.010**(2008).
60. Basso, C. et al. Arrhythmogenic right ventricular cardiomyopathy causing sudden cardiac death in boxer dogs: a new animal model of human disease. *Circulation* **109**, 1180-1185 (2004).
61. Oxford, E.M. et al. Molecular composition of the intercalated disc in a spontaneous canine animal model of arrhythmogenic right ventricular dysplasia/cardiomyopathy. *Heart Rhythm* **4**, 1196-1205 (2007).
62. Meurs, K.M., Ederer, M.M. & Stern, J.A. Desmosomal gene evaluation in Boxers with arrhythmogenic right ventricular cardiomyopathy. *Am J Vet Res* **68**, 1338-1341 (2007).
63. Mallat, Z. et al. Evidence of apoptosis in arrhythmogenic right ventricular dysplasia. *N Engl J Med* **335**, 1190-6 (1996).
64. Valente, M. et al. In vivo evidence of apoptosis in arrhythmogenic right ventricular cardiomyopathy. *Am J Pathol* **152**, 479-84 (1998).
65. Dokuparti, M.V., Pamuru, P.R., Thakkar, B., Tanjore, R.R. & Nallari, P. Etiopathogenesis of arrhythmogenic right ventricular cardiomyopathy. *J Hum Genet.* **50**, 375-381 (2005).
66. James, T.N. Normal and abnormal consequences of apoptosis in the human heart. From postnatal morphogenesis to paroxysmal arrhythmias. *Circulation* **90**, 556-73 (1994).
67. Kavantzas, N.G., Lazaris, A.C., Agapitos, E.V., Nanas, J. & Davaris, P.S. Histological assessment of apoptotic cell death in cardiomyopathies. *Pathology* **32**, 176-80 (2000).
68. Nagata, M. et al. Apoptotic cell death in arrhythmogenic right ventricular cardiomyopathy: a comparative study with idiopathic sustained ventricular tachycardia. *Jpn Heart J* **41**, 733-41 (2000).
69. Nishikawa, T. et al. Programmed cell death in the myocardium of arrhythmogenic right ventricular cardiomyopathy in children and adults. *Cardiovasc Pathol* **8**, 185-9 (1999).
70. Yamaji, K. et al. Apoptotic myocardial cell death in the setting of arrhythmogenic right ventricular cardiomyopathy. *Acta Cardiol* **60**, 465-70 (2005).
71. Yamomoto S, T.V., James TN. Morphological patterns of death by myocytes in arrhythmogenic right ventricular dysplasia. *Am J Med Sci* **320**, 310-319 (2000).
72. Runge, M.S. et al. Morphological patterns of death by myocytes in arrhythmogenic right ventricular dysplasia. *Am J Med Sci* **320**, 310-9 (2000).
73. Culbertson, M.R. RNA surveillance. Unforeseen consequences for gene expression, inherited genetic disorders and cancer. *Trends Genet* **15**, 74-80 (1999).

74. Chang, Y.F., Imam, J.S. & Wilkinson, M.F. The nonsense-mediated decay RNA surveillance pathway. *Annu Rev Biochem* **76**, 51-74 (2007).
75. Conti, E. & Izaurralde, E. Nonsense-mediated mRNA decay: molecular insights and mechanistic variations across species. *Curr Opin Cell Biol* **17**, 316-325 (2005).
76. Holbrook, J.A., Neu-Yilik, G., Hentze, M.W. & Kulozik, A.E. Nonsense-mediated decay approaches the clinic. *Nat Genet* **36**, 801-808 (2004).
77. Kuzmiak, H.A. & Maquat, L.E. Applying nonsense-mediated mRNA decay research to the clinic: progress and challenges. *Trends Mol Med* **12**, 306-316 (2006).
78. Amrani, N., Sachs, M.S. & Jacobson, A. Early nonsense: mRNA decay solves a translational problem. *Nat Rev Mol Cell Biol* **7**, 415-425 (2006).
79. Frischmeyer, P.A. & Dietz, H.C. Nonsense-mediated mRNA decay in health and disease. *Hum Mol Genet* **8**, 1893-1900 (1999).
80. Stoilov, P. et al. Defects in pre-mRNA processing as causes of and predisposition to diseases. *DNA Cell Biol* **21**, 803-818 (2002).
81. Caceres, J.F. & Kornblihtt, A.R. Alternative splicing: multiple control mechanisms and involvement in human disease. *Trends Genet* **18**, 186-193 (2002).
82. Maquat, L.E. Nonsense-mediated mRNA decay: splicing, translation and mRNP dynamics. *Nat Rev Mol Cell Biol* **5**, 89-99 (2004).
83. Lejeune, F. & Maquat, L.E. Mechanistic links between nonsense-mediated mRNA decay and pre-mRNA splicing in mammalian cells. *Curr Opin Cell Biol* **17**, 309-315 (2005).
84. Basso, C. et al. Arrhythmogenic right ventricular cardiomyopathy: clinical registry and database, evaluation of therapies, pathology registry, DNA banking. *Eur Heart J* **25**, 531-534 (2004).
85. Rampazzo, A. et al. Arrhythmogenic right ventricular cardiomyopathy type 1 (ARVD1): confirmation of locus assignment and mutation screening of four candidate genes. *Eur J Hum Genet* **11**, 69-76 (2003).
86. Kapoun, A.M. et al. B-type natriuretic peptide exerts broad functional opposition to transforming growth factor-beta in primary human cardiac fibroblasts: fibrosis, myofibroblast conversion, proliferation, and inflammation. *Circ Res* **94**, 453-61 (2004).
87. Yoshida, M. et al. Transforming growth factor-beta stimulates the expression of desmosomal proteins in bronchial epithelial cells. *Am J Respir Cell Mol Biol* **6**, 439-45 (1992).
88. Tiso, N. et al. Identification of mutations in the cardiac ryanodine receptor gene in families affected with arrhythmogenic right ventricular cardiomyopathy type 2 (ARVD2). *Hum Mol Genet* **10**, 189-94 (2001).
89. Laitinen, P.J. et al. Mutations of the cardiac ryanodine receptor (RyR2) gene in familial polymorphic ventricular tachycardia. *Circulation* **103**, 485-90 (2001).
90. Priori, S.G. et al. Mutations in the cardiac ryanodine receptor gene (hRyR2) underlie catecholaminergic polymorphic ventricular tachycardia. *Circulation* **103**, 196-200 (2001).
91. Severini, G.M. et al. A new locus for arrhythmogenic right ventricular dysplasia on the long arm of chromosome 14. *Genomics* **31**, 193-200 (1996).
92. Rampazzo, A. et al. ARVD4, a new locus for arrhythmogenic right ventricular cardiomyopathy, maps to chromosome 2 long arm. *Genomics* **45**, 259-63 (1997).
93. Ahmad, F. et al. Localization of a gene responsible for arrhythmogenic right ventricular dysplasia to chromosome 3p23. *Circulation* **98**, 2791-5 (1998).
94. Asano, Y. et al. Lamr1 functional retroposon causes right ventricular dysplasia in mice. *Nat Genet* **36**, 123-30 (2004).
95. Li, D. et al. The locus of a novel gene responsible for arrhythmogenic right-ventricular dysplasia characterized by early onset and high penetrance maps to chromosome 10p12-p14. *Am J Hum Genet* **66**, 148-56 (2000).
96. Melberg, A. et al. Autosomal dominant myofibrillar myopathy with arrhythmogenic right ventricular cardiomyopathy linked to chromosome 10q. *Ann Neurol* **46**, 684-92 (1999).
97. Selcen, D. & Engel, A.G. Mutations in ZASP define a novel form of muscular dystrophy in humans. *Ann Neurol* **57**, 269-76 (2005).
98. Nava, A. et al. Clinical profile of concealed form of arrhythmogenic right ventricular cardiomyopathy presenting with apparently idiopathic ventricular arrhythmias. *Int J Cardiol* **35**, 195-206; discussion 207-9 (1992).
99. Beffagna, G. et al. Missense mutations in Desmocollin-2 N-terminus, associated with arrhythmogenic right ventricular cardiomyopathy, affect intracellular localization of desmocollin-2 in vitro. *BMC Med Genet* **8**, 65 (2007).

100. Awad, M.M. et al. DSG2 mutations contribute to arrhythmogenic right ventricular dysplasia/cardiomyopathy. *Am J Hum Genet* **79**, 136-42 (2006).
101. Syrris, P. et al. Desmoglein-2 mutations in arrhythmogenic right ventricular cardiomyopathy: a genotype-phenotype characterization of familial disease. *Eur Heart J* (2006).
102. Syrris, P. et al. Arrhythmogenic right ventricular dysplasia/cardiomyopathy associated with mutations in the desmosomal gene desmocollin-2. *Am J Hum Genet* **79**, 978-84 (2006).
103. Heuser, A. et al. Mutant desmocollin-2 causes arrhythmogenic right ventricular cardiomyopathy. *Am J Hum Genet* **79**, 1081-8 (2006).
104. Pilichou, K. et al. Mutations in desmoglein-2 gene are associated with arrhythmogenic right ventricular cardiomyopathy. *Circulation* **113**, 1171-9 (2006).
105. Rampazzo, A. et al. The gene for arrhythmogenic right ventricular cardiomyopathy maps to chromosome 14q23-q24. *Hum Mol Genet* **3**, 959-62 (1994).
106. Rampazzo, A. et al. A new locus for arrhythmogenic right ventricular cardiomyopathy (ARVD2) maps to chromosome 1q42-q43. *Hum Mol Genet* **4**, 2151-4 (1995).
107. van Tintelen, J.P. et al. Plakophilin-2 mutations are the major determinant of familial arrhythmogenic right ventricular dysplasia/cardiomyopathy. *Circulation* **113**, 1650-8 (2006).
108. Dalal, D. et al. Clinical features of arrhythmogenic right ventricular dysplasia/cardiomyopathy associated with mutations in plakophilin-2. *Circulation* **113**, 1641-9 (2006).
109. Nagaoka, I. et al. Novel mutation of plakophilin-2 associated with arrhythmogenic right ventricular cardiomyopathy. *Circ J* **70**, 933-5 (2006).
110. Antoniades, L. et al. Arrhythmogenic right ventricular cardiomyopathy caused by deletions in plakophilin-2 and plakoglobin (Naxos disease) in families from Greece and Cyprus: genotype-phenotype relations, diagnostic features and prognosis. *Eur Heart J* **27**, 2208-16 (2006).
111. Kannankeril, P.J. et al. Arrhythmogenic right ventricular cardiomyopathy due to a novel plakophilin 2 mutation: wide spectrum of disease in mutation carriers within a family. *Heart Rhythm* **3**, 939-44 (2006).
112. Lahtinen, A.M. et al. Plakophilin-2 missense mutations in arrhythmogenic right ventricular cardiomyopathy. *Int J Cardiol.* (2007).
113. Awad, M.M. et al. Recessive arrhythmogenic right ventricular dysplasia due to novel cryptic splice mutation in PKP2. *Hum Mutat* **27**, 1157 (2006).
114. Coonar, A.S. et al. Gene for arrhythmogenic right ventricular cardiomyopathy with diffuse nonepidermolytic palmoplantar keratoderma and woolly hair (Naxos disease) maps to 17q21. *Circulation* **97**, 2049-58 (1998).
115. Jou, T.S., Stewart, D.B., Stappert, J., Nelson, W.J. & Marrs, J.A. Genetic and biochemical dissection of protein linkages in the cadherin-catenin complex. *Proc Natl Acad Sci U S A* **92**, 5067-71 (1995).
116. Stappert, J. & Kemler, R. A short core region of E-cadherin is essential for catenin binding and is highly phosphorylated. *Cell Adhes Commun* **2**, 319-27 (1994).
117. Butz, S., Stappert, J., Weissig, H. & Kemler, R. Plakoglobin and beta-catenin: distinct but closely related. *Science* **257**, 1142-4 (1992).
118. Knudsen, K.A. & Wheelock, M.J. Plakoglobin, or an 83-kD homologue distinct from beta-catenin, interacts with E-cadherin and N-cadherin. *J Cell Biol* **118**, 671-9 (1992).
119. Peifer, M., McCrea, P.D., Green, K.J., Wieschaus, E. & Gumbiner, B.M. The vertebrate adhesive junction proteins beta-catenin and plakoglobin and the Drosophila segment polarity gene armadillo form a multigene family with similar properties. *J Cell Biol* **118**, 681-91 (1992).
120. Huber, A.H., Nelson, W.J. & Weis, W.I. Three-dimensional structure of the armadillo repeat region of beta-catenin. *Cell* **90**, 871-82 (1997).
121. Huber, A.H. & Weis, W.I. The structure of the beta-catenin/E-cadherin complex and the molecular basis of diverse ligand recognition by beta-catenin. *Cell* **105**, 391-402 (2001).
122. Pokutta, S. & Weis, W.I. Structure of the dimerization and beta-catenin-binding region of alpha-catenin. *Mol Cell* **5**, 533-43 (2000).
123. Nagafuchi, A., Ishihara, S. & Tsukita, S. The roles of catenins in the cadherin-mediated cell adhesion: functional analysis of E-cadherin-alpha catenin fusion molecules. *J Cell Biol* **127**, 235-45 (1994).
124. North, A.J. et al. Molecular map of the desmosomal plaque. *J Cell Sci* **112**, 4325-36 (1999).
125. Burdett, I.D. Aspects of the structure and assembly of desmosomes. *Micron* **29**, 309-28 (1998).

126. Getsios, S., Huen, A.C. & Green, K.J. Working out the strength and flexibility of desmosomes. *NatRev Mol Cell Biol* **5**, 271-281 (2004).
127. Jamora, C. & Fuchs, E. Intercellular adhesion, signalling and the cytoskeleton. *Nat Cell Biol* **4**, E101-8 (2002).
128. Marshall, J.M. The heart. *Medical Physiology* **13th ed.**(1974).
129. Schwarz, M.A., Owaribe, K., Kartenbeck, J. & Franke, W.W. Desmosomes and hemidesmosomes: constitutive molecular components. *Annu Rev Cell Biol* **6**, 461-91 (1990).
130. Schmelz, M. & Franke, W.W. Complexus adhaerentes, a new group of desmoplakin-containing junctions in endothelial cells: the syndesmos connecting retothelial cells of lymph nodes. *Eur J Cell Biol* **61**, 274-89 (1993).
131. Stappenbeck, T.S. et al. Functional analysis of desmoplakin domains: specification of the interaction with keratin versus vimentin intermediate filament networks. *J Cell Biol* **123**, 691-705 (1993).
132. Stappenbeck, T.S. & Green, K.J. The desmoplakin carboxyl terminus coaligns with and specifically disrupts intermediate filament networks when expressed in cultured cells. *J Cell Biol* **116**, 1197-1209 (1992).
133. Meng, J.J., Bornslaeger, E.A., Green, K.J., Steinert, P.M. & Ip, W. Two-hybrid Analysis Reveals Fundamental Differences in Direct Interactions between Desmoplakin and Cell Type-specific Intermediate Filaments. *J Biol Chem* **272**, 21495-21503 (1997).
134. Huber, O. Structure and function of desmosomal proteins and their role in development and disease. *Cell Mol Life Sci* **60**, 1872-90 (2003).
135. McGrath, J.A. Hereditary diseases of desmosomes. *J Dermatol Sci* **20**, 85-91 (1999).
136. Magin, T.M., Reichelt, J. & Hatzfeld, M. Emerging functions: diseases and animal models reshape our view of the cytoskeleton. *Exp Cell Res* **301**, 91-102 (2004).
137. Borrmann, C.M. et al. The area composita of adhering junctions connecting heart muscle cells of vertebrates. II. Colocalizations of desmosomal and fascia adhaerens molecules in the intercalated disk. *Eur J Cell Biol* **85**, 469-485 (2006).
138. Franke, W.W., Borrmann, C.M., Grund, C. & Pieperhoff, S. The area composita of adhering junctions connecting heart muscle cells of vertebrates. I. Molecular definition in intercalated disks of cardiomyocytes by immunoelectron microscopy of desmosomal proteins. *Eur J Cell Biol* **85**, 69-82 (2006).
139. Severs, N.J. The cardiac gap junction and intercalated disc. *Int J Cardiol***26**, 137-173 (1990).
140. Sohl, G., Odermatt, B., Maxeiner, S., Degen, J. & Willecke, K. New insights into the expression and function of neural connexins with transgenic mouse mutants. *Brain Res Brain Res Rev* **47**, 245-259 (2004).
141. Kanter, H.L., Saffitz, J.E. & Beyer, E.C. Cardiac myocytes express multiple gap junction proteins. *Circ Res* **70**, 438-44 (1992).
142. Severs, N.J. et al. Gap junction alterations in human cardiac disease. *Cardiovasc Res* **62**, 368-77 (2004).
143. Severs, N.J. et al. Remodelling of gap junctions and connexin expression in heart disease. *Biochim Biophys Acta* **1662**, 138-48 (2004).
144. Desplantez, T., Dupont, E., Severs, N.J. & Weingart, R. Gap junction channels and cardiac impulse propagation. *J Membr Biol* **218**, 13-28 (2007).
145. Sepp, R., Severs, N.J. & Gourdie, R.G. Altered patterns of cardiac intercellular junction distribution in hypertrophic cardiomyopathy. *Heart* **76**, 412-7 (1996).
146. Severs, N.J. et al. Alterations in cardiac connexin expression in cardiomyopathies. *Adv Cardiol* **42**, 228-242 (2006).
147. Leithe, E. & Rivedal, E. Ubiquitination of gap junction proteins. *J Membr Biol* **217**, 43-51 (2007).
148. Herve, J.C., Derangeon, M., Bahbouhi, B., Mesnil, M. & Sarrouilhe, D. The Connexin Turnover, an Important Modulating Factor of the Level of Cell-to-Cell Junctional Communication: Comparison with Other Integral Membrane Proteins. *J Membr Biol* **217**, 21-33 (2007).
149. Solan, J.L. & Lampe, P.D. Key connexin 43 phosphorylation events regulate the gap junction life cycle. *J Membr Biol* **217**, 35-41 (2007).
150. Godsel, L.M., S. Getsios, A.C. Huen, and K.J. Green. . The molecular composition and function of desmosomes. *In Cell Adhesion. J.N. Behrens and W.J. Nelson, editors. Springer-Verlag New York, Inc., New York.*, 137–193. (2004).

151. Hunt, D.M. et al. Spectrum of dominant mutations in the desmosomal cadherin desmoglein 1, causing the skin disease striate palmoplantar keratoderma. *Eur J Hum Genet* **9**, 197-203 (2001).
152. Rickman, L. et al. N-terminal deletion in a desmosomal cadherin causes the autosomal dominant skin disease striate palmoplantar keratoderma. *Hum Mol Genet* **8**, 971-6 (1999).
153. Kljuic, A. et al. Desmoglein 4 in hair follicle differentiation and epidermal adhesion: evidence from inherited hypotrichosis and acquired pemphigus vulgaris. *Cell* **113**, 249-60 (2003).
154. Armstrong, D.K. et al. Haploinsufficiency of desmoplakin causes a striate subtype of palmoplantar keratoderma. *Hum Mol Genet* **8**, 143-8 (1999).
155. Whittock, N.V. et al. Striate palmoplantar keratoderma resulting from desmoplakin haploinsufficiency. *J Invest Dermatol* **113**, 940-6 (1999).
156. Norgett, E.E. et al. Early death from cardiomyopathy in a family with autosomal dominant striate palmoplantar keratoderma and woolly hair associated with a novel insertion mutation in desmoplakin. *J Invest Dermatol* **126**, 1651-1654 (2006).
157. Alcalai, R., Metzger, S., Rosenheck, S., Meiner, V. & Chajek-Shaul, T. A recessive mutation in desmoplakin causes arrhythmogenic right ventricular dysplasia, skin disorder, and woolly hair. *J Am Coll Cardiol* **42**, 319-27 (2003).
158. Uzumcu, A. et al. Loss of desmoplakin isoform I causes early onset cardiomyopathy and heart failure in a Naxos-like syndrome. *J Med Genet* **43**, e5 (2006).
159. Norgett, E.E. et al. Recessive mutation in desmoplakin disrupts desmoplakin-intermediate filament interactions and causes dilated cardiomyopathy, woolly hair and keratoderma. *Hum Mol Genet* **9**, 2761-6 (2000).
160. Whittock, N.V. et al. Compound heterozygosity for non-sense and mis-sense mutations in desmoplakin underlies skin fragility/woolly hair syndrome. *J Invest Dermatol* **118**, 232-8 (2002).
161. Jonkman, M.F. et al. Loss of desmoplakin tail causes lethal acantholytic epidermolysis bullosa. *Am J Hum Genet* 77, 653-660 (2005).
162. Norman, M. et al. Novel mutation in desmoplakin causes arrhythmogenic left ventricular cardiomyopathy. *Circulation* **112**, 636-42 (2005).
163. Yang, Z. et al. Desmosomal dysfunction due to mutations in desmoplakin causes arrhythmogenic right ventricular dysplasia/cardiomyopathy. *Circ Res* **99**, 646-55 (2006).
164. Bauce, B. et al. Clinical profile of four families with arrhythmogenic right ventricular cardiomyopathy caused by dominant desmoplakin mutations. *Eur Heart J* **26**, 1666-1675 (2005).
165. Sen-Chowdhry, S. et al. Clinical and genetic characterization of families with arrhythmogenic right ventricular dysplasia/cardiomyopathy provides novel insights into patterns of disease expression. *Circulation* **115**, 1710-1720 (2007).
166. McGrath, J.A. et al. Mutations in the plakophilin 1 gene result in ectodermal dysplasia/skin fragility syndrome. *Nat Genet* **17**, 240-4 (1997).
167. Whittock, N.V. et al. Genomic amplification of the human plakophilin 1 gene and detection of a new mutation in ectodermal dysplasia/skin fragility syndrome. *J Invest Dermatol* **115**, 368-74 (2000).
168. Amagai, M. Autoimmunity against desmosomal cadherins in pemphigus. *J Dermatol Sci* **20**, 92-102 (1999).
169. Nousari, H.C. & Anhalt, G.J. Pemphigus and bullous pemphigoid. *Lancet* **354**, 667-72 (1999).
170. Hashimoto, T. Immunopathology of paraneoplastic pemphigus. *Clin dermatol* **19**, 675-682 (2001).
171. Amagai, M., Matsuyoshi, N., Wang, Z.H., Andl, C. & Stanley, J.R. Toxin in bullous impetigo and staphylococcal scalded-skin syndrome targets desmoglein 1. *Nat Med* **6**, 1275-7 (2000).
172. Amagai, M. et al. Staphylococcal exfoliative toxin B specifically cleaves desmoglein 1. *J Invest Dermatol* **118**, 845-50 (2002).
173. Hanakawa, Y. et al. Molecular mechanisms of blister formation in bullous impetigo and staphylococcal scalded skin syndrome. *J Clin Invest* **110**, 53-60 (2002).
174. Hanakawa, Y. et al. Enzymatic and molecular characteristics of the efficiency and specificity of exfoliative toxin cleavage of desmoglein 1. *J Biol Chem* **279**, 5268-77 (2004).
175. Lewis, J.E. et al. Cross-talk between adherens junctions and desmosomes depends on plakoglobin. *J Cell Biol* **136**, 919-34 (1997).
176. Willert, K. & Nusse, R. Beta-catenin: a key mediator of Wnt signaling. *Curr Opin Genet Dev* **8**, 95-102 (1998).

177. Shtutman, M. et al. The cyclin D1 gene is a target of the beta-catenin/LEF-1 pathway. *Proc Natl Acad Sci U S A* **96**, 5522-7 (1999).
178. Orsulic, S. & Peifer, M. An in vivo structure-function study of armadillo, the beta-catenin homologue, reveals both separate and overlapping regions of the protein required for cell adhesion and for wingless signaling. *J Cell Biol* **134**, 1283-300 (1996).
179. Maeda, O. et al. Plakoglobin (gamma-catenin) has TCF/LEF family-dependent transcriptional activity in beta-catenin-deficient cell line. *Oncogene* **23**, 964-72 (2004).
180. Williams, B.O., Barish, G.D., Klymkowsky, M.W. & Varmus, H.E. A comparative evaluation of beta-catenin and plakoglobin signaling activity. *Oncogene* **19**, 5720-8 (2000).
181. Muller, J., Ritt, D.A., Copeland, T.D. & Morrison, D.K. Functional analysis of C-TAK1 substrate binding and identification of PKP2 as a new C-TAK1 substrate. *Embo J* **22**, 4431-42 (2003).
182. Mertens, C. et al. Nuclear particles containing RNA polymerase III complexes associated with the junctional plaque protein plakophilin 2. *Proc Natl Acad Sci U S A* **98**, 7795-800 (2001).
183. Chen, X., Bonne, S., Hatzfeld, M., van Roy, F. & Green, K.J. Protein binding and functional characterization of plakophilin 2. Evidence for its diverse roles in desmosomes and beta - catenin signaling. *J Biol Chem* **277**, 10512-22 (2002).
184. Hatzfeld, M. Plakophilins: Multifunctional proteins or just regulators of desmosomal adhesion? *Biochim Biophys Acta* **1773**, 69-77 (2007).
185. Bierkamp, C., McLaughlin, K.J., Schwarz, H., Huber, O. & Kemler, R. Embryonic heart and skin defects in mice lacking plakoglobin. *Dev Biol* **180**, 780-5 (1996).
186. Ruiz, P. et al. Targeted mutation of plakoglobin in mice reveals essential functions of desmosomes in the embryonic heart. *J Cell Biol* **135**, 215-25 (1996).
187. Gallicano, G.I. et al. Desmoplakin is required early in development for assembly of desmosomes and cytoskeletal linkage. *J Cell Biol* **143**, 2009-22 (1998).
188. Gallicano, G.I., Bauer, C. & Fuchs, E. Rescuing desmoplakin function in extra-embryonic ectoderm reveals the importance of this protein in embryonic heart, neuroepithelium, skin and vasculature. *Development* **128**, 929-41 (2001).
189. Vasioukhin, V., Bowers, E., Bauer, C., Degenstein, L. & Fuchs, E. Desmoplakin is essential in epidermal sheet formation. *Nat Cell Biol* **3**, 1076-85 (2001).
190. Grossmann, K.S. et al. Requirement of plakophilin 2 for heart morphogenesis and cardiac junction formation. *J Cell Biol* **167**, 149-60 (2004).
191. Eshkind, L. et al. Loss of desmoglein 2 suggests essential functions for early embryonic development and proliferation of embryonal stem cells. *Eur J Cell Biol* **81**, 592-598 (2002).
192. Allen, E., Yu, Q.C. & Fuchs, E. Mice expressing a mutant desmosomal cadherin exhibit abnormalities in desmosomes, proliferation, and epidermal differentiation. *J Cell Biol* **133**, 1367-1382 (1996).
193. Serpente, N. et al. Extracellularly truncated desmoglein 1 compromises desmosomes in MDCK cells. *Mol Membr Biol* **17**, 175-183 (2000).
194. Koch, P.J. et al. Targeted disruption of the pemphigus vulgaris antigen (desmoglein 3) gene in mice causes loss of keratinocyte cell adhesion with a phenotype similar to pemphigus vulgaris. *J Cell Biol* **137**, 1091-1102 (1997).
195. Hughes, S.E. & McKenna, W.J. New insights into the pathology of inherited cardiomyopathy. *Heart* **91**, 257-64 (2005).
196. Angst, B.D., Nilles, L.A. & Green, K.J. Desmoplakin II expression is not restricted to stratified epithelia. *J Cell Sci* **97**, 247-257 (1990).
197. Sonnenberg, A., Rojas, A.M. & de Pereda, J.M. The structure of a tandem pair of spectrin repeats of plectin reveals a modular organization of the plakin domain. *J Mol Biol* **368**, 1379-1391 (2007).
198. Jefferson, J.J., Ciatto, C., Shapiro, L. & Liem, R.K. Structural analysis of the plakin domain of bullous pemphigoid antigen1 (BPAG1) suggests that plakins are members of the spectrin superfamily. *J Mol Biol* **366**, 244-257 (2007).
199. Lapouge, K. et al. New insights into the molecular basis of desmoplakin- and desmin-related cardiomyopathies. *J Cell Sci* **119**, 4974-4985 (2006).
200. Virata, M.L., Wagner, R.M., Parry, D.A. & Green, K.J. Molecular structure of the human desmoplakin I and II amino terminus. *Proc Natl Acad Sci U.S.A* **89**, 544-548 (1992).
201. Green, K.J. et al. Structure of the human desmoplakins. Implications for function in the desmosomal plaque. *J Biol Chem* **265**, 2603-2612 (1990).

202. Gorlov, I.P., Gorlova, O.Y., Frazier, M.L. & Amos, C.I. Missense mutations in hMLH1 and hMSH2 are associated with exonic splicing enhancers. *Am J Hum Genet* **73**, 1157-1161 (2003).
203. Liu, H.X., Cartegni, L., Zhang, M.Q. & Krainer, A.R. A mechanism for exon skipping caused by nonsense or missense mutations in BRCA1 and other genes. *Nat Genet* **27**, 55-58 (2001).
204. Wang, Z. et al. Systematic identification and analysis of exonic splicing silencers. *Cell* **119**, 831-845 (2004).
205. Sironi, M. et al. Silencer elements as possible inhibitors of pseudoexon splicing. *Nucleic Acids Res* **32**, 1783-1791 (2004).
206. Unsold, B.W. et al. Abstract 1054: Severe Manifestation of Arrhythmogenic Right Ventricular Cardiomyopathy (ARVC) in a Family with a Nonsense-Mutation in the Plakophilin-2 Gene. *Circulation* **114**, II_194-a (2006).
207. Dalal, D. et al. Penetrance of mutations in plakophilin-2 among families with arrhythmogenic right ventricular dysplasia/cardiomyopathy. *J Am Coll Cardiol* **48**, 1416-24 (2006).
208. Otterspoor, L.C. et al. Arrhythmogenic right ventricular cardiomyopathy: asymptomatic to life threatening as illustrated by the cases of two sisters. *Neth Heart J* **15**, 348-353 (2007).
209. van der Smagt, J.J. et al. Abstract 2723: Large Genomic Deletions in Plakophilin-2 are a Rare Cause of ARVD/C and ARVD/C-like Disease. *Circulation* **116**, II_604-a (2007).
210. Schafer, S., Koch, P.J. & Franke, W.W. Identification of the ubiquitous human desmoglein, Dsg2, and the expression catalogue of the desmoglein subfamily of desmosomal cadherins. *Exp Cell Res* **211**, 391-399 (1994).
211. Nuber, U.A., Schafer, S., Schmidt, A., Koch, P.J. & Franke, W.W. The widespread human desmocollin Dsc2 and tissue-specific patterns of synthesis of various desmocollin subtypes. *Eur J Cell Biol* **66**, 69-74 (1995).
212. Huen, A.C. et al. Intermediate filament-membrane attachments function synergistically with actin-dependent contacts to regulate intercellular adhesive strength. *J Cell Biol* **159**, 1005-1017 (2002).
213. Corrado, D. & Thiene, G. Arrhythmogenic right ventricular cardiomyopathy/dysplasia: clinical impact of molecular genetic studies. *Circulation* **113**, 1634-1637 (2006).
214. Nava, A. et al. Clinical profile and long-term follow-up of 37 families with arrhythmogenic right ventricular cardiomyopathy. *J Am Coll Cardiol.* **36**, 2226-2233 (2000).
215. Sen-Chowdhry, S., Syrris, P. & McKenna, W.J. Role of genetic analysis in the management of patients with arrhythmogenic right ventricular dysplasia/cardiomyopathy. *J Am Coll Cardiol* **50**, 1813-1821 (2007).
216. Godsel, L.M. et al. Desmoplakin assembly dynamics in four dimensions: multiple phases differentially regulated by intermediate filaments and actin. *J Cell Biol* **171**, 1045-59 (2005).
217. Bornslaeger, E.A., Corcoran, C.M., Stappenbeck, T.S. & Green, K.J. Breaking the connection: displacement of the desmosomal plaque protein desmoplakin from cell-cell interfaces disrupts anchorage of intermediate filament bundles and alters intercellular junction assembly. *J Cell Biol* **134**, 985-1001 (1996).
218. Oxford, E.M. et al. Connexin43 Remodeling Caused by Inhibition of Plakophilin-2 Expression in Cardiac Cells. *Circ Res* **101**, 703-711 (2007).
219. Wang, Y. et al. Cellular Uptake of Exogenous Human PDCD5 Protein. *J Biol Chem* **281**, 24803-24817 (2006).
220. Dai, F.F. et al. The Neuronal Ca2+ Sensor Protein Visinin-like Protein-1 Is Expressed in Pancreatic Islets and Regulates Insulin Secretion. *J Biol Chem* **281**, 21942-21953 (2006).
221. Mertens, C., Kuhn, C. & Franke, W.W. Plakophilins 2a and 2b: constitutive proteins of dual location in the karyoplasm and the desmosomal plaque. *J Cell Biol* **135**, 1009-1025 (1996).
222. Sobolik-Delmaire, T., Katafiasz, D. & Wahl, J.K., 3rd. Carboxyl terminus of Plakophilin-1 recruits it to plasma membrane, whereas amino terminus recruits desmoplakin and promotes desmosome assembly. *J Biol Chem* **281**, 16962-70 (2006).
223. Hofmann, I. et al. Interaction of plakophilins with desmoplakin and intermediate filament proteins: an in vitro analysis. *J Cell Sci* **113**, 2471-2483 (2000).
224. Klymkowsky, M.W. Plakophilin, armadillo repeats, and nuclear localization. *Microsc Res Tech* **45**, 43-54 (1999).
225. Stappenbeck, T.S., Lamb, J.A., Corcoran, C.M. & Green, K.J. Phosphorylation of the desmoplakin COOH terminus negatively regulates its interaction with keratin intermediate filament networks. *J Biol Chem* **269**, 29351-29354 (1994).

226. Yin, T. et al. Mechanisms of plakoglobin-dependent adhesion: desmosome-specific functions in assembly and regulation by epidermal growth factor receptor. *J Biol Chem* **280**, 40355-40363 (2005).
227. Shaw, G., Morse, S., Ararat, M. & Graham, F.L. Preferential transformation of human neuronal cells by human adenoviruses and the origin of HEK 293 cells. *FASEB J* **16**, 869-871 (2002).
228. Saffitz, J.E. Adhesion molecules: why they are important to the electrophysiologist. *J Cardiovasc Electrophysiol* **17**, 225-229 (2006).
229. Hengartner, M.O. The biochemistry of apoptosis. *Nature* **407**, 770-776 (2000).
230. Bishopric, N.H., Andreka, P., Slepak, T. & Webster, K.A. Molecular mechanisms of apoptosis in the cardiac myocyte. *Curr Opin Pharmacol* **1**, 141-150 (2001).
231. Green, D.R. & Reed, J.C. Mitochondria and apoptosis. *Science* **281**, 1309-1312 (1998).
232. Wang, X. The expanding role of mitochondria in apoptosis. *Genes Dev* **15**, 2922-2933 (2001).
233. Gross, A., McDonnell, J.M. & Korsmeyer, S.J. BCL-2 family members and the mitochondria in apoptosis. *Genes Dev* **13**, 1899-1911 (1999).
234. Ashkenazi, A. & Dixit, V.M. Death receptors: signaling and modulation. *Science* **281**, 1305-1308 (1998).
235. Pan, J. et al. Mechanical stretch activates the JAK/STAT pathway in rat cardiomyocytes. *Circ Res* **84**, 1127-1136 (1999).
236. Leri, A. et al. Stretch-mediated release of angiotensin II induces myocyte apoptosis by activating p53 that enhances the local renin-angiotensin system and decreases the Bcl-2-to-Bax protein ratio in the cell. *J Clin Invest* **101**, 1326-1342 (1998).
237. Leri, A. et al. Inhibition of p53 function prevents renin-angiotensin system activation and stretch-mediated myocyte apoptosis. *Am J Pathol* **157**, 843-857 (2000).
238. van Kesteren, C.A. et al. Cultured neonatal rat cardiac myocytes and fibroblasts do not synthesize renin or angiotensinogen: evidence for stretch-induced cardiomyocyte hypertrophy independent of angiotensin II. *Cardiovasc Res* **43**, 148-156 (1999).
239. Pimentel, D.R. et al. Reactive oxygen species mediate amplitude-dependent hypertrophic and apoptotic responses to mechanical stretch in cardiac myocytes. *Circ Res* **89**, 453-460 (2001).
240. Liao, X.D., Wang, X.H., Jin, H.J., Chen, L.Y. & Chen, Q. Mechanical stretch induces mitochondria-dependent apoptosis in neonatal rat cardiomyocytes and G2/M accumulation in cardiac fibroblasts. *Cell Res* **14**, 16-26 (2004).
241. Liao, X., Wang, X., Gu, Y., Chen, Q. & Chen, L.Y. Involvement of death receptor signaling in mechanical stretch-induced cardiomyocyte apoptosis. *Life Sci* 77, 160-174 (2005).
242. Saffitz, J.E. Dependence of electrical coupling on mechanical coupling in cardiac myocytes: insights gained from cardiomyopathies caused by defects in cell-cell connections. *Ann N Y Acad Sci* **1047**, 336-344 (2005).
243. Pieperhoff, S., Schumacher, H. & Franke, W.W. The area composita of adhering junctions connecting heart muscle cells of vertebrates. V. The importance of plakophilin-2 demonstrated by small interference RNA-mediated knockdown in cultured rat cardiomyocytes. *Eur J Cell Biol* **In Press, Corrected Proof. Eur. J. Cell Biol. (2008), doi:10.1016/j.ejcb.2007.12.002**(2008).
244. Thomas, N., Dupont, E., Halliday, D., Fry, C.H. & Severs, N.J. An inducible cell system to investigate connexin co-expression and action potential propagation within the heart. *J Mol Cell Cardiol* **40**, 984 (2006).
245. Pieperhoff, S. & Franke, W.W. The area composita of adhering junctions connecting heart muscle cells of vertebrates - IV: Coalescence and amalgamation of desmosomal and adhaerens junction components - Late processes in mammalian heart development. *Eur J Cell Biol* **86**, 377-391 (2007).
246. Franke, W.W. et al. The area composita of adhering junctions connecting heart muscle cells of vertebrates - III: Assembly and disintegration of intercalated disks in rat cardiomyocytes growing in culture. *Eur J Cell Biol* **86**, 127-142 (2007).
247. Bass-Zubek, A.E. et al. Plakophilin 2: a critical scaffold for PKC{alpha} that regulates intercellular junction assembly. *J Cell Biol* **Corrected Proof. J Cell Biol. (2008), doi:10.1083/jcb.200712133**(2008).
248. Davidson, M.M. et al. Novel cell lines derived from adult human ventricular cardiomyocytes. *J Mol Cell Cardiol* **39**, 133-147 (2005).
249. Palka, H.L. & Green, K.J. Roles of plakoglobin end domains in desmosome assembly. *J Cell Sci* **110**, 2359-2371 (1997).

250. Hatzfeld, M., Green, K.J. & Sauter, H. Targeting of p0071 to desmosomes and adherens junctions is mediated by different protein domains. *J Cell Sci* **116**, 1219-1233 (2003).
251. Gumbiner, B., Stevenson, B. & Grimaldi, A. The role of the cell adhesion molecule uvomorulin in the formation and maintenance of the epithelial junctional complex. *J Cell Biol* **107**, 1575-1587 (1988).
252. Kowalczyk, A.P. et al. The amino-terminal domain of desmoplakin binds to plakoglobin and clusters desmosomal cadherin-plakoglobin complexes. *J Cell Biol* **139**, 773-784 (1997).
253. Kowalczyk, A.P. et al. The head domain of plakophilin-1 binds to desmoplakin and enhances its recruitment to desmosomes. Implications for cutaneous disease. *J Biol Chem* **274**, 18145-18148 (1999).
254. Smith, E.A. & Fuchs, E. Defining the interactions between intermediate filaments and desmosomes. *J Cell Biol* **141**, 1229-1241 (1998).
255. Schmidt, A. & Jager, S. Plakophilins--hard work in the desmosome, recreation in the nucleus? *Eur J Cell Biol* **84**, 189-204 (2005).
256. South, A.P. Plakophilin 1: an important stabilizer of desmosomes. *Clin Exp Dermatol* **29**, 161-167 (2004).
257. Hatzfeld, M., Haffner, C., Schulze, K. & Vinzens, U. The function of plakophilin 1 in desmosome assembly and actin filament organization. *J Cell Biol* **149**, 209-222 (2000).
258. Wahl, J.K., 3rd. A role for plakophilin-1 in the initiation of desmosome assembly. *J Cell Biochem* **96**, 390-403 (2005).
259. South, A.P. et al. Lack of plakophilin 1 increases keratinocyte migration and reduces desmosome stability. *J Cell Sci* **116**, 3303-3314 (2003).
260. Bornslaeger, E.A. et al. Plakophilin 1 interferes with plakoglobin binding to desmoplakin, yet together with plakoglobin promotes clustering of desmosomal plaque complexes at cell-cell borders. *J Cell Sci* **114**, 727-38 (2001).
261. Goossens, S. et al. A unique and specific interaction between alphaT-catenin and plakophilin-2 in the area composita, the mixed-type junctional structure of cardiac intercalated discs. *J Cell Sci* **120**, 2126-2136 (2007).
262. Lahtinen, A.M. et al. Plakophilin-2 missense mutations in arrhythmogenic right ventricular cardiomyopathy. *Int J Cardiol* **126**, 92-100 (2007).
263. Giepmans, B.N. Gap junctions and connexin-interacting proteins. *Cardiovasc Res* **62**, 233-245 (2004).
264. Wei, C.J., Xu, X. & Lo, C.W. Connexins and cell signaling in development and disease. *Annu Rev Cell Dev Biol* **20**, 811-838 (2004).
265. Wei, C.J., Francis, R., Xu, X. & Lo, C.W. Connexin43 associated with an N-cadherin-containing multiprotein complex is required for gap junction formation in NIH3T3 cells. *J Biol Chem* **280**, 19925-19936 (2005).
266. Gutstein, D.E. et al. Conduction slowing and sudden arrhythmic death in mice with cardiac-restricted inactivation of connexin43. *Circ Res* **88**, 333-339 (2001).
267. Jongsma, H.J. & Wilders, R. Gap junctions in cardiovascular disease. *Circ Res* **86**, 1193-1197 (2000).
268. Severs, N.J. et al. Remodelling of gap junctions and connexin expression in heart disease. *Biochim Biophys Acta* **1662**, 138-148 (2004).
269. Acehan, D. et al. Plakoglobin Is Required for Effective Intermediate Filament Anchorage to Desmosomes. *J Invest Dermatol* **Corrected Proof. J Invest dermatol. (2008), doi:10.1038/jid.2008.141**(2008).
270. Leung, C.L., Liem, R.K., Parry, D.A. & Green, K.J. The plakin family. *J Cell Sci* **114**, 3409-3410 (2001).
271. Leung, C.L., Green, K.J. & Liem, R.K. Plakins: a family of versatile cytolinker proteins. *Trends Cell Biol* **12**, 37-45 (2002).
272. Yin, T. & Green, K.J. Regulation of desmosome assembly and adhesion. *Semin Cell Dev Biol* **15**, 665-677 (2004).
273. Guiraudon, C.M. Histological diagnosis of right ventricular dysplasia: a role for electron microscopy? *Eur Heart J* **10 Suppl D**, 95-96 (1989).
274. Roncali, L., Nico, B., Locuratolo, N., Bertossi, M. & Chiddo, A. Right ventricular dysplasia: an ultrastructural study. *Eur Heart J* **10 Suppl D**, 97-99 (1989).
275. Kirchhof, P. et al. Age- and training-dependent development of arrhythmogenic right ventricular cardiomyopathy in heterozygous plakoglobin-deficient mice. *Circulation* **114**, 1799-1806 (2006).

276. Fox, P.R., Maron, B.J., Basso, C., Liu, S.K. & Thiene, G. Spontaneously occurring arrhythmogenic right ventricular cardiomyopathy in the domestic cat: A new animal model similar to the human disease. *Circulation* **102**, 1863-1870 (2000).
277. Awad, M.M., Calkins, H. & Judge, D.P. Mechanisms of disease: molecular genetics of arrhythmogenic right ventricular dysplasia/cardiomyopathy. *Nat Clin Pract Cardiovasc Med* **5**, 258-267 (2008).
278. Kong, H. et al. Skeletal and Cardiac Ryanodine Receptors Exhibit Different Responses to Ca2+ Overload and Luminal Ca2+. *Biophys J* **92**, 2757-2770 (2007).